KINETICS AND ENGINE PERFORMANCE OF BIODIESEL PRODUCED FROM SELECTED NON EDIBLESEEDSOILS USING ACTIVATED CLAY CATALYSTS

BY

UDE CALLISTUS NONSO

2014217010P

A DISSERTATION SUBMITTED TO THE DEPARTMENT OF CHEMICAL ENGINEERING
FACULTY OF ENGINEERING
SCHOOL OF POST GRADUATE STUDIES
NNAMDI AZIKIWE UNIVERSITY, AWKA, NIGERIA

IN PARTIAL FULFILLMENT OF THE REQUIREMENT FOR THE AWARD OF DOCTOR OF PHILOSOPHY (Ph.D) DEGREE IN CHEMICAL ENGINEERING

SUPERVISOR: ENGR. PROF. O. D. ONUKWULI

OCTOBER, 2019

CERTIFICATION

This is to certify that the dissertation on **"KINETICS AND ENGINE PERFORMANCE OF BIODIESEL PRODUCED FROM SELECTED NON EDIBLE (AFRICAN PEARAND GMELINA SEEDS) SEEDS OILS USING ACTIVATED CLAY CATALYSTS"** was carried out in the Department of Chemical Engineering, Nnamdi Azikiwe University, Awka by Ude Callistus Nonso under the supervision of Engr. Prof. O. D. Onukwuli.

---------- ----------

ENGR. UDE CALLISTUS .N. **DATE**

(STUDENT)

APPROVAL PAGE

We hereby certify that the dissertation titled "Kinetics and Engine Performance of Biodiesel produced from selected non edible (African pear and Gmelina seed) seeds oils by activated clay catalysts" by Ude, Callistus Nonso with Registration No. 2014217010P, satisfied the standard in partial fulfillment of the requirements for the award of Doctor of Philosophy (Ph.D) in Chemical Engineering.

_____ _____

ENGR. PROF. O. D. ONUKWULI **DATE**
(SUPERVISOR)

_____ _____

ENGR. PROF. M. C. MENKITI **DATE**
HEAD OF DEPARTMENT

_____ _____

ENGR. PROF. K. O. OKPALA
(EXTERNAL EXAMINER) **DATE**

_____ _____

ENGR. PROF. H. C. HAROLD **DATE**
(DEAN, FACULTY OF ENGINEERING)

_____ _____

ENGR. PROF. P. K. IGBOKWE **DATE**
(DEAN, SCHOOL OF POST-GRADUATE STUDIES)

DEDICATION

This work is dedicated to my parents, Mr. Ude J.N and Mrs Ude Louisa for their relentless efforts and support to give me the best of education. It is also dedicated to my lovely wife Ude Precious for her unalloyed support and my uncle Mr. Francis Ude for his propelling advice and inspiration.

ACKNOWLEDGEMENTS

My special gratitude goes to Almighty God for His guidance, blessing, wisdom and knowledge He gave to me during this programme.

My gratitude goes to the Nnamdi Azikiwe University, Awka, particularly Chemical Engineering Department for granting me the opportunity to purse a PhD programme and for all the support during the period of study.

My heartfelt appreciation goes to my supervisor,Engr. Prof. O.D. Onukwuli for the support and tutelage given to me during the study and research period. My gratitude goes to Engr. Prof. P.K. Igbokwe, Engr. Dr. R. O. Ajemba, Engr. Dr. J. T. Nwabanne, Engr. Prof. M. C. Menkiti (HOD Chemical Engineering), Engr. Dr. V.O. Ugonabo, Engr. S. O. Nwokolo, all the staff (academic and non academic staff) in Chemical Engineering Department, Nnamdi Azikiwe University, Awka, Anambra State.

The support and assistance of Engr. Dr. C. Agulanna (DG PRODA), Dr. Ezemokwe, Dr. (Mrs) Nwogu, Engr. Dr. E. C. Oriaku, Engr. C. C. Njoku, Mr. Henry Nwakama, Engr. Udeh Nnamdi, Engr. Collins Elendu and all the staff of PRODA-MET laboratory and ERDP Department are appreciated.

I thank Engr. Agbo, Mr. Orji and staff of UNN Mechanical Engineering Power Laboratory for their help. I also appreciate Mr. Yakubu Isah and staff of Central Multipurpose Laboratory Ahmed Bello University, ABU, Zaria, Kaduna State for their assistance.

I also acknowledge the support of my lovely and caring wife, Ude Precious who in diverse ways has contributed immensely to this work. I am grateful to my parents, my uncle Ude Francis and siblings for their financial, emotional, spiritual, moral and dynamic support during the programme.

“May the Almighty God richly bless everyone that share in the success of the work. Amen.”

ABSTRACT

The kinetics and engine performance of biodiesel from African pear seed oil (APO) and Gmelina seed oil (GSO) by modified clay catalysts were carried out. The catalyst was synthesized by activating it with heat, phosphoric acid and sodium hydroxide. They were characterized using American Society for Testing Materials (ASTM) D4067 (1986) standard methods to determine their phsico-chemical properties.The parameters investigated for transesterification of the oils were the reaction time 1, 2, 3, 4 and 5hours, catalysts concentration 1, 2, 3, 4 and 5 % wt,methanol/oil molar ratio 6:1, 8:1, 10:1, 12:1 and 14:1, reaction temperature 45, 50, 55, 60 and 65^{o}C and agitation speed 100, 200, 300, 400 and 500rpm. The oil were extracted by solvent extraction using two solvents: n-hexane and petroleum ether and the process parameters were optimized using response surface methodology (RSM). The physical and chemical properties of the oil and biodiesel were determinedusing (ASTM) 6751(1973) standard methods in order to investigate the effects of the properties of the triglyceride and the reaction parameters on the product characteristics and yields. The biodiesel process parameters were optimized using response surface methodology (RSM) in combination with central composite design, CCD. The heterogeneous catalysis kinetics was studied using two elementary reaction mechanisms: Eley-Rideal (ER) and Langmuir–Hinshelwood–Hougen–Watson (LHHW).The engine performance was carried out with a steady-state diesel engine test bed. Some of the experimental data were used to train and develop Artificial Neural Network (ANN) model based on optimization algorithm for the engine performance and biodiesel production. The results obtained proved that the modification of the clay improved its catalytic properties thereby facilitating the production of biodiesel. The results obtained show that n-hexane and petroleum ether are good solvents for extracting APO and GSO. The properties of the APO and GSO determined showed that they require pretretment but the use of the modified clay catalyst circumvented the process. The reaction conditions did not significantly affect the properties of the biodiesel but affected the yield. The yield increased as the process parameters increased and decreased when the reaction time, catalyst concentration, reaction temperature, methanol/oil molar ratio and agitation speed were above 3h, 3wt%, 60^{o}C, 10:1 and 350rpm respectively. The biodiesel produced generally met the criteria required for commercial biodiesel. The optimum reaction conditions were; reaction time of 3h, catalyst concentration of 3 wt%, reaction temperature of 60^{o}C, methanol/oil molar ratio 10:1 and agitation speed of 350rpm. The optimal yield rangingfrom 77-80% was obtained for activated clay catalysts. The heterogeneous kinetics result revealed that the LHHW is the most reliable representation of the experimental data using activated clay catalysts with surface reaction between adsorbed triglyceride and adsorbed methanol as rate determining step (RDS). The effective rate constantfor the reaction increased as temperature increased showing that the reactions are endothermic and proceed at temperature below the boiling point of methanol.The thermodynamic parameters showed that the reactions were feasible and spontaneous.The thermal efficiency and brake power of biodiesel blends especially B20 were almost similar to conventional diesel fuel with negligible emission of gaseous pollutants. It was observed that the ANN model can predict the engine performance and biodiesel production quite well with good correlation coefficients ($0.9 \leq R \leq 1$) and very low mean square error. The results exhibited the potential of activated clay in catalysis of transesterification of APO and GSO to methyl ester.

TABLE OF CONTENTS

LIST OF TABLES

LIST OF FIGURES

LIST OF PLATES

NOMENCLATURE

AAC: Acid activated clay

ANN : Artificial neural network

ASTM: American Society for Testing and Materials

APO: African pear seed oil

BAC: Base activated clay

BP : Brake power

BTE : Brake thermal efficiency

BSFC :Brake specific fuel consumption

CCD : Central composite design

CO : Carbon II oxide

CO_2: Carbon IV oxide

Ea: Activation energy

FAME: Fatty acid methyl ester

FFA : Free fatty acid

GSO: Gmelina seed oil

HC : Hydrocarbon

MLP: Multiplayer perceptron

MSE: Mean square error

NOx : Nitrogen oxides

RPM : Revolution per minutes

RSM : Response surface methodology

TAC: Thermally activated clay

ΔH = Change in enthalpy

ΔS = Change in enthropy

k_f = Forward rate constants

k_b = Backward rate constants

$K_1, K_2, K_3, K_4, K_5, K_6, K_7, K_8, K_9$ = Equilibrium constants

CHAPTER ONE
INTRODUCTION

1. 1 Background of the Study

Depletion of world petroleum reserves and increasing environmental concerns has stimulated the search for renewable fuels such as biodiesel in recent years. Biodiesel is the most promising alternative diesel fuel which has attracted attention worldwide (Fan *et al*., 2011). This is primarily due to its outstanding benefits over the conventional petro diesel. It is renewable, biodegradable, non-toxic, with high flash point and good reduction in greenhouse emissions (Demirbes, 2009; Kaya *et al*., 2009; Ghesti *et al*., 2009; Aderemi & Hameed, 2010). Vegetable oils can be used in diesel engines as an alternative fuel owing to its comparable and competent physicalproperties as that of diesel. On the other hand when raw vegetable oil is directly used indiesel engine, the high viscosity and volatility nature of vegetable oil caused problems suchas chocking of injector, deposits on engine cylinder and sticking of piston (Dwivedi & Sharma, 2011).These effects are reduced when vegetable oils are transesterified to biodiesel.

Biodiesel is the free fatty acid methyl esters, popularly referred to as FAME, derived from oil and fats sources (Demirbes, 2009). There are various processes that have been adopted in production of biodiesel from vegetable oils and animal fats namely; micro-emulsification with alcohols, catalytic cracking, pyrolysis and transesterification (Demirbes, 2009; Leng *et al*., 1999; Li *et al*., 2009; Aderemi & Hameed, 2010). Among these methods, transesterification is the key and foremost important process to produce the cleaner and environmentally safe fuel (Younis *et al*., 2009; Atlanatho *et al*., 2004).

Transesterification reactions have been studied for many vegetable oils such as soybean, sunflower, rapeseed, palm, palm kernel, canola or hemp, coconut seed, corn, safflower seed, olive, peanut oils, etc (Attanatho *et al*., 2004; Freedman *et al*., 1984).However, the raw material costs and limited availability of vegetable oil feedstocks are always critical issues for the biodiesel production. The high cost of vegetable oils, which could be up to 75% of the total manufacturing cost, has led to the production costs of biodiesel becoming approximately 1.5 times higher than that for diesel (Ma & Hanna, 1999; Zhang *et al*., 2003).

Biodiesel produced from non-edible feedstock can positively supplement the rapidincrease in energy requirements of the world; especially the countries which have limited fossil fuel resources. There are various sources of non-edible renewable vegetable oil

options available for production of biodiesel to augment the supply of fuel source to the huge requirements of diesel. Biodiesel is produced from non-edible seeds such as castor (Paula *et al*., 2011), tamanu (Anthony *et al*., 2014), rubber seed (Melvin Jose *et al*., 2011), *jatropha curcas* (Sunil *et al*., 2012), neem (Anyanwu et al., 2013), pongamia pinnata (Veeraprasad & Srinivas, 2012), mahua (Manjunath *et al*., 2015), cottonseed (Georgogianni *et al*., 2008) etc. Biodiesel produced from non-edible renewable resources can be a possible solution to the crisis of environmental pollution and fossil fuel depletion (Jinlin *et al*., 2011; Mythili *et al*., 2014; Sahro *et al*., 2008). Non-edible seeds oils of African pear and gmelina are gaining attention of researchers in the recent time.

The African pear, African plum or Safou, locally called 'Ube' among the Igbos in south eastern part of Nigeria belongs to the family of Burseraceae and botanically known as *Dacryodes edulis.* It is an indigenous fruit tree grown in the humid low lands and Plateau regions of West, Central African and Gulf of Guinea countries.In south-eastern Nigeria, the trees are grown around homesteads and flowering takes place from January to April. The major fruiting season is between May and October. It is an annual fruit of about 3cm in diameter and contains a leathery shelled stone surrounded by a pulpy pericarp about 5mm thick. The pericarp is butyraceous i.e, having the qualities of butter. It is this portion of the pear which is eaten, either raw or cooked that forms a sort of 'butter'. Besides, the pulp contains 48% oil and a plantation can produce 7-8 tonnes of oil per hectare. This makes it useful as feedstock for biodiesel production (Awono *et al.*, 2002). There are few reports on production of biodiesel from African pear. Ogunsuyi and Oyewo, (2015)performed evaluation of African pear (*dacryodesedulis)* seeds-oil *as a* viable feedstock for biodiesel fuel using NaOH and KOH.

Gmelina arborea Roxb, known as Gomari in Assamese, is a big forest tree popular for its wood used for making furniture and as building materials. *Gmelina arborea* is a fast growing tree, which grows on different localities and prefers moist fertile valleys with 750-5000 mm rainfall. The *Gmelina arborea* tree attains moderate to large height up to 40 m and 140 cm in diameter (Okoroigwe *et al*., 2012). It occurs naturally throughout greater part of India at altitudes up to1500m. It also occurs naturally in Myanmar, Thailand, Laos, Cambodia, Vietnam, and in southern provinces of China, and has been planted extensively in Sierra Leone, Nigeria and Malaysia (Choudhury, 2012).Researchers are focusing attention on production of biodiesel from Gmelina seed oil.Sanjay *et al*. (2012)studied composition of biodiesel from *Gmelina arborea* seed oil using a heterogeneous catalyst derived from the trunk of *Musa balbisiana Colla*.

Clay is a type of soil which is naturally available in most of the states in Nigeria. Clays are essentially alumina silicates which have resulted from weathering of rocks and aluminum silicates (Igbokwe & Ogbuagu, 2003). Clays have adsorptive and catalytic capacities. They can be used as catalysts for transesterification reaction. Some researchers worldwide have investigated clay catalysts for esterification but its application for biodiesel productionis been considered (Manut & Satit, 2007). Prakash *et al*. (2005) reported transesterifcation of dicarboxylic acid with various alcohols by Mn^{+}-montmorillonite clay catalysts. AlsoVijayakumar *et al*. (2005)had used Indian bentonite as esterification catalyst for ester synthesis.Dubios *et al*. (2006) had prepared biodegradable polyester by transesterification catalysts to improve clay exfoliation. Liu *et al*. (2004) produced ethyl/methyl β -ketoester bymontmorillonite K-10 as an efficient reusable catalyst. Manut and Satit, (2007) studied biodiesel synthesis from transesterification by clay-based catalyst. They discovered that biodiesels from clay–based catalysts have some encouraging properties to supersede low speed diesel fuel and to lower the cost of production in some extent.Calgaroto *et al*. (2013)studied production of biodiesel from soybean and *Jatropha Curcas* oils with KSF and amberlyst 15 catalysts in the presence of co-solvents.

There are some factors that affect the yield of biodiesel through transesterification of vegetable oils. The effects of alcohol/oil molar ratio, catalyst concentration, reaction temperature, reaction time and agitation speed have been widely investigated and the process parameters optimized. Some researchers have adopted different techniques of optimization. Some employ the traditional 1-factor-at-a-time approach, which is time consuming and nearly impossible to achieve the true optimal condition for a multi-variable system. Another approach employed by some researchers is response surface methodology (RSM). It is an experimental strategy described first by Box and Wilson for seeking an optimal condition for a multivariable system. It is an efficient technique for process optimization (Kong *et al*., 2004). Zabeti *et al*. (2010) used response surface methodology in production of biodiesel using alumina –supported calcium oxide. Fan (2008) employed response surface methodology in optimization of biodiesel production from crude cottonseed oil using sodium hydroxide. Nevertheless, the use of response surface methodology in optimization of biodiesel production from African pear oil and gmelina oil using modified clay is been studied.

The engine performance testing of bio-diesel is indispensable for evaluating its suitability in diesel engines. Several groups have investigated the properties of a biodiesel from vegetable oils in diesel engines and found that particulate matter (PM), CO and soot

mass emissions decreased, while NOx increased. Labeckas and Slavinskas (2006), examined the performance and exhaust emissions of rapeseed oil methyl esters in direct injection diesel engines, and found that there were lower emissions of CO, CO_2 and HC. Similar results were reported by Kalligeros *et al*.(2003) for methyl esters of sunflower oil and olive oil when they were blended with marine diesel and tested in a stationary diesel engine. Ude *et al*. (2017) obtained similar result when they studied the performance evaluation of cottonseed oil methylesters produced using CaO and prediction with anartificial neural network.

In addition, an artificial intelligence (AI) system is widely accepted as a technology offering an alternative way to tackle complex and ill-defined problems (Kalogirou, 2003). The artificial neural network (ANN) approach has been applied to predict the performance of various thermal systems (Kalogirou, 2000). A well-trained ANN can be used as a predictive model for a specific application, which is a data-processing system inspired by biological neural system. The predictive ability of an ANN results from the training on experimental data and then validation by independent data. An ANN has the ability to re-learn to improve its performance if new data are available (Hertz *et al*., 1991). The use of ANNs for modelling the operation of internal combustion engines is a more recent progress. This approach was used to predict the performance and exhaust emissions of diesel engines (Canakc *et al*., 2006; Arcaklioglu & Celitkten, 2005).Ramadhas *et al*. (2006) developed ANNs to predict the cetane number of biodiesel. Multi-layer feed-forward, radial base, generalized regression and recurrent network models were used for the prediction of cetane number. Predicted cetane numbers were found to be in agreement with the experimental data.Kumar and Bansal (2007) examined seven neural network architectures, three training algotharims and 10 different sets of weights and biases to predict the properties of diesel and biodiesel blends. The results showed that the neural network with a Levernberg– Marquard algorithm gave the best estimate for the properties of diesel and biodiesel blends.Further, Duran *et al*. (2005) used neural networks for estimation of diesel PM composition from transesterified waste oil blends. Simulation results proved that the amount of palmitic acid methyl ester in fuels was the main factor affecting the amount of insoluble material emitted, due to its higher oxygen content and cetane number.Baroutian *et al*. (2008) used a neural network to predict palm oil-based methyl ester biodiesel density. The predicted densities were found to be in agreement with the experimental data.

Most of biodiesel production from non edible oils involved more of the use of commercial homogeneous and heterogeneous catalystsbut attention is shifting to use of locally synthesized heterogeneous catalyst.Therefore, the present study focused on exploring

the potential of non-edible seed oil like African pear (*Dacryodes edulis*) andgmelina as feedstocks for the production of biodiesel by heterogeneous catalysis(activated clay catalysed reaction)of transesterification reaction.

1.2 Statement of the Problem

The increase in the consumption of electricity, the increase in use of fossil fuel for transportation and over dependence of crude oil as major source of revenue in Nigeria has led to external debt, environmental degradation and economic recession. These acute aspects have necessitated the research to find viable, environmental friendly and sustainable alternative fuel which will also help to diversify Nigerian economy.

The production of biodiesel from various seed oil using conventional homogeneous strong bases catalysts (such as alkali metal hydroxides and alkoxides (NaOH, KOH, $NaOCH_3$)) and homogeneous acids (such as H_2SO_4) has some draw backs. Basic catalysts are generally corrosive to equipment and also react with free fatty acid to form unwanted soap as by-products that require expensive separation. Homogeneous acid catalysts are difficult to recycle and operate at high temperatures, and also give rise to serious environmental and corrosion problems. Therefore, to overcome all these problems including cost, there are compelling need to developan economically viable as well as eco-friendly solid catalysts for biodiesel industries. This issue can be ameliorated by using heterogeneous catalyst from clay.Recently, several naturally derived heterogeneous catalysts have been reported in various literatures and showed potentials to be used as a low-cost biodiesel production catalyst.

However, after an exhaustive literature survey, African Pear Seed Oil (APO) and gmelina seed oil (GSO) have been discovered as promising feedstocks but have not been extensively exploited for the production of biodiesel.The availability of these plants in developing countries in Africa such as Nigeria gives the assurance that they are promising alternative feedstocks which can be utilized for biodiesel production at the global level. Therefore, biodiesel production from African pear (*Dacryodes edulis*) seed oil (non edible oil) andgmelina seed oilusing heterogeneous catalysts synthesized from clay is limited.

Researchers have adopted different techniques of optimization. Some employ the traditional 1-factor-at-a-time approach, which is time consuming and nearly impossible to achieve the true optimal condition for a multi-variable system. Response surface methodology (RSM) is an efficient technique for process optimization to achieve optimal condition for multivariable system at a faster rate.

The use of ANN to predict production of biodiesel from vegetable oils or fats is gaining the attention of researchers. The use of ANNs for modelling the production is a more recent progress. The use of ANN to predict performance and exhaust emissions of biodiesel produced from African pear (Dacryodes edulis) seed oil and Gmelina seed oilusing clay catalyst is limited. The use of ANNs for modelling the operation of internal combustion engines is a more recent progress.

Most studies for the use of clay catalysts focused on the catalyst synthesis, characterization and catalytic activity for fattyacid transesterification with short chain alcohols without measuring and properly exploring the kinetics of these mineral clay catalyzedreactions. Since the kinetics is vital in every reaction,transesterification will acquired further improvement from engineering side if the research on kinetics oftransesterification is dedicatedto experimental and kinetic modelling of fatty acid transesterification withalcohol is carried out.

Therefore this study focused on exploring the potential of non-edible seed oil like African pear (*Dacryodes edulis*) andgmelina as feedstocks for the productionof biodiesel usingactivated clay-catalysts with emphasis on the kinetics study of heterogeneous catalysis and engine performance.

1.3 Aim and Objectives of the Study

The aim of this study is the productionand engine performance of biodiesel produced from non edible seed oils (African pear seed oil and gmelinaseed oil) using activated clay.

The specific objectives are as follows:

i. To extract oil from African pear seed and gmelina seed using solvent extraction and characterize them.
ii. To synthesize catalyst by thermal, acid and base activations and characterize them.
iii. To produce biodiesel using transesterification method and investigate the effects of process parameters on the biodiesel production.
iv. To optimize the production of biodiesel using response surface methodology (RSM) andto develop model for production of a biodiesel using artificial neural network (ANN).
v. To characterize the biodiesel produced with optimal conditions.
vi. To investigate the kinetics of the biodiesel produced from African pear seed oil andgmelina seed oilusing activated clay catalysts.

vii. To predict the performance and exhaust emissions of a biodiesel engine using artificial neural network (ANN).

1.4 Scope of the Study

This work is limited to synthesis of clay catalyst for production of biodiesel from African pear seed and gmelina seed oils and the optimization of the production process using RSM; prediction of the production using ANN, kinetics studies of the heterogeneous catalyzed transesterification and engine performance of the biodiesel and its blends.

1.5 Significant of the Study

The world has shifted attention to developing countries especially Nigeria for the production of raw material for biodiesel and to encourage diversification of economy. For Nigeria to maximize the benefits from these projects, serious research should be done on biodiesel production in Nigeria so that processing of the raw material could be domesticated and biodiesel exported to the developed world thereby boasting other sector of the economy and improve our revenue. If this is not done, Nigeria will remain a producer of raw materials which will be processed by the developed countries and sold back to Nigeria at a higher price. Biodiesel has been produced from a number of sources, under various conditions, thus to optimize the yield, the best method and conditions for production should be developed.

The production of biodiesel from non-edible oil using heterogeneous catalysts will help to establish the best method for the production of biodiesel compared to use of homogeneous catalysts. This project will contribute to the promotion of heterogeneous catalysts synthesized from local and available materials as alternative viable catalysts and non-edible oil for biodiesel production and hence promote local economy and create employment.

1.6 Limitation of the study

This study was limited to transesterification reaction using flat bottom flask equipped with magnetic stirrer mounted on hot magnetic plate as an improvised reactor. It was also limited to use of two reaction mechanisms for kinetics studies and use of polymath software for determining kinetic parameters of the rate determining step. The gas chromatographymass

spectrometer was used for determining the concentrations of the reacting species, intermidates, products and bye-production in the reaction for kinetics studies instead of Nuclear Magnetic radiation (NMR) or high performance liquid chromatography. This was due to the non-availability of the equipment during the cause of the study.

CHAPTER TWO

LITERATURE REVIEW

2.1 Overview of Biodiesel Production

Energy is the prime mover for socio-economic development. The World's economic growth is affected by climatic change, fuel price hike, and the gradual depletion of fossil fuel reserves. Therefore, to increase energy security for economic development, there is need to search for an alternative source of energy such as biodiesel(Oh *et al*., 2002, Uma& Kim, 2009). Biodiesel is renewable, sustainable, biodegradable, and emits low greenhouse gases (Sharma& Singh, 2009, Lee *et al*., 2010). Furthermore, the oxygen content of 11–15% in the molecular structure speed up the combustion process in compression ignition engines and decreases pollutants such as soot, fine particles, and carbon monoxide (CO) (Lee *et al*., 2011, Kim *et al*., 2007).Thus, biodiesel is a potential substitute to replace/supplement petro-diesel fuel (Saeid *et al*., 2008, Szulczyk & McCarl, 2010).

Biodiesel fuel is mostly produced via transesterification of refined vegetable oil, waste cooking oil, and used frying oil using alkaline catalysts(Chhetri & Watts, 2008, Bai *et al*., 2011)as shown in Figure 2.1. The nature of catalyst employed during transesterification reaction is crucial in converting triglycerides to biodiesel. As a result different catalysts have being explored for converting triglycerides to biodiesel fuel. The catalysts usually employed to catalyze transesterification reaction are homogeneouscatalysts and heterogeneous catalysts. Conventionally, homogeneous alkaline catalysts such as NaOH, KOH, CH_3ONa, and CH_3OK are more often used in producing biodiesel (Sharma*et al*., 2008). The catalytic performance of these catalysts and their ability to perform under moderate conditions has led to their choice (Hideki *et al*., 2001).

Among these homogeneous alkaline catalysts, CH_3ONa is most active, providing biodiesel yield above 98wt% in short reaction time (30min) (Helwami *et al*., 2001, Demirbas, 2009). However because of low price, industrial biodiesel production process mostly employs NaOH and KOH **(**Helwami *et al*., 2001**)**. The process involving these catalysts needs high-quality feedstocks, thus the free fatty acid (FFAs) level of the feedstocks should not exceed 3wt%, beyond which the reaction will not occur. In addition, water content of the feedstocks is critical; as a result the feedstocks used in alkali-catalyzed transesterification have to be anhydrous **(**Helwami *et al*., 2001**)**. The presence of water leads to hydrolysis of oils to FFAs. Figure 2.2shows water hydrolysis of fats and oils to form free fatty acid. The FFAs react with alkaline catalysts to produce soaps. Figure 2.3presents soaps formation in homogeneous

alkali-catalyzed transesterification. Soaps formation consumes the catalyst, deactivates it and makes biodiesel purification process difficult (Van Gerpen *et al*., 2004). Therefore,preparation of biodiesel by low quality feedstocks containing huge quantity of FFAs and water needs sound technology (Chongkhong *et al*., 2009).

However, high cost of refined feedstocks result in high price of biodiesel compared to diesel fuel (Bozbas, 2008). The cost of refined feedstocks, account for over 70% of the overall cost of biodiesel production (Zullaikah *et al*., 2005). As a result, different kinds of low quality feedstocks such as: waste cooking oils, used cooking oil, greases (yellow and brown), and non-edible oils have been investigated (Lee *et al*., 2007). The price of low quality feedstocks such as waste cooking oil is 2-3 times lower than refined oils**.**Nonetheless, the feedstocks contain higher amount of FFAs and water contents. These features make their processing challenging (Balat & Balat, 2010). Therefore to augment their processingdifficulties, acid-catalyzed transesterification is first employed to decrease the content of FFAs before performing alkalicatalyzed transesterification (Chongkhong *et al*., 2009). Thus adopting two-step transesterification technique could provide large biodiesel conversion of up to 98% (Ramadhas *et al*., 2005).

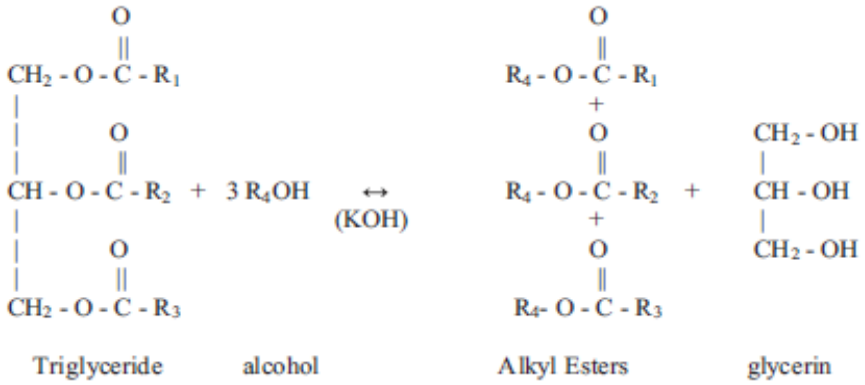

Figure 2.1: Transesterification reaction of triglycerides via alkaline catalyst.

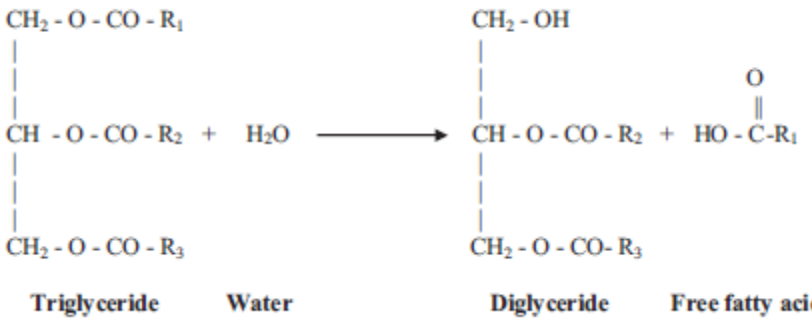

Figure 2.2: Water hydrolysis of fats and oils to form free fatty acid (FFAs)

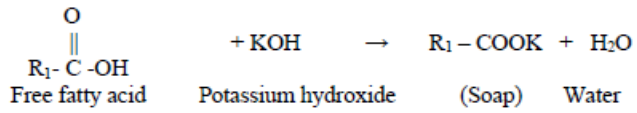

Figure 2.3: Soap formation in homogeneous alkali-catalyzed.

Recently heterogeneous catalysts such as solid catalysts and enzyme catalysts are employed to catalyze transesterification reaction for producing biodiesel. Heterogeneous catalysts offer many advantages over homogeneous catalysts such as; simple catalyst recovery, catalyst reusability, simple product purification, less energy and water consumption, less added cost of purification, and simple glycerol recovery etc. Besides, most of the heterogeneous catalysts used especially solid alkaline catalysts have provided high yields (Zabeti *et al*., 2009), though faced with problem of leaching (Zabeti *et al*., 2009). Also, the stability of enzymes catalysts in non aqueous media is significant to its excellent catalytic activity, this improves transesterification and esterification during biodiesel production (Tan *et al*., 2010), and providing high biodiesel yield (95wt%) (Watanabe *et al*., 2000). However, the problem mostly associated with enzyme catalysts is the cost of the enzymes, but immobilization of the catalyst could mitigate the cost (Shah *et al*., 2004). Therefore, to achieve biodiesel that is economically feasible, development of active and cheap catalysts for effective transesterification of different kinds of feed stocks is necessary (Thian & Bhatia, 2008).

2.2. Techniques for Biodiesel Production

Biodiesel is usually produced through different techniques such as direct/blends(Boehman, 2005, Keskin *et al*., 2008), microemulsion (Ramadhas *et al*., 2004, Khan, 2007), pyrolysis (Brennan & Owende, 2010, Naik *et al*., 2010) and transesterification (Leung & Guo, 2006, Salahi *et al*., 2010).

2.2.1 Direct use and blending (dilution)

Beginning in 1980, there was considerable discussion regarding use of straight vegetable oil as a fuel. Caterpillar Brazil used pre – combustion chamber engines with a mixture of 10% vegetable oil to maintain total power without any alterations or adjustment to the engine(Boehman, 2005, Keskin *et al*., 2008). At that point, it was not practical to substitute

100% vegetable oil but 80% diesel fuel was successful. Some short-term experiment used up to a 50/50 ratio.

Direct use of vegetable oil and/or the use of blends of the oils have generally been considered to be not satisfactory and impractical for both direct and indirect diesel engines. The high viscosity, acid composition, free fatty acid contents as well as gum formation due to oxidation and polymerization during storage and combustion, carbon deposits and lubricating oil thickening are obvious problems (Fanguri & Milford, 1999).

2.2.2 Thermal cracking (pyrolysis)

Pyrolysis is defined as the conversion of one substance into another by means of heat with the aid of a catalyst. It involves heating in the absence of air or oxygen and cleavage of chemical bonds to yield small molecules. Pyrolytic chemistry is difficult to characterize because of the variety of reaction paths and the variety of reaction products that may be obtained from the reactions that occur. The pyrolyzed material can be vegetable oils, animal fats, natural fatty acids and methyl esters of fatty acids. The pyrolysis of fats has been investigated for more than 100 years, especially in those areas of the world that lack deposits of petroleum (Fangrui & Milford, 1999).

The first pyrolysis of vegetable oil was conducted in an attempt to synthesize petroleum from vegetable oil. Since World War 1, many investigators have studied the pyrolysis of vegetable oils to obtain products suitable for fuel. The mechanisms for the thermal decomposition of triglycerides are given in Figure 2.4. The chemical compositions (heavy hydrocarbons) of the diesel fractions were similar to fossil fuels. The process was simple and effective compared with other cracking processes. There was no waste water or air pollution (Fangrui & Milford, 1999).

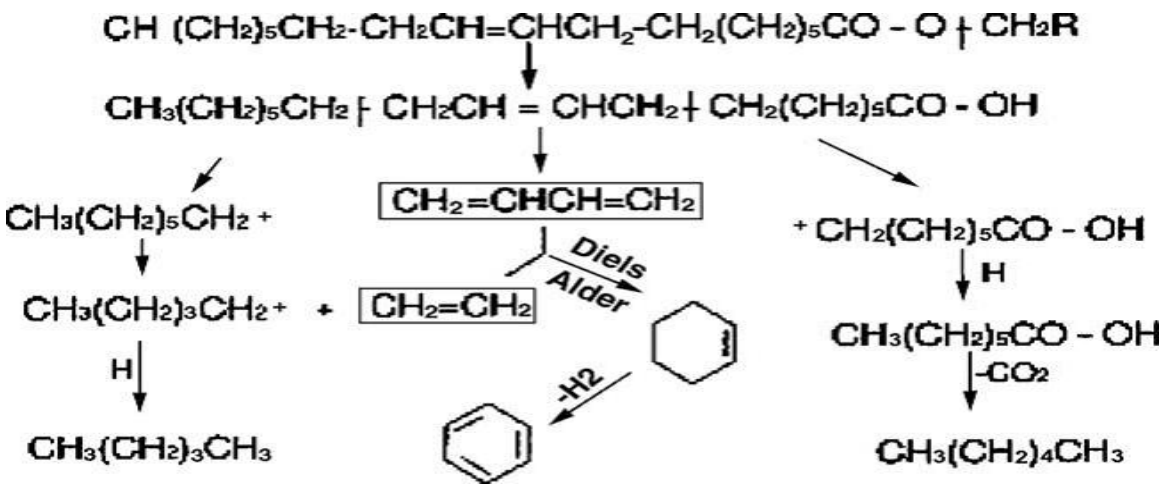

Figure 2.4: The mechanism of thermal decomposition of triglycerides

2.2.3. Micro-emulsion process

A micro-emulsion is defined as a colloidal equilibrium dispersion of optically isotropic fluid microstructure with dimensions generally into 1–150 range formed spontaneously from two normally immiscible liquids and one or more ionic or non ionic amphiphiles. They can improve spray characteristics by explosive vaporization of the low boiling constituents in micelles. The engine performances were the same for a micro-emulsion of 53% sunflower oil and the 25% blend of sunflower oil in diesel. A micro-emulsion prepared by blending soyabean oil, methanol, and 2-octanol and cetane improver in ratio of 52.7:13.3:33.3:1.0 also passed the 200 h EMA test (Singh & Singh, 2010).

2.2.4 Transesterification

Transesterification (also known as alcoholysis) is the reaction of a fat or oil with an alcohol to form esters and glycerol. A catalyst is usually used to improve the reaction rate and yield. Excess alcohol is used to shift the equilibrium toward the product because of reversible nature of reaction. For this purpose primary and secondary monohybrid aliphatic alcohols having 1-8 carbon atoms are used.

13

2.2.4.1*Chemistry of transesterification process*

Transesterification consists of a number of consecutive, reversible reactions. The triglycerides are converted step wise to diglycerides, monoglyceride, fatty acid esters and finally glycerol (Singh & Singh, 2010). The overall process is normally a sequence of three consecutive steps that are reversible reactions. In the first step, from triglycerides, diglyceride is obtained, from diglyceride, monoglyceride is produced and in the last step, from monoglycerides, glycerin is obtained. In all these reactions esters are produced (Marchetti *et al*., 2007). In other words, a mole of ester is librated at each step. The stoichiometric relation between alcohol and the oil is 3:1. However, an excess of alcohol is usually more appropriate to improve the reaction towards the desired product (Figure 2.5).

Triglycerides + ROH ⟶ Diglyceride + R'COOR

Diglycerides + ROH ⟶ Monoglyceride + R"COOR

Monoglyceride + ROH ⟶ Glycerol + R"'COOR

Figure 2.5: Transestrification reaction.

2.2.4.2*Catalyst used in transesterification*

A wide range of catalysts may be used for biodiesel production, such as homogenous and heterogeneous acids and bases, sugars, lipases, ion exchange resins, zeolites, and other heterogeneous materials. A recent exotic example is that of KF/Eu2O3, which was used to prepare rapeseed oil methyl esters with 92.5% conversion. The homogenous base-catalyzed transesterification reaction is about 4,000 times faster than the corresponding acid-catalyzed process. Base-catalyzed reactions are performed at generally lower temperatures, pressures, and reaction times and are less corrosive to industrial equipment than acid-catalyzed methods. Therefore, fewer capital and operating costs are incurred by biodiesel production facilities in the case of the base-catalyzed transesterification methods.

In general, acids are more appropriate for feedstocks high in FFA content. Homogenously catalyzed reactions generally require less alcohol, shorter reaction times, and more complicated purification procedures than heterogeneously catalyzed transesterification reactions. Heterogeneous lipases are generally not tolerant of methanol, so production of ethyl or higher esters is more common with enzymatic methods.

Furthermore, non catalytic transesterification of biodiesel may be accomplished in supercritical fluids such as methanol, but at very high pressure (45–65 bar), temperature (350°C), and amount of alcohol (42:1 molar ratio) are required (Moser, 2009). Advantages of

supercritical transesterification versus various catalytic methods are that only very short reaction times (4 min, for instance) are needed, and product purification is simplified because there is no need to remove a catalyst. Disadvantages of this approach include limitation to a batch-wise process, elevated energy and alcohol requirements during production, and increased capital expenses and maintenance associated with pressurized reaction vessels (Moser, 2009).

(i) Base or Alkali catalyzed transesterification: The reaction mechanism for alkali catalyzed transesterification was formulated in three steps as explained in Figure2.6. The first step is an attack on the carbonyl carbon atom of the triglycerides molecule by the anion of the alcohol (methoxide ion) to form a tetrahedral intermediate. In the last step, rearrangement of tetrahedral intermediate results in the formation of a fatty acid ester and a diglyceride. When NaOH, KOH, K_2CO_3 or other similar catalysts were mixed with alcohol, the actual catalysts, alkoxide group is formed. Processes have been developed for the production of biodiesel from vegetable oils using heterogeneous catalyst, CaO, MgO, Na/NaOH/Al_2O_3 etc (Moser, 2009). These catalysts showed almost the same activity under the optimized reaction conditions compared to conventional homogeneous NaOH catalyst. For an alkali catalyzed transesterification, the glyceride and alcohol must be substantially anhydrous because water makes the reaction partially change to saponification, which produces soap. A number of researchers have worked with feed stocks that have elevated FFA (free fatty acid) levels. However, in most cases, alkaline catalysts have been used and the FFAs (Free fatty acids) were removed from the process stream as soap and considered waste. Waste greases typically contain from 10 to 25%FFAs. This is far beyond the level that can be converted to biodiesel using an alkaline catalyst.

(ii) Acid catalyst transesterification: An alternative process is to use acid catalyst that some researchers have claimed are more tolerant of free fatty acid. The mechanism of acid catalyzed transesterification of vegetable oil (for a monoglyceride) is shown in Figure 2.7. However, it can be extended to di- and triglycerides. The protonation of carbonyl group of the ester leads to the carbonation, which after a nucleophilic attack of the alcohol produces a tetrahedral intermediate. This intermediate eliminates glycerol to form a new ester and toregenerate the catalyst. We can use acid alkali and biocatalyst in transesterification method. If more water and free fatty acids are in triglycerides, acid catalyst can be used. Transemethylation occur approximately 4000 times faster in the presence of an alkali catalyst than those catalyzed by the same amount of acidic catalyst (Sing & Singh, 2010)

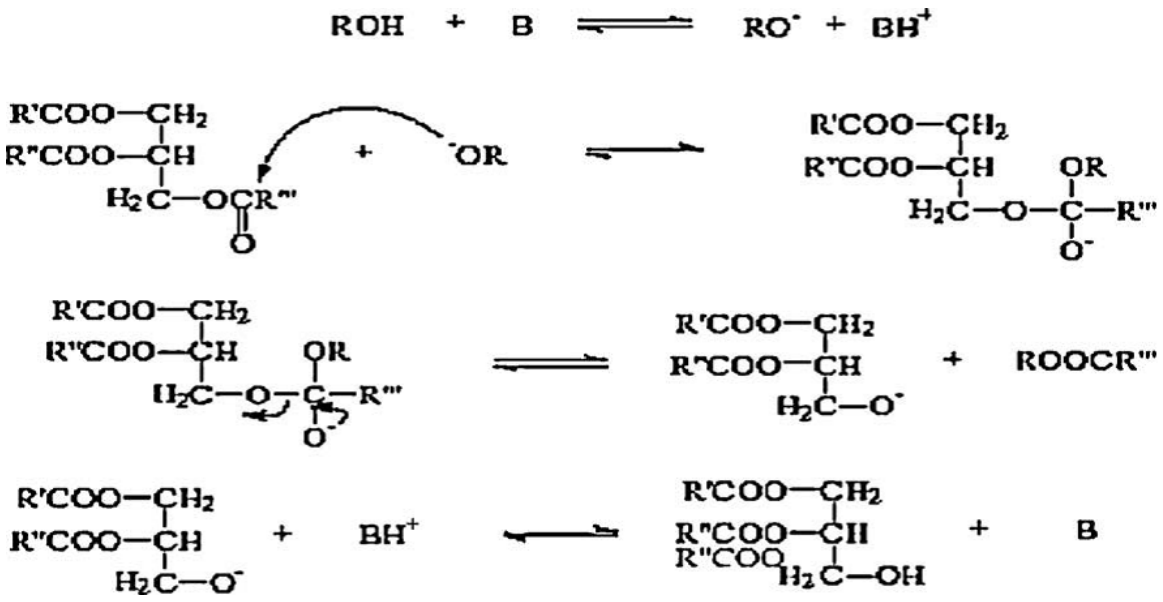

Figure 2.6: Mechanism of the alkali-catalyzed transesterification of vegetable oils.

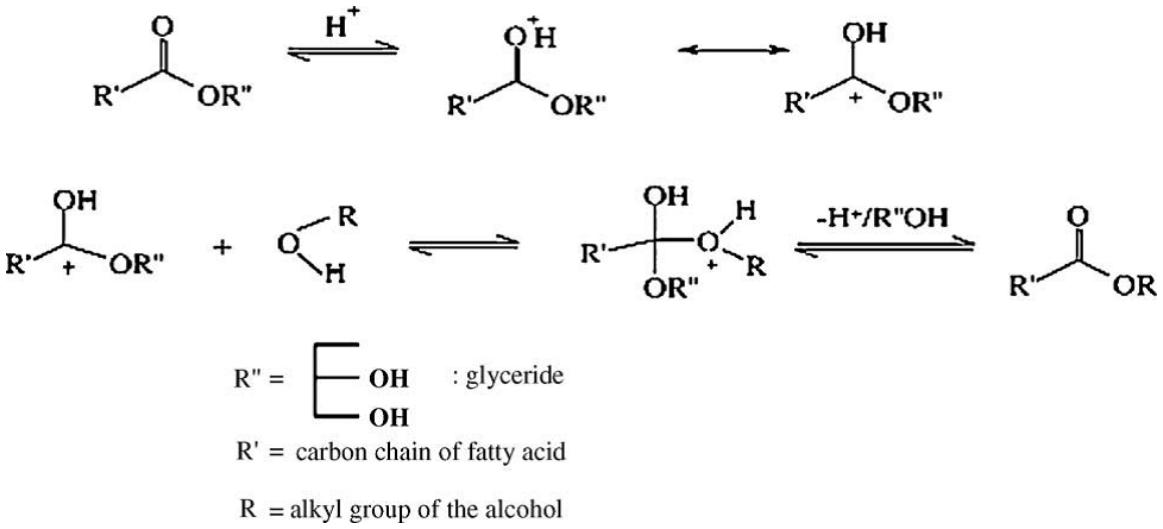

Figure 2.7: Mechanism of acid catalyzed transesterification.

(iii) *Enzyme- catalyzed transesterification:* Biodiesel can be obtained from enzyme or biocatalytic transesterification methods. Transesterification can be carried out chemically or enzymatically (Ayhan, 2009). Lipases are enzymes used to catalyze some reaction such as hydrolysis of glycerol, alcoholysis and acidolysis, but it has been discovered that they can be used as catalyst for transesterification and esterification reactions too.

Biocompatibility, biodegradability and environmental acceptability of the biotechnical procedure are the desired properties in agricultural and medical applications. The extra

cellular and the intracellular lipases are also able to catalyze the transesterification of triglycerides effectively (Marchetti *et al*., 2007). The process is explained in Figure 2.8. Lipases are known to have a propensity to act on long-chain fatty alcohols better than on short-chain ones. Thus, in general, the efficiency of the transesterification of triglycerides with methanol (methanolysis) is likely to be very low compared to that with ethanol in systems with or without a solvent (Singh & Singh, 2010).

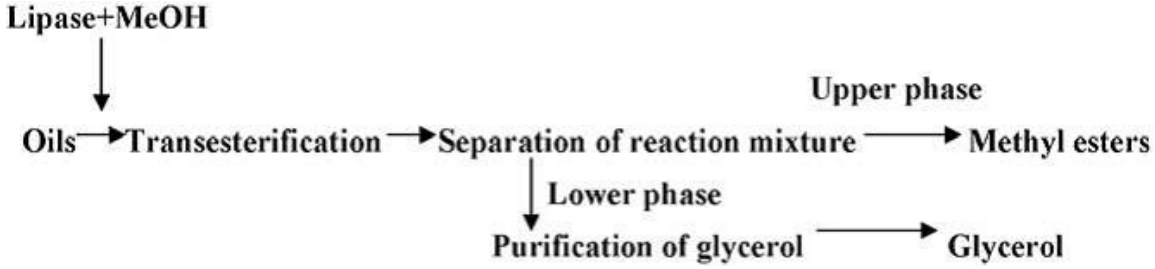

Figure 2.8: Flow diagrams comparing biodiesel production using lipase-catalysis

(iv) *Catalytic supercritical methanol transesterification*

Although this is a new relevant topic, there is an uncertainty regarding whether tranesterification or alkyl esterification is a better way of production and which one has a faster reaction rate.In the case where supercritical alcohol was used, it was demonstrated that one gets a higher reaction rate for esterification than for transesterification. Another advantage of this process is that the free fatty acid will be changed completely into esters (Marchetti *et al*., 2007).

Catalytic supercritical methanol transesterification is carried out in an autoclave in the presence of 1–5% NaOH, CaO, and MgO as catalyst at 520K. In the catalytic supercritical methanol transesterification method, the yield of conversion rises to 60–90% for the first minute (Ayhan, 2009).

A summary of the advantages and disadvantages of each technological possibility to produce biodiesel could be found in Table 2.1.

17

Table 2.1: Comparison of the different technologies of transesterification to produce biodiesel (Marchetti *et al*., 2007).

Variable	Alkali catalysis	Lipase catalysis	Supercritical alcohol	Acid catalysis
Reaction temperature(^{o}C)	60–70	30–40	239–385	55–80
Free fatty acid in raw materials	Saponified products	Methyl esters	Esters	Esters
Water in raw materials No	Interference with reaction	No influence	_____	Interference with reaction
Yield of methyl esters	Normal	Higher	Good	Normal
Recovery of glycerol	Difficult	Easy	_____	Difficult
Purification of methyl esters	Repeated washing	None	_____	Repeated washing
Production cost of catalyst	Cheap	Relatively Expensive	Medium	Cheap

2.3 Feedstocks for Biodiesel Production.

Biodiesel production is achieved via different kinds of feed stocks. The nature of feedstock used is dependent on their geographical position and climate of the place. For instance Europe employs sunflower and rapeseed oils, palm oil predominates in tropical countries, soybean in United States and canola oil in Canada (Cao *et al*., 2008). Singh and Singh (2010) reported the major feedstocks employed in producing biodiesel are cotton seed, palm oil, sunflower, soybean, canola, rapeseed, and *Jatropha curcas*. Additionally, Zhang *et al*. (2003) remarked that employing feedstocks such as waste frying oils, nonedible oils, and animal fats, as feedstocks could be useful in producing biodiesel. Although, Banerjee and Chakraborty

(2009) stated that FFAs contents in the waste cooking oil should be kept within certain limit for reaction involving both acid- and alkali-catalyzed transesterification reactions.Otherwise these substances may cause severe difficulties in refining of biodiesel products. Table 2.2presents the recommended FFAs values for alkali-catalyzed transesterification method while Table 2.3shows FFAs contents of different vegetable oils

.

Table 2.2: FFAs recommended for alkali-catalyzed transesterification.

FFAs recommended (%)	**Reference**
≤1	Demirbas (2009)
≤1	Chongkhong *et al*., (2009)
<3	Ramadhas *et al*., (2005)
<0.5	Khan (2007)
<3	Canakci and Van Gerpan, 1999
<0.5	Zhang *et al*., (2003)
<0.5	Martino *et al*., (2008)
≤2	Sahoo *et al*., (2007)
<1	Ma and Hanna (1999)
<2	Huang and Chang (2010)
≤0.5	Szczesna Antczak *et al*., (2009)
≤1	Marchetti *et al*., (2007)
<1	Tiwari *et al*., (2007)

In addition, Table 2.4presents FFAs levels of most of the feedstocks used to produce biodiesel**.** The cost of feedstocks decreases as FFAs content increases. In case of industrial biodiesel production, there is need for low-cost (high FFAs) feedstocks such as used cooking oils, waste cooking oils, and non-edible vegetable oils since biodiesel fuels from refined oils are costly when compared to petro-diesel fuel. Besides, the application of such feedstocks in biodiesel production could minimize competition between demand of edible vegetable oils

and cost of biofuel (Zabeti *et al.*, 2009). In addition, application of vegetable oils as sources of biodiesel needs great efforts to either develop more productive plant species with a high yield of oil or to increaseoilseeds' production (Uma & Kim, 2009).Further, many studies have reported microalgal oil asfeedstocks for producing biodiesel (Khan *et al*., 2009; Mata *et al*., 2010).Demirbas (2010)noted that microalgal oil is the only feedstock that can meetthe global demand for transport fuels. The author alsoreported that soon, microalgal oil will become the mostimportant feedstocks for biofuel production. Singh and Gu(2010) reported that microalgae feedstocks are receiving greatattention as sources of energy because of their quick growthpotential coupled with reasonably high lipid, carbohydrateand nutrients contents. In addition, Demirbas (2011) highlighted that microalgae possess much quicker growth-rates than terrestrial crops. The author noted the per unit area yield of oil from algae is estimated to be from 20,000 to 80,000 L per acre, per year. In deed this is 7–31 times more than the next best crop, palm oil.

Table 2.3: Values of FFAs content of different vegetable oils (Atadashi *et al*., 2012).

Vegetable oils	FFA Levels (%)
Polanga oil	22.0
Cottenseed oil	0.11
Tobacco oil	35.0
Spent bleaching earth	24.1
Rubber oil	17.0
Palm fatty acid distillate (PFAD)	93
Pongamia pinnata	≤ 20
Palm oil	5.3
Rape seed oil	2.0
Tall oil	100
Jatropha oil	14.0
Tung oil	9.55
Soybean oil	>90
Pongamia oil	0.61
Salvadora oil	1.76

Moringa oleifera	2.9
Karanja oil	2.53
Sorghum bag oil	10.5
Mahua oil	21.0
Madhua indica	20.0
Zanthoxylum bungeanum	45.5
Acid oil	59.3
Karanja oil	2.53
Trap grease	50-100
Finished greases	8.8-25
Crude soybean oil	0.4-0.7
Restaurant waste grease	0.7-41.8
Waste palm oil	>20
Municipal sludge	Up to 65
Animal fat	5-30
Trap grease	75-100
Use cooking oil	2-7
Waste oil	46.75

Table 2.4: FFAs levels in feed stocks

Feed stocks	FFA Level	Reference
Trap grease	50-100%	Sharma and Singh (2009)
Refined vegetable oils	<0.05%	Davies (2005)
Finished greases	8.8% - 25.5%	Canakci and Gerpen (1999)
Crude soybean oil	0.4 – 0.7%	Canakci and Gerpen (1999)
Restaurant waste grease	0.7% - 41.8%	Canakci and Gerpen (1999)
Waste palm oil	>20%	Balat and Balat (2010)
Municipal sludge	Up to 65%	Sureshkumara et al., (2008)
Animal fat	5-30%	Garpen (2005), Davies (2005)
Trap grease	75 – 100%	Garpen (2005), Davies (2005)
Use cooking oil	2 – 7%	Garpen (2005),
Waste oil	46.75%	Nie *et al*., (2006)

2.4 Catalysts for Biodiesel Production

2.4.1 The effects of homogeneous catalyst in biodiesel production

2.4.1.1 The effects of alkaline catalysts in biodiesel production

Application of alkali-catalyzed transesterification reaction provide faster rate, nearly 4000 times faster than that catalyzed by the same amount of an acid catalyst (Hideki *et al*., 2001). Some of the alkaline catalysts used for the transesterification reaction include among others; NaOH (Chongkhong *et al*., 2009, Behzadi & Farid, 2009), KOH (Haq *et al*., 2008, Casa *et al*., 2011), and sodium methoxide (Demirbas, 2009, Behzadi & Farid, 2009). Other alkaline catalysts include; sodium ethoxide (Bryan, 2009), potassium methoxide (Sharma *et al*., 2009, Sharma *et al*., 2008), sodium propoxide (Bryan, 2009), sodium butoxide (Thiam & Bhatia, 2008))and carbonates (Thiam & Bhatia, 2008, Khan *et al*., 2009) etc. Based on biodiesel yield, CH_3ONa or CH_3OK are better and more suitable catalyst than NaOH and KOH. Thus, CH_3ONa and CH_3OK are more suitable due to their ability to dissociate into CH_3O- and Na^+ and CH_3O^- and K^+ respectively. Besides, the catalysts do not form water during transesterification reaction (Sharma *et al*., 2009). For these reason, alkaline catalyst is mostly preferred in commercial production of biodiesel fuel (Sharma *et al*., 2008).

Transesterification of refined oils with less than 0.5 wt% FFAs via alkaline catalysts could lead to high quality biodiesel fuel with better yield within short time of 30–60 min (Wang et al., 2007). Figure 2.9 presents the mechanism of base catalyzed transesterification reaction (Davies, 2005). Vicente *et al*. (2004) have compared different basic catalysts (sodium hydroxide, potassium hydroxide, sodium methoxide and potassium methoxide,) to produce biodiesel fuel using sunflower oil. The reactions were conducted at temperature of 65^{o}C, methanol to oil molar ratio of 6:1 and basic catalyst by weight of vegetable oil of 1%. They achieved 85.9 and 91.67 wt% yield of esters for NaOH and KOH and 99.33 and 98.4 6 wt% yields of esters for CH_3ONa and CH_3OK respectively. The authors recorded 98 wt% yields of esters for methoxides after separation and purification steps were completed. Further, less yields losses and negligible ester dissolution in glycerol were observed with methoxides compared to hydroxides. Umer et al. (2008) used alkali catalyst to produce sunflower oil methyl esters. They reported notable yield of 97.1wt% at 60^{o}C. In addition, alkaline catalysts concentrations ranging from 0.5-1wt% could yield 94–99wt% conversion of vegetable oils to alkyl esters. However, increase in catalyst concentration above 1wt% does not increase the conversion but could add to extra costs of production. Since it is essential to get rid of the catalyst from the products after the reaction is completed (Srivastava & Prasad, 2000, Agarwal, 2007).

Chung,(2010) transesterified *V. fordii* and *C. japonica* seed oils with methanol using alkaline catalysts (KOH, NaOH, and CH_3ONa) to produce biodiesel. The authors noted that KOH provided higher catalytic activity to the seed oils in the reaction. The optimum reaction conditions used were: 6:1 molar ratio of methanol to the seed oils, 1 wt% loading amount of catalyst, 65^{o}C reaction temperature, and reaction time of 3hrs. The biodiesel contents of the *C. japonica* and *V. fordii* seed oils under these reaction conditions were 97.7% and 96.1% on KOH catalyst. In another study, Sahoo *et al*. (2007) employed alkaline transesterification after reducing the FFAs value from 44 mg KOH/g a below 4 mg KOH/g through acid catalyzed transesterification. The author found that 1.5 wt% of KOH was adequate to obtained maximum biodiesel yield.

Marchetti and Errazu (2008) revealed that ethanol and sulphuric acid are suitable to carry out both direct esterification and transesterification reactions simultaneously. These processes could effectively convert waste cooking oil containing high amount of FFAs ranging from 3% to 40% to biodiesel. The authors noted the FFAs content was reduced via esterification process from 10.684% to a value close to 0.54wt%. Though, the final FFAs concentration

was slightly more than the recommendable quantity. They reported minimized soaps formation during alkali-catalyzed transesterification reaction.

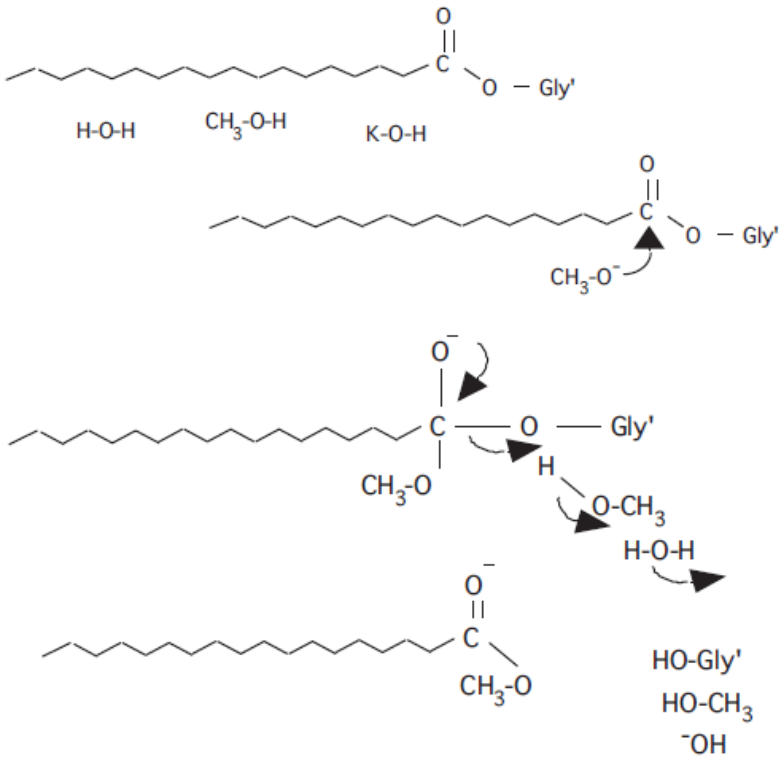

Figure 2.9: Mechanism of base-catalyzed transesterification reaction (Atadashi *et al*., 2012).

Further, to improve biodiesel production process, Refaat *et al*. (2008)studied microwave irradiation technique to produce biodiesel. They employed sunflower oil (used 3 times at a cooking temperature of 130°C) and methanol to oil ratio of 6:1 in the presence of 1wt% of potassium hydroxide at 65^{o}C. The authors used a normal pressure glass reactor 500 mL flask and reflux condenser. Using the microwave system, the vegetable oil was preheated to a desired temperature of 65^{o}C. The mixture of alcohol and catalyst then charged into the flask through the condenser. The power output adjusted to 500 watt and under reflux the mixture irradiated via different reaction times of 0.5, 1, 1.5, 2, 2.5, 3 and 6 min. Using microwave irradiation technique, reaction time was reduced by 97% and the separation time reduced by 94%. They recorded biodiesel yield of 100% within 2 min and separation time of 30 min.

Also, Saifuddin and Chua (2004) optimized transesterification of used frying oil to ethyl ester using microwave irradiation. They used a microwave oven equipped with non-contact infrared continuous feedback temperature system and magnetic stirrer to heat the oil and the alcohol at 60^{o}C. Twenty five percent (25%) of an exit power of 750 W was used to irradiate the reaction mixture. The authors experimented different concentrations of sodium methoxide

(0.3wt% to 0.5wt%) and achieved maximum conversion (87wt%) at 0.5wt%. During transesterification process, both sodium ethoxide and potassium hydroxide provided good conversions. However, due simplicity in products phase separation, sodium ethoxide was viewed as most promising catalyst for producing biodiesel.

2.4.1.2 The effects of acid catalysts in biodiesel production

The most notable acids commonly employed in transesterification reaction include among others; sulfuric acid (Sharma *et al*., 2008, Chongkhong *et al*., 2009), sulfonic acid (Hideki *et al*., 2001) hydrochloric acid (Demirbas, 2009) organic sulfonic acid (Hideki *et al*., 2001) and ferric sulphate (Sharma *et al*., 2008)etc. Among these acids, hydrochloric acid, sulfonic acid and sulfuric acid are usually favoured as catalysts for the production of biodiesel.

The catalyst and the alcohol are vigorously mixed with a stirrer in a small reactor. The oil is first charged into the biodiesel reactor and then the mixture of catalyst/alcohol is fed into the oil. Brønsted acids preferably sulfuric acid or sulfonic acid is used to catalyze the reaction. Although the catalysts give high yield of biodiesel, but the reaction rates are slow. The alcohol to oil molar ratio is the main factor influencing the reaction.

Therefore addition of excess alcohol speeds up the reaction and favours the formation biodiesel products. The steps involve during acid-catalyzed transesterification are: (1) initial protonation of the acid to give an oxonium ion (2) The oxonium ion and an alcohol undergo an exchange reaction to give the intermediate (3) and this in turn can lose a proton to become an ester. Reversibility of each of the above step is possible but the equilibrium point of the reaction is displaced in the presence of excess large alcohol, by allowing esterification to advance to completion (Demirbas, 2009). Leung *et al*. (2010) reported that esterification by acid-catalysis makes the best use of the FFAs in the animal fats and vegetable oils and converts them into fatty acid alkyl esters. The authors noted that one-step esterification pretreatment may not reduce the FFAs efficiently, if the acid value of the oils or fats is very high. This is because of the high content of water produced during the reaction. In this case, addition of mixture of alcohol and sulphuric acid into the oils or fats three times (three-step pre-esterification) is required. The time needed for this process is about 2hrs and removal of water is necessary by a separation funnel before adding the mixture into the oils or fats for esterification again.

Further, Palligarnai and Briggs (2008) reported sulfuric acid catalyzed transesterification to provide a few advantages over base-catalyzed technique such as one-step process as opposedto a two-step transesterification. The authors also reported that feedstock with a high

FFAs content could be easily handle, downstream separation is straightforward, and a high-quality glycerol by-product is achievable.

2.4.2 The effects of homogeneous catalysts on the yield of biodiesel fuel.

The nature of catalyst used plays a great role during transformation of vegetable oil to biodiesel (Atandash, 2010). As a result, catalyst is among the key factors determining the rate andyield of biodiesel during biodiesel production process (Atandash, 2010).

Thus, Table 5 presents reaction yield as function of the homogeneous catalyst weight. The data obtained shows that production of biodiesel via homogeneous catalyst could yield more than 99%.

2.4.3 The effects of heterogeneous catalysts in biodiesel production

Despite the problems surrounding alkali-catalyzed transesterification, the process is still favourable in producing biodiesel fuel. The main reason is due to their faster kinetic rate and economic viability (Wang & Yang, 2007). Recently several researches were conducted on heterogeneous catalysts with the aim of finding solutions to problems caused by using homogeneous catalysts in producing biodiesel. As a result a good number of heterogeneous catalysts were explored and many of the catalysts have displayed very good catalytic performances (Zabeti *et al*., 2009).

Some of these catalysts include among others; oxides (Chementator, 2008), hydrotalcides (Georgogianni *et al*., 2009), zeolites (Suppes *et al*., 2004) etc. Currently, majority of heterogeneous catalysts used in producing biodiesel are either oxides of alkali or oxides of alkaline earth metals supported over large surface area (Helwani *et al*., 2001). Further, biodiesel is commercially produced using heterogeneous catalyst through the Esterfip-H process. This biodiesel process is commercialized by Axens. The process needs neither catalyst recovery nor aqueous treatment steps, which are major bottlenecks from the current homogeneous catalytic processes. Additionally the Esterfip-H process displays high biodiesel yields and directly produces salt-free glycerol at purities exceeding 98% compared to 80% glycerol purity from homogeneous catalyzed process (Atadashi *et al*., 2012).

Thus, the effects of these catalysts are discussed as follows:

2.4.3.1 The effects of solid alkaline and acid catalysts in biodiesel production

Surbhi *et al*.(2011) reported that many studies on solid acidic catalysts for producing biodiesel were carried out, however lower reaction rates and unfavorable side reactions have limited their uses. The authors noted that a good number of investigations on basic heterogeneous catalysts were also conducted but their activity gets degraded in the presence of water. They stated that acid–base catalysts are among the most promising catalysts to employ in biodiesel production; this is because they can catalyze both esterification and transesterification simultaneously. Further, Lee and Shiro (2010) reported simultaneous esterification and transesterification of waste cooking oil using solid catalyst ZnO– La_2O_3, which combines acid (ZnO) and base sites (La_2O_3). Although the process provided high conversion of 96% in 3hrs, but like zirconia, lanthanum is a rare and expensive metal, therefore cost of the catalyst would prohibit its usage in the production of biodiesel. Further gelular resin catalysts having covalently bound sulfonic groups are developed and employed to simultaneously esterify and transesterify variety of feedstocks including beef tallow and soybean oil of high acid number. The authors noted the key factors influencing the feasibility and performance of solid catalysts, are durability, catalytic activity and cost of production. Therefore the main challenges to R&D in using solid catalyst in production of biodiesel are exploring the impacts of those chemical properties of supports on the catalytic activity. And designing specifically tailored deactivation–prevention and/or renewal techniques for each catalyst and developing less expensive supports.

2.4.3.2 The effects of solid alkaline catalysts in biodiesel production

In recent times there is a great development in the preparation of solid alkaline catalysts for producing biodiesel. Solid alkaline catalysts such as CaO provides many advantages for instance higher activity, long catalyst life times, and could run under only moderate reaction conditions (Kouzu *et al*., 2008). However, use of CaO in biodiesel production presents slow reaction rate (Thiam & Bhatia, 2008). Antunes *et al*, (2008) noted that like homogeneous catalysts, solid alkaline catalysts present more catalytic activity than solid acid catalysts. Meher *et al*., (2006) examined methanolysis of karanja oil via solid basic catalysts. They remarked that increased in FFAs content of karanja oil from 0.48 to 5.75% decreased the yield of biodiesel produced from 94.9 to 90.3 wt%. The authors achieved an acid value of 0.36 mg KOH/g and an ester content of 98.6 wt%, after purification of the esters. The

properties of the esters produced met both American and European standard specifications for biodiesel fuels.

Also, Liu *et al*., (2008) have produced biodiesel fuel from soybean oil using CaO as a solid base catalyst. The authors reported that use of CaO as a catalyst could provide a numbers of advantages such as: high activity, lengthen catalyst life and moderate condition of reaction. In a similar study, Masato *et al*. (2008) produced biodiesel fuel via solid base-catalyzed transesterification at a reaction time of 1hr and obtained esters yield of 93wt% for CaO, 12wt% for $Ca(OH)_2$, and 0% for $CaCO_3$. The authors stated that CaO will probably provide good productivity as NaOH as well as easy recovery of products and environmental benignity. They used CaO to transesterify waste cooking oil with an acid value of 5.1 mg-KOH/g. The yield of esters was above 99% at a reaction time of 2hrs. But a fraction of the catalyst transformed into calcium soap. Thus, solving this problem will entail removal of FFAs before transesterification reaction. The authors also noted that due to neutralization reaction of the catalyst, concentration of calcium in the produced biodiesel increased from 187 ppm to 3065 ppm. Conversely, Lim *et al*. (2009)noted that transesterification reaction involving CaO needs longer reaction time. But the benefits gained from the process such as elimination of neutralization process, less waste generation and prospect of catalyst reusability compensates the delay. The authors also achieved biodiesel purity of 98.6 ± 0.8% within 2.5hrs. Besides for CaO catalyst, the process generated 90.4% biodiesel yield compared to biodiesel yield of 45.5% for NaOH and 61.0%for KOH catalysts. Further, it was observed that compared to biodiesel yield of 80% under anhydrous conditions using CaO, addition of 2.03 wt% water into the reaction medium of 8 wt.%catalysts, 12:1 alcohol/oil molar ratio and at 3hr of reaction time, could provide biodiesel yield above 95%. Besides the catalyst active sites were found not to and the activity of the catalyst was stable after 20 cycles of the reaction (Zabeti *et al*., 2009).

Similarly, Puna *et al*.,(2010) conducted an experimental study to produce biodiesel via CaO and CaO modified with Li catalysts. Both catalysts showed good catalytic performances with high activity and stability. In fact yields of biodiesel were higher than 92% in two consecutive reaction batches without expensive intermediate reactivation procedures. As a result, the catalysts are suitable for producing biodiesel. In another study,Sharma *et al*. (2011) remarked that the regeneration and resuse of CaO for many times (for instance, 20 runs) makes the catalyst most favourite among the oxides. These characteristics are useful from economic analysis. Further, moderate conversion and yield could be obtained using mixed oxides as catalyst therefore oxides of calcium and magnesium is preferred. Besides presence

of some amount of water/moisture in the reaction mixture has fewer effects on the activity of CaO, this reduces pretreatment cost of feedstock and alcohol.

However, Hsin *et al*. (2010) reported that the high solubility of CaO in methanol makes it a less attractive candidate for recyclable heterogeneous catalysis. Consequently the authors have produced biodiesel fuel from soybean oil (SBO) and poultry fat using new calcium containing silicate mixed oxide based heterogeneous catalysts. The catalysts are; PME templated calcium containing silicate mixed oxide catalysts (PMCS 1-9) and mesoporous calcium containing silicates (CS1-9). The authors reported transesterification of SBO via PMCS-5 consisting of total surface area of $150m^2/g$ to provide 100% yield within 2hrs. This catalyst could be recycled and reused for 8 times after regeneration by calcinations. They remarked that transesterification of soybean oil using CS-9 improved the reaction kinetics by a factor of 6. Also this catalyst could be recycled and reused for 3 times without any decrease in reactivity for poultry fat and 9 times for soybean oil. To further examine the potential of solid alkaline catalysts, Ilgen and Akin (2009) studied different heterogeneous catalysts such as K_2CO_3/γ-Al_2O_3, Na_2CO_3/γ- Al_2O_3, LiOH/γ Al_2O_3, NaOH/γ-Al_2O_3, $\gamma-Al_2O_3$, and KOH/γ-Al_2O_3 and reported FAME yield of 89.40%.

In recent years hydrotalcites materials are receiving great attention because they can be applied as precursors (Schulze *et al*., 2001) and as catalyst (Shumaker *et al*., 2008). Hydrotalcite-like compounds (HTlcs) are a category of anionic and basic clays referred as layered double hydroxides (LDH) with the formula $Mg_6Al_2(OH)_{16}CO_3.4H_2O$ (Helwani *et al*., 2001). Thus production of biodiesel was experimented using different hydrotalcites such as activated Mg–Al hydrotalcites (Barakos *et al*., 2008). Zeng *et al*. (2008) have examined activation of Mg– Al hydrotalcite catalysts for rape oil, and achieved 90.5% conversion. The production of biodiesel from soybean oil via Mg–Al hydrotalcite was patented by Siano *et al*. (2006). The ratio of Mg/Al was found to affect the performance of the catalyst. And the catalytic activity was highest at 3 to 8 ratio of Mg/Al. The authors remarked that the catalyst is best suitable for oils containing up to 10,000ppm quantity of water. They achieved 92% conversion at a reaction condition: reaction time of 1hr, temperature of 180 °C, catalyst concentration of 5wt.% and alcohol/oil weight ratio of 0.45. Similarly the catalytic performance of Mg–Al hydrotalcite for the transesterification of vegetable oil to biodiesel was investigated by Di Serio *et al*. (2006). The authors noted that at higher reaction temperatures (215–225°C); Mg–Al hydrotalcite displayed high catalytic activity. The transesterification was then conducted at methanol/oil weight ratio of 0.45 and catalyst concentration of 1wt%, and esters yield of 94wt% was achieved. Xie *et al*. (2006) have

experimented methanolysis of soybean using Mg–Al hydrotalcite as solid base catalyst. The synthesis of the Mg–Al hydrotalcite was carried out by employing co-precipitation technique of aqueous solution of NaOH, Na_2CO_3, Al $(NO_3)_3 \cdot 9H_2O$, and Mg $(NO_3)_2 \cdot 6H_2O$ under intense stirring.

Increased in catalytic performance and improved basicity were observed by improving temperature of calcinations to 500^oC. But the catalyst showed very low catalytic activity. And a conversion of 67% was recorded at an operating condition of 9hrs, catalyst concentration 7.5 wt%, temperature of 65°C, and alcohol/oil molar ratio of 15:1. Further, Georgogianni *et al*. (2009) have employed heterogeneous catalyst to produce biodiesel fuel using used frying oil. The authors conducted comparison between the catalytic activities of MgO supported on MCM-41 and Mg–Al hydrotalcite base catalyst in the production of biodiesel fuel from soybean frying oil with alcohol (methanol). They reported the conversion of oil to biodiesel to be 97% and 85% respectively after 24hrs under the same reaction conditions. Further the hydrotalcite showed greater activity which was attributed to its high basicity. Even though Mg-MCM 41 has higher specific surface area of 1289 m^2/g compared to the low specific surface area of Mg–Al hydrotalcite of 820m^2/g.

Furthermore, Suppes *et al*. (2004) have transesterified soybean oil with zeolites (ETS-10 zeolite, NaX faujasite zeolite) and metal catalysts. The transesterification reaction was performed at 6:1 molar ratio of alcohol and temperatures of 60, 120, and 150^oC. The conversion to esters increases from 60-150^oC with an average conversion of 90% achieved at 125^oC. Thus, ETS-10 gave better conversions of triglycerides than zeolite-X type catalysts. This was attributed to the higher activity of ETS-10 zeolites and larger pore structures that improved intra-particle diffusion. The catalyst activity was not affected after reused. However, FFAs loadings in excess of 25% quench the catalyst activity. Meyer *et al*. (2008) conducted experimental studies on heterogeneous catalysts to produce biodiesel. The reaction occurred at temperature of 90°C and a methanol to triglyceride ratio of 9:1. The authors stated that among the studied catalysts the potassium exchanged low silica zeolite of the faujasite type (K-LSX) has shown the best results and reached ester formation of over 90 wt.% after 1hr. The result obtained was comparable to those of homogeneous catalysts such as alkali metal hydroxides. Another study conducted by Ramos*et al*. (2008) examined different zeolite catalysts such as NaX for the parent zeolite in sodium form: 0.3MNaX, 1MNaX, 3MNaX, 3MNaXB, and samples from modenite and beta zeolite were named as 3NaM and 3Nab for the transesterification of sunflower oil with alcohol (methanol).

Hence, zeolite X provided greater activity compared to other zeolites (mordenite and beta) due to its higher concentration of super-basic sites. The authors reported that biodiesel contents of 93.5 and 95.1 wt% were achieved at 60^{o}C for zeolite X with and without sodium bentonite, respectively. Though, during the course of the reaction, the active species were observed to be leached out to the product (Ramos*et al*., 2008). Additionally, Supamathanon *et al*.,(2011) have transesterified jatropha oil using heterogeneous catalysts consisting of potassium supported on NaY (K/NaY) with potassium loading of 4, 8 and 12 wt% to produce biodiesel. The experiments were conducted in a 50 mL round-bottom flask equipped with a water-cooled condenser and heated with a water bath. They remarked that under reaction temperature of 65^{o}C, methanol to oil molar ratio of 16:1 and at a reaction time of 3hrs, the catalyst with 12 wt% of potassium loading yielded optimum biodiesel yield of 73.4%.

2.4.3.3 The effects of solid acid catalysts in biodiesel production

The replacement of homogenous catalysts by the solid acid catalysts is useful for green chemistry (Supareak *et al*., 2010). Helwani *et al*. (2001) reported that compared to homogeneous acid, solid acid catalysts are preferred although their catalytic activities are low. This is due to fact that they contain a multiple sites with different strength of Bronsted or Lewis acidity. Kathlene *et al*. (2008) reported solid acid catalysts to have strong capacity to substitute liquid acids, thus wiping out separation, corrosion and environmental problems. The authors evaluated different solid catalysts for the production of biodiesel from high FFAs feedstocks (waste cooking oil). The catalysts investigated include; Zinc stearate/SiO_2, MoO_3/ZrO_2, WO_3/ZrO_2, $WO_3/ZrO_2–Al_2O_3$, MoO_3/SiO_2, TPA/ZrO_2, and Zinc ethanoate/SiO_2. They stated that zinc stearate immobilized on silica gel was most active and stable. The catalyst recycled several times at optimized conditions of reaction temperature of 470 K, 1:18 molar ratio of oil to alcohol, and 3wt% catalyst loading without being deactivated. The authors recorded a maximum ester content of 98 wt%. Catalyst recycling reduces the biodiesel processing cost. In another study, Ngo *et al*. (2010) have esterified FFAs in greases (12–40 wt% FFA) using a diphenylammonium triflate acid catalyst immobilized onto two robust and highly porous solid silica supports (MCM-48 and SBA-15). The authors evaluated the catalytic activities of the catalysts. The catalysts were reported to be effective for the esterification of FFAs in greases with a conversion to biodiesel of 95–99%, resulting in a pretreated grease with a final FFAs content of <1 wt%. Also, Furuta *et al*. (2004)studied biodiesel fuel production via transesterification using soybean oil and methanol with solid

superacid catalysts (sulfated tin oxide (SO_4/SnO_2) and zirconium oxide (SO_4/ZrO_2) and tungstated zirconia (WO_3/ZrO_2) at 200-300^oC. And conducted esterififcation of n-octanoic acid with methanol at 175–200^oC in fixed bed reactor under atmospheric pressure. The authors noted that out of the catalysts prepared, tungstated zirconia– alumina catalyst (WZA) showed high performance, yielding over 90% conversion for esterification processes although detail analysis for the acidity of WZA has not yet been determined.

Besides, Jitputti*et al*. (2006) studied transesterification of palm and coconut oils using solid catalysts such as KNO_3/ZrO_2, KNO_3/KL zeolite, SO_4 2-/ZrO_2, SO_4 2-/SnO_2, and ZrO_2, ZnO. The authors noted that transesterification of crude palm kernel oil using SO_4 2−/SnO_2 and SO_4/ZrO_2catalysts provided highest yield of methyl esters (90.3 wt%). The purities of the esters were 95.4wt% for SO_4 2−/SnO_2 and 95.8wt% for SO_4 2−/ZrO_2, respectively. However, for ZnO the highest content of the esters was 98.9wt%. In addition, owing to the availability of enough acid site strength, solid acid catalysts for example sulfated zirconia, tungstated zirconia and Nafion-NR50 were selected to catalyze transesterification (Wongmaneenil *et al*., 2010). However, due to its acid strength, the selectivity of Nafion-NR50 towards biodiesel and glycerol production was higher, compared to both sulfated zirconia and tungstated zirconia (Lopez *et al*., 2007). Nonetheless, Chai, *et al*. (2007) remarked that major drawbacks of Nafion as catalyst to produce biodiesel, is its lower catalytic activity and high cost compared to liquid acids. Further, application of amberlyst^{tm} BD20 catalyst has provided more impetus for the development of biodiesel fuel.

The amberlyst^{tm} BD20 process can effectively convert any feedstock containing 0.5-100% FFAs to biodiesel. Further amberlyst^{tm} BD20 presents fast solid esterification catalyst. Besides high biodiesel yield can be obtained with improved biodiesel and glycerol purity (Atadashi *et al*., 2012). Additionally the search for a suitable solid catalyst has lead to the development of vanadium phosphate catalyst by Di Serio *et al*. (2007) for biodiesel production. The authors reported 2–4 m^2/g as specific surface area of the catalyst. However, despite the surface area of the catalyst is low, the catalyst was found to be active in producing biodiesel from soybean oil. They reported ester yield of 80% at 150 °C and observed catalysts deactivation at elevated temperatures owing to reduction of V5+ to V3+ with the alcohol (methanol).Although regenerating process of the catalyst after use is simple and could be achieved without complexities.

Also, zeolites are used as a catalyst for esterification and as a support material for transesterification catalysts (Uma & Kim, 2009, Supamathanon *et al*., 2011). Zeolites are microporous crystalline solids with well defined structures and that they contain aluminum,

silicon and oxygen in their framework and cations. As catalysts, unlike the compositionally equivalent amorphous catalysts, zeolites demonstrate substantial acid activity and shape selective features (Chung *et al*., 2008, Park *et al*., 2007, Kim *et al*., 2004). Chung *et al*. (2008) employed different Si/Al molar ratio to remove FFAs in waste frying oil by esterification with methanol using different zeolite catalysts.

The catalysts used include mordenite (MOR), faujasite (FAU), beta (BEA) zeolites, ZSM-5 (MFI), and silicalite. The pore structure and the acidic properties of the zeolites were particular useful in the removal of FFAs. These properties influenced the catalytic activity in FFAs removal. High conversion of FFAs was comparatively induced by strong acid sites of zeolites. The MFI zeolite induced an improvement of the FFAs removal efficiency by cracking to the FFAs in its pore structure owing to its constricted pore mouth. Converting FFAs on HMFI and HMOR zeolites provided 80% at a reaction temperature of 60^{o}C. In addition, HMOR zeolites showed almost a similar conversion of FFAs with different Si/Al molar ratio, but with decreased acidity. Decreased in acid strength of the zeolites lowered the catalytic performance for FFAs removal (Atadashi *et al*., 2012).

2.4.4 The effects of enzymes catalysts in biodiesel production

Transesterification reaction can be catalyzed with enzymes catalysts such as *Candida antarctica* lipase (Tan *et al*., 2010),*Pseudomonas cepacia* (Salis *et al*., 2008), *candida sp*. 99–125 (Tan *et al*., 2010, Nie *et al*., 2006),*Pseudomonas fluorescens* (Salis *et al*., 2008), *Rhizomucor Miehei and Chromobacterium viscosum*(Bozbas, 2008, Shieh *et al*., 2003) and *Rhizopus oryzae* lipase (Piazarro & Park, 2003) etc. Casimir *et al*. (2007) noted that biodiesel can be excellently produced via enzymatic-transesterification reactions involving lipases. They suggested that large quantities of lipases can be produced using recombinant DNA technology. The authors believed that application of immobilized lipase may reduce the overall cost of biodiesel production and lower downstream processing problems.

Besides, enzymatic approach is environmentally friendly (Casimir *et al*., 2007). Watanabe *et al*. (2000) explored use of immobilized *Candida antarctica* lipase for continuous production of biodiesel fuel from vegetable oil. The transesterification of vegetable oil was conducted using 4% immobilized *Candida lipase* as a catalyst at 30°C in a 20- or 50-mL screw-capped vessel, shaking at 130 oscillations/min. The authors noted the activity of *Candida antarctica* lipase was not affected in a mixture of vegetable oil and more than 1:2 molar equivalent of methanol against the total fatty acids. They discovered inactivation of the lipase to be eradicated via three consecutive additions of 1:3 molar equivalent of methanol. And then

developed a three-step methanolysis by which over 95% of the oil triacylglycerols (TAG) transformed to their corresponding esters.

Additionally, Shah *et al*. (2004) have prepared biodiesel from jatropha oil using lipase catalyst. The authors have screened *Pancreas porcine*, *Candida rugosa, Chromobacterium viscosum* and in a solvent-free system for the production of biodiesel. They employed a screw-capped vial and jatropha seed oil (0.5 g) and ethanol were taken in the ratio of 1:4 (mol mol-1). Also 50 mg of enzyme preparation (tuned or immobilized) was added and incubated at 40°C with constant shaking at 200 rpm. The immobilization of lipase (*Chromobacterium viscosum*) on Celite-545 improved yield of esters from 62% to 71% by free tuned enzyme preparation with a process time of 8hr at 40°C. Additionally to explore more information on the use of enzymes for the production of biodiesel, Tan *et al*. (2010) reviewed biodiesel production using immobilized lipase. The immobilized lipase as biocatalyst draws great interest because that process is environmentally friendly. The authors noted different techniques for lipase immobilization, such as covalent bonding, cross-linking, encapsulation, entrapment and adsorption. Lipase immobilization technique is commonly used to increase the stability of lipase in biodiesel production. They stated that, for biodiesel (fatty acid methyl esters) preparation, at least a stoichiometric amount of methanol is needed for the complete conversion of triglycerides to their resultant fatty acid methyl ester. But, methanolysis is reduced considerably by adding >1/2 molar equivalent of methanol at the commencement of the enzymatic process. Usually, the polar short chain alcohols causes inactivation of enzymes and this is the major obstacle for the enzymatic-transesterification reaction. Therefore to overcome this difficulty one of these options is selected: acyl acceptor alterations, solvent engineering and methanol stepwise addition. The authors reported that biodiesel yield of 97wt% was obtained after 24 hrs at temperature of 50°C with a reaction mixture containing 13.5% methanol, 32.5% t-butanol, 54% oil and 0.017 g enzyme (g oil)−1. With the same mixture, a 95% biodiesel yield was achieved using a one step fixed bed continuous reactor with a flow rate of 9.6 ml h^{-1} (g enzyme)$^{-1}$. The authors concluded that low cost of immobilized *Candida sp*. 99–125 lipases is rather competitive for industrial use (Tan *et al*., 2010). More so, Hideki *et al*. (2001) noted use of enzymatic-catalyzed transesterification to avoid problems associated with homogeneous catalysts. Therefore the production processes are compared in Figures 2.10 and 2.11. The authors reported conversion of high FFAs feedstocks to biodiesel using immobilized *antarctica* lipase (Novozym-435) with ease of separation process.

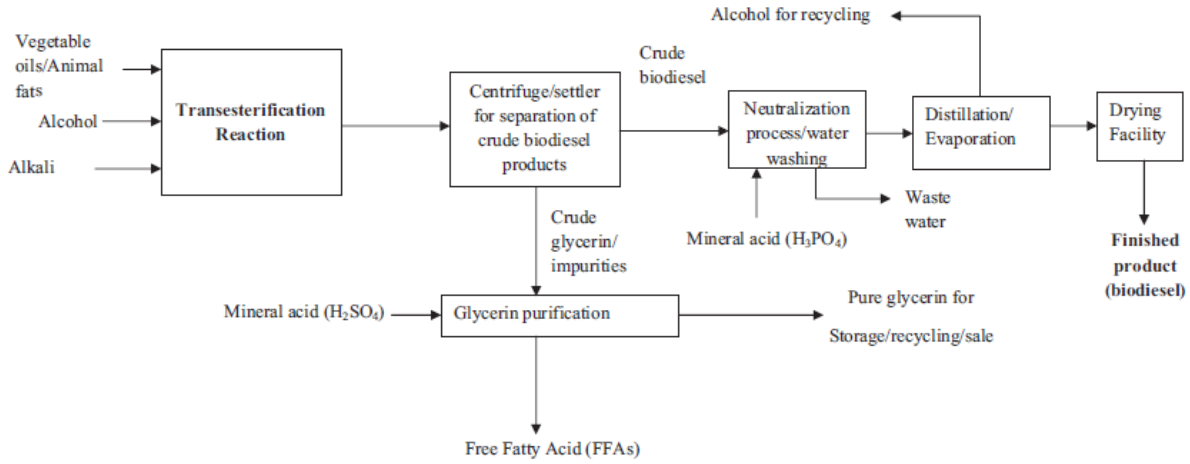

Figure 2.10: Traditional alkali biodiesel production (Atadashi *et al*., 2012)

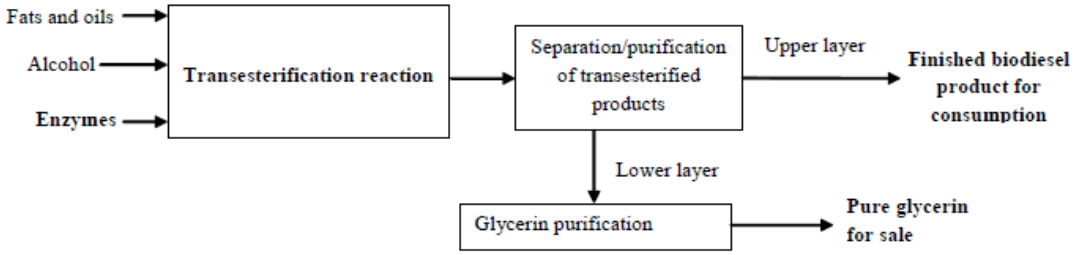

Figure 2.11: Enzymatic biodiesel production (Atadashi *et al*., 2012).

2.4.5 The effects of heterogeneous catalysts on the yield of biodiesel

As earlier stated great efforts have being made by several researchers and industries to explore and exploit use of heterogeneous catalysts in the production of biodiesel. Some ofthe reasons for the recent growth and development of heterogeneous catalysts include among others: biodiesel yield of 98wt% and simplicity in catalyst separation process (Zabeti *et al*., 2010), high-purity by-products, less cost of separation and low energy consumption (Thiam & Bhatia, 2008). Table 2.5presents reaction yield as function of the heterogeneous catalyst weight.

Table 2.5: Reaction Yield as Function of Heterogeneous Catalyst Weight (Atadashi *et al*., 2012).

Feedstock	Catalyst	Conc (wt)	Reaction time (hr)	Reaction temp (^oC)	Yield (wt%)	Molar ratios
Soybean oil	CaO	25	1	-	93	-
Vegetable oil	M(3-hydroxy-2-methyl-4-pyrone)2(H_2O)2	-	3	60	93	-
Sunflower oil	CaO/SBA-14	-	5	160	95	12
Sunflower oil	ZeoliteX	4.2	-	60	95.1	-
Soybean oil	ETS-10 zeolite	0.03	24	125	90	-
Palm oil	CaO/Al_2O_3	3.5	5	65	98.64	12:1
Waste bleaching earths	Rhizopus oryzae	-	96	35	55	1:4
Soybean	$Na/NaOH/Al_2O_3$	1	2	60	96	9:1
Crude palm kernel oil	$SO42-/ZrO_2$	1	1	200	90.3	6:1
Waste cooking oil	ZS/Si	3	10	200	98	1:18
Soybean oil	Lipase	0.9	6.3	36.5	92.2	3.4:1
Palm oil	CaO/Al_2O_3	3.5	5	65	95	12:1
Canola oil	Nano-g-Al_2O_3	-	8	65	97.7 ± 2.1	15:1
Mixture of soybean and rapeseed oils	*Candida* lipase	4	24	30	93	1:3
Jatropha oil	*Chromobacterium viscosum* lipase	5	8	40	92	1:4
Soybean oil	*Pseudomonas cepacia* lipase	47.5	1	35	67mol%	1:17.5
Sunflower oil	WO_3/ZrO_2	3	5	200	97	20:1

2.4.6 The advantages and disadvantages of homogeneous catalysts and heterogeneous catalysts

The choice of catalyst to use in the production of economically viable biodiesel fuel is one of the most critical issues that arebeing discussed by futurists and industries (Georgogianni *et al*., 2009). As discussed earlier, NaOH and KOH are mostly preferred because they are cheaper than alkoxides, but are less active (Atadashi *et al*., 2012). Leung and Guo (2006) revealed that industrially, separation of esters is much easier when KOH catalyst is used compared to NaOH or CH_3ONa. Because potassium soap formation is much softer and does

not sink into glycerol phase. Owing to this reason, KOH is most often employed to produce biodiesel from waste recycled feedstocks (Leung & Guo, 2006). Saka and Isayama (2009)reported that even though the alkaline catalyst technique has the advantage of using moderate reaction conditions, several water washings are needed to remove the catalysts. Zhang *et al*. (2003) conducted economic analysis of four continuous processes to produce biodiesel such as alkali- and acid-catalyzed processes, with virgin vegetable oil and waste cooking oil. The authors revealed that acid-catalyzed transesterification with waste cooking oil were more economically viable. The process gave lesser total production cost, a more attractive after-tax rate of return and a less biodiesel break-even price.

In contrast both alkali- and acid catalyzed transesterification are associated with a number of problems. Madras *et al*. (2004)reported that alkali-catalyzed transesterification present high cost of biodiesel production and large energy consumption during down-stream biodiesel refining process. Ferella *et al*. (2010) stated that potassium hydroxide produces soaps formation by neutralizing FFAs.

Additionally, due to the tendencies to produce soaps formation and mono- and di-glycerides during transesterification, direct use of sodium and potassium alkylates as catalysts is raising serious issues in the industries. The soaps formations cause formation of gels and makes separation and purification of biodiesel hard. Also, Cardoso *et al*. (2009) reported that the problems associated with H_2SO_4 catalyst include much reactor corrosion and huge wastewater discharges resulting from the neutralization of mineral acid. Another investigation conducted by Helwani *et al*. (2001) revealed that application of homogeneous catalysts in biodiesel production presents difficulty in biodiesel product separation and makes recovery of used catalyst cumbersome. The authors reported that biodiesel production via homogeneous alkaline catalysts needs multi-steps of production and purification, since such catalysts do not tolerate presence of moisture or FFAs. In addition, there are many notable issues surrounding the existing transesterification processes such as; difficulties in processing low quality feedstocks and refining of transesterified products (Leung *et al*., 2010).

Further heterogeneous catalysts provide many advantages compared to homogeneous catalysts such as: catalyst re-usability, less separation and purification difficulties, high purity glycerol (above 99%), and catalyst recoverability etc (Martin Alonso *et al*., 2007). Additionally no neutralization step is required (Janaun, 2010). Thus, in biodiesel production, the overall economy can be improved through the use or sale of by-product, glycerol (Atadashi *et al*., 2012). Mariscal *et al*. (2007) reported that heterogeneous catalysts are less corrosive, leading to safer, less costly and more environmentally friendly operations.

Watanabe *et al*. (2000) reported enzymatic-transesterification reaction to overcome problems associated with chemical processes.Palligarnai and Briggs (2008)found glycerol from enzymatic-catalyzed transesterification not to show negative effects on biodiesel fuel property. The authors stated that the major advantage of employing enzyme catalysts is lack of soaps formation. They reported application of insoluble solid catalysts (immobilized enzymes) to speed up catalyst removal from both glycerol and alkyl esters. Zabeti *et al*. (2009) showed solid-catalyzed transesterification reaction to yield biodiesel products with no catalyst impurities. Therefore absence of leaching improves separation process and lowers the cost of final refining. Martino *et al*. (2008) noted that heterogeneous catalysts can be separated more easily, besides low processing costs and zero waste streams. Hameed *et al*. (2009) stated that heterogeneous catalysts are searched over time to achieve environmentally benign and economically viable biodiesel production and purification processes. However, issues such as leaching of catalysts especially when solid alkaline catalysts such as CaO, MgO, La_2O_3, ZnO, SrO, Li-promoted CaO, $CaCO_3$, $Ba(OH)_2$, K_xX/Al_2O_3 (X-halide ion or other mono/di-valent anion), zinc aluminates, metal salts of amino acids, Mg–Al hydrocalcites and K- and Cs-exchanged zeolites are used in producing biodiesel creates great deal of concern during separation process. The leaching of active sites of solid alkaline catalysts into liquids results from its change in characteristic turning it partly "homogeneous". This change in the properties of the catalysts affects biodiesel quality, makes catalyst separation and biodiesel purification difficult, thus bringing extra cost of production (Helwani *et al*., 2009). Mariscal *et al*. (2007) reported significant leaching of potassium during transesterification of triglyceride via K/c-Al_2O_3 catalysts. The authors reported 99wt% biodiesel yield which was attributed to homogeneous contribution from active basic species dissolved in the methanol. In addition, the homogeneity of this catalyst complicates its separation process. Also leaching of solid acid catalyst (sulfate species) was reported to restrict its reusability (Mittelbach *et al*., 1996). Moreover, a study carried out by Lee *et al*. (2009) remarked that leaching of base active species caused great negative effects on the degree of purity of biodiesel and glycerol. Another investigation conducted through optimization of catalytic activity of CaO/Al_2O_3 for producing biodiesel with response surface methodology showed insignificant leaching of catalyst into the reaction medium (Zabeti *et al*., 2009, Zabeti *et al*., 2010). Table 2.6summarizes the merits and demerits of homogeneous catalysts and heterogeneous catalysts for biodiesel production.

Table 2.6: Advantages and disadvantages of homogeneous catalysts and heterogeneous catalysts (Atadashi *et al*., 2012)

Type of catalyst	Example	Merits	Demerits
Homogeneous catalyst			
Alkaline catalyst	NaOH, KOH, CH_3ONa, CH_3OK	Less corrosive, high reaction rate	Formulation of saponified product, emulsion formation, high water and energy consumption, huge, high wastewater discharges, high purification cost. Feedstocks are limited to 0.5wt FFAs, not recycle
Acid catalysts	H_2SO_4	Zero soap formation, the catalyst can be used to catalyze both esterification and transesterification simultaneously	More waste as a result of neutralization, recycling difficulty, high purification cost, energy consuming, low reaction rates.
Heterogeneous catalyst			
Solid alkaline catalysts and solid acid catalyst	MgO, CaO, ZnO, KOH/NaY. CaO/MgO, Al_2O_3,-SnO, KOH/K_2CO_3,CaO/ Al_2O_3, KOH/ Al_2O_3, Al_2O_3/KI, $Sr(NO_3)_2$/ZnO, ZrO_2/SO_4^{2-}, $TiO_2//SO_4^{2-}$,ETS-10 zeolite, zeolite HY, and zeolite X	Environmentally friendly, easily recycle, less discharge, less separation difficulty, high purity glycerol, lower cost of separation, insignificant leaching of CaO/ Al_2O_3	Leaching effects, catalysts preparation is complicated and expense relatively slow rates
Enzymes catalysts	Candida Antarctica B. lipase, Rhizomucor meihel lipase, candida rugosa Pseudonas cepacia, M. meihei (Lypozyme), M. meihei (Lypozyme IM60), Aspergillus niger,	Zero saponification products nonpoHuting, easily separable, lesser separation cost, high purity glycerol and biodiesel products, environmentally benign.	Catalysts inhbiton by water.
	P. fluorescenes, R. Oryzae	Simple glycerol recovery	High cost of enzymes

2.5 Alcohols used in the Production of Biodiesel

As previously mentioned, methanol is the most common alcohol used in the production of biodiesel. Other alcohols may also be used in the preparation of biodiesel, such as ethanol, propanol, iso-propanol, and butanol. Ethanol is of particular interest primarily because it is less expensive than methanol in some regions of the world, and biodiesel prepared from bio-ethanol is completely bio-based. Butanol may also be obtained from biological materials, thus yielding completely bio-based biodiesel as well. Methanol, propanol, and iso-propanol are normally produced from petrochemical materials such as methane obtained from natural gas in the case of methanol.

2.5.1 Methanolysis of triglyceride

The classic reaction conditions for the methanolysis of vegetable oils or animal fats are 6:1 molar ratio of methanol to oil, 0.5 wt.% alkali catalyst (with respect to TAG), 600+ rpm, 60°C reaction temperature, and 1 h reaction time to produce FAME and glycerol . A number of recent studies have described optimal reaction conditions for biodiesel production from various feed stocks using response surface methodology (RSM). Parameters that are normally optimized to produce the most biodiesel include catalyst type and amount, reaction time and temperature, amount of alcohol, and/or agitation intensity. Table 2.7 shows the summary of recent examples of biodiesel process optimization employing RSM. A representative example of reaction conditions optimized by RSM is the work in which Jatropha curcas oil methyl esters were produced (after acid pretreatment) using 0.55 wt.% KOH, 60°C reaction temperature, 5:1 molar ratio of methanol to oil, and 24 min reaction time to provide biodiesel in 99% yield (Moser, 2009). The reaction parameters do not vary by a significant amount, as seen by comparison of the classic reaction conditions to that of and others listed in Table 2.7.

2.5.2 Ethanolysis of triglyceride

The classic conditions for ethanolysis of vegetable oils or animal fats are 6:1 molar ratio of ethanol to oil, 0.5 wt.% catalyst (with respect to TAG), 600+ rpm, 75°C reaction temperature, and 1 h reaction time to produce fatty acid ethyl esters (FAEE) and glycerol. Ethyl esters have been prepared from a number of feedstocks for use or evaluation as potential biodiesel fuels. In addition, mixtures of methyl and ethyl esters have been reported whereby the transesterification reaction was conducted with both methanol and ethanol. Table 2.7 shows two recent examples. A representative example is that of the ethanolysis of crude *Raphanus*

sativus oil in which 0.60 wt.% NaOH, 11.7:1 molar ratio of ethanol to oil, 380°C reaction temperature, and a 1-h reaction time afforded the corresponding ethyl esters in 99.1% yield.

Table 2.7: Recent examples of optimization of reaction conditions for production of biodiesel from various feedstocks using response surface methodology (Moser, 2009).

Feedstock	Catalyst	Temp. ^{o}C	MeOH	Time (mins)	Yield (%)
Pork Lard	1.26KOH	65	7.5:1	20	97.8
Rapeseed	1.0KOH	65	6:1	120	95.96
Sunflower	1.0NaOH	60	6:1	120	97.1
Safflower	1.0NaOH	60	6:1	120	98
Jojobo	1.35NaOH	25	6:1	60	83.5
Rice brain	0.75NaOH	55	9:1	60	90.2
Waste cooking oil	1.0NaOH	50	9:1	90	89.9
Jatropha Curacas	0.55NaOH	60	5:1	24	99
Madhuca Indica	0.70KOH	60	6:1	30	99
Pongamia Indicia	1.0KOH	65	6:1	180	97-98
Brassica Carinata	1.2KOH	25	6:1	60	97
Used Frying oil	1.1NaOH	60	5:1	20	88.8
Canola	1.07KOH	40	6:1	60	93.5
Cotton seed	1.07KOH	25	20:1	30	98
Raphanus Satiuus	0.6NaOH	38	1:7	60	99.1

The reaction temperature and amount of ethanol in this case varied considerably from the conditions initially reported.

Ethanolysis proceeds at a slower rate than methanolysis because of the higher reactivity of the methoxide anion in comparison to ethoxide. As the length of the carbon chain of the alkoxide anion increases, a corresponding decrease in nucleophilicity occurs, resulting in a reduction in the reactivity of ethoxide in comparison to methoxide. These results indicate that methyl esters are preferentially formed at both ambient and elevated reaction temperatures, but at elevated temperatures, the preference is diminished.

Even though the formation of ethyl esters is comparatively slow, the overall rate of formation of esters is faster than with methanol alone due to the better solubility of TAG in a mixture of methanol and ethanol, which results in a reduction of mass transfer limitations (Moser, 2009).

2.5.3 Butanolysis of triglyceride

The classic conditions for butanolysis of vegetable oils or animal fats are 6:1 molar ratio of butanol to oil, 0.5 wt. % catalyst (with respect to TAG), 600+ rpm, 114°C reaction temperature, and 1 h reaction time to produce fatty acid butyl esters and glycerol. Butyl esters have been prepared from a variety of feedstocks for use or evaluation as potential biodiesel fuels. Based on the available literature, the butanolysis reaction has not yet been optimized by RSM. Butanol is completely miscible with vegetable oils and animal fats because it is significantly less polar than methanol and ethanol. Consequently, transesterification reactions employing butanol are monophasic throughout.The monophasic nature of butanolysis reactions influences the rate and extent of the reaction. There are no mass transfers limitations in the case of butanolysis, since all reactants and catalysts are contained in a single phase. As a result, the initial rate of butanolysis is considerably faster than that of methanolysis.

In the case of butanolysis, the reverse reactions are more likely to occur because all materials are in contact throughout the reaction. The monophasic nature of butanolysis reactions also complicates purification of the resultant butyl esters, as gravity separation of glycerol at the conclusion of the reaction is not possible. The weaker nucleophilicity of butoxide versus methoxide is another factor that affects the extent of reaction. Although butanolysis proceeds at a faster initial rate than methanolysis, the final conversion to products after 1 h reaction (114°C and 60°C reaction temperatures, respectively) is 96 wt.% versus 98 wt.% for methanolysis. In addition, after 1 h (at 23°C), 14.4 wt.% of bound glycerol (TAG +DAG + MAG) remained, whereas only 11.7 and 7.2 wt. % remained in the cases of methanolysis and ethanolysis, respectively.

In summary, the butanolysis reaction is monophasic throughout, which results in a faster initial rate of reaction but may yield lower overall conversion to butyl esters in comparison to methyl or ethyl esters (Moser, 2009).

2.6 Biodiesel Separation from Glycerol

Several researchers had studied extensively numerous conventional techniques for the separation of biodiesel. A brief review for the biodiesel separation techniques is presented here. Most of the researchers reported that high quality biodiesel that is economically viable can be achieved when suitable biodiesel separation process is employed. After transesterification, separation of biodiesel and by-product, glycerol is usually first carried out. This process of biodiesel separation is based on the facts that the biodiesel and glycerol produced are typically sparingly mutually soluble, and that there is palpable difference in density between biodiesel (880 kg/m^3) and glycerol (1050 kg/m^3, or more) phases respectively. More so, this difference in density is sufficient enough for the application of simple techniques such as gravitational settling or centrifugation for the separation of biodiesel and glycerol phases (Atadashi *et al*., 2010)

2.7 Biodiesel Washing

A critical step in the production of biodiesel, particularly when the feed vegetable oil contains free fatty acids, is the removal of the soap that is formed as part of the transesterification reaction and is dissolved in the biodiesel if homogeneous catalyst (NaOH or KOH) is used. Soap is the salt of fatty acids; and during the biodiesel esterification reaction, the free fatty acids in the oils react with the sodium (or potassium) ions of the methoxide or ethoxide to form the soap. Two approaches have been advanced for performing this chemical process separation task: extraction of the soap with water, and extraction of the soap with absorbents. The former extraction task is often described, in local biodiesel production operations, as washing the biodiesel fuel. However, the two approaches are based on the same chemical science; and the washing science application is better reflected through the extraction with water; besides, for large scale biodiesel production operation, the extraction with water supports more stable operation.

Water is generally known to be immiscible with biodiesel and is also heavier than oil. However, it is the latter characteristics that define the most the design rationale for the biodiesel washing.

The ionic end of the soap molecule is termed hydrophilicwhile the other end is hydrophobic or lipophilic and the molecule itself is described as amphiphilic, and called amphiphile. Water, of course, is slightly polar at the hydrogen location, and as such the hydrophilic group of the soap molecule is attracted to the water molecules when exposed to water molecules.

This affinity for water then is the basis of separation of the soap from the biodiesel. When water comes into contact with the biodiesel after the transesterification reaction, the hydrophilic group of the soap gets attached with the water molecules while the hydrophobic group remains in the biodiesel.

However, the impact of the variation of length of soap molecules is relatively more intrinsic in the case of biodiesel washing than the other factors. The intrinsic feature of the biodiesel transesterification reaction is that the soap molecules are of varying carbon chain lengths: a vegetable oil is generally a mixture of oils of different carbon chain lengths; hence the free fatty acids produced from such oils also have different carbon chain lengths and consequentially result in soap of varying carbon chain lengths as well.

So first an understanding of the formation of structures as a function of carbon chain length: essentially, when several molecules of soap are added to water, the hydrophilic groups of the molecules attach themselves to water molecules and forces an isolation of the hydrophobic end from association with any water molecule; as a result a small structure of the form of a ball is formed in which the surface of the ball consists of the hydrophilic groups of the soap molecules but with the hydrophobic ends being encased or encapsulated within the sphere. This structure is commonly called a micelle.

Effectively then, if a droplet of biodiesel with soap molecules were bubbling up through water medium, then the soap molecules will reoriented themselves by jotting the hydrophilic ends into the water while keep the hydrophobic ends in the biodiesel droplet. Conceptually, the biodiesel droplet should appear to be occluded by the soap molecules as the droplet bubbles up to the top of the water medium. Inferentially then, in this case the structure that gets to be formed is of the form of micelles.

However, this relation between the water and the biodiesel droplet is not preserved. The soap molecules will ultimately get pulled out of the biodiesel droplet into the water medium because of the strength of electrostatic attraction between the ionic charges of the water and soap molecules; and effectively there comes about a separation of the soap molecules and biodiesel.

2.8 Biodiesel Characterization

Biodiesel fuel quality depends upon composition of feedstock, production process, storage and handling (Reo *et al.*, 2010). Vegetable oils and animal fats of differing origin have dissimilar fatty acid composition. A typical fatty acid composition of common feedstock oils and fats for biodiesel production is shown on Table 2.8.

Table 2.8: Typical fatty acid composition (wt %) of common feedstock oils and fats used for biodiesel production.

Fatty acid	Castor oil CO	Palm oil PO	Soybean oil SBO	Sunflower oil SFO	COO	Cottonseed oil CSO	Coconut oil CCO	CF	BT
C6:0							1		
C8:0							7		
C10:0							7		
C12:0							47		1
C14:0		1				1	18	1	4
C16:0		4	11	6	11	23		25	26
C18:0			4	5	2	2	3	6	20
C20:0									
C22:0				1					
C16:1	61	23				1		8	4
C18:1			23	29	28	17	6	41	28
C18:2			54	58	58	56	2	18	3
C18:3			8	1	1				
C20:1									
Others									14

Source: Moser, 2009.

The fatty ester composition of biodiesel is identical to that of parent oil or fat from which it was produced. Feed stocks for biodiesel production vary with location according to climate and availability (Moser, 2009).

Biodiesel quality is evaluated through the determination of chemical composition and physical properties of the fuel. Contaminants and other minor components due to incomplete reaction are the major issues in the quality of biodiesel i.e., glycerol, mono, di, triglycerides, alcohol, catalysts and free fatty acid present in the biodiesel. Moreover, biodiesel composition could be changed during storage and handling. Biodiesel can absorb water or undergoes oxidation during storage. Therefore, significance of these parameters and their analytical or engine test methods are addressed in standards. Biodiesel standard are in place in a number of countries in an effort to ensure that only high quality biodiesel reaches the market place. The most important standard, ASTM D6571 in the United State and EN 14214 (European Committee for Standardization, CEN) in European Union are summarized below in Table 2.9(a) and 2.9(b) respectively. In addition, a petrol diesel - biodiesel blend standard, ASTM D7467 was recently introduced that covers blends of biodiesel in petro diesel from 6 to 20 vol. % and is summarized also in Table 2.9(c) (Moser, 2009).

Table 2.9(a): ASTM D6751 biodiesel fuel standard.

	Property		Method	Limit	Units
1.	Flash point (Closed Cup)		ASTM 093	93 min	^{0}C
2.	Alcohol control: one of The following must be meet				
	• Methanol content		EN14110	0.2 max	% volume
	• Flash point		ASTM D93	130.0 min	^{0}C
3.	Water and sediment		ASTM D 2709	0.050 max	%volume
4.	Kinematic Viscosity		ASTM D 445	1.9-60	mm^2/S @ (40^0c)
5.	Sulfated ash		ASTM D874	0.020 max	% mass
6.	Sulfur		ASTM D5453	0.0015max	%mass (ppm)
7.	Copper strip corrosion		ASTM D130	No.3 max	
8.	Cetane number		ASTM D613	47 min	
9.	Cloud point		ASTM D2500	Report	^{0}C
10.	Cold soak filterability		Annex A1	360 max	S
11.	Carbon residue		ASTM D4530	0.050 max	% mass
12.	Acid value		ASTM D664	0.050 max	mgKOH/g
13.	Free glycerin		ASTM D65	0.020	% mass
14.	Total glycerin		ASTM D6584	0.0240	% mass
15.	Oxidation stability		EN 14112	3.0 min	H
16.	Phosphorous content		ASTM D4951	0.00/max	% mass
17.	Sodium & potassium Combine		EN 14538	5 max	Ppm
18.	Calcium & magnesium Combined		EN 14538	5 max	Ppm
19.	Distillation temperature equivalent, Temp, 90% recovered	Atmospheric	ASTM D1160	360 max	^{0}C

Fuel properties can be grouped conveniently into physical, chemical and thermal properties. The important properties of biodiesel are classified into three groups, viz.

i. Physical properties - viscosity, cloud point, pour point, flash point etc.

ii. Chemical properties - chemical structure, acid value, saponification value, sulphur content, copper corrosion, oxidation resistance and thermal degradation etc.

iii. Thermal properties- distillation temperature, thermal conductivity, carbon residue and calorific value.

2.8.1 Physical Properties

2.8.1.1*Kinematic Viscosity*

Kinematic viscosity is the resistance to flow of a fluid under gravity. It is the time taken for a fixed volume of fuel to flow undergravity through the capillary tube viscometer immersed in a thermostatically controlled bath at 40ºC. It isthe product of measured time flow and

calibration constant of viscometer. From ASTM 6751 Table, standard values of kinematic viscosity of biodieselare in the range of 1.9-6.0mm^2/s. The kinematic viscosity is a basic design parameter for the fuelinjectors used in diesel engines.

Table 2.9(b) European Committee for Standardization EN 14214 biodiesel fuel standards

	Property	Test method	Limits	Units
1.	Ester content	EN 14103	96.5 min	%(mol/mol)
2.	Density, 15^oC	EN 150 3675, EN 150 12185	860-900	Kg/m^3
3.	Kinematic viscosity 40^oC	EN 150 3104, 180 3105	3.5 -5.0	mm^2/S
4.	Flash point	EN 180 3679	120 min	^0C
5.	Sulfur content	EN 150 20846, EN 150 20884	100 max	mg/kg
6.	Carbon residue (10% distillation residue)	EN 180 10310	0.30 max	% (mol/mol)
7.	Cetane number	EN 150 5165	51 min	
8.	Sulfated ash	150 3987	0.02 max	% (mol/mol)
9.	Water content	EN 150 12937	500 max	Mg/kg
10.	Total contamination	EN 12662	24 max	Mg/kg
11.	Copper strip corrosion (3h, 50^{o}c)	EN 150 2160	1	Mpy
12.	Oxidation stability, 110^oC	EN 1412	6.0	H
13.	Acid value	EN 14104	0.50 max	mKOH/g
14.	Iodine value	EN 14111	120 max	g½ /100g
15.	Linolenic acid content	EN 14103	12.0 max	% (mol/mol)
16.	polyunsaturated (7/4 double bonds) methyl ester	EN 14103	1 max	% (mol/mol)
17.	Methanol content	EN 14110	0.20 max	% (mol/mol)
18.	MAG content	EN 14105	0.80 max	% (mol/mol)
19.	DAG content	EN 14105	0.20 max	% (mol/mol)
20.	TAG content	EN 14105	0.20 max	% (mol/mol)
21.	Free glyercol	EN 14105 EN 14106	0.020 max	%(mol/mol)
22.	Total glycerol	EN 14105	0.25 max	%(mol/mol)
23.	Group I metal (Na,k)	EN 14108 EN 14109	5.0 max	mg/kg.
24.	Group II metal (CA,mg)	EN 14538	5.0 max	mg/kg
25.	Thosphorous	EN 14107	10.0 max	mg/kg

Table 2.9(c): ASTM 7467 biodiesel – petrodiesel blend (B6-B20) fuel standard

	Property	Test method	Limits	Units	Limits	Units
1.	Biodiesel content	ASTM D7371	6.20	% volume		
2.	Flash point (close cup)	ASTN D93	52	^{o}C		
	One of the following must be met:					
	• Cetane index	ASTM D876	40 min	% volume		
	• Aromaticity	ASTM 01319	35 max	% volume		
3.	Water and sediment	ASTM D2709	0.050 max	% volume		
4.	Kinematic viscosity, 40^{o}C	ASTM D445	1-9-401	mm^2/S		
5.	Sulfur content	ASTM D5453 ASTM D2622	15 max (S15) 500 max (5500)	Ppm		
6.	Copper strip corrosion	ASTM D130	No. 3 max			
7.	Cetane number	ASTM D613	40 min			
8.	carbon residue	ASTM D524	0.35 max	% max		
9.	Acid value	ASTM D664	0.30 max	Mg KoHg		
10.	Oxidative stability	EN 14112	6.0 min			
11.	Ash content	ASTM D482	0.01 max	% max		
12.	Cubraily, HFRR, 60^{o}C	ASTM D6079	520 max	Pm		
13.	Cloud point or LTFT/CFPP	ASTM D2500, D4539, D6371	Only guidance provided	^{o}C		
14.	Distillation temperature 90% received	ASTM D56	343 max	^{o}C		

Source: Moser, 2009.

Fuel viscosity has influence on fuel droplet size and spraycharacteristics. Viscosity is inversely proportional to temperature. Viscosity increases with chain length and degree of saturation. Higher viscosity leads to poor atomization, incomplete combustion and increases carbon deposits. Higher viscosity fuel needs higher pumping power also. Fuels with lower viscosity leaks past plunger through the clearance between plunger and barrel during fuel compression (Reo *et al*., 2010).

2.8.1.2*Density*

Density is another important property of biodiesel. It is the weight of a unit volume of fluid. Specific gravity is the ratio of density of the liquid to the density of the water. Oils that are denser contain more energy. For example, petrol and diesel fuels give comparable energy by

weight, but diesel is denser and hence gives more energy per litre. The aspects listed above are the key aspects that determine the efficiency of a fuel for diesel engines. The specific gravity of biodiesels ranges from 0.87 to 0.89 (Ayhan, 2006).

2.8.1.3*Cetane number*

Cetane number (CN) is determined in accordance with ASTM D613 and is one of the primary indicators of diesel fuel quality. It is related to the ignition delay time which a fuel experiences once it has been injected into a diesel engine's combustion chamber. Generally, shorter ignition delay times result in higher CN and vice versa. CN is based on two compounds, namely hexadecane and heptamethylnonane. Hexadecane, also known as cetane (trivial name), which gives the cetane scale its name, is the high-quality reference standard with a short ignition delay time and an arbitrarily assigned CN of 100. The compound 2,2,4,4,6,8,8-heptamethylnonane is the low-quality reference standard with a long ignition delay time and an arbitrarily assigned CN of 15 (Moser, 2009).

2.8.1.4*Flash point*

Flash point is defined as the lowest temperature corrected to a barometric pressure of 101.3 kPa (760 mmHg), at which application of an ignition source causes the vapors of a specimen to ignite under specified conditions of test. Flash point of the fuel is evaluated as per ASTM D93 test method. Flash point of biodiesel is higher than that of diesel (>130 ºC) which makes biodiesel safer than diesel in handling and storage point of view. A minimum flash point for biodiesel is specified in restricting the alcohol content. Flash point of biodiesel will reduce drastically if the alcohol used in production of biodiesel is not completely removed from it. Moreover, it reduces the combustion quality of fuel. Excess methanol in the fuel may also affect engine seals and elastomers and corrode metal components. Hence, alcohol content in biodiesel is given in biodiesel specification to a limit value of 0.24 mg/kg (Reo *et al*., 2010).

2.8.1.5 *Cloud point and Pour point*

Two important parameters for low temperature application of a fuel are cloud point (CP) and pour point (PP). The CP is temperature at which wax first become visible when fuel is cooled. The PP is the temperature at which the amount of wax out of solution is sufficient to gel the fuel, thus it is the lowest temperature at which the fuel can flow. Biodiesel has higher CP and PP compared to conventional diesel (Ayhan, 2006).

2.8.2 Chemical properties

2.8.2.1*Water and sediment*

This refers to free water droplets and sediment particles. The allowable level for biodiesel is set at the same level allowed for conventional diesel fuel. Poor drying techniques during manufacturing or contact with excessive water during transport or storage can cause biodiesel to be out of specification for water content. Excess water can lead to corrosion and provides an environment for microorganisms. Fuel oxidation can also raise sediment levels, so this test can be used in conjunction with acid number and viscosity to determine if fuels have oxidized too much during storage (Gerpen, 2005).

2.8.2.2*Sulfated ash test*

This test measures the amount of residual alkali catalyst in the biodiesel as well as any other ash-forming compounds that could contribute to injector deposits or fuel system fouling (Gerpen, 2005).

2.8.2.3*Sulfur*

This is limited to reduce sulfate and sulfuric acid pollutant emissions and to protect exhaust catalyst systems when they are deployed on diesel engines in the future. Sulfur content of 15 ppm or lower is also required for proper functioning of diesel particle filters. Biodiesel generally contains less than 15 ppm sulfur. The test for low-sulfur fuel (ASTM D5453) should be used for accurate results instead of D2622, which will provide falsely high results caused by the test's interference with the oxygen in the biodiesel (Biodiesel Handling and Use Guide, 2009).

2.8.2.4*Copper strip corrosion test*

This test is used to indicate potential difficulties with copper and bronze fuel system components. The requirements for biodiesel and conventional diesel are identical, and biodiesel meeting other D6751 specifications always passes this test. Copper and bronze may not corrode in the presence of biodiesel fuel, but prolonged contact with these catalysts can degrade the fuel and cause sediment to form (Biodiesel Handling and Use Guide, 2009).

2.8.2.5*Carbon residue*

This measures the carbon-depositing tendency of a fuel and is an approximation of the tendency for carbon deposits to form in an engine. For conventional diesel fuel, the carbon residue is measured on the 10% distillation residue. Because biodiesel boils entirely at the high end of the diesel fuel range and in a very narrow temperature range, it is difficult to leave only a 10% residual when distilling biodiesel. So, bio diesel carbon residue specifies

that the entire biodiesel sample be used rather than the 10% distilled residue (Biodiesel Handling and Use Guide, 2009).

2.8.2.6*Acid number*

The acid number for biodiesel is primarily an indicator of free fatty acids (natural degradation products of fats and oils) and can be elevated if a fuel is not properly manufactured or has undergone oxidative degradation. Acid numbers higher than 0.50 have been associated with fuel system deposits and reduced life of fuel pumps and filters (Biodiesel Handling and Use Guide, 2009).

2.8.2.7 *Free and total glycerin*

These numbers measure the amount of unconverted or partially converted fats and by-product glycerin in the fuel. Incomplete conversion of the fats and oils into biodiesel can lead to high total glycerin. Incomplete removal of glycerin can lead to high free glycerin and total glycerin. If these numbers are too high, the storage tank, fuel system, and engine can be contaminated. Fuels that exceed these limits are highly likely to plug filters and cause other problems. One of the major shortcomings of the D6584 gas chromatograph (GC) method is its sensitivity to diesel fuel. Diesel fuel components react differently on the column used in the GC—they make the determination of free glycerin very difficult and may damage the column. Thus, many labs are unable to determine free and total glycerin by this method in samples with even small amounts of diesel fuel, such as B99.9 (Biodiesel Handling and Use Guide, 2009).

2.8.2.8 *Phosphorus content*

This is limited to 10 ppm maximum in biodiesel because it can damage catalytic converters; phosphorus above 10 ppm can be present in some plant oils. Biodiesel produced in the United States generally has phosphorus levels of about 1 ppm (Biodiesel Handling and Use Guide, 2009).

2.8.2.9*T90 distillation specification*

This specification was incorporated to ensure that fuels have not been contaminated with high boiling materials such as used motor oil. Biodiesel exhibits a boiling point rather than a distillation curve. The fatty acids from which biodiesel are produced are mainly straight-chain HCs with 16 to 18 carbons that have similar boiling point temperatures. The atmospheric boiling point of biodiesel is generally 626º to 675ºF (330º to 357ºC).

2.8.2.10 *Oxidation stability*

Biodiesel can oxidize during storage and handling, leading to the formation of peroxides, acids, gums, and deposits. The minimum oxidation stability requirement is intended to ensure the storage stability of B100 and biodiesel blends (Biodiesel Handling and Use Guide, 2009).

2.8.2.11 *Cold soak filterability*

This is the newest requirement. It was added in 2008 in response to data indicating that some B100 could, in blends with petroleum diesel of up to 20%, form precipitates above the cloud point. B100 meeting the cold soak filterability requirements does not form these precipitates. This, along with cloud point, is needed to predict low-temperature operability (Biodiesel Handling and Use Guide, 2009).

2.8.2.12 *High levels of Group I and II metals*

Sodium (Na), potassium (K), calcium (Ca), and magnesium (Mg) can cause deposits to form, catalyze undesired side reactions, and poison emission control equipment (Biodiesel Handling and Use Guide, 2009).

2.8.3 Thermal properties

2.8.3.1*Calorific value*

Calorific value is an important property that defines the energy content in the biodiesel and hence thermal efficiency and specific fuel consumption.

2.8.3.2 *Heat of combustion*

Heat of combustion is determined according to ASTM D240, but it is not specified in ASTM D6741 or EN 14214. Heat of combustion is the thermal energy that is liberated upon combustion, so it is commonly referred to as energy content. Factors that influence the energy content of biodiesel include the oxygen content and carbon to hydrogen ratio. Generally, as the oxygen content of FAAE is increased, a corresponding reduction in energy content is observed.

2.8.4 Gas chromatography analysis (GC)

Gas chromatograph (GC) analysis is a technique which is used to determine the fatty acid composition of oils. It offers quantitative and qualitative analysis for carbon atoms/bonds in oil. It is an effective analytical instrument for detecting free fatty acid compositions in vegetable oils.

2.9 Biodiesel–Petrodiesel Blends and Its Effects

Biodiesel can be used as a blend component in petro diesel in any proportion because it is completely miscible with ultra-low sulfur diesel (ULSD). However, ASTM D975 and D7467 only allow up to 5 and 20 vol. % biodiesel, respectively. Biodiesel and petro diesel are not chemically similar: biodiesel is composed of long-chain FAAE, whereas petro diesel is a mixture of aliphatic and aromatic hydrocarbons that contain approximately 10 to 15 carbons. Because biodiesel and petro diesel have differing chemical compositions, they have differing fuel properties. Once mixed, the blend will exhibit properties different from neat biodiesel or petro diesel fuels. Specifically, the most important fuel properties influenced by blending of biodiesel with petro diesel are lubricity, exhaust emissions, CN, flash point, oxidative stability, low-temperature operability, kinematic viscosity, and energy content. Lubricity of petro diesel is positively impacted through blending with biodiesel. Specifically, B2 and B20 blends of SME (soybeans methyl esters) in ULSD (contains no lubricity enhancing additives) significantly improve lubricity (60°C according to ASTM D6079) from 551 to 212 and 171 μm, respectively.

Exhaust emissions of ULSD, with the exception of NOx, are reduced through blending with biodiesel. The CN of petro diesel is increased upon blending with biodiesel. For example, the CN of petro diesel, tall oil methyl esters, and the corresponding B50, B60, and B70 blends are 47, 54, 52, 52, and 53, respectively. The flash point of petro diesel is increased upon blending with biodiesel. The flash points of FAME are much higher than those of petro diesel and range from around 110 to 200°C versus 50 to 60°C for petro diesel. When blended with petro diesel, biodiesel does not impact flash point up to B20, but beyond B20, the flash point increases significantly. The oxidative stability of petro diesel is negatively impacted upon blending with biodiesel. This is because the hydrocarbon constituents of petro diesel are more stable to oxidation than FAME (especially in the case of unsaturated FAME). The amount of gravimetric solids formed (indicators of oxidative degradation) according to ASTM D5304 in the cases of petro diesel and the corresponding B10 and 20 blends (SME) were 0.6, 4.2, and 9.0 mg/100 ml, respectively. The low-temperature operability of petro diesel is negatively impacted once blended with biodiesel. For instance, the CFPP of petro diesel, tall oil methyl esters, and the corresponding B50, 60, and 70 blends were −8°C, −3°C, −7°C, −6°C, and −6°C, respectively. In another example, the PP of ULSD and B2, 5, 20, and 100 blends palm oil methyl ester (PME) were −21°C, −21°C, −18°C, −12°C, and 18°C, respectively.

The kinematic viscosity of petro diesel increases upon blending with biodiesel. For example, the kinematic viscosities (40°C) of ULSD and B1,2, 5, and 20 soybean methyl esters (SME)

blends are 2.32, 2.40, 2.48, 2.57, and2.71 mm2/s, respectively. In another example, the kinematic viscosities (40°C) of petro diesel and B50, 60, 70, and 100 (tall oil methyl esters) blends are 2.60, 4.50, 4.82, 5.12, and 7.10 mm2/s, respectively.

Lastly, the heat of combustion (energy content) of petro diesel is reduced upon blending with biodiesel. Specifically, the energy contents of petro diesel and B50, 60, 70, and 100 (tall oil methyl esters) blends are 43.760, 41.901, 41.511, 41.145, and 40.023 kJ/kg respectively. In another example, the energy contents of petro diesel and B2, 5, 10, 20, and 100 (SME) blends are 46.65, 46.01, 45.46, 44.48, 43.75, and 39.09 MJ/kg, respectively (Moser, 2009).

2.10 Economic Benefit of Biodiesel over Conventional Fuel

2.10.1 Use of biodiesel provides a high energy return and displaces petroleum- derived diesel fuel.

Life-cycle analyses show that biodiesel contains 2.5 to 3.5 units of energy for every unit of fossil energy input in its production. This is because very little petroleum is used in its production. Biodiesel usage displaces petroleum at nearly a 1-to-1 ratio on a life-cycle basis. This value of energy of biodiesel over fossil fuel used in its production includes energy used in diesel farm equipment and transportation equipment (trucks, locomotives); fossil fuels used to produce fertilizers, pesticides, steam, and electricity; and methanol used in the manufacturing process. Because biodiesel is an energy-efficient fuel, it can substitute petroleum supplies (Biodiesel Handling and Use Guide, 2008).

2.10.2Biodiesel reduces greenhouse gas emissions

The use of biodiesel can significantly reducethe greenhouse effect caused by emissions from use of petroleum based diesel. By one estimate, GHG emissions (including carbon dioxide [CO_2], methane, and nitrogen oxide (NOx) are reduced by 41%, if biodiesel is produced from crops harvested from fields that were already in production. When plants such as soybeans grow, they take CO_2 from the air to make the stems, roots, leaves, and seeds (soybeans). After the oil is extracted from the soybeans, it is converted into biodiesel. When the biodiesel is burned, CO_2 and other emissions are released and return to the atmosphere. This cycle does not add to the net CO_2 concentration in the air because the next soybean crop will reuse the CO_2 as it grows. When fossil fuels such as coal or diesel fuel are burned, however, 100% of the CO_2 released adds to the CO_2 concentration levels in the air (Biodiesel Handling and Use Guide, 2008).

2.10.3Biodiesel reduces tailpipe emissions

Biodiesel reduces tailpipe particulate matter (PM), hydrocarbon (HC), and carbon monoxide (CO) emissions from most modern four-stroke CI or diesel engines. These benefits occur because biodiesel contains 11% oxygen by weight. The fuel oxygen allows the fuel to burn more completely, so fewer unburned fuel emissions result. This same phenomenon reduces air toxics, which are associated with the unburned or partially burned HC and PM emissions. Testing has shown that PM, HC, and CO reductions are independent of the biodiesel feedstock. The EPA reviewed 80 biodiesel emission tests on CI engines and has concluded that the benefits are real and predictable over a wide range of biodiesel blends. EPA's review also indicated that B20 increased NOx by about 2% relative to petroleum diesel use. A more detailed analysis of the database examined by EPA, plus more recently published results, confirms the positive impact of B20 on emissions of HC, CO, and PM.

However, examination of the NOx results shows that the effect of biodiesel can vary with engine design, calibration, and test cycle. At this time, the data are insufficient for users to conclude anything about the average effect of B20 on NOx, other than that it is likely very close to zero. In contrast, when biodiesel is used in boilers or home heating oil applications, NOx tends to decrease because the combustion process is different (open flame for boilers, enclosed cylinder with high-pressure spray combustion for engines). The NOx reduction seen with biodiesel blends used in boilers appears to be independent of the type of biodiesel used. In blends with heating oil up to 20% biodiesel, NOx is reduced linearly with increasing biodiesel content. For every 1% biodiesel added, NOx decreases by 1%. B20 heating oil fuel will reduce NOx by about 20%.

Sulfur dioxide (SO_2) emissions were also reduced when the two fuels were blended, because biodiesel contains much less sulfur than typical heating oil does. A 20% blend of biodiesel in heating oil will reduce SO_2 by about 20% (Biodiesel Handling and Use Guide, 2008).

2.10.4 Biodiesel and human health

Biodiesel is non toxic, biodegradable and suitable for sensitive environment. Some PM and HC emissions from diesel fuel combustion are toxic or carcinogenic. Using B100 can eliminate as much as 90% of these air toxics. B20 reduces air toxics by 20% to 40%. The positive effects of biodiesel on air toxics have been shown in numerous studies.

Recently, the U.S. Department of Labor Mining Safety Health Administration (MSHA) has implemented rules for underground mines that limit workers' exposure to diesel PM. MSHA found that switching from petroleum diesel fuels to high blend levels of biodiesel (B50 to

B100) significantly reduced PM emissions from underground diesel vehicles and substantially reduced workers' exposure. However, even low concentrations of biodiesel reduce PM emissions and provide significant health and compliance benefits wherever humans receive higher levels of exposure to diesel exhaust (Biodiesel Handling and Use Guide, 2008).

2.10.5 Biodiesel improves engine operation

Even in very low concentrations, biodiesel improves fuel lubricity and raises the cetane number of the fuel. Diesel engines depend on the lubricity of the fuel to keep moving parts, especially fuel pumps, from wearing prematurely. One unintended side effect of the federal regulations, which have gradually reduced allowable fuel sulfur to only 15 ppm and lowered aromatics content, has been to reduce the lubricity of petroleum diesel. The hydro treating processes used to reduce fuel sulfur and aromatics contents also reduces polar impurities such as nitrogen compounds, which provide lubricity. To address this, the ASTM D975 diesel fuel specification was modified to add a lubricity requirement (a maximum wear scar diameter on the high-frequency reciprocating rig [HFRR] test of 520 microns). Biodiesel can impart adequate lubricity to diesel fuels at blend levels as low as 1% (Biodiesel Handling and Use Guide, 2008).

2.10.6 Biodiesel is easy to use

Finally, one of the biggest benefits to using biodiesel is that it is easy to produce and use. Blends of B20 or lower are literally a "drop in" technology. No new equipment and no equipment modifications are necessary. B20 can be stored in diessel fuel tanks and pumped with diesel equipment. B20 does present a few unique handling and use precautions, but most users can expect a trouble-free B20 experience (Biodiesel Handling and Use Guide, 2008).

2.11 Clay

Clay is a type of soil which is naturally available in most of the states in Nigeria. Clays are essentially alumina silicates which have resulted from weathering of rocks and aluminum silicates (Igbokwe & Ogbuagu, 2003). Clays have adsorptive and catalytic capacities. They can be used as catalysts for transesterification reaction. Some researchers worldwide have investigated clay catalysts for esterification and transesterification but very few for biodiesel production (Manuit & Statit, 2007). Prakash *et al*. (2005) reported transesterifcation of dicarboxylic acid with various alcohols by Mn+-montmorillonite clay

catalysts and then, his group Vijayakumar *et al*. (2005) had continuously used Indian bentonite as esterification catalyst for ester synthesis.Duboius *et al*. (2006) had prepared biodegradable polyester by transesterification catalysts to improve clay exfoliation. Liu *et al*. (2004) produced ethyl/methyl β -ketoester bymontmorillonite K-10 as an efficient reusable catalyst. Manuit and Statit, (2007) studied biodiesel synthesis from transesterification by clay-based catalyst. They discovered that biodiesels from clay–based catalysts have some encouraging properties to supersede low speed diesel fuel and to lower the cost of production in some extent.Calgaroto et al. (2013)studied production of biodiesel from soybean and *Jatropha curcas* oils with KSF and amberlyst 15 catalysts in the presence of co-solvents.

2.11.1 Classification of clay

There are different types of clay. They are illite; glauconite; chlorite; kaolinite; vermiculite; smectite; sepiolite; palygorskite and halloysite (Brigatti *et al.*, 2006; Obaje *et al.*, 2013). As a whole, clay consists of a layer of silicates and alumina that joins and links each other (Brigatti *et al.*, 2006). The types of bond determine the characteristics of clay in binding the colloids in water treatment processes.

To have a clear view of the type of clay minerals, they are grouped into the followings:

2.11.1.1*Kaolinite group*

Include kaolinite; dickite; nacrite and halloysite. The chief member of this group is kaolinite which has the composition $(OH)_3Al_4Si_4O_{10}$. They are formed by the decomposition of orthoclase feldspar as in granite. Kaoline is the principal constituent in china clay. It absorbs toxins and materials and acts as bulky agent.They include hydrous micas; phengite; brammalite and glauconite (Brigatti *et al.*, 2006).

2.11.1.2 *Illite group*

They include hydrous micas; phengnite; bramalite and glauconite. They are formed by the decomposition of some micas and feldspar. They are predominant in marine clays and shales (Brigatti *et al.*, 2006; Obaje *et al.*, 2013).

2.11.1.3 *Montmorillonite/Smectite group*

They include montmorillonite; bentonite; nontronite; hectorite; saponite and sauconite. This group takes its name from the mineral montmorillonite with the composition

$(OH)_4Al_4Si_3O_{20}.XH_2O$. Magnesium is practically always present although it is not usually written in the formula. Beidellite which has a SiO_2 to Al_2O_3 molecular ratio of 3 and nontronite, in which aluminum has been replaced by ferric iron are reputedly members of the montmorillonite group. Saponite in which the aluminum has been replaced by magnesium can be classed as a montmorillonite (Brigatti *et al.*, 2006).

2.11.1.4 *Vermiculite group*

They are generally regarded as weathering products of micas. It is hydrated and sometimes expansible (Obaje *et al.*, 2013).

2.11.2 Locations of clay in Nigeria

Clay has a wide spread occurrence in the world. In Nigeria, clay is widely distributed though not always found in sufficient quantity or suitable quality for modern industrial purposes. It occurs both as residual and sedimentary clay (Akhirevbulu & Ogunbajo, 2011). More than 80 clay deposits have been reported from all parts of the country. Clay deposits occur in Abak, Akwa Ibom State, Uruove near Ughelli in Delta State, Ifon in Ondo State, Mokola in Oyo State, Sokoto in Sokoto State, Gombe in Gombe State, Dangara in Niger State, Umuahia in Abia State, Onitsha in Anambra State e.t.c (Akhirevbulu & Ogunbajo, 2011). Almost every State in Nigeria has at least one known deposit of kaolin. In Anambra State there is the Ozubulu deposit, Darazo kaolin deposit in Bauchi, Akpene-Obom deposit in Cross River State, Kankara in Kaduna State e.t.c. The three most extensively studied deposits are the Ozubulu kaolin deposits, Kankara deposits and the Major Porter deposits, in Plateau State (Akhirevbulu & Ogunbajo, 2011).

2.11.3 Properties of clay

2.11.3.1 *Physical properties of clay*

The clay minerals are probably monoclinic in form, though an orthorhombic form has been suggested for some of them, and have as their prime characteristic a pronounced basal cleavage. Kaolinite has a hardness of 2.5 and a density of 2.58-2.59 g/cm^3. The hardness and density of the other clay minerals have not been determined precisely. Kaolinite and the halloysite minerals are white; the other clay minerals vary from white to yellow or green (Brigatti *et al.*, 2006).

2.11.3.2*Optical properties of clay*

The optical properties of the clay minerals showed that clay minerals commonly occur in particles too small for optical study. The individuals can, however, be aggregated together uniformly and fairly precise measurements can be obtained from the aggregates. Many scientists have shown that the indices of refraction of some clay minerals vary for different immersion liquids. The variation is greatest for minerals of high base-exchange capacity.

The indices of refraction of some clay minerals vary when they are heated to relatively low temperatures (200°C). Kaolinite seems to be less affected than the other clay minerals (Brigatti *et al.*, 2006).

2.11.3.3*Chemical properties of clay*

The kaolinite and halloysite minerals do not contain alkalies or alkali earths and no definite examples of iron replacing aluminum have been found. In the kaolinite minerals the molecular silica to alumina ratio varies, and there seems also to be a variation in the water content. The composition of members of the illite and montmorillonite groups varies between wide limits because of replacement of aluminum by ferric iron, a variable molecular silica to R_2O_3 ratio, and the presence of variable amounts of alkalies and alkali earths (Brigatti *et al.*, 2006).

Allophane may vary within wide limits. Little is known of the precise composition of the magnesium clay minerals, but considerable variability will no doubt be found. The general similarity of the chemical makeup of all clay minerals and the variability of the composition of individuals cause it to be difficult or impossible to interpret the mineral composition of a clay from its chemical composition alone.

2.11.3.4 *Dehydrating properties of clay*

Recent researches indicate that there is appreciable variation in dehydration properties depending on particle size, this means that dehydration characteristics must be used with considerable caution in the mineralogical analyses of clays. The hydration characteristics of montmorillonite at low temperatures have indicated that water is lost in units providing a step-like curve. The hydration characteristics in this temperature range vary with the character of the exchangeable cation.

Montmorillonite is reported as rehydrating after heating to 550°C, kaolinite after heating to 500°C. Few precise data are available on this point although the property is important in determining certain commercial utilizations of clays (Brigatti *et al.*, 2006).

2.11.4 Uses of clay

Clay has been of great importance to man since ancient times. Its use mainly depends on what the user has in mind. Due to its properties and composition, clay has been used under the followings (Obaje *et al.*, 2013):

2.11.4.1*Building materials*

From the beginning of time clay was used for making blocks and building houses in the form of cement paste (clay cement).

2.11.4.2*Drilling mud*

Bentonite and other clays have been used in the drilling of water and oil wells as drilling mud. The clays are turned into mud which seals the walls of the borehole, lubricates the drill head and removes drill cuttings

2.11.4.3*Contaminant removal*

Clay slurries have been used effectively to remove a range of contaminants including lead and heavy metals and overall water clarification.

2.11.4.4 *Adsorption*

Clays are used to decolourise, filter and purify animal, mineral and vegetable oils and greases due to their high adsorbing properties.

2.11.4.5 *Environmental sealants*

Bentonite is used to establish low permeability liners in landfills, sewage, lagoons, water retention ponds, golf course, ponds and hazardous waste sites.

2.11.4.6 *Pharmaceuticals/Cosmetics*

Bentonite is used as a binder in tablet manufacturing and diarrhea medications. Clays are used as thickeners in a wide variety of cosmetics including facial creams, shampoos etc.

2.11.4.7*Peletizing*

Bentonite is used to bind tiny particles of iron ores which are then formed into pellets for use as feed materials for blast furnaces.

2.11.4.8 *Paints*

Finely ground clays are used in the paint industry to disperse pigments evenly throughout the paint. Without clays, it would be extremely difficult to evenly mix the paint base and colour pigment.

2.11.5 Characterization of clay

Peculiar characteristics of clays which include thioxotropic, swelling and adsorption properties have accounted for their demands for various industrial uses. These properties have been attributed to the type of clay minerals, the nature of exchangeable cations present and its cation-exchange capacity (Obaje *et al.,* 2013). Clay comprises of mineral groups which contain certain hydrous aluminum, magnesium and iron silicates in addition to sodium, potassium, calcium and magnesium ions etc. The applicability and acceptability of clay is however dependent on an appreciable knowledge of its mineral contents and chemical composition (Galan *et al*., 2005). In most countries of the world like Nigeria, non-black fillers which include clays are largely imported whereas clay deposits abound but there is paucity of information about their potentials. The method being employed to characterize clays include: the chemical analysis, XRF, Fourier Transform Infra Red (FTIR), Scanning Electron Microscope (SEM) and High Resolution Transmission Electron Microscope (HRTEM). A combination of different methods is needed for sufficient characterization of the material obtained.

2.11.5.1 *Characterization techniques*

In this study, various characterization techniques were used to analyze the properties of the clay samples. In this section, a brief overview of the characterization techniques is described.

a.*Atomic absorption spectroscopy (AAS)*

Atomic absorption spectrometry (AAS) is an analytical technique that measures the concentrations of elements. Atomic absorption is so sensitive that it can measure down to parts per billion of a gram (µg dm^{-3}) in a sample. The technique makes use of the wavelengths of light specifically absorbed by an element. They correspond to the energies needed to promote electrons from one energy level to another, higher, energy level. Atomic absorption spectrometry has many uses in different areas of chemistry (American Public Health Association, 2005).

i. *Clinical analysis*: - Analyzing metals in biological fluids such as blood and urine.

Environmental analysis - Monitoring our environment – eg finding out the levels of various elements in rivers, seawater, drinking water, air, petrol and drinks such as wine, beer and fruit drinks.

ii. *Pharmaceuticals*:- In some pharmaceutical manufacturing processes, minute quantities of a catalyst used in the process (usually a metal) are sometimes present in the final product. By using AAS the amount of catalyst present can be determined (American Public Health Association, 2005).

iii. *Industry*: - Many raw materials are examined and AAS is widely used to check that the major elements are present and that toxic impurities are lower than specified – eg in concrete, where calcium is a major constituent, the lead level should be low because it is toxic.

iv. *Mining* : - By using AAS the amount of metals such as gold in rocks can be determined to see whether it is worth mining the rocks to extract the gold.

b.*Fourier transforms infrared spectroscopy*

The region of the infrared spectrum which is of great interest to most of the chemists is the wavelength range 2.5 to 15 µm. In practice, units proportional to frequency, (wave number in units of cm^{-1}) rather than wavelength are commonly used and the region 2 – 15 µm corresponds to approximately 4000 to 400 cm^{-1}. The atoms in a molecule are constantly oscillating around average positions. Bond lengths and bond angles are continuously changing due to this vibration. A molecule absorbs infrared radiation when the vibration of the atoms in the molecule produces an oscillating electric field with the same frequency as the frequency of incident infrared radiation when they are in resonance. Each molecule has its own characteristic spectrum. The bands that appear depend on the types of bonds and the

structure of the molecule (Madejova, 2003). Fourier transform infrared (FTIR) spectroscopy measures dominant vibrations of functional groups and highly polar bonds. Thus, these chemical fingerprints are made up of the vibration features of all the samples components. FTIR spectrometer records the interaction of IR radiation with experimental samples, measuring the frequencies at which the sample absorbs the radiation and the intensities of the absorptions. Determining these frequencies allows identification of the sample's chemical makeup, since chemical functional groups are known to absorb light at specific frequencies (Madejova, 2003). FTIR experiments generally can be classified into the following two categories: (a) Qualitative analysis, where the aim is to identify the sample and (b) Quantitative analysis, where the intensity of absorptions is related to the concentration of the component.

c.*Scanning electron microscopy (SEM)*

Scanning electron microscopy (SEM) is a type of microscope that uses electrons rather than light to form an image. There are many advantages in using the SEM instead of light microscope. The SEM has a large depth of field, which allows a large amount of the sample to be in focus at one time (Willis *et al.*, 2002). . The SEM also produces images of high resolution, which means that small spaced features can be examined at a high magnification. Preparation of the samples is relatively easy since most SEM instruments only require the sample to be conductive. The combination of higher magnification, larger depth of focus, greater resolution, and ease of sample observation makes the SEM one of the most heavily used instruments in present-day research. By using the wave-particle duality, SEM creates the magnified images by using electrons instead of light waves. The SEM shows very detailed 3-dimensional images at much higher magnifications than is possible with a light microscope. The images created without light waves are rendered black and white. By the nature of electron beam, the vacuum is required during the operation, therefore the sample has to be prepared carefully to withstand the vacuum inside the microscope. The samples must be conductive materials in order to be able to interact with electron; SEM samples are coated with a very thin layer of gold by a machine called a sputter coater. The sample is placed inside the microscope's vacuum column through an air-tight door. After the air pumped out of the column, an electron gun emits a beam of high energy electrons. This beam travels downward through a series of magnetic lenses designed to focus the electrons to a very fine spot. Near the bottom, a set of scanning coils moves the focused beam back and forth across the specimen, row by row. As the electrons beam hits each spot on the sample, secondary electrons and back scattered electrons are knocked loose from its surface. A detector counts

these electrons and sends the signals to an amplifier. The final image is built up from the number of electrons emitted from each spot on the sample. By this way the morphology of the sample can be seen directly from the micrograph (Willis *et al.*, 2002).

2.12 African Pear (*Dacryodes edulis*)

The African pear, African plum or Safou (French), ube (Igbo), elemi (Yoruba), eben (Efik) and orumu (Benin) belongs to the family of Burseraceae and botanically known as *Dacryodes edulis*. It is an indigenous fruit tree they are found in Cabinda, Cameroon, Congo (Brazzaville and Kinshasa), Gabon, Ghana, Equatorial Guinea, Nigeria and Sao Tome. It is grown in the humid low lands. In south-eastern Nigeria, the trees are grown around homesteads and flowering takes place from January to April. The major fruiting season is between May and October. It is an annual fruit of about 3 cm in diameter and contains a leathery shelled stone surrounded by a pulpy pericarp of about 5 mm thick. The pericarp is butyraceous, i.e., it has the qualities of butter. It is this portion of the pear which is eaten, either raw or cooked that forms a sort of 'butter'. Besides, as a percentage of dry matter, the pulp contains 31.9% oil, 25.9% proteins and 17.9% fiber. They could be an important source of pulp oil, seed oil and even whole fruit oil. The seeds are not economically useful and are often discarded as a waste into the environment. A plantation can produce 7-8 tonnes of oil per hectare. This makes it useful as feedstock for biodiesel production (Awono *et al.*, 2002).

2.13 Gmelina

Gmelina arborea Roxb, known as Gomari in Assamese, is a big forest tree popular for its wood used for making furnitures and as building materials. *Gmelina arborea* is a fast growing tree, which grows on different localities and prefers moist fertile valleys with 750-5000 mm rainfall. The *Gmelina arborea* tree attains moderate to large height up to 40 m and 140 cm in diameter (Okoroigwe et al., 2012). It is occurring naturally throughout greater part of India at altitudes up to1500m. It also occurs naturally in Myanmar, Thailand, Laos, Cambodia, Vietnam, and in southern provinces of China, and has been planted extensively in Sierra Leone, Nigeria and Malaysia (Choudhury, 2012).

`

2.14 Kinetic Study of Transesterification

The goal of kinetic experiments is to measure the concentration of a species at a particular time during a reaction so that a rate law can be determined. Chemical kinetics is the study of the rates and rate parameters of chemical reactions. Such reaction rates range from the almost

instantaneous, as in an explosion, to the almost unnoticeably slow, as in corrosion. The aim of chemical kinetics is to make predictions about the composition of reaction mixtures as a function of time, to understand the processes that occur during a reaction, and to identify what controls its rate. A fundamental challenge in chemical kinetics is the determination of the reaction order (or, in general, the rate law) from experimental information. It is known that the rate law is closely related to the reaction mechanism, and the knowledge of the mechanism of a given reaction allows the control of the reaction. The rate of a chemical reaction is defined as the rate of change of the concentration of one of its components, either a reactant or a product. The experimental investigation of reaction rates, therefore, depends on being able to monitor the change of concentration with time. Classical procedures for reactions that take place in hours or minutes make use of a variety of techniques for determining concentration, such as spectroscopy and electro-chemistry. Very fast reactions are studied spectroscopically. Spectroscopic procedures are available for monitoring reactions that are initiated by a rapid pulse of electromagnetic radiation and are over in a few femtoseconds (1 fs = 10−15 s). The analysis of kinetic data commonly proceeds by establishing a rate law, a mathematical expression for the rate in terms of the concentrations of the reactants (and sometimes products) at each stage of the reaction. For instance, it may be found that the rate of consumption of a reactant is proportional to the concentration of the reactant, in which case the rate law is Rate = k [Reactant] where [Reactant] denotes the concentration of the reactant and k is called the rate constant. The rate constant is independent of the concentrations of any species in the reaction mixture but depends on the temperature. A reaction with a rate law of this form is classified as a first-order rate law. More generally, a reaction with a rate law of the form Rate = k[Reactant A]^a[Reactant B]^{b}is said to be of order a in A, of order b in B, and to have an overall order of a + b + …. Some rate laws are far more complex than these two simple examples and many involve the concentrations of the products. The advantage of identifying the reaction order is that all reactions with the same rate law (but different characteristic rate constants) behave similarly. The identification of a rate law provides valuable insight into the reaction mechanism, the sequence of elementary steps by which a reaction takes place. The aim is to identify the reaction mechanism by constructing the rate law that it implies. This procedure may be simplified by identifying the rate-determining step of a reaction, the slowest step in a sequence that determines the overall rate. In general, for a mechanism of many steps (including their reverse), the construction of the overall rate law is quite difficult, requiring an approximation or a computer for a numerical analysis. A hazard of using kinetic information to identify a reaction mechanism,

however, is that more than one mechanism might result in the same rate law, especially when approximate solutions are derived. For this reason, a proposed reaction mechanism must be supported by additional evidence. Once a reaction mechanism has been identified, attention turns to the molecular properties that govern the values of the rate constants that occur in the individual elementary steps. A clue to the factors involved is provided by the experimental observation that the rate constants of many reactions depend on temperature according to the Arrhenius expression where *E*a is called the activation energy. The simplest model that accounts for the Arrhenius expression is the collision theory of gas-phase reaction rates, in which it is supposed that reaction occurs when two reactant molecules collide with at least a minimum kinetic energy (which is identified with the activation energy). A more sophisticated theory is the activated complex theory (also known as the transition state theory), in which it is supposed that the reactants encounter each other, form a loosened cluster of atoms, then decompose into products. Reactions in solution require more detailed consideration than reactions in gases. The rate of a reaction may also be increased by using a catalyst (a substance that takes part in a reaction by providing an alternative pathway with lower activation energy but is regenerated in the process and is therefore not consumed). Catalysis is the foundation of the chemical industry and a great effort is made to discover or fabricate efficient and economical catalysts for the production of biodiesel lately. It is also necessary to optimize all the parameters involved in the production of biodiesel to reduce cost and maximize profit.

There are several studies on kinetic modeling of transesterification using homogeneous catalysts and most of them have suggested that the reaction is second-order kinetics at the initial stages (Noureddini & Zhu, 1997; Vicente *et al.*, 2005; Karmee *et al.*,2006) and followed by first-order or zero-order kinetics as the reaction proceeds (Darnoko & Cheryan, 2000). However, there is less studies on kinetic modeling using heterogeneous catalysts. One of the literatures was Hattori *et al.* (2000) who proposed a five-step mechanism for transesterification of ethyl acetate using heterogeneous alkaline earth metal oxides by considering the rate-determining steps based on the basicity of the catalyst.

On the other hand, Dossin *et al.*(2006) studied the simulation of heterogeneously MgO-catalzed transesterification by comparing with three different models. The Langmuir-Hinshelwood-Hougen-Watson (LHHW), Eley-Rideal and the previous model proposed by Hattori *et al.* (2000). Dossin *et al.* (2006) proposed a kinetic model based on a three-step

mechanism of Eley-Rideal and suggested that the rate-determining step for the MgO is methanol adsorption on its active sites.

Lopez *et al.* (2005) studied kinetics of heterogenous catalyst and stated that the rate-determining step is either methanol adsorption on its active sites, or the reaction at the catalyst surface which is similar in both heterogeneous and homogeneous base-catalyzed transesterification.

In chemical reaction, a power law model is the most popular model. However, rate laws in heterogeneous catalysis rarely follow power law models and hence are inherently more difficult to formulate from the data (Fogler, 2011). In order to develop an in-depth understanding and in sight as to how the rate laws are formed from heterogeneous catalytic data, catalytic mechanisms and derive rate laws for the various mechanisms was postulated. The mechanisms will typically have an adsorption step, a surface reaction step, and a desorption step, one of which is usually a rate-determining step. Knowing the different forms that catalytic rate equations can take, it will be easier to view the trends in the data and deduce the appropriate rate law. After knowing the form of the rate law, one can then numerically evaluate the rate law parameters and postulate a reaction mechanism and rate determining step that is consistent with the rate data.

2.15 Engine Performance

2.15.1. Effect of biodiesel on engine power/torque

The effect of biodiesel on engine power and/or torque was investigated. It is shownthat 70.4% of authors agreed that, with biodiesel (especially with pure biodiesel), engine power will drop due to the loss of heating value of biodiesel (Aydin & Bayindir, 2010). However, the results reported show some fluctuation. Some authors (Aydin & Bayindir, 2010; Karabektas, 2009; Utlu & Kocak, 2008) found that the power loss was lower than expected (the loss of heating value of biodiesel compared to diesel) because of power recovery. Utlu and Kocak (2008)found that the respective average decrease of torque and power values of WFOME (waste frying oil methyl ester) was 4.3% and 4.5% due to higher viscosity and density and lower heating value (8.8%). Hansen et al., (2006)observed that the brake torque loss was 9.1% for B100 biodiesel relative to D2 diesel at 1900rpm as the results of variation in heating value (13.3%), density and viscosity. And Murillo et al. (2007)found that the loss of power was 7.14% for biodiesel compared to diesel on a 3-cylinder, naturally aspirated

(NA), submarine diesel engine at full load, but the loss of heating value of biodiesel was about 13.5% compared to diesel.

Of course, it was reported that there were surprising increases in power or torque of engine for pure biodiesel (Al-Widyam et al., 2002). Songand Zhang (2008)observed that the engine brake power and torque increased with the increase in biodiesel percentage in the blends. And they contributed to the higher oxygen content, the higher biodiesel consumption, an advance of injection timing and a shorter ignition delay time. But it is the most unbelievable that the increased power of the pure biodiesel could reach 70% relative to diesel fuel.

2.15.2. Factors of effect on biodiesel engine power

2.15.2.1. Content of biodiesel

Content of biodiesel blended with diesel results in the difference in engine power performance, which has become the common sense. Engine power will decrease with the increase of content of biodiesel (Aydin & Bayindir, 2010; Karabektas, 2009; Hansen et al., 2006). For example, Carraretto et al. (2004)found that the increase of biodiesel percentage in the blends resulted in a slight decrease of both power and torque over the entire speed range for different blends (B20, B30, B50, B70, B80, B100) of biodiesel and diesel on a 6-cylinder DI diesel engine. Aydin & Bayindir(2010)reported that the torque was decreased with the increase in CSOME (cottonseed oil methyl ester) in the blends (B5 B20 B50 B75 B100) due to higher viscosity and lower heating value of CSOME. And Murillo et al. (2007)observed that increasing the amount of biodiesel in the fuel decreased engine power on a single-cylinder, 4-stroke, DI and NA diesel engine.

Some authors (Gumus & Kasifoglu, 2010; Al-Widyam et al., 2002; Usta et al., 2005)found that the use of biodiesel blends did not meet this trend. For instance, Gumus and Kasifoglu (2010)found the power increased with the addition of biodiesel content in the blends until the B20 blend and reached a maximum value, when the biodiesel content continued to increase in the blends, the power would decrease below that of the diesel fuel and reached minimum value for B100, which was obtained on a single cylinder, 4-stroke, DI, air-cooled (AC) diesel engine. Likewise, Usta et al. (2007)showed that the power initially increased with the addition of biodiesel, reached a maximum value, and then decreased with further increase of the biodiesel content.

Of course, a small number of authors thought that the power between biodiesel blends appeared similar. Pal et al. (2010)foundthe variation of brake power was almost negligible for

all types of Thumba oil biodiesel blends (B10, B20, B30) within a whole enginespeed range on a 4-cylinder, DI, water-cooled (WC) diesel engine. Lapuerta et al. (2008)obtained that there were very small variations in effective torque among waste cooking oil methyl ester and ethyl ester (WCOM and WCOE) and their blends (WCOM30, WCOM70, WCOE30, WCOE70) on a 4-cylinder, 4-stroke, turbocharged (TU), intercooled, DI, 2.2 L Nissan diesel engine. Also, the similar results were obtained by Ghobadian et al. (2009)who tested the waste cooking biodiesel blends (B10, B20, B30, B40, B50) at full load on a 2-cylinder, 4-stroke diesel engine.

2.15.2.2. Properties of biodiesel and its feedstock

Properties of biodiesel, especially in heating value, viscosity and lubricity, have an important effect on engine power.Heating value of fuels is an important measure of its releasing energy for producing work. So, the lower heating value of biodiesel is attributed to the decrease in engine power, which is commonly agreed by the authors who reported that engine power reduced with biodiesel. Higher viscosity of biodiesel, which enhances fuel spray penetration, and thus improves air–fuel mixing, is used to explain the recovery in torque and power for biodiesel related to diesel in some literatures (Oner & Altum, 2009; Monyem et al., 2001). However, a few authors (Aydin & Bayindir, 2010; Utlu & Kocak, 2008)thought that the higher viscosity results in the power losses, because the higher viscosity decreases combustion efficiency due to bad fuel injection atomization.High lubricity of biodiesel might result in the reduced friction loss and thus improve the brake effective power. Ramadhas et al.(2005)used this argument to explain the recovery in the rated power, although they did not explain how this improvement occurred.

There may be no significant effect of biodiesel feedstock on engine power. Lin et al. (2009)mentioned above, found that the maximum and minimum differences in engine power and torque at full load between the PD and VOMEs were only 1.49% and −0.64%, 1.39% and −1.25%, respectively, which indicates that using VOME yields the same engine power as PD at full load conditions as well as at average load conditions for various engine speeds. Additionally, Ozsezen et al. (2009) who compared waste palm oil and canola oil methyl esters (WPOME and COME) with diesel on a WC, NA, DI diesel engine at 1500rpm under full load, and O˘guz et al. (2007) who compared biodiesel from soybean, rapeseed and palm on a 3- cylinder, 4-stroke, 30kW diesel engine, all found that there were no significant differences in power.

2.15.2.3. Engine type and its operating conditions

Factors on engine type and its operating conditions, such as engine load, engine speed, injection timing and injection pressure, etc., have been studied to illustrate their effects on biodiesel engine power. Karabektas (2009)compared the naturally aspirated (NA) conditions to the TU conditions on a 4-stroke, DI diesel engine and found that the mean increase in torque for biodiesel with the TU conditions was determined as 18.7% with regard to the NA conditions.

Has¸ imo˘glua et al. (2008)observed that the engine power and torque were increased by the application of the low heat rejection (LHR) engine, mainly due to the increased exhaust gas temperatures before the turbine inlet in LHR engine. Similarly, the comparison of power between the coated engine (CE) and uncoated engine (UE) was conducted by Hazar (2009). The author reported that the increase values in power for the CE are 3.5% and 1.6% for pure biodiesel and its blend, respectively.

Although the basic trends of engine power performance with load or speed were similar for biodiesel engine and diesel engine,there existed offset of maximum value of torque and power for biodiesel compared to diesel (Rahema & Phadatau, 2004; Aydin & Bayindir, 2010).

2.15.2.4. Additives.

A few authors investigated the effect of additives on the power performance of biodiesel. Although Keskin et al. (2008)found no significant effect of Mo and Mg as the additives into B60 biodiesel blend on engine torque and power tested on a single cylinder, 4-stroke, AC, DI diesel engine, Guru et al. (2010)obtained the positive effect of a blend of 10% chicken fat biodiesel and diesel fuel with an additive 12mol Mg, which improved the performance of biodiesel in flash point, viscosity and pour point. And Kalam and Masjuki (2008)found that B20X with 1% 4-nonyl phenoxy acetic acid (NPAA) additive produced higher brake power over the entire speed range in comparison to B20 and B0 (diesel), and the maximum brake power obtained at 2500rpm is 12.28kW from B20X followed by 11.93kW (B0) and 11.8kW (B20). They contributed to the increase of fuel conversion efficiency by improving fuel ignition and combustion quality due to the effect of fuel additive in B20 blend.

2.15.3 Brake power

The brake power of an engine is the useful power available at the crank shaft and it is called brake power. It is less than indicated power and denoted by B.P.

2.15.4 Brake thermal efficiency

This is a property that determines how efficiently the fuel is being used in the engine. This efficiency shows the portion of the energy consumed by the engine that is converted into useful work.

2.15.5 Brake specific fuel consumption

This is the mass of fuel required to develop 1kW brake power for a period of one hour. It is inversely proportional to brake thermal efficiency.

2.15.6 Volumetric efficiency

Volumetric efficiency in the internal combustion engine design refers to the efficiency with which the engine can move the charge into and out of the cylinders. It is a ratio of the quantity of air that is trapped by the cylinder during induction over the swept volume of the cylinder under state conditions.

2.15.7 Air-fuel ratio

This is the mass ratio of air to fuel present in an internal combustion engine. It is an important measure for anti-pollution and performance turning reasons. The lower the AFR, the “richer” the flame.

2.16 Neural Network

Neural networks or simply neural nets are computing systems which can be trained to learn a complex relationship between two or more variables or data sets. Basically, they are parallel computing systems composed of interconnecting simple processing nodes (Lau, 1991). Neural networks utilize a matrix programming environment making most nets mathematically challenging. The neuron model and the architecture of a neural network describe how a network transforms its input to output. This transformation can be viewed as a computation. Each model and architecture generate limitations on what a particular neural

net can compute. The way a network computes its output, is in such a way that the products of neurons' output and weight are summed with the neurons' bias and passed through the transfer function to get the neuron's output. Neurons may be simulated with or without biases.Artificial neural networks make use of artificial neurons. Artificial neural networks (ANNs) simulate the manner of operation of natural neurons in the human body. The basic unit of operation of an ANN is the neuron shown in Figure 2.12.

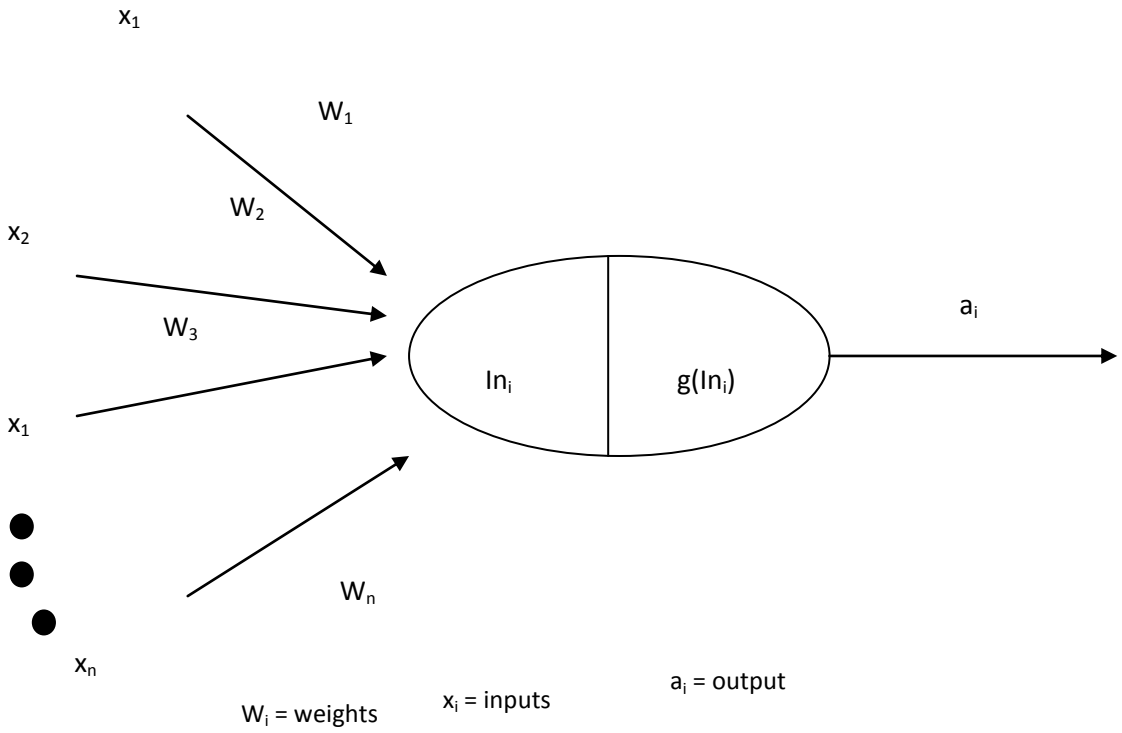

Figure 2.12: An artificial neuron

In a typical neuron shown in Figure 2.12, the input to the neuron x_i is multiplied by a weighting function W_i to generate the transformed input W_ix_i. The transformed inputs are summed to obtain the summed input. The summed input constitutes the variables to the activation/transfer function, g, which generates the output a_i. The output of the transfer function is compared to a threshold value. If the output is greater than the threshold value, the neuron is activated and signal is transferred to the neuron output, alternatively, if it is less the signal is blocked.

Given an input vector $X = (x_1, x_2, ...x_n)$, the activations of the input units are set to $(a_1, a_2, ...a_n) = (x_1, x_2, ...x_n)$ and the network computes to:

$$In_i = \sum_{j=1}^{n} W_{j,i} a_j \quad (2.1)$$

$$a_i = g(In_i) \quad (2.2)$$

The transfer function could be a threshold transfer function, a sin function, a sigmoid function, hyperbolic tangent function etc. Differentiable transfer functions are preferred. Similarly, non linear transfer functions perform better than linear transfer function. Bearing these in mind, in this particular application we chose the sigmoid function. The sigmoid activation function which is given by the equation:

$$a_i = g(In_i) = \frac{1}{1 - e^{-In_i}} \quad (2.3)$$

Training the network (learning) could be supervised or unsupervised training. In supervised training, the network is provided with the inputs and appropriate outputs; hence the network is trained with a set of examples in a specified manner. In unsupervised/adaptive learning, the network is provided with inputs but not the outputs.

2.17 Design of Experiment (DoE)

Design of experiment (DoE) is a data analyses tool that researchers employ in planning experiments in the best economical and chronological path for easy interpretation. This tool depicts the desirable parameters and responses and best process combination that gives the most effective arrangement.

Experimental factor levels and analysis of the study defines the runs of experiments that make up the design of experiments. The tool gives perfect study of experiment for quick, accurate resultand saves cost. The use of design of experiment has increased invariably in the chemical, mechanical and electrical engineering industries.

Fischer (1920) developed the first design of experiment. The tool was used for a simultaneous study of multiple variables effect.The tool was created for study of rain water, sunshine, fertilizer and location effect on crop production, since the variables are much the experiment design gave the best combination of parameters to aid in running the experiment. (Gep *et al.,* 2005).The tool technique now has become very useful in statisticsas it aidin understanding of the process characteristics and in investigation ofthe numerous ways in which inputs parameters affect responses (results) in statistical field based experiments. Furthermore, lots of optimal values of both parameters and responses have been attained using the design of experiment tool with less number of trial and error. Sivaraos *et al*. (2014)listed some of the gains of design of experiment as:

i. More information are provided than in the unplanned experiment
ii. The data collection is more organized and analyzed better
iii. Reliability of information assessment.
iv. Study of interaction of curves and significance of variables and correlation coefficient. The tool is also useful in viewing of contour and three dimensional response surface curves.

2.17.1 Response surface method (RSM)

Response surface design is among several techniques of experimental design. Sivaraos *et al*., (2014) statedresponse surface methodology is used to achieve the following goals;

- To attain an optimal value of parameter and response.
- To optimize the obtained optimal value by either maximization or minimization.
- To minimize trial and error in experimental analysis by locating the actual point of management by pick optimal value from the most highlighted region of the contour by colour.
- To achieve a very organized system of experimental process, data collection and collation

The method is also used for analysis ofcases whereby response is influenced by numerous parameters and it quantifies the quality of the studied system properties. This approach is

based on analysis of polynomial interface and it is a method of statistical and mathematical datagatheringwhich are useful for problem modeling and analysis in situations wherebya lot of factors influence the response. Dey *et al.* (2001) in his study foung out thatthe use of response surface methodology in optimizing the experimental factors and response were efficient.

Response surface design has two types of quadratic models and they include: central composite design (CCD) and Box-Behnken design. The curvature is estimated by augmenting the center pointed fractional factorial design level with a group of star point contained in CCD. The Box-Behnken design contains negative fractional factorial design that is embedded thus it is regarded as a quadratic design of independent nature. In this design the analysis combinations are at the process edge center points of contour space and at the center of ridge. Three levels of each of the variable (factor) are required in the design of experiment since the method is rotatable. The method has less right angle structure intersection (limited orthogonal structure) than the Central composite design. Thus, central composite design was applied for this study considering the fact that the Box-Behnken Design is less capable of attaining orthogonal blocking.

2.17.2 Central composite design (CCD)

In statistical data collection and collation, considering the need for high orthogonal blocking, designed training data analysisgives better result than random experimental analysis. Central Composite Design (CCD) is more desirableto researchersfor training data set design and analysis ofparametric influence owing to the ability to depictthe significance, effect and extent of every parameter on the responses(Sivaraos *et al*., 2014).The general requirements of response surface approach as satisfied by central composite design include:

1. Possibility of estimation of model parameters
2. Possibility of working with less cumbersome combination of treatment.
3. Even distribution of data observation over the regions where information is required on the surface.

Studies by majority of researchers pointed out that, to have a vigorousoptimization model, the CCD is the best technique for optimization, using RSM. CCD is used for depictingthe best parametric and parametric combinations that affecteach response significantly and maximize or minimize the significant parameter.

2.18 Review of related works

Sanjay *et al*. (2012)examinedcomposition of biodiesel from *Gmelina arborea* seed oil using a heterogeneous catalyst derived from the trunk of *Musa balbisiana Colla*.Composition of biodiesel prepared from *Gmelina arborea* seed oil was determined by IR, NMR and GC-MSanalysis. Biodiesel from Gmelina arborea was found to consist of 15.09 wt.% of methyl palmitate (C16:0), 44.88 wt.% of methyloleate (C18:1), 11.16 wt.% of methyl stearate (18:0), 15.95 wt.% of methyl gondoate (C20:1), 4.21 wt.% of methylarachidate (C20:0) and 8.67 wt.% of methyl behenate (C22:0).

Ogunsuyi and Oyewo (2015)performed evaluation of African pear (*dacryodes edulis)* seeds-oil *as a* viable feedstock for biodiesel fuel using NaOH and KOH.The authors obtained yield of the extracted oil as 59% of the total seed. Gas-chromatographic analysis of the oil extract showed that the oil was predominantly mono-unsaturated fatty acid (Oleic acid, 76%) while the percentage of the saturated fatty acids was 24% (palmtic acid 6.1% ,Stearic acid 7.5% and others 10.4%). Biodiesel yield of the seed oil attained optimum yields of 90% at the methanol/oil molar ratio of 7:1,catalyst concentration of 1.00%, reaction temperature of 60^{o}C, agitation speed of 850rpm and effective contact time of 120min. They found out that the fuel properties such as smoke point, flash point, fire point, viscosity and specific gravity exhibited by the biodiesel of African pear (*Dacryodes edulis*) were comparable with those of the petrol-diesel and the values fall within the acceptable limits of ASTM and EN standards.

Manuit and Statit (2007) studied biodiesel synthesis from transesterification by clay-based catalyst. The catalysts were prepared by impregnation between aqueous solution and Suratthanee black (SB) clay and Ranong kaolin (RK) with a controlling catalyst. All biodiesel products were characterized by gas chromatography, viscosity, flash point, cloud point, pour point and carbon residue consecutively. They opined that biodiesels from clay–based catalysts have some encouraging properties to supersede low speed diesel fuel and to lower the cost of production to some extent.

Soetaredjo *et al*. (2011) worked on the use of KOH/bentonite catalysts for transesterification of palm oil to biodiesel. They prepared series of KOH/bentonite catalysts by impregnation of bentonite from Pacitan with potassium hydroxide with theratios between KOH and bentonite as 1:20, 1:10, 1:5, 1:4, 1:3, and 1:2. The characterization of KOH/bentonite and natural bentonite was conducted by nitrogen adsorption and XRD analysis. The effects ofvarious reaction variables on the yield of biodiesel were investigated. The authors obtained the highest yield of 90.70±2.47% biodiesel over KOH/bentonite

catalyst at KOH/bentonite 1:4, reaction time of 3 h, 3% catalyst,methanol to oil ratio of 6, and the reaction temperature at 60°C.

Dang *et al*. (2013) investigated the application of kaolin-based catalysts in biodiesel production via transesterification of vegetable oils in excess methanol. The heterogeneous catalyst was successfully prepared from natural kaolin firstly by dehydroxylation at 800^{o}C for 10 h and, subsequently, by NaOH-activation hydrothermally at 90^{o}C for 24 h and calcined again at 500^{o}C for 6 h. The authors characterized the catalytic material with instruments, including FT-IR, XRD, SEM, and porosimeter (BET/BJH analysis). They obtained conversion efficiencies of soybean and palm oils to biodiesel over the as-prepared catalysts reached 97.0 ± 3.0% and 95.4 ± 3.7%, respectively, under optimal conditions with activation energies of transesterification reactions of soybean and palm oils in excess methanol using these catalysts are 14.09 kJ/mol and 48.87 kJ/mol, respectively.

Calgaroto *et al*. (2013)studied production of biodiesel from soybean and *Jatropha curcas* oils with KSF and amberlyst 15 catalysts in the presence of co-solvents.They foundthat the use of co-solvents led to a reduction in the FAME conversion and that higher conversions were obtained for *Jatropha curcas* compared to soybean oil. The Amberlyst15 presented an enhancement in the catalytic activity after regeneration, providing high biodiesel conversions compared to the fresh resin. The catalyst also presented stability after 5 cycles of reuse. Activity lostwas observed for KSF after 2 successive batch experiments, probably due to a deactivation of acid sites.

Rutto (2013) investigated the use of thermally modified koalin as a heterogeneous catalyst for producing biodiesel. He optimized the production using response surface methodology based on a central composite design (CCD) varrying four transesterification variables namely: temperature, (30-120°C), reaction time, (2- 6hr), methanol to oil ratio, (10-50 wt %) and amount of catalyst, (1-6 grams). He measured the important fuel properties such as viscosity, density and flash point and compared with American Society for Testing and Material (ASTM) standards for biodiesel. The optimum conditions for biodiesel production were found as follows: temperature 49.31°C, amount of catalyst of 2.03 wt %, methanol to oil ratio 18.26 wt %, reaction time of 4.56 hr with optimum yield of biodiesel 95.06%. The results showed that the important fuel properties of the biodiesel produced at optimum conditions met the biodiesel ASTM standard. It was also observed that thermally modified kaolin heterogeneous catalyst can be recycled up to three times.

There is less studies on kinetic modeling using heterogeneous catalysts. One of the studies was Hattori *et al.* (2000) who proposed a five-step mechanism for transesterification

of ethyl acetate using heterogeneous alkaline earth metal oxides by considering the rate-determining steps based on the basicity of the catalyst.Moreso, Dossin *et al.* (2006) studied the simulation of heterogeneously MgO-catalyzed transesterification by comparing three different kinetic models. The Langmuir-Hinshelwood-Hougen-Watson (LHHW), Eley-Rideal and the previous model proposed by Hattori *et al.* (2000). They proposed a kinetic model based on a three-step mechanism of Eley-Rideal and suggested that the rate-determining step for the MgO is methanol adsorption on its active sites. Overall, Lopez *et al.* (2005) stated that the rate-determining step is either methanol adsorption on its active sites, or the reaction at the catalyst surface which is similar in both heterogeneous and homogeneous base-catalyzed transesterification.

Schizaki dos Santos *et al*. (2016) examined the kinetics of ethylic esterification of lauric acid on acid activated montmorillonite (STx1-b) as catalyst. The catalyst consists of a clay mineral (montmorillonite STx1-b) prepared with acid activation. The acid activation was confirmed by X-ray diffraction (XRD) and Fourier transform infrared spectroscopy (FTIR). The authors used Eley–Rideal to describe the kinetic reaction. They obtained that the catalyst montmorilloniteSTx1-b was able to lead the system to high conversions in shorter time when compared to the noncatalyzedreaction.

2.19 Knowledge Gap

From the literature reviewed, it was discovered that the production of biodiesel from African pear seed and gmelina seed oils using clay catalyst and the reaction mechanism of transesterification of these oils via heterogeneous catalysis are limited. The present study therefore focused on production of biodiesel and its kinetics from African pear seed oil using activated clay catalyst.

CHAPTER THREE

MATERIALS AND METHODS

3.1 Materials

Gmelina arborea Roxb. seeds were collected from Energy Centre Avenue, University of Nigeria Nsukka, Enugu State, Nigeria and African pear seeds were bought from Odegba in New Market Enugu, Enugu State, Nigeria. The seeds were dried in sunlight, deshelled and the kernel crushed using a grinder prior to oil extraction.

Methanol used was of analytical grade (Merck, Mumbai, India). All other solvents and chemicals used were ofanalytical grade, and they were procured from commercial sources and used as such without further treatment.

3.2 Oil Extraction

The methods employed by Sanjay et al.(2012) and Uzoh & Onukwuli (2014) were used in extraction of oil from the seeds. Extractability of oil was evaluated by solvent extraction of the100g of crushed kernel. Crushed kernel in petroleum ether and n-hexane (bp 40-60 ºC) with solvent/solute ratio of 0.5ml/g to 2.5ml/g and constant particle size of 900 µm were magnetically stirred at a constant speed of 200rpm at temperature range of 30ºC to 70ºC for time 15minutes to 75minutes. At the end of the extraction, the micelle was filtered using a vacuum filtration (Millipore glass base and funnel) to remove suspended solids. Subsequently, the solvent was separated from the oil using rotary vacuum evaporator (Laborota 4000) and was collected in the receiving flask. The oil which was remained in the sample flask was weighed after the process was completed.

The yield of the crude oil extracted was calculated using Equation (3.1).

$$Y = \frac{W_o}{W} * 100 \qquad (3.1)$$

Where, Y is the oil yield (%),

W_o is the weight of pure oil extracted (g) and

W is the weight of the sample of seed used in the experiment

3.2.1 Optimization of oil extraction

The optimization of the oil extraction was done using central composite design of response surface methodology.

3.2.2: Design of experiment for the optimization process of oil extraction

Minitab version 17 was used in this study to design the experiment and to optimize the extraction conditions. The experimental design employed in this work was a two-level-five factor fractional factorial design, involving 32 experiments. Extraction temperature, solvent/solute ratio, extraction time, particle size and agitation speed were selected as independent factors for the optimization study. The response chosen was the oil yield obtained from solvent extraction. Six replications of centre points were used in order to predict a good estimation of errors and experiments were performed in a randomized order. The actual and coded levels of each factor are shown in Table 3.1. The coded values are designated by −1 (minimum), 0 (centre), and +1 (maximum). It is noteworthy to point out that the software uses the concept of the coded values for the investigation of the significant terms, thus equation in coded values is used to study the effect of the variables on the response. The empirical equation is represented as shown below:

$$Y = \beta_0 + \sum_{i=1}^{3} \beta_i X_i + \sum_{i=1}^{3} \beta_{ii} X^2{}_i + \sum_{i=1}^{3} \sum_{j=i+1}^{3} \beta_{ij} X_i X_j \quad (3.2)$$

Where, β_0 = constant term, β_i = coefficient of linear term, β_{ij} = coefficient of interaction term, β_{ii} = coefficient of quadratic term; X_i, X_{ij} and X_{ii} are the variables for linear, interactive and quadratic terms respectively.

Table 3.1: Studied range of each factor in actual and coded form.

Independent variables	**Symbols**	**Range and levels**				
		-2	-1	0	+1	+2
Solvent/solute ratio (ml/g)	A	0.5	1	1.5	2	2.5
Time (Minutes)	B	15	30	45	60	75
Temperature (^{o}C)	C	30	40	50	60	70
Particle size (mm)	D	0.31	0.44	0.57	0.70	0.83
Agitation speed (rpm)	E	100	150	200	250	300

Table 3.2: Experimental design matrix for extraction of oil from African pear and gmelina using n-hexane and petroleum ether.

Run order	Solvent/Solid ratio (mL/g) A		Time (Minutes) B		Temperature (^{o}C) C		Particle size (mm) D		Agitation Speed (rpm) E		Yield of oil (%)
	Coded	Real	Coded	Real	Coded	Real	Coded	Real	Coded	Real	
1	-1	1	-1	30	-1	40	-1	0.44	+1	250	
2	+1	2	-1	30	-1	40	-1	0.44	-1	150	
3	-1	1	+1	60	-1	40	-1	0.44	-1	150	
4	+1	2	+1	60	-1	40	-1	0.44	+1	250	
5	-1	1	-1	30	+1	60	-1	0.44	-1	150	
6	+1	2	-1	30	+1	60	-1	0.44	+1	250	
7	-1	1	+1	60	+1	60	-1	0.44	+1	250	
8	+1	2	+1	60	+1	60	-1	0.44	-1	150	
9	-1	1	-1	30	-1	40	+1	0.70	-1	150	
10	+1	2	-1	30	-1	40	+1	0.70	+1	250	
11	-1	1	+1	60	-1	40	+1	0.70	+1	250	
12	+1	2	+1	60	-1	40	+1	0.70	-1	150	
13	-1	1	-1	30	+1	60	+1	0.70	+1	250	
14	+1	2	-1	30	+1	60	+1	0.70	-1	150	
15	-1	1	+1	60	+1	60	+1	0.70	-1	150	
16	+1	2	+1	60	+1	60	+1	0.70	+1	250	
17	-2	0.5	0	45	0	50	0	0.57	0	200	
18	+2	2.5	0	45	0	50	0	0.57	0	200	
19	0	1.5	-2	15	0	50	0	0.57	0	200	
20	0	1.5	+2	75	0	50	0	0.57	0	200	
21	0	1.5	0	45	-2	30	0	0.57	0	200	
22	0	1.5	0	45	+2	70	0	0.57	0	200	
23	0	1.5	0	45	0	50	-2	0.31	0	200	
24	0	1.5	0	45	0	50	+2	0.83	0	200	
25	0	1.5	0	45	0	50	0	0.57	-2	100	
26	0	1.5	0	45	0	50	0	0.57	+2	300	
27	0	1.5	0	45	0	50	0	0.57	0	200	
28	0	1.5	0	45	0	50	0	0.57	0	200	
29	0	1.5	0	45	0	50	0	0.57	0	200	
30	0	1.5	0	45	0	50	0	0.57	0	200	
31	0	1.5	0	45	0	50	0	0.57	0	200	
32	0	1.5	0	45	0	50	0	0.57	0	200	

3.2 Kinetics and Thermodynamics of Oil Extraction

3.2.1 Kinetics of oil extraction

The analysis and design of an extraction process for industrial scale requires a relevant kinetic data. Extraction is a process controlled by diffusion due to an oil concentration gradient in the solid phase (particles). The use of a diffusive model to explain mass transfer requires finding solution to Fick's second law. However, mass flow by diffusion entails knowledge of the concentration gradient inside the particles, which is difficult to determine. At the solid-liquid interface, mass flow by diffusion is equal to mass flow by convection. For these reasons, the model of mass transfer by convection has been used to represent kinetics of the vegetable oil extraction process (Liauw, et al., 2008; Adeib, et al., 2010; Sulaiman et al., 2013; Silmara Bispo dos Santos et al., 2015).

Considering the fact that extraction process occurs at non steady state and there are no chemical reactions, mass transfer kinetic model was adopted to study extraction of oil from African pear seed and gmelina seed with both petroleum ether and n-hexane. The rate of variation of the oil concentration in the liquid phase (g L^{-1} min^{-1}) can be written as follows:

$$\frac{dC_L}{dt} = k\,(C_{Le} - C_L) \qquad (3.3)$$

WhereC_L and C_{Le} are the oil concentrations (g L^{-1}) in the liquid phase at time t (minutes) and at equilibrium, respectively and k is the mass transfer coefficient (min^{-1}).

The following boundary conditions were applied in order to solve Equation (3.3):

(i) At the beginning of the extraction process (t = 0), the oil concentration in the liquid phase is equal to zero ($C_L = C_{Lo}$).

(ii) At any time t, concentration of either African pear oil or Gmelina oil in the liquid phase is $C_{Lo} = C_{Le}$.

The integration of Equation (3.3) considering the boundary conditions, gives Equation (3.4).

$$C_L = C_{Le}\,(1 - e^{-kt}) \qquad (3.4)$$

Rewriting Equation (3.4) in terms of percentage yield of extracted oil, (Y_t), it gives Equation (3.5).

$$Y_t = Y_{Le}\,(1 - e^{-kt}) \quad (3.5)$$

Re-arranging equation (3.5), gives Equation (3.6).

$$\ln Y_t = \ln Y_{Le} + kt \quad (3.6)$$

Where Y_{Le} is the percentage of oil contained in the liquid phase at equilibrium in relation to the total oil contained in the sample at time t = 0.

The percentage of oil contained in the liquid phase at equilibrium and mass transfer coefficient (k) were obtained from the intercept and slope of plot of $\ln Y_t$ against t respectively.

The activation energy was calculated with the Arrhenius equation:

$$k = Ae^{-\frac{E_a}{RT}} \quad (3.7)$$

Re-arranging Equation (3.7) produces Equation (3.8)

$$\ln k = \ln A - \frac{E_a}{RT} \quad (3.8)$$

where k is the reaction rate (extraction) constant, A is the Arrhenius constant or frequency factor; Ea is the activation energy; R is the universal gas constant, and T is the absolute temperature. A plot of ln k vs 1/T gives a straight line whose slope represents the activation energy of extraction, −Ea/R, and whose intercept is the Arrhenius constant, A.

3.2.2 Thermodynamics of oil extraction

The thermodynamic parameters enthalpy change (ΔH) and entropy change (ΔS) for the oil extraction process were estimated using the Van't Hoff and Erying equations:

$$\ln K = -\frac{\Delta H}{RT} + \frac{\Delta S}{R} \quad (3.9)$$

$$K = \frac{Y_{Le}}{Y_{se}} \quad (3.10)$$

$$\Delta G = \Delta H - T\Delta S \quad (3.11)$$

Where k = rate constant/mass transfer coefficient, Y_{Le} is the average yield percent of oil at temperature *T*, Y_{Se} is percent of oil remaining in the seeds, T = temperature used in the

extraction process (K), K is the equilibrium constant of extraction process, and R is the universal gas constant (8.314 J mol^{-1} K^{-1}).

The changes in enthalpy and entropy were calculated from the slope and intercept of plot of $\ln K$ against $\frac{1}{T}$ respectively while ΔG was calculated using Equation (3.11).

3.3 Characterization of Oil

The extracted oil from both African pear seed and gmelina seed were characterized using appropriate American Society for Testing Material, ASTM 6751(1973) and ASTM D4067(1986) for physiochemical properties and instrumentation such as Fourier Transform infra- red spectrometer, FTIR and gas chromatography mass spectrometer, GC-MS for functional group and fatty acid profile respectively.

3.3.1 Physiochemical properties of the extracted oil

The physicochemical properties of the extracted oils were determined using standard method ASTM 6751(1973) and ASTM D4067(1986).

3.3.1.1. Specific gravity

This was determined using a 25ml specific gravity bottle. The bottle was washed dried and weighed and the weight was noted and recorded as M_1. It was then filled oil sample and weighed again. The weight was also noted and recorded as M_2. The bottle was then washed, dried, filled with water and weighed. The weight was noted and recorded as M_3. Thus:

$$\text{Specific gravity (S.G)} = \frac{M_2 - M_1}{M_3 - M_1} \quad (3.12)$$

3.3.1.2. Melting point

This was determined using a mercury in glass thermometer which was immersed in the oil as the sample was poured into a petridish and heated in a hot air oven in a closed system until the sample completely liquidated without giving off time. Then the temperature at that point, the value was noted and recorded as the melting point.

3.3.1.3. Flash point

This was determined by measuring 20ml of the oil sample into a crucible and a thermometer was inserted into the crucible as the crucible was heated gently on a moving flame until the sample was ignited. Then, the temperature was noted and recorded as flash point.

3.3.1.4. Moisture content

1ml of the oil sample was measured and poured into a clean dried petri-dish. The petri-dish containing the sample was weighed and recorded as W_1. The sample in the petri-dish was then placed in hot air oven at 105^{o}C. The sample was monitored closely to determine the loss in moisture without allowing it to burn until moisture was completely lost. Then, the petri-dish containing the sample was allowed to cool in a desiccators with its weight noted and recorded as W_2 using an electronic weighting balance; thus

$$\% \text{ moisture content} = \frac{W_1 - W_2}{Weight of sample} * 100 \quad (3.13)$$

3.3.1.5. Saponificaton value

This was determined by weighing 0.2g of the oil sample into a conical flask. 50ml of 0.5N ethanoic potassium hydroxide was added and heated in a refluxed round bottom flask for 30mins. The essence of the reflux was to get a perfect dissolution of the oil sample in the ethanoic potassium hydroxide thereafter. The heated mixture was allowed to cool for another 30mins after which 3 drops of phenolphthalein was added to the mixture, and the mixture was titrated against a 0.5N hydrochloric acid (HCl) until there was a change from pink to colorless. Then a blank (without the oil sample) solution was also prepared and this titrated until the colour change was observed, hence.

$$\text{Saponification value (number)} = \frac{56.1 * N(V_2 - V_1)}{W} \quad (3.14)$$

Where

56.1 = Molecular mass of potassium hydroxide,N = Normality = 0.5

V_2 = Titre value of blank, V_1 = Titre value of sample,W = Weight of the sample used

3.3.1.6. Iodine value

The iodine number was determined based on ASTM D4067-86 (1986) by using the sodium thiosulphate volumetric method. This was determined by measuring 0.5g of the oil sample which was poured into a 25ml conical flask and dissolved with 15ml of chloroform. 25ml of the Wifi's solution was added also into the conical flask and mixed properly. The flask was covered and kept in a dark place for 30mins at room temperature. At the end of the 30minutes, the flask was brought out and 20ml of 10% potassium iodide solution and 150ml water were added into the flask and the solution turned reddish. Thus, the reddish solution was titrated with 0.1N sodium thiosulphate until the reddish colour cleared.

Then, 5ml of 1% starch solution was added to the solution as an indicator and the solution turned bluish-black, then the bluish-black solution was further titrated against 0.1N sodium thiosulphate until the sample again turned colorless.

A blank (without oil sample) solution was also prepared and titrated with the titre values of both the sample and blank noted and recorded respectively, thus,

$$\text{Iodine value} = \frac{12.69 * N(V_2 - V_1)}{Weight of sample \ (W)} \quad (3.15)$$

Where

12.69 = Molecular mass of iodine, N = Normality, V_2 = Blank titre value

V_1= Sample titre value, W = Weight of sample

3.3.1.7. Peroxide value

This was determined by measuring 0.5g of sample with a beaker; thereafter, 25ml of acetic acid and chloroform in the ratio of 2:1 was added to the sample and mixed. Then 1ml of 4grams of potassium iodine dissolved in 3ml of distilled water was also added to the mixture and mixed vigorously. It was covered and kept in a dark place for a minute, after which 35ml of distilled water was added followed by 5ml of starch indicator. The color changed to purple. Then, the purple mixture was titrated against 0.02N sodium thiosulphate until it became colorless. Thereafter the blank solution was also prepared and titrated with the titre value in each case noted and recoded, hence

$$\text{Peroxide value} = \frac{100 * N\ (V_1 - V_2)}{Weight of sample \ (W)} \quad (3.16)$$

Where

N = Normality of sodium thiosulphate ($Na_2S_3O_3$),100 = Peroxide value constant

V_1 = Titre value of sample, V_2 = Titre value of blank,W = Weight of the sample

3.3.1.8. Free fatty acid (FFA) value

0.5g of the oil sample was weighed and purred into a conical flask and 3 drops of phenolphthalein indicator was added, this was followed by 20ml of complete ethanol and the mixture was titrated with 0.1N sodium hydroxide until a pink coloration was observed thus,

$$\text{Free fatty acid value FFA} = \frac{Tr*N*56.1}{Weight of sample} \quad (3.17)$$

Where

T = Titre value,N = Normality, W = Weight of sample used i.e. 0.5 x specific gravity ofsample oil

3.3.1.9. Calorific value

The energy value of the oil sample and its combustion ability was determined by measuring 0.5g of the sample into a distillation flask, this flask containing the sample was heated in a hot air oven to vaporize, the vapors coming out was condensed using a glass condenser with water acting as condensing liquid. The weight of the distillate and the weight of residue after condensation were noted and recorded for each case of weighing, thus,

$$\text{Calorific value} = (W_s - W_r) * 9 \quad (3.18)$$

Where

W_s= weight of sample, W_r= weight of residue,9 = Conversion factor

3.3.1.10. Cloud point

50ml of the sample was introduced into a test jar and closed with a cork filled with a thermometer. The position of the cork was adjusted so that it fits tightly and the thermometer dipped inside to be in contact with the sample.

The test jar was placed in a conical flask supported with a cotton wool in an ice bath. The sample was inspected at regular internal for any smallest observations on formation of

Chister of wax crystals. Upon formation of crystals, the temperature was noted as the "Cloud point".

3.3.1.11. Viscosity

Viscosity is a measure of the internal fluid friction or resistance to flow, which tends to opposeany dynamic change in the fluid motion. As thetemperature of oil is increased its viscosity decreases andit is therefore able to flow more readily.The viscosity was measured with a digital viscometer made by Searchtech instruments, England. The spindle was selected and fixed on the instrument. The spindle was inserted in the sample to be analyzed till the level mark on the spindle reached the surface of the sample. The*Enter* button on the instrument was pressed and the dynamic viscosity, μ, of the sample was displayed on the screen and recorded.

3.3.1.12 Molecular weight of vegetable oils

The molecular weight of the triglyceride was determined using the free fatty acid profile obtained using Gas Chromatography in Section 3.3.2 (II).

$$\text{Molecularweightofatriglyceride} = 3 \times \text{Averagemolecularweight} + 38.049 \qquad 3.19$$

Where,

$3 = \text{Numberofchainsofeachfattyacidinatriglyceride}$

$38.049 = \text{Molecularmassofglycerolinthetriglyceride}\,(\text{Glycerolbackbone})$

3.3.2 Instrumentation characterization

3.3.2.1 Fourier transform infra-red spectrometer (FTIR) analysis of the extracted oil samples

The extracted oil samples from African pear seed and gmelina seed were analyzed using FTIR to determine functional group present in the oils. The infrared spectra were recorded in the mid-infrared region (500-5000cm^{-1}) in an evacuated chamber of Shimadzu FTIR-8400S spectrophotometer using potassium bromide discs as matrices. A spectral resolution of 2cm^{-1} was used and the spectral was accumulated over the scans. The FTIR spectroscopy was applied to the samples. Only 2mg of each of the samples were mixed with 100mg of KBr and pressed under 6 tones for 2minutes in making disk. At first, the sample was crushed and ground before making the KBr pellets. The fitting of peaks and smoothing was done with OPUS 2000 software on the Shimadzu 8400S over the working window, 500-5000cm^{-1}.

3.3.2.2 Gas chromatography mass spectrometer GC-MS

The determination of free fatty acid composition of the oil samples were done with GC-MS by adopting the method employed by Uzoh and Onukwuli (2014). The analysis of the oil was performed with a Thermo Finnigan Trace GC/Trace DSQ/A1300, (E.IQuadropole) equipped with a SGE-BPX5 MS fused silica capillary column (film thickness 0.25μm)for GC-MS detection, and an electron ionization system with ionization energy of 700eV was used.Carrier gas was helium at a flow rate of 10mL/min. injector and MS transfer line temperatures wereset at 220^{o}C and 290^{o}C respectively. The oven temperature was programmed from 50^{o}C to 150^{o}C at3^{o}C/min, then held isothermal for 100min, and raised to 250^{o}C at 10^{o}C/min. Diluted samples (1/100,v/v, in methylene chloride) of 1.00 μL were injected manually in the slitless mode. The identificationof individual components was based on the comparison of their relative retention times with those ofauthentic samples on SGE-BPX5 capillary column, and by matching their mass spectral of peaks withthose obtained from authentic samples and/ or the Wiley 7N and TRLIB libraries spectra and publisheddata.

3.4 Synthesis of Catalyst

The catalyst employed in this study is clay heterogeneous catalyst and was synthesized using the method employed by Manuit and Statit (2007). The clay was immersed in hydrogen peroxide solution (30%) at 30^{o}C for 24h to remove organic impurities in the ratio of 1:2 wt/wt. The mixture was gently heated in a boiling water bath to remove excess H_2O_2 and subsequently separated from the clay. The purified clay was then suspended in distilled water in the ratio of 1:4 wt/wt and allowed to settle. The water was removed and the purified clay was dried in an oven at a temperature of 110^{o}C until its moisture content reached 10%. Then the clay was crushed and sieved with 80/100mesh.

The dried clay catalyst was modified with thermal, acid and alkaline activation to improve its catalytic activity. Their catalytic activities were compared with one another by biodiesel production.

3.4.1 Thermal activation of clay

The dried clay was subjected to heat treatment in a muffle furnace under inert condition at temperatures of 500^{o}C, 600^{o}C, 700^{o}C, 800^{o}C, 900^{o}C and 1000^{o}C for 1hr as reported by many researchers (Nwabanne and Igbokwe, 2011) as temperatures for thermal activation.

3.4.2 Alkaline activation of the clay

The impregnation of NaOH on the dried clay was carried out using method employed by Soetaredjo et al. (2011). The dried clay was mixed with sodium hydroxide (NaOH) 0.5M in the ratio of 1:1, 1:2, 1:3, 1:4, 1:5 (clay:NaOH, g/ml) in a three-neck round bottom flask (500ml) equipped with a reflux condenser, temperature indicator and mechanical stirrer. The mixture was placed in a water bath and heated to a temperature of 60^{o}C for 3h with a constant speed of 300rpm. After the impregnation process, the catalyst was then heated in a muffle furnace at a temperature of 200^{o}C for 2h.

3.4.3 Acid activation of the clay

The method employed by Schizaki dos Santos et al. (2016) was adopted in acid activation of the clay. The dried clay sample was mixed with a solution of phosphoric acid, H_3PO_4 0.5M (Vetec 85) in ratio of 1:1 (g/ml). The reaction was carried out in a round bottom flask at the condition under vigorous stirring and at the temperature of 100^{o}C during 2h. The system was heated in glycerine bath connected to a reflux condenser. Then the acid activated clay was washed with distilled water until the pH was close to 7 and dried at 110^{o}C for 6h. It was finally grounded into a fine powder. The procedure was repeated with ratio of 1:2, 1:3, 1:4, 1:5 (g/ml).

3.5 Characterization of the Clay Sample

The raw and activated clay samples were characterized with ASTM D4067 (1986) method to determine their physiochemical properties; Atomic absorption spectrometer (AAS) to determine metallic compositions, Fourier transform infra-red spectrometer to determine the functional group andBrønsted and Lewis acid sites; Scanning Electron Microscope to determine the morphology of the clay samples and X-ray Diffractometer to determine the mineralogy/type of the clay.

3.5.1 Physiochemical characterization of the clay

3.5.1.1. Surface area measurement

The surface area of the raw clay catalyst and prepared clay catalysts were measured using BET surface area analyser (Autosorb AS-1 MP, USA) at Chemical Engineering Laboratory, Federal University of Technology, Minna, Niger State, Nigeria. The samplewas degassed at

568K for 3 h and the physi-sorption analysis was carried out with nitrogen gasas an adsorbate and liquid nitrogen as a coolant. The multi-point BET correlation technique was used to measure the surface area of the catalysts.

3.5.1.2. Determination of bulk density

The apparent or bulk density of raw and activated clay was determined by the tapping procedure (Nwabanne & Igbokwe, 2011). A known weight of each sample, after being dried at 110^{o}C, was packed into a 100ml capacity graduated cylinder. The bottom of the cylinder was tapped gently on the laboratory bench top several times until there was no further diminution of the sample level. The bulk density was then calculated using the following equation.

$$\text{Bulk density(g/ml)} = \frac{W_{mat}}{V_{mat}} \qquad (3.20)$$

Where:

W_{mat} is the weight of dry material (g)

V_{mat} is the volume of drymaterial (ml)

3.5.1.3 Determination of iodine number

According to ASTM D4067-86 (1986) as reported by Nwabanne and Igbokwe (2011), the iodine number was determined by using the sodium thiosulphate volumetric method. The amount of iodine adsorbed from aqueous solution was estimated by titrating a blank with standard thiosulphate solution and starch indicator compared with titrating against iodine containing 0.5g of the clay.

Typically 0.5g of the clay sample was weighed into a centrifuge tube which was added 25ml of 0.1m iodine solution. The tube was immediately stoppered, shaken for 10mins and then centrifuges at 1000ppm for 5mins.

A 20ml of aliquot of supernatant liquid was pipette into a conical flask and the residual amount of iodine determined by titrating with standard thiosulphate solution in which starch was used as an indicator. Blank determination was carried out without the activated carbon sample. The iodine number is given by the relationship;

$$\text{I(mg/g)} = \frac{\text{(B-S)}}{\text{B}} \times \frac{\text{VM}}{\text{W}} \times 126.91 \qquad (3.21)$$

Where:

B and S are the volumes of thiosulphate solution required for blank and sample titration respectively, W is the mass of the clay sample sample, M is the concentration (mol/L) of the iodine solute and 126.91 is the atomic mass of iodine.

3.5.2 X-ray fluorescence analysis

X-ray fluorescence was performed to know the chemical compositions of the minerals that are present in the raw clay samples. The samples were mined from the various locations and then fractionated into the required different fractions of varying particle sizes using standard sieves of mesh sizes. An ARL 9400XP + Wavelength-dispersed XRF spectrometer with Rh source was used for the x-ray fluorescence analyses of the samples. The NBSGSC fundamental parameter programme was used for matrix correction of the major elements as well as Cl, Co, Cr, V, Sc and S. The Rh Compton peak ratio method was used for the other trace elements. Samples were dried and fired at 1000^{o}C to determine the percentage loss on ignition. Major elements analyzed were carried out on fused beads. A pre-fired sample of 1 and 6g of lithium tetra-borate flux was mixed in a 5% Au/Pt crucible and fused at 1000^{o}C in a muffle furnace with occasional swirling. The glass disk was transferred into a preheated Pt/Au mould and the bottom surface was analyzed.

3.5.3 Fourier transforms infra red (FTIR) analysis

The method employed by Nwabanne and Igbokwe (2011) was adopted to carry out FTIR analysis of raw and activated clay using BUCK model 500 M infra red spectrophotometer. The sample was prepared using KBr and the analysis was done by scanning the sample through a wave number range of 700 to 4000 cm^{-1}.

3.5.4 Surface morphological studies

The surface morphology of the raw and activated clay was studied using Carl Zeiss sigma field emission scanning electron microscope and the images at 1mm and 150 magnification.

3.5.5 X-ray diffraction (XRD) of the clay samples

The method employed by Schizaki dos Santoset al. (2016) was adopted in characterization of the clay sampled with XRD. The X-ray diffraction measurements were obtained in a Shimadzu diffractometer model XRD-7000 with Cu Ka X-ray source (40 kV, 30 mA, λ = 1.5418 Å), interval of 2θ = 3–40^{o}, at a speed of 2^{o} min^{-1} and scanning pace of 0.02^{o}.

3.5.6 Thermogravimetric analysis of the clay catalysts

A Mettler-Toledo TG850 thermo-analyser was used to record DTA and TGA curves simultaneously. The thermo-analytical investigation was carried out in a high purity dried nitrogen gas with a flow rate of 5.0 L/h under continuous evacuation at 1.33 x 10 -6 mbar between 0 - 1000 °C. The heating rate was 10 °C/min. Al_2O_3 was used as reference material.

3.5.7 Brauner Emmet Teller analysis (BET)

The Brunauer-Emmett-Teller (BET) method was used to calculate the surface area, average pore diameter and total pore volume of the clay. Surface area, pore volume and average pore diameter were determined from adsorption isotherms using a micrometrics ASAP 2020 surface analyzer. The samples were degassed using two-stage temperature ramping under a vacuum of <10 mm Hg, followed by sample analysis at 77 K using nitrogen gas prior to analysis in order to remove moisture and other adsorbed gases from the catalyst surface.

3.6 Transesterification Reaction

The extracted oils from African pear seed and gmelina seed reacted with methanol in the presence of thermal, acid and alkaline activated clay to produce methyl esters of fatty acids (biodiesel) and glycerol.

The oil sample was precisely quantitatively transferred into a flat bottom flask placed on a hot magnetic stirrer. Then specific amount of catalyst (by weight of oil sample) mixed with the required amount of methanol was added. The reaction flask was kept on a hot magnetic stirrer under constant temperature with defined agitation throughout the reaction. At the defined time, sample was taken out, cooled, and the biodiesel (i.e. the methyl ester in the upper layer) was separated from the by-product (i.e. the glycerol in the lower layer) by settlement overnight under ambient condition. The percentage of the biodiesel yield was determined by comparing the volume of layer biodiesel with the volume of oil used.

$$Y = \frac{Volume\ of\ biodiesel}{Volume\ of\ oil\ used} \times 100 \qquad (3.22)$$

The procedure was repeated by varying the factors affecting the transesterification reaction catalyzed by thermally, acid and alkaline activated clay such as; time (1 – 5h), catalyst concentration (1 – 5wt%), temperature (40 – 80^{o}C), alcohol/oil molar ratio (6:1 – 14:1) and agitation speed (100 – 500rpm).

3.7. Design of Experiment for Transesterification Reaction

Minitab version 17 was used in this study to design the experiment and to optimize the transesterification conditions. The experimental design employed in this work was a two-level-five factor fractional factorial design, including 32 experiments. Reaction temperature, catalyst concentration, methanol/oil molar ratio, reaction time and agitation speed were selected as independent factors for the optimization study. The responses chosen were the methyl ester yields obtained from transesterification of African pear seed and gmelina seed oil. Eight replications of centre points were used in order to predict a good estimation of errors and experiments were performed in a randomized order. The actual and coded levels of each factor are shown in Table 3.3. The coded values were designated by −1 (minimum), 0 (centre), +1 (maximum), −α and +α. Alpha is defined as a distance from the centre point which can be either inside or outside the range, with the maximum value of 2n/4, where n is the number of factors. Hereby the value of alpha is set at 0.5. It is noteworthy to point out that the software uses the concept of the coded values for the investigation of the significant terms, thus equation in coded values is used to study the effect of the variables on the response. The empirical equation is represented as shown below:

$$Y = \beta_0 + \sum_{i=1}^{5} \beta_i X_i + \sum_{i=1}^{5} \beta_{ii} X^2{}_i + \sum_{i=1}^{5} \sum_{j=i+1}^{5} \beta_{ij} X_i X_j \quad (3.23)$$

Selection of levels for each factor was based on the experiments performed to study the effects of process variables on the application of solid catalysts for transesterification reaction of African pear seed and gmelina seeds oil.

Table 3.3: Studied range of each factor in actual and coded form for heterogeneous catalysts.

Factor	**Units**	**Low level**	**High level**	**-α**	**+α**	**0 level**
Catalyst conc. (A)	Wt%	2(-1)	4(+1)	1(-2)	5(+2)	3
Methanol, (B)	Mol/mol	8(-1)	12(+1)	6(-2)	12(+2)	10
Temperature, (C)	°C	50(-1)	70(+1)	40(-2)	80(+2)	60
Reaction time (D)	Hours	2(-1)	4(+1)	1(-2)	5(+2)	3
Agitation speed (E)	Rpm	200(-1)	400(+1)	100(-2)	500(+2)	300

Table 3.4: Experimental design Matrix for transesterification studies catalyzed by activated clay catalysts

Run order	Catalyst conc. (wt %) A		Methanol/Oil molar ratio B		Temperature (^{o}C) C		Time (Hours) D		Agitation Speed (Rpm) E	
	Coded	Real	Coded	Real	Coded	Real	Coded	Real	Coded	Real
1	-1	2	-1	8	-1	50	-1	2	+1	400
2	+1	4	-1	8	-1	50	-1	2	-1	200
3	-1	2	+1	12	-1	50	-1	2	-1	200
4	+1	4	+1	12	-1	50	-1	2	+1	400
5	-1	2	-1	8	+1	70	-1	2	-1	200
6	+1	4	-1	8	+1	70	-1	2	+1	400
7	-1	2	+1	12	+1	70	-1	2	+1	400
8	+1	4	+1	12	+1	70	-1	2	-1	200
9	-1	2	-1	8	-1	50	+1	4	-1	200
10	+1	4	-1	8	-1	50	+1	4	+1	400
11	-1	2	+1	12	-1	50	+1	4	+1	400
12	+1	4	+1	12	-1	50	+1	4	-1	200
13	-1	2	-1	8	+1	70	+1	4	+1	400
14	+1	4	-1	8	+1	70	+1	4	-1	200
15	-1	2	+1	12	+1	70	+1	4	-1	200
16	+1	4	+1	12	+1	70	+1	4	+1	400
17	-2	1	0	10	0	60	0	3	0	300
18	+2	5	0	10	0	60	0	3	0	300
19	0	3	-2	6	0	60	0	3	0	300
20	0	3	+2	14	0	60	0	3	0	300
21	0	3	0	10	-2	40	0	3	0	300
22	0	3	0	10	+2	80	0	3	0	300
23	0	3	0	10	0	60	-2	1	0	300
24	0	3	0	10	0	60	+2	5	0	300
25	0	3	0	10	0	60	0	3	-2	100
26	0	3	0	10	0	60	0	3	+2	500
27	0	3	0	10	0	60	0	3	0	300
28	0	3	0	10	0	60	0	3	0	300
29	0	3	0	10	0	60	0	3	0	300
30	0	3	0	10	0	60	0	3	0	300
31	0	3	0	10	0	60	0	3	0	300
32	0	3	0	10	0	60	0	3	0	300

3.8 Prediction of Biodiesel Production using Artificial Neural Network

ANNs are composed of simple elements operating in parallel. ANNs are trained to perform a particular function by adjusting the values of the connections, or weights, between elements until a particular input leads to a specific output. ANN operates like a black box model and does not require detailed information about the system being tested. Instead, it learns the relationship between the input parameters and controlled and uncontrolled variables by studying previously recorded data, similar to the way a non-linear regression might perform. Another advantage of using an ANN is its ability to handle large and complex systems with many inter-related parameters. Moreover, it predicts quite well even if the sample size is small.

The ANN consists of three layers: input layer, hidden layer, and output layer. These layers are connected with each other .The input layer receives the input data outside the network and sends them to the hidden layer .The hidden layer contains interconnected neurons for pattern recognition and the relevant information interpretation for adjusting the weights on the connections. Afterwards, the results from the hidden layer are sent to the output layer for the output. The neurons contain several functions and variables including weights, non-linear transfer functions, methods to add up all inputs and bias values. The sum of all products of all the inputs multiplying the weights and the bias values pass through a non-linear transfer function as the output of each neuron.

By adjusting the weights of an ANN we obtained the output we want for specific inputs. Back propagation algorithm was used to adjust the weights of the ANN in order to obtain the desired output from the network. This process of adjusting the weights is called (learning or Training). ANN which learns using the back propagation algorithm for learning the appropriate weight is one of the common models used in ANNs. The back propagation algorithm is used in layered feed forward ANNs. This means that artificial neurons are organized in layer and send their signals forward and then the errors are propagated backward. The back propagation algorithm uses supervised learning which means that we provide the algorithm with examples of inputs and outputs we want the network to compute, and then the error (difference between actual and expected result is calculated. The idea of the back propagation algorithm is to reduce this error, until the ANN learns the training data. The activation function of ANNs implementing the back propagation algorithm is a weighted sum (the sum of the inputs $x_i$multiplied by their respective weightsw_{ji}).

$$A_j(\bar{x}, \bar{w}) = \sum_i^n x_i w_{ji} \quad (3.24)$$

Output function: The most common output function is sigmoidal function

$$O_j(\bar{x}, \bar{w}) = \frac{1}{1 + e^{A_j(\bar{x}, \bar{w})}} \quad (3.25)$$

The goal of the training process is to obtain a desired output when certain inputs are given. Error function:

$$E_j(\bar{x}, \bar{w}, d) = \left(O_j(\bar{x}, \bar{w}) - d_j\right)^2 \quad (3.26)$$

Where:

$$O_j(\bar{x}, \bar{w}) = \text{Actual Output}$$

$$A_j(\bar{x}, \bar{w}) = \text{input vector}$$

$$d_j = \text{Desired output}$$

The error of the network is:

$$\bar{E}(\bar{x}, \bar{w}, \bar{d}) = \sum_j \left(O_j(\bar{x}, \bar{w}) - d_j\right)^2 \quad (3.27)$$

The propagation algorithms then calculate how the error depends on the outputs, inputs and weights. Weights will then be adjusted using the method of gradient descendent.

$$\Delta w_{ji} = \beta \frac{\partial E}{\partial w_{ji}} \quad (3.28)$$

$$\beta = Learning\ rate$$

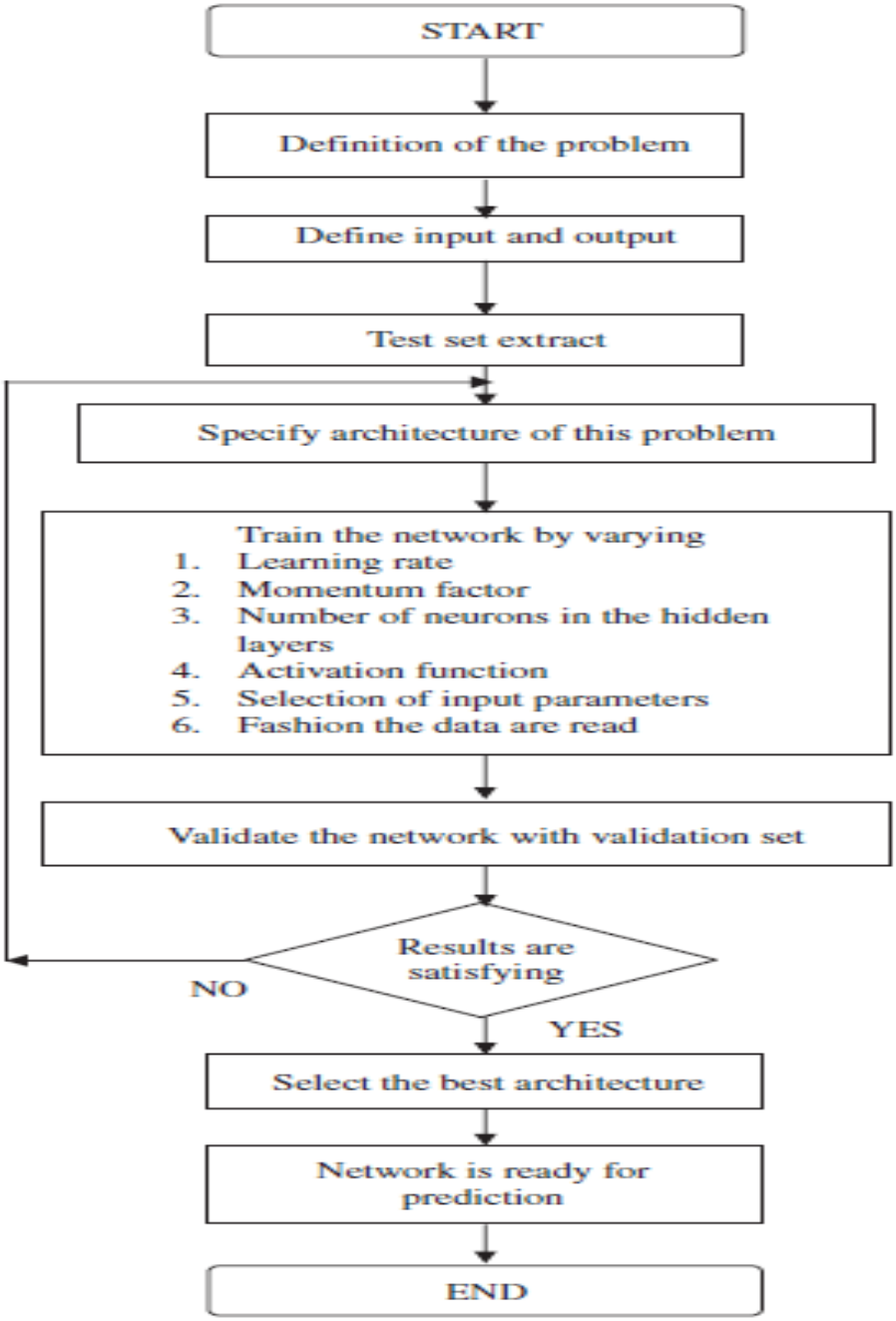

Figure 3.1: ANN flow chart depicting the modelling procedure.

3.9 Characterization of Biodiesel Produced using Optimal Conditions

The properties of the produced biodiesel fuels were determined after the production. The determined properties of the biodiesel include: Acid value, FFA, saponification value, iodine value, density, viscosity, calorific value, flash point, cloud point, pour point and cetane number.

3.9.1 Determination of acid value and FFA

Acid value indicates the proportion of free fatty acid present in biodiesel or fat and may be defined as the number of milligrams of caustic potash required to neutralize the acid in 1 gram of the sample. About 5 gram of each biodiesel was poured into a conical flask. About 50ml of neutralized ethanol solution was added to the biodiesel and the solution heated for about 10 minutes at temperature of 45^{o}C. After the heating, two drops of phenolphthalein indicator was added. The mixture was then titrated against $0.25\ moldm^{-3}$sodium hydroxide (NaOH) solution from the burette until the appearance of pink colour. The acid value (A.V) was then calculated using the equation:

$$\mathrm{A.V} = \frac{\mathrm{T} \times \mathrm{N} \times 56.1}{\mathrm{W}} \quad (3.29)$$

Where,

$$\mathrm{T} = \text{Titre value}$$

$$\mathrm{N} = \text{Normality of NaOH}$$

$$\mathrm{W} = \text{Weight of the biodiesel}$$

The FFA was determined using the equation:

$$\%\mathrm{FFA} \approx \frac{1}{2}\mathrm{A.V} \quad (3.30)$$

3.9.2 Determination of saponification value

Saponification value is a measure of the alkali reactive groups in biodiesel and fatty acids and is expressed as the number of milligrams of KOH that react with 1 gram of sample. About 2 gram of biodiesel was put into a flask. 25ml of ethanol-KOH solution, which is 75% ethanol was added to the sample. The flask was heated on a rotary evaporator for 1 hour at temperature of 40^{o}C. After the heating, the solution was cooled and 2 drops of phenolphthalein indicator was added into the flask and titrated against $0.5\mathrm{mol\,dm^{-3}}$ of tetraoxosulphate (VI) (H_2SO_4) acid from the burette until the pink colour disappeared. The procedure was repeated without the biodiesel and the corresponding reading was noted for the blank titration. The saponification value (S.V) was calculated using the equation:

$$\mathrm{S.V} = \frac{(\mathrm{B} - \mathrm{T}) \times \mathrm{N} \times 56.1}{\mathrm{W}} \quad (3.31)$$

Where,

$$\mathrm{B} = \text{Titre value of Blank}$$

$$\mathrm{T} = \text{Titre value of sample containing biodiesel}$$

$\mathrm{N} = \text{Normality of the acid}$, $\mathrm{W} = \text{Weight of biodiesel used}$

3.9.3 Determination of iodine value

Iodine value is the number of grams of iodine which will be consumed by 100 grams of fat or oil. About 0.25 grams of biodiesel was put into a flask.10ml of chloroform was added and the mixture was warmed slightly for 10 minutes at temperature of 40^{o}C and cooled thereafter. 25ml of iodine tetrachloride-glacial acetic acid solution was added to the flask and the mixture shaken vigorously. The flask was kept in a dark place for 30 minutes. Thereafter, 10 ml of potassium iodide solution was added and the mixture was titrated against $0.1 mol\ dm^{-3}$ sodium thiosulphate solution from the burette until the appearance of yellow colour. 1ml of starch indicator was added to the initially titrated mixture and the colour changed to blue and the mixture was again titrated against sodium thiosulphate until the blue colour disappeared. The procedure was repeated without the oil and the corresponding reading was noted for the blank titration. The iodine value (I.V) was calculated using the equation:

$$\mathrm{I.V} = \frac{(\mathrm{B} - \mathrm{T}) \times \mathrm{N} \times 12.69}{\mathrm{W}} \tag{3.32}$$

Where,

$\mathrm{B} = \text{Titre value of Blank}$

$\mathrm{T} = \text{Titre value of sample containing biodiesel}$

$\mathrm{N} = \text{Normality of the acid}$

$\mathrm{W} = \text{Weight of biodiesel used}$

3.9.4 Determination of density and specific gravity

A clean empty specific gravity bottle was weighed on an electronic balance and the mass (W_1) noted. It was then filled with the biodiesel, in turn, at the required temperature and its mass (W_2) and volume noted.The mass of each oil (W_s) was the difference between W_2 andW_1. The density of biodiesel, ρ, was calculated using the equation:

$$\text{Density} = \frac{\text{Mass}}{\text{Volume}} \tag{3.33}$$

The bottle was washed, dried and filled with equal volume of water at the required temperature and the mass (W_3) was noted. The mass of water (W_w) was the difference between W_3 and W_1. The specific gravity of biodiesel was determined using the equation:

$$\text{Specific gravity} = \frac{\text{Weight of biodiesel}}{\text{Weight of equal volume of water}} \tag{3.34}$$

That is:

$$\text{Specific gravity} = \frac{W_2 - W_1}{W_3 - W_1} \quad (3.35)$$

3.9.5 Determination of viscosity

Viscosity is a measure of the internal fluid friction or resistance to flow, which tends to opposeany dynamic change in the fluid motion. As the temperature of biodiesel is increased its viscosity decreases andit is therefore able to flow more readily.The viscosity was measured with a digital viscometer made by Searchtech instruments, England. The spindle was selected and fixed on the instrument. The spindle was inserted in the sample to be analyzed till the level mark on the spindle reached the surface of the sample. The*Enter* button on the instrument was pressed and the dynamic viscosity, μ, of the sample was displayed on the screen. The kinematic viscosity, υ, was then determined by using the equation:

$$\upsilon = \frac{\mu}{\rho} \quad (3.36)$$

3.9.6 Determination of calorific value

Calorific value of a fuel is the thermal energyreleased per unit quantity of fuel when the fuel is burnedcompletely. It measures the energy content in a fuel.To determine the calorific value, a bomb calorimeter was used to measure the calorific value of the biodiesel. The weight of the biodiesel was measured in grams. The sample was poured into a crucible. Two ends of the ignition thread (nichrome wire) of noted length were fixed on two electrode poles and they were made to keep a good touch on the sample to be evaluated. 10ml of distilled water was poured into the oxygen bomb and the cover was screwed down. Oxygen at a pressure of 2.9MPa was made to flow into, and fill the bomb. The oxygen bomb was put onto the clamp in the inner canister. The temperature sensor was put into the canister. The power was turned on and the stir button was pressed. The water was allowed to stir until the temperature reading stabilized and the initial temperature was noted as T_0. The fire button was pressed and the instrument automatically measured and saved the data. When testing counts got to about 31 counts, the experiment was finished. The final temperature was noted as T_f. The stirring was stopped and the temperature sensor was pulled out. The lid was opened and the bomb was removed. The oxygen inside was releasedbefore opening the bomb. The length of the unburned firing wire was measured.The inner lining of the oxygen bomb and crucible were washed with distilled water. 2 drops of methyl red indicator were

added into the solution and titrated with 0.0709N sodium carbonate. The titre volume V was recorded. The calorific value was calculated using the equation:

$$\text{Calorific value} = \frac{E\Delta T - \emptyset - V}{w} \quad (3.37)$$

Where,

$w = \text{Weight of sample}$

$E = \text{Energy equivalent of the calorimeter per degree Celsius}$

$\Delta T = \text{Change in temperature}$

$\emptyset = \text{Correction for heat of combustion of firing wire } 2.3 * \text{burnt length (cm)}$

$V = \text{Volume of titre used during titration}$

3.9.7 Determination of flash point

The flash point temperature of biodiesel fuel isthe minimum temperature at which the fuel will ignite(flash) on application of an ignition source. It is a determinant for flammability classification of materials. To determine the flash point of the biodiesel, a sample of the biodiesel were poured into the test cup up to the specified level. The cover was then fitted into position on the cup and the sample was heated and stirred at a slow and constant rate. At every 2^oC temperature rise, a flame was introduced over the test cup at a very slow rate for a moment with the help of a shutter. The temperature at which a flash appeared in the form of sound and light was recorded as the flash point.

3.9.8 Determination of cloud point

The cloud point is the temperature at which crystals first start to form in the fuel. The cloud point is reached when the temperature of the sample is low enough to cause wax crystals to precipitate. To determine the cloud point, a sample of biodiesel was put into a test tube containing a thermometer and sealed with a cork. After being heated to within 48^oC, the sample was cooled in a series of cooling baths. The temperature at which a haze or cloud was first seen at the bottom of the test tube was noted as the cloud point.

3.9.9 Determination of pour point

The pour point is the temperature at which the fuel contains so many agglomerated crystalsthat it is essentially a gel and will no longer flow. This occurs if the temperature of the fuel drops below cloud point, when the crystals merge and form large clusters, which may disrupt the flow of the fuel through the pipes of the engine's fuel system. To determine the

pour point, a sample of biodiesel was put into a test tube containing thermometer and sealed with a cork. After being heated to within 48^{o}C, the sample was cooled in a series of cooling baths. At each 3^{o}C reduction in temperature, the tube was removed and tilted until no movement of the sample occurred for 5 seconds.The pour point was recorded as the temperature 3^{o}C above the temperature at which no movement was observed.

3.9.10 Determination of cetane number

The physical and chemical properties of fuel play very important role in ignition delay period. The Cetane Number of the fuel is one such important parameter which is responsible for the delay period. Cetane number is a measure of ignition performance of a fuel. A fuel of higher cetane number gives lower delay period and provides smoother engine operation. Biodiesel has a higher cetane number than petrodiesel because of its higher oxygen content. The cetane number was determined using degree API at specific gravity at 60°F (15.56℃) of the sample and its aniline point (AP). To determine the aniline point of biodiesel, $10ml$ of aniline solution was added to 10ml of the biodiesel in a beaker. The mixture was heated on a heater while being stirred until the two merge into a homogeneous solution. Heating was stopped and thermometer was inserted into the beaker while the beaker and its content were allowed to cool. The temperature at which the two phases separated was observed and was recorded as the aniline point. The degree API and Diesel index of the sample were determined using the formula below.

$$\text{DegreeAPI} = \frac{141.5}{\text{Specificgravityat } 60℃} - 131.5 \tag{3.38}$$

$$\text{DieselIndex(DI)} = \frac{\text{DegreeAPI} \times \text{Anilinepoint}}{100} \tag{3.39}$$

Finally, the cetane number of the sample was determined using the formula:

$$\text{CetaneNumber} = 0.72\text{DI} + 10 \tag{3.40}$$

3.9.11 FTIR and GC-MS of the biodiesel

The FTIR and GC-MS of the biodiesel was carried out using the methods in Section 3.3.2.

3.10Kinetic Studies of Biodiesel Synthesis using Clay Catalyst

3.10.1 Elementary Reaction Mechanism

The mechanism proposed by Langmuir-Hinshelwood-Hougen-Watson (LHHW)forheterogeneous reactionwas employed for the kinetic model. Basically, the Langmuir-Hinshelwood-Hougen-Watson (LHHW) mechanism is a mechanism that involves adsorption, surface reaction and desorption of atoms and molecules on the surfaces (Fogler, 2011). From Equation (3.42), it is proposed that both reactant molecule A (methanol) and T (triglyceride) are adsorbed at different free sites on the catalyst surface. Then, the reaction takes place between chemisorbed (chemical bond between the surface and an atom or a molecule) molecules to give the products B (biodiesel) and G (glycereol). Finally, the adsorbed products B and G are desorbed.

$$T + A \underset{k_b}{\overset{k_f}{\longleftrightarrow}} B + G \qquad (3.41)$$

Assumptions

The following assumptions were made in using LHHW mechanism to model transesterification reaction catalyzed by heterogeneous reaction (Hattori et al., 2000; Dossin et al., 2006):

i. The pellet size of the catalyst is small such that the reaction is not diffusion limited.

ii. The activity of the surface toward adsorption, desorption or surface reaction is independent of coverage such that the surface is essentially uniform as far as the various steps in the reaction are concerned.

The elementary steps of LHHW are derived in nine-step sequence as presented in Equation (3.42) to (3.50) according to Hattori et al., (2000).

$$A + S \underset{k_2}{\overset{k_1}{\longleftrightarrow}} AS \qquad \text{(Adsorption of alcohol)} \qquad (3.42)$$

$$T + S \underset{k_4}{\overset{k_3}{\longleftrightarrow}} TS \qquad \text{(Adsorption of triglyceride)} \qquad (3.43)$$

$$TS + AS \underset{k_6}{\overset{k_5}{\longleftrightarrow}} DS + BS \text{(Surface reaction between adsorbed triglyceride \& alcohol)} (3.44)$$

$$DS + AS \underset{k_8}{\overset{k_7}{\longleftrightarrow}} MS + BS \text{(Surface reaction betweenadsorbed diglyceride \& alcohol)} (3.45)$$

$$MS + AS \underset{k_{10}}{\overset{k_9}{\longleftrightarrow}} BS+GS \text{(Surface reaction betweenAdsorbed monoglyceride \& alcohol)} (3.46)$$

$$BS \underset{k_{12}}{\overset{k_{11}}{\longleftrightarrow}} B + S \text{(Desorption of biodiesel)} \qquad (3.47)$$

DS $\underset{k_{14}}{\overset{k_{13}}{\longleftrightarrow}}$ D + S(Desorption of diglyceride) (3.48)

MS $\underset{k_{16}}{\overset{k_{15}}{\longleftrightarrow}}$ M + S(Desorption of Monoglyceride) (3.49)

GS $\underset{k_{18}}{\overset{k_{17}}{\longleftrightarrow}}$ G + S(Desorption of glycerol) (3.50)

The '*S'* represents the active site of catalyst surface and *D* represents diglyceride, M represents monoglyceride molecules.

From Equation (3.42): $r_1 = k_1$[A][S] - k_2[AS] (3.51)

At equilibrium: $K_1 = \frac{k_1}{k_2} = \frac{[AS]}{[A][S]}$; [AS] = K_1[A][S] (3.52)

From Equation (3.43): $r_2 = k_3$[T][S] - k_4[TS] (3.53)

At equilibrium: $K_2 = \frac{k_3}{k_4} = \frac{[TS]}{[T][S]}$; [TS] = K_2[T][S] (3.54)

From Equation (3.44): $r_3 = k_5$[TS][AS] - k_6[DS][BS] (3.55)

At equilibrium: $K_3 = \frac{k_5}{k_6} = \frac{[DS][BS]}{[TS][AS]}$ (3.56)

From Equation (3.45): $r_4 = k_7$[DS][AS] - k_8[MS][BS] (3.57)

At equilibrium: $K_4 = \frac{k_7}{k_8} = \frac{[MS][BS]}{[DS][AS]}$ (3.58)

From Equation (3.46): $r_5 = k_9$[MS][AS] - k_{10}[GS][BS] (3.59)

At equilibrium: $K_5 = \frac{k_9}{k_{10}} = \frac{[GS][BS]}{[MS][AS]}$ (3.60)

From Equation (3.47): $r_6 = k_{11}$[BS] - k_{12}[B][S] (3.61)

At equilibrium: $K_6 = \frac{k_{11}}{k_{12}} = \frac{[B][S]}{[BS]}$; [BS] = $\frac{[B][S]}{K_6}$ (3.62)

From Equation (3.48): $r_7 = k_{13}$[DS] - k_{14}[D][S] (3.63)

At equilibrium: $K_7 = \frac{k_{13}}{k_{14}} = \frac{[D][S]}{[DS]}$; [DS] = $\frac{[D][S]}{K_7}$ (3.64)

From Equation 3.49: $r_8 = k_{15}$[MS] - k_{16}[M][S] (3.65)

At equilibrium: $K_8 = \frac{k_{15}}{k_{16}} = \frac{[M][S]}{[MS]}$; [MS] = $\frac{[M][S]}{K_8}$ (3.66)

From Equation 3.50: $r_9 = k_{17}$[GS] - k_{18}[G][S] (3.67)

At equilibrium: $K_9 = \frac{k_{17}}{k_{18}} = \frac{[G][S]}{[GS]}$; [GS] = $\frac{[G][S]}{K_9}$ (3.68)

I. Assuming alcohol adsorption as rate determining step (Equation 3.42)

$r_1 = k_1$[A][S] - k_2[AS] (Eq. 3.51)

From Equation 3.56, [AS] = $\frac{[DS][BS]}{K_3[TS]}$

But [DS] = $\frac{[D][S]}{K_7}$ (Eq. 3.64), [BS] = $\frac{[B][S]}{K_6}$ (Eq. 3.62),[TS] = K_2[T][S] (Eq. 3.54)

[AS] = $\frac{[D][B][S]}{K_2K_3K_6K_7[T]}$ (3.69)

$r_1 = k_1$[A][S] - $k_2 \frac{[D][B][S]}{K_2K_3K_6K_7[T]}$ (3.70)

$r_1 = (k_1$[A] - $k_2 \frac{[D][B][S]}{K_2K_3K_6K_7[T]})$ [S] (3.71)

L = [S] + [AS] + [TS] + [DS] + [MS] + [BS] + [GS] = 1 (3.72)

L = Total active site = 1

[S] = $\frac{1}{1+\frac{[D][B]}{K_2K_3K_6K_7[T]}+K_2[\mathrm{T}]+\frac{[D]}{K_7}+\frac{[M]}{K_8}+\frac{[B]}{K_6}+\frac{[G]}{K_9}}$ (3.73)

$\boldsymbol{r_1}=\frac{\boldsymbol{k_1}[\mathbf{A}]-\frac{\boldsymbol{k_2}[\boldsymbol{D}][\boldsymbol{B}]}{\boldsymbol{K_2K_3K_6K_7}[\boldsymbol{T}]})}{\mathbf{1}+\frac{[\boldsymbol{D}][\boldsymbol{B}]}{\boldsymbol{K_2K_3K_6K_7}[\boldsymbol{T}]}+\boldsymbol{K_2}[\mathbf{T}]+\frac{[\boldsymbol{D}]}{\boldsymbol{K_7}}+\frac{[\boldsymbol{M}]}{\boldsymbol{K_8}}+\frac{[\boldsymbol{B}]}{\boldsymbol{K_6}}+\frac{[\boldsymbol{G}]}{\boldsymbol{K_9}}}$(3.74)

II. Assuming triglyceride adsorption as rate determining step (Equation 3.43)

$r_2 = k_3$[T][S] - k_4[TS] (Eq. 3.51)

From Equation 3.56, [TS] = $\frac{[DS][BS]}{K_3[AS]}$

But [DS] = $\frac{[D][S]}{K_7}$ (Eq. 3.64), [BS] = $\frac{[B][S]}{K_6}$ (Eq. 3.62),[AS] = K_1[A][S] (Eq. 3.52)

[TS] = $\frac{[D][B][S]}{K_1K_3K_6K_7[A]}$ (3.75)

$r_2 = k_3$[T][S] - $k_4 \frac{[D][B][S]}{K_1K_3K_6K_7[A]}$ (3.76)

$r_2 = (k_3$[T] - $k_4 \frac{[D][B][S]}{K_1K_3K_6K_7[A]})$ [S] (3.77)

[S] = $\frac{1}{1+K_1[\mathrm{A}]+\frac{[D][B]}{K_1K_3K_6K_7[A]}+\frac{[D]}{K_7}+\frac{[M]}{K_8}+\frac{[B]}{K_6}+\frac{[G]}{K_9}}$ (3.78)

$\boldsymbol{r_2} = \frac{\boldsymbol{k_3}[\mathbf{T}]-\frac{\boldsymbol{k_4}[\boldsymbol{D}][\boldsymbol{B}]}{\boldsymbol{K_1K_3K_6K_7}[\boldsymbol{A}]}}{\mathbf{1}+\boldsymbol{K_1}[\mathbf{A}]+\frac{[\boldsymbol{D}][\boldsymbol{B}]}{\boldsymbol{K_1K_3K_6K_7}[\boldsymbol{A}]}+\frac{[\boldsymbol{D}]}{\boldsymbol{K_7}}+\frac{[\boldsymbol{M}]}{\boldsymbol{K_8}}+\frac{[\boldsymbol{B}]}{\boldsymbol{K_6}}+\frac{[\boldsymbol{G}]}{\boldsymbol{K_9}}}$ (3.79)

III. Assuming surface reaction between adsorbed triglyceride and adsorbed alcohol as rate determining step (Equation 3.44)

$r_3 = k_5$[TS][AS] - k_6[DS][BS] (Eq. 3.55)

But [TS] = K_2[T][S] (Eq. 3.56), [DS] = $\frac{[D][S]}{K_7}$ (Eq. 3.64), [BS] = $\frac{[B][S]}{K_6}$ (Eq. 3.62),

[AS] = K_1[A][S] (Eq. 3.52), [GS] = $\frac{[G][S]}{K_9}$ (Eq. 3.68)

$r_3 = k_5K_1K_2$[T][A]$[S]^2$ - $k_6 \frac{[D][B][S]^2}{K_6K_7}$ (3.80)

$r_3 = (k_5K_1K_2$[T][A] - $k_6 \frac{[D][B]}{K_6K_7})[S]^2$ (3.81)

[S] = $\frac{1}{1+K_1[\mathrm{A}]+K_2[\mathrm{T}]+\frac{[D]}{K_7}+\frac{[M]}{K_8}+\frac{[B]}{K_6}+\frac{[G]}{K_9}}$ (3.82)

$$[S]^2 = \frac{1}{(1 + K_1[\mathrm{A}] + K_2[\mathrm{T}] + \frac{[D]}{K_7} + \frac{[M]}{K_8} + \frac{[B]}{K_6} + \frac{[G]}{K_9})^2} \quad (3.83)$$

$$\boldsymbol{r_3 = \frac{k_5 K_1 K_2 [\mathrm{T}][\mathrm{A}] - \frac{k_6 [D][B]}{K_6 K_7}}{(1 + K_1[\mathrm{A}] + K_2[\mathrm{T}] + \frac{[D]}{K_7} + \frac{[M]}{K_8} + \frac{[B]}{K_6} + \frac{[G]}{K_9})^2}} \quad (3.84)$$

IV. Assuming surface reaction between adsorbed diglyceride and adsorbed alcohol as determining step (Equation 3.45)

$r_4 = k_7[\mathrm{DS}][\mathrm{AS}] - k_8[\mathrm{MS}][\mathrm{BS}]$ (Eq. 3.57)

But $[\mathrm{DS}] = \frac{[D][S]}{K_7}$ (Eq. 3.64), $[\mathrm{BS}] = \frac{[B][S]}{K_6}$ (Eq. 3.62),$[\mathrm{AS}] = K_1[\mathrm{A}][\mathrm{S}]$ (Eq. 3.52),

$[\mathrm{GS}] = \frac{[G][S]}{K_9}$ (Eq. 3.68)

$$r_4 = k_7 \frac{K_1}{K_7}[\mathrm{D}][\mathrm{A}][S]^2 - k_8 \frac{[M][B][S]^2}{K_6 K_8} \quad (3.85)$$

$$r_4 = (k_7 \frac{K_1}{K_7}[\mathrm{D}][\mathrm{A}] - k_8 \frac{[M][B]}{K_6 K_8})[S]^2 \quad (3.86)$$

Recalls $[S]^2 = \frac{1}{(1 + K_1[\mathrm{A}] + K_2[\mathrm{T}] + \frac{[D]}{K_7} + \frac{[M]}{K_8} + \frac{[B]}{K_6} + \frac{[G]}{K_9})^2}$

$$\boldsymbol{r_4 = \frac{k_7 \frac{K_1}{K_7}[\mathrm{D}][\mathrm{A}] - \frac{k_8 [D][B]}{K_6 K_8}}{(1 + K_1[\mathrm{A}] + K_2[\mathrm{T}] + \frac{[D]}{K_7} + \frac{[M]}{K_8} + \frac{[B]}{K_6} + \frac{[G]}{K_9})^2}} \quad (3.87)$$

V. Assuming surface reaction between adsorbed monoglyceride and adsorbed alcohol as rate determining step (Equation 3.46)

$r_5 = k_9[\mathrm{MS}][\mathrm{AS}] - k_{10}[\mathrm{GS}][\mathrm{BS}]$ (Eq. 3.59)

$$r_5 = k_9 \frac{K_1}{K_8}[\mathrm{M}][\mathrm{A}][S]^2 - k_{10} \frac{[B][G][S]^2}{K_6 K_9} \quad (3.88)$$

$$r_5 = (k_9 \frac{K_1}{K_8}[\mathrm{M}][\mathrm{A}] - k_{10} \frac{[B][G]}{K_6 K_9})[S]^2 \quad (3.89)$$

Recalls $[S]^2 = \frac{1}{(1 + K_1[\mathrm{A}] + K_2[\mathrm{T}] + \frac{[D]}{K_7} + \frac{[M]}{K_8} + \frac{[B]}{K_6} + \frac{[G]}{K_9})^2}$

$$\boldsymbol{r_5 = \frac{k_9 \frac{K_1}{K_8}[\mathrm{M}][\mathrm{A}] - \frac{k_{10} [D][B]}{K_6 K_9}}{(1 + K_1[\mathrm{A}] + K_2[\mathrm{T}] + \frac{[D]}{K_7} + \frac{[M]}{K_8} + \frac{[B]}{K_6} + \frac{[G]}{K_9})^2}} \quad (3.90)$$

VI. Desorption of biodiesel as rate determining step (Equation 3.47)

$r_6 = k_{11}[\mathrm{BS}] - k_{12}[\mathrm{B}][\mathrm{S}]$ (Eq. 3.61)

From Equation (3.52), $[\mathrm{BS}] = \frac{K_3[TS][AS]}{[DS]}$

But $[\mathrm{DS}] = \frac{[D][S]}{K_7}$ (Eq. 3.64),$[\mathrm{TS}] = K_2[\mathrm{T}][\mathrm{S}]$ (Eq. 3.54), $[\mathrm{AS}] = K_1[\mathrm{A}][\mathrm{S}]$ (Eq. 3.52)

$$[\mathrm{BS}] = \frac{K_1 K_2 K_3 K_7 [T][A]}{[D]} \quad (3.91)$$

$r_6 = k_{11} \frac{K_1K_2K_3K_7[T][A][S]}{[D]} - k_{12}[\mathrm{B}][\mathrm{S}]$ (3.92)

$r_6 = (k_{11} \frac{K_1K_2K_3K_7[T][A]}{[D]} - k_{12}[\mathrm{B}])[\mathrm{S}]$ (3.93)

$[\mathrm{S}] = \frac{1}{1 + K_1[\mathrm{A}] + K_2[\mathrm{T}] + \frac{K_1K_2K_3K_7[T][A]}{[D]} + \frac{[D]}{K_7} + \frac{[M]}{K_8} + \frac{[G]}{K_9}}$ (3.94)

$\boldsymbol{r_6 = \frac{k_{11}\frac{K_1K_2K_3K_7[T][A]}{[D]} - k_{12}[\mathrm{B}]}{1 + K_1[\mathrm{A}] + K_2[\mathrm{T}] + \frac{K_1K_2K_3K_7[T][A]}{[D]} + \frac{[D]}{K_7} + \frac{[M]}{K_8} + \frac{[G]}{K_9}}}$ (3.95)

VII. Desorption of diglyceride as rate determine step (Equation 3.48)

$r_7 = k_{13}[\mathrm{DS}] - k_{14}[\mathrm{D}][\mathrm{S}]$ (Eq. 3.63)

From Equation (3.52), $[\mathrm{DS}] = \frac{K_3[TS][AS]}{[BS]}$

But $[\mathrm{TS}] = K_2[\mathrm{T}][\mathrm{S}]$ (Eq. 3.54), $[\mathrm{AS}] = K_1[\mathrm{A}][\mathrm{S}]$ (Eq. 3.52), $[\mathrm{BS}] = \frac{[B][S]}{K_6}$ (Eq. 3.62),

$[\mathrm{DS}] = \frac{K_1K_2K_3K_6K_7[T][A][S]}{[B]}$ (3.96)

$r_7 = k_{13} \frac{K_1K_2K_3K_6K_7[T][A][S]}{[B]} - k_{14}[\mathrm{D}][\mathrm{S}]$ (3.97)

$r_7 = (k_{13} \frac{K_1K_2K_3K_6K_7[T][A]}{[B]} - k_{14}[\mathrm{D}])[\mathrm{S}]$ (3.98)

$[\mathrm{S}] = \frac{1}{1 + K_1[\mathrm{A}] + K_2[\mathrm{T}] + \frac{[B]}{K_6} + \frac{K_1K_2K_3K_6K_7[T][A]}{[B]} + \frac{[M]}{K_8} + \frac{[G]}{K_9}}$ (3.99)

$\boldsymbol{r_7 = \frac{k_{13}\frac{K_1K_2K_3K_6[T][A]}{[B]} - k_{14}[\mathrm{D}]}{1 + K_1[\mathrm{A}] + K_2[\mathrm{T}] + \frac{[B]}{K_6} + \frac{K_1K_2K_3K_6[T][A]}{[B]} + \frac{[M]}{K_8} + \frac{[G]}{K_9}}}$ (3.100)

VIII. Desorption of monoglyceride as rate determining step (Equation 3.49)

$r_8 = k_{15}[\mathrm{MS}] - k_{16}[\mathrm{M}][\mathrm{S}]$ (Eq. 3.65)

From Equation (3.58), $[\mathrm{MS}] = \frac{K_4[DS][AS]}{[BS]}$

But $[\mathrm{DS}] = \frac{[D][S]}{K_7}$ (Eq. 3.64),$[\mathrm{BS}] = \frac{[B][S]}{K_6}$ (Eq. 3.62), $[\mathrm{AS}] = K_1[\mathrm{A}][\mathrm{S}]$ (Eq. 3.52)

$[\mathrm{MS}] = \frac{K_1K_4K_6[D][A][S]}{K_7[B]}$(3.101)

$r_8 = k_{15} \frac{K_1K_4K_6[D][A][S]}{K_7[B]} - k_{16}[\mathrm{M}][\mathrm{S}]$ (3.102)

$r_8 = (k_{15} \frac{K_1K_4K_6[D][A]}{K_7[B]} - k_{16}[\mathrm{M}])\ [\mathrm{S}]$ (3.103)

$[\mathrm{S}] = \frac{1}{1 + K_1[\mathrm{A}] + K_2[\mathrm{T}] + \frac{[B]}{K_6} + \frac{K_1K_4K_6[D][A]}{K_7[B]} + \frac{[D]}{K_7} + \frac{[G]}{K_9}}$ (3.104)

$\boldsymbol{r_8 = \frac{k_{15}\frac{K_1K_4K_6[D][A]}{K_7[B]} - k_{16}[\mathrm{M}]}{1 + K_1[\mathrm{A}] + K_2[\mathrm{T}] + \frac{[B]}{K_6} + \frac{K_1K_4K_6[D][A]}{K_7[B]} + \frac{[D]}{K_7} + \frac{[G]}{K_9}}}$ (3.105)

IX. Desorption of glycerol as rate determining step (Equation 3.50)

$r_9 = k_{17}$[GS] - k_{18}[G][S] (Eq. 3.67)

From Equation (3.60), [GS] = $\frac{K_5[MS][AS]}{[BS]}$

But [MS] = $\frac{[M][S]}{K_8}$ (Eq. 3.66),[BS] = $\frac{[B][S]}{K_6}$ (Eq. 3.62), [AS] = K_1[A][S] (Eq. 3.52)

[GS] = $\frac{K_1K_5K_6[M][A][S]}{K_8[B]}$(3.106)

$r_9 = k_{17}\frac{K_1K_5K_6[M][A][S]}{K_8[B]} - k_{18}$[G][S] (3.107)

$r_9 = (k_{17}\frac{K_1K_5K_6[M][A]}{K_8[B]} - k_{18}$[G]) [S] (3.108)

[S] =$\frac{1}{1 + K_1[\mathrm{A}] + K_2[\mathrm{T}] + \frac{[B]}{K_6} + \frac{[D]}{K_7} + \frac{[M]}{K_8} + \frac{K_1K_5K_6[M][A]}{K_8[B]}}$(3.109)

$$\boldsymbol{r_9 = \frac{k_{17}\frac{K_1K_5K_6[M][A]}{K_8[B]} - k_{18}[\mathrm{G}]}{1 + K_1[\mathrm{A}] + K_2[\mathrm{T}] + \frac{[B]}{K_6} + \frac{[D]}{K_7} + \frac{[M]}{K_8} + \frac{K_1K_5K_6[M][A]}{K_8[B]}}} \quad (3.110)$$

Concentration of T, D, M, A, B and G were determined from GC analysis using equation adopted by Olutoye and Hameed (2016).

C_i (g/l) = 5 * 10^{-7} A + 2.1272 (3.111)

Where

C_i = concentration of triglyceride or diglyceride or monoglyceride or glycerol or alcohol or biodiesel

A = peak area of the triglyceride/diglyceride/monoglyceride/glycerol/alcohol/biodiesel component as was determined by GC.

The derived rate equations (Equations (3.74), (3.79), (3.84), (3.87), (3.90), (3.95), (3.100), (3.105) and (3.110)) were used as models for the transesterification of African seed oil and Gmelina seed oil by thermally, acidic and alkaline modified clay catalyst. The rate and equilibrium constants were determined by using nonlinear regression analysis of POLYMATH 5.1 to search for those parameter values that minimize the sum of the squares of difference between the measured rates and the calculated rates for all the data pointsas shown in Equation (3.112) with initial guess of 0.01 and 10 for rate constant and equilibrium constant respectively. Each reaction rate was determined using POLYMATH 5.1 by developing polynomial equation with concentration of various species in the reaction obtained by GC-MS analysis. The models were compared by using their individual variances calculated using Equation (3.113) at 95% confidence level. The model with lowest variance

and positive parameter suits the experimental data while the model with lowest rate constant becomes the rate determining step.

$S^2 = \sum(r_{im} - r_{ic})^2$(3.112)

$\sigma^2 = \frac{S^2}{N-K} = \sum_{i=1}^{N} \frac{(r_{im} - r_{ic})^2}{N-K}$ (3.113)

Where S^2 = sum of squares, N = no of runs, K = no of parameters to be determine,

r_{im} = measured reaction rate for run i, r_{ic} = calculated reaction rate of run i,

σ^2 = variance

The mechanism proposed by Eley-Rideal was also used to model the kinetics of the transesterification reaction catalyzed by activated clay catalyst. The mechanism involves the reaction between an adsorbed molecule and non-adsorbed molecule. In this study, T, D and M were assumed to be adsorbed while methanol was non-adsorbed.

The elementary steps of Eley-Rideal are derived in seven-step sequence as presented in Equation (3.114) to (3.120) according to Dossin et al., (2006).

T + S $\underset{k_2}{\overset{k_1}{\leftrightarrow}}$ TS (Adsorption of triglyceride) (3.114)

TS + A $\underset{k_4}{\overset{k_3}{\leftrightarrow}}$ DS + B (Surface reaction between adsorbed triglyceride and alcohol)(3.115)

DS + A $\underset{k_6}{\overset{k_5}{\leftrightarrow}}$ MS + B (Surface reaction betweenadsorbed diglyceride and alcohol)(3.116)

MS + A $\underset{k_8}{\overset{k_7}{\leftrightarrow}}$ B+GS(Surface reaction betweenadsorbed monoglyceride andalcohol)(3.117)

GS $\underset{k_{10}}{\overset{k_9}{\leftrightarrow}}$ B + S (Desorption of glycerol) (3.118)

DS $\underset{k_{12}}{\overset{k_{11}}{\leftrightarrow}}$ D + S(Desorption of diglyceride) (3.119)

MS $\underset{k_{14}}{\overset{k_{13}}{\leftrightarrow}}$ M + S(Desorption of Monoglyceride) (3.120)

The '*S'* represents the active site of catalyst surface and *D* represents diglyceride, M represents monoglyceride molecules.

From Equation (3.114): $r_1 = k_1$[T][S] - k_2[TS] (3.121)

At equilibrium: $K_1 = \frac{k_1}{k_2} = \frac{[TS]}{[T][S]}$; [TS] = K_1[T][S] (3.122)

From Equation (3.115): $r_2 = k_3$[TS][A] - k_4[DS][B] (3.123)

At equilibrium: $K_2 = \frac{k_3}{k_4} = \frac{[DS][B]}{[TS][A]}$; [DS] = $\frac{K_2[A][TS]}{[B]}$(3.124)

From Equation (3.116): $r_3 = k_5$[DS][A] - k_6[MS][B] (3.125)

At equilibrium: $K_3 = \frac{k_5}{k_6} = \frac{[MS][B]}{[DS][A]}$; [MS] = $\frac{K_3[A][DS]}{[B]}$ (3.126)

From Equation (3.117): $r_4 = k_7$[MS][A] - k_8[GS][B] (3.127)

At equilibrium: $K_4 = \frac{k_7}{k_8} = \frac{[GS][B]}{[MS][A]}$ (3.128)

From Equation (3.118): $r_5 = k_9$[GS] - k_{10}[G][S] (3.129)

At equilibrium: $K_5 = \frac{k_9}{k_{10}} = \frac{[G][S]}{[GS]}$; [GS] = $\frac{[G][S]}{K_5}$(3.130)

From Equation (3.119): $r_6 = k_{11}$[DS] - k_{12}[D][S] (3.131)

At equilibrium: $K_6 = \frac{k_{11}}{k_{12}} = \frac{[D][S]}{[DS]}$; [DS] = $\frac{[D][S]}{K_6}$ (3.132)

From Equation (3.120): $r_7 = k_{13}$[MS] - k_{14}[M][S] (3.133)

At equilibrium: $K_7 = \frac{k_{13}}{k_{14}} = \frac{[M][S]}{[MS]}$; [MS] = $\frac{[M][S]}{K_7}$ (3.134)

I. Assuming alcohol adsorption as rate determining step (Equation 3.114)

$r_1 = k_1$[T][S] - k_2[TS] (Eq. 3.121)

From Equation (3.124), [TS] = $\frac{[DS][B]}{K_2[A]}$

But [DS] = $\frac{[D][S]}{K_6}$ (Eq. 3.132), [MS] = $\frac{[M][S]}{K_7}$ (Eq. 3.134),[GS] = $\frac{[G][S]}{K_5}$ (Eq. 3.130)

[TS] = $\frac{[D][B][S]}{K_2K_6[A]}$(3.135)

$r_1 = k_1$[T][S] - $k_2 \frac{[D][B][S]}{K_2K_6[A]}$(3.136)

$r_1 = (k_1$[T] - $k_2 \frac{[D][B][S]}{K_2K_6[A]})$ [S] (3.137)

L = [S] + [TS] + [DS] + [MS] + [GS] = 1 (3.138)

L = Total active site = 1

[S] = $\frac{1}{1 + \frac{[D][B]}{K_1K_6[A]} + \frac{[G]}{K_5} + \frac{[D]}{K_6} + \frac{[M]}{K_7}}$ (3.139)

$$\boldsymbol{r_1 = \frac{k_1[A] - \frac{k_2[D][B]}{K_2K_6[A]}}{1 + \frac{[D][B]}{K_2K_6[A]} + \frac{[G]}{K_5} + \frac{[D]}{K_6} + \frac{[M]}{K_7}}} \quad (3.140)$$

II. Assuming surface reaction between adsorbed triglyceride and non adsorbed alcohol as rate determining step (Equation 3.115)

$r_2 = k_3$[TS][A] - k_4[DS][B] (Eq. 3.123)

[TS] = K_1[T][S] (Eq. 3.122),

$r_2 = k_3K_1$[T][A][S] - $k_4 \frac{[D][B][S]}{K_6}$ (3.141)

$r_2 = (k_3K_1$[T][A] - $k_4 \frac{[D][B]}{K_6})$ [S] (3.142)

[S] = $\frac{1}{1 + K_1[T] + \frac{[G]}{K_5} + \frac{[D]}{K_6} + \frac{[M]}{K_7}}$ (3.143)

$$\boldsymbol{r_2} = \frac{\boldsymbol{k_3 K_1[\mathrm{T}][\mathrm{A}] - \frac{k_4[D][B]}{K_6}}}{\boldsymbol{1 + K_1[\mathrm{T}] + \frac{[G]}{K_5} + \frac{[D]}{K_6} + \frac{[M]}{K_7}}} \qquad (3.144)$$

III. Assuming surface reaction between adsorbed diglyceride and non adsorbed alcohol as determining step (Equation 3.116)

$r_3 = k_5[\mathrm{DS}][\mathrm{A}] - k_6[\mathrm{MS}][\mathrm{B}]$ (Eq. 3.125)

$$r_3 = k_5 \frac{[D][A][S]}{K_6} - k_6 \frac{[M][B][S]}{K_7} \qquad (3.145)$$

$$r_3 = (k_5 \frac{[D][A]}{K_6} - k_6 \frac{[M][B]}{K_7})[\mathrm{S}] \qquad (3.146)$$

Recalls $[\mathrm{S}] = \frac{1}{1 + K_1[\mathrm{T}] + \frac{[G]}{K_5} + \frac{[D]}{K_6} + \frac{[M]}{K_7}}$

$$\boldsymbol{r_3} = \frac{\boldsymbol{k_5 \frac{[D][A]}{K_6}] - \frac{k_6[M][B]}{K_7}}}{\boldsymbol{1 + K_1[\mathrm{T}] + \frac{[G]}{K_5} + \frac{[D]}{K_6} + \frac{[M]}{K_7}}} (3.147)$$

IV. Assuming surface reaction between adsorbed monoglyceride and non adsorbed alcohol as rate determining step (Equation 3.117)

$r_4 = k_7[\mathrm{MS}][\mathrm{A}] - k_8[\mathrm{GS}][\mathrm{B}]$ (Eq. 3.127)

$$r_4 = k_7 \frac{[M][A][S]}{K_7} - k_8 \frac{[B][G][S]}{K_5} \qquad (3.148)$$

$$r_4 = (k_7 \frac{[M][A]}{K_7} - k_8 \frac{[B][G]}{K_5})\,[S] \qquad (3.149)$$

Recalls $[\mathrm{S}] = \frac{1}{1 + K_1[\mathrm{T}] + \frac{[G]}{K_5} + \frac{[D]}{K_6} + \frac{[M]}{K_7}}$

$$\boldsymbol{r_4} = \frac{\boldsymbol{k_7 \frac{[M][A]}{K_7} - \frac{k_8[G][B]}{K_5}}}{\boldsymbol{1 + K_1[\mathrm{T}] + \frac{[G]}{K_5} + \frac{[D]}{K_6} + \frac{[M]}{K_7}}} \qquad (3.150)$$

V. Desorption of glycerol as rate determining step (Equation 3.118)

$r_5 = k_9[\mathrm{GS}] - k_{10}[\mathrm{G}][\mathrm{S}]$ (Eq. 3.129)

From Equation (3.128), $[\mathrm{GS}] = \frac{K_4[MS][A]}{[B]}$

$$[\mathrm{GS}] = \frac{K_4[M][A][S]}{K_7[B]} (3.151)$$

$$r_5 = k_9 \frac{K_4[M][A][S]}{K_7[B]} - k_{10}[\mathrm{G}][\mathrm{S}] \qquad (3.152)$$

$$r_5 = (k_9 \frac{K_4[M][A]}{K_7[B]} - k_{10}[\mathrm{G}])\,[\mathrm{S}] \qquad (3.153)$$

$$[\mathrm{S}] = \frac{1}{1 + K_1[\mathrm{T}] + \frac{[B]}{K_6} + \frac{[D]}{K_7} + \frac{[M]}{K_8} + \frac{K_4[M][A]}{K_7[B]}} \qquad (3.154)$$

$$\boldsymbol{r_5} = \frac{\boldsymbol{k_9 \frac{K_4[M][A]}{K_7[B]} - k_{10}[G]}}{\boldsymbol{1 + K_1[\mathrm{T}] + K_2[\mathrm{T}] + \frac{[D]}{K_6} + \frac{[M]}{K_7} + \frac{K_4[M][A]}{K_7[B]}}} \qquad (3.155)$$

VI. Desorption of diglyceride as rate determine step (Equation 3.119)

$r_6 = k_{11}[\text{DS}] - k_{12}[\text{D}][\text{S}]$ (Eq. 3.131)

From Equation (3.124), $[\text{DS}] = \frac{K_2[TS][A]}{[B]}$

$$[\text{DS}] = \frac{K_1K_2[T][A][S]}{[B]} \quad (3.156)$$

$$r_6 = k_{11}\frac{K_1K_2[T][A][S]}{[B]} - k_{12}[\text{D}][\text{S}] \quad (3.157)$$

$$r_6 = (k_{11}\frac{K_1K_2[T][A]}{[B]} - k_{12}[\text{D}])\,[\text{S}] \quad (3.158)$$

$$[\text{S}] = \frac{1}{1 + K_1[\text{T}] + \frac{K_1K_2[T][A]}{[B]} + \frac{[M]}{K_7} + \frac{[G]}{K_5}} \quad (3.159)$$

$$\boldsymbol{r_6 = \frac{k_{11}\frac{K_1K_2[T][A]}{[B]} - k_{12}[\text{D}]}{1 + K_1[\text{T}] + \frac{K_1K_2[T][A]}{[B]} + \frac{[M]}{K_7} + \frac{[G]}{K_5}}} \quad (3.160)$$

VII. Desorption of monoglyceride as rate determining step (Equation 3.120)

$r_7 = k_{13}[\text{MS}] - k_{14}[\text{M}][\text{S}]$ (Eq. 3.133)

From Equation (3.126), $[\text{MS}] = \frac{K_3[DS][A]}{[B]}$

$$[\text{MS}] = \frac{K_8[D][A][S]}{K_6[B]} \quad (3.161)$$

$$r_7 = k_{13}\frac{K_8[D][A][S]}{K_6[B]} - k_{14}[\text{M}][\text{S}] \quad (3.162)$$

$$r_7 = (k_{13}\frac{K_8[D][A]}{K_6[B]} - k_{14}[\text{M}])\,[\text{S}] \quad (3.163)$$

$$\boldsymbol{r_7 = \frac{k_{13}\frac{K_8[D][A]}{K_6[B]} - k_{14}[\text{M}]}{1 + K_1[\text{T}] + \frac{K_8[D][A]}{K_6[B]} + \frac{[D]}{K_6} + \frac{[G]}{K_5}}} \quad (3.164)$$

The rate constants and equilibrium constants were determined using nonlinear regression analysis method adopted under LHHW mechanisms.

3.10.2 Determination of Activation Energy

The temperature dependent term (Activation energy) for the rate determining step (RDS) was calculated using well known Arrhenius equations given in Equation (3.165).

$$k = Ae^{\frac{-E_a}{RT}} \quad (3.165)$$

Linearization of Equation (3.165) resulted in Equation (3.166). A plot of *ln k* against *(1/T)* gives slope=*Ea/R* and intercept = *lnA.*

$$\ln k = \left(\frac{-E_a}{RT}\right) + \ln A \quad (3.166)$$

k = rate constant (the unit depends on the reaction order); A = pre-exponential factor (same unit as that of k); Ea = activation energy ($Jmol^{-1}$); R = gas constant (8.314 $Jmol^{-1}K^{-1}$); and T = temperature (K).

3.10.3Determination of conversion

The measured and predicted rates of reaction of rate determining step (RDS) obtained for both LHHW and ER model were used to determine conversions at various time intervals for the three temperatures under study using batch reactor rate equation as shown in Equation (3.167).

$$-\frac{dN_T}{dt} = -r_T V \quad (3.167)$$

$$N_T = N_{To}(1 - X) \quad (3.168)$$

$$\frac{N_{To}\, dX}{dt} = -r_T V \quad (3.169)$$

$$X = \int_0^t \left(\frac{V}{N_{To}}(-r_T)\right)dt \quad (3.170)$$

Where $-r_T = rateofdisapperanceoftriglyceride = r_3(LHHWRDS)\ or r_2\ (EileyRidealRDS)$

$N_T = molesoftriglycerideinthereactoratanytime$

$N_{To} = molesoftriglycerideinitiallyfedtothereactor$

V = volume of the batch reactor = 250mL

t = time

X = conversion

The Equation (3.170) was evaluated using trapezoidal rule (two-point) simplest numerical evaluation method of integral expressed in Equation 3.171.

$$X = \int_{t_o}^{t_1} f(t)dt = \frac{h}{2}\left[f(t_o) + f(t_1)\right] \quad (3.171)$$

$f(t) = \left(\frac{V}{N_{To}}(-r_T)\right)$ at t = t, $f(t_o) = \left(\frac{V}{N_{To}}(-r_T)\right)$ at t = 0 (3.172)

$$h = t_1 - t_o \quad (3.173)$$

3.11 Engine Test Analysis

The performance of the bio-diesel produced by the transesterification process was evaluated on a Perkins 4:108 Diesel engine mounted on a steady state engine test bed. The engine is four cylinders, water-cooled, naturally aspirated and 4-stroke compression ignition (CI) engine. The engine has the following specification represented in Table 3.5 and the set up is shown in Plates 3.1 and 3.2. The experiments were conducted with standard diesel fuel,

biodiesel and blends. The ambient temperature and pressure were noted. A short trial run was done in order to ensure that all essential accessories were in the working order before the actual test. The experiments for engine performance were carried out with different engine speeds ranging from 1400 to 2200rpm at constant load of 100kg. Because of the viscosities of APO and GSO methyl esters produced were within the ASTM acceptable limit for biodiesel, high blends of biodiesel-diesel (B20, B40, B60, B80 and B100) were used in the experiment. Precautionary measure taken was the warming of engine with pure diesel, until the cooling water temperature reached 80^{o}C. The engine was subjected to the above-mentioned speeds and load. The time taken for a given volume (50ml) of the fuel to be consumed at each speed was noted using stop watch. The manometer reading, the torque and exhaust temperature were measured. Then the brake power, brake specific fuel consumption (BSFC), and brake thermal efficiency were calculated.

Furthermore, the engine was reloaded with different loads (50, 100, 150, 200 and 250kg) at a constant speed of 2000rpm. The load on the engine was varied using the dynamometer loading wheel. The exhaust gases including NO_x, CO and HC were measured with a portable digital gas analyzer (Testo XL 450). The data of exhaust emissions were taken from the end of the pipe of the engine.

The fuel consumption is estimated by measuring the fuel consumed per unit time and the calculated values of the density of each blend using measured densities of biodiesel and diesel through Eqs. (3.174) and (3.175):

$$\dot{m}_f = \rho_b Q_f \qquad (3.174)$$

$$\rho_b = \sum \rho_i v_i \qquad (3.175)$$

Where $\dot{m}_f$= mass flow rate of the fuel, (kg/s), ρ_b= density of fuel, (kg/m^3), Q_f=volumetric flow rate of fuel, (m^3/s), ρ_i = density of biodiesel or diesel, (kg/m^3), v_i= composition of biodiesel or diesel, (%).

The brake power is calculated by measuring the engine speed and the engine torque and is given by Eq. (3.176). The specific consumption is defined as the ratio of the fuel consumption to the brake power, as shown in Eq. (3.177). The brake thermal efficiency is defined as the ratio of the brake power to the heat input for each blend, as shown in Eq. (3.178).

$$bp = \frac{TxN}{9549.3} (3.176)$$

$$BSFC = \frac{3600 x m_f}{bp} \quad (3.177)$$

$$n_{bt} = \frac{bp}{m_f x LHV} \times 100 \quad (3.178)$$

Where T= torque (N), N= engine speed (rpm), LHV= Lower Heating Value (J/kg).

The lower heating values of the biodiesel and its blends were found using a "bomb calorimeter.

Table 3.5: Engine Specifications

Components	Values
Type	Perkins 4:108
Bore	79.735mm
Stroke	80.9mm
Swept volume	1.76 L/cycle
Compression ratio	22:1
Maximum BHP	38 hp
Maximum speed	3000 rpm
Number of cylinder head	4
Diameter of exhaust	$1\frac{1}{2}''$
Length of exhaust pipe	$36'31''$
Dynamometer capacity	112 kW/150 hp
Dynamometer Max. Speed	7500 rpm
Power	(N_m x rev/min)/9549.305 (kW)
Fuel guage	50-100cc

Plate 3.1: Diesel Engine Test Bed in UNN

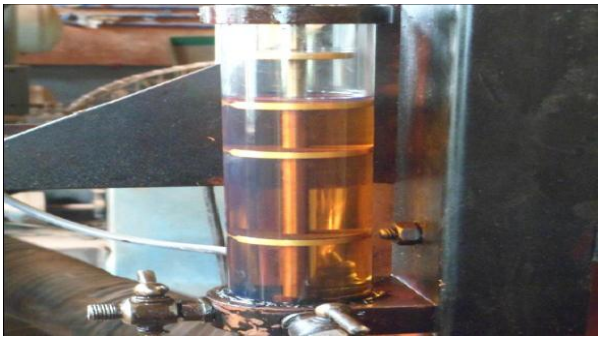

Plate 3.2: Fuel Gauge containing biodiesel blends

116

3.12Prediction of Engine Performance using Feed Forward Network Architecture

Artificial neural network was used to predict the engine performance of biodiesel produced from APO and GSO using TAC, AAC and BAC catalysts. The developed neural network models are feed forward multiplayer perceptron networks (MLP). The hidden units adopted the sigmoid activation function. The network model is shown in Figure 3.1.In the feed forward network shown in Figure 3.1, the output of the network is compared with the desired output. The difference between the output and the desired output is known as the error, E. ANNs learn by trying to minimize this error. The learning process uses optimisation algorithms such as gradient descent algorithm, genetic algorithm or some other natural optimisation algorithm. These algorithms work by adjusting the weights, W_i, such that the error, E, is minimized. Most ANNs use the simple gradient descent optimisation algorithm. In this work, the algorithm was adopted. This algorithm uses the supervised training technique where the network weights and biases are initialized randomly at the beginning of the training phase. The error minimization process is achieved using a gradual descent rule. There were two input and three output parameters in the experimental tests. The two input variables are engine speed in rpm and the percentage of biodiesel blending with the conventional diesel fuel. The three outputs for evaluating engine performance are Brake Power in kW, Specific Fuel Consumption (SFC) in kg/kWh and Brake Thermal Efficiency in %. Therefore the input layer consisted of two neurons which corresponded to engine speed and levels of biodiesel blends and the output layer had three neurons (Fig. 3.1). Hence, the learning process uses the sum of squares error criterion E to measure the effectiveness of the learning algorithm.

$$E = \frac{1}{2} Err^2 \equiv \frac{1}{2} (y - h_W(x))^2 \tag{3.179}$$

Where, y = Y= the true/experimental value

$$\hat{Y} = h_W(x) \tag{3.180}$$

$h_W(x)$ is the output of the perceptron.

The learning process, as previously mentioned, uses Cauchy's steepest descent or gradient descend algorithm optimisation method given by the formula:

$$W_j(t+1) = W_j(t) + \gamma \times \nabla E(W_j) \tag{3.181}$$

Here γ = non negative scalar that minimizes the function, $E(W_j)$, in the direction of the gradient and it is equal to the network learning rate.

While

$$\nabla E(W_j) = \frac{\partial E}{\partial W_j} \tag{3.182}$$

But

$$\frac{\partial E}{\partial W_j} = \frac{\partial E}{\partial Err} \times \frac{\partial Err}{\partial W_j} \tag{3.183}$$

Since

$$\frac{\partial E}{\partial Err} = Err \tag{3.184}$$

Hence,

$$\frac{\partial E}{\partial W_j} = Err \times \frac{\partial Err}{\partial W_j} \tag{3.185}$$

But

$$\frac{\partial Err}{\partial W_j} = \frac{\partial}{\partial W_j}\left(y - g\left(\sum_{j=1}^{n} W_j x_j\right)\right) \tag{3.186}$$

$$\frac{\partial Err}{\partial W_j} = -g'(in) \times x_j \tag{3.187}$$

Substituting equation (3.187) into equation (3.183), equation (3.188) is obtained:

$$\frac{\partial E}{\partial W_j} = -Err \times g'(in) \times x_j \tag{3.188}$$

$$W_j(t+1) = W_j(t) + \gamma \times Err \times g'(in) \times x_j \tag{3.189}$$

3.13 Modelling of Physical Properties of Biodiesel

Linear and multiple linear regressions (MLR) were employed to model the physical properties of biodiesel produced in this study. MLR is a multivariate statistical technique for examining the linear correlation between two or more independent variable and a single dependent variable. Linear dependence was developed to model physical properties of biodiesel produced from African pear oil (APO) and gmelina seed oil (GSO). Linear regression was carried out to fit the following linear equations with unknown coefficients.

For density

$$\rho = a_0 + a_1 x \tag{3.190}$$

Where ρ = density, x = fraction of biodiesel

For viscosity

$$\gamma = a_0 + a_1 x \quad (3.191)$$

$$\gamma = a_0 + a_1 T \quad (3.192)$$

Where γ = kinematics viscosity, x = fraction of biodiesel, T = temperature in Kelvin

For cetane number

$$CN = a_0 + a_1\rho + a_2\gamma + a_3 FP + a_4 LHV \quad (3.193)$$

Where CN is the cetane number, FP = flash point, LHV = lower heating value.

To predict the physical properties of biodiesel from blends and temperature, linear regression LR and multiple linear regression, MLR models were developed using polymath version 6.0 software by processing the full experimental data obtained in this work as shown in Appendix M. The developed models performances were justified by comparing their statistical values such as; root-mean-square error (RMSE) and coefficients of determination, (R-square).

CHAPTER FOUR

RESULTS AND DISCUSSION

4.1 Oil Yield of African Pear and Gmelina Seeds

African pear (*D. edulis*) and Gmeina oils extracted by solvent extraction using both n-hexane and petroleum etherwere liquid at room temperature. This implies that they could be classified as oil. The oil yield of both seeds using n-hexane and petroleum ether is presented in Table 4.1. The percentage oil yield of the African pear oil, APO was 53.1 and 52% using n-hexane and petroleum ether respectively and they fall within the range reported by Umoti and Okyi (1987). Umoti and Okyi (1987) in Isaac *et al*., (2014) gave the range of oil yield of African pear oil extracted by solvent extraction as 40 – 65% depending on the maturity of the fruits, while the range of yield obtained by press extraction was given as 25 – 49 %. It has been established that the oil content of African pear (*D. edulis*) varies from species to species (Isaac & Ekpa, 2009). The yield was also relatively higher than the yields reported for other nonedible seed oil like mangifera indica; 30.7% (Ogunsuyi, 2012) almond seed oil; 47%, (Ogunsuyi & Daramola,2013). The observed oil content of edulis was also found comparable to the yields of some edible oil such as soybeans 65% and cottonseed 60% (Rashid et al., 2009). The relatively high oil content of *Dacryodes* will encourage less dependence on edible oils as feedstock for biodiesel production, therefore promotes food security and food availability. Besides, the cost of producing biodiesel will be minimized, since the major feedstock is cheaply available, hence making biodiesel economically pleasant.

In addition, the oil yield of *gmelina arborea* seed (GSO) obtained using n-hexane and petroleum ether was found to be 51% and 50% respectively (Table 4.1). The oil content aresignificant and compare favourably with seed oil of other plants such as *Hevea brasiliensis* (51%wt), *Hematostaphis berter* (54.5%wt), *Jatropha curcas* (30-50%wt), *Sapindus mukorossi* (51%wt), *Mellia azadirachta* (33-45%wt), and 55-65% wt for *Simarouba glauca* (Basumatary et al., 2012). On the basis of the oil content, *gmelina arborea* seed would be highly suitable and economical for industrial applications, as any oil bearing seed that can produce up to 30% oil are regarded as suitable (Okolie et al., 2012). The oil content obtained in this study using both solvent (n-hexane and petroleum ether) is similar to the yield of oil obtained by Ricardo and Acquairus, (2008) and Uzoh and Onukwuli, (2014).

It could be observed that the oil content obtained from each seed using n-hexane and petroleum ether are very close and it implies that either of the solvent is efficient for extraction of oil from the seeds.

Table 4.1: Oil yield from African pear and Gmelina seeds using different solvents

Type of Seed Oil	n-hexane	Petroleum ether
APO Yield (%)	53.1	52
GSO Yield (%)	51	50

4.2 Statistical Analysis of Oil Extraction by Using Different Solvents

Minitab version 17 was employed to develop model, statistically analyze the model for the extraction of oil from both African pear and gmelina seeds using n-hexane and petroleum ether.

4.2.1 Statistical analysis of oil extraction from seeds using n-hexane and petroleum ether

Central composite design of response surface methodology in Minitab v.17 was used to develop models for extraction of oil from African pear seed and gmelina seed. The experimental design employed was a two-level-five factor fractional factorial design, involving 32 experiments. Extraction temperature, solvent/solute ratio, extraction time, particle size and agitation speed were selected as independent factors for the optimization study. The response chosen was the oil yield obtained from solvent extraction.The response surface design table for the oil extraction study is given in Table A1 of Appendix A. The models developed by the software in terms of coded values are shown in Equations 4.1, 4.2, 4.3 and 4.4 for the yield of APO by n-hexane, yield of GSO by n-hexane, yield of APO by petroleum ether and yield of GSO by petroleum ether respectively.

$$\text{Yield of APO by n} - \text{hexane} = 53.402 + 0.75\text{A} - 0.8167\text{B} + 0.2667\text{C} - 0.100\text{D} - 0.0833\text{E} - 0.500\text{AB} + 1.00\text{AC} - 0.250\text{AD} + 0.700\text{AE} - 2.050\text{BC} + 2.550\text{BD} + 0.750\text{BE} - 3.70\text{CD} - 0.250\text{CE} + 0.250\text{DE} - 3.4295\text{A}^2 - 6.9295\text{B}^2 - 3.9295\text{C}^2 - 5.1795\text{D}^2 - 6.9295\text{E}^2 \quad (4.1)$$

$$\text{Yield of GSO by n} - \text{hexane} = 50.616 - 0.20\text{A} - 0.883\text{B} - 0.408\text{C} - 0.033\text{D} + 0.133\text{E} + 0.388\text{AB} + 0.612\text{AC} + 0.988\text{AD} - 0.637\text{AE} + 0.825\text{BC} + 0.950\text{BD} + 0.825\text{BE} - 1.200\text{CD} - 1.325\text{CE} + 0.550\text{DE} - 2.741A^2 - 4.428B^2 - 2.866C^2 - 3.803D^2 - 4.553E^2 \quad (4.2)$$

$$\text{Yield of APO by petroleum ether} = 51.352 + 0.683\text{A} + 0.683\text{B} - 0.600\text{C} + 0.633\text{D} - 0.392\text{E} - 0.488\text{AB} + 0.550\text{AC} + 0.837\text{AD} + 0.113\text{AE} + 0.788\text{BC} + 1.00\text{BD} - 0.275\text{BE} + 0.563\text{CD} + 0.588\text{CE} + 1.250\text{DE} - 2.140A^2 - 1.977B^2 - 2.540C^2 - 2.227D^2 - 3.290E^2 \quad (4.3)$$

$$\text{Yield of GSO by petroleum ether} = 50.438 + 1.146\text{A} + 0.938\text{B} - 0.187\text{C} + 1.271\text{D} - 0.021\text{E} + 0.156\text{AB} + 0.344\text{AC} + 0.531\text{AD} + 0.469\text{AE} + 0.156\text{BC} + 0.719\text{BD} - 0.219\text{BE} - 1.469\text{CD} + 0.219\text{CE} + 0.906\text{DE} - 2.438A^2 - 3.813B^2 - 2.938C^2 - 2.687D^2 - 4.563E^2 \quad (4.4)$$

$$\text{WhereA} = \text{solventtosolidratio}\left(\frac{\text{mL}}{\text{g}}\right), \text{B} = \text{Time(Minutes)},$$

$$\text{C} = \text{Temperature}(^{\circ}\text{C}), \text{D} = \text{particlesize(mm)}, \quad \text{E} = \text{Agitationspeed (rpm)}$$

4.2.2 Adequacy analysis of the models

The analysis of variance for the model of the extraction process parameters are shown in Tables 4.2 – 4.5. The coefficient of determination and error standard deviation of the models are shown in Table 4.6.

Table 4.2: ANOVA for the model of Yield of APO by n – hexane (%)

Source	DF	Adj SS	Adj MS	F-Value	P-Value
Model	20	991.284	49.564	312.32	0.001
Linear	5	31.620	6.324	39.85	0.001
Square	5	852.124	170.425	1073.89	0.002
Interaction	10	107.540	10.754	67.76	0.003
Error	11	1.746	0.159		
Lack-of-Fit	6	0.537	0.090	0.37	0.871
Pure Error	5	1.208	0.242		
Total	31	993.030			

Table 4.3: ANOVA for the model of Yield of GSO by n – hexane (%)

Source	DF	Adj SS	Adj MS	F-Value	P-Value
Model	20	1727.47	86.373	95.91	0.002
Linear	5	24.14	4.828	5.36	0.010
Square	5	1580.63	316.125	351.01	0.001
Interaction	10	122.70	12.270	13.62	0.003
Error	11	9.91	0.901		
Lack-of-Fit	6	0.57	0.096	0.05	0.999
Pure Error	5	9.33	1.867		
Total	31	1737.37			

Table 4.4: ANOVA for the model of Yield of APO by petroleum ether (%)

Source	DF	Adj SS	Adj MS	F-Value	P-Value
Model	20	813.846	40.692	124.03	0.001
Linear	5	44.362	8.872	27.04	0.020
Square	5	686.699	137.340	418.60	0.002
Interaction	10	82.785	8.279	25.23	0.004
Error	11	3.609	0.328		
Lack-of-Fit	6	0.276	0.046	0.07	0.997
Pure Error	5	3.333	0.667		
Total	31	817.455			

Table 4.5: ANOVA for the model of Yield of GSO by petroleum ether(%)

Source	DF	Adj SS	Adj MS	F-Value	P-Value
Model	20	1448.62	72.431	127.48	0.002
Linear	5	92.22	18.444	347.42	0.010
Square	5	1288.24	257.648	453.46	0.003
Interaction	10	68.16	6.816	12.00	0.001
Error	11	6.25	0.568		
Lack-of-Fit	6	0.75	0.125	0.11	0.990
Pure Error	5	5.50	1.100		
Total	31	1454.87			

Table 4.6: Coefficients of determination and ESD for the models

Responses	S	R-sq	R-sq(adj)
Yield of APO by n – hexane (%)	0.398370	99.82	95.34
Yield of GSO by n – hexane (%)	0.949006	99.43	99.13
Yield of APO by petroleum ether (%)	0.572793	99.56	99.07
Yield of GSO by petroleum ether (%)	0.753778	99.57	98.46

From Tables4.2 – 4.5, it could be observed that the coefficient of determination and error standard deviation of the models indicate that the models fit the data. This could beas a result of the interaction and square terms that improved the adequacy of the models.

Test of significance of individual terms in the models are shown in Tables 4.7 to 4.10 and it was carried out at 95% level of confidence or 5% significance level. Individual terms in the model are said to be statistically significant to the responses if $P - val < 0.05$ and therefore, those statistically insignificant terms were eliminated from the model as shown in Equations 4.6 – 4.9.

Table 4.7: Effects and coefficients for model of Yield of APO by n − hexane (%)

Term	Effect	Coef	SE Coef	T-Value	P-Value
Constant		53.402	0.159	336.09	0.001
A	1.5000	0.7500	0.0813	9.22	0.001
B	-1.6333	-0.8167	0.0813	-10.04	0.001
C	0.5333	0.2667	0.0813	3.28	0.007
D	-0.2000	-0.1000	0.0813	-1.23	0.024
E	-0.1667	-0.0833	0.0813	-1.02	0.032
A^2	-3.4295	-0.3851	0.0645	-5.97	0.001
B^2	0.6965	0.3482	0.0645	5.40	0.001
C^2	-1.4266	-0.7133	0.0645	-11.06	0.003
D^2	-1.1989	-0.5994	0.0645	-9.29	0.002
E^2	0.3767	0.1883	0.0645	2.92	0.007
A*B	0.1513	0.0756	0.0879	0.86	0.398
A*C	-0.3200	-0.1600	0.0879	-1.82	0.080
A*D	0.0675	0.0337	0.0879	0.38	0.704
A*E	0.4100	0.2050	0.0879	2.33	0.028
B*C	-0.0425	-0.0212	0.0879	-0.24	0.811
B*D	1.3675	0.6838	0.0879	7.78	0.002
B*E	-0.3950	-0.1975	0.0879	-2.25	0.033
C*D	0.0412	0.0206	0.0879	0.23	0.816
C*E	-0.5837	-0.2919	0.0879	-3.32	0.003
D*E	-0.1537	-0.0769	0.0879	-0.87	0.390

Table 4.8: Effects and coefficients for model of Yield of GSO by n – hexane (%)

Term	Effect	Coef	SE Coef	T-Value	P-Value
Constant		50.616	0.379	133.72	0.001
A	-0.400	-0.200	0.194	-1.03	0.032
B	-1.767	-0.883	0.194	-4.56	0.001
C	-0.817	-0.408	0.194	-2.11	0.039
D	-0.067	-0.033	0.194	-0.17	0.047
E	0.267	0.133	0.194	0.69	0.026
A^2	-5.482	-2.741	0.175	-15.64	0.001
B^2	-8.857	-4.428	0.175	-25.27	0.001
C^2	-5.732	-2.866	0.175	-16.36	0.001
D^2	-7.607	-3.803	0.175	-21.71	0.001
E^2	-9.107	-4.553	0.175	-25.99	0.001
A*B	0.775	0.388	0.237	1.63	0.131
A*C	1.225	0.612	0.237	2.58	0.026
A*D	1.975	0.988	0.237	4.16	0.002
A*E	-1.275	-0.637	0.237	-2.69	0.021
B*C	1.650	0.825	0.237	3.48	0.005
B*D	1.900	0.950	0.237	4.00	0.002
B*E	1.650	0.825	0.237	3.48	0.005
C*D	-2.400	-1.200	0.237	-5.06	0.002
C*E	-2.650	-1.325	0.237	-5.58	0.004
D*E	1.100	0.550	0.237	2.32	0.041

Table 4.9: Effects and coefficients for model of Yield of APO by petroleum ether (%)

Term	Effect	Coef	SE Coef	T-Value	P-Value
Constant		51.352	0.228	224.77	0.001
A	1.367	0.683	0.117	5.84	0.002
B	1.367	0.683	0.117	5.84	0.001
C	-1.200	-0.600	0.117	-5.13	0.003
D	1.267	0.633	0.117	5.42	0.001
E	-0.783	-0.392	0.117	-3.35	0.006
A^2	-4.280	-2.140	0.106	-20.23	0.001
B^2	-3.955	-1.977	0.106	-18.70	0.001
C^2	-5.080	-2.540	0.106	-24.01	0.001
D^2	-4.455	-2.227	0.106	-21.06	0.001
E^2	-6.580	-3.290	0.106	-31.11	0.001
A*B	-0.975	-0.488	0.143	-3.40	0.006
A*C	1.100	0.550	0.143	3.84	0.003
A*D	1.675	0.837	0.143	5.85	0.000
A*E	0.225	0.113	0.143	0.79	0.449
B*C	1.575	0.788	0.143	5.50	0.002
B*D	2.000	1.000	0.143	6.98	0.001
B*E	-0.550	-0.275	0.143	-1.92	0.081
C*D	1.125	0.563	0.143	3.93	0.002
C*E	1.175	0.588	0.143	4.10	0.002
D*E	2.500	1.250	0.143	8.73	0.003

Table 4.10: Effects and coefficients for model of Yield of GSO by petroleum ether(%)

Term	Effect	Coef	SE Coef	T-Value	P-Value
Constant		50.438	0.301	167.76	0.000
A	2.292	1.146	0.154	7.45	0.000
B	1.875	0.938	0.154	6.09	0.000
C	-0.375	-0.187	0.154	-1.22	0.248
D	2.542	1.271	0.154	8.26	0.000
E	-0.042	-0.021	0.154	-0.14	0.895
A^2	-4.875	-2.438	0.139	-17.51	0.000
B^2	-7.625	-3.813	0.139	-27.39	0.000
C^2	-5.875	-2.938	0.139	-21.11	0.000
D^2	-5.375	-2.687	0.139	-19.31	0.000
E^2	-9.125	-4.563	0.139	-32.78	0.000
A*B	0.313	0.156	0.188	0.83	0.425
A*C	0.687	0.344	0.188	1.82	0.095
A*D	1.062	0.531	0.188	2.82	0.017
A*E	0.938	0.469	0.188	2.49	0.030
B*C	0.312	0.156	0.188	0.83	0.425
B*D	1.438	0.719	0.188	3.81	0.003
B*E	-0.438	-0.219	0.188	-1.16	0.270
C*D	-2.938	-1.469	0.188	-7.79	0.000
C*E	0.438	0.219	0.188	1.16	0.270
D*E	1.813	0.906	0.188	4.81	0.001

The reduced empirical relationships between the factors and responses developed and analysed using the MINITAB 17 are shown in Equations (4.5), (4.6), (4.7) and (4.8) for the yield of APO by n − hexane, yield of GSO by n − hexane, yield of APO by petroleum ether and yield of GSO by petroleum ether of the oil extraction process respectively.

$$\text{Yield of APO by n} - \text{hexane} = 53.402 + 0.75\text{A} - 0.8167\text{B} + 0.2667\text{C} - 0.100\text{D} - 0.0833\text{E} + 0.700\text{AE} + 2.550\text{BD} + 0.750\text{BE} - 0.250\text{CE} - 3.4295A^2 - 6.9295B^2 - 3.9295C^2 - 5.1795D^2 - 6.9295E^2 \quad (4.5)$$

$$\text{Yield of GSO by n} - \text{hexane} = 50.616 - 0.20\text{A} - 0.883\text{B} - 0.408\text{C} - 0.033\text{D} + 0.133\text{E} + 0.612\text{AC} + 0.988\text{AD} - 0.637\text{AE} + 0.825\text{BC} + 0.950\text{BD} + 0.825\text{BE} - 1.200\text{CD} - 1.325\text{CE} + 0.550\text{DE} - 2.741A^2 - 4.428B^2 - 2.866C^2 - 3.803D^2 - 4.553E^2 \quad (4.6)$$

$$\text{Yield of APO by petroleum ether} = 51.352 + 0.683\text{A} + 0.683\text{B} - 0.600\text{C} + 0.633\text{D} - 0.392\text{E} - 0.488\text{AB} + 0.550\text{AC} + 0.837\text{AD} + 0.113\text{AE} + 0.788\text{BC} + 1.00\text{BD} - 0.275\text{BE} + 0.563\text{CD} + 0.588\text{CE} + 1.250\text{DE} - 2.140A^2 - 1.977B^2 - 2.540C^2 - 2.227D^2 - 3.290E^2 \quad (4.7)$$

$$\text{Yield of GSO by petroleum ether} = 50.438 + 1.146\text{A} + 0.938\text{B} - 0.187\text{C} + 1.271\text{D} - 0.021\text{E} + 0.344\text{AC} + 0.531\text{AD} + 0.719\text{BD} - 1.469\text{CD} + 0.906\text{DE} - 2.438A^2 - 3.813B^2 - 2.938C^2 - 2.687D^2 - 4.563E^2 \quad (4.8)$$

The models adequacy were confirmed graphically using the residual plots which include the normal probability plot, histogram, residual versus fitted values and residual versus observation order in a 4-in-1 format as shown in Figures 4.1– 4.4. An analytical view of the figures shows the adequacy of the models and the plots of the normal probability tend to fall in a straight line and residuals were uniformly distributed. Hence, the models were adequate and statistically fit the data with little outliers and reduced skewness. Figure 4.1 shows that the residuals or the errors for APO extraction using nhexane were uniformly distributed but occurred more at the negative values while Figure 4.2 shows that the residuals or errors for GSO extraction using nhexane were also uniformly distributed with lesser errors.This suggests that n-hexane performed better in extraction of GSO. Similarly, Figure 4.3 shows that the residuals or the errors for APO extraction using petroleum ether were uniformly distributed but occurred more at the positive valueswhile Figure 4.4 shows that the residuals or errors for GSO extraction using petroleum ether were also uniformly distributed with more errors indicating that pethroleum ether performed better in extraction of APO.

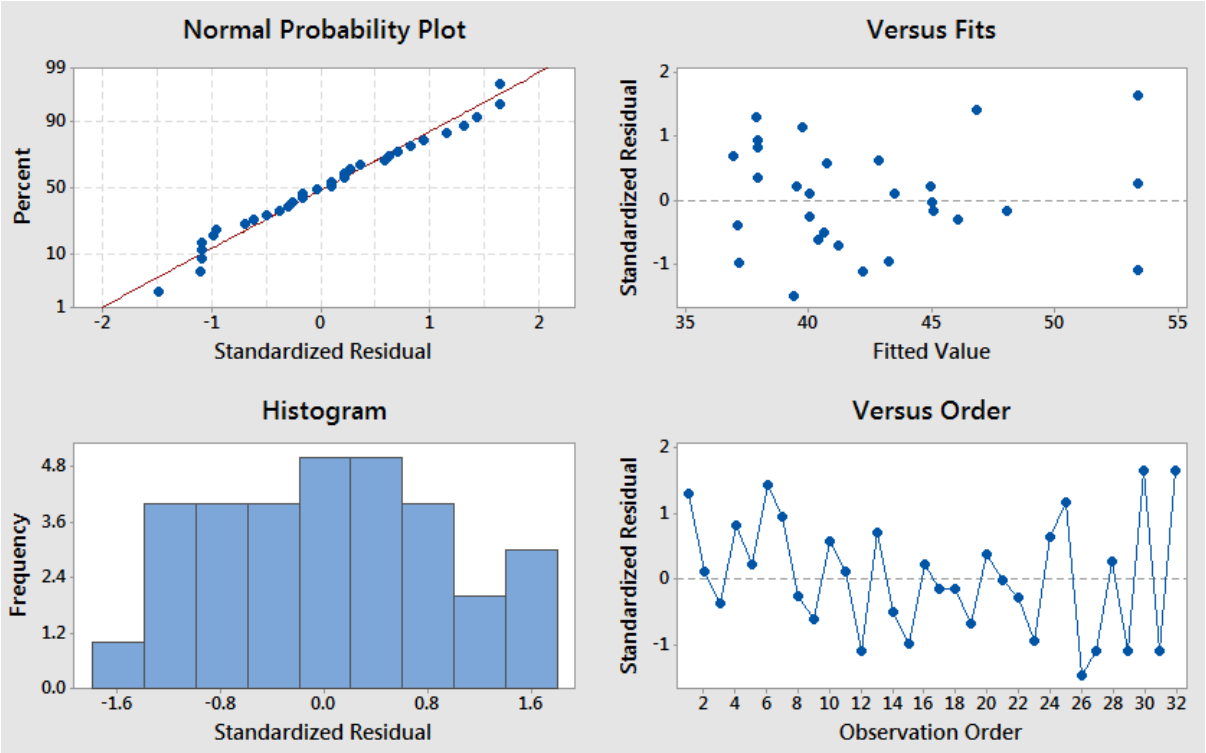

Figure 4.1: Residual plots for the model of the yield of APO with n-hexane.

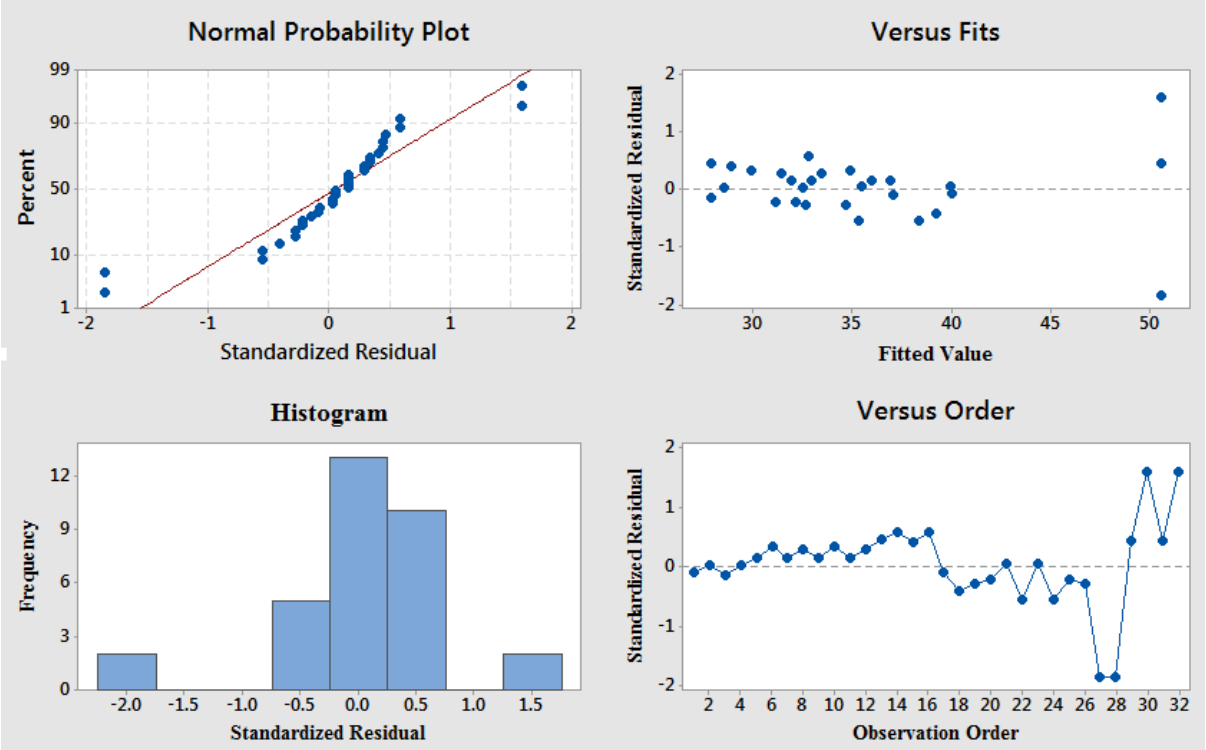

Figure 4.2: Residual plots for model of the yield of GSO with n-hexane.

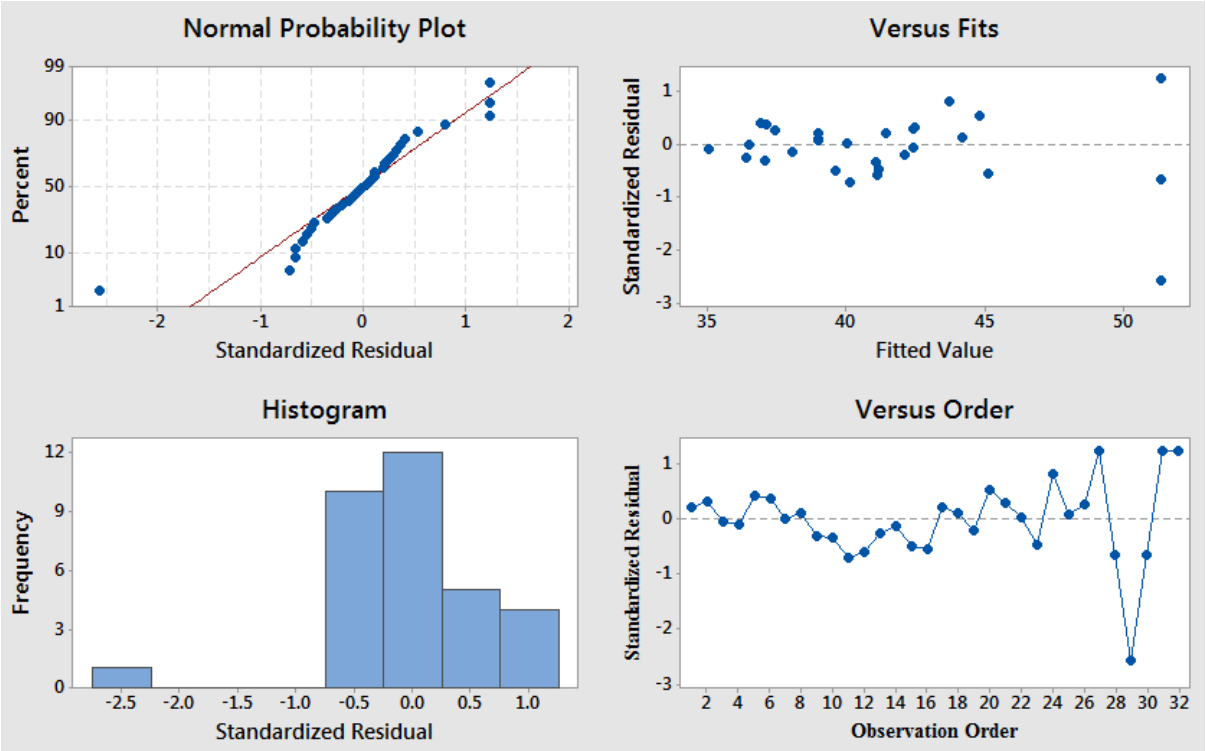

Figure 4.3: Residual plots for model of the yield of APO with petroleum ether.

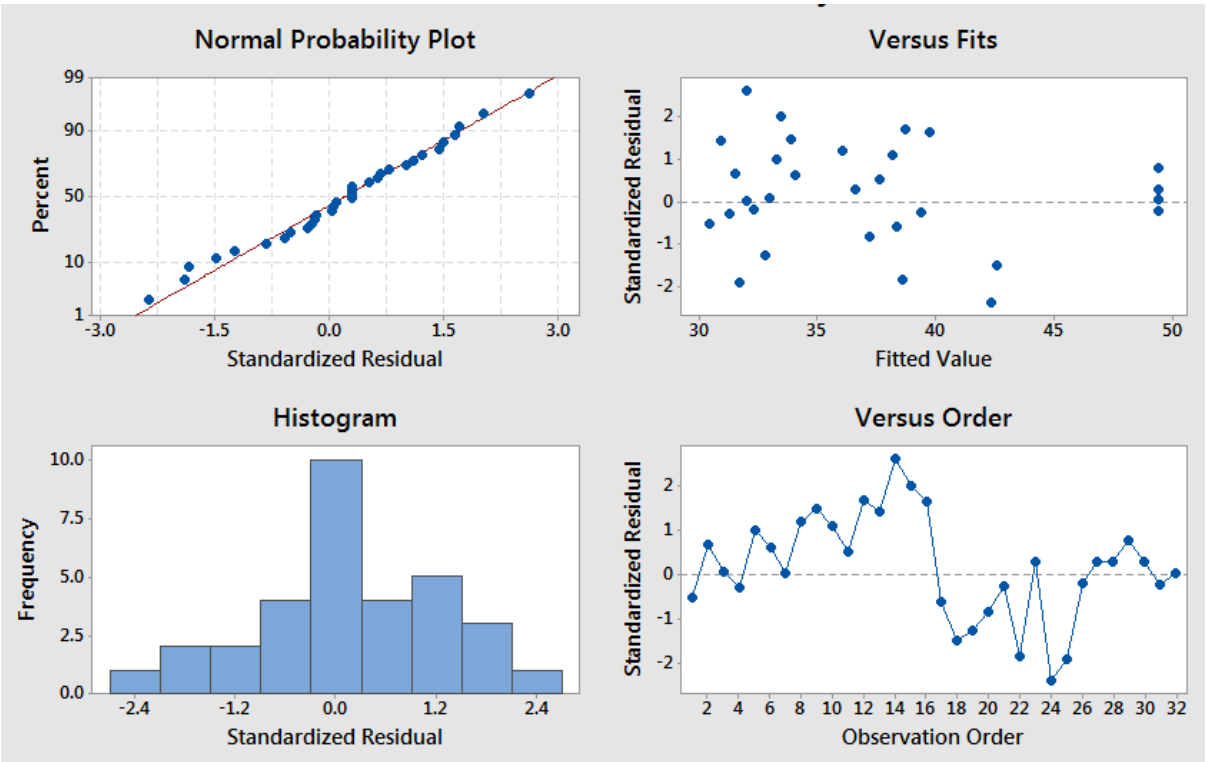

Figure 4.4: Residual plots for model of yield of GSO with petroleum ether.

4.2.3 Surface response plots of the model

Optimization using the contour and surface plots can be used to estimate the optimal relationship between each of the responses and any combination of the factors. Only statistically significant terms were considered in the plots and the topography of each plot indicates the effect each factor pair has on the response with other factors kept constant. The response surface plots are used to describe the potential relationship between five variables. The predictors are plotted in the x- axis and y- axis while the response variable is represented in the z- axis. The contour plots can be represented with shaded area or contour lines as shown in the figures.

The response surface plots for the various factors/predictor pairs and APO yield and GSO yield with n-hexane are shown in Figures 4.5 to 4.17. These show minimax response surface pattern. The desirable response is obtained at the factor pair values or range where the value of APO and GSO yields are optimal. From Figures 4.5, 4.7, 4.8, 4.9, 4.10, 4.11, 4.12 and 4.16, it can be observed that as the factor pairs increase the yield increases and decreased after the midpoint therefore desirable response of optimal oil yield with n-hexane is obtained at the centre point values of time, temperature, solvent/solid ratio and agitation speed respectively while the yield of oil decreased as particle size increases as shown in Figures 4.6, 4.13, 4.15 and 4.17.

Figures 4.5 and 4.11 show the interaction effect of solvent/solute ratio and agitation speed on the yields of APO and GSO extracted with n-hexane respectively. It could be observed from the figure that as both solvent/solute ratio and agitation speed increase, the yield of the oil increased but decreased beyond 1.6mL/g and 200rpm. This reduction in yield may be attributed to the fact that the quadratic terms of the two factors are more significant with a negative effect (Eqs. 4.5, 4.6).

Figures 4.6 and 4.13 present the interaction effect of time and particle size on the yield of APO and GSO extracted with n-hexane respectively. It could be observed from the figure that the oil yield increases as time increases and particle size decreases.This may be attributed to large surface area of the seed exposed for oil extraction at smaller particle size.

Figures 4.7 and 4.14 show the interaction effect of time and agitation speed on the yields of APO and GSO extracted with n-hexane respectively. It could be observed from the figure that as both time and agitation speed increase, the yield of the oil increased but decreased when time and agitation speed were beyond 50minutes and 200rpm respectively. This reduction in yield may be attributed to the fact that the quadratic terms of the two factors are more significant with a negative effect (Eqs. 4.5, 4.6).

Figures 4.8 and 4.16 show the interaction effect of temperature and agitation speed on the yields of APO and GSO extracted with n-hexane respectively. It could be observed from the figure that as both temperature and agitation speed increase, the yield of the oil increased but decreased when temperature and speed were beyond 60^{o}C and 200rpm respectively. This reduction in the oil yield at high temperature may be attributed to the evaporation of the solvent at higher temperature above its boiling point.

Figure 4.9 shows the interaction effect of temperature and solvent/solute ratio on the yield of GSO extracted with n-hexane. It could be observed from the figure that as both temperature and agitation speed increase, the yield of the oil increased but decreased when temperature and speed were beyond 60^{o}C and 1.6ml/g respectively. This reduction in the oil yield at high temperature may be attributed to the evaporation of the solvent at higher temperature above its boiling point.

Figure 4.10 presents the interaction effect of solvent/solute ratio and particle size on the yield of GSO extracted with n-hexane. It could be observed from the figure that the oil yield increases as solvent/solute ratio increases and particle size decreases. This may be attributed to large surface area of the seed exposed for oil extraction at smaller particle size.

Figure 4.12 depicts the interaction effect of time and temperature on the yield of GSO extracted with n-hexane. It could be observed from the figure that the oil yield increases as

both time and temperature increase the yield of the oil increased but decreased when time and temperature were beyond 60minutes and 60^{o}C respectively. This reduction in the oil yield at high temperature may be attributed to the evaporation of the solvent at higher temperature above its boiling point and negative effect of their quadratic terms (Eqs. 4.5, 4.6).

Figure 4.15 present the interaction effect of temperature and particle size on the yield of GSO extracted with n-hexane. It could be observed from the figure that the oil yield increases as temperature increases and particle size decreases. This may be attributed to large surface area of the seed exposed for oil extraction at smaller particle size.

Figure 4.17 present the interaction effect of agitation speed and particle size on the yield of GSO extracted with n-hexane. It could be observed from the figure that the oil yield increases as speed of agitation increases and particle size decreases. This may be attributed to large surface area of the seed exposed for oil extraction at smaller particle size.

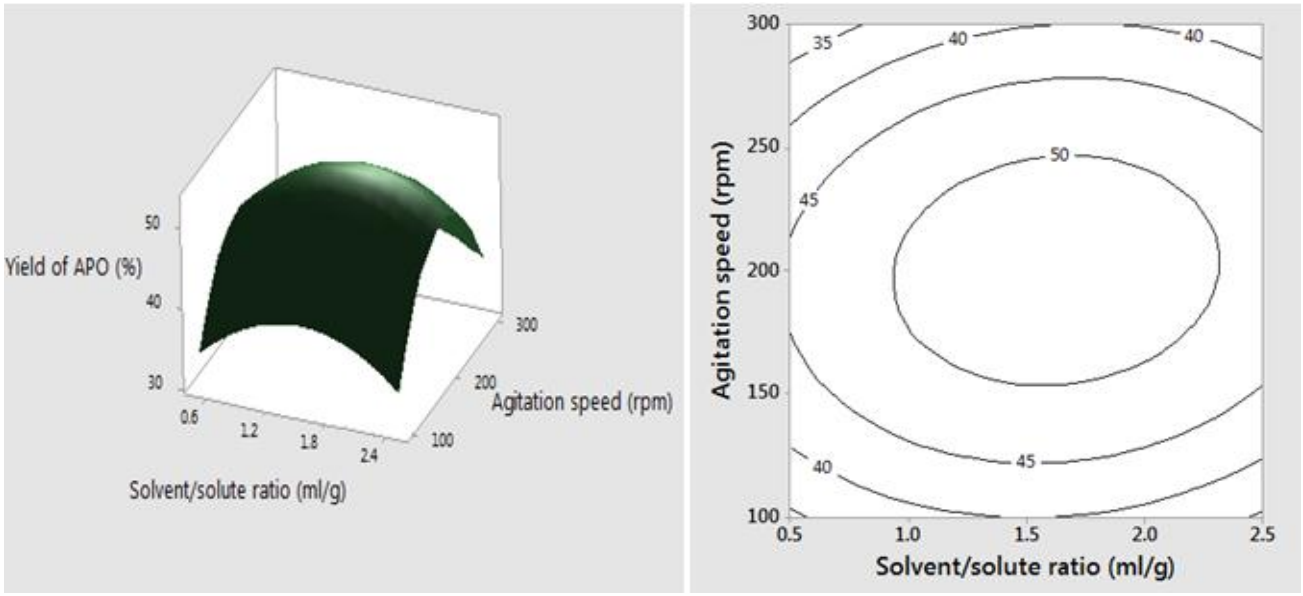

Figure 4.5: Response surface plots of APOyield (%) with n-hexane against solvent/solid ratio (A) (mL/g) and agitation speed, (E) (rpm).

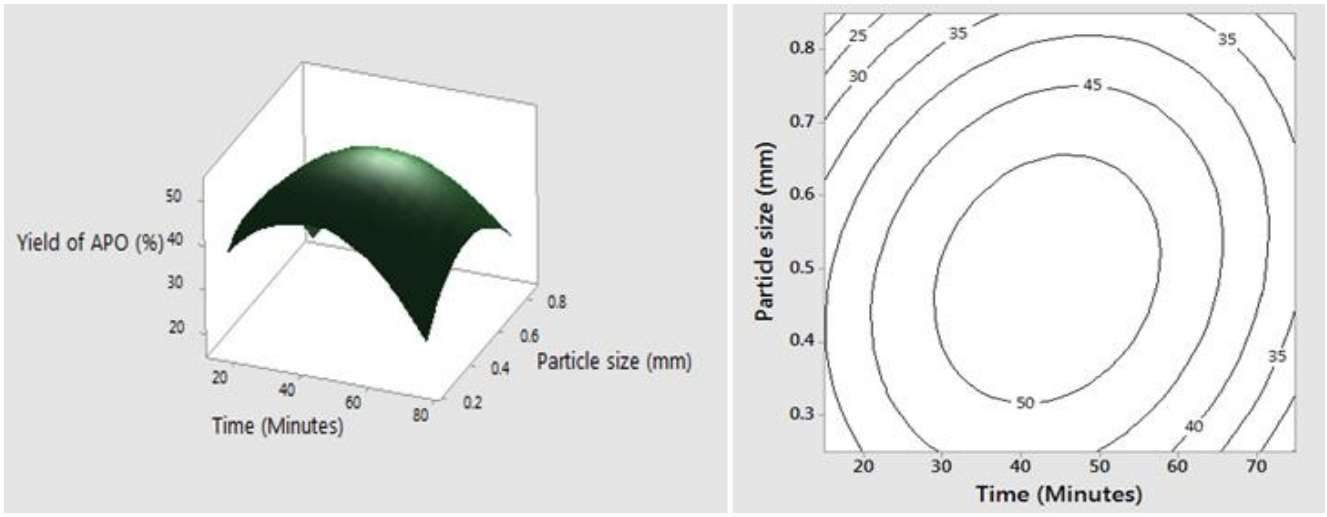

Figure 4.6: Response surface plots of APOyield (%) with n-hexane against time (B) (Minutes) and particle size, (D) (mm).

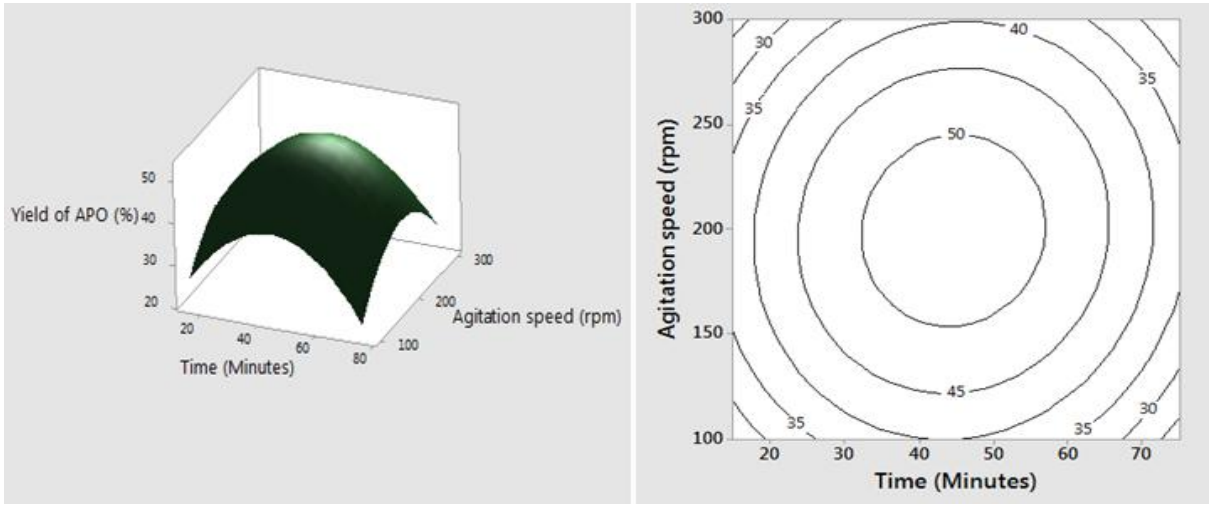

Figure 4.7: Response surface plots of APOyield (%) with n-hexane against time (B) (Minutes) and agitation speed, (E) (rpm).

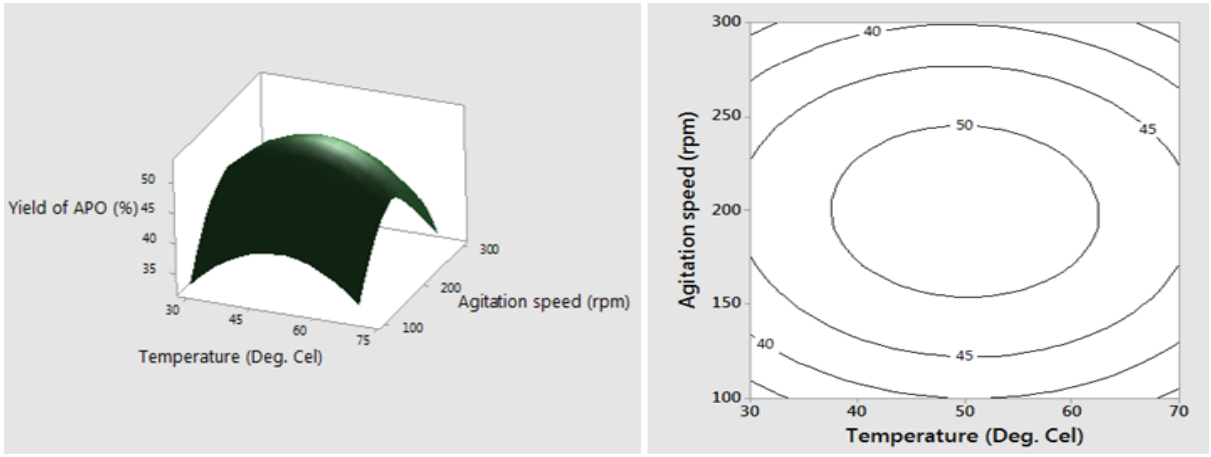

Figure 4.8: Response surface plots of APOyield(%) with n – hexane against temperature (C) (^{o}C) and agitation speed, (E) (rpm).

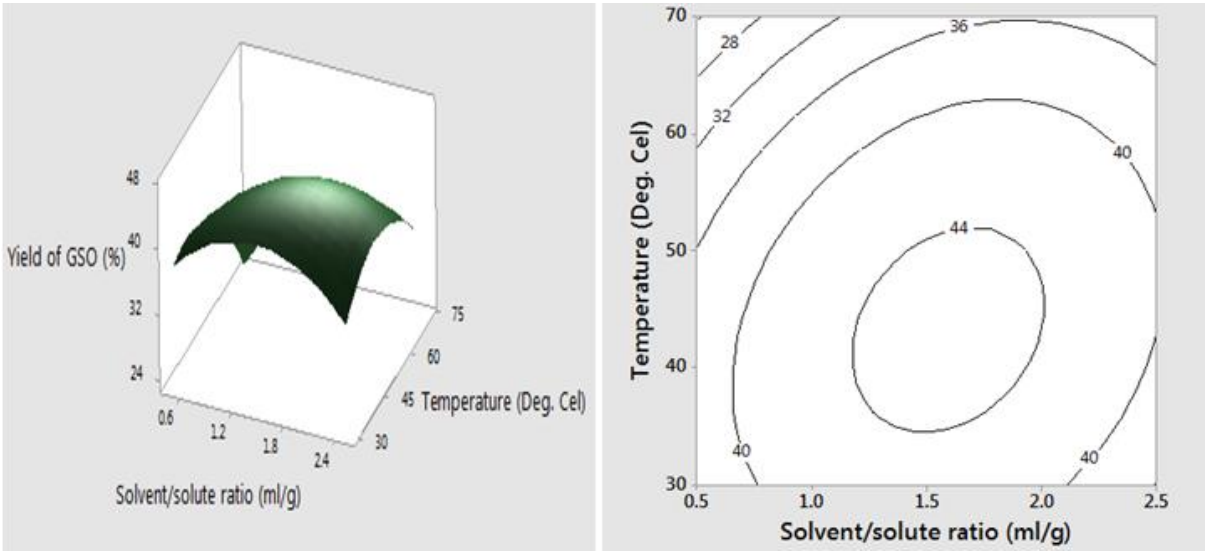

Figure 4.9: Response surface plots ofGSOyield(%) with n − hexaneagainst solvent/solid ratio (A) (mL/g) and temperature, (C) (^{o}C).

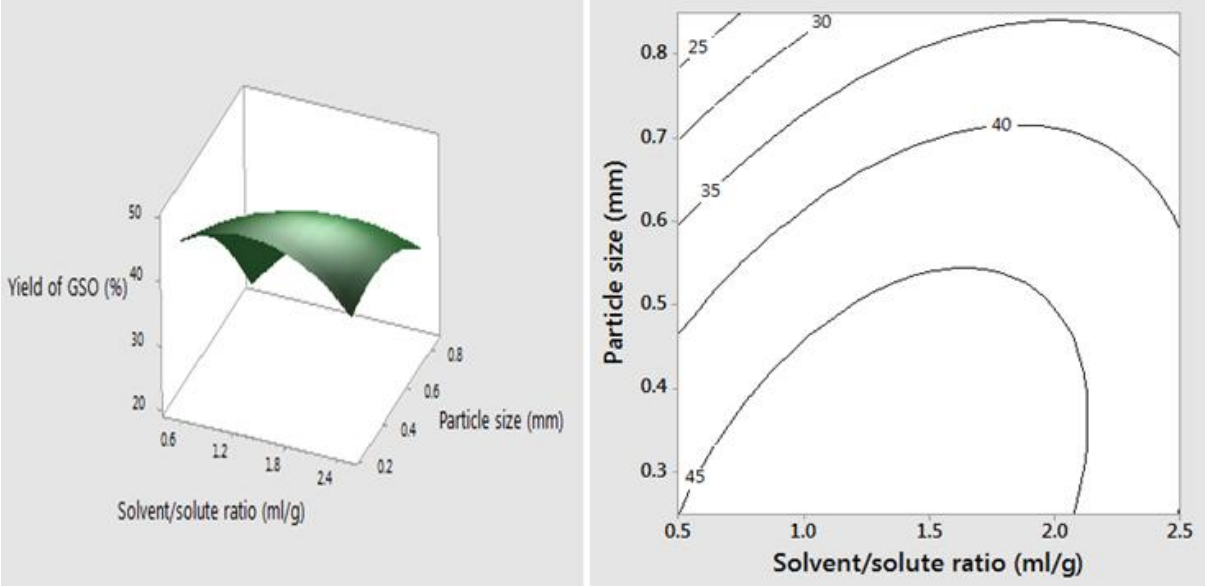

Figure 4.10: Response surface plots of GSOyield (%) with n-hexane against solvent/solid ratio (A) (mL/g) and particle size, (D) (mm).

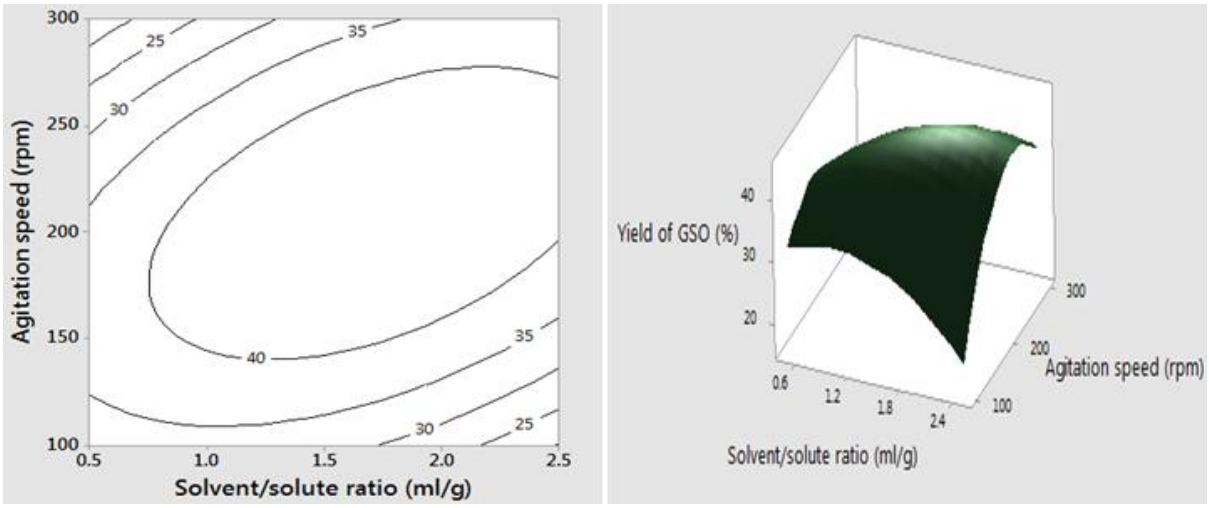

Figure 4.11: Response surface plots of GSOyield(%) with n – hexane against solvent/solid ratio (A) (mL/g) and agitation speed, (E) (rpm).

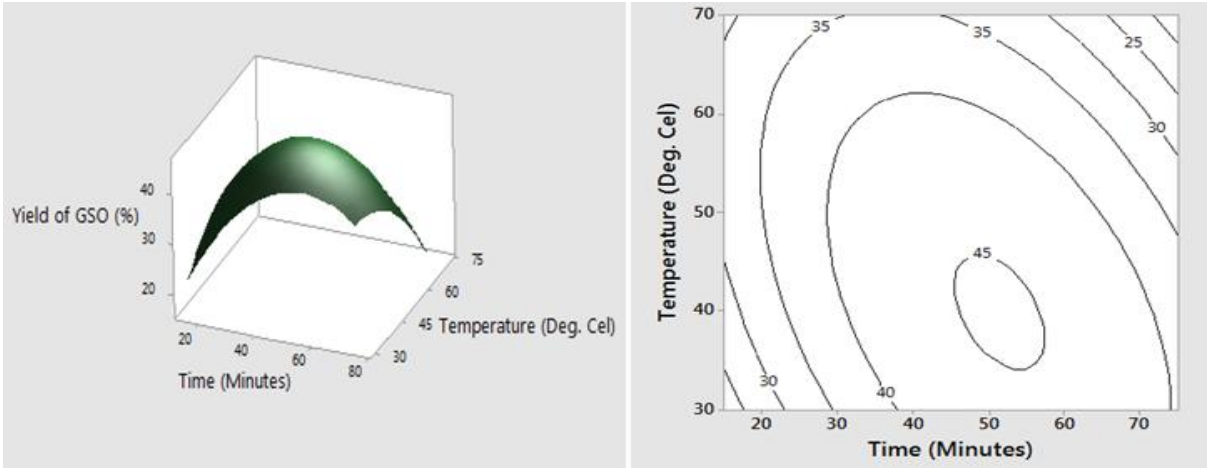

Figure 4.12: Response surface plots of GSOyield(%) with n – hexane against time (B) (Minutes) and temperature, (C)(^{o}C).

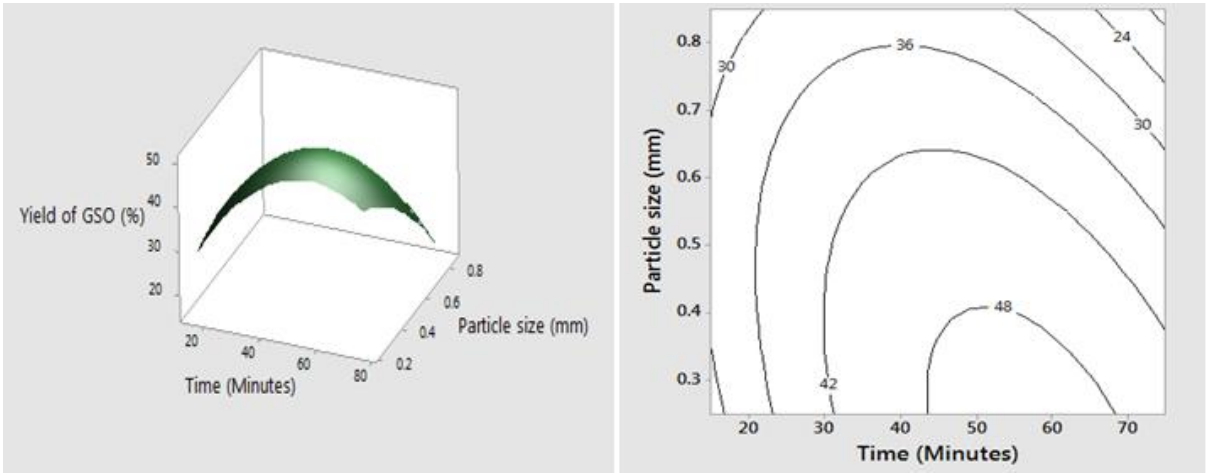

Figure 4.13: Response surface plots of GSOyield(%) with n – hexane against time (B) (Minutes) and particle size, (D) (mm).

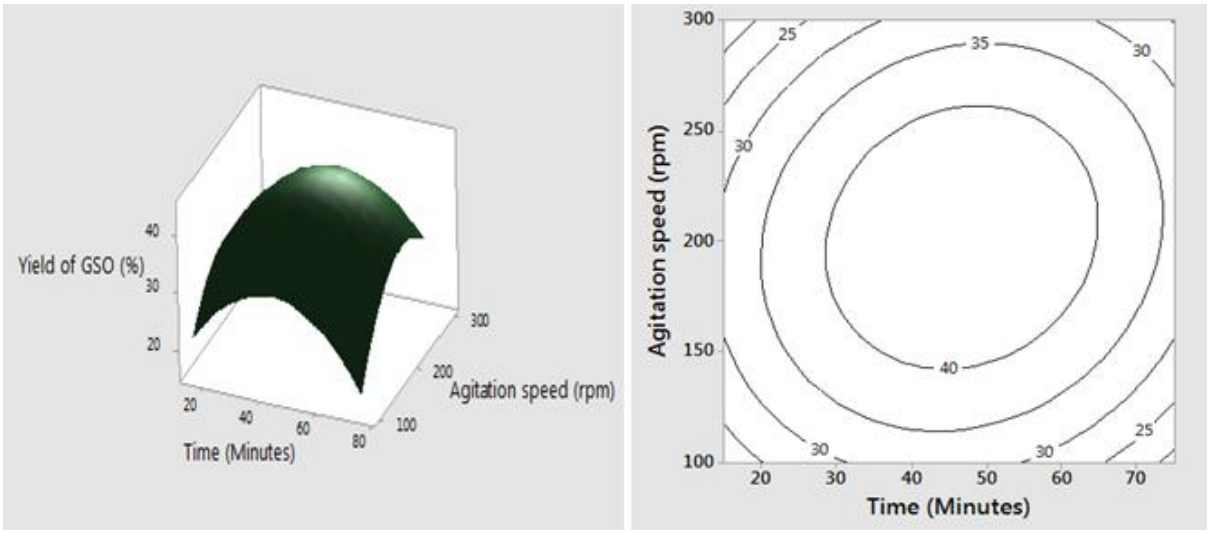

Figure 4.14: Response surface plots of GSOyield(%) with n − hexane against time (B) (Minutes) and agitation speed, (E) (rpm).

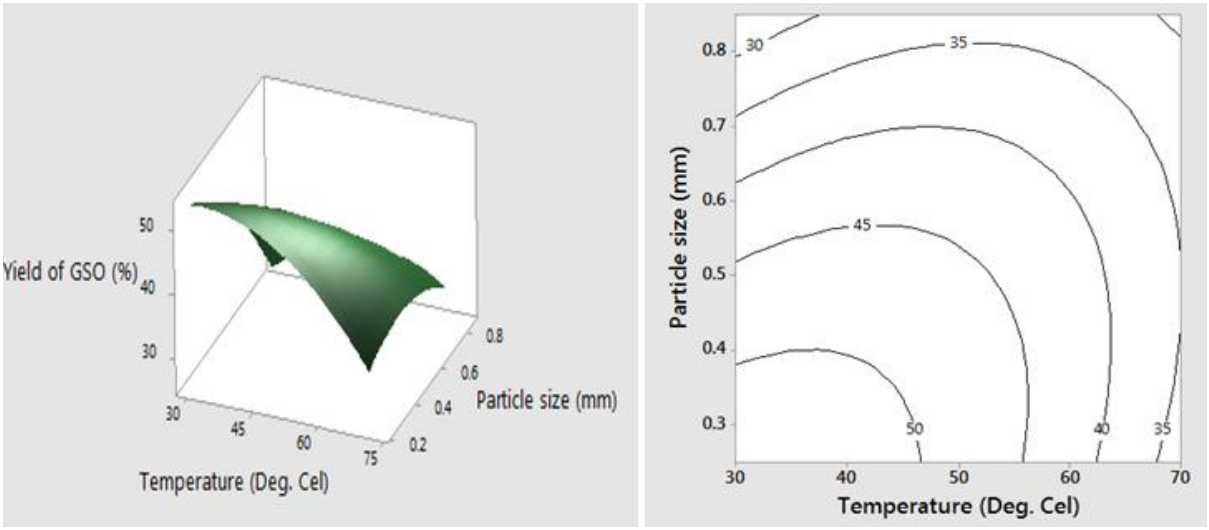

Figure 4.15: Response surface plots of GSOyield(%) with n − hexane against temperature (C) (^{o}C) and particle size, (D) (mm).

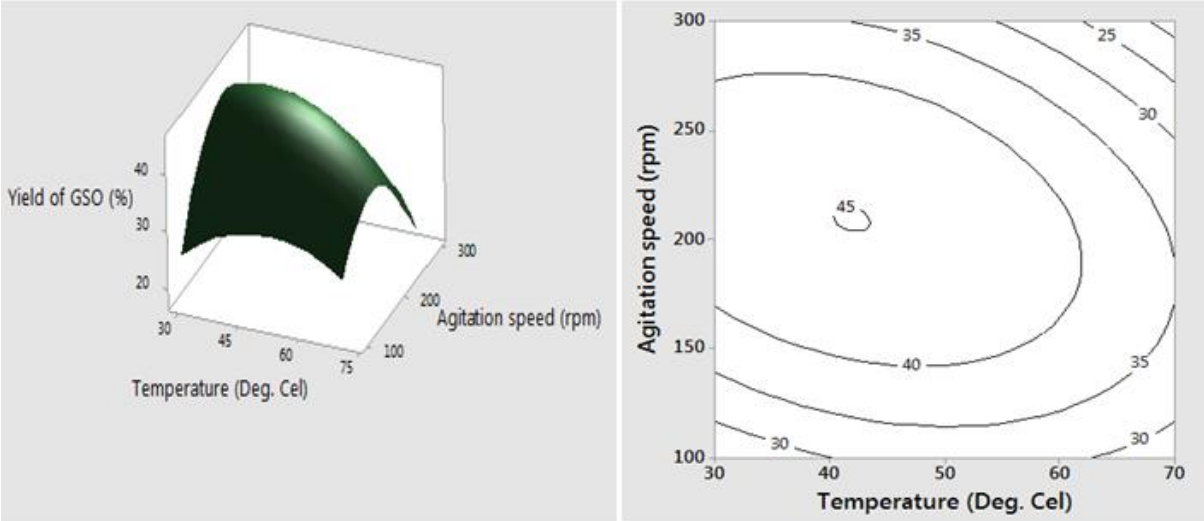

Figure 4.16: Response surface plots of GSOyield(%) with n – hexaneagainst temperature (C) (^{o}C) and agitation speed, (E) (rpm).

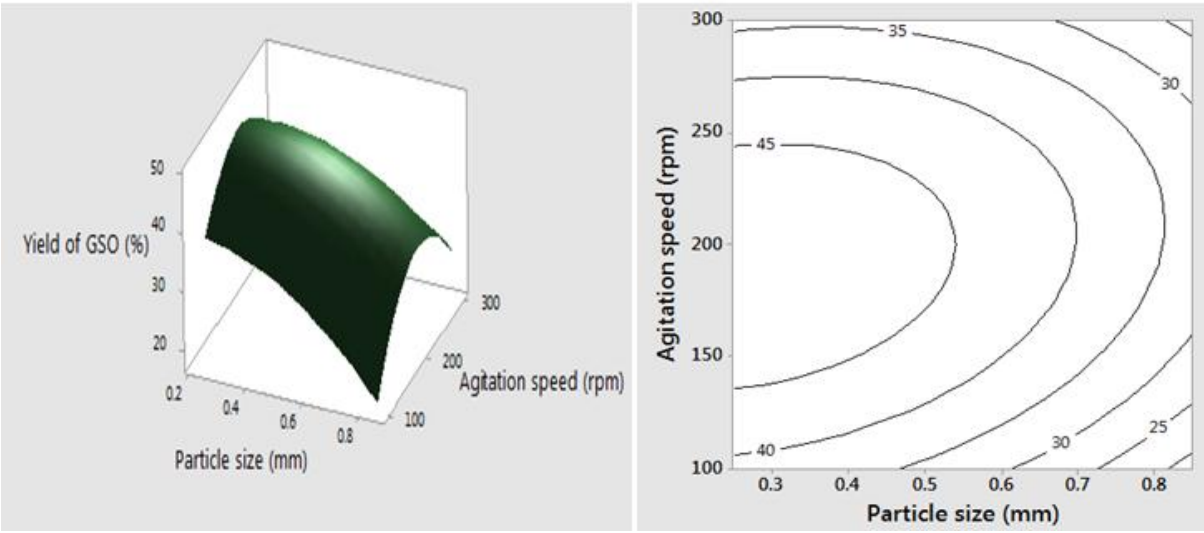

Figure 4.17: Response surface plots of GSOyield(%) with n – hexane against particle size (D) (mm) and agitation speed, (E) (rpm).

Response surface plots for the various pair of predictor variables and the APO yield and GSO yield with petroleum ether are shown in Figures 4.18 to 4.32. The desirable response is the factor pair which maximises the oil yield. Similarly as discussed for extraction of oil using n-hexane, it is observed from Figures 4.18, 4.19, 4.21, 4.22, and 4.26that the factor pairs increase as the yield increases and decreased after the midpoint therefore desirable response of optimal oil yield with petroleum ether is obtained at the centre point values of time, temperature, solvent/solid ratio and agitation speed respectively while the yield of oil decreased as particle size increases as shown in Figures 4.20, 4.23, 4.25, 4.27, 4.29, 4.30, 4.31 and 4.32.

Figures 4.18 shows the interaction effect of solvent/solute ratio and time on the yield of APO extracted with petroleum ether. It could be observed from the figure that as both solvent/solute ratio and time increased, the yield of the oil increased but decreased beyond 1.6mL/g and 60minutes. This reduction in yield may be attributed to the fact that the quadratic terms of the two factors are more significant with a negative effect (Eqs. 4.7, 4.8).

Figures 4.19 and 4.28 present the interaction effect of temperature and solvent/solute ratio on the yields of APO and GSO extracted with petroleum ether. It could be observed from the figure that as both temperature and agitation speed increase, the yield of the oil increased but decreased when temperature and speed were beyond 60^{o}C and 1.6ml/g respectively. This reduction in the oil yield at high temperature may be attributed to the evaporation of the solvent at higher temperature above its boiling point.

Figures 4.20 and 4.29 depict the interaction effect of solvent/solute ratio and particle size on the yield of APO and GSO extracted with petroleum ether respectively. It could be observed from the figure that the oil yield increases as solvent/solute ratio increases and particle size decreases. This may be attributed to large surface area of the seed exposed for oil extraction at smaller particle size.

Figure 4.21 shows the interaction effect of solvent/solute ratio and agitation speed on the yield of APO extracted with petroleum ether. It could be observed from the figure that as both solvent/solute ratio and agitation speed increase, the yield of the oil increased but decreased beyond 1.6mL/g and 200rpm. This reduction in yield may be attributed to the fact that the quadratic terms of the two factors are more significant with a negative effect (Eqs. 4.7, 4.8).

Figure 4.22 depicts the interaction effect of time and temperature on the yield of GSO extracted with petroleum ether. It could be observed from the figure that the oil yield increases as both time and temperature increase but decreased when time and temperature were beyond 60minutes and 60^{o}C respectively. This reduction in the oil yield at high temperature may be attributed to the evaporation of the solvent at higher temperature above its boiling point and negative effect of their quadratic terms (Eqs. 4.7, 4.8).

Figures 4.23 and 4.30 present the interaction effect of time and particle size on the yield of APO and GSO extracted with petroleum ether respectively. It could be observed from the figure that the oil yield increases as time increases and particle size decreases. This may be attributed to large surface area of the seed exposed for oil extraction at smaller particle size.

Figure 4.24 shows the interaction effect of time and agitation speed on the yield of APO extracted with petroleum ether. It could be observed from the figure that as both time and agitation speed increase, the yield of the oil increased.

Figures 4.25 and 4.31 present the interaction effect of temperature and particle size on the yields of APO and GSO extracted with petroleum ether respectively. It could be observed from the figure that the oil yield increases as temperature increases and particle size decreases. This may be attributed to large surface area of the seed exposed for oil extraction at smaller particle size.

Figure 4.26 depicts the interaction effect of temperature and agitation speed on the yield of APO extracted with petroleum ether. It could be observed from the figure that as both temperature and agitation speed increase, the yield of the oil increased but decreased when temperature and speed were beyond 60^{o}C and 200rpm respectively. This reduction in the oil yield at high temperature may be attributed to the evaporation of the solvent at higher temperature above its boiling point.

Figures 4.27 and 4.32 present the interaction effect of agitation speed and particle size on the yields of APO and GSO extracted with petroleum ether respectively. It could be observed from the figure that the oil yield increases as agitation speed increases and particle size decreases. This may be attributed to large surface area of the seed exposed for oil extraction at smaller particle size.

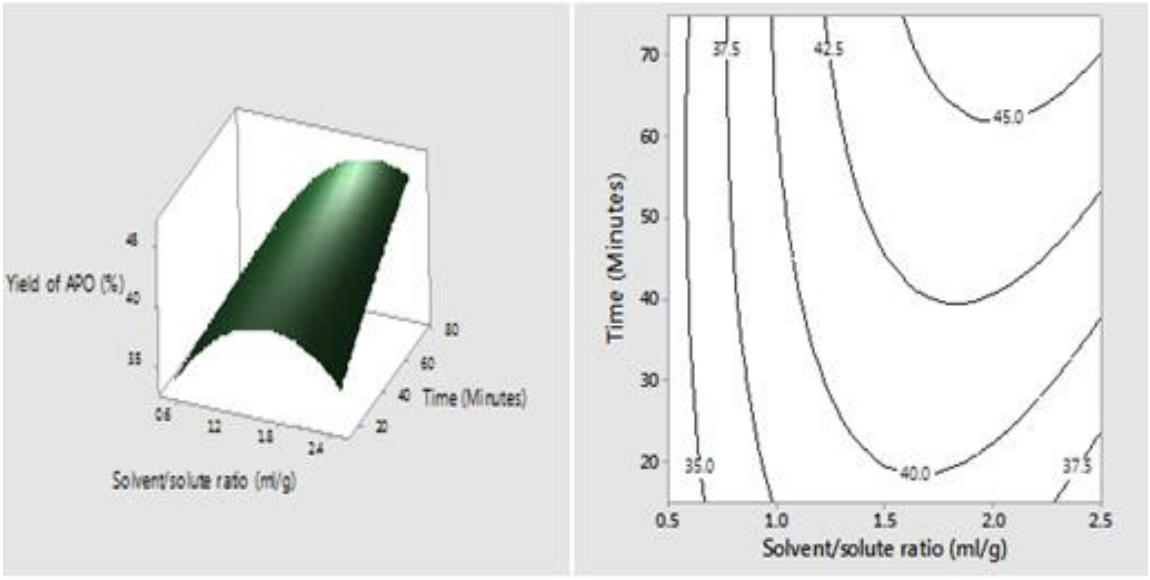

Figure 4.18: Response surface plots of APOyield(%)with n – petroleum ether against solvent/solid ratio (A) (mL/g) and time, (B) (Minutes).

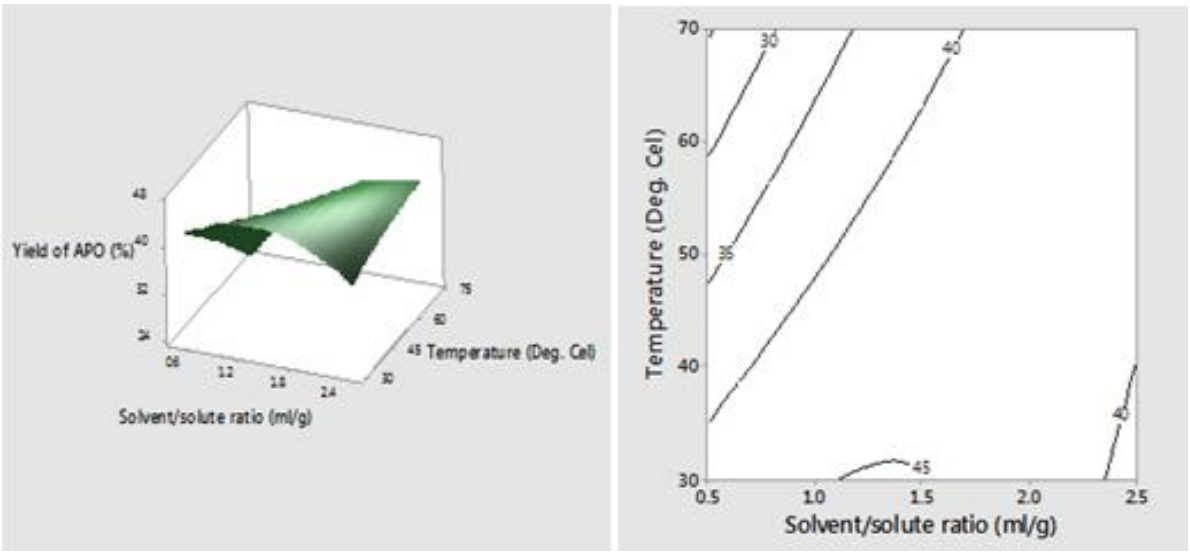

Figure 4.19: Response surface plots of APOyield(%)with n – petroleum etheragainst solvent/solid ratio (A) (mL/g) and temperature, (C) (^{o}C).

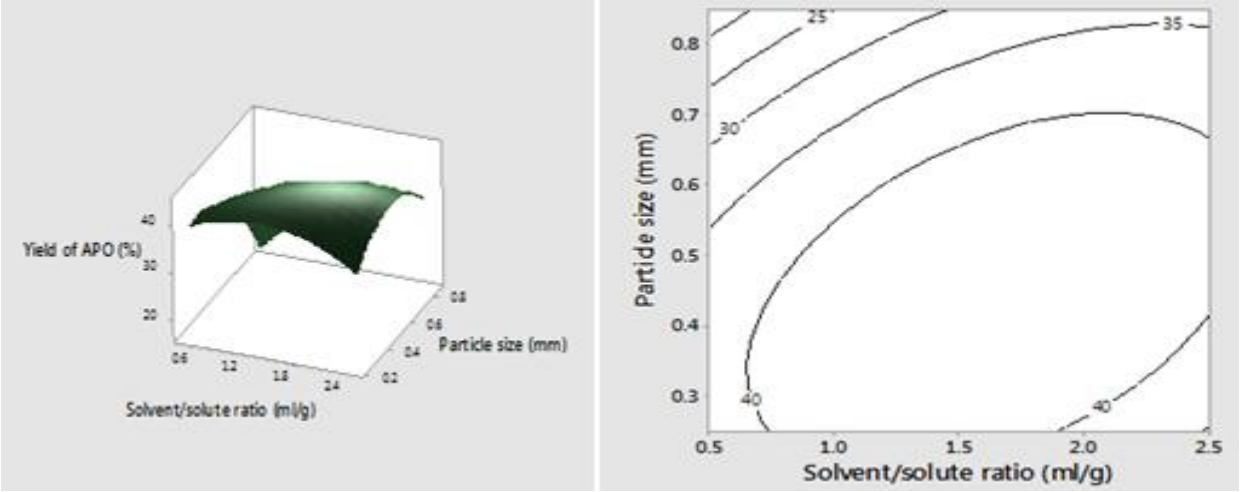

Figure 4.20: Response surface plots of APOyield(%) with n – petroleum ether against solvent/solid ratio (A) (mL/g) and particle size, (D) (mm).

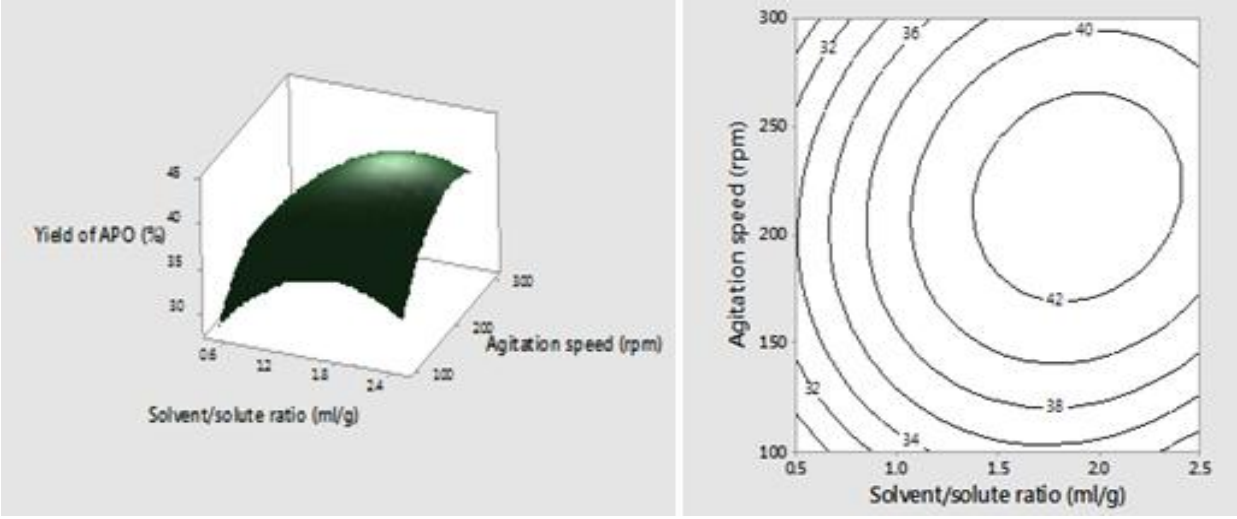

Figure 4.21: Response surface plots of APOyield(%)with n – petroleum ether against solvent/solid ratio (A) (mL/g) and agitation speed, (E) (rpm).

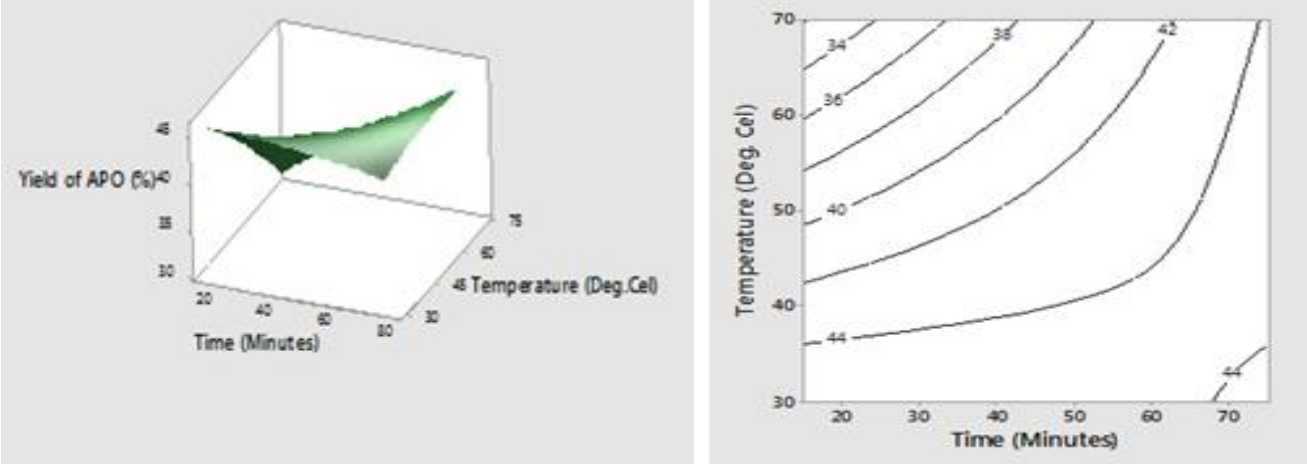

Figure 4.22: Response surface plots of APOyield(%)with n – petroleum ether against time (B) (Minutes) and temperature, (C) (^{o}C).

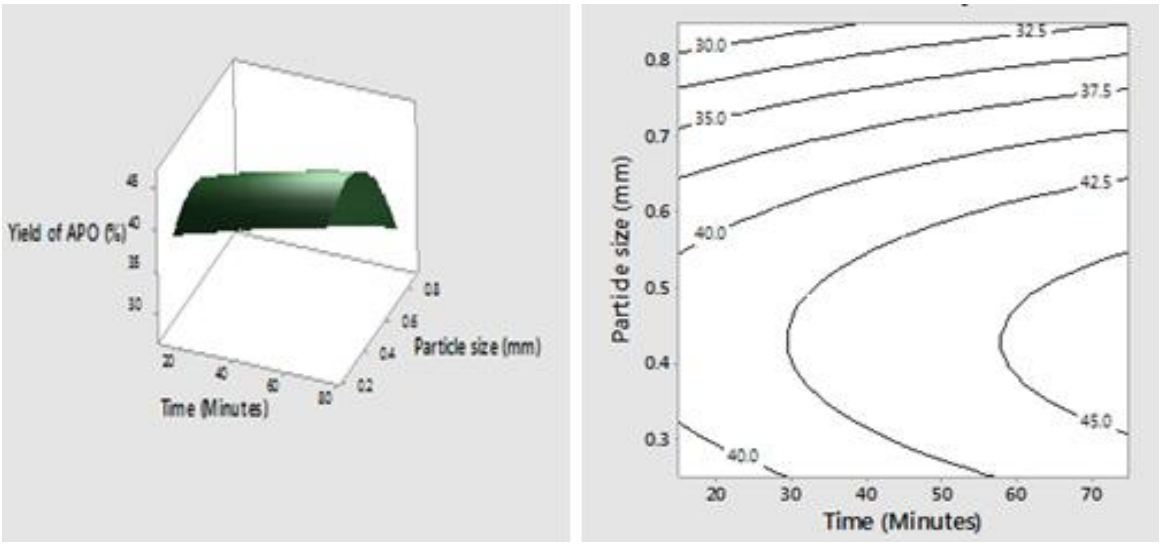

Figure 4.23: Response surface plots of APOyield(%)with n – petroleum ether against time (B) (Minutes) and particle size, (D) (mm).

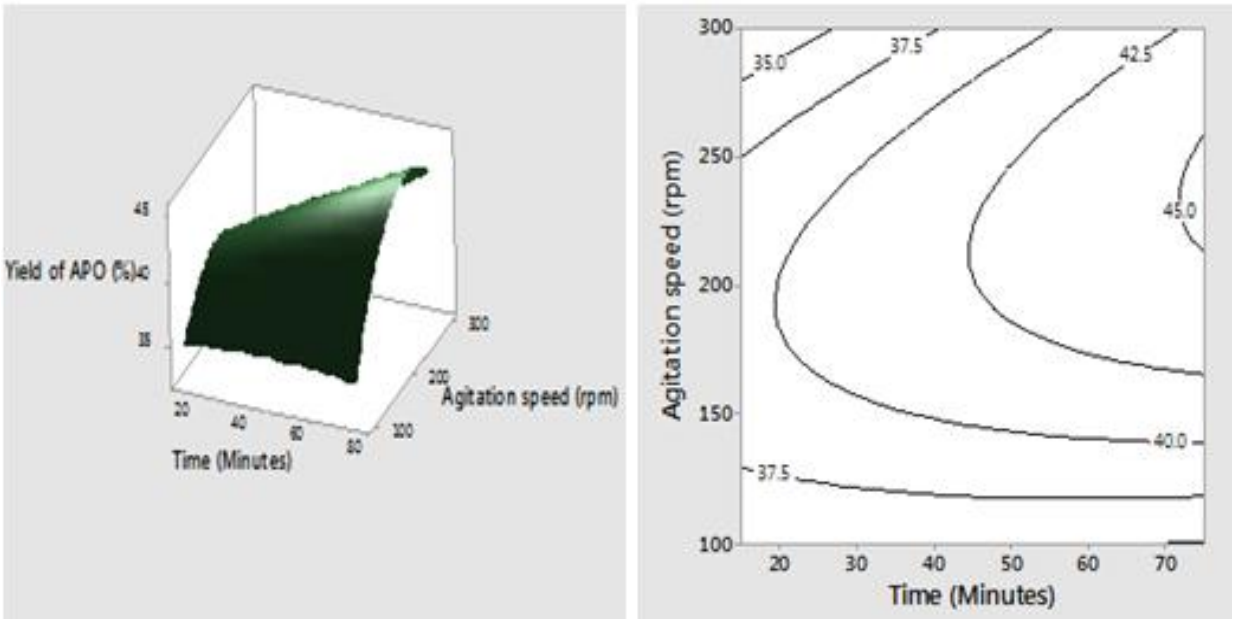

Figure 4.24: Response surface plots of APOyield(%)with n – petroleum ether against time (B) (Minutes) and agitation speed, (E) (rpm).

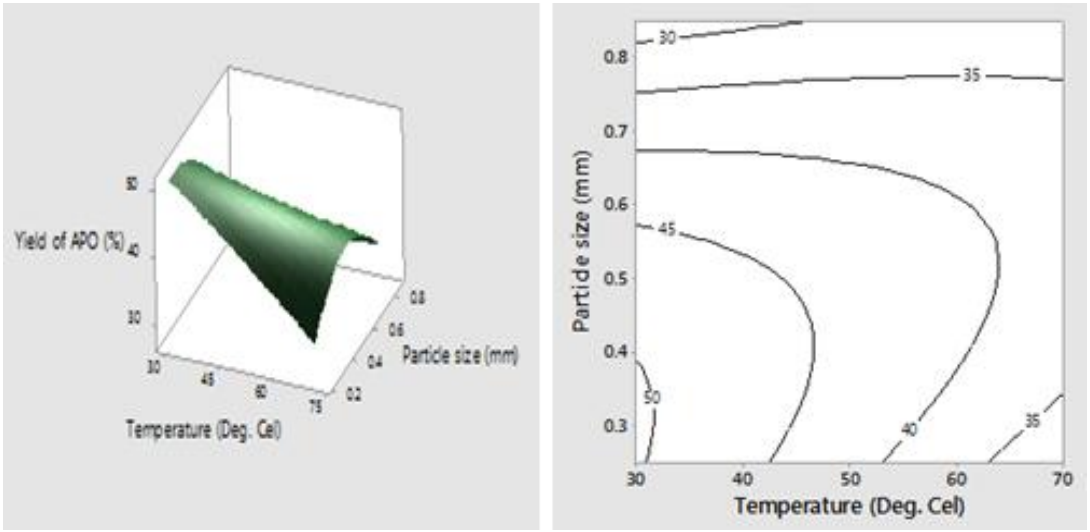

Figure 4.25: Response surface plots of APOyield(%)with n – petroleum ether against temperature (C) (^{o}C) and particle size, (D) (mm).

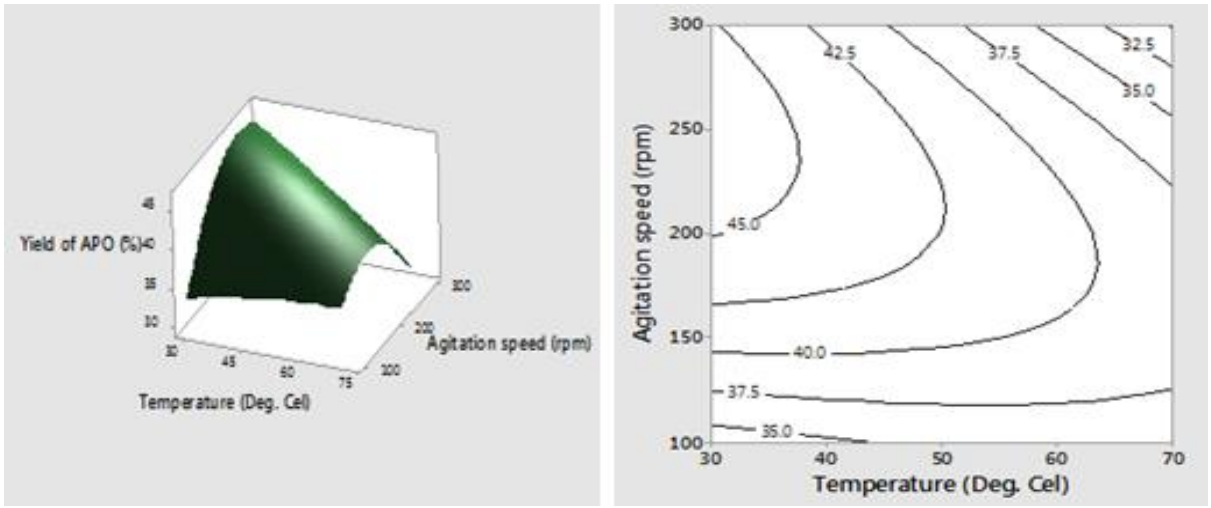

Figure 4.26: Response surface plots of APOyield(%)with n – petroleum ether against temperature (C) (^{o}C) and agitation speed, (E) (rpm).

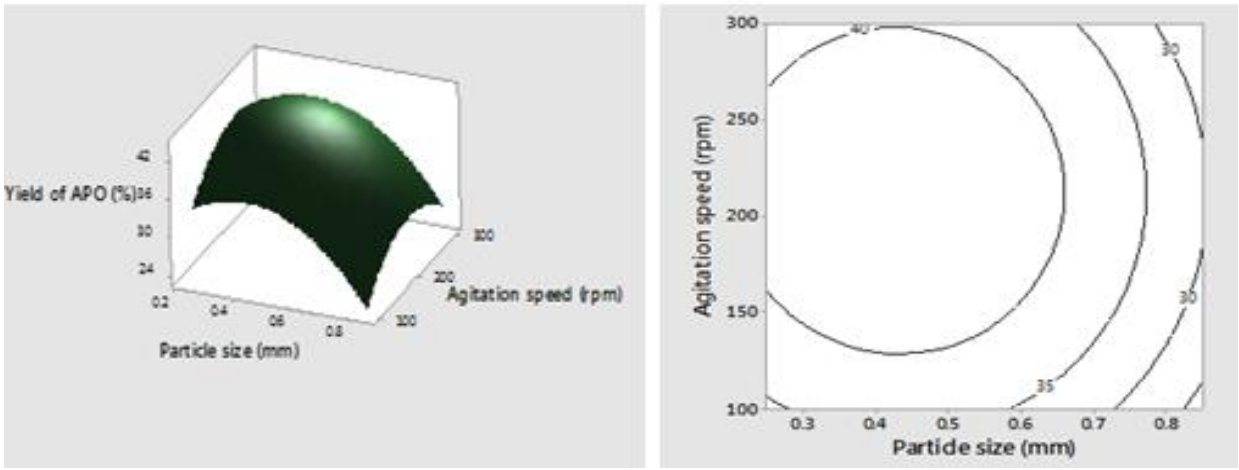

Figure 4.27: Response surface plots of APOyield(%)with n – petroleum ether against particle size (D) (mm) and agitation speed, (E) (rpm).

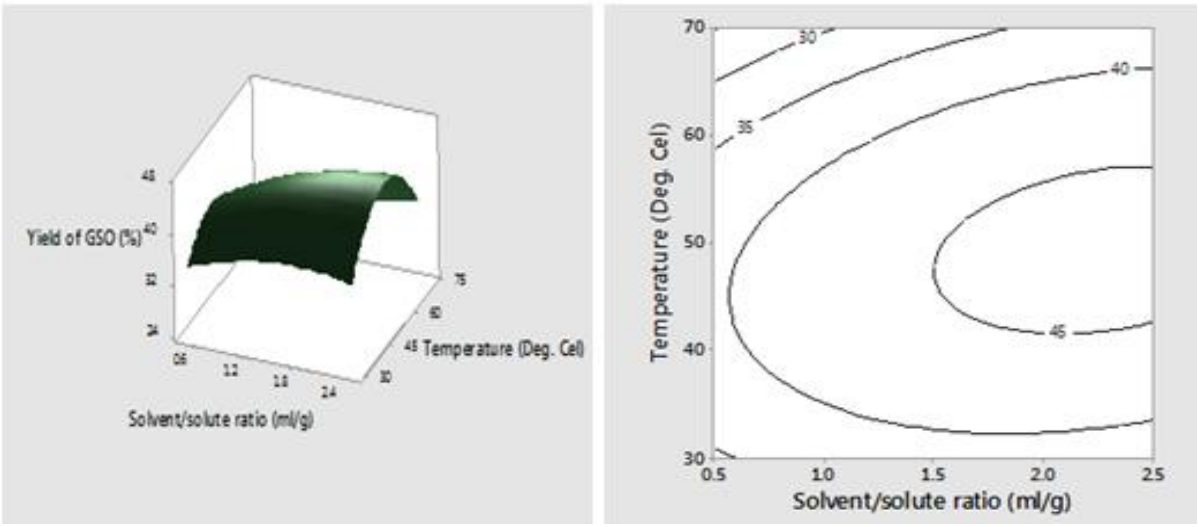

Figure 4.28: Response surface plots of GSOyield(%)with n – petroleum ether against solvent/solid ratio (A) (mL/g) and temperature, (C) (^{o}C).

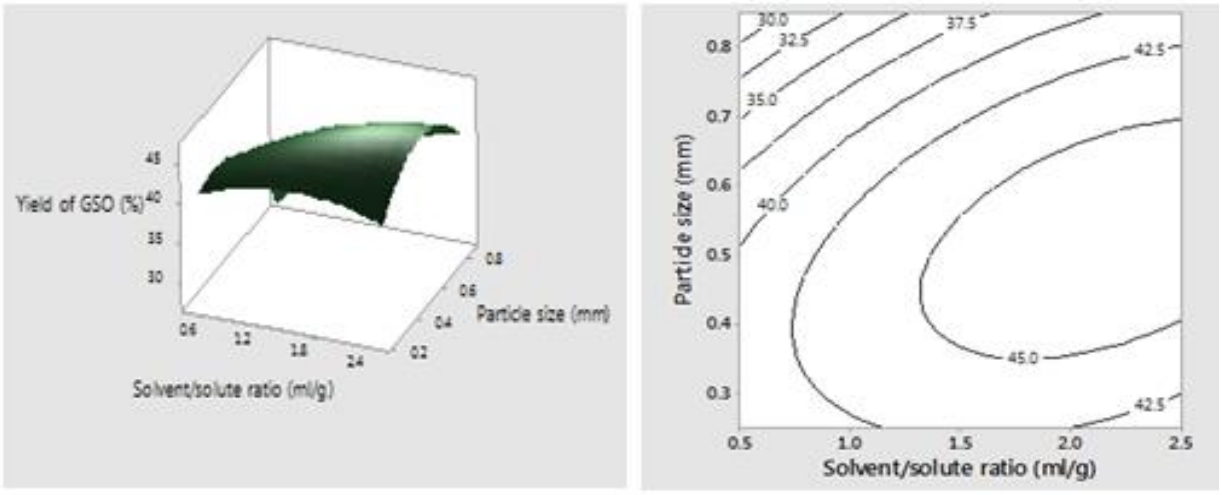

Figure 4.29: Response surface plots of $GSOyield(\%) with\ n-petroleum\ ether$ against solvent/solid ratio (A) (mL/g) and particle size, (D) (mm).

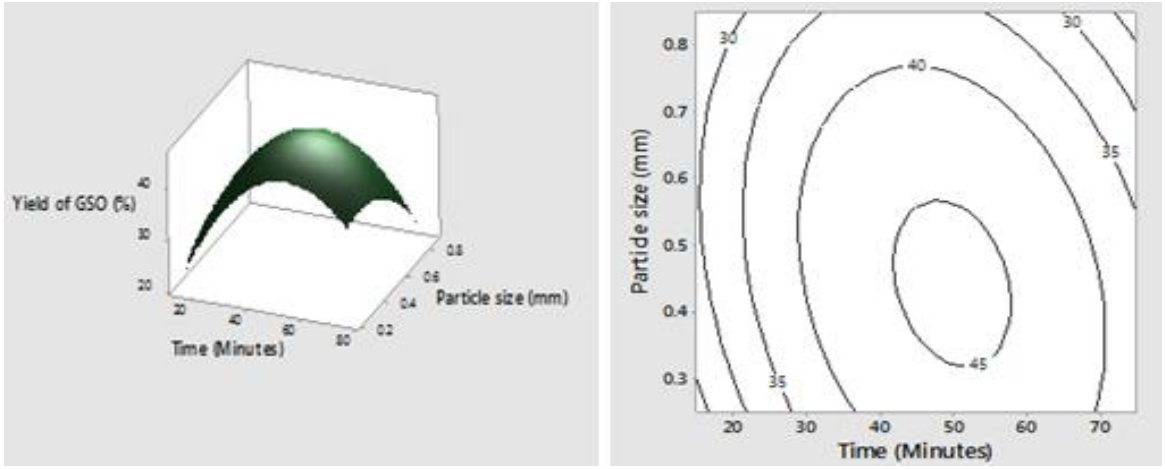

Figure 4.30: Response surface plots of GSOyield(%)with n − petroleum ether against time (B) (Minutes) and particle size, (D) (mm).

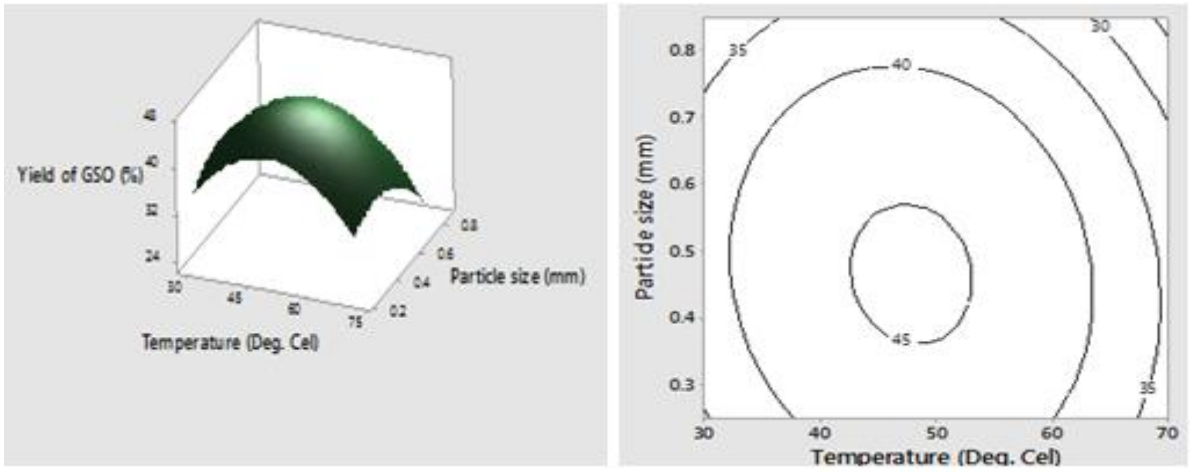

Figure 4.31: Response surface plots of GSOyield(%)with n − petroleum ether against temperature (C) (^{o}C) and particle size, (D) (mm).

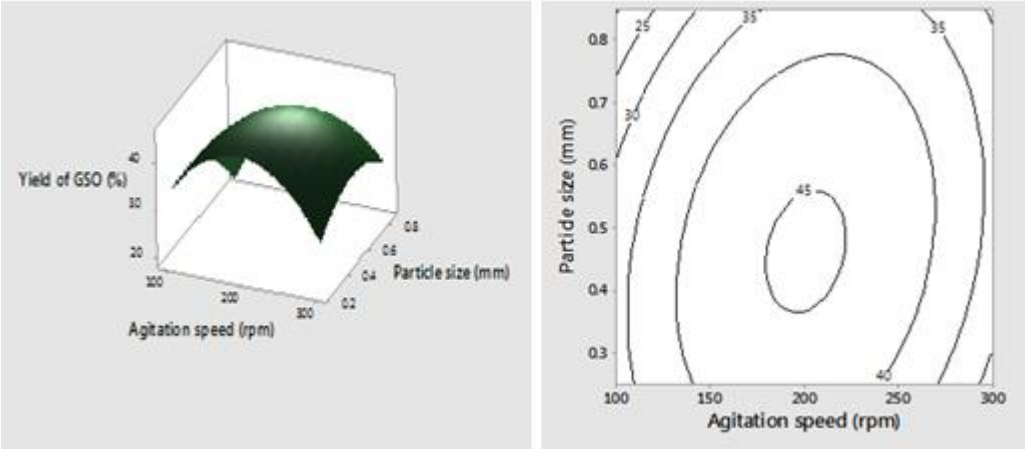

Figure 4.32: Response surface plots of GSOyield(%)with n – petroleum ether against particle size (D) (mm) and agitation speed, (E) (rpm).

Optimization using the response surface – contour and surface plots could be technically unreliable when there are more than one response and multiple predictors. Thus it can lead to multiplicity of optimal settings established for one response. Inspection of the contour and surface graphs revealed that for a particular response, some factor pairs are in the maximum region while others indicate minimum optimal region. The indeterminate tendency of this approach gave rise to the need to adopt a more suitable optimization approach which can define the optimal settings of the operational parameters for all the responses.

4.2.4 Optimization of the oil extraction using desirability function approach

Desirability function approach eliminates the rigour associated with most other optimization techniques such as the optimization using contour and surface plots. It is a multi -response multi -factor optimization technique which operates on the principle established by Derringer Harrington (Fan, 2008). It optimizes a set of responses and defines the best factor settings for a solution of a multivariate objective function. The objective of this study is to determine the optimum solvent/solid ratio, time, temperature, particle size and agitation speed to optimize the oil yield extracted from African pear seed and gmelina seed using both n-hexane and petroleum ether. The response optimizer capability of MINITAB 17 was employed for this purpose and the optimization values are presented in Table 4.10.The value of individual desirability and the yield desirability respectively approximate to 1 which signifies that the optimization result is highly desirable. It is observed that the African pear oil (APO) and gmelina seed oil (GSO) yield using n-hexane and petroleum ether at the factor settings of 1.57mL/g, 45minutes, 45^{o}C, 0.57mm and 200rpm for solvent/solid ratio, time, temperature, particle size and agitation speed respectively gave the optimal responses of50.7% GSO yield

with petroleum ether, 51.5% APO yield with petroleum ether, 50.5% GSO yield with n-hexane and 53.4% APO yield with n-hexane. Table 4.11also depicts the validation of the optimal results of the extraction process, from the table it could be observed that the percentage error of each response was less 2%. This shows that the model was adequate in predicting the responses.

Table 4.11: Validation of the optimal values for oil extraction

S/N	Responses	Solvent/solid ratio (ml/g)	Time (Minutes)	Temperature (^{o}C)	Particle size (mm)	Agitation speed (rpm)	Experimental Yield (%)	Predicted Yield (%)	% Error
1	Yield of APO with n-hexane	1.57	45	45	0.57	200	53	53.4	0.75
2	Yield of GSO with n-hexane	1.57	45	45	0.57	200	50	50.5	1.0
3	Yield of APO With petroleum ether	1.57	45	45	0.57	200	51	51.5	0.98
4	Yield of APO With petroleum ether	1.57	45	45	0.57	200	50	50.7	1.4

4.3 Characterization of the Extracted Oil

4.3.1 Physicochemical properties of the oil

Table 4.12 shows the physiochemical properties of the rawoil of *Dacryodes edulis*(African pear seed) and gmelina seeds. The oils have moderate acid number and free fatty acid values of 5.49mgKOH/g (African pear seed oil, APO); 5.56mgKOH/g (gmelina seed oil, GSO)and 2.75% (APO); 2.78% (GSO) respectively. These values suggest the pretreatment step on the raw-oil before the transesterification step using homogeneous catalyst but the process could be circumvented using heterogeneous catalysts. The physicochemical properties of the raw oil compare favourably with those of some other non–edible oils such as *Pongamia pinnata*(Agarwal & Garima, 2011), *Jatropha curcas* (Adebayo et al., 2011), *Madhuca indica*(Azam et al., 2005).

The densities and high viscosities of both oil will make their atomization difficult in internal combustion engine, hence they cannot be used directly as bio-fuel. The low pour point shows that the oil will hardly solidify at room temperature hence can be stored for a long time. The oxidation stability of the oil was high and is good for production of biodiesel. The high oxidation stability of the oils could be as a result of method used in extracting the oils. Solvent refining results in the production of base oils, which retain some sulphur compounds that are natural antioxidants. These base oils retain a natural ability to prevent oxidation, while hydro treated base oils must be further fortified with antioxidants in order to maintain thermal and oxidation stability.

Table 4.12: Physicochemical properties of APO and GSO

S/N	Physicochemical properties	African pear seed oil	Gmelina seed oil
1	Specific gravity	0.930	0.895
2	Acid value (mgKOHg)	5.49	5.56
3	Free fatty acid (FFA) (%)	2.75	2.78
4	Spanofication value (mgKOH/g)	130	40.58
5	Iodine value (gI_2/100g)	24.23	35.12
6	Kinematic viscosity at 40^oC (mm^2/s)	7.8	8.01
7	Peroxide value	4.6	8.79
8	Flash point	230	212
9	Cloud point	-3	-2
10	Pour point	13	15
11	Moisture content (%)	7	8
12	Refractive index	1.46	1.43
13	Oxidation stability 11^oC (Hour)	5	5.5
14	Molecular weight	868.8	826.63

4.3.2 Fatty acid profile of African pear seed oil (*D. edulis*) and gmelina seed oil (GC –MS)

The fatty acid composition/profile of *D.edulis* oil and Gmelina seed oil were carried out with the aid of Gas Chromatography Mass Spectrometry (GC-MS). The fatty acid composition of *D. edulis* seed and Gmelinaseed oil are shown in Table 4.13 and Figures C1 and C2 of Appendix C. From Figure C1 and Table 4.13, it could be observed that *D. edulis* oil comprises 14.34% of saturated acids (Lauric Acid, Myristics Acid, Palmitic acid

andArachidic Acid) and 85.66% unsaturated acids (oleic andlinoleic). The dominantmonounsaturated fatty acid of the oil was oleic, which accounted for 74.78% of thetotal fatty acid content, hence, the oil belongs to oleic acid category (Sonntag, 2012). This is in consonance with 76% oleic acid content reported by Ogunsuyi (2015). Theoleic acid content of *Dacryodes* is comparatively higher than 7-40% reported forcoconut oil, palm oil, cottonseed oil and soya beans oil (Ampaitepin *et al.*,2006;Rashid *et al*., 2009). This shows that *D. edulis* seed oil is highly unsaturatedtriglycerides (Triolein). Nevertheless, the fatty acid components of the *Dacryodes*seed oil were found to be consistent with the fatty acids present in typical oils usedfor producing biodiesel.

The fatty acid composition of gmelina seed oil was also presented in Table 4.13and Figure C2. GC-MS analysis of the oil showed abundance of oleic acid (38.78%wt), magaric acid (12.84%wt), palmitic acid (14.15%wt) and stearic acid (12.75%wt). The most abundant saturated and unsaturated fatty acids were palmitic acid (14.15%wt) and oleic acid(38.78%wt) respectively. The oil contains 52.67% saturated fatty acid and 47.32% unsaturated fatty acid.

Table 4.13: Fatty acid composition of African pear seed (*D. edulis*) and Gmelina seed oil.

S/N	FFA Profile		African pear seed oil	Gmelina seed Oil
	Fatty Acid	Component	Composition (%)	Composition (%)
1	Capric acid	C_{10}	-	1.72
2	Lauric acid	C_{12}	2.52	-
3	Myristic acid	C_{14}	3.148	8.62
4	Palmitic acid	$C_{16:0}$	8.105	14.15
5	Magaric acid	C_{17}	-	14.84
6	Stearic acid	$C_{18:0}$	-	12.75
7	Oleic acid	$C_{18:1}$	74.78	38.78
8	Linoleic acid	$C_{18:2}$	10.88	-
9	Linolenic acid	$C_{18:3}$	-	6.82
10	Arachidic acid	C_{20}	0.567	0.64
11	Euric acid	C_{21}	-	1.67
	Total		100	99.99

4.3.3 Fourier transform infra-red spectra of African pear seed oil (*D. edulis*) and gmelina seed oil

The FTIR spectrum of African pear seed oil is shown in Figure C3 of Appendix C and Table 4.14. This was carried out to determine the different functional groups present in thefeedstock. From the result, discernible peaks of note were recorded .The region679.61 cm^{-1} – 886.65 cm^{-1} indicate the presence of =C-H(alkenes) functional groups.They possess bending type of vibrations appearing at low energy and frequencyregion in the spectrum and they are all double bounded. They are attributed toolefinic (alkenes) functional groups and are unsaturated. They could be part of fattyacid methyl esters with unsaturated bond in the biodiesel, such as methyl oleate andmethyl linoleate (Saifuddin *et al*., 2014; Jimoh *et al*., 2012). The characteristicspeaks found in the region 1050.15–1297.23cm^{-1} indicate stretching vibrations ofC-O and C-O-C. They can also indicate the bending vibration of O-CH_3 in thespectrum (John *et al*., 2000; Isah *et al.*, 2015).The band region of 1387.88 cm^{-1} can be ascribed to the bending vibration of C-H methyl groups, while the band at 1631.85cm^{-1} is ascribed to C=C bending vibrations(Shuit *et al*.,2010). The region 1861-2003 cm^{-1} indicates the presence of aromaticcombination. Region 2179.68-2281 cm^{-1} indicates the presence of O-H groupstretched in carboxylic acid. The peaks at 2874.75 cm^{-1} and 2982.07cm^{-1}indicate symmetric and asymmetric stretching vibrations of C-H alkane groupsrespectively. They could be methyl (CH_3) or methylene groups and they requirehigh energy to cause stretching vibrations within their bond when compared to theordinary C-H bending vibrations of alkene groups detected at low energy andfrequency region (Saifuddin *et al.*, 2014; Jimoh *et al.*, 2012). The peak at 3160.41cm^{-1} is attributed to the stretching vibration of =C-H alkene groups. They are detected above wavenumber 3000 cm^{-1} in the spectrum compared tocorresponding alkane C-H stretching groups detected below 3000 cm^{-1}. The peak at3911.89 cm^{-1} with stretching mode of vibration is ascribed to the presence of O-Hgroups. They are single bounded and at high energy region in the spectrum (Michael *et al*., 2010).

The structural organization of extracted gmelina seed oil was investigated by FTIR as shown in Figure C4 and Table 4.14. In the spectrum of gmelina raw oil, 3498.02cm^{-1}correspond to the hydroxyl group (O-H) of the unsaturated fatty acid in the oil. The carboxyl group (C=O) is indicated at 1646.3cm^{-1}. The straight chain of –CH- stretch in aliphatic compound is found at the band 2924.18cm^{-1}. Alkene group (CH=CH) is attributed to the band of 3206.78cm^{-1}.

Table 4.14: FTIR analysis of the extracted oil

	Group Frequency (cm^{-1}) of extracted oil		Functional group/Asigment
S/N	Raw African pear seed oil	Raw Gmelina seed oil	
1	679.61-886.65	679.61-886.65	=C-H Alkenes
2	1050.15-1297.23	1050.15-1297.23	C-O, C-O-C stretching vibration, O-CH_3bending vibration
3	1387.88	1345.57	C-H methyl groups
4	1631.85	1425.44-1724.42	-C=C- bending vibration
5	1861-2003	2011.97	Aromatic combination
6	2179.68-2281	2351.30	O-H group stretched in carboxylic acid
7	2874.75-2982.07	-	Symmetric and asymmetric strectching vibrations of C-H alkane groups
8	3000-3160.41	-	=C-H alkene group, C-H alkane
9	3498.02	3475.84	–OH stretch of unsaturated fatty acid.
10	3911.89	3700.89	Double bond C = C, primary alcohol – OH stretch

4.4 Kinetics of Oil Extraction

Figures 4.33, 4.34 and 4.35 show the kinetics plots of extraction of oil from African pear seed and gmelina seed using n-hexane and petroleum ether at temperatures of 30^{o}C, 40^{o}C and 50^{o}C respectively. It could be observed from the figures that high coefficient of determinations were obtained which implied that the extraction of oil from the seeds using n-hexane and petroleum ether obeyed mass transfer kinetic model (Equations 3.4 & 3.5 in sub-section 3.2.1). The kinetic parameters are shown in Table 4.15. It could be deduced from the table that the rate constant increases as temperature increases which suggests that the extraction of oil from the seeds (African pear seed & gmelina seed) using n-hexane and petroleum ether occurs at moderate temperature. The activation energy of the extraction was determined from Figure 4.36 and depicted in Table 4.16. It could be observed that the activation energy obtained was low showing that the extraction of oil from the seeds using n-hexane and petroleum ether requires lesser energy consumption which makes the process economical.

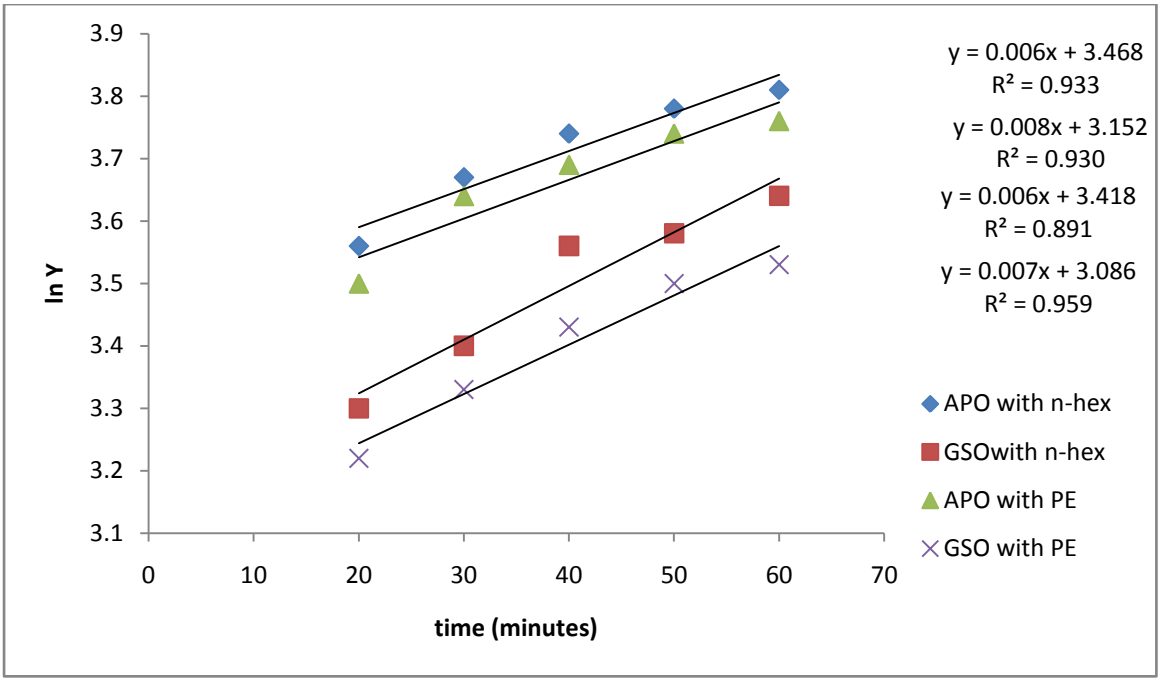

Figure 4.33: Kinetic plot for oil extraction from two seeds using two solvents at 30^{o}C.

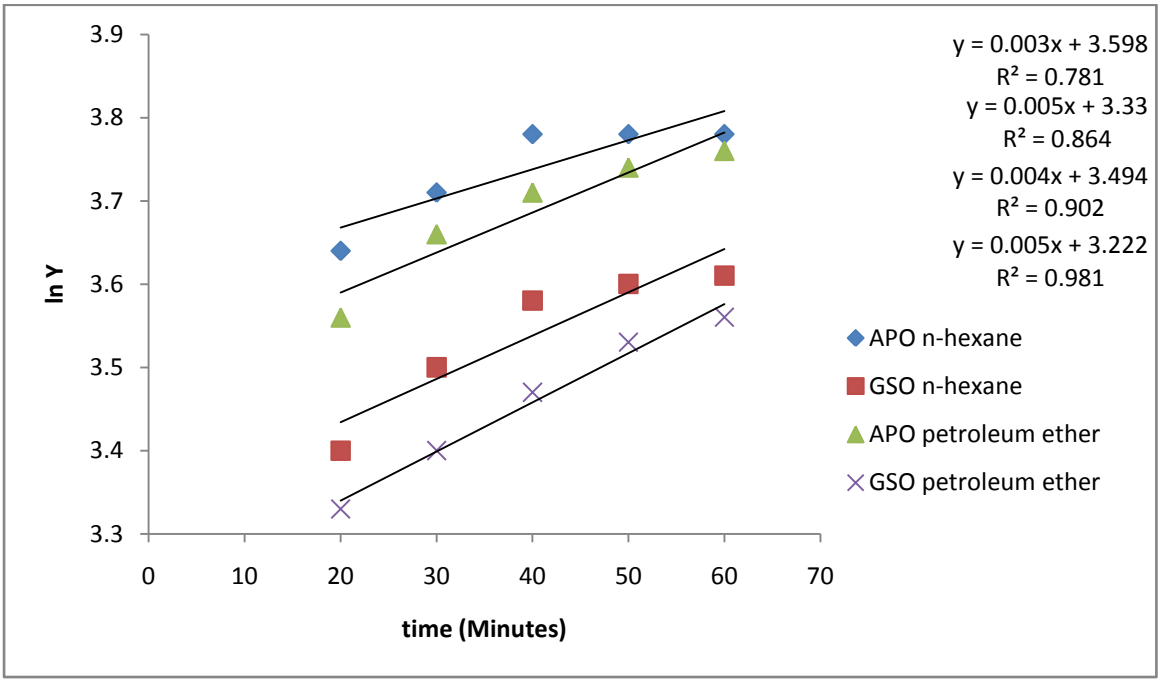

Figure 4.34: Kinetic plot for oil extraction from two seeds using two solvents at 40^{o}C.

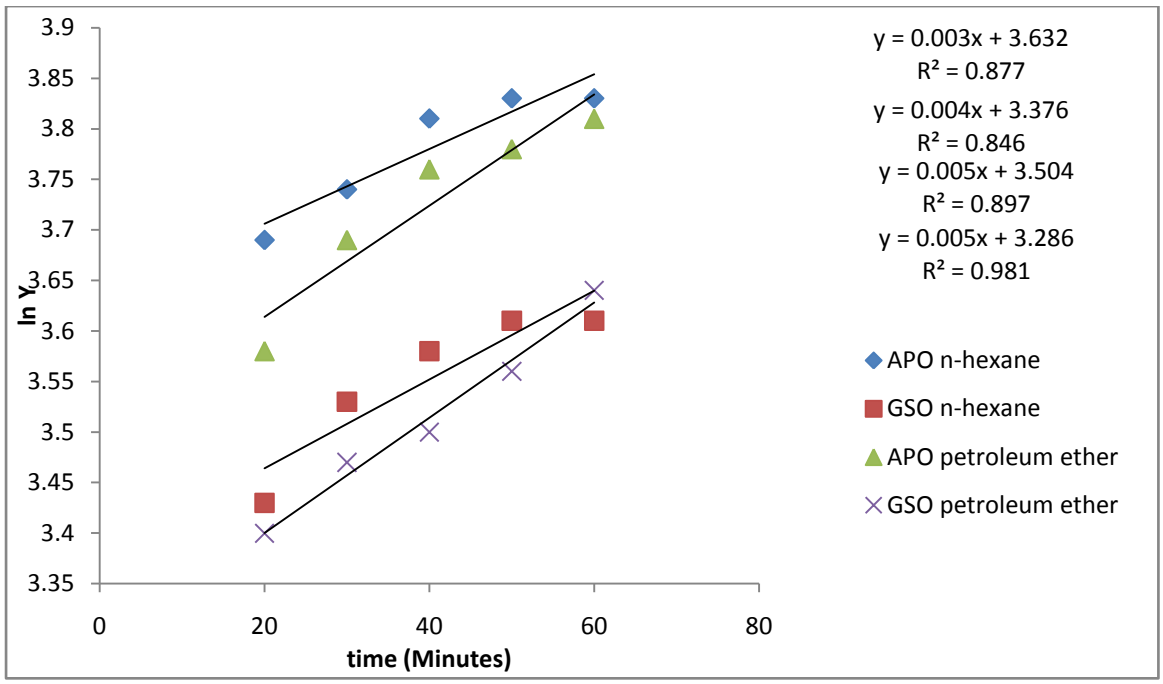

Figure 4.35: Kinetic plot for oil extraction from two seeds using two solvents at 50^{o}C.

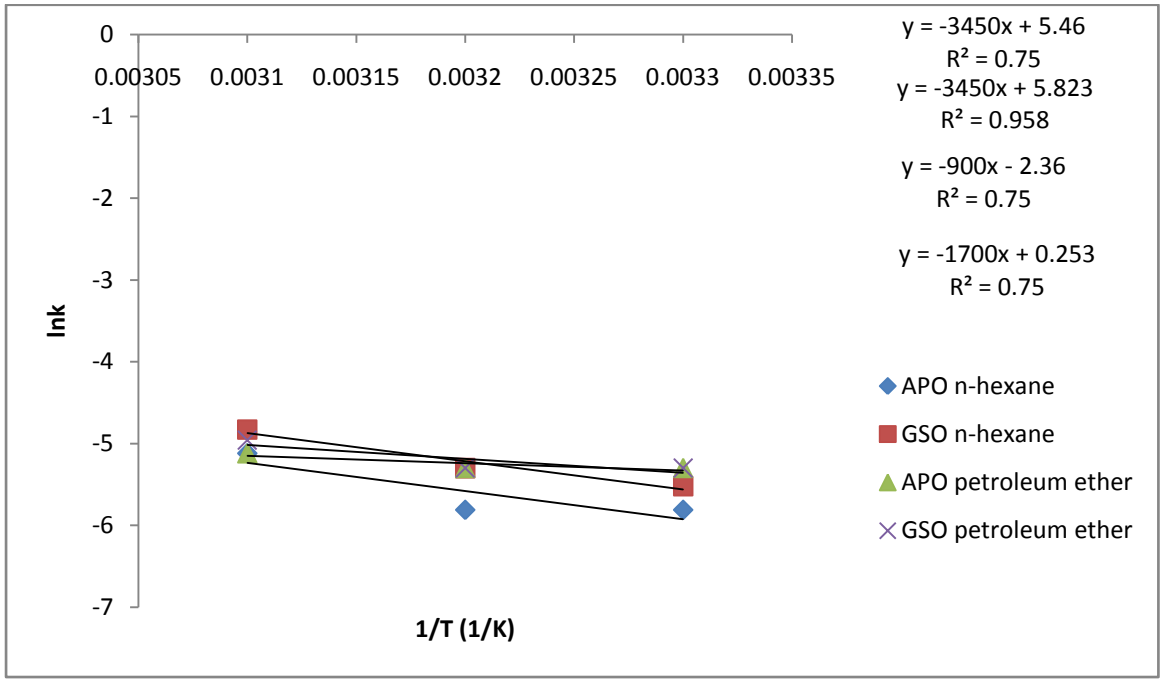

Figure 4.36: Activation energy plot for oil extraction from two seeds using two solvents.

Table 4.15: Kinetic data of oil extraction

	303K		313K		323K		Ea (kJ/mol)
Oil/solvent	k(min^{-1})	R^2	k(min^{-1})	R^2	k(min^{-1})	R^2	
APO/ n-hexane	0.003	0.933	0.003	0.781	0.006	0.877	28.68
GSO/ n-hexane	0.004	0.930	0.005	0.864	0.008	0.846	28.68
APO petroleum ether	0.006	0.891	0.005	0.902	0.005	0.897	7.48
GSO/petroleum ether	0.005	0.959	0.005	0.981	0.007	0.981	14.13

4.5 Thermodynamics Studies of Extraction Process

The values of K, ΔH, andΔS for extraction of African pear oil (APO) and gmelina seed oil (GSO) using n-hexane and petroleum ether as solvents were determined from Figure 4.37 while $\Delta G$was calculated using Equation (3.10) and given in Table 4.16. The positive value of enthalpy indicates that the process is endothermic which implied that the extraction process requires heat energy but at low temperature. The negative values of ΔG indicate that the extraction of oil using n-hexane and petroleum ether are spontaneous process and feasible.

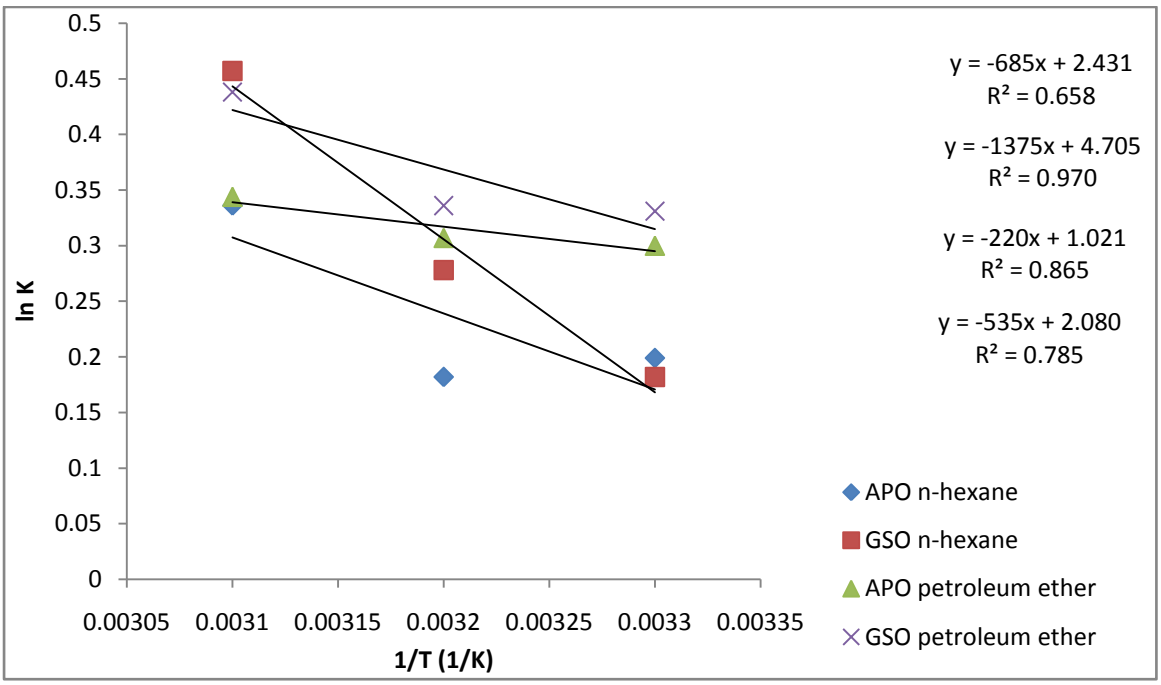

Figure 4.37: Thermodynamic data for oil extraction

Table 4.16: Thermodynamics data for APO and GSO extraction.

Oil/solvent	ΔH (kJ/mol)	ΔS (J/molK)	Temperature (K)	ΔG (J/mol)
APO/ n-hexane	5.695	19.46	303	-201.29
			313	-395.89
			323	-590.49
GSO/ n-hexane	11.432	39.12	303	-422.36
			313	-812.81
			323	-1204.01
APO petroleum ether	1.829	8.49	303	-743.39
			313	-828.29
			323	-913.19
GSO/petroleum ether	4.447	17.29	303	-790.88
			313	-963.78
			323	-1136.68

4.6 Catalytic Activity of Synthesized Catalysts

Catalytic activities of the synthesized catalysts were compared in production of biodiesel at catalyst concentration of 3wt%, 3hours time interval, temperature of 55^{o}C, agitation speed of 300rpm and alcohol/methanol oil molar ratio of 10:1 and shown in Figure 4.38. It could be observed from the figure that biodiesel yield was affected by increase in activation temperature, alkali/clay ratio and acid/clay ratio. The catalysts performed better at activation temperature of 700^{o}C, clay/acid ratio of 1:4g/ml and clay/alkali ratio of 1:3 g/ml. The catalyst at these conditions produced higher biodiesel yield with African pear seed oil and this could be as a result of different nature of the FFA profile of the seed. Therefore, the catalysts used in this study were prepared by using temperature of 700^{o}C for thermal activation, clay to acid ratio of 1:4g/ml at a concentration as stated in section 3.4.2 and clay to base/alkaline ratio of 1:3g/ml at a concentration stated in section 3.4.3 of chapter three.

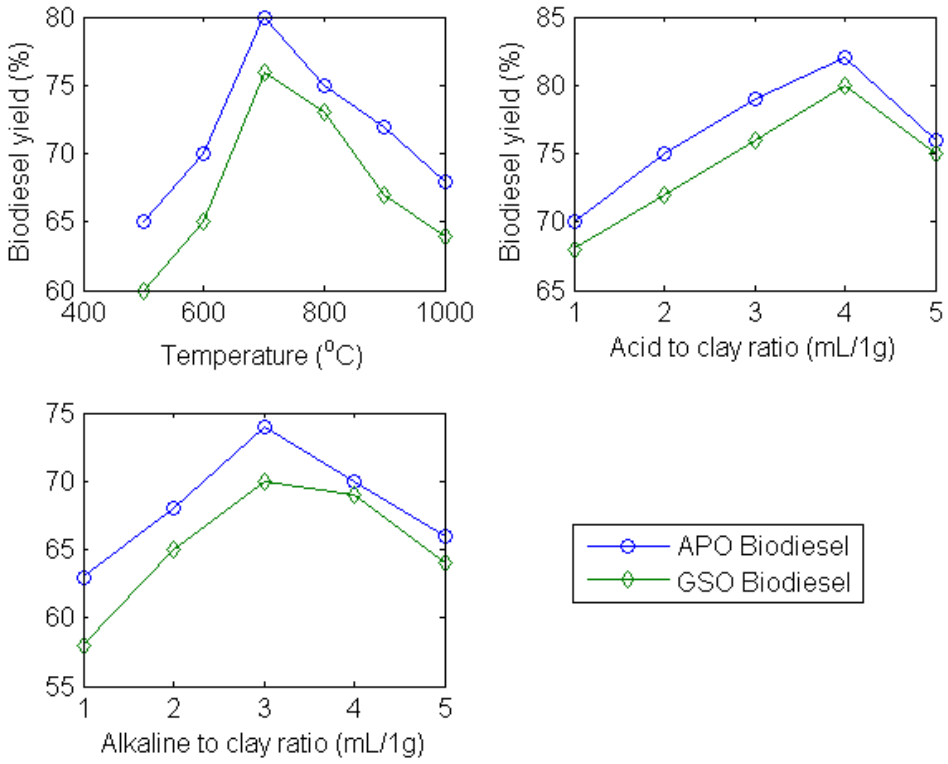

Figure 4.38: Catalytic activities of catalysts prepared with different methods.

4.7 Catalyst Characterization

4.7.1 Physiochemical properties of the synthesized catalyst

The physical properties of the raw clay catalyst and modified clay catalysts are presented in Table 4.17. From the table, it could be observed that the properties of the clay catalyst improved after activation with acid activated clay catalyst (AAC) having more surface area. The pore size of the raw clay increased after different mode of activation and this may be attributed to opening of pores by the activation. The raw clay has higher iodine value than the activated clay. This is could be attributed to the presence of carbonated material presence in the clay before activation.

Table 4.17: Physiochemical properties synthesized clay catalysts

Parameters	Raw clay	Thermally activated clay (TAC)	Base activated clay (BAC)	Acid activated clay (ACC)
Surface area (m^2/g)	286.3	487.6	436.4	526.2
Pore size (nm)	2.647	4.523	2.864	5.901
Total pore volume (cm^3/g)	13.67	25.3	17.33	26.0
Bulk density (g/cm^3)	2.4	1.92	1.42	1.71
pH	7.12	7.12	8.07	6.34
Iodine number (mg/g)	5	0.2	0.15	0.12

4.7.2 X-ray fluorescence analysis of the clay catalysts

The chemical composition of the raw clay, thermally activated clay, acid activated clay and base/alkaline activated clay used in this study is summarized in Table 4.18. The main compositions of the clay are Si, Al, Ti and Fe. It contains metallic oxides such as MgO, Al_2O_3, SiO_2, K_2O, CaO, TiO_2, Cr_2O_3, Mn_2O_3, Fe_2O_3, ZnO and SrO which are constituents of heterogeneous catalysts (Sani et al., 2014). Clay had high amounts of SiO_2, Al_2O_3 and Fe_2O_3. The modification of the raw clay by thermal, acid and base/alkaline activation increased the quantity of SiO_2, Al_2O_3 and reduced the quantity of Fe_2O_3 classifying the modified clay as Brønsted and Lewis acids whose acidity and catalytic properties are largely dependent on the electronegativity of interlamellar spacing ofexchangeable cations attached to the negatively charged aluminosilicate sheets.Consequently, the activation enhanced the amount and strength ofBrønsted and Lewis acid sites (Sani et al., 2014).

Table 4.18: X-ray fluorescence (XRF) of clay catalysts

	Concentration (wt%)			
Elements	Raw clay	Thermally activated clay	Acid activated clay	Base/alkaline activated clay
Na_2O	0.000	0.000	0.000	0.163
MgO	0.321	0.386	0.326	0.235
Al_2O_3	23.123	23.565	27.642	25.743
SiO_2	57.115	57.403	64.556	67.197
P_2O_5	0.310	0.311	1.118	0.286
SO_3	0.246	0.269	0.303	0.343
Cl	0.018	0.019	0.010	0.017
K_2O	0.080	0.089	0.122	0.114
CaO	0.756	0.773	0.024	0.020
TiO_2	4.217	4.098	3.606	3.644
Cr_2O_3	0.028	0.030	0.029	0.028
Mn_2O_3	0.055	0.052	0.013	0.014
Fe_2O_3	13.682	12.963	2.230	2.178
ZnO	0.023	0.021	0.003	0.002
SrO	0.025	0.023	0.019	0.017

4.7.3 Fourier transform infra red (FTIR) analysis of the catalysts

Fourier transform infra-red (FTIR) spectroscope of the raw clay catalyst and the acid, base and thermally modified clay catalysts were done to ascertain the functional groups present in them and depicted in Figures C5, C6, C7, and C8 respectively of Appendix C. The results are shown in Table 4.19. From the figures and table, it was observed that the catalysts have common functional groups such as Si-O-Si, C-Cl of alphatic chloro compounds, C-H stretch of aromatic bend, C-H stretch of vinyl, Organic silicone Si-O-C, Si-O, double bond C=C, -OH stretch of primary alcohol, Al–OH–Al, Al–OH–Mg and Al–OH–O–Si vibrations. Comparing the raw clay to the thermally activated clay, acid and base/alkaline leached clay catalysts,it could be observed that there was no significantdecrease in intensity of bands 998.9 and 685 cm^{-1}, suggesting that the structural changes attributed to the modifications are

small. According to Zatta et al. (2013), the FTIR bands at 998.9,909.5, and 685 cm^{-1} are attributed to Al–OH–Al, Al–OH–Mg and Al–OH–O–Si vibrations respectively. These bands decreased in intensity after the modification process due to the leaching of octahedral cations (Al^{3+} and Mg^{2+}) from the clay structure.The presence of free silica is corresponded to the Si–O–Si deformation (685.6 cm^{-1}) and in-the-plane stretching of Si–O (1114.5 cm^{-1}). The raw clay catalyst contains cyanide ion which can hinder catalytic activity of the clay but the modification of the clay with acid, base and heat removed the cyanide content.

Table 4.19: FTIR analysis of the catalysts

	Group Frequency (cm^{-1}) of catalyst				Functional group/Asigment
S/N	Raw clay	Thermally activated clay (TAC)	Acid activated clay (AAC)	Base activated clay (BAC)	
1	678.4	678.4	678.4	685.8	Si-O-Si deformation
2	752.9	749.2	752.9	-	Aliphatic chloro compounds, C-Cl
3	797.7	797.7	797.7	779.0	Aliphatic chloro compounds, C-Cl
4	909.5	909.5	909.5	909.5	Aromatic C-H out-of-plane bend, Al-OH-Al
5	998.9	998.9	998.9	998.9	Vinyl C-H out-of-plane bend, Al-OH-Mg
6	1118.2	1118.2	1114.5	1114.5	Organic siloxane/silicone (Si-O-C), Si-O
7	-	-	1640.0	-	Conjugated ketone
8	2009.0	-	-	-	Cyanide ion
9	3652.8	3652.8	3652.8	3652.8	Double bond C = C, primary alcohol –OH stretch
10	3693.8	3693.8	3693.8	3652.8	Double bond C = C, primary alcohol –OH stretch

4.7.4 Scanning electron microscopes (SEM) of the clay catalysts

The morphologiesof the raw clay catalyst, thermally activated clay catalyst, acid activated clay catalyst and base/alkaline activated clay catalyst were performed by SEM, as shown in Plates 4.1, 4.2, 4.3 and 4.4 respectively. Micrographs of the clay catalyst samples synthesized bythermal activation, acid activation and base/alkaline activation showed increase in number of poresand pore size on the clay. For the acid activated clay, the formation of more poreson the clay particles was observed and this supports the fact that it has more surface area with lower pore size as reported in sub-section 4.7.1.

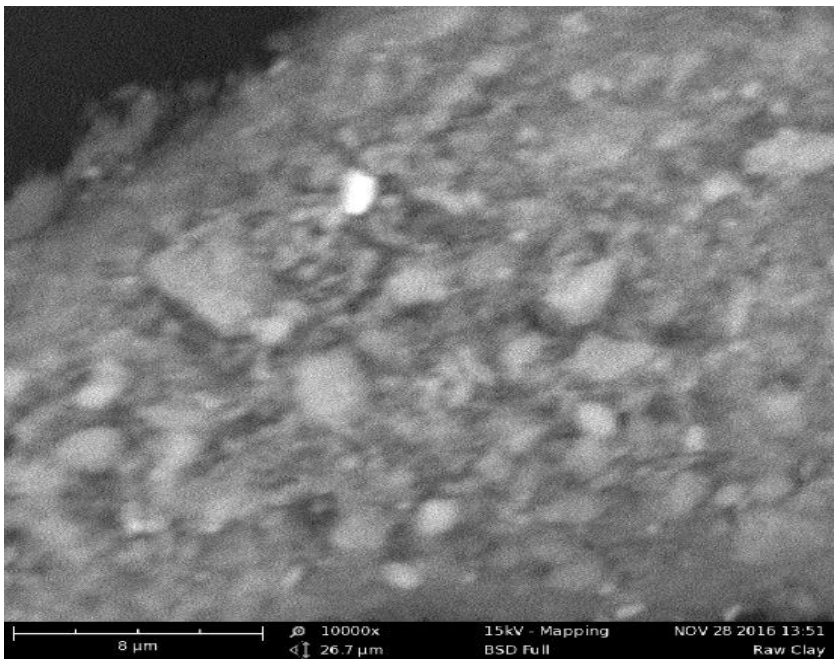

Plate 4.1: SEM image of raw clay catalyst.

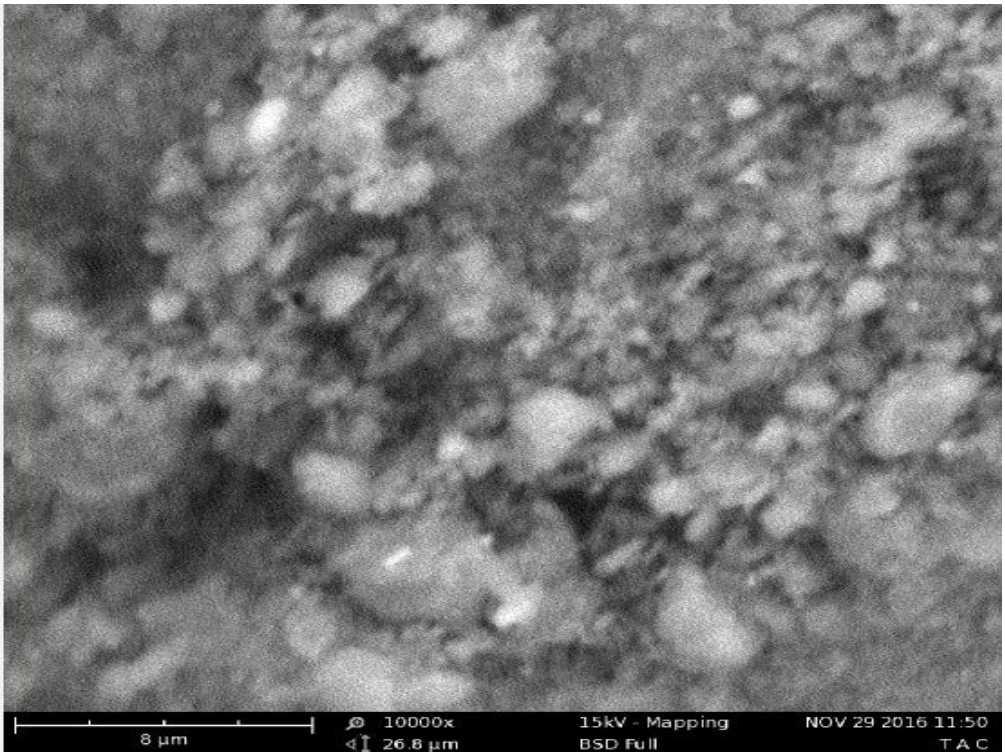

Plate 4.2: SEM image of thermally activated clay catalyst.

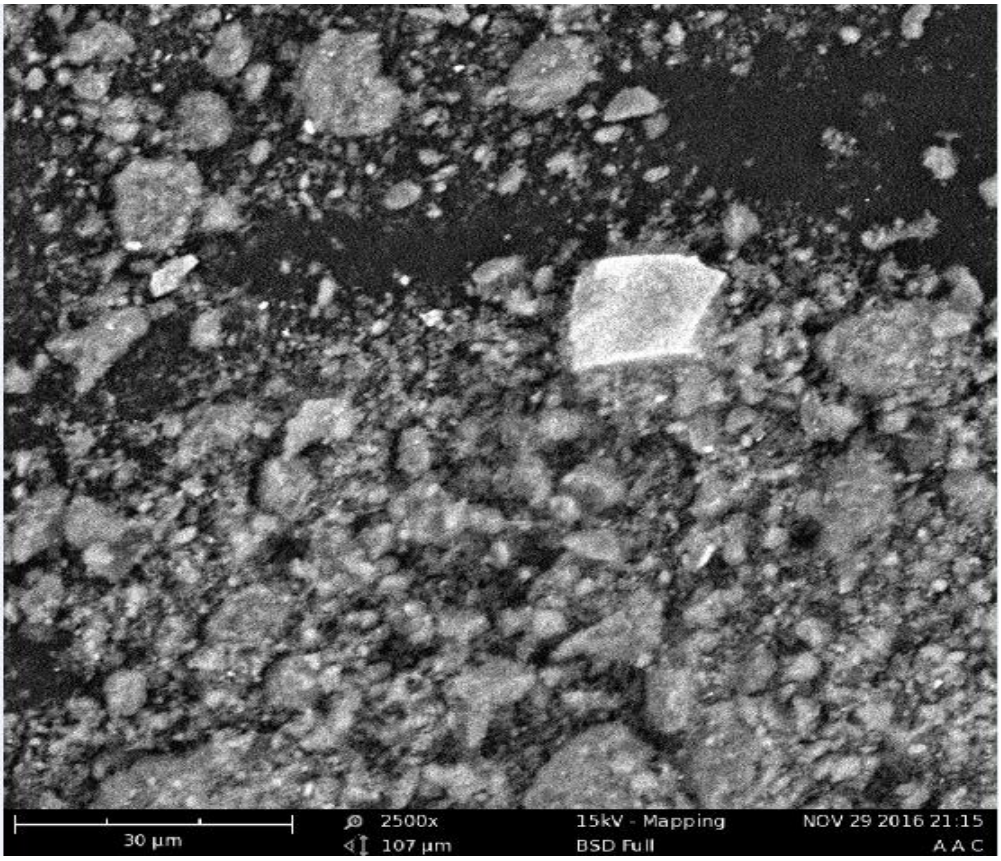

Plate 4.3: SEM image of acid activated clay catalyst.

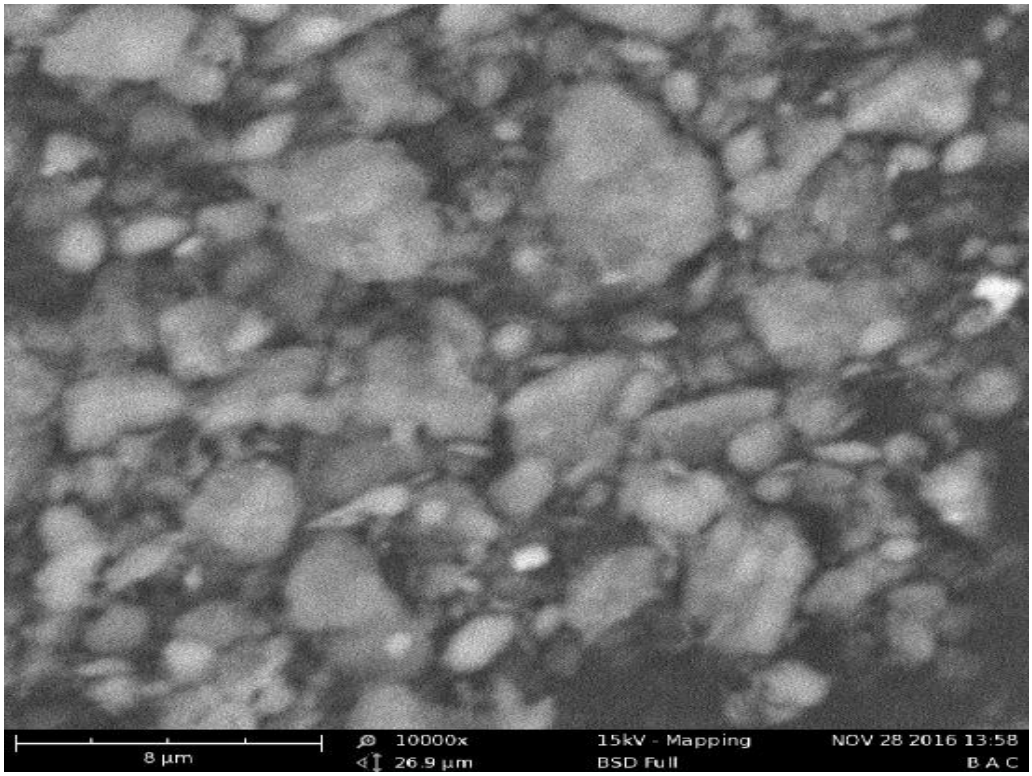

Plate 4.4: SEM image of base/alkaline activated clay catalyst.

4.7.5 X-ray diffraction pattern of the clay catalysts

Figures 4.39, 4.40, 4.41 and 4.42 depict XRD of the raw clay, thermally activated clay, acid activated clay and alkaline activated catalysts. Figure 4.39 shows that the clay belongs to kaolinite group confirming the presence of Alumina and silica and contains quartz which is a residual clay indicating that the clay is from the place of origin. It is observed that the activation of the clay by thermal, acid and alkaline methods modified the clay composition. Figure 4.40 shows that thermal activation introduced phengite, acid activation introduced muscovite (Figure 4.41) while alkaline activation introduced illite (Figure 4.42) and this may be attributed to presence of sodium metal from the alkaline used.

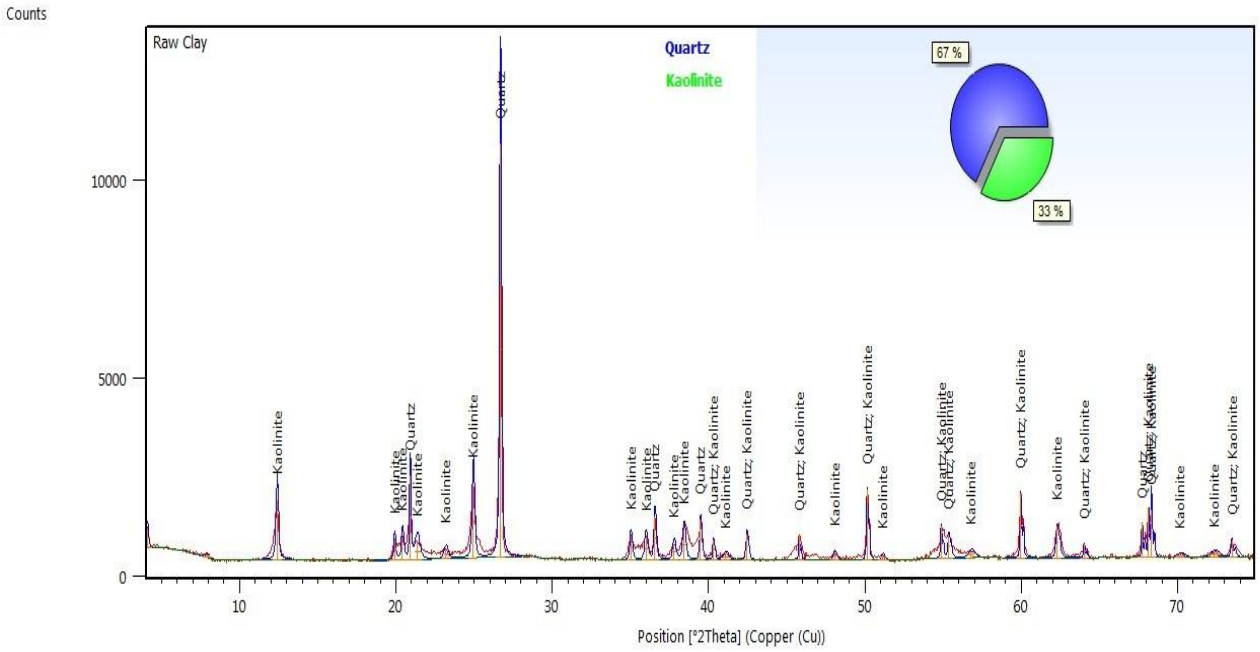

Figure 4.39: XRD of raw clay.

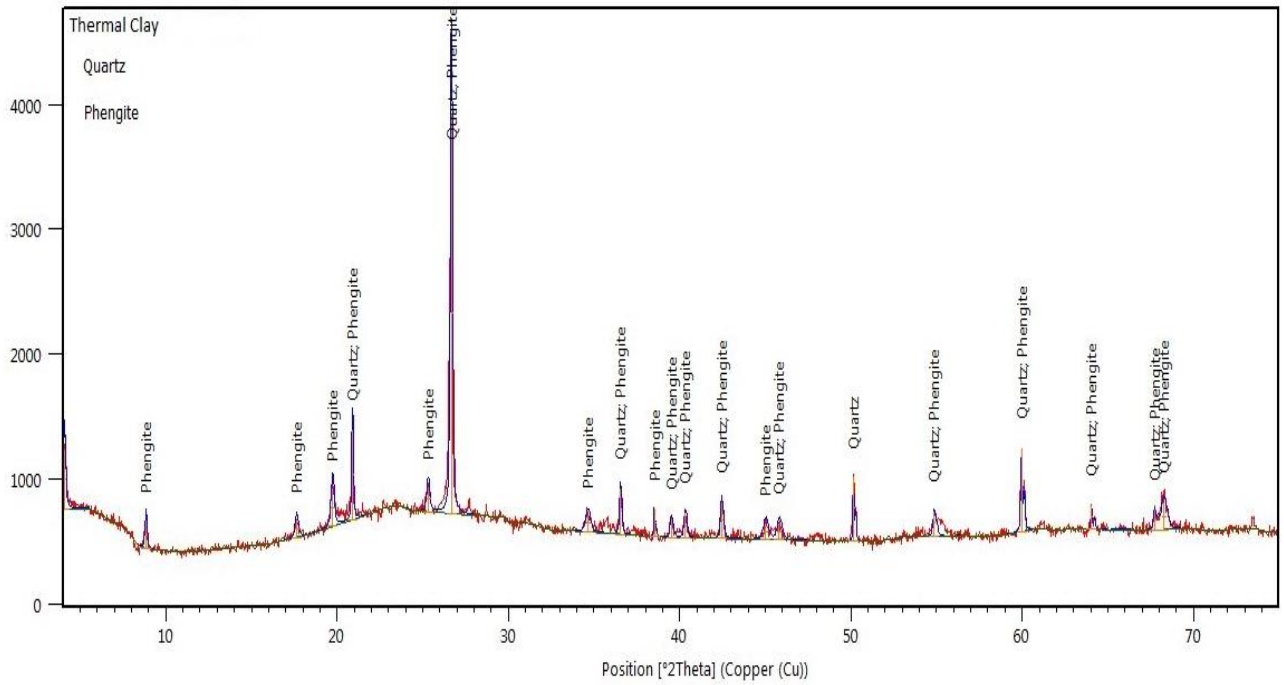

Figure 4.40: XRD of thermally activated clay

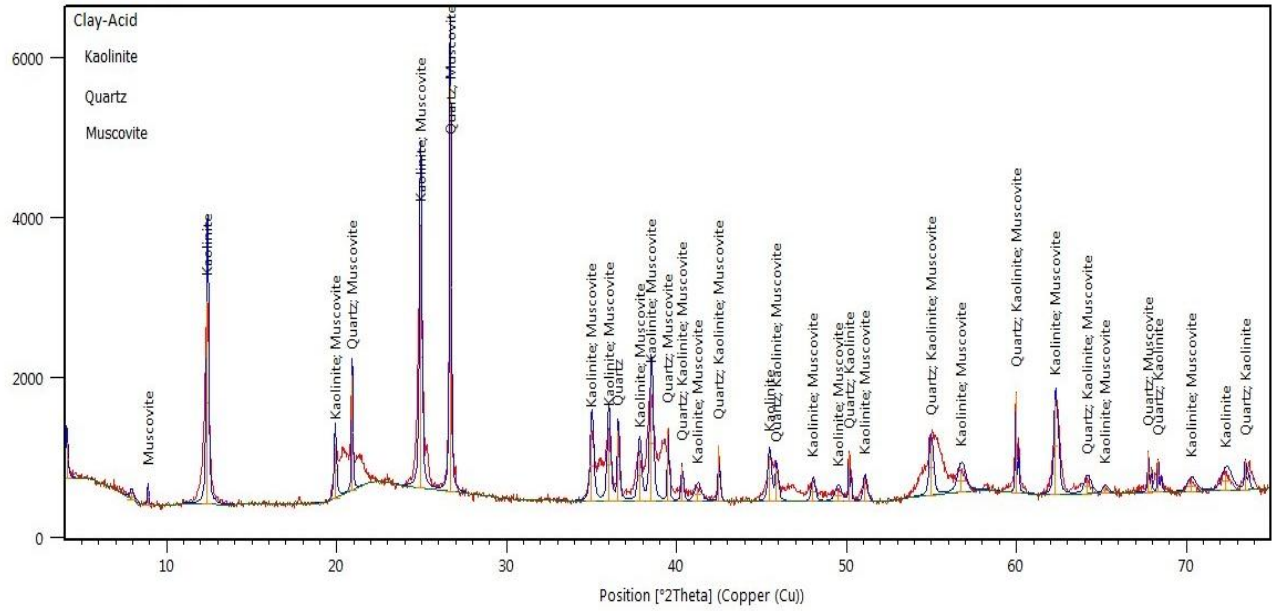

Figure 4.41: XRD of acid activated clay catalyst.

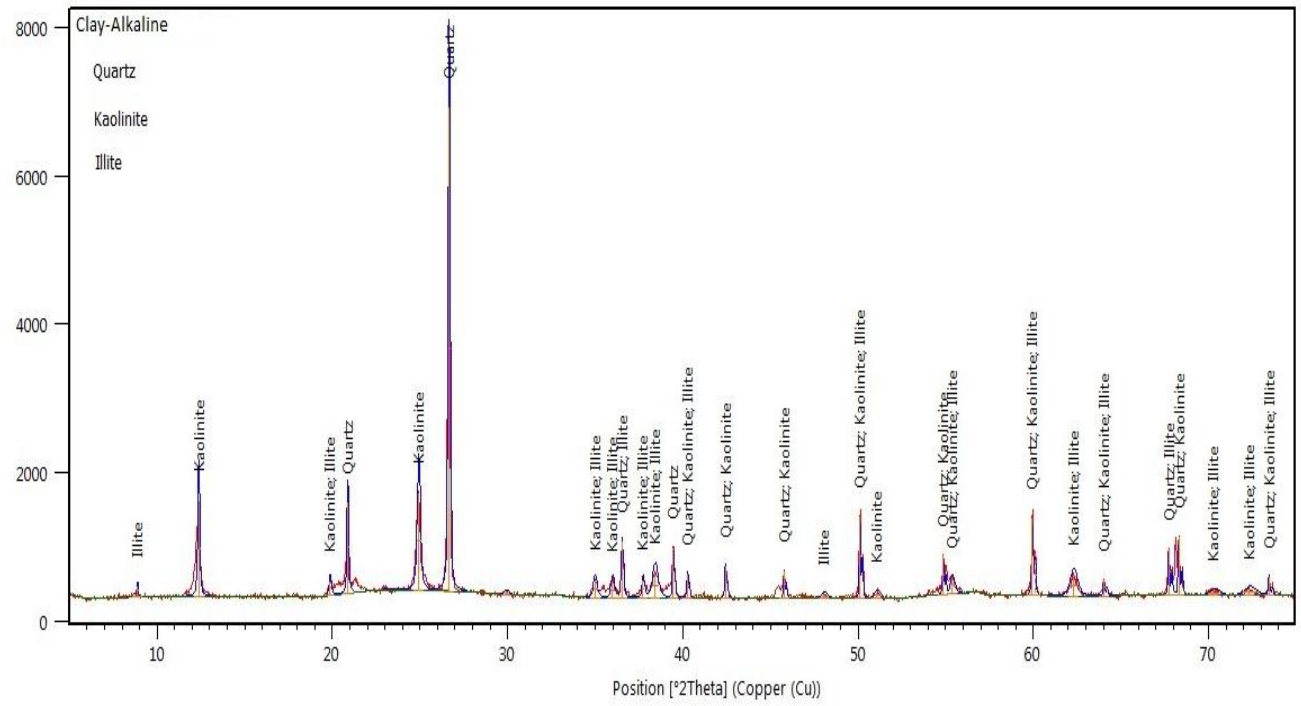

Figure 4.42: XRD of base/alkaline activated clay catalysts.

4.7.6 Thermo gravimetric analysis (TGA) of the clay catalysts

The thermo gravimetric analysis-differential thermal analysis curves obtained in the present study for raw clay catalyst, thermally activated clay catalyst, acid activated clay catalyst and base/alkaline activated clay catalyst are presented in Figures 4.43, 4.44, 4.45 and

4.46respectively. It could be observed from the figures that there were mass losses in the clay catalysts within the temperature range of 150-280^{o}C and weight gainwithin temperature range of 150 - 400^{o}C. The weight of the clay became stableat temperature above 400^{o}C. The decomposition of the catalysts was not complete until 280^{o}C as indicated by endothermic peaks at 270^{o}C in DTA curves. This implied that the clay catalysts can perform well at low temperature below 100^{o}C and high temperature above 400^{o}C without degrading.

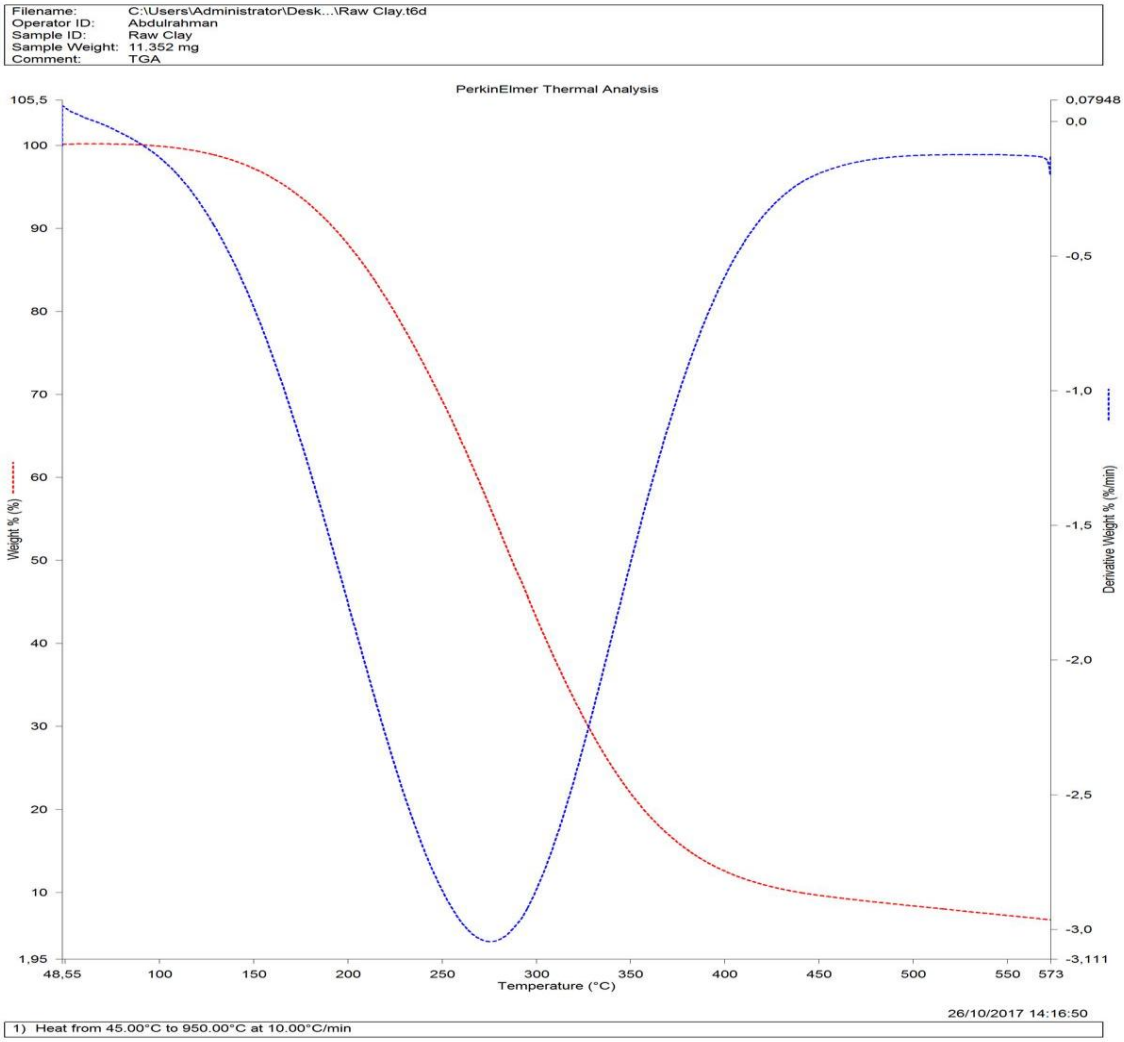

Figure 4.43: TGA-DTA analysis of raw clay catalyst.

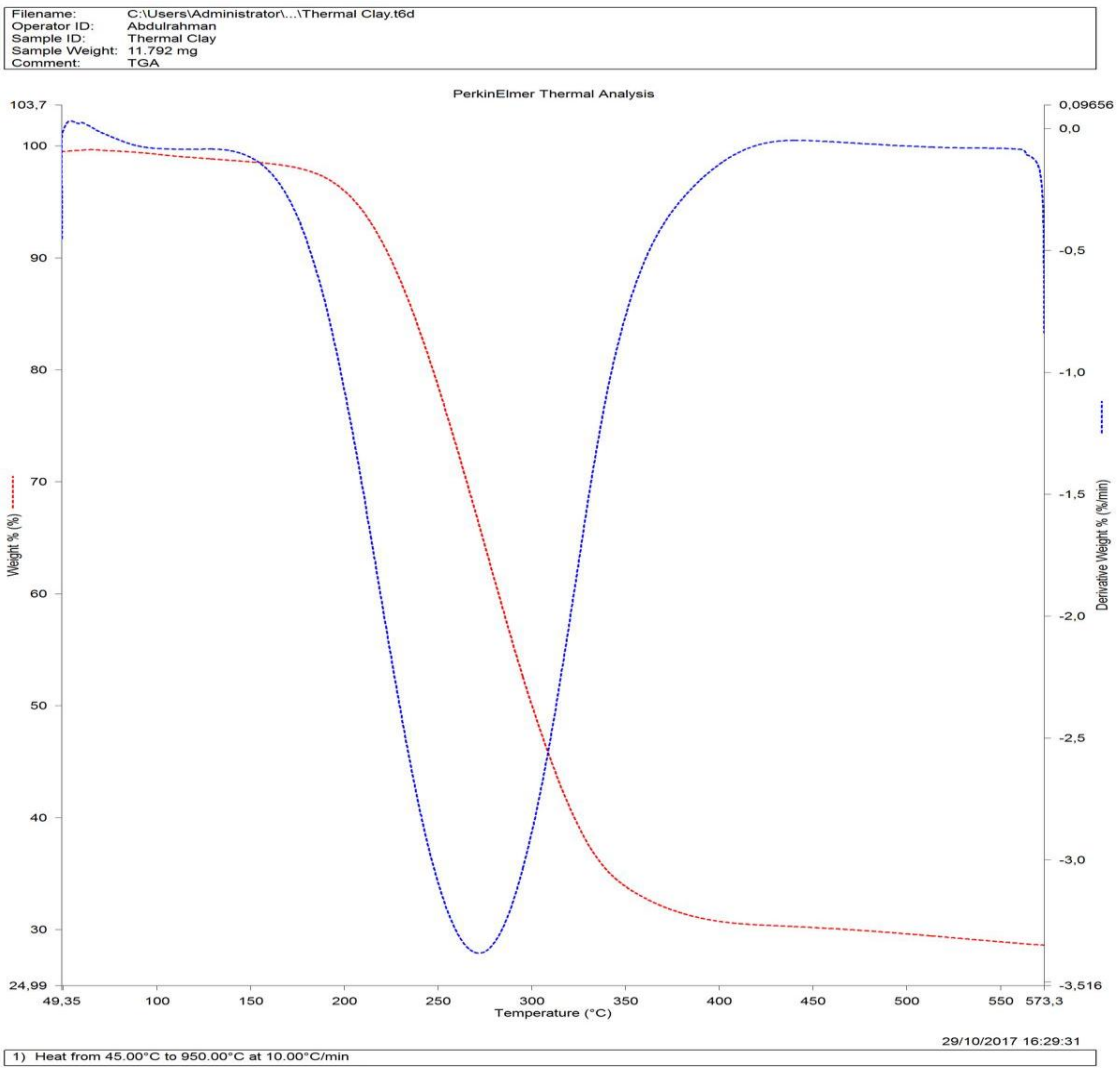

Figure 4.44: TGA-DTA analysis of thermally activated clay catalyst.

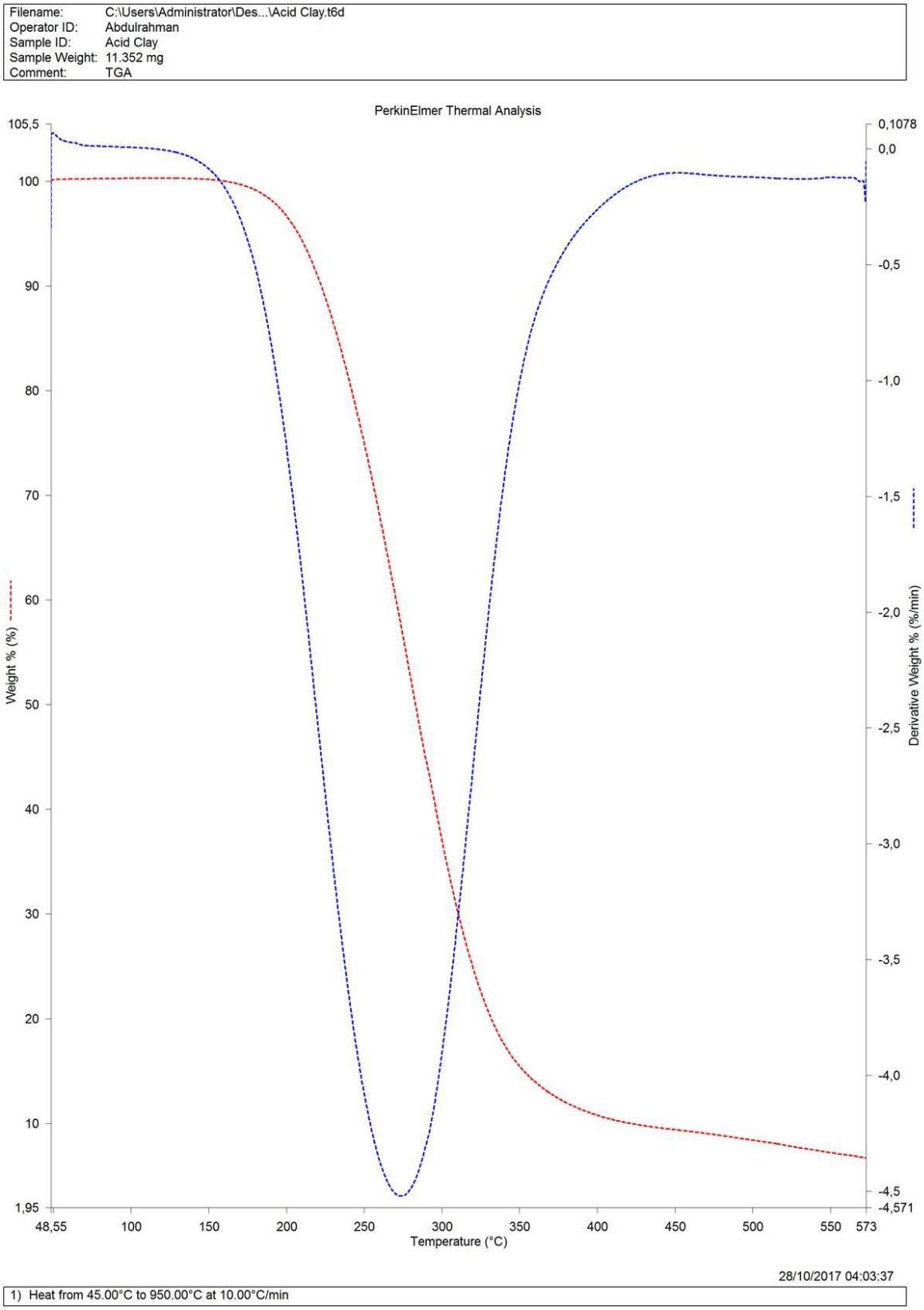

Figure 4.45: TGA-DTA analysis of acid activated clay catalyst.

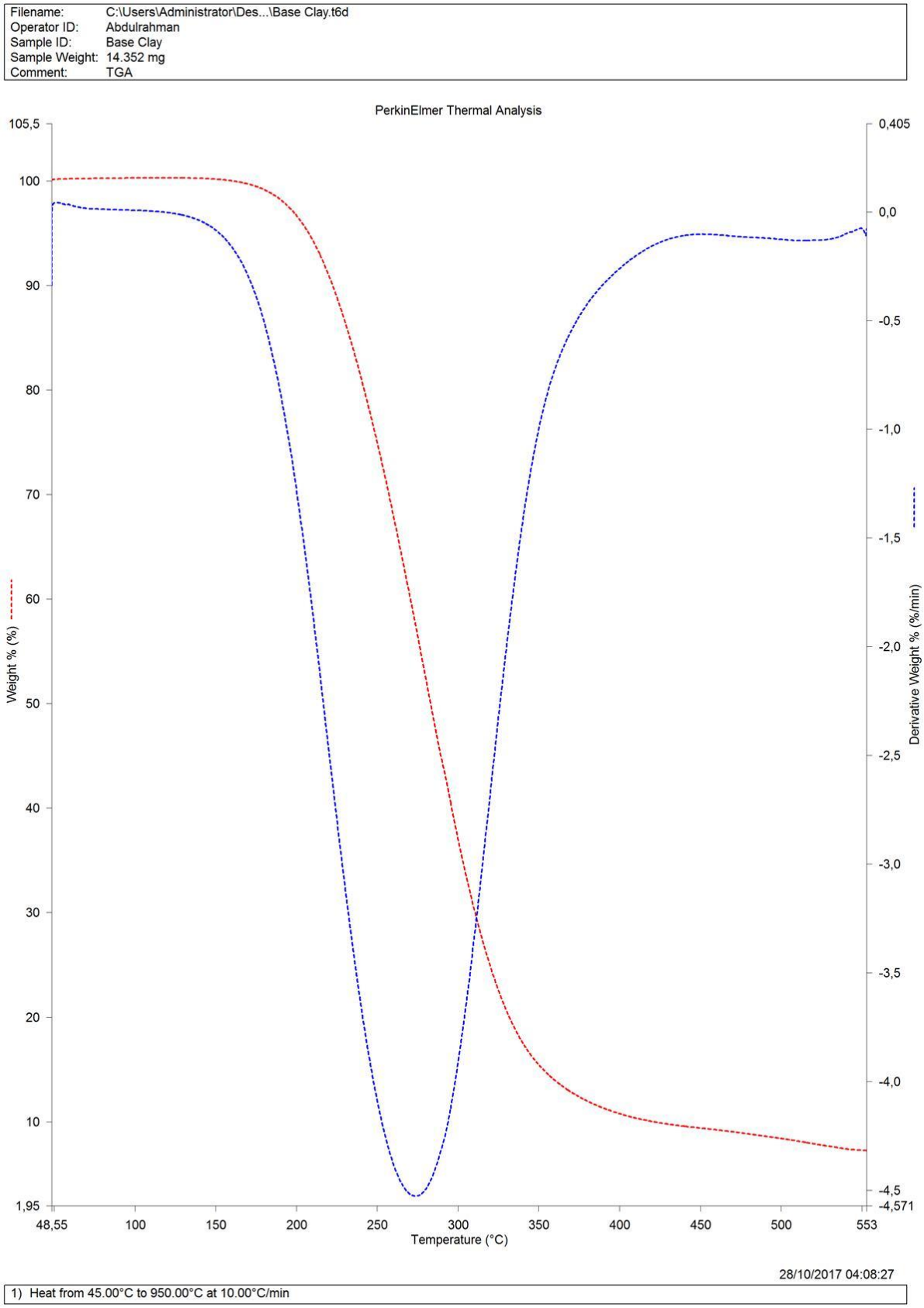

Figure 4.46: TGA-DTA analysis of base/alkaline activated clay catalyst.

4.8 Effects of Process Parameters on Biodiesel Yield

4.8.1 Effect of time on biodiesel yield

The percentage yieldof biodiesel increased with reaction time. In this work, the effect of reaction time from 1h to 5h on the reaction yield using raw clay catalyst, thermally activated clay catalyst, acid activated clay catalyst and base/alkaline activated clay catalystwere investigated and shown in Figure 4.47. It was found that higher yield occurred at reaction time of 3h for both African pear seed oil biodiesel and gmelina seed oil biodiesel and beyond it the yield decreased (as shown in Figure 4.47). The reaction was very slow due to diffusion of methanol and triglyceride into the active site of the catalysts is slow and the decreased in the yield after 3h reported above may be due to reversible reaction of transesterification resulting in loss of esters. The yield obtained by thermally, acid and base/alkaline activated clay was found to be greater than the yield by raw clay and this could be attributed to the activation.

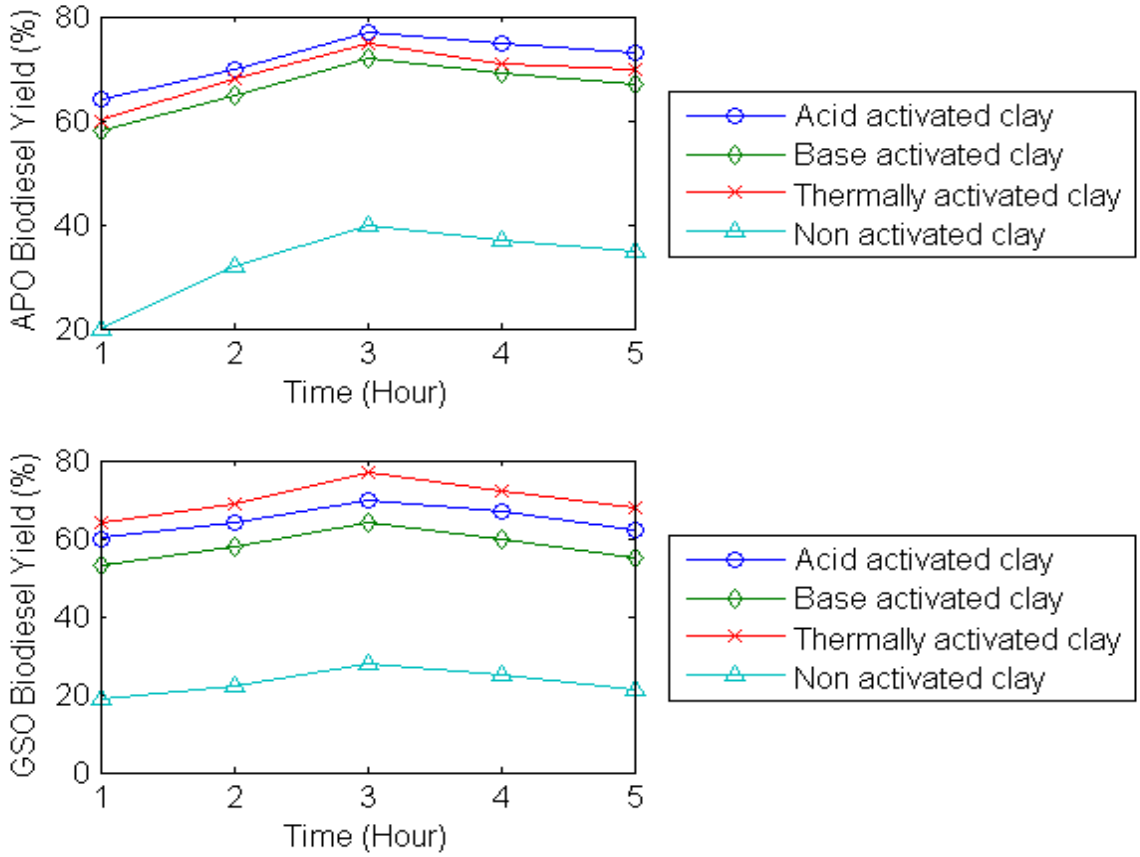

Figure 4.47: Effect of time on biodiesel by clay catalysts. Conditions: temperature = 55^{o}C, catalyst conc. = 3wt%, methanol/oil molar ratio = 12:1, speed = 300rpm.

4.8.2 Effect of catalyst concentration on biodiesel yield

In a chemical reaction, the bonds holding the reactants together must first be broken before the reaction can begin. Breaking bonds requires energy, and the minimum energy needed to start a reaction is referred to as activation energy. Catalysts provide alternative reaction pathways for breaking and remaking of bonds. The activation energy for this new pathway is often less than the activation energy of the normal pathway. Raw clay, thermally activated clay, acid activated clay and base/alkaline activated clay catalysts were used as heterogeneous catalysts for the transesterification reaction in this work. The effect of catalysts concentrations expressed as weight percentage of the African pear seed oil and gmelina seed oil on the production yield is presented in Figure 4.48. From Figure 4.48, it could be observed that the yield of methyl ester increased with increase in catalyst weight up to 3 wt% for the raw clay catalyst and the activated clay catalysts in both African pear seed oil and gmelina seed oil and then began to decrease. Initially the amount of catalyst helped to accelerate the reaction by increasing the reaction rate. The higher yield of ester with increase in catalyst weight is due to the higher availability of catalyst in the reaction medium. Increasing the catalyst weight beyond the catalyst weight of 3 wt% led to the decrease in ester yield. This may be due to excess catalyst causing dispersion and mixing problems, thereby inhibiting the formation of end product (Zhang et al., 2003).

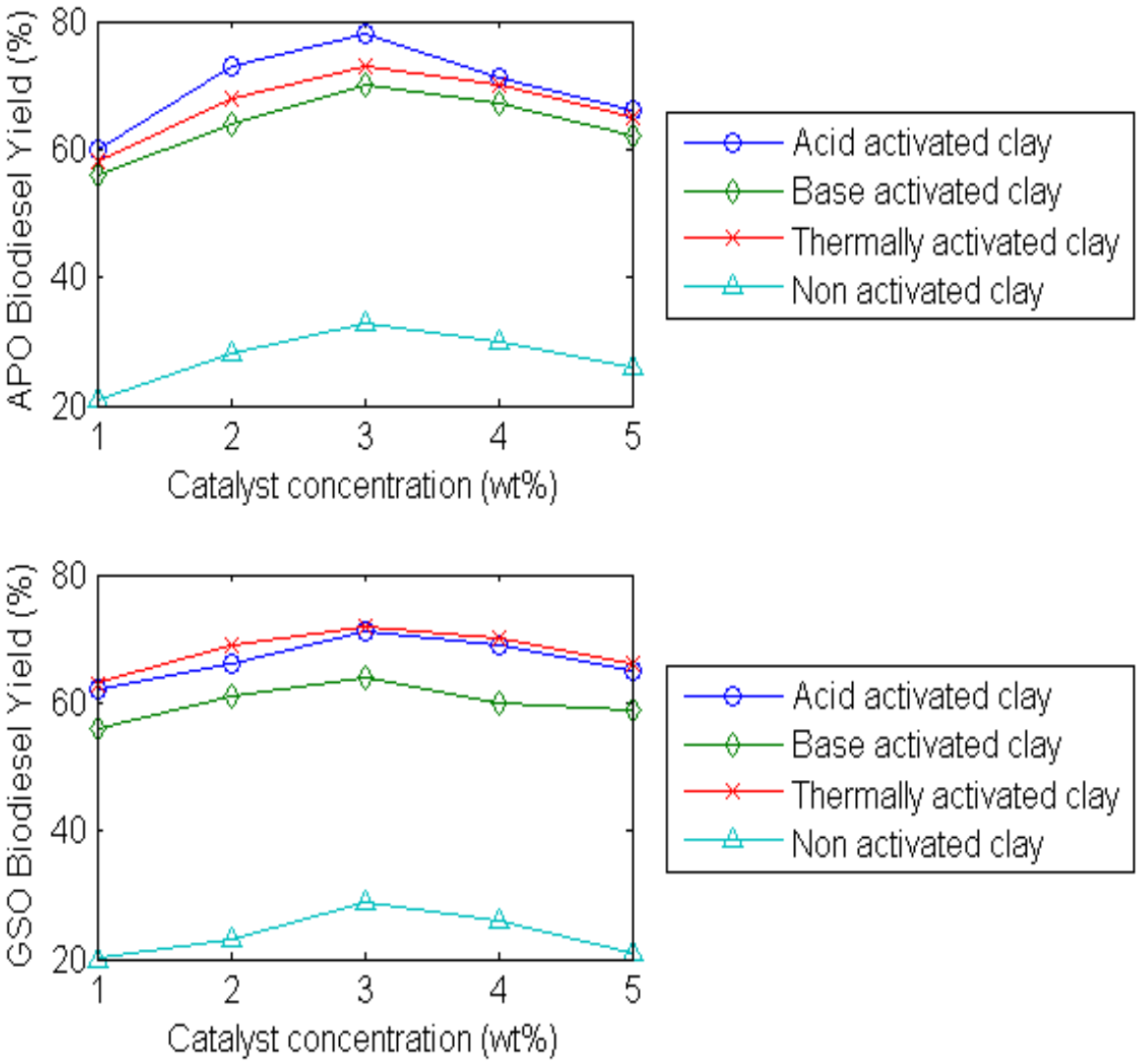

Figure 4.48: Effect of catalyst concentration by clay catalysts.Conditions: temperature = 55^{o}C, methanol/oil molar ratio = 12:1, speed = 300rpm, time = 3h.

4.8.3 Effect of methanol/oil molar ratio on biodiesel yield

The alcohol to oil molar ratio is one of the most important factors that can affect the yield of esters. The stoichiometry of the transesterification reaction requires 3:1 molar ratio to yield 3 moles of ester and 1 mole of glycerol, but most researchers have found that excess alcohol was required to drive the reaction close to completion. In this research, methanol was preferred alcohol and the effect its molar ratio in the range of 6:1 to 14:1 for the clay catalysts were investigated, keeping other process parameters fixed. The yield of methyl esters to the

different molar ratio of methanol/oil of raw clay, thermally activated clay, acid activated clay and base/alkaline activated clay catalysts in African pear seed oil and gmelina seed oil is shown in Figure 4.49. The results indicated that methanol oil molar ratio has significant impact on biodiesel yield. The maximum ester yield was obtained at a methanol/oil molar ratio of 10:1 for all the four catalysts considered with raw clay catalyst having lowest yield. The higher molar ratio resulted in higher yield of ester. The yield reduced when the molar ratio was beyond 10:1. This may be due to decrease in the catalyst activity with increased in methanol content and difficulty in glycerol separation. Also it could be that methanol has polar hydroxyl group which act as an emulsifier causing emulsification that made the separation of the ester layer from the water layer very difficult at high volume of the methanol thus, causing loss in the yield of the ester (Leung and Guo, 2006). The results obtained are in agreement with the reports of earlier works of Zhang et al. (2003).

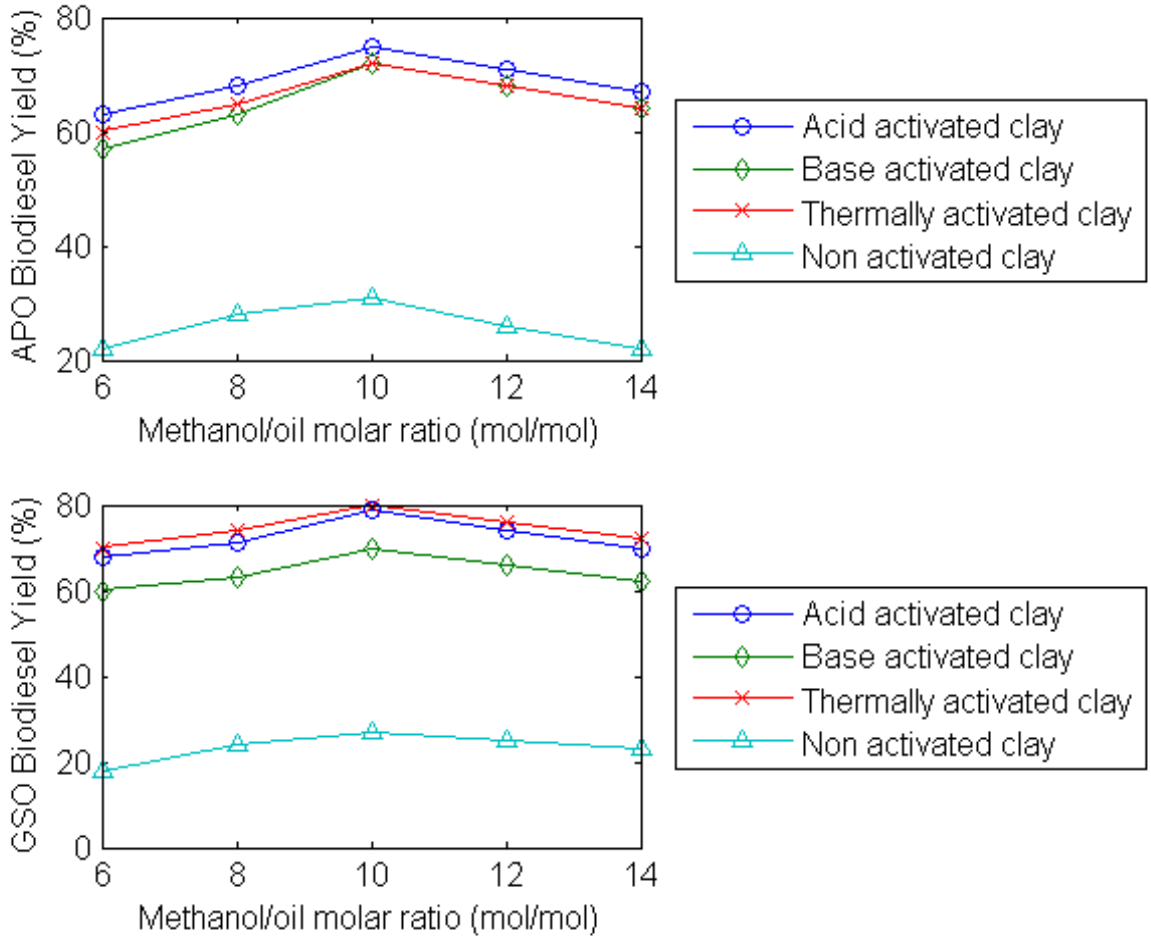

Figure 4.49: Effect of methanol/oil molar ratio on biodiesel yield by clay catalysts. Conditions: temperature = 55^{o}C, speed = 300rpm, time = 3h, catalyst conc.= 3 wt %.

4.8.4 Effect of temperature on biodiesel yield

In the presence of heterogeneous catalyst, the reaction mixture constitutes a two-phase system, oil/methanol-catalyst in which the reaction would be slowed down because of the diffusion resistance between oil/methanol mixture and the catalyst unlike with homogeneous catalyzed reaction that constitutes one-phase. However the reaction rate can be accelerated at higher reaction temperatures. For studying the effect of temperature on the yield of the transesterification reaction of African pear seed oil and gmelina seed oil with raw clay, thermally activated clay, acid activated clay and base/alkaline activated clay catalysts, the reaction temperature was varied as 45, 50, 55, 60, 65 and 70^{o}C, while the other parameters were kept constant. As shown in Figure 4.50, the reaction rate was slow at low temperatures, but biodiesel yield first increased and then decreased with the increased of the reaction temperature beyond 60^{o}C. Generally, a more rapid reaction rate could be obtained at high temperatures, but at high temperatures, methanol was vaporised and formed a large number of bubbles, which inhibited the reaction on the two-phase interface. Similar result was reported by Liu et al.,(2008).

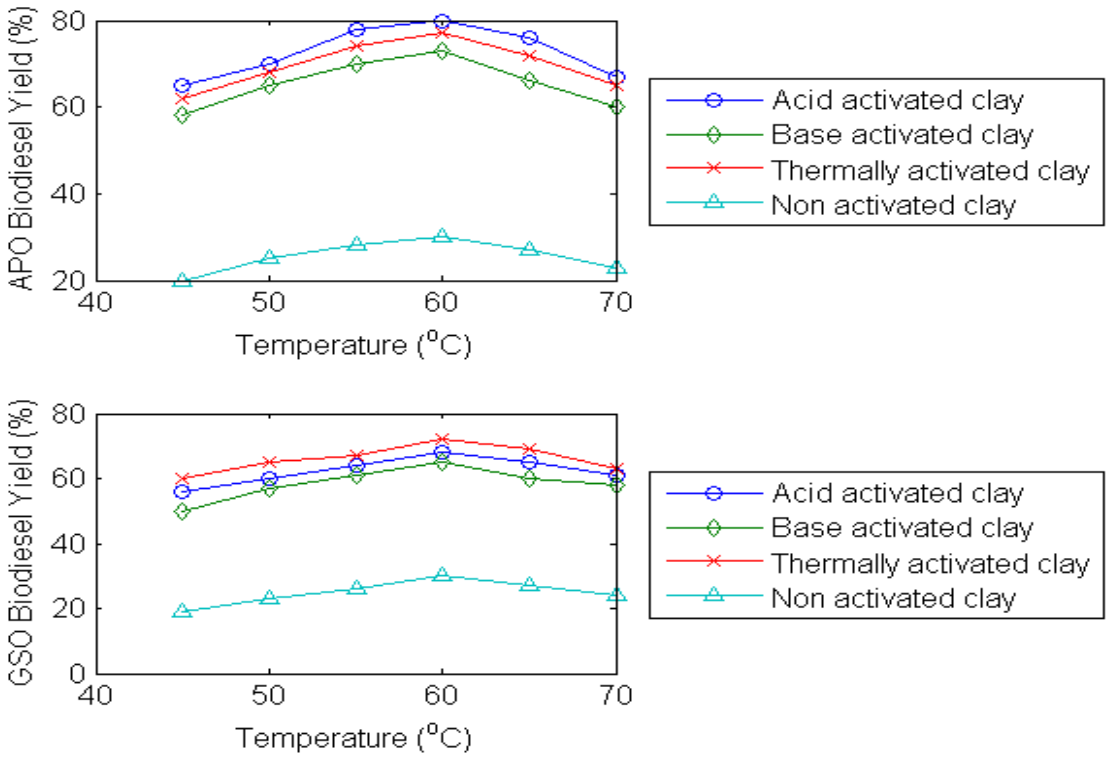

Figure 4.50: Effect of temperature on biodiesel yield by clay catalysts. Conditions: speed = 300rpm, time = 3h, catalyst conc. = 3 wt %, methanol/oil molar ratio = 10:1

4.8.5 Effect of speed of agitation on biodiesel yield

The mixing appears to be of particular importance for the transesterification process: it ensures homogeneity within the reaction mixture. It increased the contact area between oils and catalyst or methanol solution (Liu et al., 2008). Mixing also facilitates the reaction. In this study, methanolysis was conducted with different rate of stirring such as 100, 200, 300, 400 and 500 revolutions per minutes (rpm).The yield of methyl esters produced fromAfrican pear seed oil and gmelina seed oil with raw clay, thermally activated clay, acid activated clay and base/alkaline activated clay catalysts at different rate of mixing is shown in Figure 4.51. It was observed from the figure that the reaction of methanolysis was low at 100rpm and only exhibited a yield which was difficult to separate. The yield was observed to decrease as the stirring rate went above 300rpm for all the catalysts in both oils; the backward reaction may have been favoured when mixing intensity was accelerated.

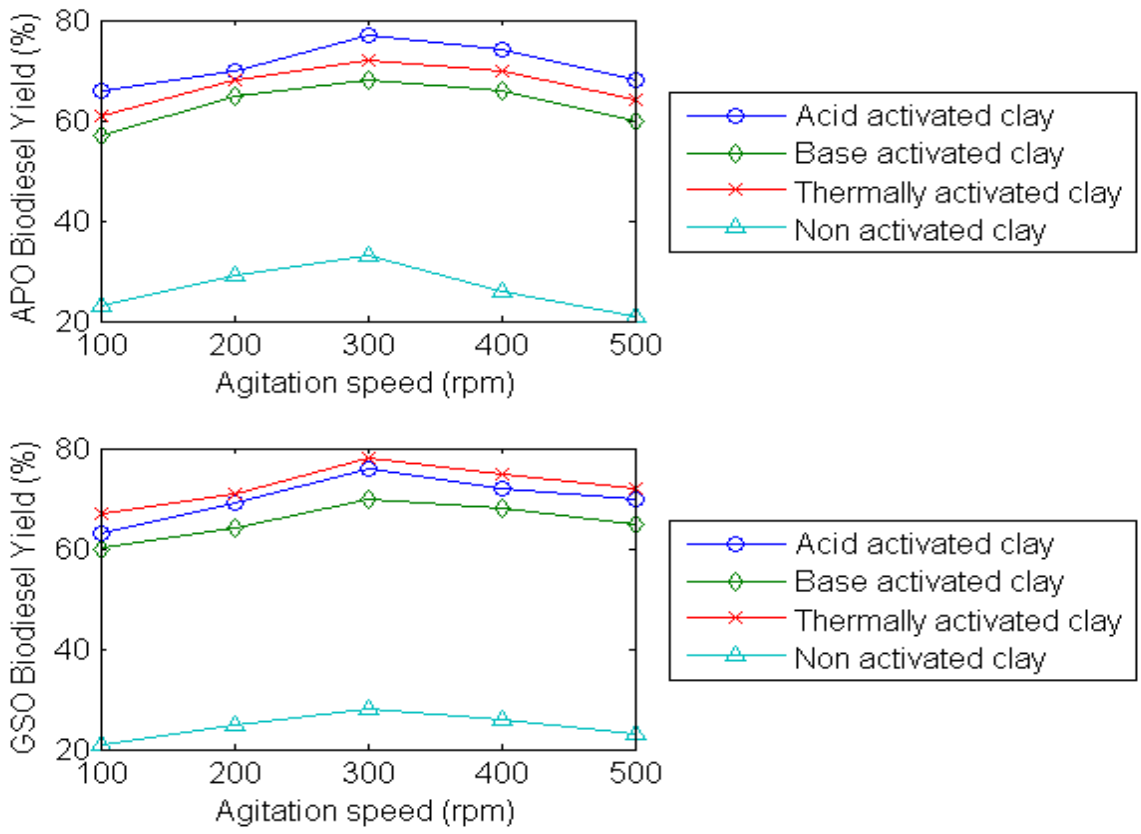

Figure 4.51: Effect of agitation speed on biodiesel yield by clay catalysts. Conditions: time = 3h, catalyst conc. = 3 wt %, methanol/oil molar ratio = 10:1, temperature = 60^{o}C.

Conclusively, acid activated clay catalyst was observed to give more biodiesel yield than other catalysts in African pear seed oil while thermally activated clay catalysts perform better than other catalysts in gmelina seed oil. This could be attributed to higher content of unsaturated free fatty acid in African pear seed oil than gmelina seed oil. Raw clay catalyst performed lowest which suggests the need for improving its catalytic activity by activation. Therefore, it was not used in the next section of this study. The heterogeneous catalysts used are readily available, cheap and converted triglyceride to methyl ester without treating the oils to lower the FFA value. The separation of biodieseland the catalyst wasvery easy to separate because of their heterogeneous nature. It gave yield above 70%, therefore it can serve as a close substitute for homogeneous catalyst.

4.9 Statistical Analysis of Biodiesel Production from African Pear Seed Oil and Gmelina Seed oil.

Minitab version 17 was employed to develop model and statistically analyze the model for the production of biodiesel from both African pear and gmelina seeds oils using thermally activated clay (TAC) catalyst, acid activated clay (AAC) catalyst and base/alkaline activated clay (BAC) catalyst.

4.9.1 Statistical analysis of biodiesel production from African seed oil using different catalysts.

Central composite design of response surface methodology in Minitab v.17 was used to develop models for biodiesel production from African pear seed oil using thermally activated clay (TAC) catalyst, acid activated clay (AAC) catalyst and base/alkaline activated clay (BAC) catalyst. The experimental design employed was a two-level-five factor fractional factorial design, involving 32 experiments. Catalyst concentration, methanol/oil molar ratio, reaction temperature, reaction time and agitation speed were selected as independent factors for the optimization study. The response chosen was the biodiesel yield obtained from transesterification.The response surface design table for the transesterification study is given in Tables 3.4(a) and the responses are presented in Table G1 of Appendix G. The models developed by the software in terms of coded values are shown in Equations 4.9, 4.10, 4.11 and 4.12 for the yields of biodiesel from African seed oil by thermally activated clay (TAC) catalyst, acid activated clay (AAC) catalyst and base/alkaline activated clay (BAC) catalyst.

Yield of FAME by TAC =
$$70.48 + 1.06A + 1.27B + 0.90C + 0.73D + 0.31E - 1.91AB + 0.28AC - 0.250AD + 0.700AE - 2.050BC + 2.550BD + 0.750BE - 3.70CD - 0.250CE + 0.250DE - 4.05A^2 - 3.42B^2 - 2.30 - 2.92D^2 - 0.670E^2 \quad (4.9)$$

Yield of FAME by AAC
$$= 76.03 + 1.13A + 1.21B + 0.71C + 0.63D + 0.71E - 1.06AB + 0.69AC + 1.19AD - 0.31AE + 0.56BC - 0.94BD + 0.56BE - 2.44CD - 0.69CE + 2.56DE - 4.91A^2 - 4.41B^2 - 2.41C^2 - 3.28D^2 - 1.16E^2 \quad (4.10)$$

Yield of FAME by BAC
$$= 69.26 + 0.92A + 1.00B + 0.58C + 0.58D + 0.33E - 1.38AB + 0.25AC + AD - 0.5AE + 0.63BC - 1.38BD + 0.63BE - CD - 0.75CE + 1.50DE - 4.57A^2 - 4.07B^2 - 2.82C^2 - 3.32D^2 - 0.95E^2 \quad (4.11)$$

$$\text{WhereA} = \text{Catalyst concentration(wt\%)}, \text{B} = \frac{\text{methanol}}{\text{oil}} \text{molar ratio (mol/mol)},$$

$$\text{C} = \text{Temperature(°C)}, \text{D} = \text{Time(Hour)}, \qquad \text{E} = \text{Agitationspeed (rpm)}$$

4.9.2 Adequacy analysis of the models

The analysis of variance for the model of the transesterification process parameters are shown in Tables 4.20 – 4.22. From the tables, it could be observed that square terms have more significant effect as they have highest F-values followed by interaction terms while the single terms have least significant effect with lowest F-values. The coefficient of determination and error standard deviation of the models are shown in Table 4.22.From table, it could be observed that the coefficient of determination and error standard deviation of the models indicate that the models fit the data. This could beas a result of the interaction and square terms that improved the adequacy of the models.

Table 4.20: ANOVA for the model of Yield of FAME by TAC catalyst

Source	DF	Adj SS	Adj MS	F-Value	P-Value
Model	20	1466.32	73.316	156.67	0.002
Linear	5	100.22	20.044	42.83	0.001
Square	5	997.45	199.489	426.28	0.003
Interaction	10	368.66	36.866	78.78	0.004
Error	11	5.15	0.468		
Lack-of-Fit	6	3.94	0.657	0.37	0.871
Pure Error	5	1.21	0.242		
Total	31	1471.47			

Table 4.21: ANOVA for the model of Yield of FAME by AAC (%)

Source	DF	Adj SS	Adj MS	F-Value	P-Value
Model	20	1824.63	91.231	245.31	0.003
Linear	5	98.88	19.775	53.17	0.005
Square	5	1444.13	288.826	776.62	0.001
Interaction	10	281.63	28.163	28.163	0.002
Error	11	4.09	0.372		
Lack-of-Fit	6	2.09	0.348	0.87	0.572
Pure Error	5	2.00	0.400		
Total	31	1828.72			

Table 4.22: ANOVA for the model of Yield of FAME by BAC (%)

Source	DF	Adj SS	Adj MS	F-Value	P-Value
Model	20	1560.45	78.023	385.66	0.001
Linear	5	63.17	12.633	62.45	0.004
Square	5	1342.29	268.458	1326.98	0.006
Interaction	10	155.00	15.500	76.62	0.002
Error	11	2.23	0.202		
Lack-of-Fit	6	0.35	0.058	0.16	0.979
Pure Error	5	1.88	0.375		
Total	31	1562.68			

Table 4.23: Coefficients of determination and ESD for the models

Responses	S	R-sq	R-sq(adj)	R-sq (pred)
Yield of FAME by TAC (%)	0.344808	99.90	99.73	99.68
Yield of FAME by AAC (%)	0.609837	99.78	99.37	96.81
Yield of FAME by BAC (%)	0.449786	99.86	99.60	99.23

From Tables 4.24, 4.25 and 4.26, it could be observed that all the five variables: catalyst conc. (A), methanol/oil molar ratio (B), reaction temperature (C), time (D) and agitation

speed (E) have significant effect on yield of fatty acid methyl ester (FAME) produced by heterogeneous catalyzed reaction. Also from Tables 4.24, 4.25 and 4.26 it was clearly shown that among the five variables studied for heterogeneous catalysts, methanol/oil molar ratio (B) has the largest effect on the yield of FAME as it has the highest F-test value. There were also significant interaction effects between variables; as shown by those between catalyst concentration and methanol/oil molar ratio, catalyst concentration and reaction time, methanol/oil molar ratio and reaction temperature, methanol/oil molar ratio and reaction time, methanol/oil molar ratio and agitation speed, reaction temperature and time, reaction temperature and agitation speed, time and agitation speed for transesterified reaction by TAC and AAC catalysts while for BAC transeterified reaction, all the interactions were significant. The test of significance terms in the models as shown in Tables 4.24 to 4.26 was carried out on 95% level of confidence or 5% significance level. Individual terms in the model are said to be statistically significant to the responses if $P - val < 0.05$ and therefore, those statistically insignificant terms were eliminated from the model as shown in Equations 4.12 – 4.15.

Table 4.24: Effects and coefficients for model of Yield of FAME by TAC catalyst (%)

Term	Effect	Coef	SE Coef	T-Value	P-Value
Constant		70.483	0.273	258.32	0.001
A	2.125	1.063	0.140	7.61	0.003
B	2.542	1.271	0.140	9.1	0.005
C	1.792	0.896	0.140	6.42	0.001
D	1.458	0.729	0.140	5.22	0.002
E	0.625	0.313	0.140	2.24	0.047
A^2	-8.091	-4.045	0.126	-32.03	0.001
B^2	-6.841	-3.420	0.126	-27.08	0.001
C^2	-4.591	-2.295	0.126	-18.17	0.003
D^2	-5.841	-2.920	0.126	-23.12	0.002
E^2	-1.341	-0.670	0.126	-5.31	0.001
A*B	-3.813	-1.906	0.171	-11.15	0.002
A*C	0.563	0.281	0.171	1.64	0.128
A*D	0.812	0.406	0.171	2.38	0.037
A*E	-0.437	-0.219	0.171	-1.28	0.227
B*C	1.187	0.594	0.171	3.47	0.005
B*D	-3.563	-1.781	0.171	-10.42	0.003
B*E	2.187	1.094	0.171	6.40	0.005
C*D	-5.687	-2.844	0.171	-16.63	0.006
C*E	-1.437	-0.719	0.171	-4.20	0.001
D*E	4.812	2.406	0.171	14.07	0.007

Table 4.25: Effects and coefficients for model of Yield of FAME by AAC (%)

Term	Effect	Coef	SE Coef	T-Value	P-Value
Constant		76.034	0.243	312.59	0.003
A	2.250	1.125	0.124	9.04	0.001
B	2.417	1.208	0.124	9.71	0.002
C	1.417	0.708	0.124	5.69	0.006
D	1.250	0.625	0.124	5.02	0.005
E	1.417	0.708	0.124	5.69	0.002
A^2	-9.818	-4.909	0.113	-43.60	0.001
B^2	-8.818	-4.409	0.113	-39.16	0.003
C^2	-4.818	-2.409	0.113	-21.40	0.004
D^2	-6.568	-3.284	0.113	-29.17	0.001
E^2	-2.318	-1.159	0.113	-10.29	0.003
A*B	-2.125	-1.063	0.152	-6.97	0.001
A*C	1.375	0.687	0.152	4.51	0.001
A*D	2.375	1.188	0.152	7.79	0.006
A*E	-0.625	-0.312	0.152	-2.05	0.065
B*C	1.125	0.563	0.152	3.69	0.004
B*D	-1.875	-0.938	0.152	-6.15	0.002
B*E	1.125	0.562	0.152	3.69	0.004
C*D	-4.875	-2.437	0.152	-15.99	0.003
C*E	-1.375	-0.688	0.152	-4.51	0.001
D*E	5.125	2.562	0.152	16.81	0.002

Table 4.26: Effects and coefficients for model of Yield of FAME by BAC (%)

Term	Effect	Coef	SE Coef	T-Value	P-Value
Constant		69.261	0.179	386.07	0.004
A	1.833	0.917	0.0918	9.98	0.002
B	2.000	1.000	0.0918	10.89	0.005
C	1.167	0.583	0.0918	6.35	0.001
D	1.167	0.583	0.0918	6.35	0.002
E	0.667	0.333	0.0918	3.63	0.003
A^2	-9.148	-4.574	0.0830	-55.08	0.001
B^2	-8.148	-4.074	0.0830	-49.05	0.001
C^2	-5.648	-2.834	0.0830	-34.00	0.007
D^2	-6.648	-3.234	0.0830	-40.02	0.005
E^2	-1.898	-0.949	0.0830	-11.43	0.001
A*B	-2.750	-1.375	0.112	-12.23	0.010
A*C	0.500	0.250	0.112	2.22	0.048
A*D	2.000	1.000	0.112	8.89	0.002
A*E	-1.000	-0.500	0.112	-4.45	0.001
B*C	1.250	0.625	0.112	5.56	0.003
B*D	-2.750	-1.375	0.112	-12.23	0.004
B*E	1.250	0.625	0.112	5.56	0.001
C*D	-2.000	-1.000	0.112	-8.89	0.002
C*E	-1.500	-0.750	0.112	-6.67	0.003
D*E	3.000	1.500	0.112	8.73	0.006

The reduced empirical relationships between the factors and responses developed and analysed using the MINITAB 17 are shown in Equations 4.12, 4.13 and 4.14 for the Yield of FAME by TAC catalyst,Yield of FAME by AAC catalystand
Yield of FAME by BAC catalyst of the transesterification process respectively.

$$\text{Yield of FAME by TAC} = 70.48 + 1.06\text{A} + 1.27\text{B} + 0.90\text{C} + 0.73\text{D} + 0.31\text{E} - 1.91\text{AB} - 0.250\text{AD} - 2.050\text{BC} + 2.550\text{BD} + 0.750\text{BE} - 3.70\text{CD} - 0.250\text{CE} + 0.250\text{DE} - 4.05A^2 - 3.42B^2 - 2.30 - 2.92D^2 - 0.670E^2 \quad (4.12)$$

$$\text{Yield of FAME by AAC} = 76.03 + 1.13\text{A} + 1.21\text{B} + 0.71\text{C} + 0.63\text{D} + 0.71\text{E} - 1.06\text{AB} + 0.69\text{AC} + 1.19\text{AD} - 0.31\text{AE} + 0.56\text{BC} - 0.94\text{BD} + 0.56\text{BE} - 2.44\text{CD} - 0.69\text{CE} + 2.56\text{DE} - 4.91A^2 - 4.41B^2 - 2.41C^2 - 3.28D^2 - 1.16E^2 \quad (4.13)$$

$$\text{Yield of FAME by BAC} = 69.26 + 0.92\text{A} + 1.00\text{B} + 0.58\text{C} + 0.58\text{D} + 0.33\text{E} - 1.38\text{AB} + 0.25\text{AC} + \text{AD} - 0.5\text{AE} + 0.63\text{BC} - 1.38\text{BD} + 0.63\text{BE} - \text{CD} - 0.75\text{CE} + 1.50\text{DE} - 4.57A^2 - 4.07B^2 - 2.82C^2 - 3.32D^2 - 0.95E^2 \quad (4.14)$$

The models adequacy are confirmed graphically using the residual plots which include the normal probability plot, histogram, residual versus fitted values and residual versus observation order in a 4-in-1 format as shown in Figures 4.52 (a, b & c) for TAC, AAC and BAC respectively.It was observed that the figures have similar trend. An analytical view of the figures shows the adequacy of the models and the plots of the normal probability tend to fall in a straight line and residuals were uniformly distributed (Figures 4.52 (a, b & c)). Hence, the models are adequate to statistically fit the data with little outliers and reduced skewness. Residuals or errors obtained in TAC catalyzed reaction (Figure 4.52) is lowest compared to AAC and BAC catalyzed reactions (Figures 4.5b and 4.5c).

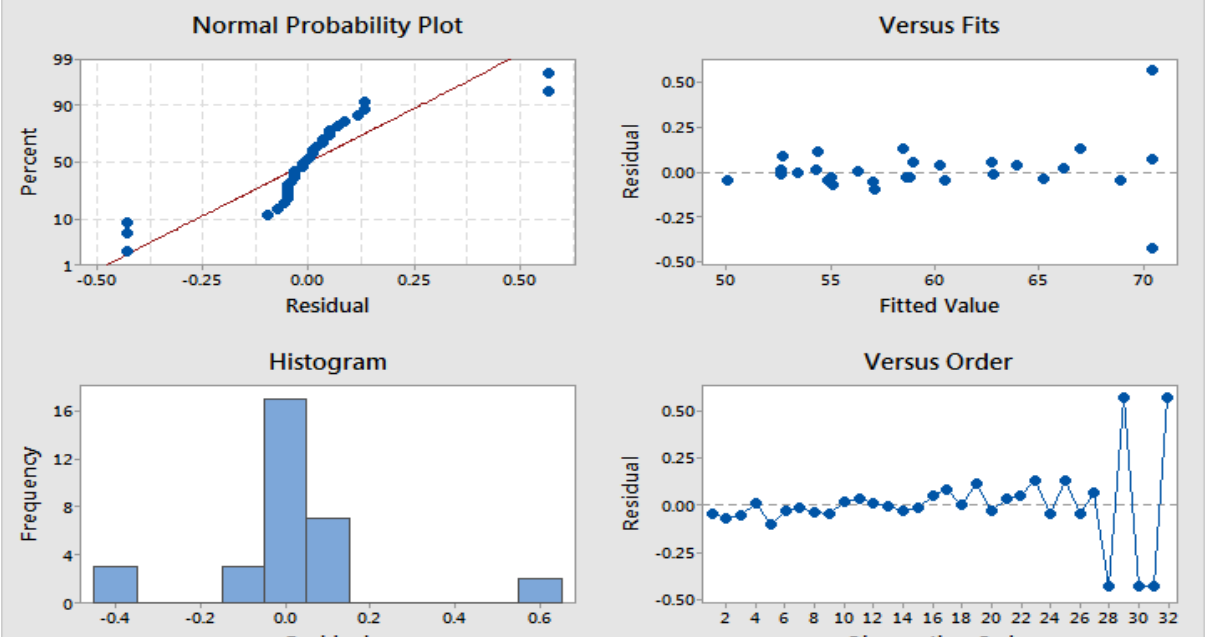

Figure 4.52a: Residual plots for the model of the yield of FAME by TAC.

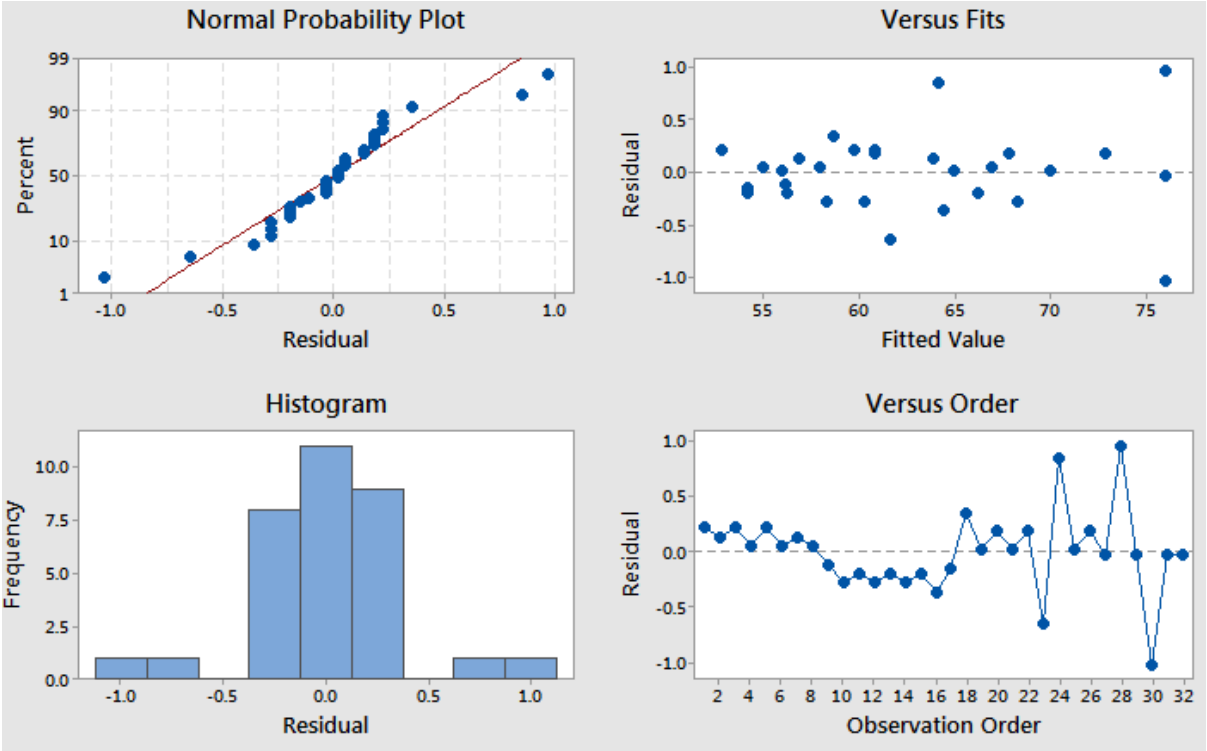

Figure 4.52b: Residual plots for model of the yield of FAME by AAC.

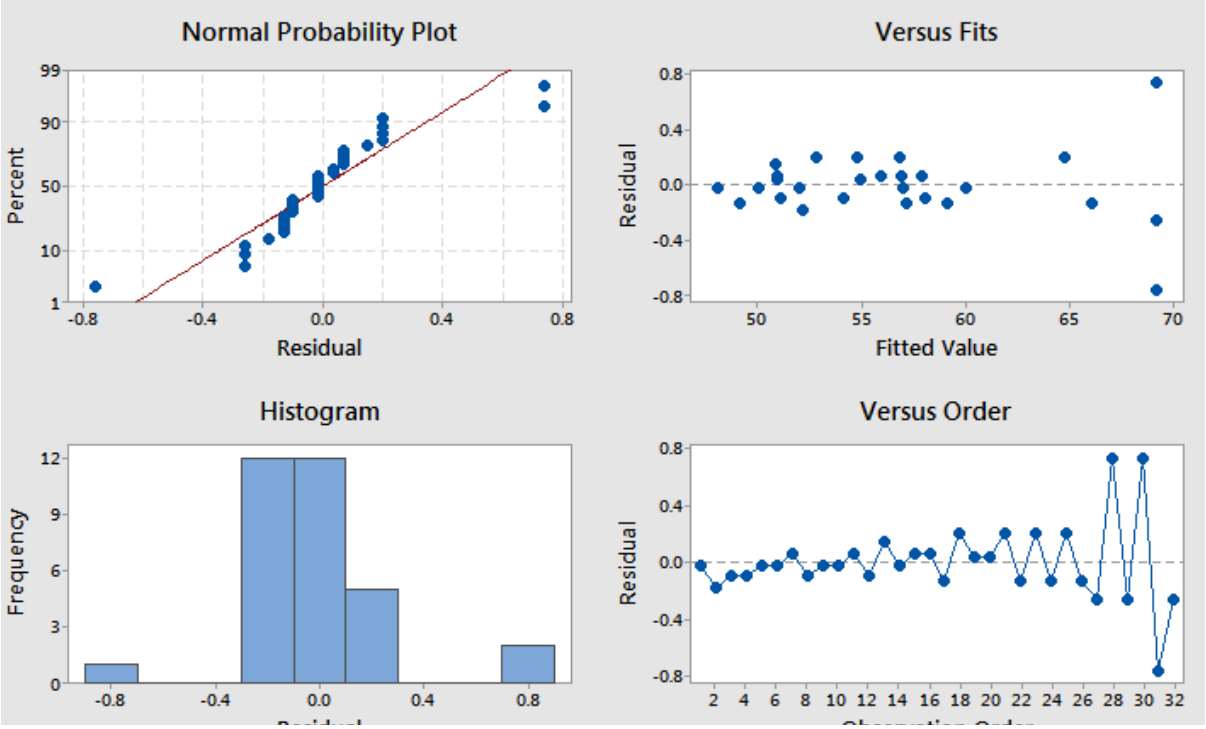

Figure 4.52c: Residual plots for model of the yield of FAME with BAC.

4.9.3 Surface response plots of the model

Figures 4.53 to 4.62 are the surface plots of the predicted FAME yield which can be generated by Equations 4.12 to 4.14 for heterogeneous catalysts TAC, AAC & BAC.The interaction effect of catalyst conc. and methanol/oil molar ratio on yield of FAME is shown in Figures 4.53 (a, b & c) for TAC, AAC and BAC catalyzed reactions respectively. It could be observed from the figures that the effect follow similar trend on the yield for all the catalysts. The figures show that the amount of methyl ester yield increases with methanol/oil molar ratio and catalyst concentration. However, at higher catalyst concentrations and methanol/oil molar ratio, a reduction in the yield can be observed due to the fact that the quadratic terms of the two factors are more significant with a negative effect (Eqs.(4.12), (4.13), (4.14)).

The interaction effect of catalyst conc. and time on yield of FAME is shown in Figures 4.54 (a, b & c) for TAC, AAC and BAC catalyzed reactions respectively. It could be observed from the figures that the effect is similar on the yield for all the catalysts. The figures indicate that increase in reaction time and catalyst concentration increases the yield of FAME. However, at higher reaction time and catalyst concentration, reduction in the yield can be observed due to the fact that the quadratic terms of the two factors are more significant with a

negative effect (Eqs.(4.12), (4.13), (4.14)) which may be as a result of more active sites with lesser reacting species.

The interaction effect of methanol/oil molar ratio and reaction temperature on yield of FAME is shown in Figures 4.55 (a, b & c) for TAC, AAC and BAC catalyzed reactions respectively. It could be observed from the figures that the effect is similar on the yield for all the catalysts. At lower temperature, below 60^{o}C, the yield increases with methanol/oil molar ratio. However, at a temperature above 60^{o}C, there was reduction in yield. This may be as a result of evaporation of methanol which inhibits the reaction on the three-phase interface.

The interaction effect of methanol/oil molar ratio and time on yield of FAME is shown in Figures 4.56 (a, b & c) for TAC, AAC and BAC catalyzed reactions respectively. It could be observed from the figures that the effect is similar on the yield for all the catalysts.The figures indicate that the amount of FAME yields increase with methanol/oil molar ratio and reaction time. This may be as a result of adequate time provided for conversion of the triglyceride. At higher methanol/oil molar ratio and reaction time, a reduction in FAME yield can be observed due to the fact that the quadratic terms of the two factors are more significant with a negative effect (Eqs.(4.12), (4.13), (4.14)).

The interaction effect of methanol/oil molar ratio and agitation speed on yield of FAME is shown in Figures 4.57 (a, b & c) for TAC, AAC and BAC catalyzed reactions respectively.The figures show that the FAME yield increases with methanol/oil molar ratio and agitation speed as a result of a positive significant effect of methanol/oil molar ratio-agitation speed interaction term, BE on response. However, at higher methanol/oil molar ratio and agitation speed a reduction in the yield can be observed due to the fact that the quadratic terms of the two factors are more significant with a negative effect and the high speed could not allow further conversion of triglyceride.

The interaction effect of reaction temperature and time on yield of FAME is shown in Figures 4.58 (a, b & c) for TAC, AAC and BAC catalyzed reactions respectively. At lower temperature, below 60^{o}C the yield increase with increase in time. However, at a temperature above 60^{o}C, there was reduction in yield. This may be as a result of evaporation of methanol which inhibits the reaction on the three-phase interface.

The interaction effect of reaction temperature and agitation speed on yield of FAME is shown in Figures 59 (a, b & c) for TAC, AAC and BAC catalyzed reactions respectively.The figures

indicate that the yield of FAME increases with reaction temperature and agitation speed. However, at higher reaction temperature and agitation speed, there was a decrease in FAME yield because there is a negative significant effect of reaction temperature-agitation speed interaction term, (CE) on response (Tables 4.23 to 4.25).

The interaction effect of time and agitation speed on yield of FAME is shown in Figures 60 (a, b & c) for TAC, AAC and BAC catalyzed reactions respectively.The figures indicate that the yield of FAME increases with reaction time and agitation speed. However, at higher reaction time and agitation speed, there was a reduction in FAME yield which may be attributed to reversible reaction of transesterification resulting in loss of esters.

The interaction effect of catalyst conc. and temperature on yield of FAME is only significant for AAC and BAC catalyzed reactions and shown in Figures 61 (a & b) respectively.The figures indicate that the yield of FAME increases with reaction temperature and catalyst concentration. This is as a result of a postive significant effect of catalyst concentration and temperature interaction, AC (Tables 4.23 & 4.24). However, at higher catalyst concentration and reaction temperature, a decrease in the yield can be observed due to evaporation of methanol at higher temperature and the fact that the quadratic terms of the two factors are more significant with a negative effect (Tables 4.23 & 4.25).

The interaction effect of catalyst conc. and agitation speed on yield of FAME is only significant for BAC catalyzed reaction and shown in Figure 62. The figures show that the FAME yield increases with catalyst conc. and agitation speed which may be as a result of a proper mixing. However, at higher catalyst concentration and agitation speed a reduction in the yield can be observed due to the fact that the quadratic terms of the two factors are more significant with a negative effect and the high speed could not allow further conversion of triglyceride.

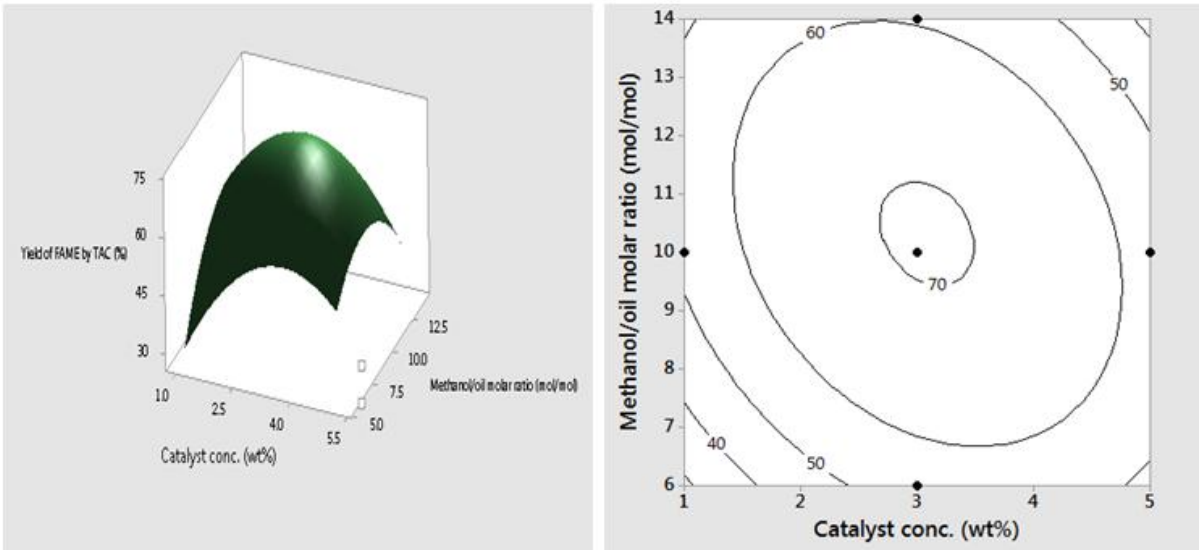

Figure 4.53a: Surface and contour plots of catalyst conc. and methanol/oil molar ratio by TAC.

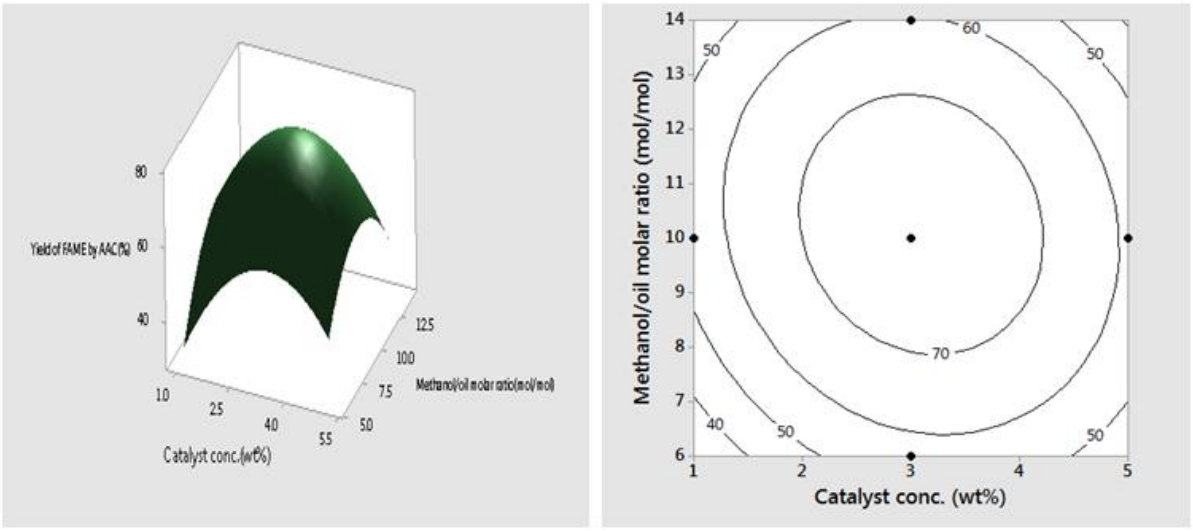

Figure 4.53b: Surface and contour plots of catalyst conc. and methanol/oil molar ratio by AAC.

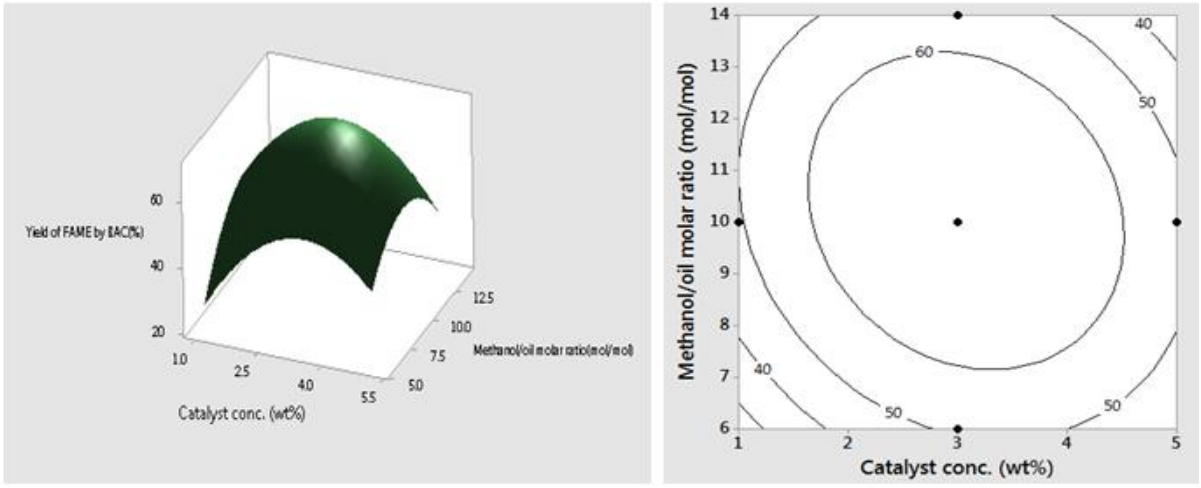

Figure 4.53c: Surface and contour plots of catalyst conc. and methanol/oil molar ratio by BAC.

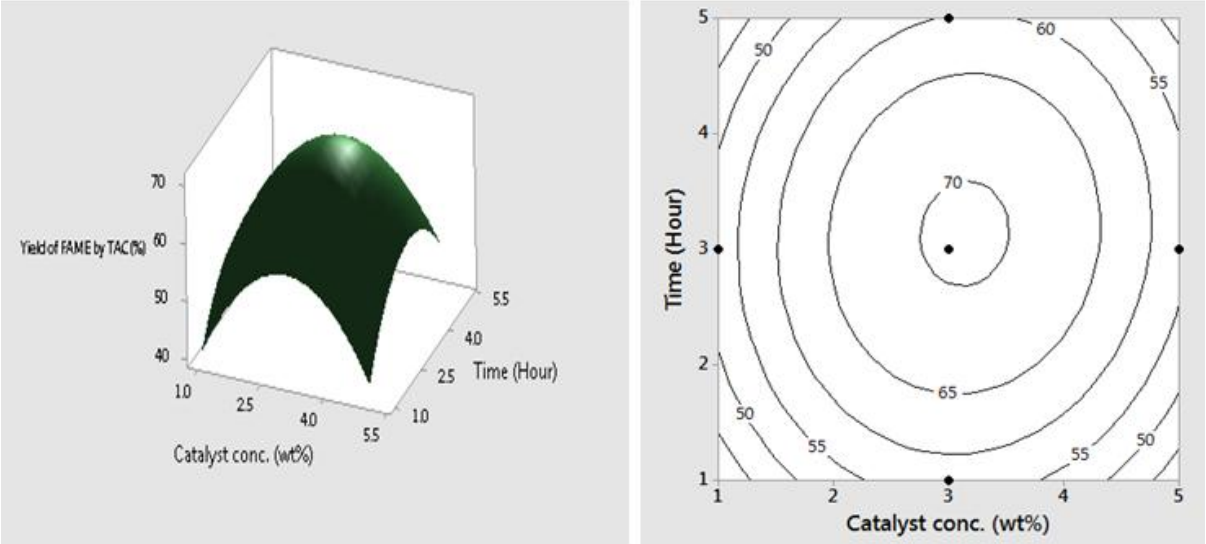

Figure 4.54a: Surface and contour plots of catalyst conc. and time by TAC.

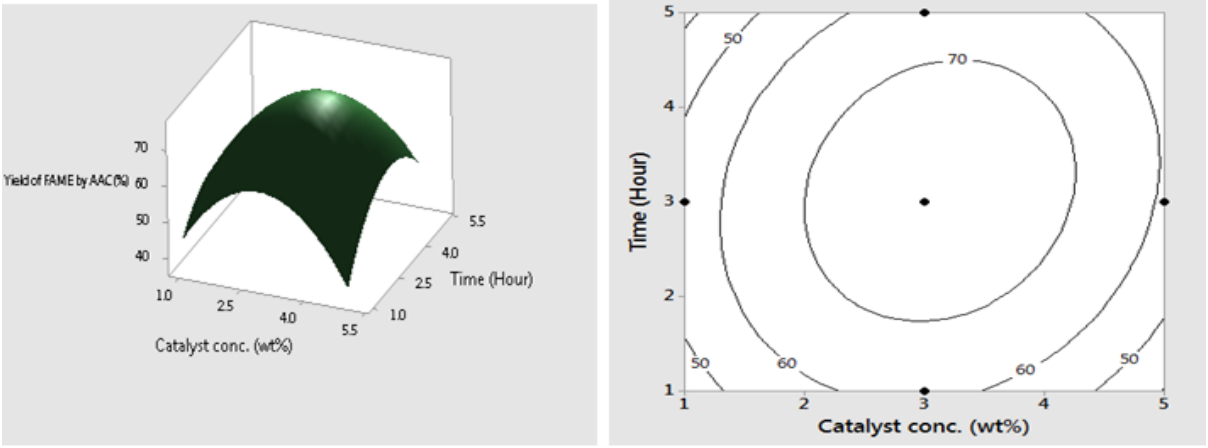

Figure 4.54b: Surface and contour plots of catalyst conc. and time by AAC.

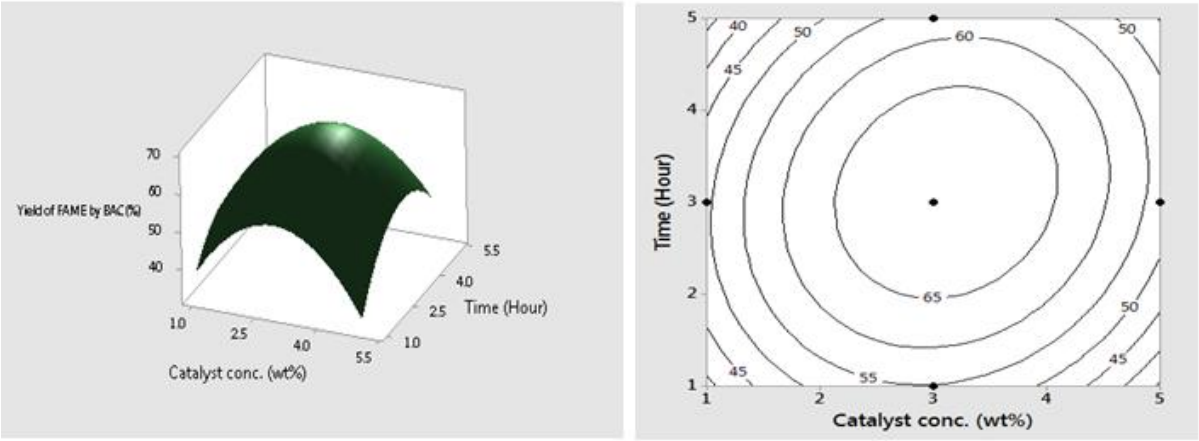

Figure 4.54c: Surface and contour plots of catalyst conc. and time by BAC.

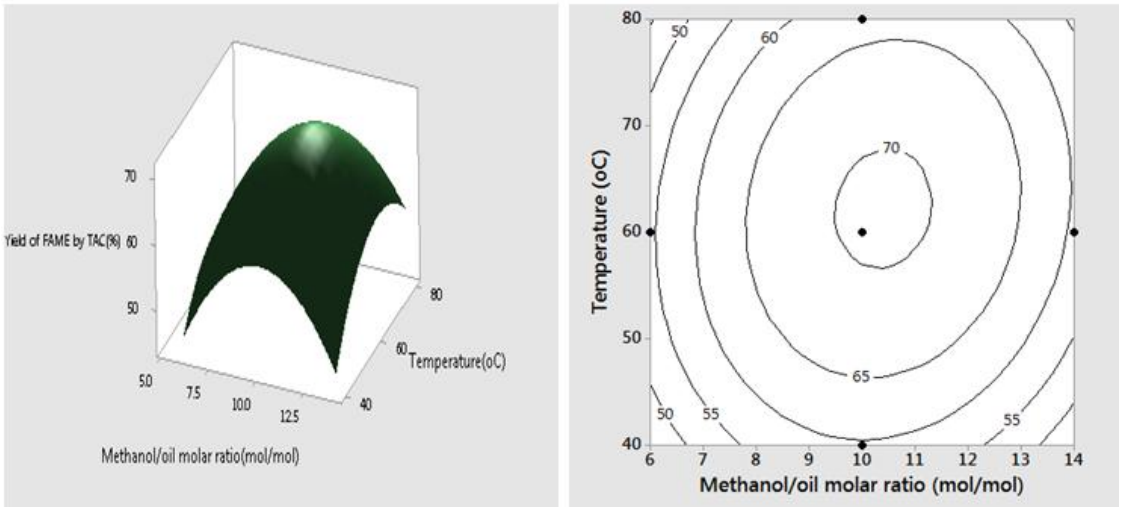

Figure 4.55a: Surface and contour plots of temperature and methanol/oil molar ratio by TAC.

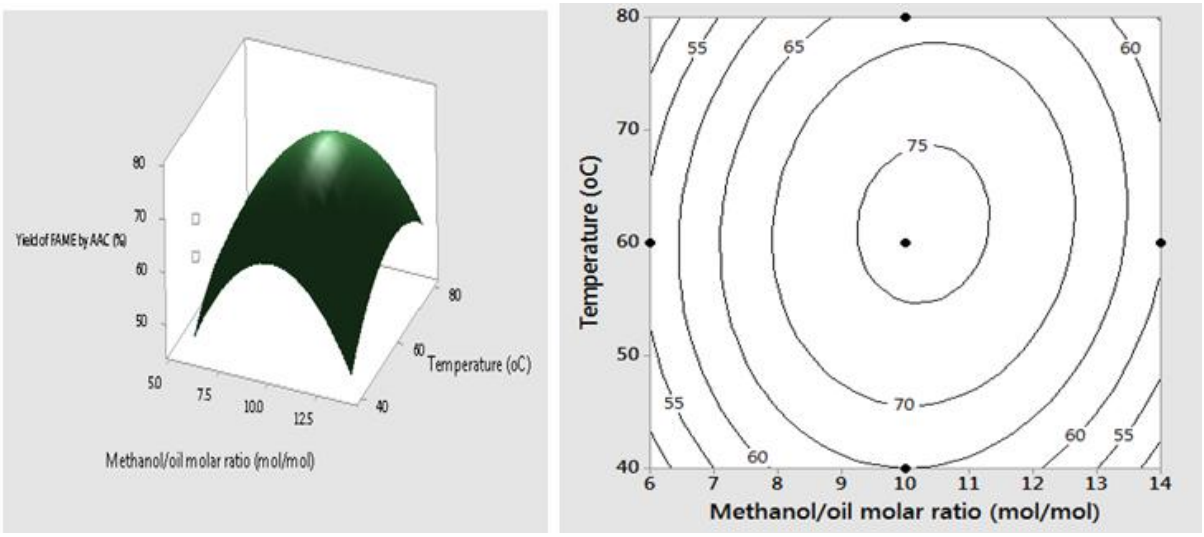

Figure 4.55b: Surface and contour plots of temperature and methanol/oil molar ratio by AAC.

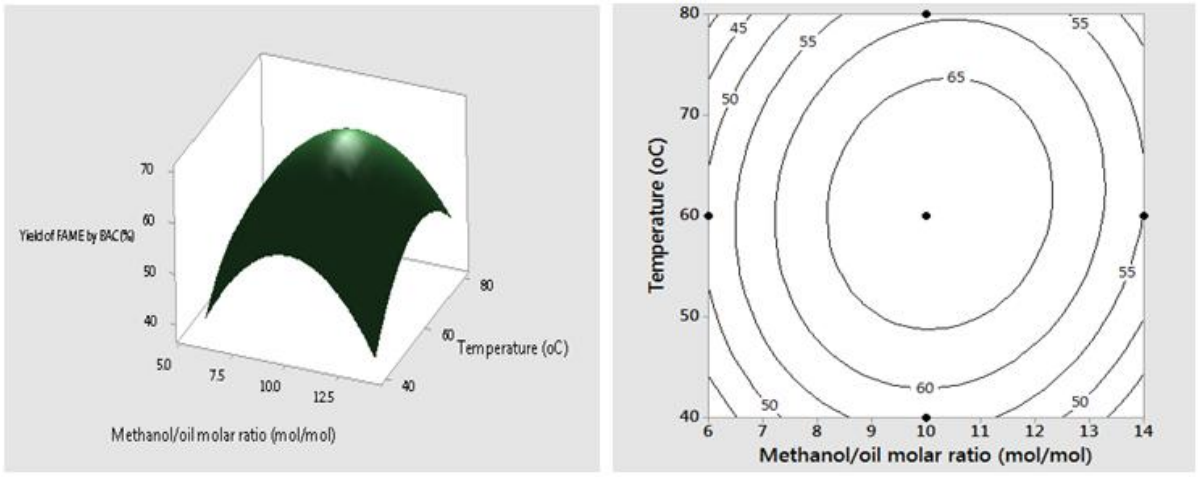

Figure 4.55c: Surface and contour plots of temperature and methanol/oil molar ratio by BAC.

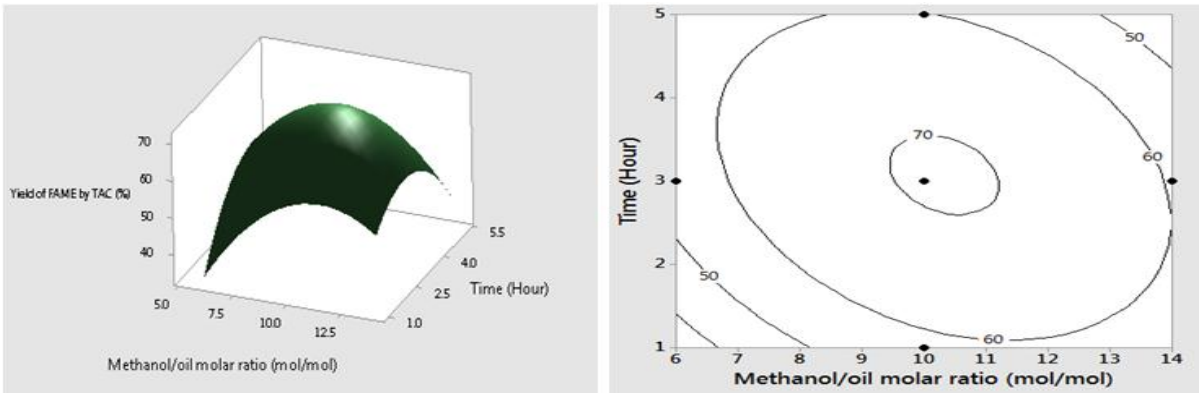

Figure 4.56a: Surface and contour plots of time and methanol/oil molar ratio by TAC.

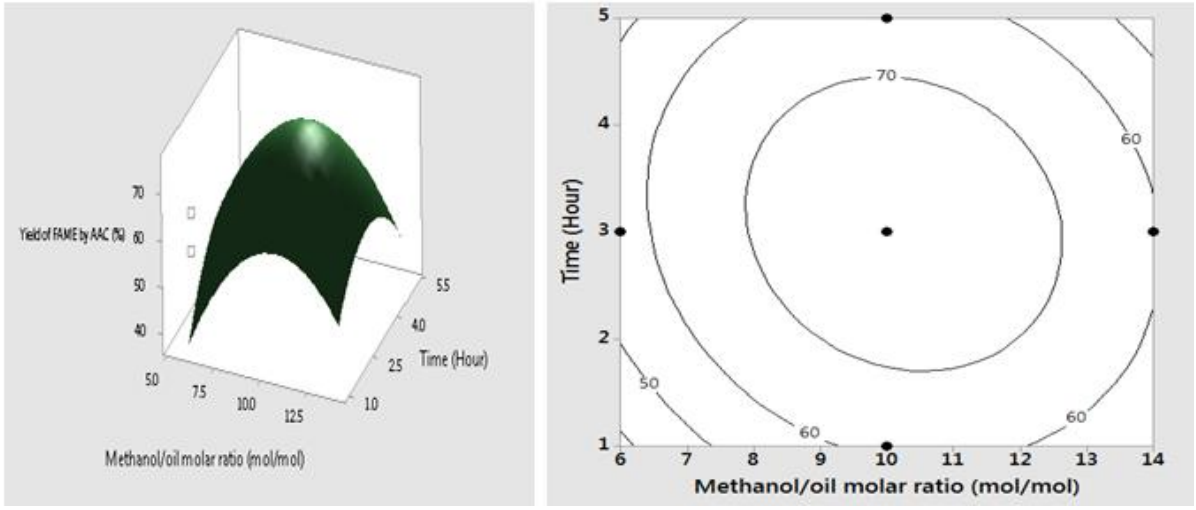

Figure 4.56b: Surface and contour plots of time and methanol/oil molar ratio by AAC.

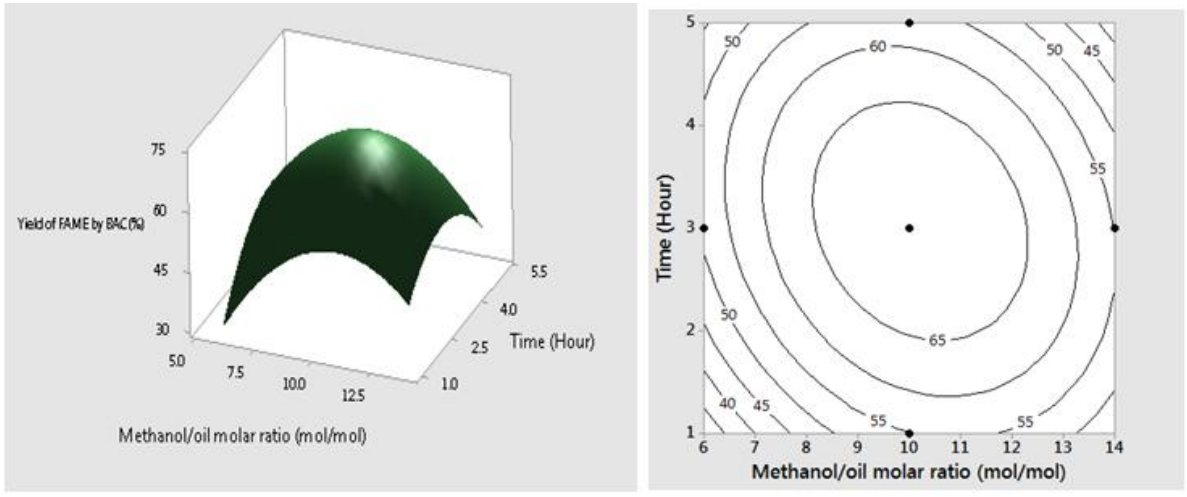

Figure 4.56c: Surface and contour plots of time and methanol/oil molar ratio by BAC.

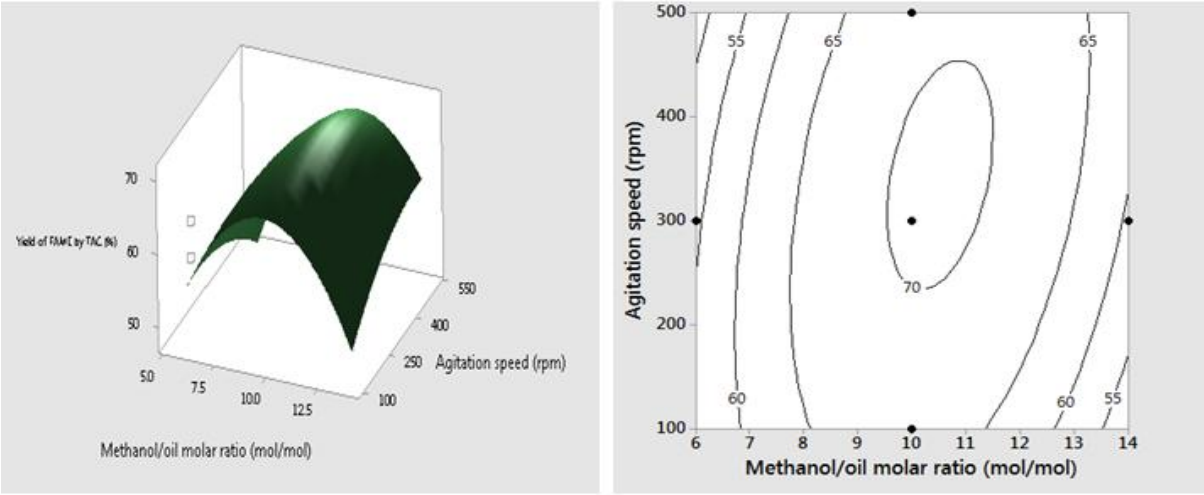

Figure 4.57a: Surface and contour plots of agitation speed and methanol/oil molar ratio by TAC.

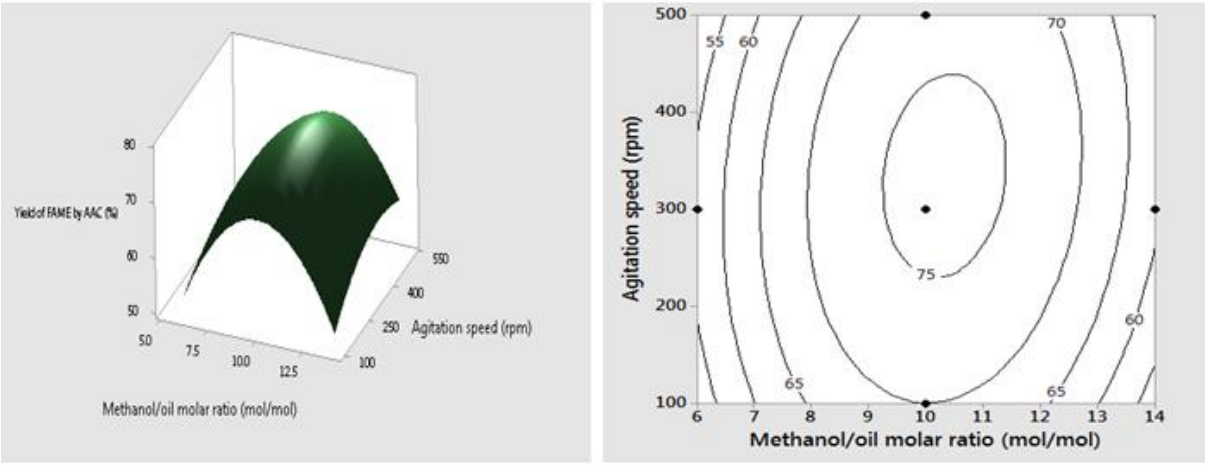

Figure 4.57b: Surface and contour plots of agitation speed and methanol/oil molar ratio by AAC.

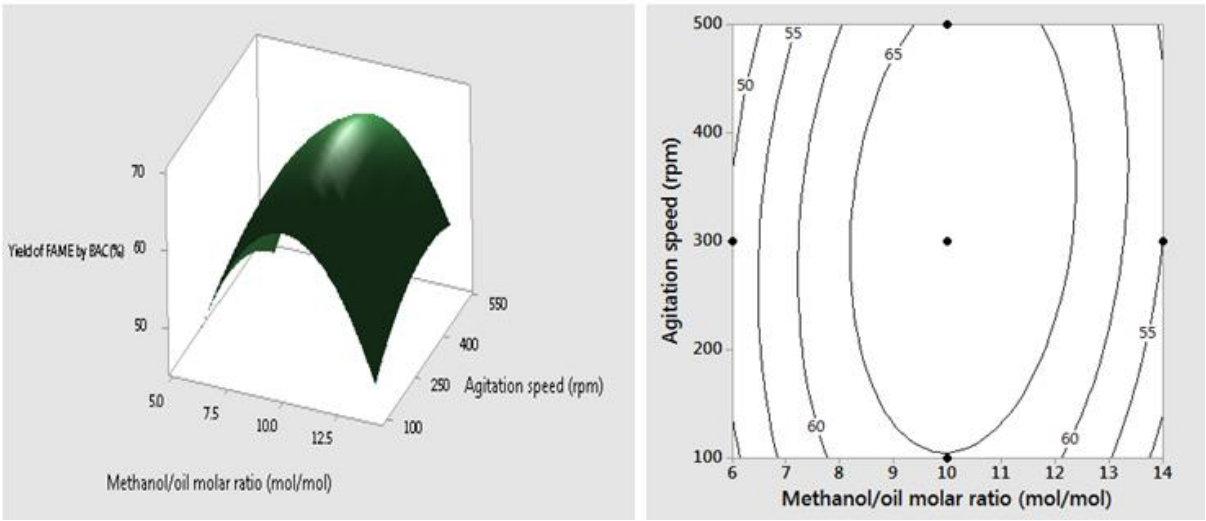

Figure 4.57c: Surface and contour plots of agitation speed and methanol/oil molar ratio by BAC.

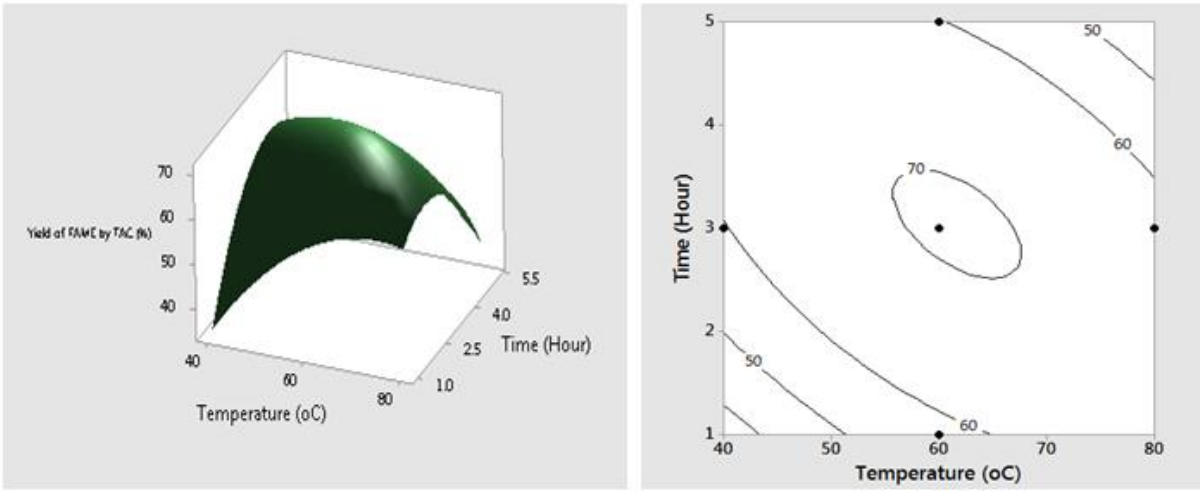

Figure 4.58a: Surface and contour plots of time and temperature by TAC.

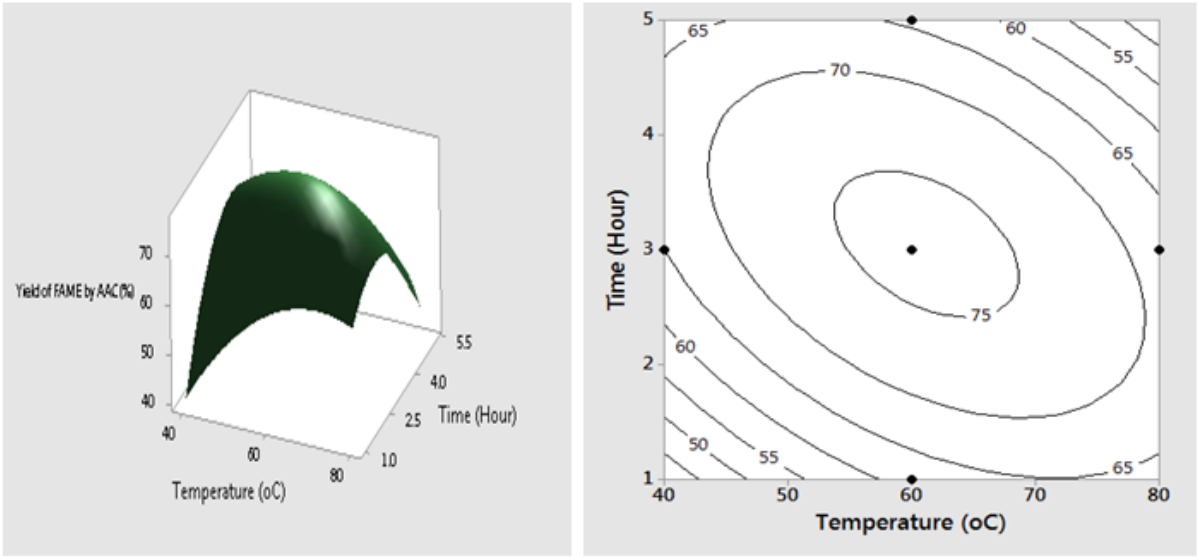

Figure 4.58b: Surface and contour plots of time and temperature by AAC.

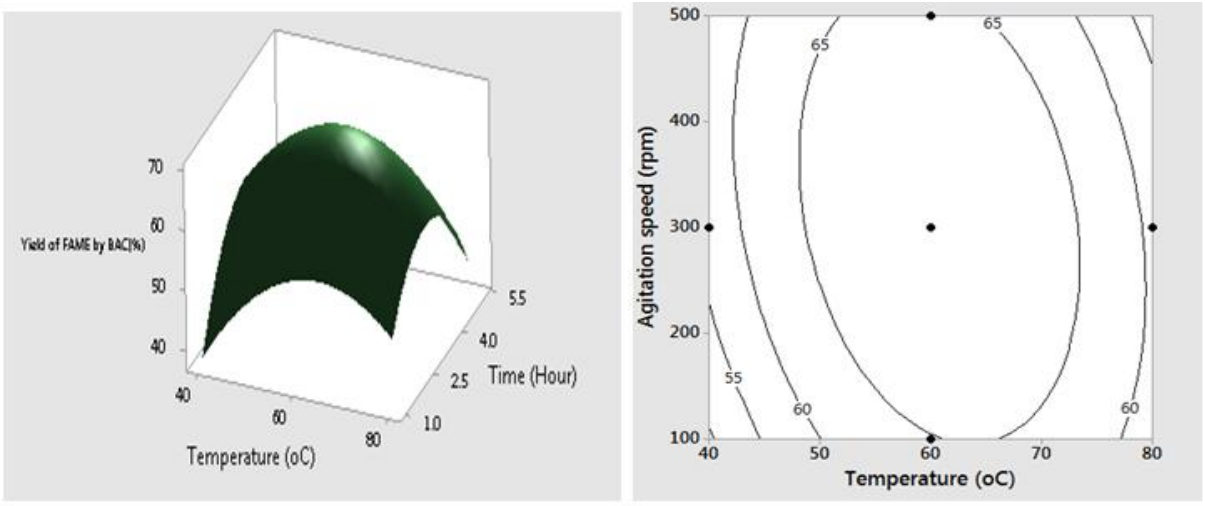

Figure 4.58c: Surface and contour plots of time and temperature by BAC.

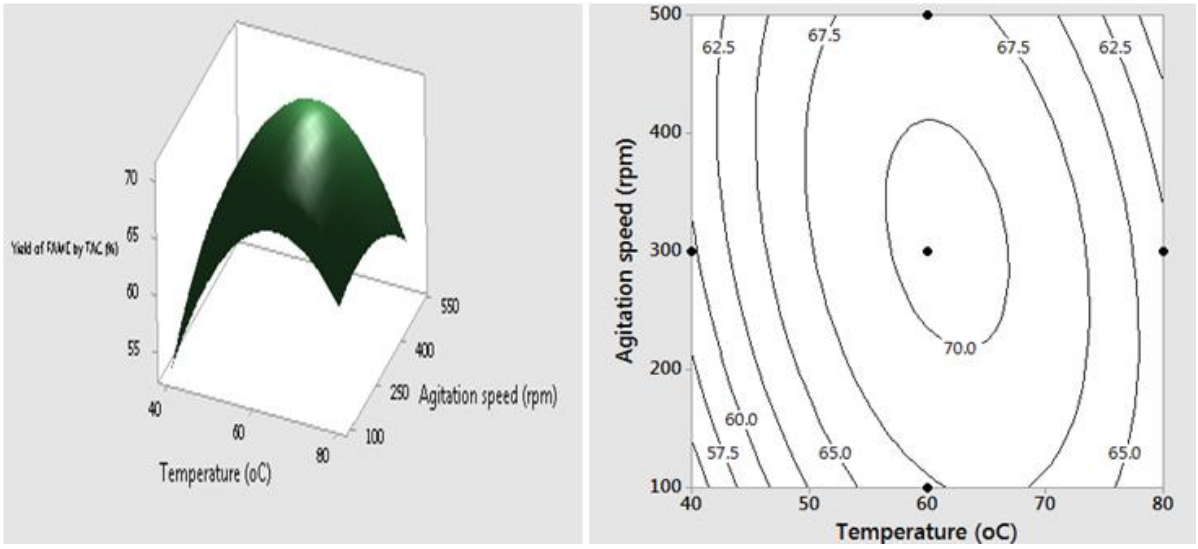

Figure 4.59a: Surface and contour plots of agitation speed and temperature by TAC.

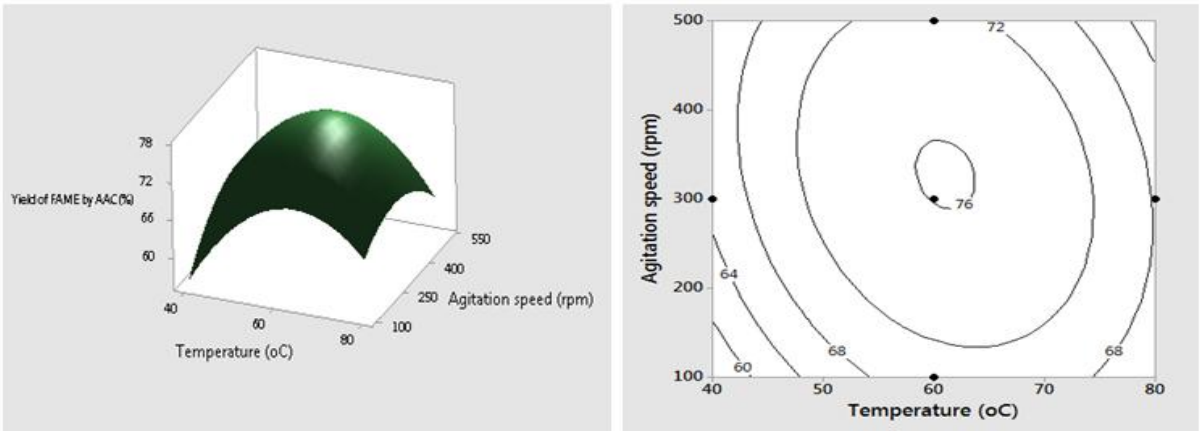

Figure 4.59b: Surface and contour plots of agitation speed and temperature by AAC.

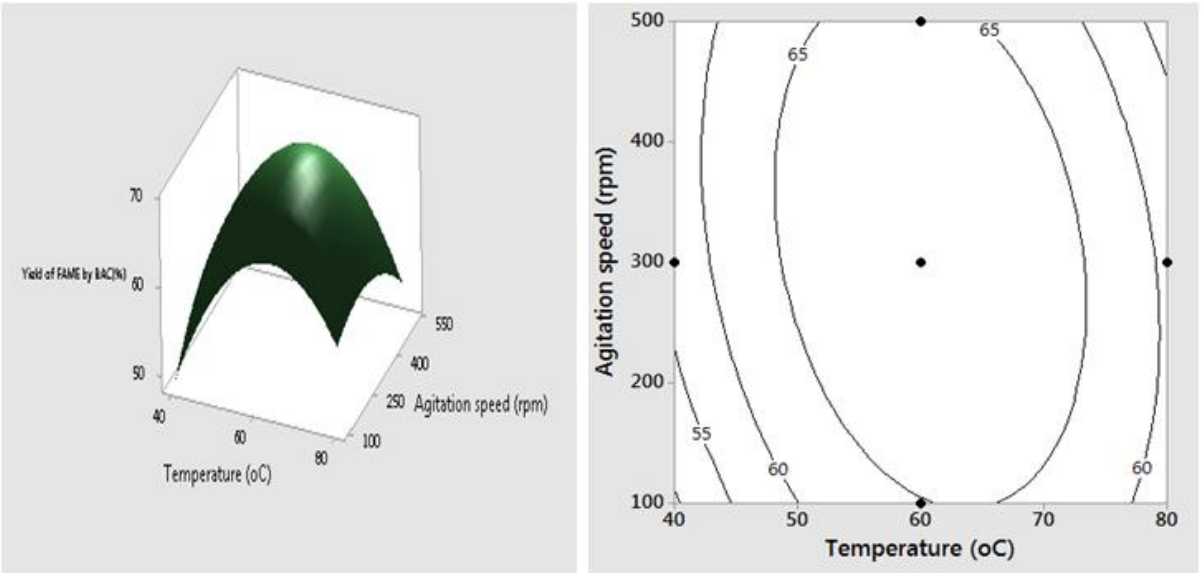

Figure 4.59c: Surface and contour plots of agitation speed and temperature by BAC.

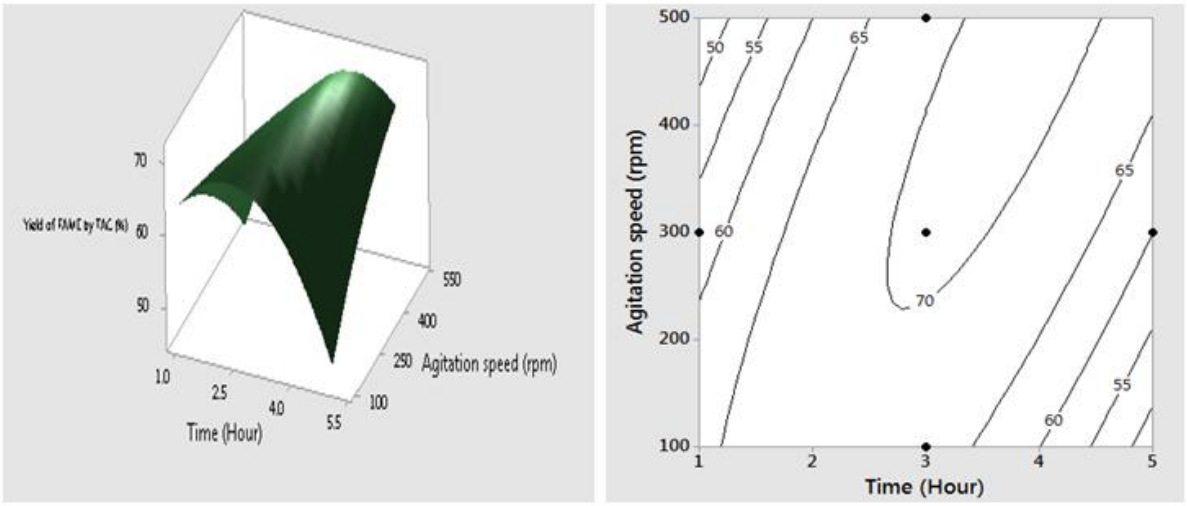

Figure 4.60a: Surface and contour plots of agitation speed and time by TAC.

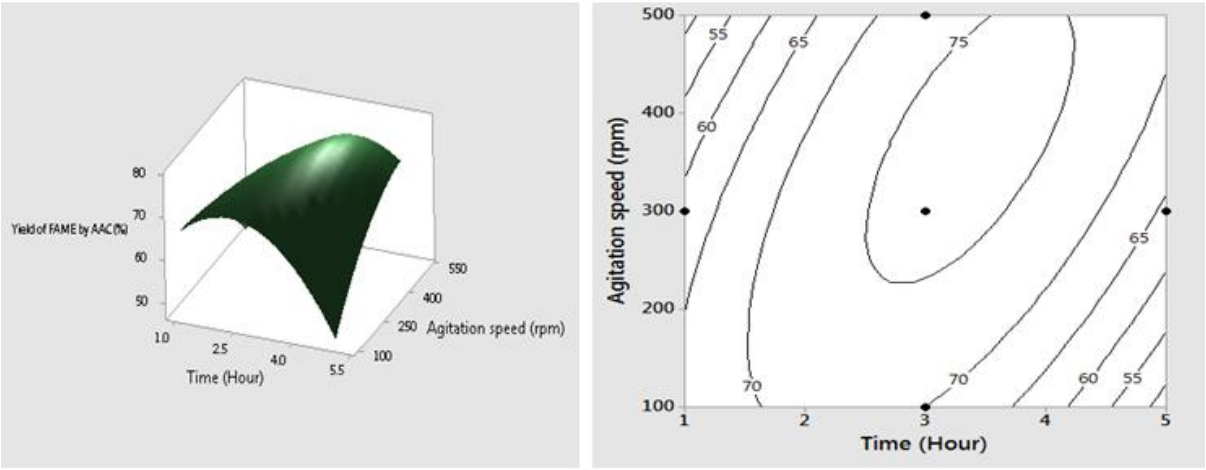

Figure 4.60b: Surface and contour plots of agitation speed and time by AAC.

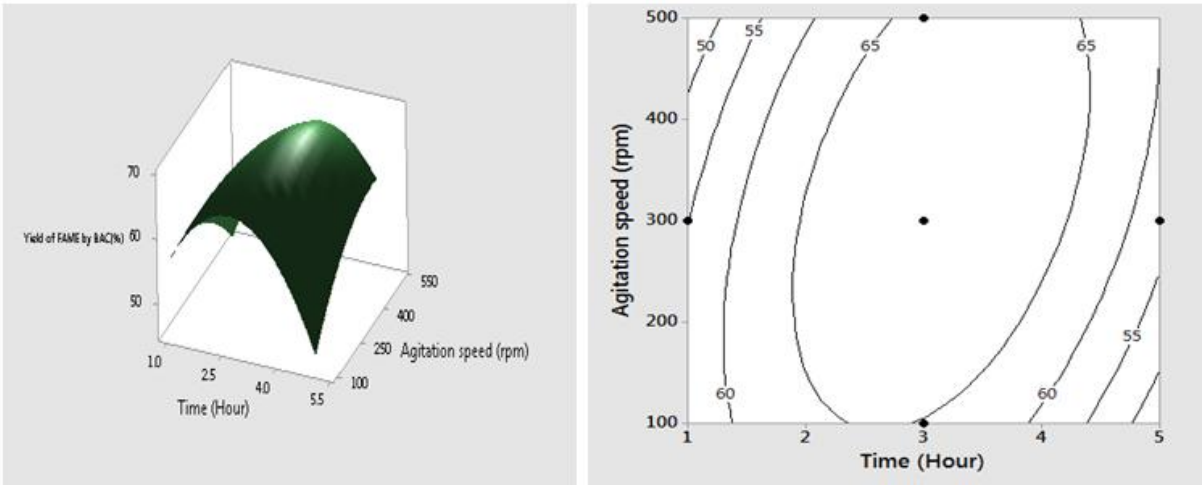

Figure 4.60c: Surface and contour plots of agitation speed and time by BAC.

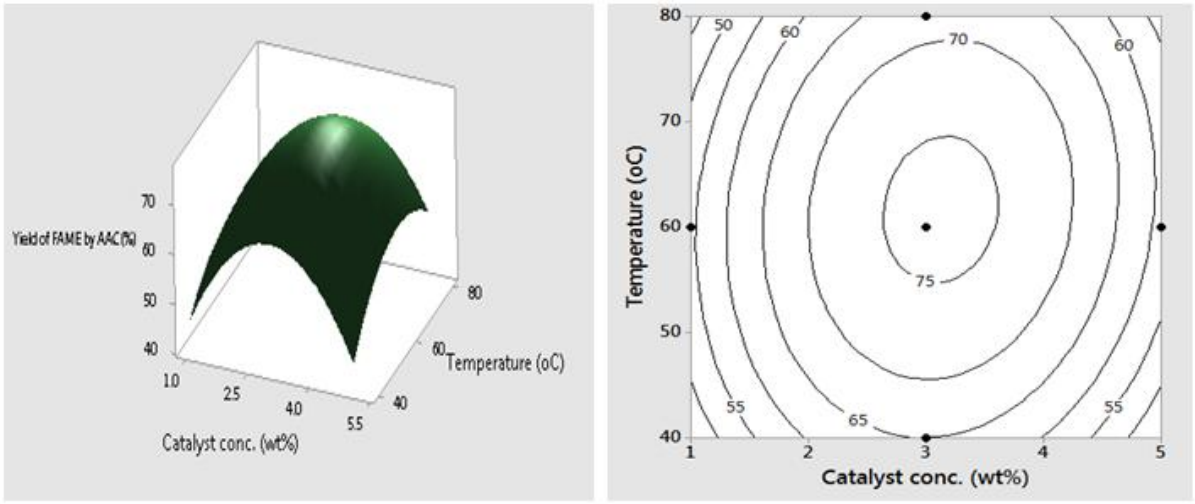

Figure 4.61a: Surface and contour plots of catalyst conc. and temperature by AAC.

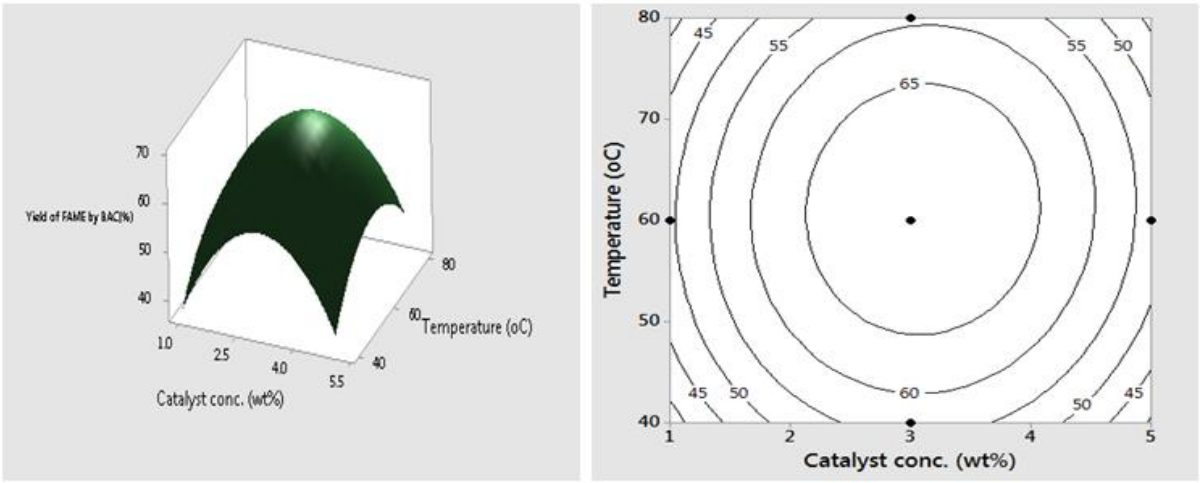

Figure 4.61b: Surface and contour plots of catalyst conc. and temperature by BAC.

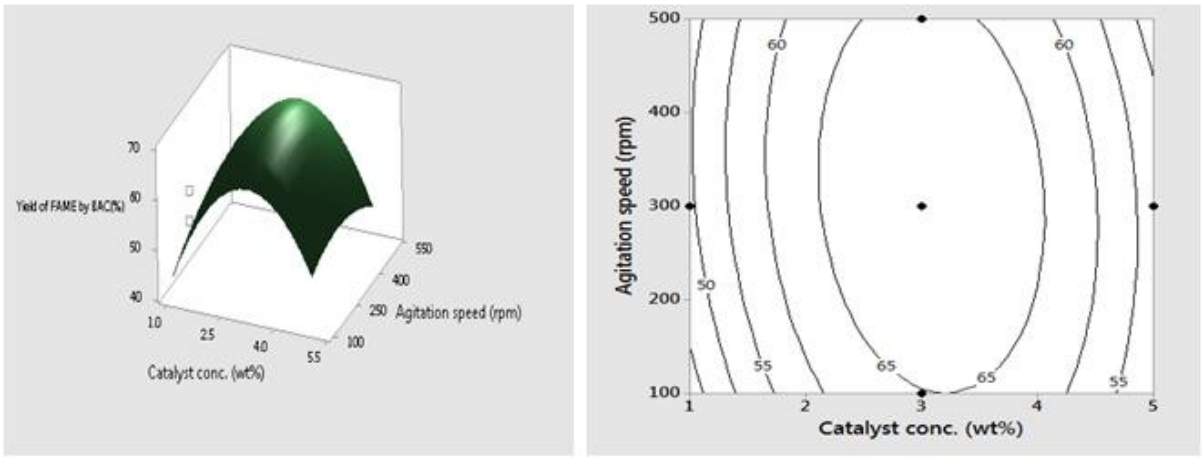

Figure 4.62: Surface and contour plots of catalyst conc. and agitation speed by BAC.

4.9.4 Statistical analysis of biodiesel production from gmelina seed oil using different catalysts.

Similar analysis used in section 4.9.1 was employed to develop models for biodiesel production from gmelina seed oil using thermally activated clay (TAC) catalyst, acid activated clay (AAC) catalyst and base/alkaline activated clay (BAC) catalyst. The response surface design tables for the transesterification study are given in Table H1 (Appendix H) for heterogeneous catalysts. The models developed by the software in terms of coded values are shown in Equations 4.15, 4.16 and 4.17 for the yields of biodiesel from gmelina seed oil by thermally activated clay (TAC) catalyst, acid activated clay (AAC) catalyst and base/alkaline activated clay (BAC) catalyst respectively.

$$\text{Yield of Gmelina FAME by TAC} = 74.65 + 1.13A + 0.71B + 1.13C + 0.54D + 0.46E - 2.06AB + 0.81AC + 0.81AD + 0.19AE + 1.06BC - 1.19BD + 0.94BE - 2.31CD - 1.44CE + 1.81DE - 4.65A^2 - 4.02B^2 - 1.77C^2 - 1.90D^2 - 0.90E^2 \quad (4.15)$$

$$\text{Yield of Gmelina FAME by AAC} = 71.97 + 0.79A + 0.79B + 0.79C + 0.13D + 0.46E - 1.69AB + 0.19AC + 0.94AD - 0.19AE + 0.56BC - 1.81BD + 0.56BE - 2.06CD - 0.94CE + 1.94DE - 4.47A^2 - 3.97B^2 - 2.72C^2 - 2.84D^2 - 1.22E^2 \quad (4.16)$$

$$\text{Yield of Gmelina FAME by BAC} = 69.81 + 0.96A + 0.71B + 0.38C + 0.79D + 0.29E - 1.44AB + 0.31AC + 1.06AD - 0.31AE + 0.44BC - 1.56BD + 0.31BE - 1.06CD - 0.69CE + 1.56DE - 4.81A^2 - 4.31B^2 - 3.06C^2 - 3.43D^2 - 1.31E^2 \quad (4.17)$$

$$\text{Where A} = \text{Catalyst concentration (wt\%)}, \text{B} = \frac{\text{methanol}}{\text{oil}} \text{molar ratio (mol/mol)},$$

$$\text{C} = \text{Temperature (°C)}, \text{D} = \text{Time (Hour)}, \qquad \text{E} = \text{Agitation speed (rpm)}$$

4.9.5 Adequacy analysis of the models for gmelina seed oil biodiesel

The analysis of variance for the model of the transesterification process parameters are shown in Tables 4.27 – 4.29. From the tables, it could be observed that square terms have more significant effect as they have highest F-values followed by interaction terms while the single terms have least significant effect with lowest F-values. The coefficient of determination and error standard deviation of the models are shown in Table 4.30.From the table, it could be observed that the coefficient of determination and error standard deviation of the models indicate that the models fit the data. This could beas a result of the interaction and square terms that improved the adequacy of the models.

Table 4.27: ANOVA for the model of Yield of Gmelina FAME by TAC catalyst

Source	DF	Adj SS	Adj MS	F-Value	P-Value
Model	20	1500.65	75.033	453.95	0.002
Linear	5	84.88	16.975	102.70	0.001
Square	5	1100.15	220.030	1331.18	0.004
Interaction	10	315.63	31.563	190.95	0.003
Error	11	1.82	0.165		
Lack-of-Fit	6	0.48	0.081	0.30	0.911
Pure Error	5	1.33	0.267		
Total	31	1502.47			

Table 4.28: ANOVA for the model of Yield of Gmelina FAME by AAC (%)

Source	DF	Adj SS	Adj MS	F-Value	P-Value
Model	20	1546.95	77.348	172.78	0.001
Linear	5	50.54	10.108	22.58	0.002
Square	5	1220.78	244.157	545.41	0.004
Interaction	10	275.63	27.563	61.57	0.003
Error	11	4.92	0.448		
Lack-of-Fit	6	2.92	0.487	1.22	0.423
Pure Error	5	2.00	0.400		
Total	31	1551.87			

Table 4.29: ANOVA for the model of Yield of Gmelina FAME by BAC (%)

Source	DF	Adj SS	Adj MS	F-Value	P-Value
Model	20	1708.80	85.440	348.48	0.002
Linear	5	54.54	10.908	44.49	0.003
Square	5	1491.64	298.327	1216.77	0.001
Interaction	10	162.63	16.263	66.33	0.005
Error	11	2.70	0.245		
Lack-of-Fit	6	1.86	0.311	1.86	0.256
Pure Error	5	0.83	0.167		
Total	31	1711.50			

Table 4.30: Coefficients of determination and ESD for the models of Gmelina seed oil biodiesel

Responses	S	R-sq	R-sq(adj)	R-sq (pred)
Yield of Gmelina FAME by TAC (%)	0.406558	99.88	99.66	99.02
Yield of Gmelina FAME by AAC (%)	0.6669073	99.68	99.11	94.80
Yield of Gmelina FAME by BAC (%)	0.495156	99.84	99.56	97.03

From Tables 4.31, 4.32 and 4.33, it could be observed that all the five variables: catalyst conc. (A), methanol/oil molar ratio (B), reaction temeperature (C), time (D) and agitation speed (E) have significant effect on yield of fatty acid methyl ester (FAME) produced by TAC, AAC and BAC catalyzed reaction. Also from Tables 4.31, 4.32 and 4.33 it was clearly shown that among the five variables studied for the three catalysts, methanol/oil molar ratio (B) has the largest effect on the yield of FAME as it has the highest F-test value while in There were also significant interaction effects between variables; as shown by those between catalyst concentration and methanol/oil molar ratio, catalyst concentration and reaction time, methanol/oil molar ratio and reaction temperature, methanol/oil molar ratio and reaction time, methanol/oil molar ratio and agitation speed, reaction temperature and time, reaction temperature and agitation speed, time and agitation speed for transesterified reaction by TAC and AAC catalysts while for BAC transeterified reaction, all the interactions were significant. The test of significance terms in the models as shown in Tables 4.31 to 4.33 was carried out on 95% level of confidence or 5% significance level. Individual terms in the model are said to be statistically significant to the responses if $P - val < 0.05$ and therefore, those statistically insignificant terms were eliminated from the model as shown in Equations 4.18 – 4.20.

Table 4.31: Effects and coefficients for model of Yield of Gmelina FAME by TAC catalyst (%)

Term	Effect	Coef	SE Coef	T-Value	P-Value
Constant		74.648	0.162	460.33	0.001
A	2.250	1.125	0.0830	13.56	0.005
B	1.417	0.708	0.0830	8.54	0.006
C	2.250	1.125	0.0830	13.56	0.002
D	1.083	0.542	0.0830	6.53	0.003
E	0.917	0.458	0.0830	5.52	0.001
A^2	-9.296	-4.645	0.0751	-61.92	0.002
B^2	-8.046	-4.023	0.0751	-53.59	0.003
C^2	-3.546	-1.773	0.0751	-23.62	0.007
D^2	-3.796	-1.898	0.0751	-25.28	0.001
E^2	-1.796	-0.898	0.0751	-11.96	0.001
A*B	-4.125	-2.063	0.1020	-20.29	0.010
A*C	1.625	0.813	0.1020	7.99	0.020
A*D	1.625	0.813	0.1020	7.99	0.003
A*E	0.375	0.187	0.1020	1.84	0.092
B*C	2.125	1.063	0.1020	10.45	0.002
B*D	-2.375	-1.188	0.1020	-11.68	0.001
B*E	1.875	0.937	0.1020	9.22	0.003
C*D	-4.625	-2.313	0.1020	-22.75	0.004
C*E	-2.875	-1.437	0.1020	-14.14	0.001
D*E	3.625	1.812	0.1020	17.83	0.005

Table 4.32: Effects and coefficients for model of Yield of Gmelina FAME by AAC (%)

Term	Effect	Coef	SE Coef	T-Value	P-Value
Constant		71.966	0.267	269.67	0.001
A	1.583	0.792	0.137	5.80	0.002
B	1.583	0.792	0.137	5.80	0.010
C	1.583	0.792	0.137	5.80	0.020
D	0.250	0.125	0.137	0.92	0.380
E	0.917	0.458	0.137	3.36	0.006
A^2	-8.932	-4.466	0.124	-36.15	0.001
B^2	-7.932	-3.966	0.124	-32.10	0.001
C^2	-5.432	-2.716	0.124	-21.98	0.002
D^2	-5.682	-2.841	0.124	-23.00	0.003
E^2	-2.432	-1.216	0.124	-9.84	0.002
A*B	-3.375	-1.688	0.167	-10.09	0.001
A*C	1.625	0.813	0.167	4.86	0.001
A*D	1.875	0.938	0.167	5.60	0.001
A*E	-0.375	-0.188	0.167	-1.12	0.286
B*C	1.125	0.563	0.167	3.36	0.006
B*D	-3.625	-1.812	0.167	-10.84	0.003
B*E	1.125	0.562	0.167	3.66	0.006
C*D	-4.125	-2.062	0.167	-12.33	0.002
C*E	-1.875	-0.937	0.167	-5.60	0.004
D*E	3.875	1.938	0.167	11.58	0.000

Table 4.33: Effects and coefficients for model of Yield of Gmelina FAME by BAC (%)

Term	Effect	Coef	SE Coef	T-Value	P-Value
Constant		69.807	0.197	353.45	0.001
A	1.917	0.958	0.101	9.48	0.002
B	1.417	0.708	0.101	7.01	0.003
C	0.750	0.375	0.101	3.71	0.003
D	1.583	0.792	0.101	7.83	0.001
E	0.583	0.292	0.101	2.89	0.015
A^2	-9.614	-4.807	0.0914	-52.58	0.002
B^2	-8.614	-4.307	0.0914	-47.11	0.003
C^2	-6.114	-3.057	0.0914	-33.44	0.002
D^2	-6.864	-3.432	0.0914	-37.54	0.004
E^2	-2.614	-1.307	0.0914	-14.29	0.002
A*B	-2.875	-1.438	0.124	-11.61	0.003
A*C	0.625	0.313	0.124	2.52	0.028
A*D	2.125	1.062	0.124	8.58	0.012
A*E	-0.625	-0.312	0.124	-2.52	0.028
B*C	0.875	0.438	0.124	3.53	0.005
B*D	-3.125	-1.562	0.124	-12.62	0.006
B*E	0.625	0.312	0.124	2.52	0.028
C*D	-2.125	-1.063	0.124	-8.58	0.005
C*E	-1.375	-0.688	0.124	-5.55	0.003
D*E	3.125	1.562	0.124	12.62	0.004

The reduced empirical relationships between the factors and responses developed and analysed using the MINITAB 17 are as follows:

$$\text{Yield of Gmelina FAME by TAC} = 74.65 + 1.13A + 0.71B + 1.13C + 0.54D + 0.46E - 2.06AB + 0.81AC + 0.81AD + 1.06BC - 1.19BD + 0.94BE - 2.31CD - 1.44CE + 1.81DE - 4.65A^2 - 4.02B^2 - 1.77C^2 - 1.90D^2 - 0.90E^2 \quad (4.18)$$

$$\text{Yield of Gmelina FAME by AAC} = 71.97 + 0.79A + 0.79B + 0.79C + 0.46E - 1.69AB + 0.19AC + 0.94AD + 0.56BC - 1.81BD + 0.56BE - 2.06CD - 0.94CE + 1.94DE - 4.47A^2 - 3.97B^2 - 2.72C^2 - 2.84D^2 - 1.22E^2 \quad (4.19)$$

$$\text{Yield of Gmelina FAME by BAC} = 69.81 + 0.96A + 0.71B + 0.38C + 0.79D + 0.29E - 1.44AB + 0.31AC + 1.06AD - 0.31AE + 0.44BC - 1.56BD + 0.31BE - 1.06CD - 0.69CE + 1.56DE - 4.81A^2 - 4.31B^2 - 3.06C^2 - 3.43D^2 - 1.31E^2 \quad (4.20)$$

The models adequacy are confirmed graphically using the residual plots which include the normal probability plot, histogram, residual versus fitted values and residual versus observation order in a 4-in-1 format as shown in Figures 4.63 (a, b & c). An analytical view

of the Figures 4.63 (a, b and c) showthe adequacy of the models and the plots of the normal probability tend to fall in a straight line and residuals were uniformly distributed with Figure 4.63(b) has better distribution of errors. Hence, the models are adequate to statistically fit the data with little outliers and reduced skewness.

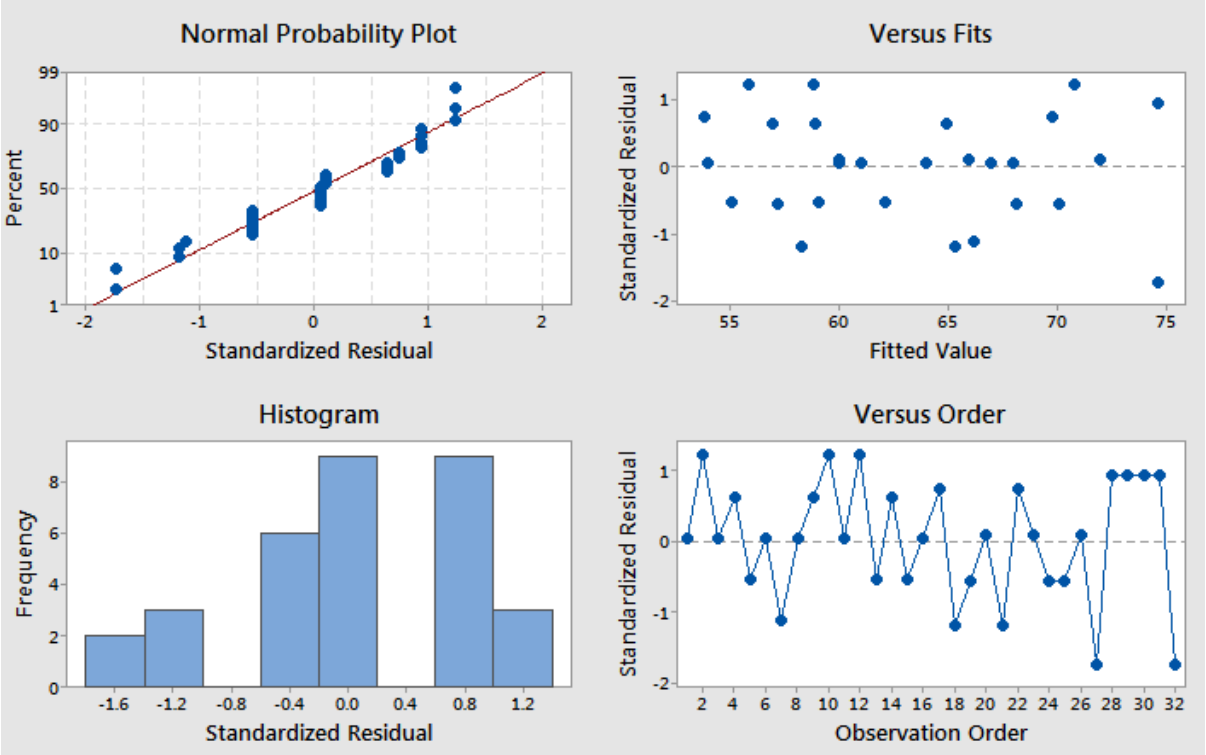

Figure 4.63a: Residual plots for the model of the yield of gmelina FAME by TAC

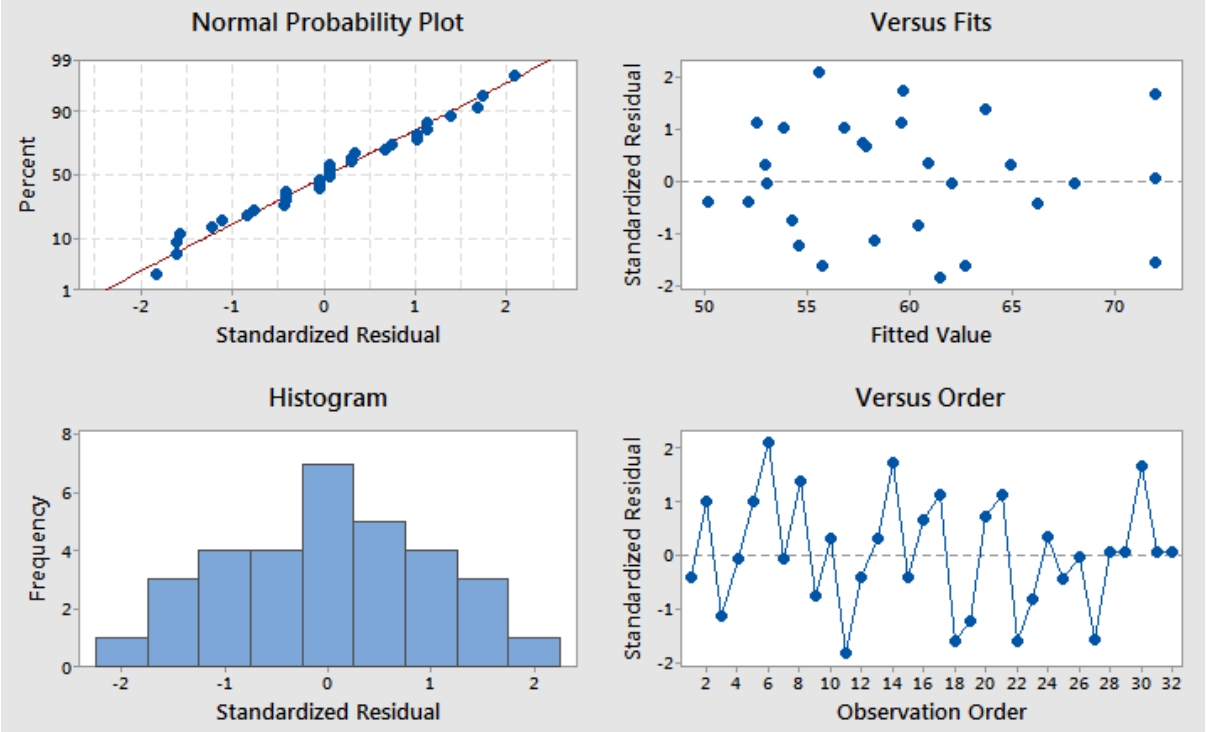

Figure 4.63b: Residual plots for model of the yield of gmelina FAME by AAC

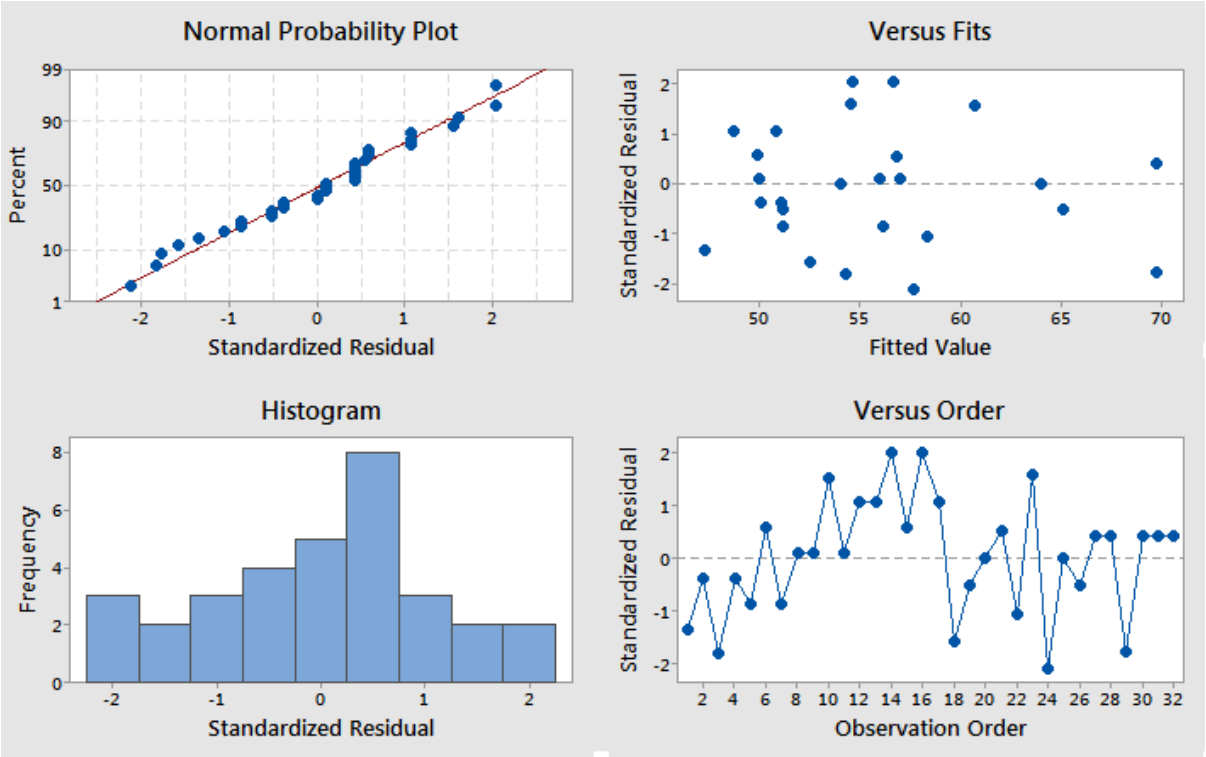

Figure 4.63c: Residual plots for model of the yield of gmelina FAME with BAC

4.9.6 Surface response plots of biodiesel production from gmelina seed oil

Figures 4.64 to 4.73 are the surface plots of the predicted FAME yield which can be generated by Equations 4.18 to 4.20 for the three heterogeneous catalysts (TAC, AAC & BAC).

The interaction effect of catalyst conc. and methanol/oil molar ratio on yield of FAME is shown in Figures 4.64 (a, b & c) for TAC, AAC and BAC catalyzed reactions respectively. It could be observed from the figures that the effect follow similar trend on the yield for all the catalysts. The figures show that the amount of methyl ester yield increases with methanol/oil molar ratio and catalyst concentration. However, at higher catalyst concentrations and methanol/oil molar ratio, a reduction in the yield can be observed due to the fact that the quadratic terms of the two factors are more significant with a negative effect (Eqs.(4.18), (4.19), (4.20)).

The interaction effect of catalyst conc. and time on yield of FAME is shown in Figures 4.65 (a, b & c) for TAC, AAC and BAC catalyzed reactions respectively. It could be observed from the figures that the effect is similar on the yield for all the catalysts. The figures indicate that increase in reaction time and catalyst concentration increases the yield of FAME. However, at higher reaction time and catalyst concentration, reduction in the yield can be observed due to the fact that the quadratic terms of the two factors are more significant with a negative effect (Eqs.(4.18), (4.19), (4.20)) which may be as a result of more active sites with lesser reacting species.

The interaction effect of methanol/oil molar ratio and reaction temperature on yield of FAME is shown in Figures 4.66 (a, b & c) for TAC, AAC and BAC catalyzed reactions respectively. It could be observed from the figures that the effect is similar on the yield for all the catalysts. At lower temperature, below 60^{o}C, the yield increase with methanol/oil molar ratio. However, at a temperature above 60^{o}C, there was reduction in yield. This may be as a result of evaporation of methanol which inhibits the reaction on the three-phase interface.

The interaction effect of methanol/oil molar ratio and time on yield of FAME is shown in Figures 4.67 (a, b & c) for TAC, AAC and BAC catalyzed reactions respectively. It could be observed from the figures that the effect is similar on the yield for all the catalysts.The figures indicate that the amount of FAME yields increase with methanol/oil molar ratio and reaction time. This may be as a result of adequate time provided for conversion of the triglyceride. At higher methanol/oil molar ratio and reaction time, a reduction in FAME yield

was observed due to the fact that the quadratic terms of the two factors are more significant with a negative effect (Eqs.(4.18), (4.19), (4.20)).

The interaction effect of methanol/oil molar ratio and agitation speed on yield of FAME is shown in Figures 4.68 (a, b &c) for TAC, AAC and BAC catalyzed reactions respectively.The figures show that the FAME yield increases with methanol/oil molar ratio and agitation speed as a result of a positive significant effect of methanol/oil molar ratio-agitation speed interaction term, BE on response. However, at higher methanol/oil molar ratio and agitation speed a reduction in the yield can be observed due to the fact that the quadratic terms of the two factors are more significant with a negative effect and the high speed could not allow further conversion of triglyceride.

The interaction effect of reaction temperature and time on yield of FAME is shown in Figures 4.69 (a, b & c) for TAC, AAC and BAC catalyzed reactions respectively. At lower temperature, below 60^{o}C the yield increase with increase in time. However, at a temperature above 60^{o}C, there was reduction in yield. This may be as a result of evaporation of methanol which inhibits the reaction on the three-phase interface.

The interaction effect of reaction temperature and agitation speed on yield of FAME is shown in Figures 4.70 (a, b & c) for TAC, AAC and BAC catalyzed reactions respectively.The figures indicate that the yield of FAME increases with reaction temperature and agitation speed. However, at higher reaction temperature and agitation speed, there was a decrease in FAME yield because there is a negative significant effect of reaction temperature-agitation speed interaction term, (CE) on response (Tables 4.30 to 4.32).

The interaction effect of time and agitation speed on yield of FAME is shown in Figures 4.71 (a, b & c) for TAC, AAC and BAC catalyzed reactions respectively.The figures indicate that the yield of FAME increases with reaction time and agitation speed. However, at higher reaction time and agitation speed, there was a reduction in FAME yield which may be attributed to reversible reaction of transesterification resulting in loss of esters.

The interaction effect of catalyst conc. and temperature on yield of FAME is only significant for TAC, AAC and BAC catalyzed reactions and shown in Figures 4.72 (a, b & c) respectively.The figures indicate that the yield of FAME increases with reaction temperature and catalyst concentration. This is as a result of a postive significant effect of catalyst concentration and temperature interaction, AC (Tables 4.30, 4.31 & 4.32). However, at

higher catalyst concentration and reaction temperature, a decrease in the yield can be observed due to evaporation of methanol at higher temperature and the fact that the quadratic terms of the two factors are more significant with a negative effect (Eqs 4.18, 4.19 & 4.20).

The interaction effect of catalyst conc. and agitation speed on yield of FAME is only significant for BAC catalyzed reaction and shown in Figure4.73. The figure show that the FAME yield increases with catalyst conc. and agitation speed which may be as a result of a proper mixing. However, at higher catalyst concentration and agitation speed a reduction in the yield can be observed due to the fact that the quadratic terms of the two factors are more significant with a negative effect and the high speed could not allow further conversion of triglyceride.

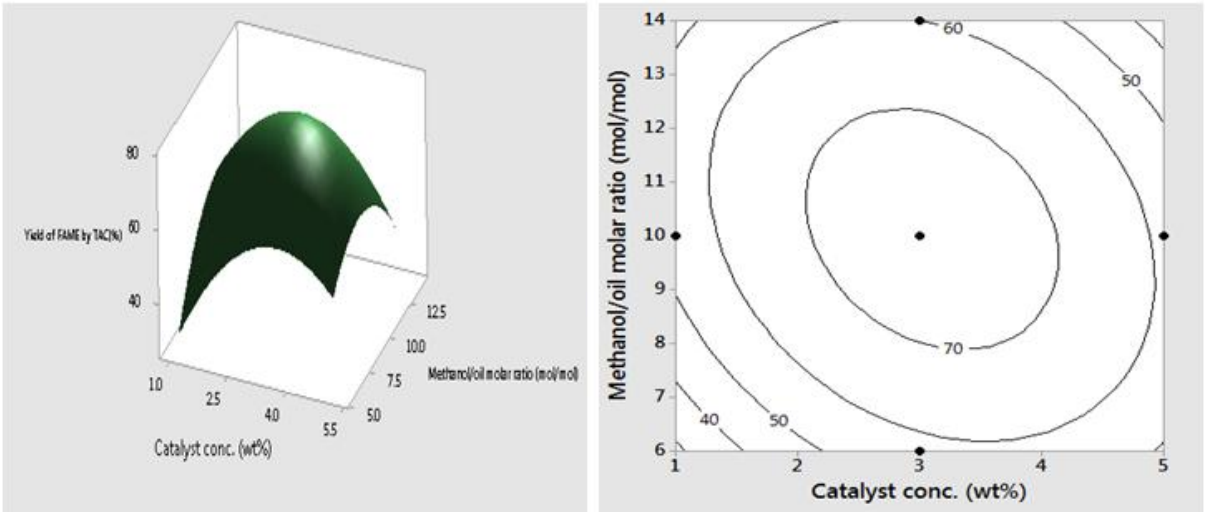

Figure 4.64a: Surface and contour plots of catalyst conc. and methanol/oil molar ratio by TAC.

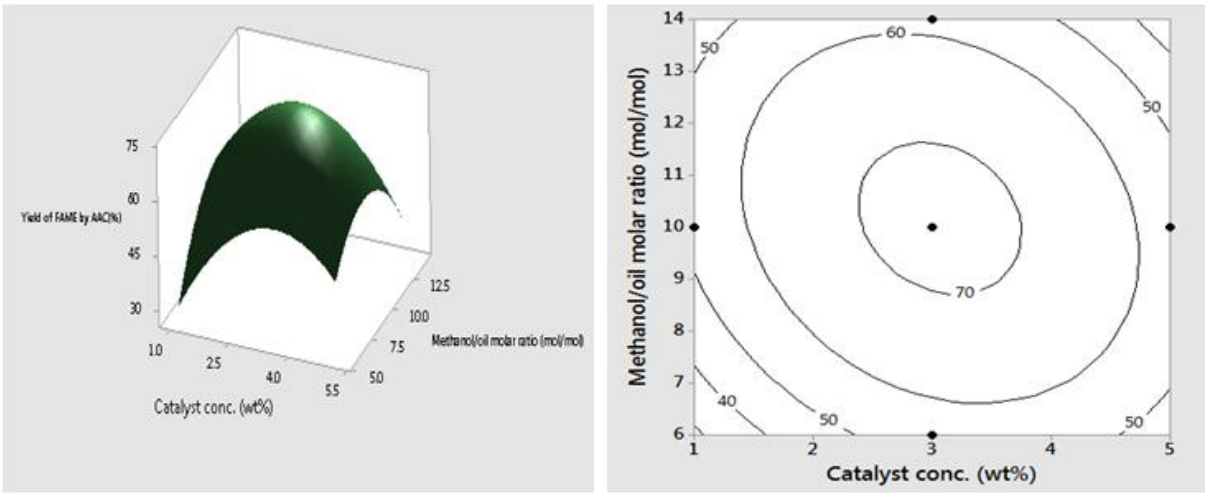

Figure 4.64b: Surface and contour plots of catalyst conc. and methanol/oil molar ratio by AAC.

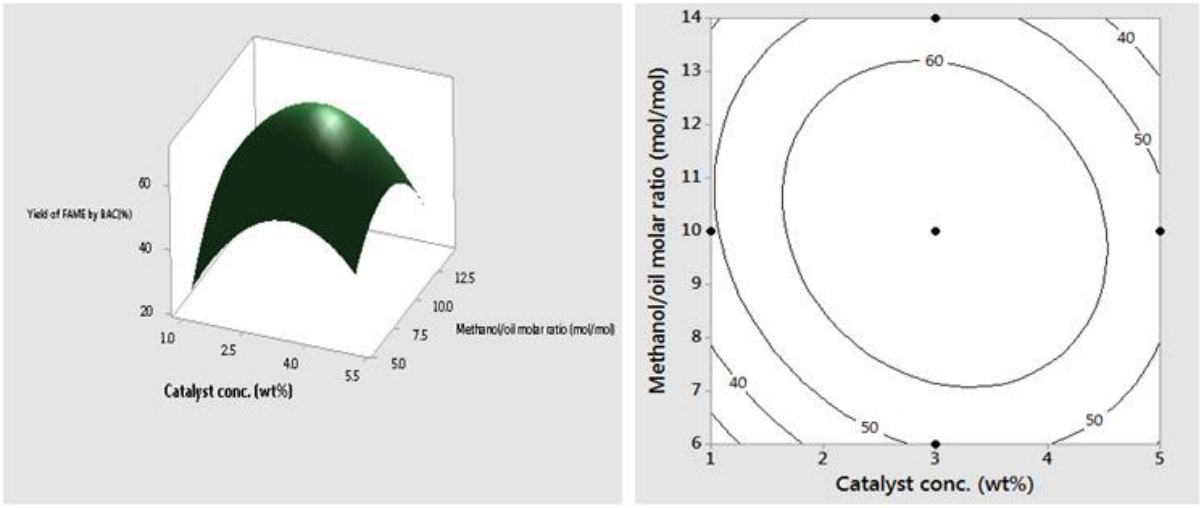

Figure 4.64c: Surface and contour plots of catalyst conc. and methanol/oil molar ratio by BAC.

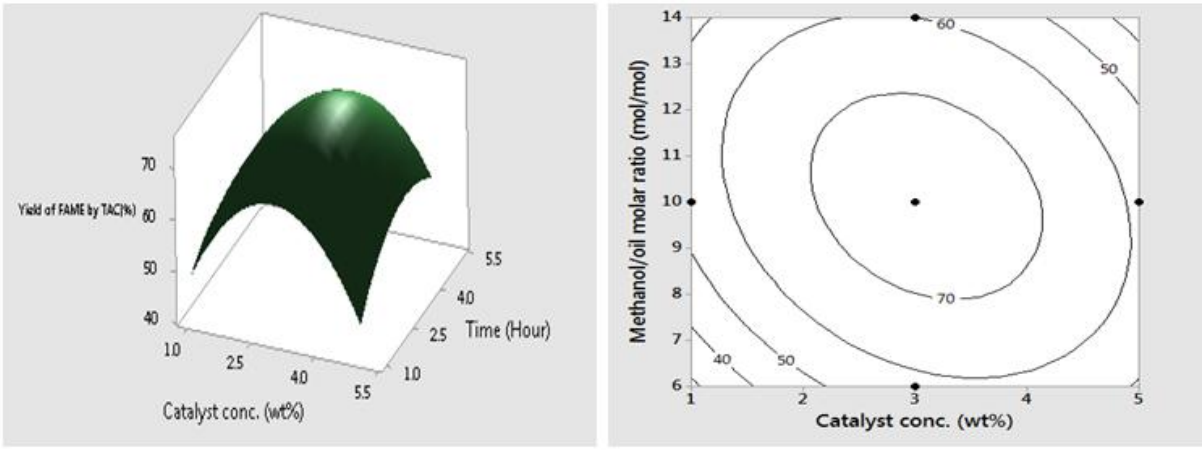

Figure 4.65a: Surface and contour plots of catalyst conc. and time by TAC.

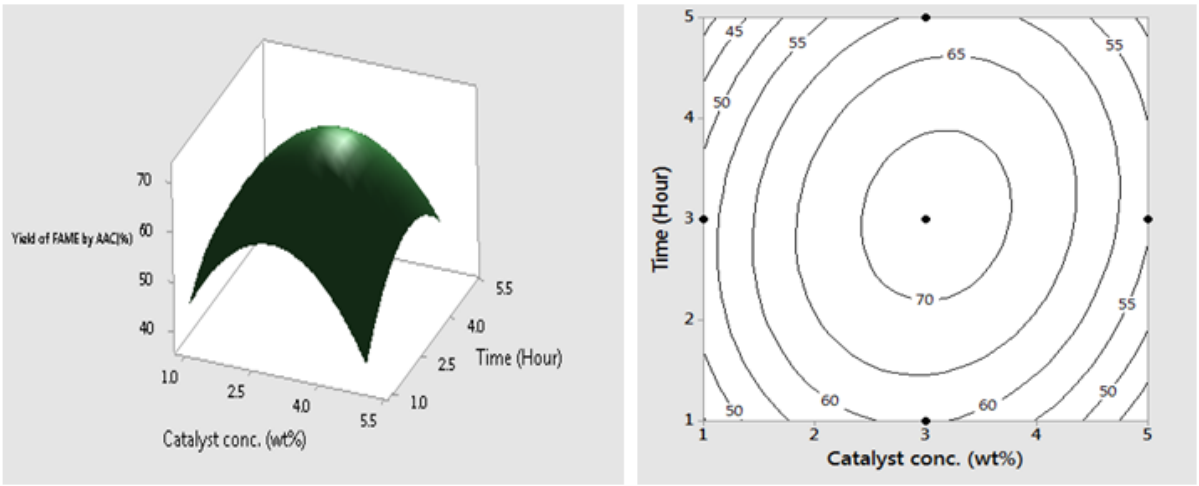

Figure 4.65b: Surface and contour plots of catalyst conc. and time by AAC.

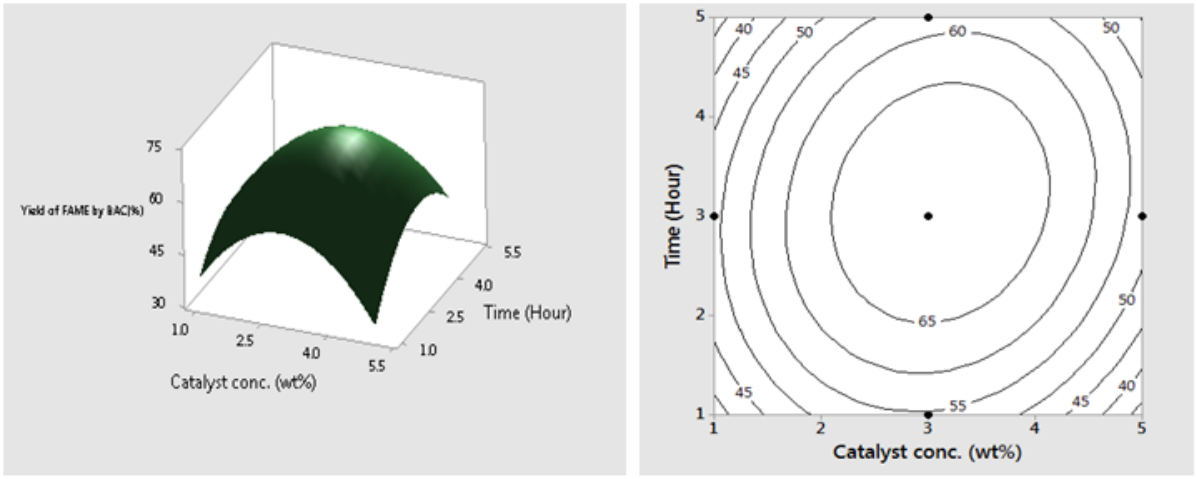

Figure 4.65c: Surface and contour plots of catalyst conc. and time by BAC.

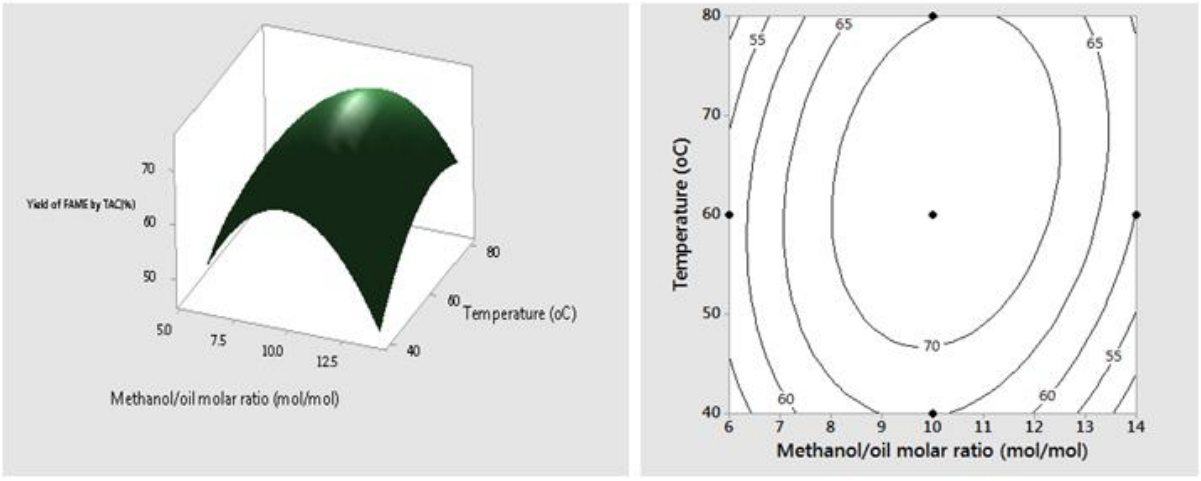

Figure 4.66a: Surface and contour plots of temperature and methanol/oil molar ratio by TAC.

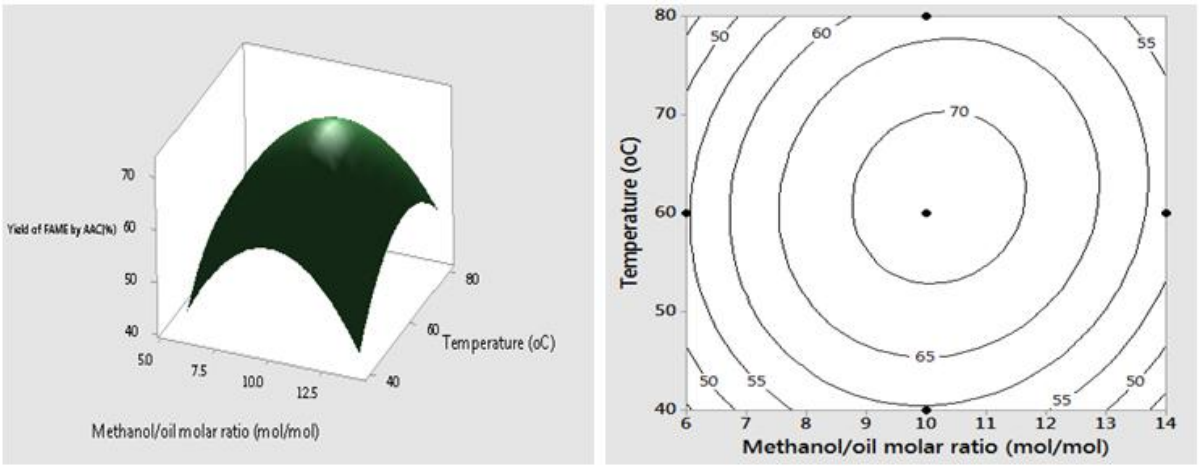

Figure 4.66b: Surface and contour plots of temperature and methanol/oil molar ratio by AAC.

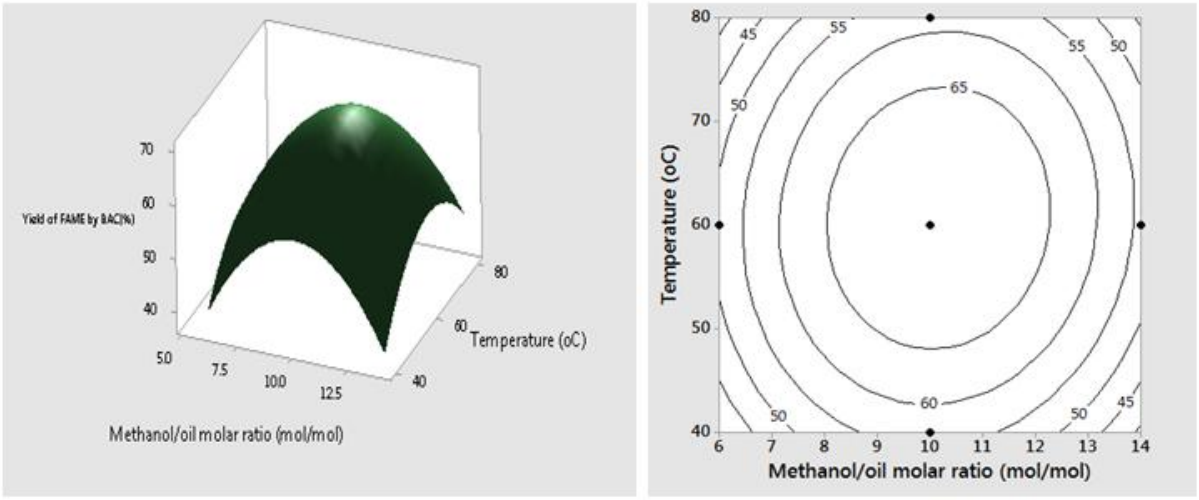

Figure 4.66c: Surface and contour plots of temperature and methanol/oil molar ratio by BAC.

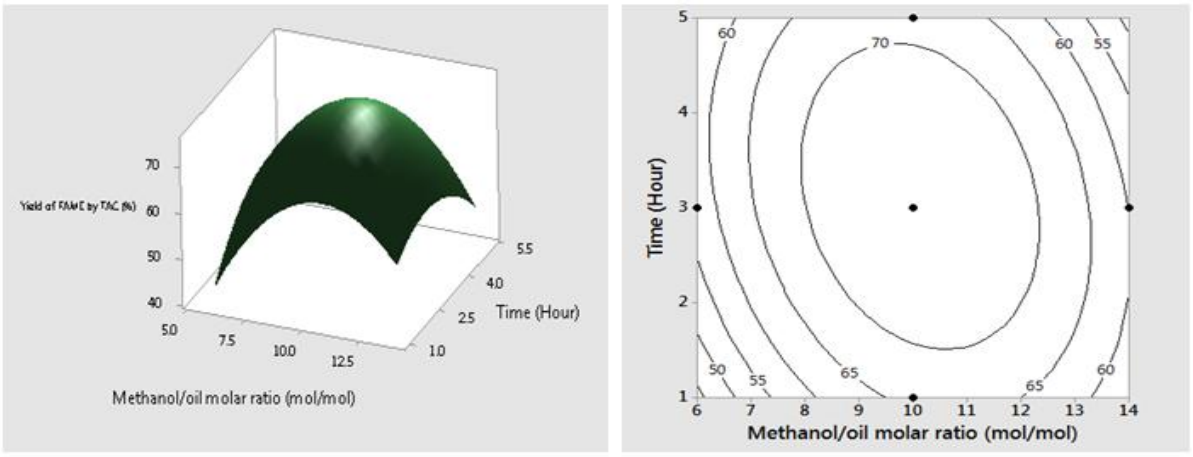

Figure 4.67a: Surface and contour plots of time and methanol/oil molar ratio by TAC.

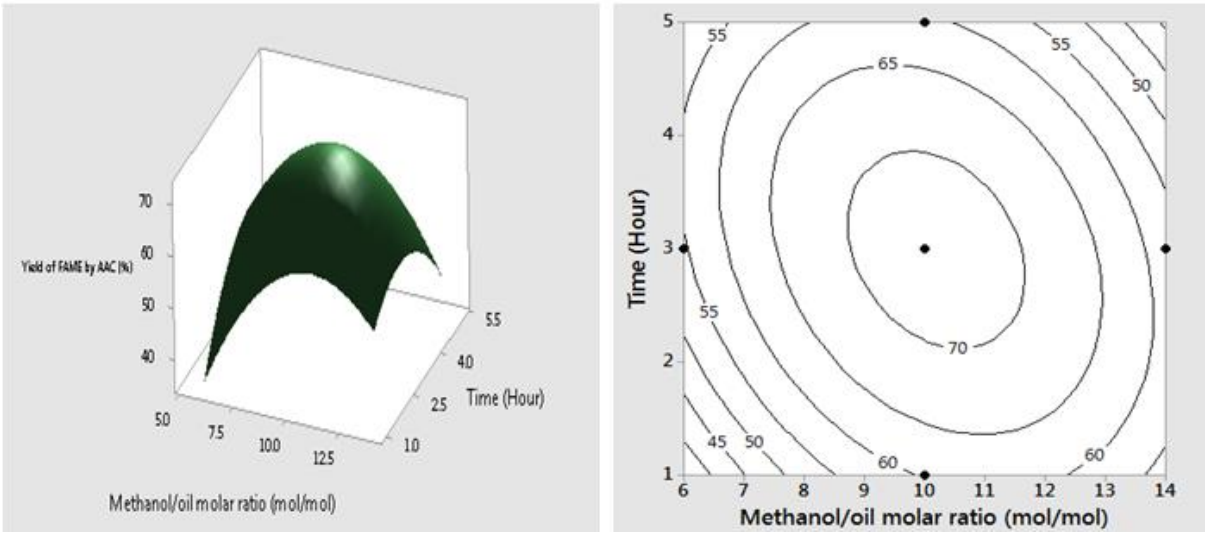

Figure 4.67b: Surface and contour plots of time and methanol/oil molar ratio by AAC.

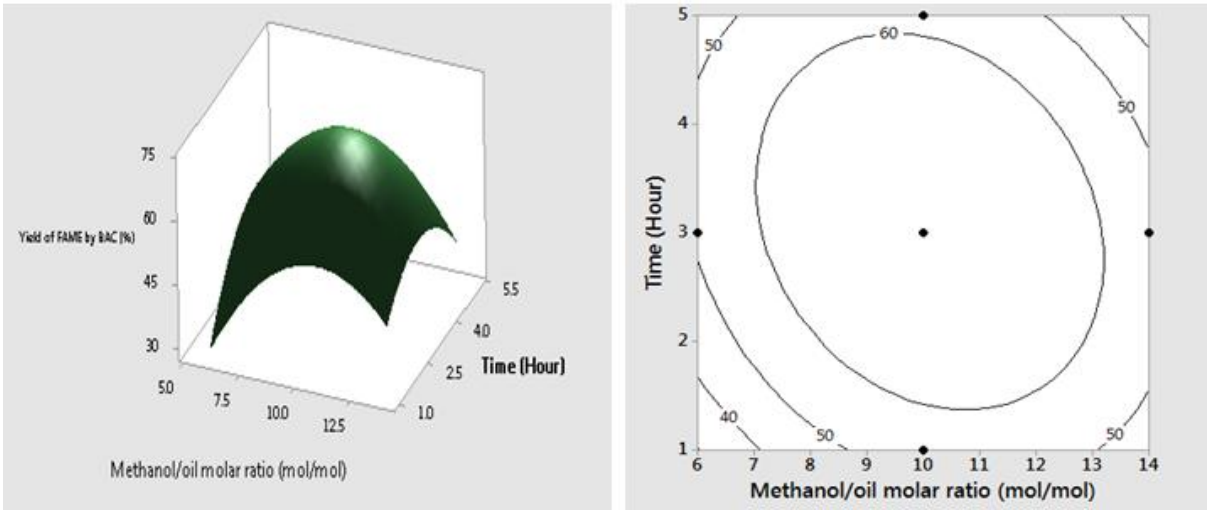

Figure 4.67c: Surface and contour plots of time and methanol/oil molar ratio by BAC.

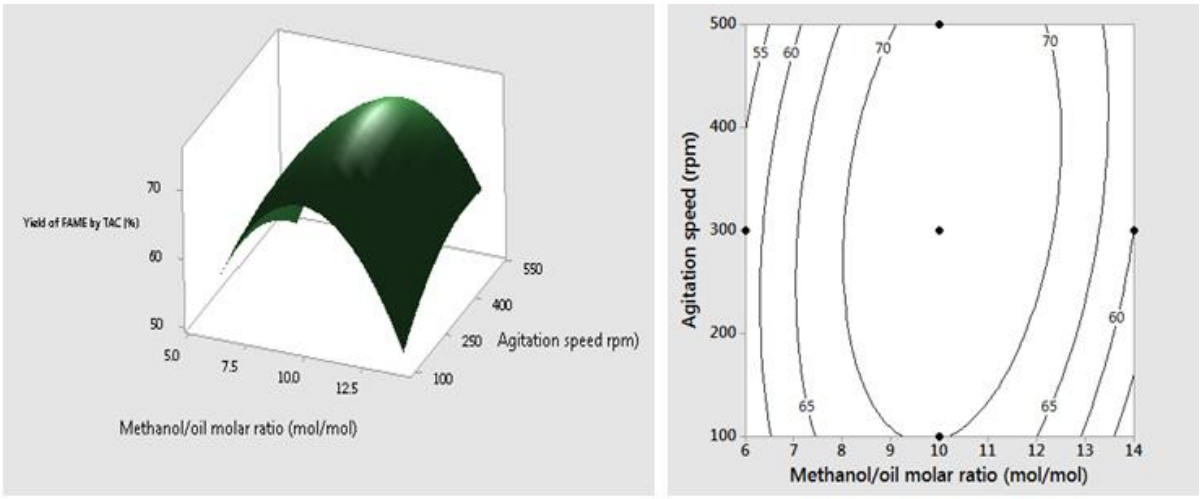

Figure 4.68a: Surface and contour plots of agitation speed and methanol/oil molar ratio by TAC.

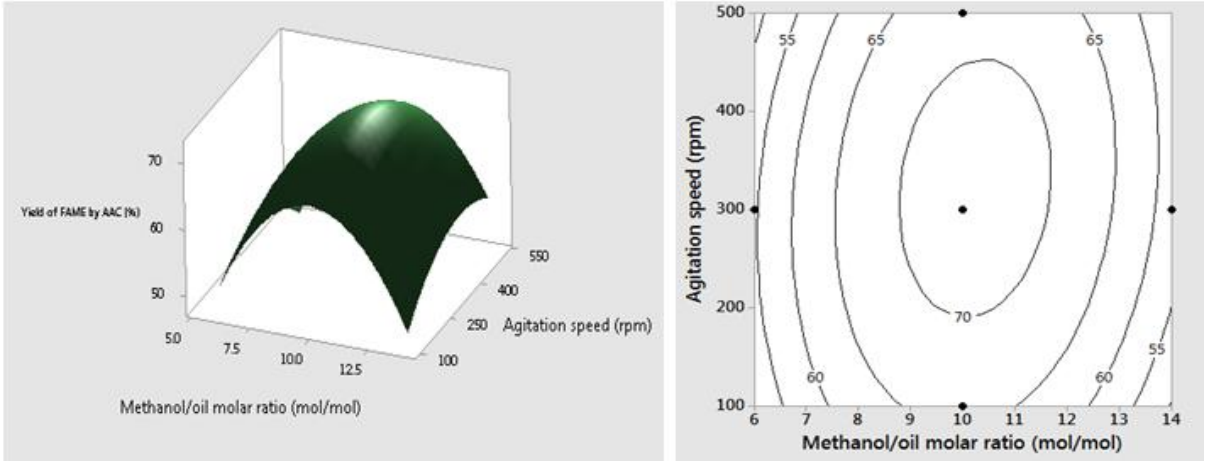

Figure 4.68b: Surface and contour plots of agitation speed and methanol/oil molar ratio by AAC.

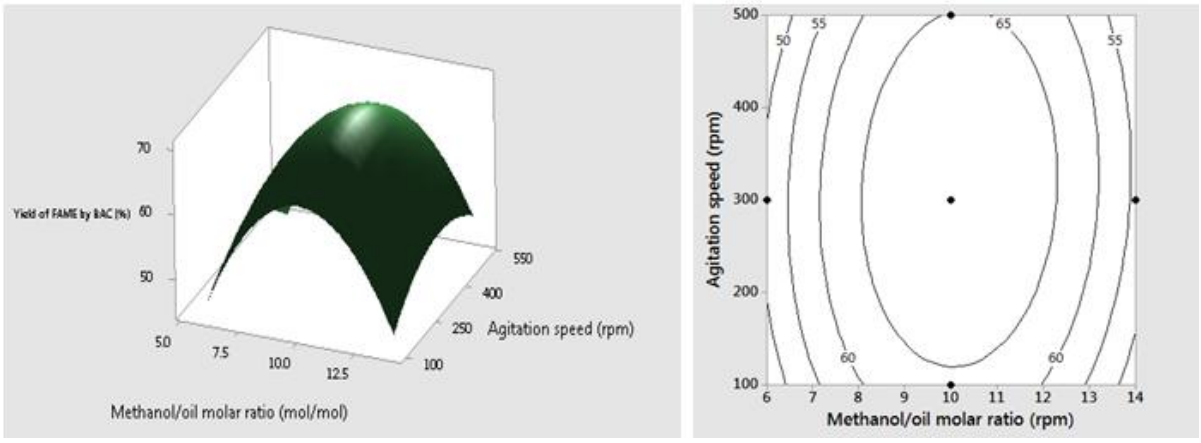

Figure 4.68c: Surface and contour plots of agitation speed and methanol/oil molar ratio by BAC.

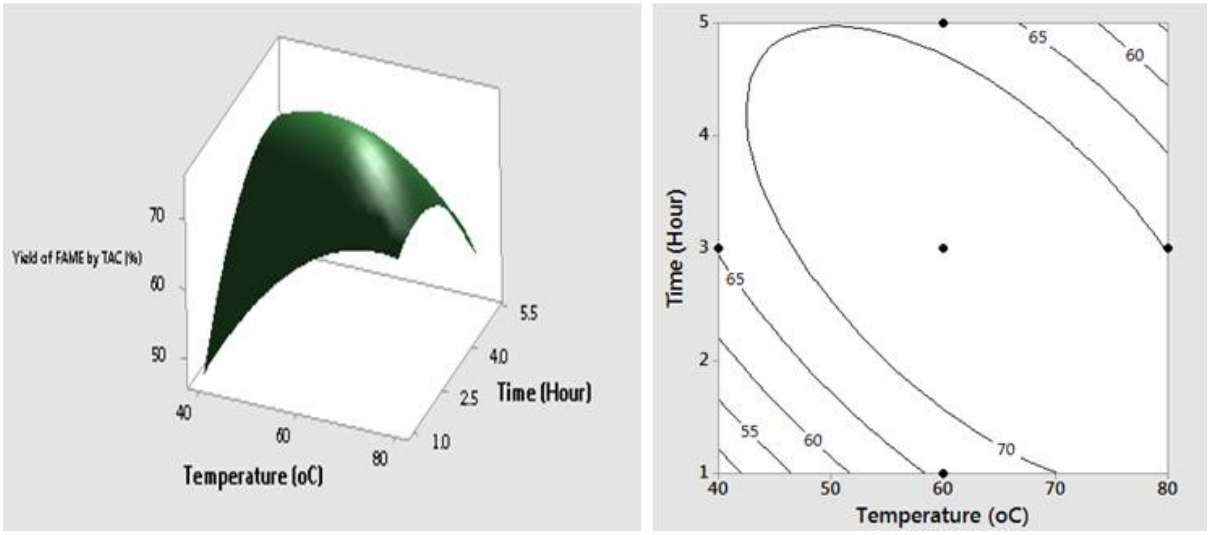

Figure 4.69a: Surface and contour plots of time and temperature by TAC.

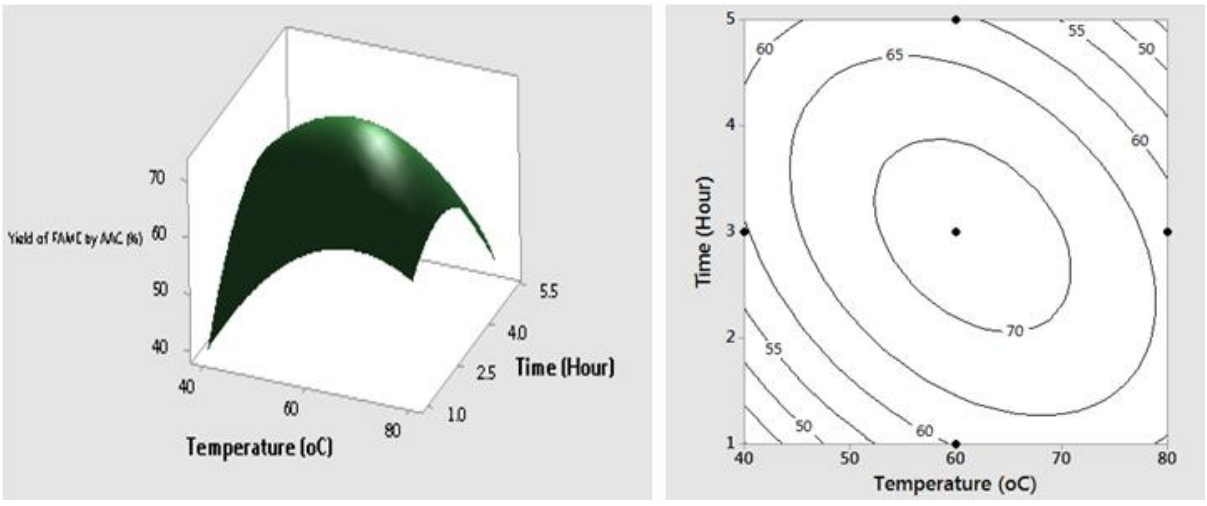

Figure 4.69b: Surface and contour plots of time and temperature by AAC.

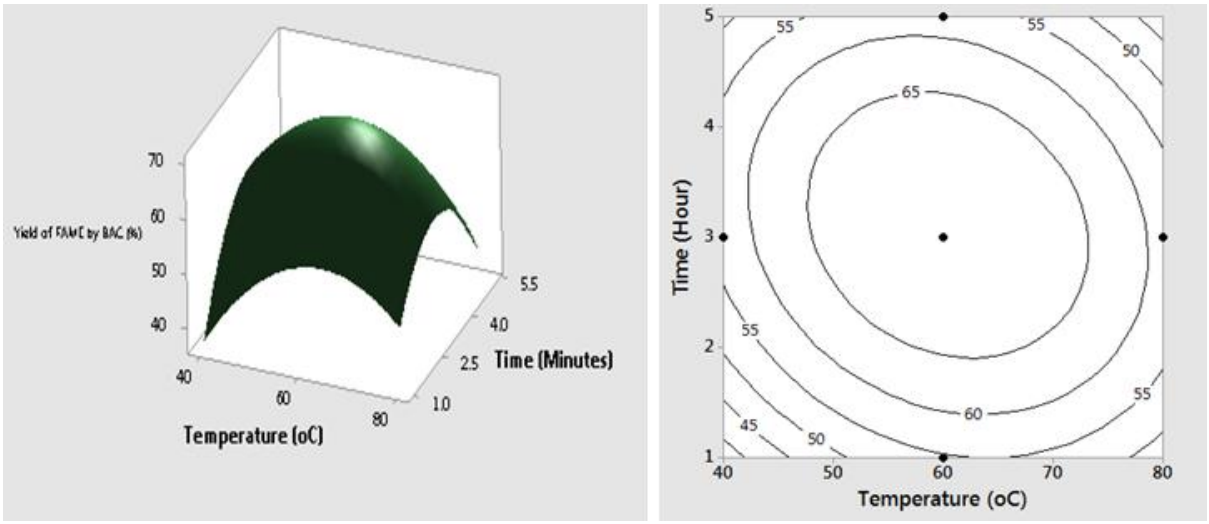

Figure 4.69c: Surface and contour plots of time and temperature by BAC.

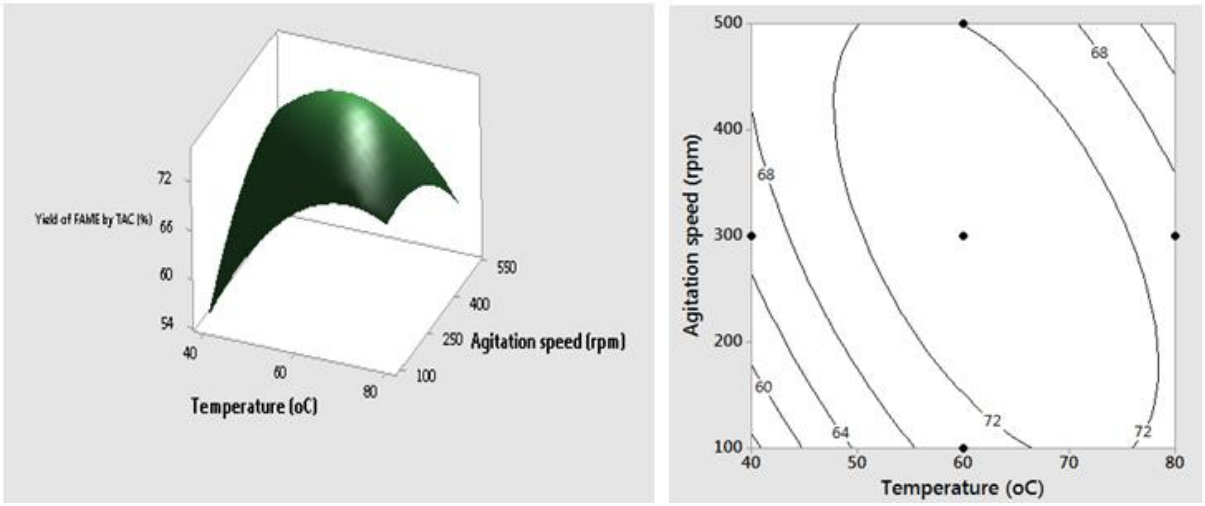

Figure 4.70a: Surface and contour plots of agitation speed and temperature by TAC.

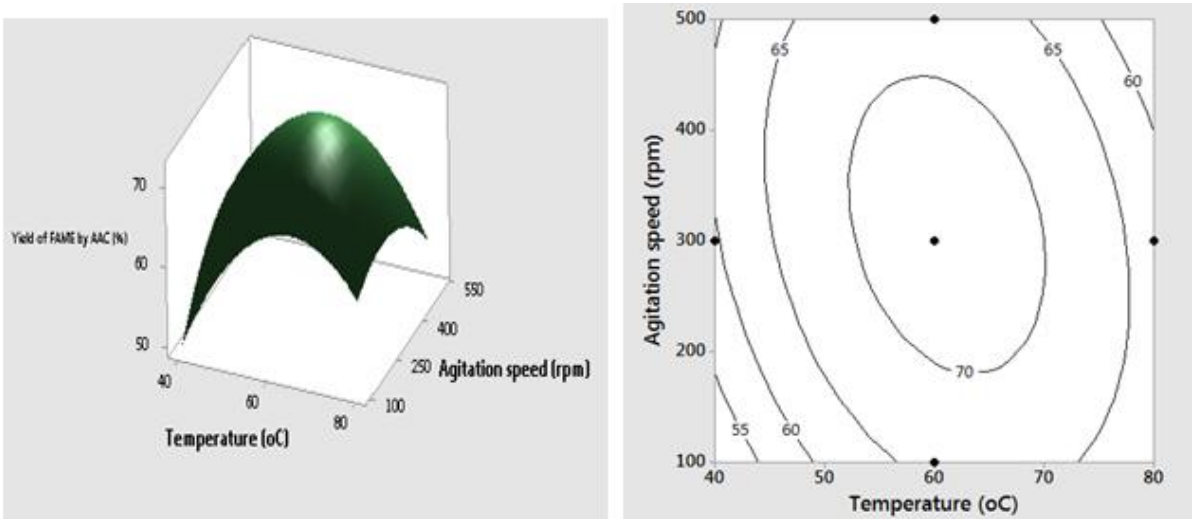

Figure 4.70b: Surface and contour plots of agitation speed and temperature by AAC.

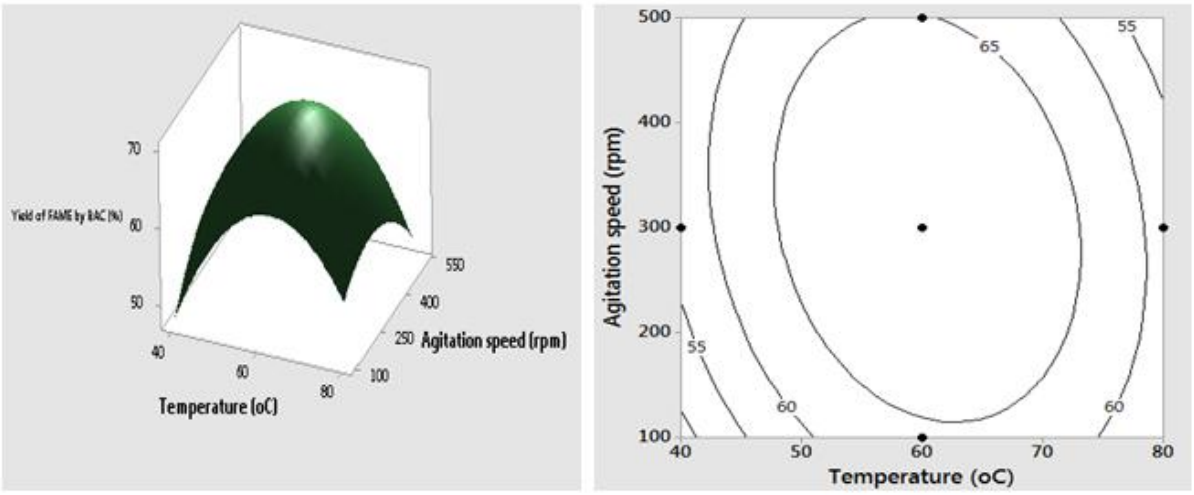

Figure 4.70c: Surface and contour plots of agitation speed and temperature by BAC.

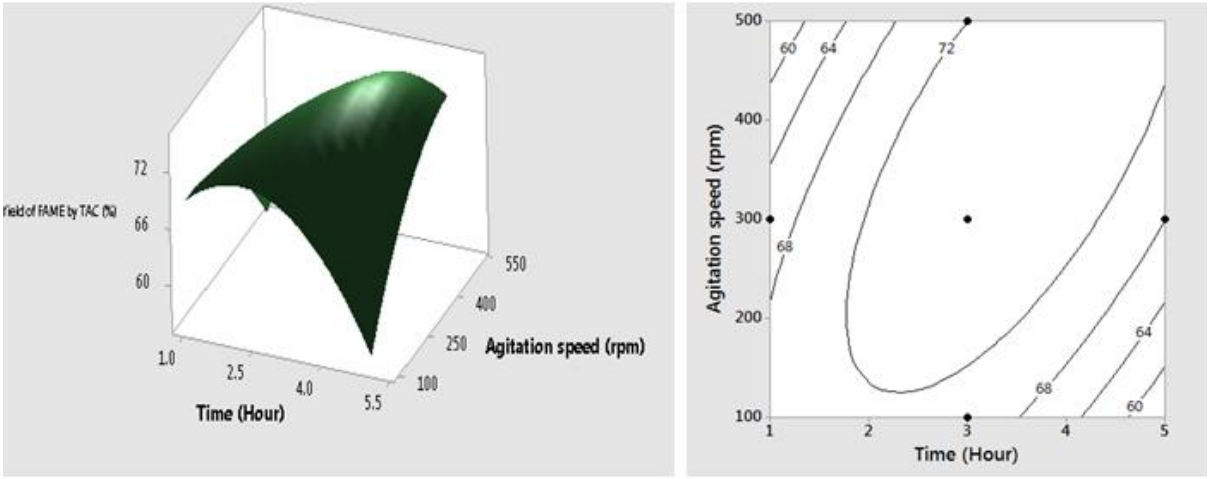

Figure 4.71a: Surface and contour plots of agitation speed and time by TAC.

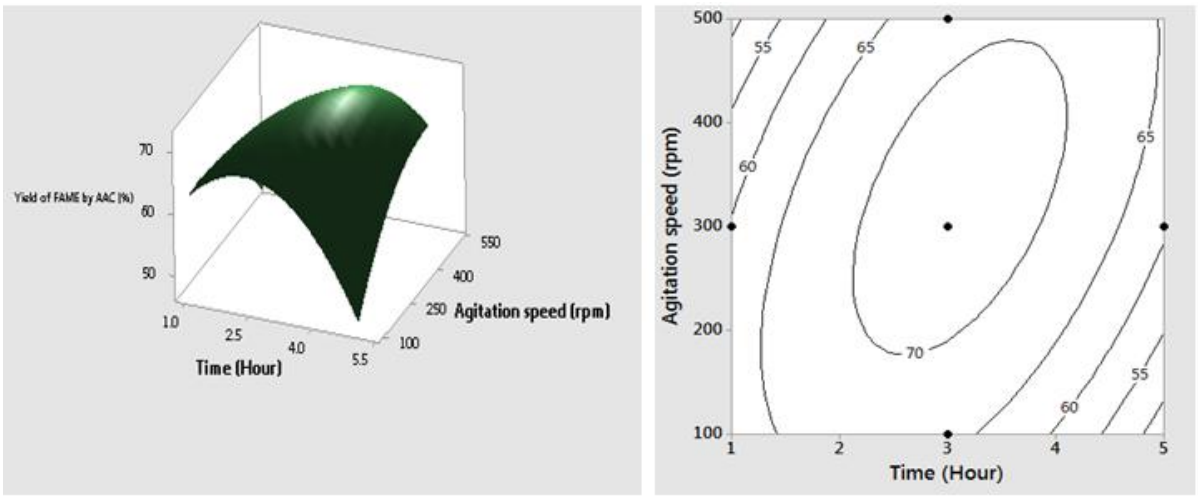

Figure 4.71b: Surface and contour plots of agitation speed and time by AAC.

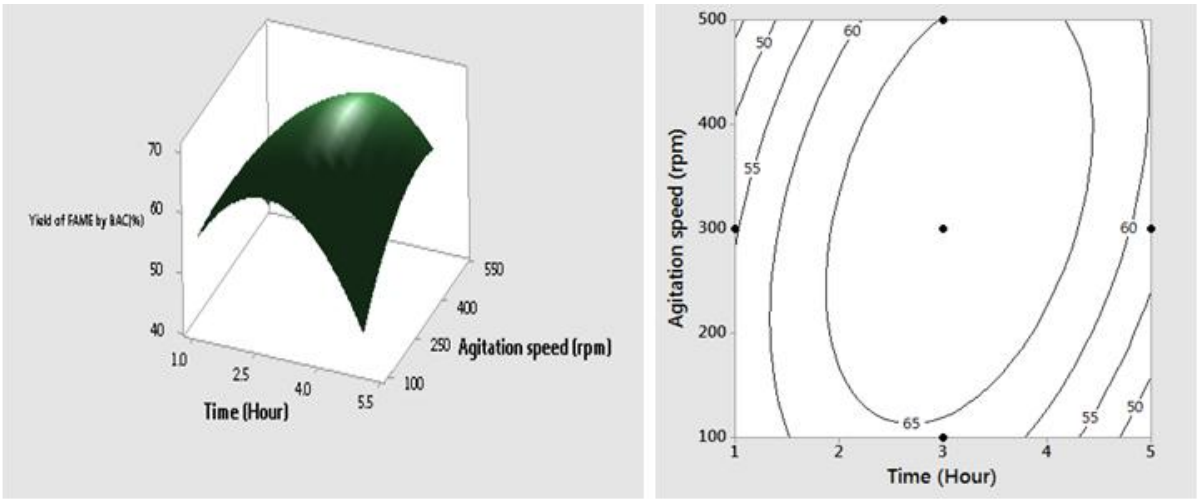

Figure 4.71c: Surface and contour plots of agitation speed and time by BAC.

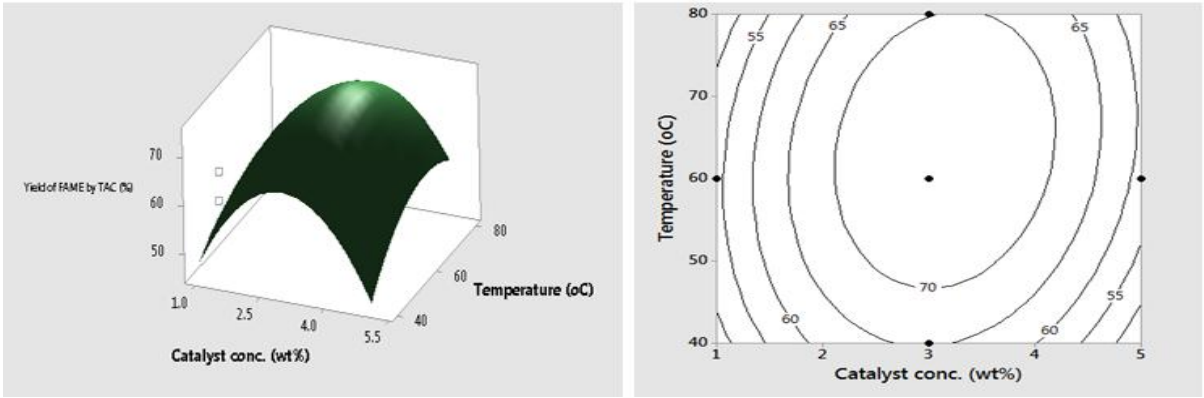

Figure 4.72a: Surface and contour plots of catalyst conc. and temperature by TAC.

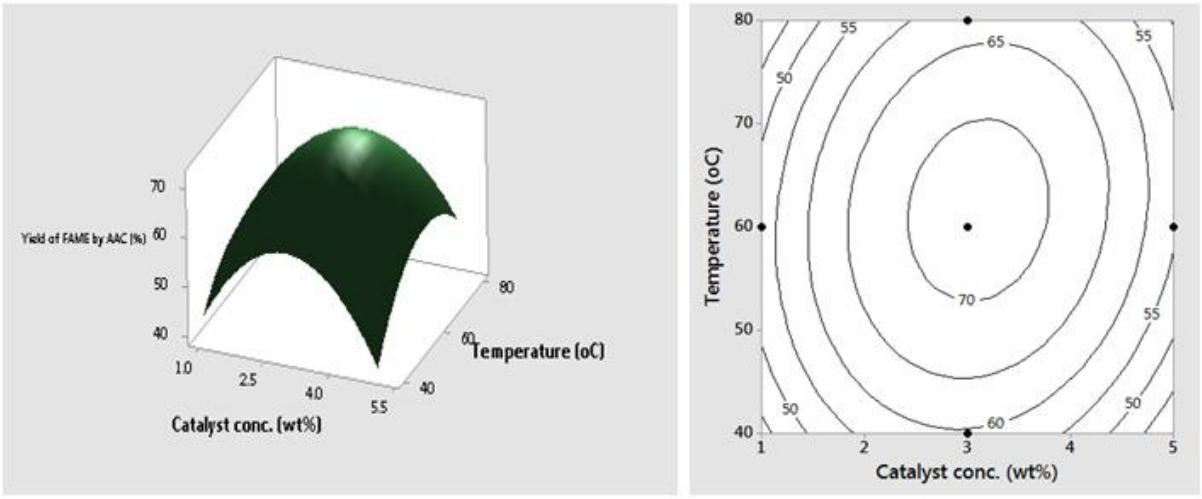

Figure 4.72b: Surface and contour plots of catalyst conc. and temperature by AAC.

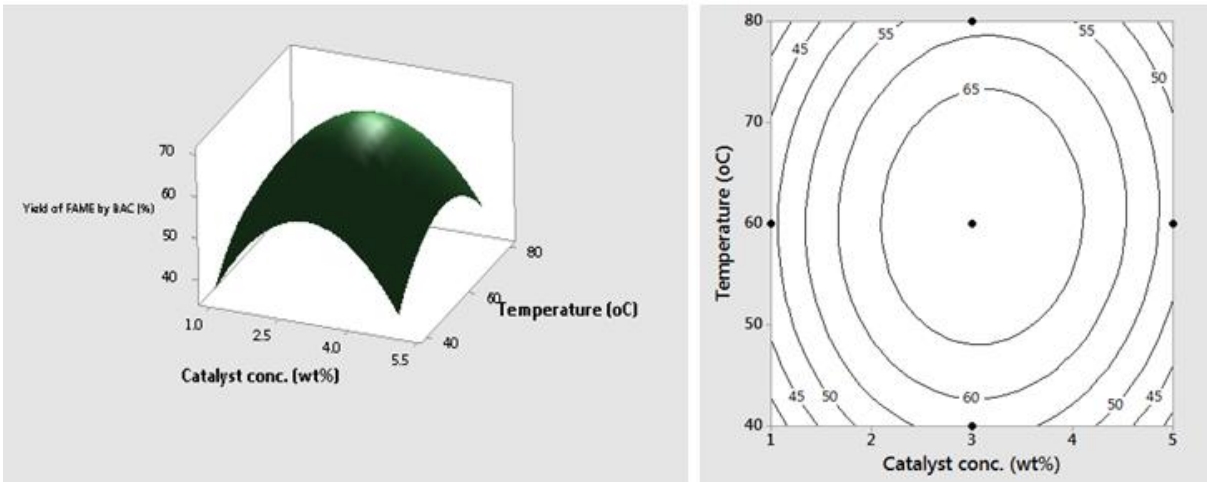

Figure 4.72c: Surface and contour plots of catalyst conc. and temperature by BAC.

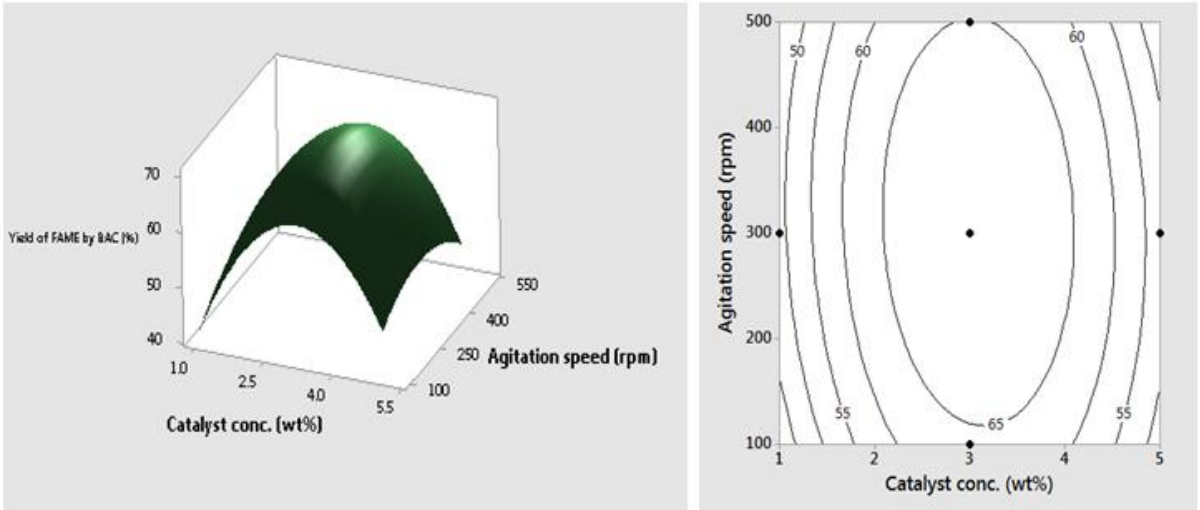

Figure 4.73: Surface and contour plots of catalyst conc. and agitation speed by BAC.

4.10 Optimization of Biodiesel Production using Desirability Function Approach

Biodiesel production from African pear seed oil and Gmelina seed oil catalyzed by three heterogeneous catalysts was optimized using desirability function approach of response surface methodology in Minitab 17. Desirability function approach eliminates the rigour associated with most other optimization techniques such as the optimization using contour and surface plots. It is a multi -response multi -factor optimization technique which operates on the principle established by Derringer Harrington. It optimizes a set of responses and defines the best factor settings for a solution of a multivariate objective function.

4.10.1 Optimization of biodiesel produced from African pear seed oil

The value of individual desirability and the composite desirability respectively approximate to 1 which signifies that the optimization result is highly desirable. The optimal conditions are shown in desirability plot (Figure G1of Appendix G) and presented in Table 4.34. Therefore, it is seen from figure and tablethat the optimalyields of biodiesel or fatty acid methyl ester (FAME) from BAC, AAC, TAC catalyzed African pear seed oil are 69.43, 76.45 & 70.89% respectively at optimized conditions of catalyst conc. = 3.1wt%, methanol/oil molar ratio = 10.2, temperature = 60.2^{o}C, time = 3.2h and agitation speed = 346rpm.
Table 4.33 also depicts the validation of the optimal results of the transesterification process, from the table it could be observed that the percentage error of each response was less than 1%. This shows that the model was adequate in predicting the responses.

Table 4.34: Validation of the optimal values for APO FAME

S/N	Responses	Catalyst conc (wt%)	Methanol/oil molar ratio (mol/mol)	Temperature (^{o}C)	Time	Agitation speed (rpm)	Experimental Yield (%)	Predicted Yield (%)	% Error
1	Yield of FAME by BAC	3.1	10.2	60.2	3.2h	346	69.0	69.43	0.61
2	Yield of FAME by TAC	3.1	10.2	60.2	3h	346	70.5	70.89	0.55
3	Yield of FAME by AAC	3.1	10.2	60.2	3.2h	346	77	76.45	0.71

4.10.2 Optimization of biodiesel produced from Gmelina seed oil

Similarly, desirability function was used to optimize the production of biodiesel from gmelina seed oil.The optimal conditions are shown in desirability plot (Figure H1 of Appendix H) and presented in Table 4.35. Therefore, it is seen from Figure H1 of Appendix AFO and Table 4.35that the optimalyields of biodiesel or fatty acid methyl ester (FAME) from BAC, TAC, AAC catalyzed gmelina seed oil are 69.95, 74.9 & 72.12% respectively at optimized conditions of catalyst conc. = 3.1wt%, methanol/oil molar ratio = 10.2, temperature = 60.6^{o}C, time = 3.1h and agitation speed = 326rpm

Table 4.35equally depicts the validation of the optimal results of the transesterification process, from the table it could be observed that the percentage error of each response was less than 1%. This shows that the model was adequate in predicting the responses.

Table 4.35: Validation of the optimal values for GSO FAME

S/N	Responses	Catalyst conc (wt%)	Methanol/oil molar ratio (mol/mol)	Temperature (^{o}C)	Time	Agitation speed (rpm)	Experimental Yield (%)	Predicted Yield (%)	% Error
1	Yield of FAME by BAC	3.1	10.2	60.6	3h	326	70	69.95	0.071
2	Yield of FAME by TAC	3.1	10.2	60.6	3h	326	75	74.9	0.13
3	Yield of FAME by AAC	3.1	10.2	60.6	3h	326	72	72.12	0.17

4.11 Prediction of Biodiesel Production using Artificial Neural Network

ANN model was developed to predict the production of biodiesel from the African pear seed oil and gmelina seed oil. The data used for the training and prediction of biodiesel production were the yields obtained from experimental response of design matrix shown in Appendices G and H. Altogether, 32 data sets of biodiesel yieldwere selected to use in this study. Supervised learning was used and data sets were randomly divided by the network; 70% of the data was used for training, while 15% each was allocated for testing and validation. The

maximum number of epoch was set to 100. The epoch was set to 100 to ensure that there is sufficient number of iterations during the learning process. Learning was very fast at this level and the optimum performance was obtained in all cases when the epoch was more than 10.

The network architecture consists of five input units, two hidden layers with ten hidden units (nodes) and three output unit as shown in Figure 4.74. The sigmoid transfer function was used in the processing units in the hidden layer. The input $(x_1, x_2, \ldots x_5)$ to the neural network are the weight percentage of process parameter for production of biodiesel. The targets were the biodiesel yields obtained from the three modified clay catalysts.

The performance parameters of the network in training for biodiesel yield prediction are shown in Figure 4.75 and 4.76 respectively. As shown in Figure 4.75, the network mean square error falls from a very high value to 0.006478 which is the best validation performance at epoch 7. The maximum numbers of epochs for best validation performance was 13, and also from Figure 4.76 the error histogram shows that the network errors were concentrated toward zero indicating a good performance. The network model output for the trained data sets is shown in Appendix M.

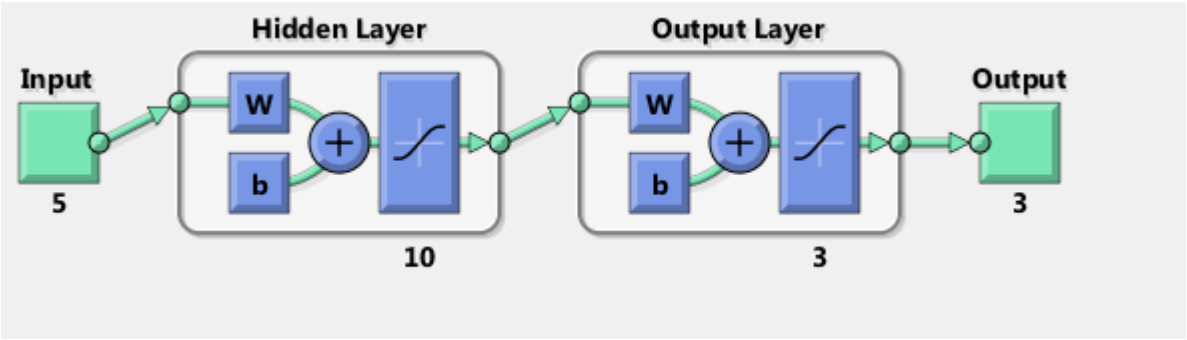

Figure 4.74: ANN architecture used in training data for biodiesel yield prediction.

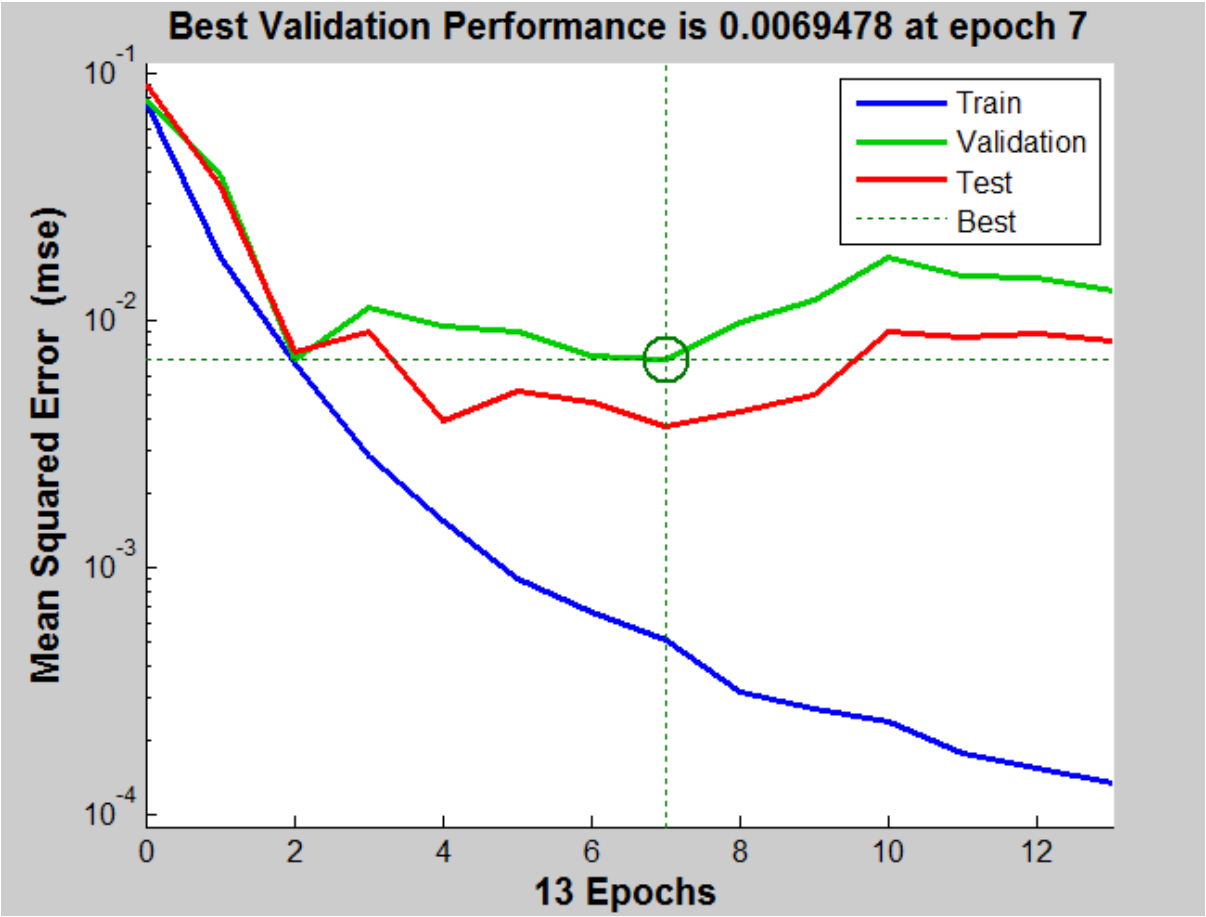

Figure 4.75: Training error (MSE) curve for biodiesel yield prediction.

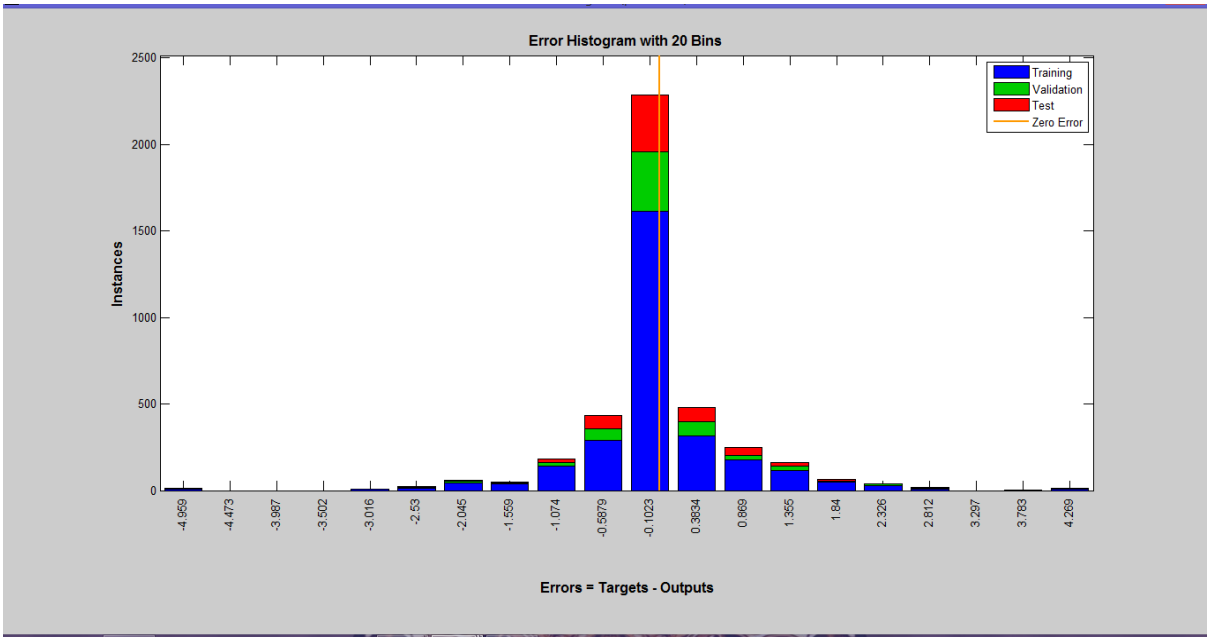

Figure 4.76: The network data sets Training Error distribution Histogram for prediction of biodiesel yield.

A further analysis of the trained model performance was done using regression analysis as shown in Figure4.77. The correlation coefficient value is an indication of how far the network is able to learn the training data sets. It can be observed from the figure that there is a very high correlation between the ANN predicted values and targeted values determined experimentally. The overall correlation coefficient for the trained model used in predicting yield was 0.98739; also the correlation coefficients for the validation and test data sets were recorded as 0.99195 and 0.99387 as shown in Figure 4.77.

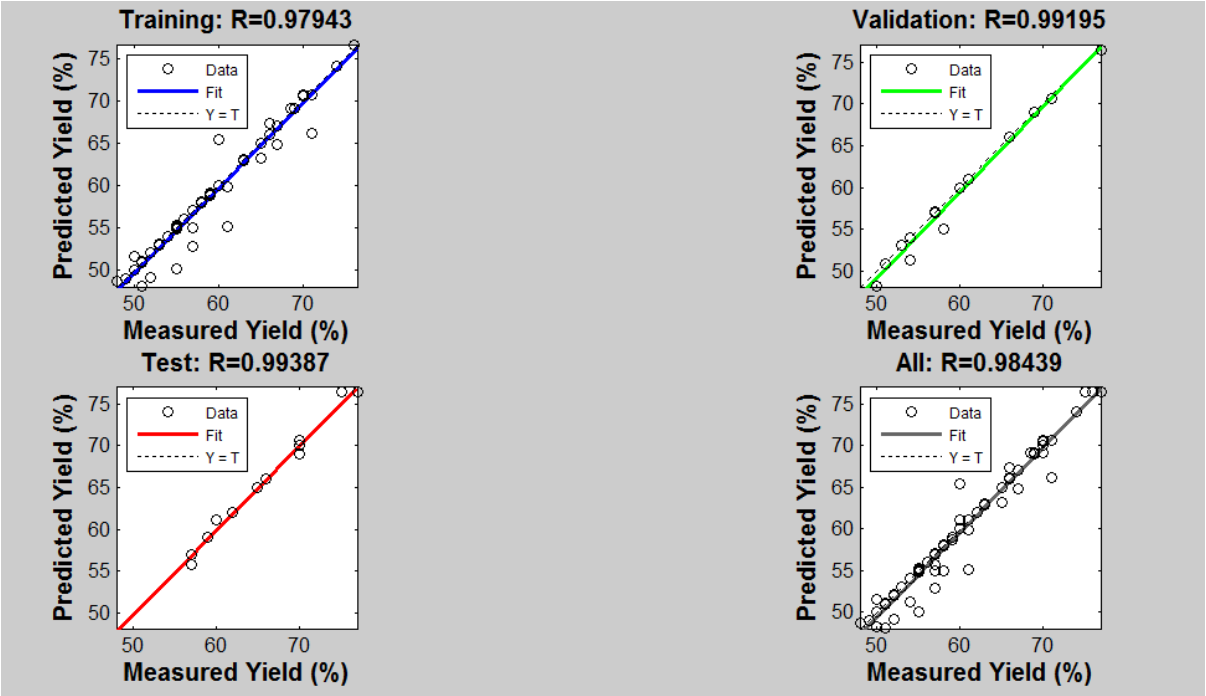

Figure 4.77: Regression plot analysis for the trained ANN model used in prediction of biodiesel yield.

4.12 Characterization of Biodiesel Produced using Optimal Conditions

Table 4.35 gives a summary of all the fuel properties analyzed and the limits that they were compared with (ASTM D 6751 (2002) standards).

4.12.1 Density

Biodiesel generally has a higher density than petro-diesel. This can impact on fuel consumption as fuel introduced into the combustion chamber is determined volumetrically. The densities of the APO and GSO FAME producedby TAC, AAC and BAC catalysts evaluated at 30^{o}C were within the ASTM limits for biodiesel (Table 4.36).

4.12.2 Viscosity

Viscosities of neat vegetable oils are always highand they cause serious problems in unmodified engines. The increase in viscosity results in poor atomization and incomplete combustion which leads to coking of injector tips. This results in engine power loss. Biodiesel still has higher viscosity than petro-diesel. Viscosity decreases with unsaturation but increases markedly with contamination by mono, di or triglycerides. It could be observed from Table 4.36 that the viscosity of APO FAME was lower than that of GSO FAME for all the catalyst and this could be as a result of its higher percentage of unsaturation as shown in Table 4.36.It is also observed that the viscosities of the FAME fall within the ASTM limits (1.6-6.0 Cst) for biodiesel.

4.12.3 Flash point

The flash point is a determinant for flammability classification of materials. The typical flash point of pure methyl ester is >200^{o}C, classifying them as "non-flammable". However, during production and purification of biodiesel, not all the methanol may be removed, making the fuel flammable and dangerous to handle and store if the flash point falls below 130^{o}C. The flash point of the APO and GSO FAME is >170^{o}C, which falls within the ASTM standard and makes it safe for storage.

4.12.4 Acid value

Acid value is a measure of mineral acids and free fatty acids contained in a fuel sample. It is expressed in mg KOH required to neutralize 1g of FAME. High fuel acidity is linked with corrosion and engine deposits. The APO and GSO FAME have acid value <0.5mgKOH/g. The ASTM value for TAN is 0.5mgKOH/g; this implies that the acid value of the biodiesel is acceptable.

4.12.5 Cetane number

This serves as a measure of ignition quality. This is the most pronounced change from vegetable oil to the transesterified product. Fuels with low cetane numbers show an increase in emission due to incomplete combustion. The lower limit for cetane index is 47 by ASTM standards. The cetane number of the APO and GSO FAME was>50, which is above the lower limit for cetane number. Thus the result obtained is acceptable.

4.12.6 Oxidation stability

Oxidation stability is one of the most important factors used to determine how long an oil/diesel will last in a particular application. Oxidation, a chemical reaction between the hydrocarbon lubricant/diesel and oxygen in the air, is the most common cause of lubricating oil degradation. The process causes an increase in oil viscosity, increased acidity, filter plugging, corrosion and the formation of varnish, sludge and rust, among other issues. From Table 4.36, it could be observed that the oxidation stabilities of all the biodiesel produced were within the ASTM acceptable limits for biodiesel. This shows that the biodiesel is good for application in a diesel engine but blending it with little disel it will improve its engine performance.

Table 4.36: Fuel properties of GSO and APO methyl esters compared with ASTM limits.

PROPERTY	UNITS	ASTM METHODS	APO FAME by TAC	APO FAME by AAC	APO FAME by BAC	GSO FAME by TAC	GSO FAME by AAC	GSO FAME by BAC	ASTM LIMITS
Density	kg/m^3	ASTM D-1298	860	858	859	859	859	860	830-880
Kinematics Viscosity	Cst	ASTM D-445	3.6	3.7	3.8	4.0	3.9	4.1	1.6-6.0
Flash Point	^oC	ASTM D-93	177	180	178	180	182	181	≥130
Pour Point	^oC	ASTM D-97	2	3	1	3	2	0.5	+15 max
Cloud Point	^oC	ASTM D-2500	1.3	1.4	1.4	1.4	1.2	1.3	-15 to 5
Acid Value	mgKOH/g	ASTM D-974	0.3	0.15	0.21				≤ 0.80
Low Heating Value	MJ/kg		40.1	41	41	41	42	41	≥ 35
Aniline Point	(^oC)	ASTM D-4737	175	194	184	186	180	184	
Higher Heating Value	MJ/Kg		51	52	52	52	53	53	
Oxidative stability	Hour	ASTM D-6751/EN 14112	5.0	5.5	5.2	5.25	5.75	5.2	3 min
Cetane number		ASTM D-130	52	56	54	55	53	54	47 min

4.13 GS-MS RESULT

Figures 4.78- 4.84 show the conversion of triglyceride of APO and GSO to methyl ester by TAC, AAC and BAC respectively. From the figure, it is observed that the triglyceride was converted to methyl esters. The highest peaks indicate the presence of methyl esters while the lower peaks at the right hand side indicate the presence of monoglyceride, diglyceride and unconverted triglyceride.

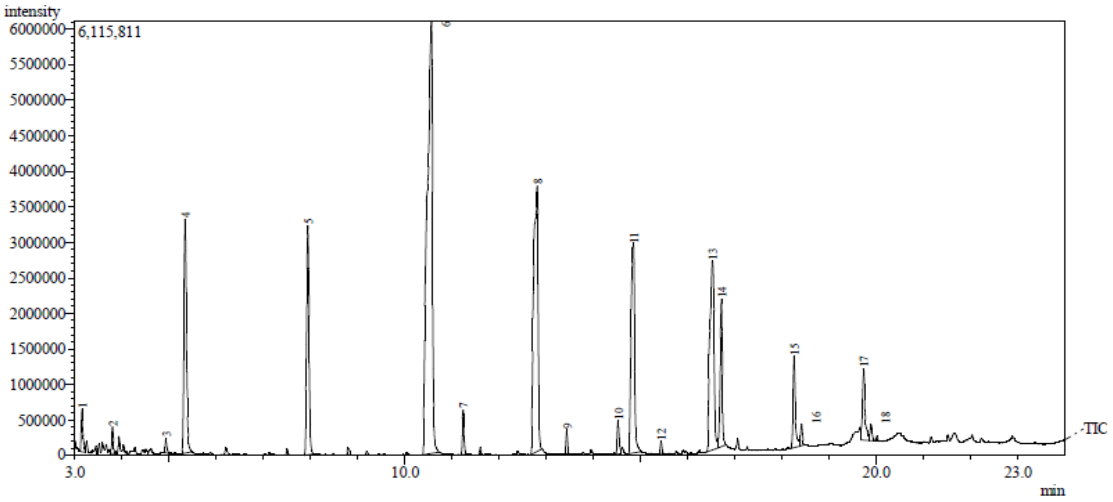

Figure 4.78: GC-MS of APO FAME produced by TAC catalyzed reaction at optimal conditions.

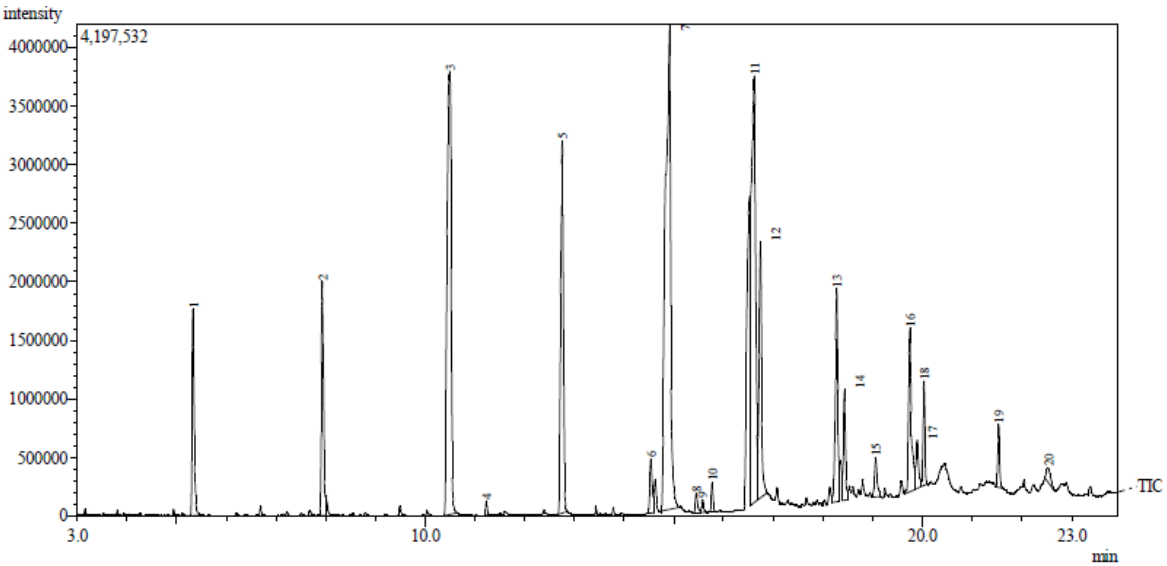

Figure 4.79: GC-MS of APO FAME produced by AAC catalyzed reaction at optimal conditions.

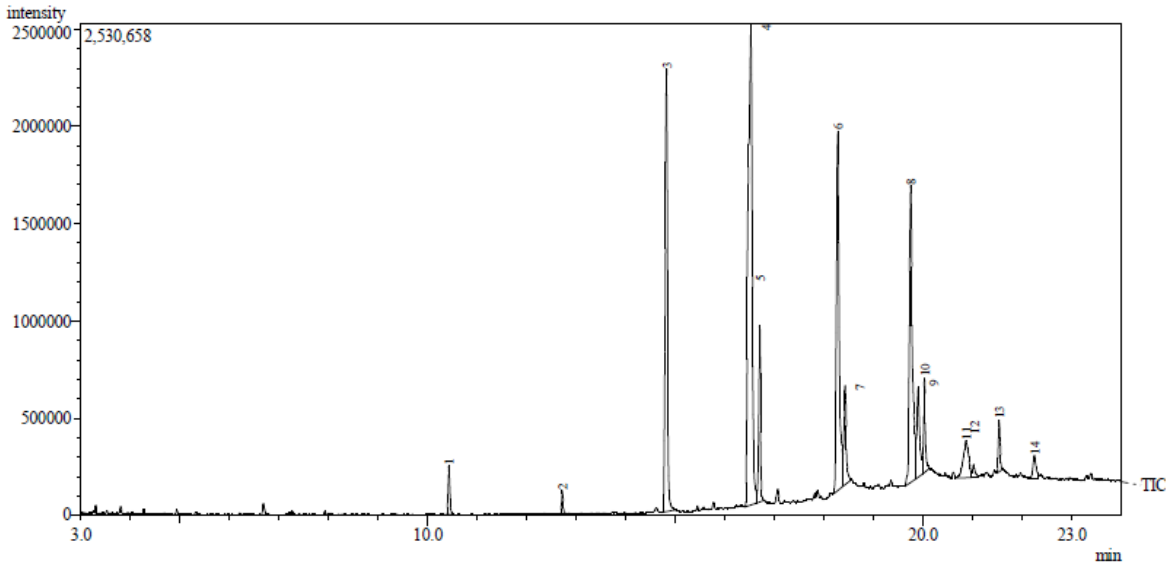

Figure 4.80: GC-MS of APO FAME produced by BAC catalyzed reaction at optimal conditions.

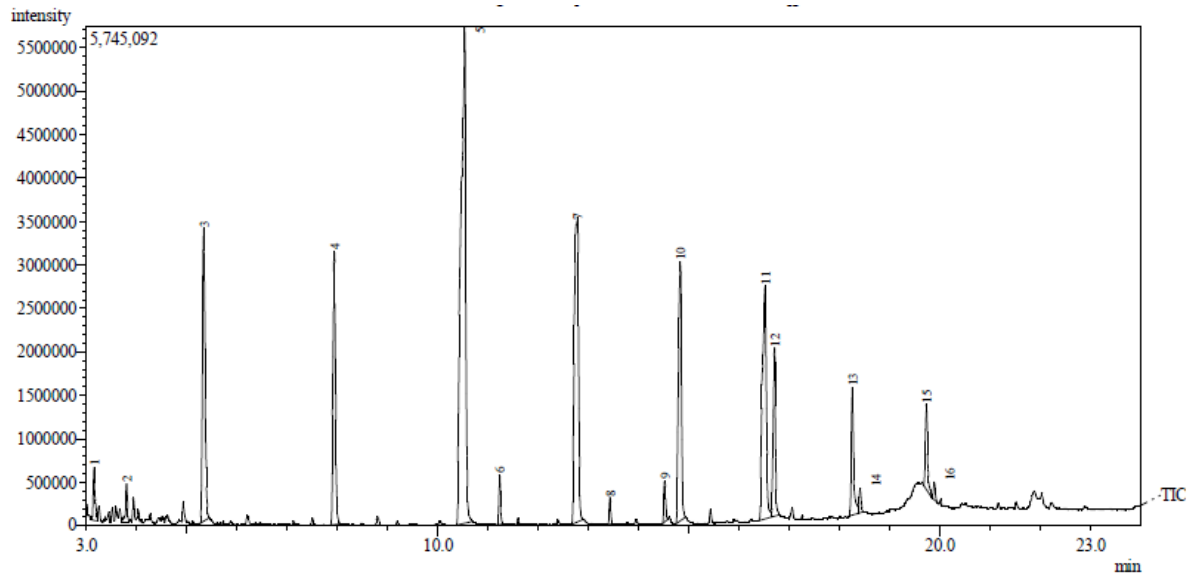

Figure 4.81: GC-MS of GSO FAME produced by TAC catalyzed reaction at optimal conditions.

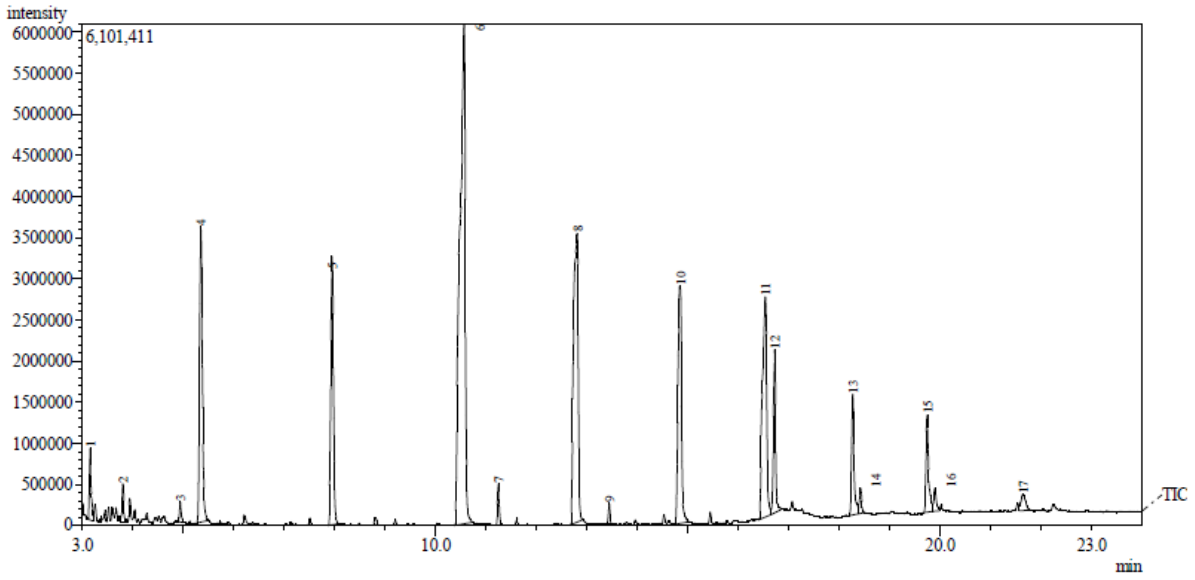

Figure 4.82: GC-MS of GSO FAME produced by AAC catalyzed reaction at optimal conditions.

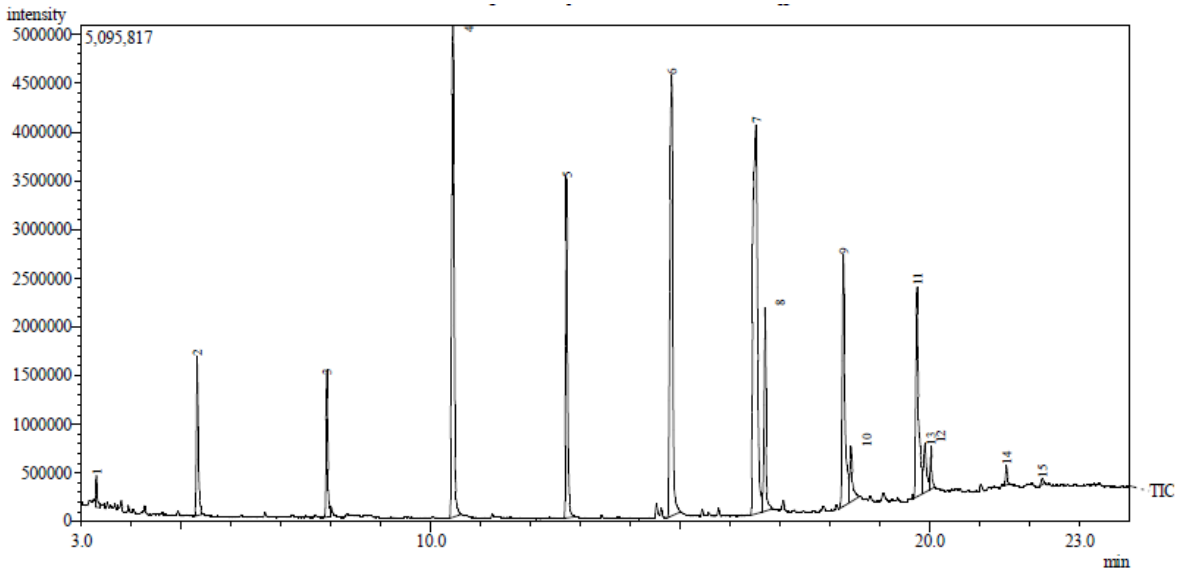

Figure 4.83: GC-MS of GSO FAME produced by BAC catalyzed reaction at optimal conditions.

4.14 FTIR Characterization of Biodiesel

Figures 4.84-89 show Fourier Transform Infra-red Spectrophotometer for the conversion of triglyceride of APO and GSO to methyl ester by TAC, AAC and BAC respectively. From the figures, the IR peak at 3100–3890 cm^{-1} is attributed to the stretching ofhydroxyl (OH) groups in the biodiesel. This functional group is predominant in biodiesel produced from APO catalyzed by TAC and biodiesel from GSOcatalyzed by AAC. This could be as a result better conversion of triglyceride. The IR peaks at 1300–1900 cm^{-1} are assigned to the peaks of bending vibration of O=C=O group. The two bands within the range of 2100–2890 $cm^{-1}$and

peak at 1750 cm^{-1} on the IR spectra of reused catalyst are ascribed to the C-H stretching of the alkyl group and C=O stretching of the esters group, respectively. These bands occurred because of the unconverted triglyceride in the oils.

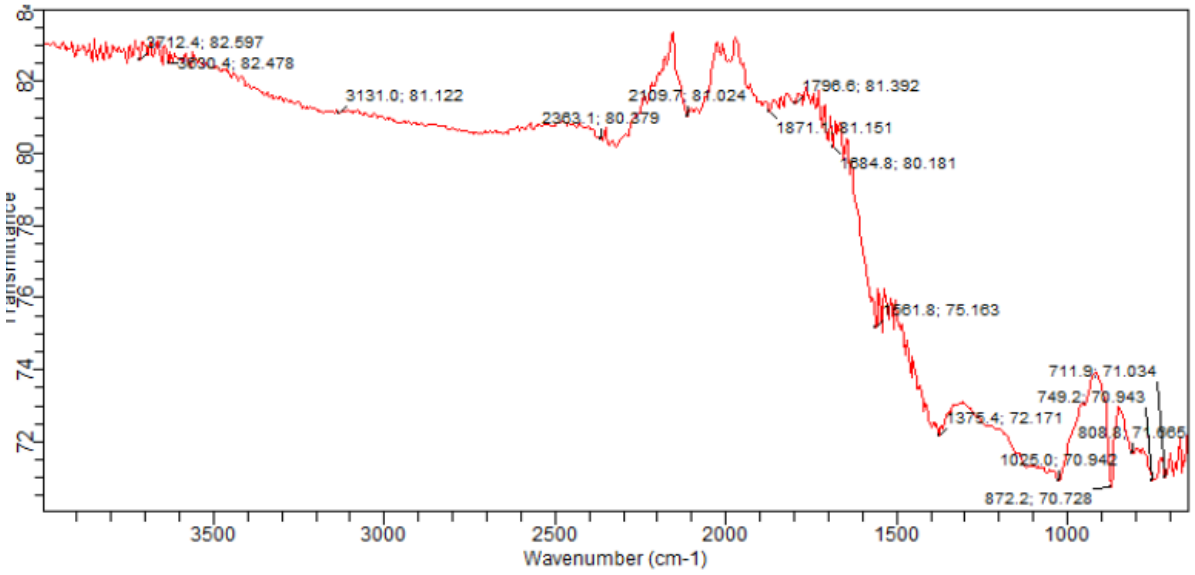

Figure 4.84:FTIR of APO FAME produced by TAC catalyzed reaction at optimal conditions.

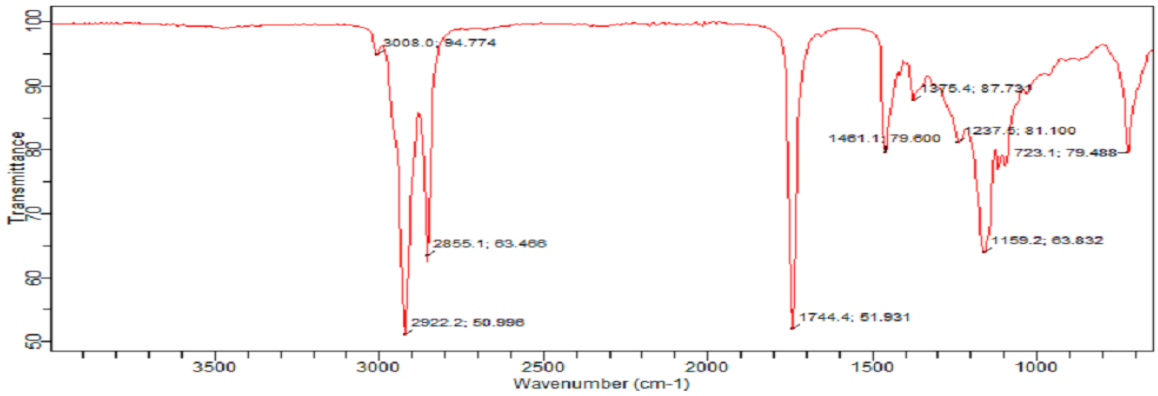

Figure 4.85:FTIR of APO FAME produced by AAC catalyzed reaction at optimal conditions.

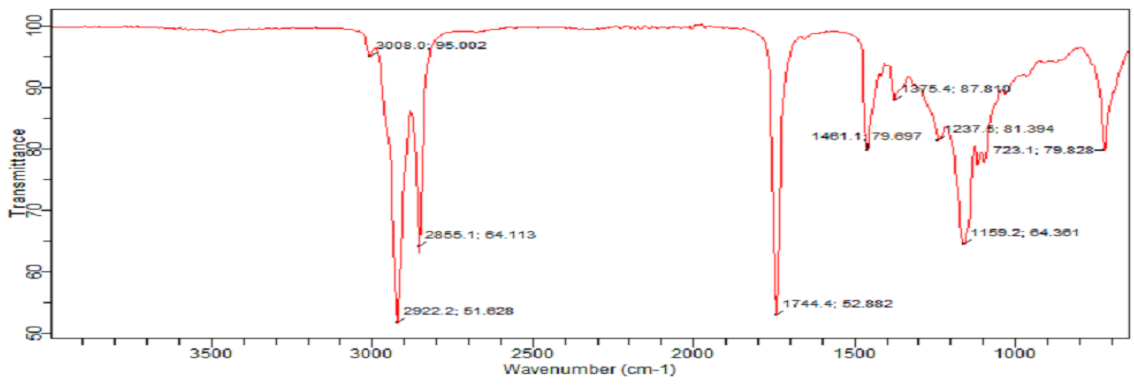

Figure 4.86:FTIR of APO FAME produced by BAC catalyzed reaction at optimal conditions.

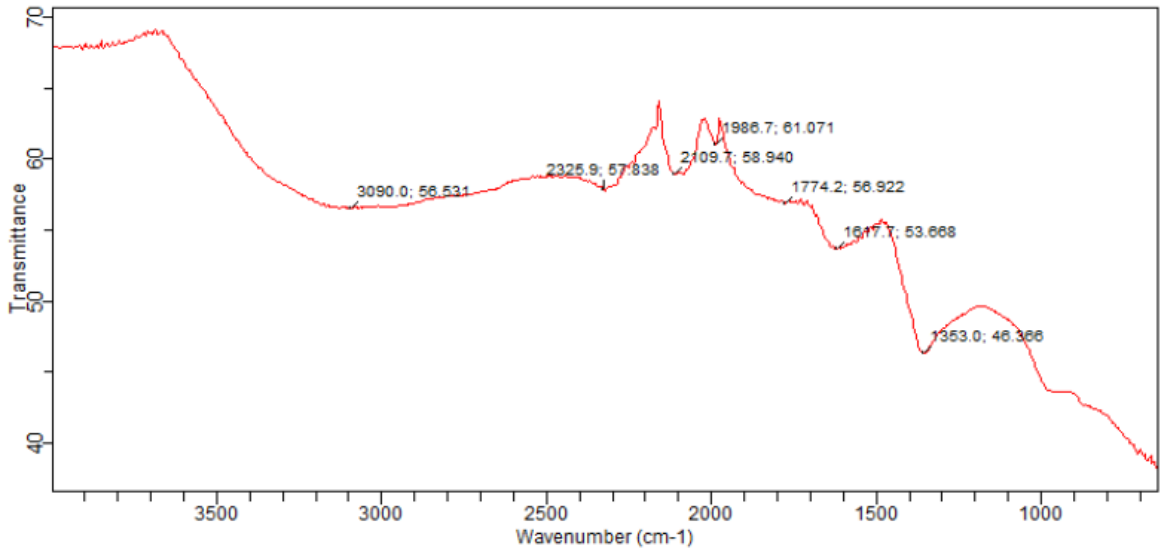

Figure 4.87:FTIR of GSO FAME produced by TAC catalyzed reaction at optimal conditions.

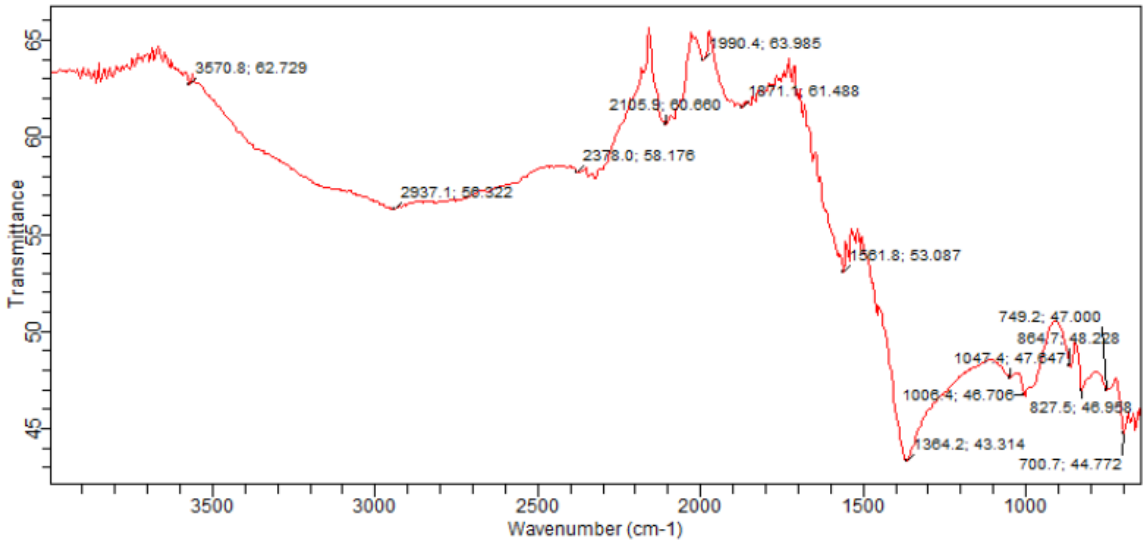

Figure 4.88:FTIR of GSO FAME produced by AAC catalyzed reaction at optimal conditions.

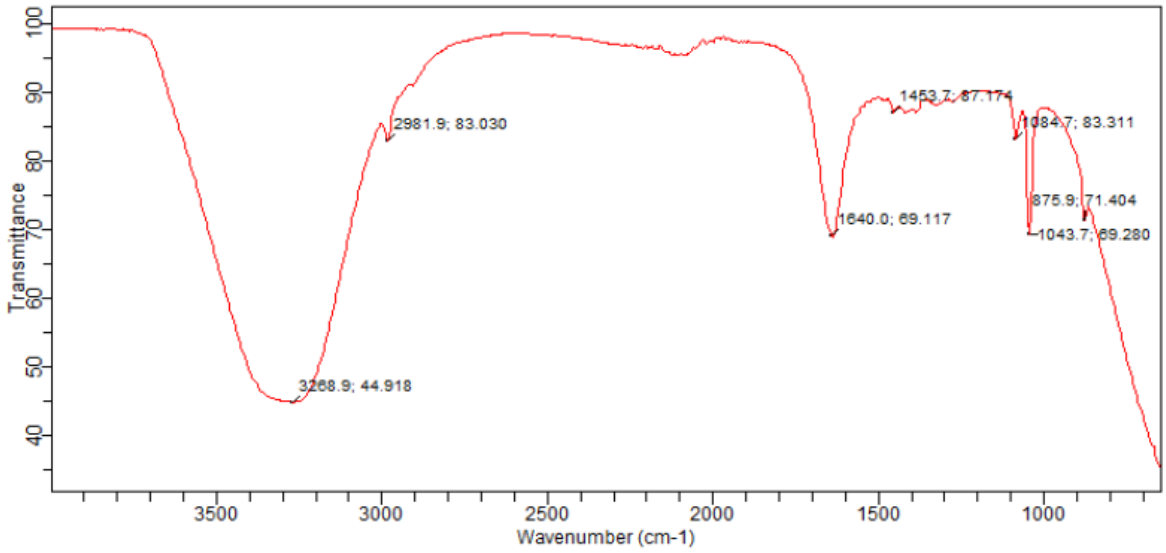

Figure 4.89:FTIR of GSO FAME produced by BAC catalyzed reaction at optimal conditions.

4.15 Product Distribution

The formation of products and disappearance of reactants at temperatures of 45, 50, 55^{o}C for transesterification of APO and GSO using TAC, AAC and BAC catalysts are depicted in Figures 4.90(a, b and c) and Figures 4.91(a, b & c)respectively. From the graphs, it could be observed that the products (biodiesel and glycerol) concentration increase as time increases and the reactants (triglyceride, diglyceride, monoglyceride and methanol) concentration decrease as time increases. The change in concentration of products and reactants became constant after 3hours for the three catalysts at all the temperatures. This could be that the reaction reached its end point at 3hours. The figures also show that biodiesel is more predominate in the product with a higher concentration at temperature of 55^{o}C. This shows that higher yield is obtained at temperature of 55^{o}C. It is also observed that the yield of biodiesel obtained from transesterification of APO is slightly higher than that obtained from GSO. This may be attributed to higher content of unsaturated free faty acid present in APO.

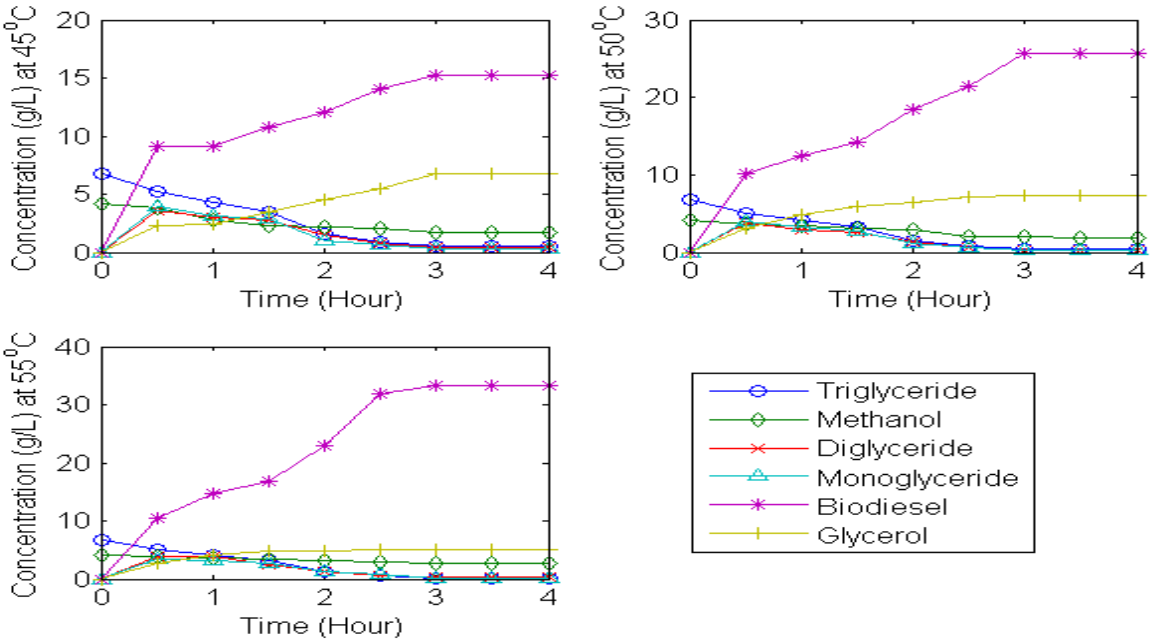

Figure 4.90(a):Concentration of species against time for TAC catalyzed transesterification of APO.

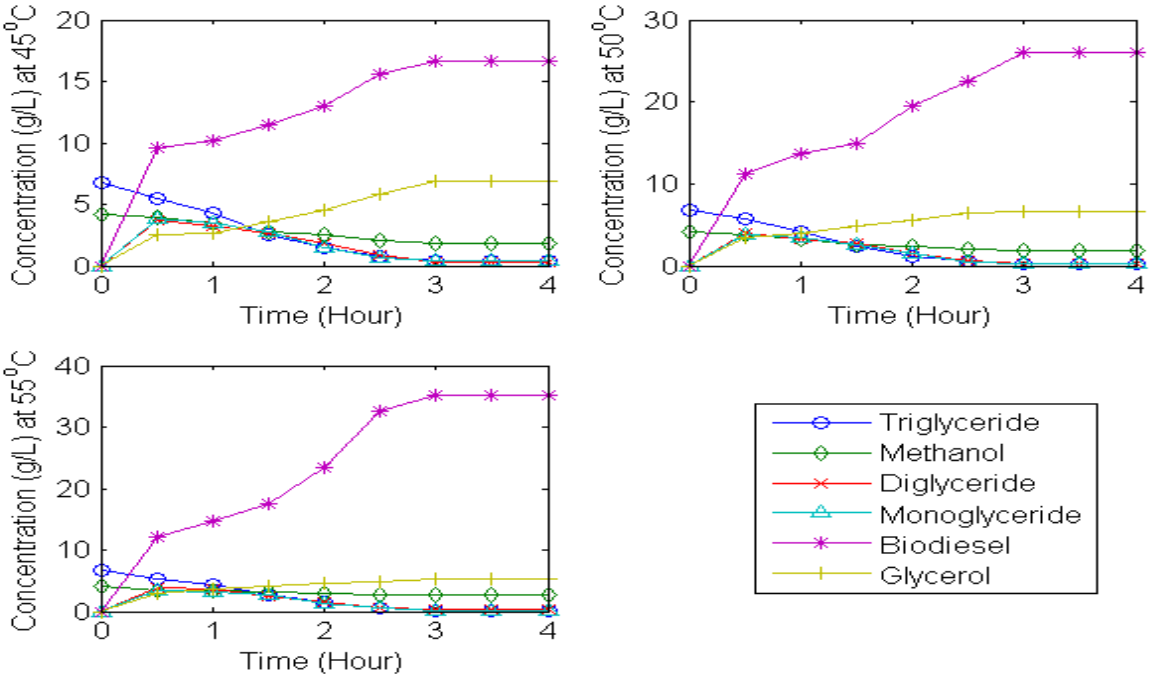

Figure 4.90(b):Concentration of species against time for AAC catalyzed transesterification of APO.

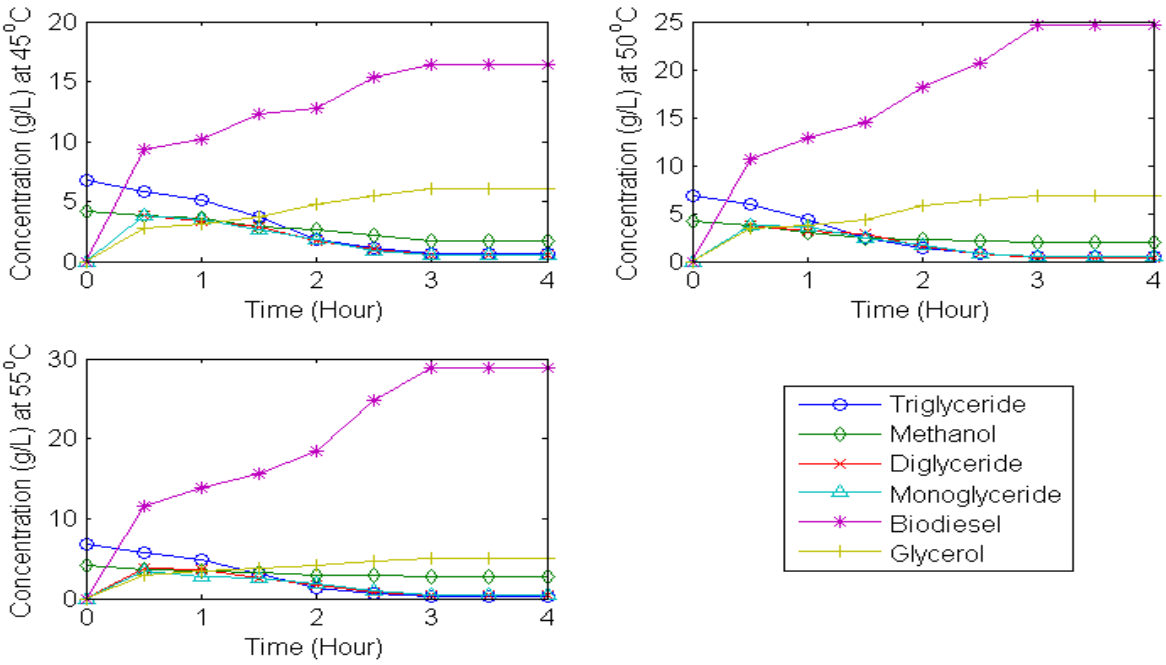

Figure 4.90(c):Concentration of species against time for BAC catalyzed transesterification of APO.

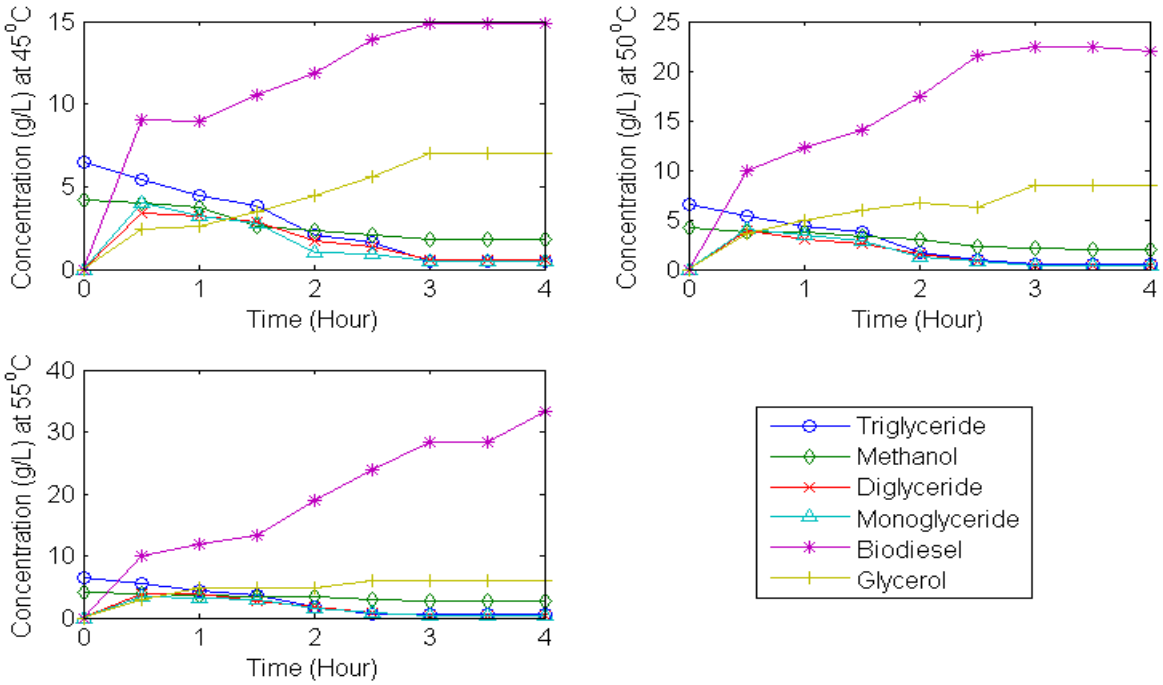

Figure 4.91(a):Concentration of species against time for TAC catalyzed transesterification of GSO.

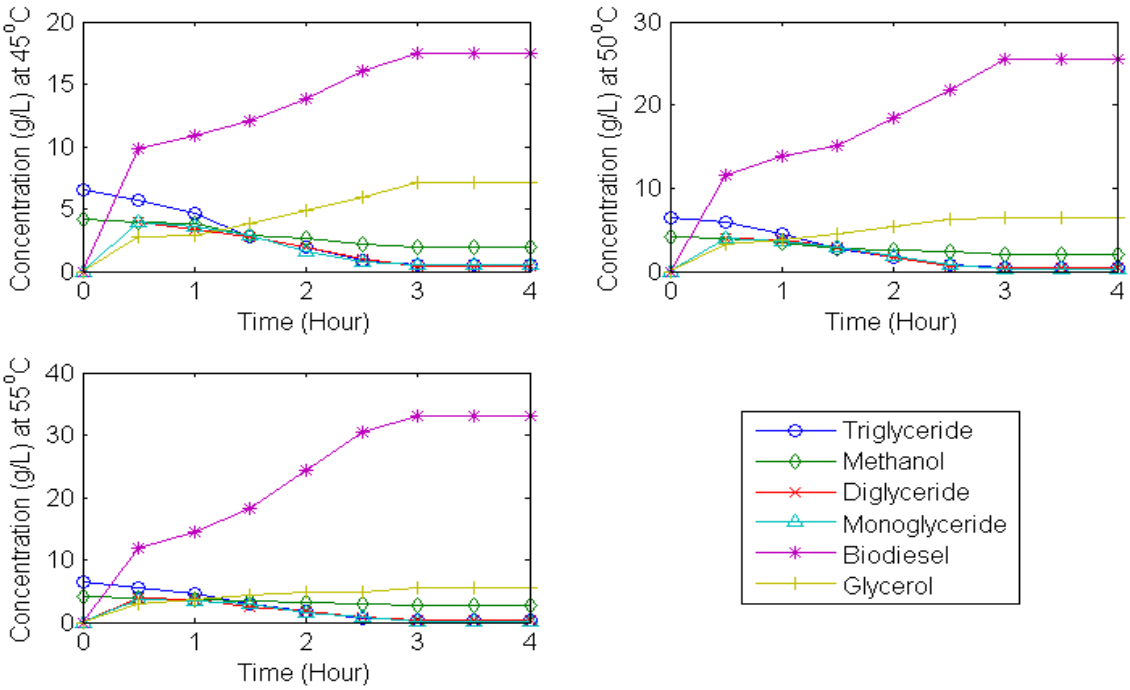

Figure 4.91(b):Concentration of species against time for AAC catalyzed transesterification of GSO.

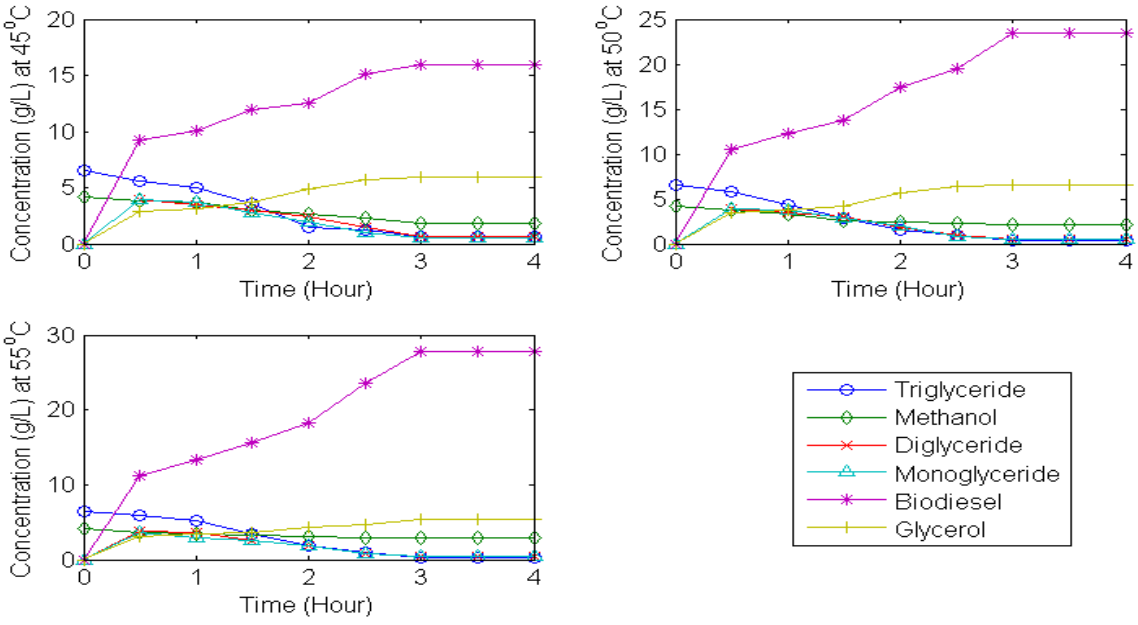

Figure 4.91(c):Concentration of species against time for BAC catalyzed transesterification of GSO.

4.16 Kinetics Study of Transesterification of APO and GSO

The kinetics study of transesterification of APO and GSO catalyzed by heterogeneous (TAC, AAC and BAC) catalysts were investigated.

The kinetics study of the APO and GSO FAME production using TAC, AAC, and BAC was done using two non-elementary reaction mechanisms: Langmuir-Hinshelwood-Hougen-Watson (LHHW) and Eley-Rideal (ER). Nine kinetic models with assumptions of adsorption of species, surface reaction and desorption of species were investigated for LHHW and seven models for Eley-Rideal (ER). The rate and equilibrium constants were determined by using nonlinear regression of POLYMATH 5.1 to search for those parameter values that minimize the sum of the squares of difference between the measured rates and the calculated rates for all the data pointsas shown in Equation (3.113) with initial guess of 0.01 and 10 respectively. Each reaction rate was determined using POLYMATH 5.1 by developing polynomial equation with concentration of various species in the reaction obtained by GC-MS analysis. The models were compared by using their individual variances calculated using Equation (3.113) at 95% confidence level. The model with lowest variance and positive parameter suits the experimental data while the model with lowest rate constant becomes the rate determining step. The rate and equilibrium constants obtained at different temperatures for each catalyst are presented in Tables J1 – J19 (Appendix J) for LHHW model and Tables K1 – K18 (Appendix K) for ER model. It was observed from the tables that for all the temperatures considered and catalysis of APO and GSO by TAC, AAC and BAC the rate constants and variances for surface reaction between adsorbed triglyceride and adsorbed methanol were lowest for LHHW model with best fitting of the experimental data in terms of conversion as shown in Figures 4.92 (a & b) while rate constant and variances between non adsorbed methanol and adsorbed triglyceride for ER model were lowest withbest fitting of the experimental data in terms of conversion as depicted in Figure 4.93 (a&b). These can be considered as rate determining step (RDS) and it is in agreement with assumption that approximately 75% of all heterogeneous reaction mechanism are surface-reaction-limited (Fogler, 2011).The rate and equilibrium constants with thermodynamics parameters of the rate determining step are presented in Tables 4.37 and 4.38 (LHHW model); Tables 4.39 and 4.40 (ER model).It was observed from the tables that the rate constant increase as temperature increases showing that the reaction is endothermic and proceeds at higher temperature below the boiling point of methanol. The activation energies for the forward and backward reactions of the rate determining steps for TAC, AAC and BAC catalyzed

transesterified APO and GSOpresentedin the tables indicate that the catalystswere able to lower the energy barrier of the reaction which is masstransfer resistance. Also the reaction was slow because triglyceride is a heavy molecule with higher potential energy than the reactant methanol.From the tables, it is also observed that the adsorption energies of step 1 is dominantly exothermic while that of step 2 is dominantly endothermic in LHHW model for both APO and GSO transesterified reactions by all the catalysts. The desorption energies for steps 6 and 8 are exothermic while the desorption energies for steps 7 and 9 are endothermic. The temperature sensitivity of step 9 for LHHW model was inconsistent for all the catalysts. Moreso, desorption energies for steps 5, 6 and 7 are endothermicwhile the adsorption energy of step 1 for both APO and GSO transesterified reactions by all the catalysts in ER model is exothermic.Comparing LHHW model and ER model, it can be observed that the variances of the RDS (surface reaction) for LHHW are smaller with better fitting as shown in Tables 4.41 and 4.42 showing that the LHHW model best describes the kinetic data. The activity of the catalysts for the RDS was compared using analysis of variance in Minitab 17. This was done at 5% level of significance to determine if there is statistical difference in performance of the catalysts and displayed in Tables 4.43 and 4.44. From the tables, it could be observed that the P-values for each catalyst is greater than 0.05 showing that their performance are different but similar at each temperature with catalyst 2 (AAC) having better performance at 55^{o}C (comparing their means in Table 4.43 and 4.444). It was also observed that the rate constant of forward reactions, k_5 for AAC catalyzed reaction was highest at all temperature and this may be attributed to its ability to catalyze the reaction faster.

Table 4.37**:** Rate and equilibrium constants with thermodynamics parameters of RDS for APO FAME using LHHW model

TAC catalyzed transesterification					
	45°C	50°C	55°C	$\Delta E, \Delta H$ (kJ/mol)	A, ΔS
k_5 (hr^{-1})	8.89E-3	9.37E-3	9.99E-3	10.77	0.52[a]
k_6 (hr^{-1})	7.97E-4	9.37E-4	7.08E-3	207.28	5.89E31[a]
K_1	11.61	10.50	10.18	- 11.86	- 0.017[b]
K_2	10.54	11.30	16.60	42.86	0.154[b]
K_6	8.79	10.23	6.90	- 22.95	- 0.054[b]
K_7	8.50	8.97	11.75	30.52	0.113[b]
K_8	15.60	9.89	10.94	- 32.28	0.079[b]
K_9	12.33	10.30	8.91	- 29.76	0.076[b]
AAC catalyzed transesterification					
k_5 (hr^{-1})	8.91E-3	9.5E-3	9.98E-3	10.08	1.05[a]
k_6 (hr^{-1})	1.03E-3	1.17E-3	1.22E-3	0.0172	1.01[a]
K_1	10	9.99	10.10	0.96	0.022[b]
K_2	9.86	9.75	8.19	- 17.61	- 0.036 [b]
K_6	8.25	13.40	7.20	-16.29	- 0.032 [b]
K_7	9.42	18.30	10.40	62.68	0.214 [b]
K_8	21.2	31.40	15.90	-30.12	- 0.068 [b]
K_9	12.41	12.40	16.60	27.75	0.108 [b]
BAC catalyzed transesterification					
k_5 (hr^{-1})	8.80E-3	9.5E-3	9.92E-3	10.91	0.547[a]
k_6 (hr^{-1})	9.17E-3	1.47E-3	9.73E-3	18.12	4.35[a]
K_1	10.53	11.10	9.20	-13.24	-0.0217[b]
K_2	7.70	9.45	12.89	47.76	0.167 [b]
K_6	7.25	13.40	6.20	- 19.11	-0.041 [b]
K_7	8.42	28.30	11.40	20.64	0.085 [b]
K_8	15.20	11.40	14.90	- 27.30	- 0.063 [b]
K_9	12.41	12.30	15.60	21.88	0.089 [b]

[a]-Unit of A is given by hr^{-1}, [b]-Unit of ΔS is given by kJ/mol. K

Table 4.38: Rate and equilibrium constants of RDS with thermodynamics parameters of RDS for GSO FAME using LHHW model

	45°C	50°C	55°C	ΔE,ΔH(kJ/mol)	A, ΔS
TAC catalyzed transesterification					
k_5 (hr^{-1})	8.79E-3	9.21E-3	9.78E-3	9.86	0.365[a]
k_6 (hr^{-1})	8.25E-4	9.70E-4	7.18E-4	73.32	12.43[a]
K_1	11.11	10.00	9.68	-12.42	- 0.019[b]
K_2	10.04	10.80	16.10	44.55	0.159[b]
K_6	8.29	9.73	6.40	-25.77	-0.063[b]
K_7	8.35	8.47	11.25	28.34	0.106[b]
K_8	15.10	9.39	10.44	- 31.97	- 0.079[b]
K_9	11.83	9.80	8.41	- 31.27	-0.078[b]
AAC catalyzed transesterification					
k_5 (hr^{-1})	8.88E-3	9.6E-3	9.99E-3	10.70	0.51[a]
k_6 (hr^{-1})	1.09E-3	1.26E-3	1.01E-3	8.26	5.14E-5[a]
K_1	9.50	9.49	8.65	- 8.93	- 0.009[b]
K_2	9.36	9.25	7.69	- 18.66	- 0.040[b]
K_6	7.75	12.90	6.70	- 17.36	- 0.036[b]
K_7	8.92	17.80	9.90	5.24	0.037[b]
K_8	20.70	30.90	15.40	-30.94	-0.070[b]
K_9	11.91	11.90	16.10	28.76	0.110[b]
BAC catalyzed transesterification					
k_5 (hr^{-1})	8.99E-3	9.23E-3	9.99E-3	9.88	0.373[a]
k_6 (hr^{-1})	9.88E-4	1.55E-3	1.02E-3	44.11	18471[a]
K_1	10.03	10.60	8.70	- 13.94	- 0.024[b]
K_2	7.20	8.95	12.39	50.30	0.174[b]
K_6	6.75	12.90	5.70	- 20.54	- 0.046[b]
K_7	7.92	27.80	10.90	24.95	0.098[b]
K_8	14.70	10.90	14.40	-40.61	- 0.106[b]
K_9	11.91	11.80	15.10	22.70	0.092[b]

[a]-Unit of A is given by hr^{-1}, [b]-Unit of ΔS is given by kJ/mol. K

Table 4.39: Rate and equilibrium constants of RDS with thermodynamics parameters of RDS for APO FAME using ER model

TAC catalyzed transesterification					
	45°C	50°C	55°C	ΔE,ΔH (kJ/mol)	A, ΔS
k_3 (hr^{-1})	8.60E-3	9.17E-3	9.34E-3	7.43	0.144[a]
k_4 (hr^{-1})	1.0E-3	1.0E-3	1.0E-3	2.82	0.003[a]
K_1	11.59	11.02	10.87	- 5.77	0.002[b]
K_5	7.97	8.79	9.06	11.56	0.054 [b]
K_6	72.4	96.37	79.47	6.94	0.058 [b]
K_7	16.27	15.40	14.38	-11.41	- 0.013 [b]
AAC catalyzed transesterification					
k_3 (hr^{-1})	8.45E-3	8.99E-3	9.34E-3	9.13	0.268[a]
k_4 (hr^{-1})	1.0E-3	1.0E-3	1.0E-3	2.82	0.003[a]
K_1	11.75	11.42	10.87	- 7.23	0.002[b]
K_5	7.51	7.81	9.06	17.64	0.072 [b]
K_6	57.03	94.30	79.47	28.23	0.123 [b]
K_7	15.82	14.05	14.38	- 10.85	- 0.011 [b]
BAC catalyzed transesterification					
k_3 (hr^{-1})	8.39E-3	8.79E-3	8.84E-3	4.67	0.049[a]
k_4 (hr^{-1})	1.07E-3	1.0E-3	1.0E-3	3.17	3.16E-4[a]
K_1	11.82	11.42	11.49	2.47	0.046[b]
K_2	7.19	7.81	7.34	1.41	0.021 [b]
K_6	91.96	94.30	88.26	4.09	0.025 [b]
K_7	15.02	14.05	13.63	- 8.80	- 0.005 [b]

[a]-Unit of A is given by hr^{-1}, [b]-Unit of ΔS is given by kJ/mol. K

Table 4.40**:**Rate and equilibrium constants of RDS with thermodynamics parameters of RDS for GSO FAME using ER model

TAC catalyzed transesterification					
	45^{o}C	50^{o}C	55^{o}C	ΔE,ΔH (kJ/mol)	A, ΔS
k_3 (hr^{-1})	8.78E-3	9.01E-3	9.20E-3	4.28	0.044[a]
k_4 (hr^{-1})	9.79E-4	9.74E-4	9.60E-4	1.83	4.90E-4[a]
K_1	12.12	12.56	11.76	-3.12	0.011[b]
K_2	8.23	8.88	8.99	7.91	0.042[b]
K_6	75.60	83.37	80.71	5.57	0.054[b]
K_7	15.12	16.10	16.38	7.21	0.045[b]
AAC catalyzed transesterification					
k_3 (hr^{-1})	8.39E-3	8.68E-3	8.99E-3	6.36	0.093[a]
k_4 (hr^{-1})	9.33E-4	1.00E-3	1.00E-3	6.14	0.010[a]
K_1	12.45	11.99	11.23	- 9.58	- 0.009[b]
K_2	9.10	9.45	9.70	5.83	0.038[b]
K_6	60.32	73.31	70.84	14.00	0.078[b]
K_7	14.39	15.45	15.10	4.11	0.035[b]
BAC catalyzed transesterification					
k_3 (hr^{-1})	8.59E-3	8.71E-3	8.86E-3	2.86	0.025[a]
k_4 (hr^{-1})	9.56E-4	1.0E-3	9.96E-4	3.60	0.0038[a]
K_1	12.32	12.04	12.01	-2.27	- 0.014[b]
K_2	9.10	8.67	7.98	- 12.20	- 0.02[b]
K_6	60.32	78.90	82.60	28.16	0.123[b]
K_7	14.39	15.40	14.30	1.06	0.019[b]

[a]-Unit of A is given by hr^{-1}, [b]-Unit of ΔS is given by kJ/mol.

Table 4.41: Statistical Parameters for rate equation 3(r_3) of LHHW model and rate equation 1(r_1) of ER model for APO transesterification

	Temperature (^oC)	Variance	P-value	Coefficient of determination (R^2)
TAC				
LHHW	45	0.318	0.74	0.789
	50	0.348	0.88	0.830
	55	0.345	0.90	0.900
ER	45	0.512	0.60	0.720
	50	0.531	0.79	0.771
	55	0.543	0.81	0.800
AAC				
LHHW	45	0.256	0.70	0.803
	50	0.323	0.89	0.880
	55	0.212	0.92	0.901
ER	45	0.465	0.61	0.751
	50	0.524	0.81	0.799
	55	0.462	0.88	0.815
BAC				
LHHW	45	0.234	0.72	0.791
	50	0.301	0.81	0.890
	55	0.245	0.91	0.899
ER	45	0.502	0.63	0.751
	50	0.523	0.78	0.801
	55	0.534	0.89	0.800

Table 4.42**:** Statistical Parameters for rate equation 3(r_3) of LHHW model and rate equation 1(r_1) of ER model for GSO transesterification

	Temperature (^oC)	Variance	P-value	Coefficient of determination (R^2)
TAC				
LHHW	45	0.308	0.78	0.800
	50	0.328	0.86	0.850
	55	0.356	0.93	0.910
ER	45	0.498	0.71	0.700
	50	0.531	0.78	0.800
	55	0.514	0.83	0.890
AAC				
LHHW	45	0.265	0.74	0.830
	50	0.234	0.91	0.900
	55	0.213	0.94	0.930
ER	45	0.487	0.68	0.790
	50	0.511	0.80	0.830
	55	0.419	0.89	0.888
BAC				
LHHW	45	0.213	0.71	0.800
	50	0.312	0.80	0.900
	55	0.321	0.92	0.931
ER	45	0.512	0.68	0.780
	50	0.502	0.76	0.890
	55	0.513	0.90	0.900

Table 4.43: Analysis of variance for the rate constant of various catalyst for APO FAME

Source	DF	Mean	F-value	P-value
Catalyst type	2	0.000032	1.81	0.275
1 (TAC)	3	0.000021		
2 (AAC)	3	0.000042		
3 (BAC)	3	0.000034		
Temperature	2	0.000032	65.10	0.001
45	3	0.000022		
50	3	0.000032		
55	3	0.000043		

Table 4.44: Analysis of variance for the rate constant of various catalyst for GSO FAME

Source	DF	Mean	F-value	P-value
Catalyst type	2	0.000036	2.49	0.198
1 (TAC)	3	0.000022		
2 (AAC)	3	0.000035		
3 (BAC)	3	0.000043		
Temperature	2	0.000022	49.50	0.002
45	3	0.000032		
50	3	0.000043		
55	3	0.000052		

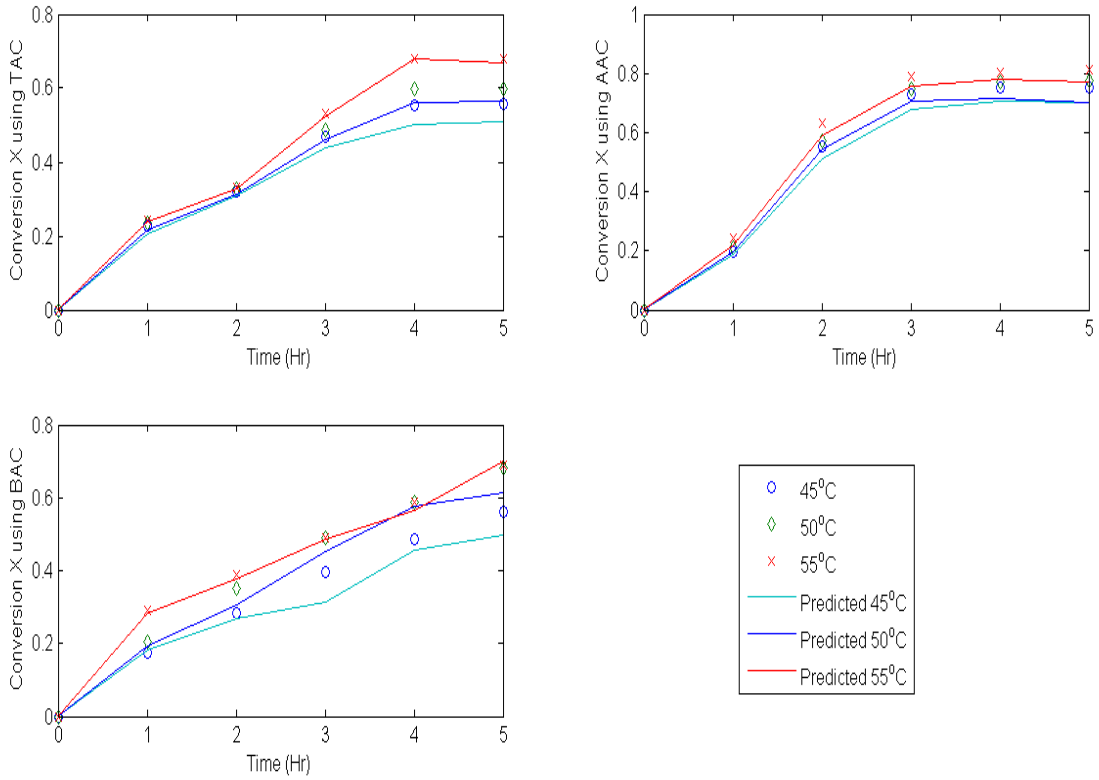

Figure 4.92a: Prediction of conversion of APO against time for LHHW model.

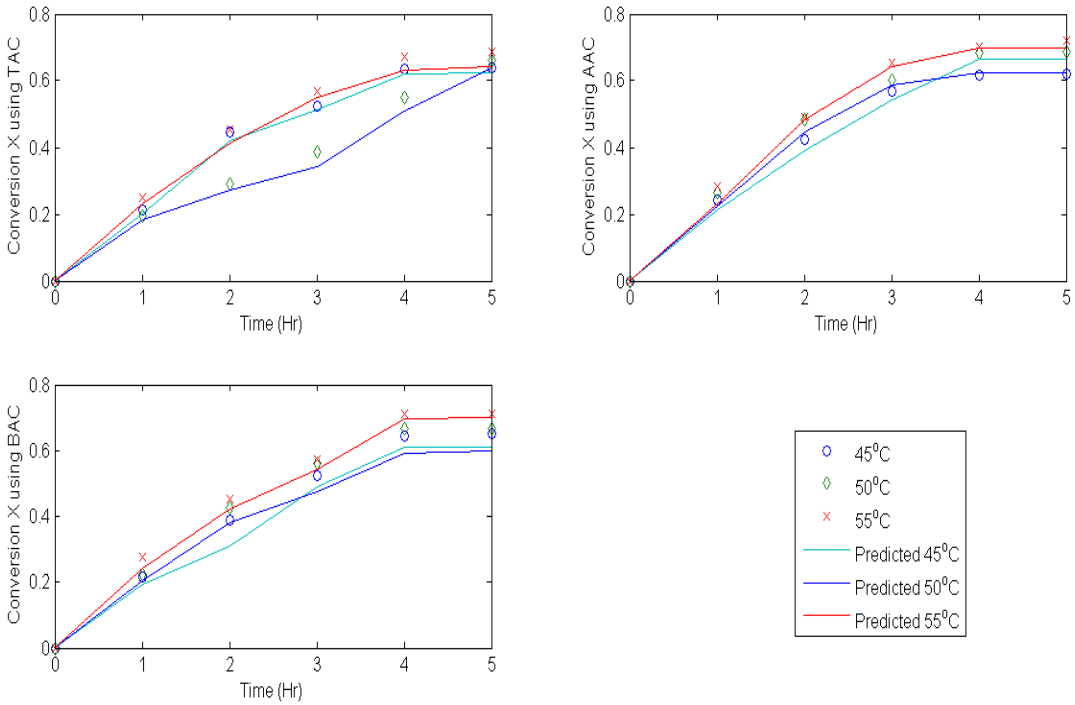

Figure 4.92b: Prediction of conversion of GSO against time for LHHW model.

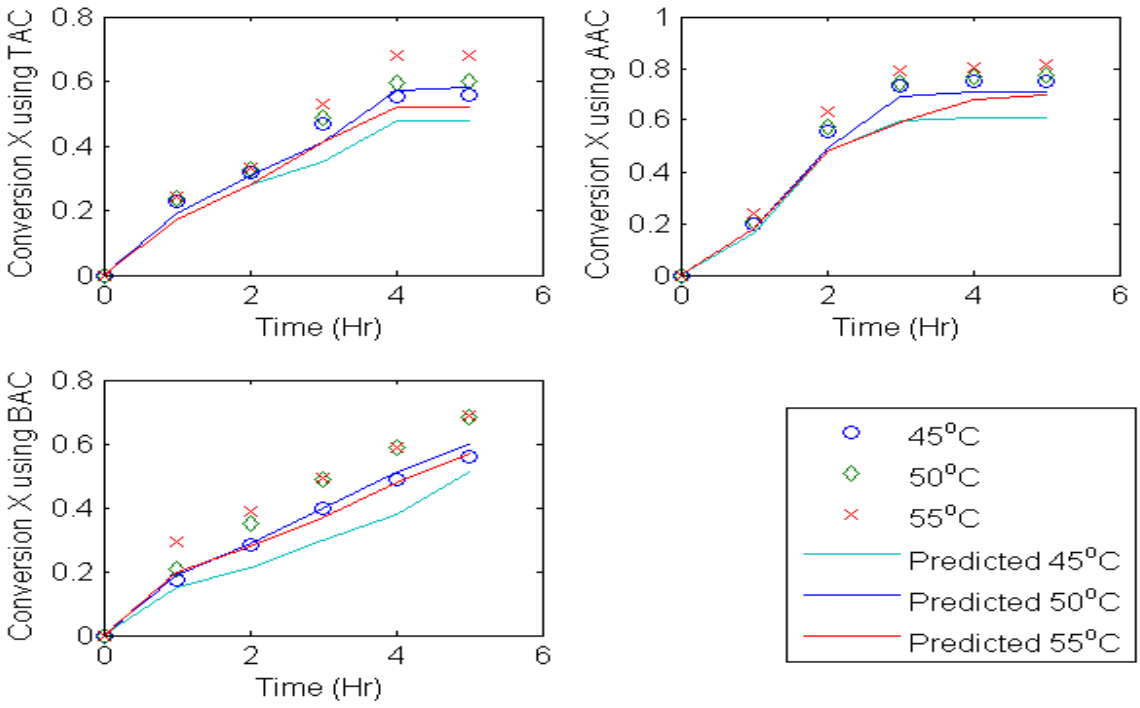

Figure 4.93a: Prediction of conversion of APO against time for ER model.

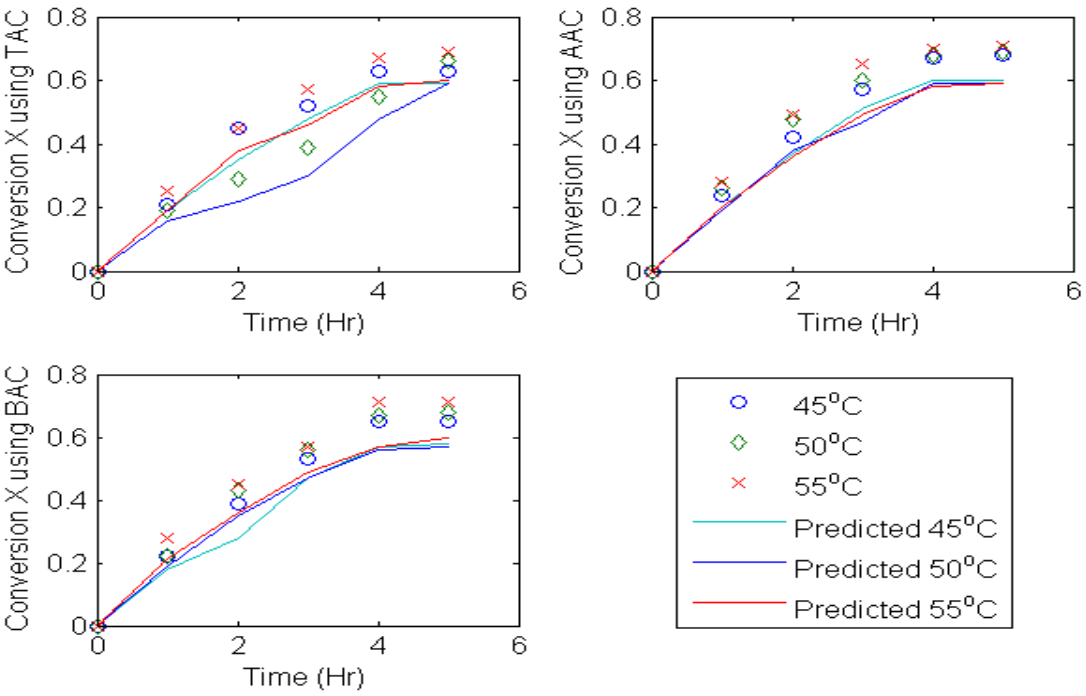

Figure 4.93b: Prediction of conversion of GSO against time for ER model.

4.17 Engine Performance of APO and GSO FAME

Performance of the APO and GSO FAME produced by the transesterification of their respective oil with heterogeneous catalysts (TAC, AAC and BAC) were investigated using diesel engine test rig.

4.17.1 Variation of torque with engine speed

Figures 4.94 (a & b) show the plot of engine torque against speed for standard diesel, biodiesel and blends from African pear seed and gmelina seed oil at full load. From the figures, the torque increases as the engine speed increased. This could be as a result of increase in the fuel temperature and reduction in the viscosity and the lubricity which resulted in increase in friction. However, the torque of the engine with standard diesel was higher than for biodiesel and its blends. This may be attributed to low calorific value and high viscosity of biodiesel. The result is in consonance with the result obtained by Abdullah et.al (2011). It could be observed from the figures that APO FAME and GSO FAME obtained using TAC, AAC and BAC show similar trend in the variation of torque with engine speed. This may be as a result of similar characteristics of the FAMEs produced as presented in Table 4.35.

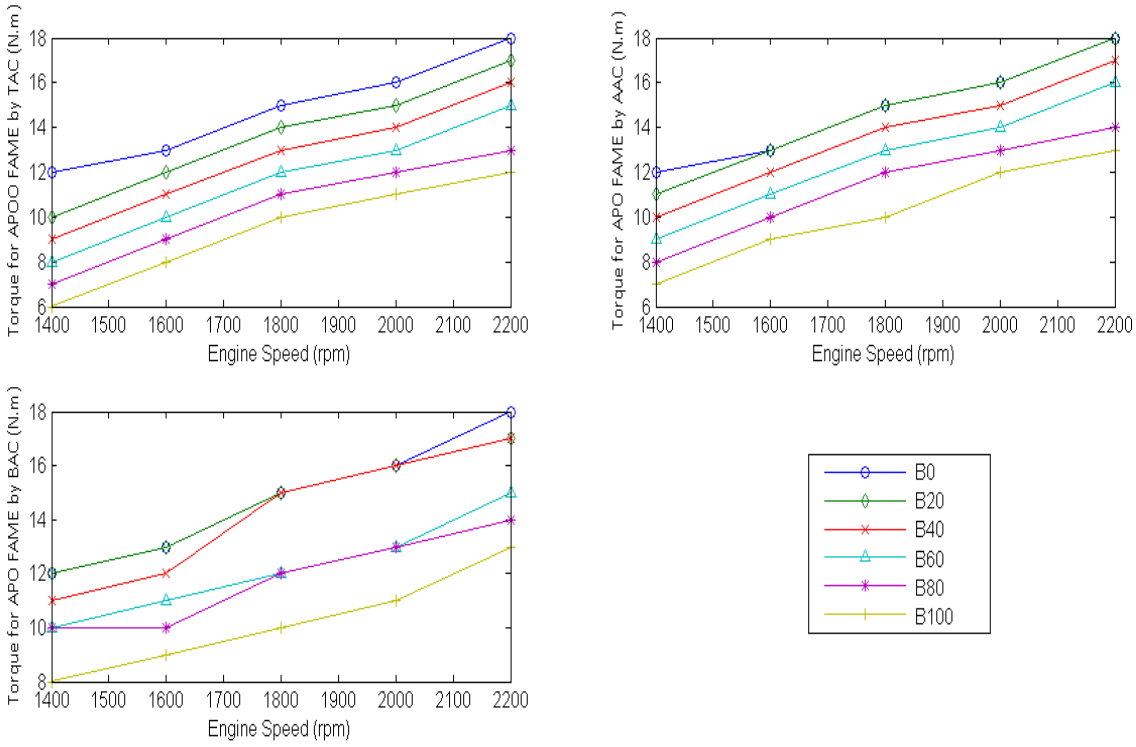

Figure 4.94a: Variation of torque with engine speed for APO FAME.

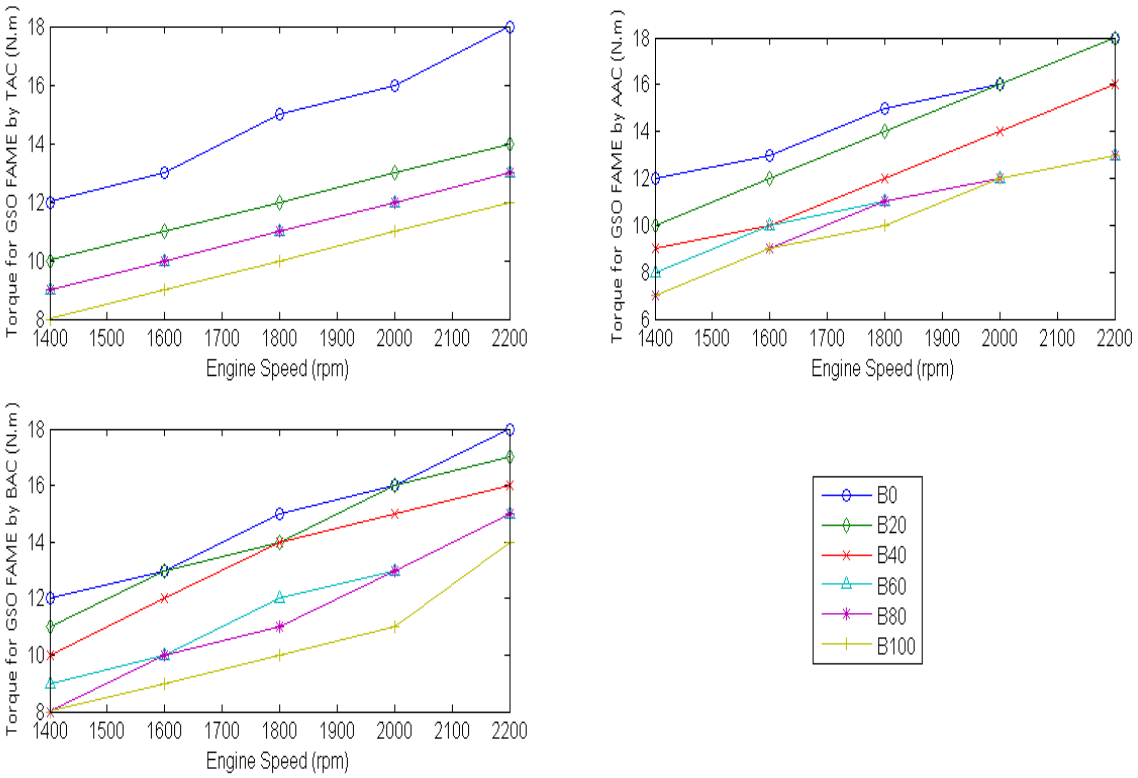

Figure 4.94b:Variation of torque with engine speed for GSO FAME.

4.17.2 Variation of brake thermal efficiency (BTE) with engine speed

Figures 4.95 (a & b) show that the brake thermal efficiency of the engine gradually increases with increase in engine speed at full load. After reaching the maximum value, it then decreased. This is due to the fact that, initially with the increase in engine speed, the torque produced by the engine increased, hence efficiency increases. But at higher rpm (>2000rpm) more amount of fuel is injected into the engine cylinder per cycle and due to higher engine speed this fuel does not get sufficient time to burn completely which reduce the efficiency of the engine. Moreso, it was observed that B20 blend has highest thermal efficiency while biodiesel and some blends have higher thermal efficiency than standard diesel. This may be attributed to their oxygen content, low calorific value and high cetane number. The result is in agreement with that obtained by Abdullah et.al (2011).It could be observed from the figures that APO FAME and GSO FAME obtained using TAC, AAC and BAC show similar trend in the variation of brake thermal efficiency with engine speed. This may be as a result of similar characteristics of the FAMEs produced as presented in Table 4.35.

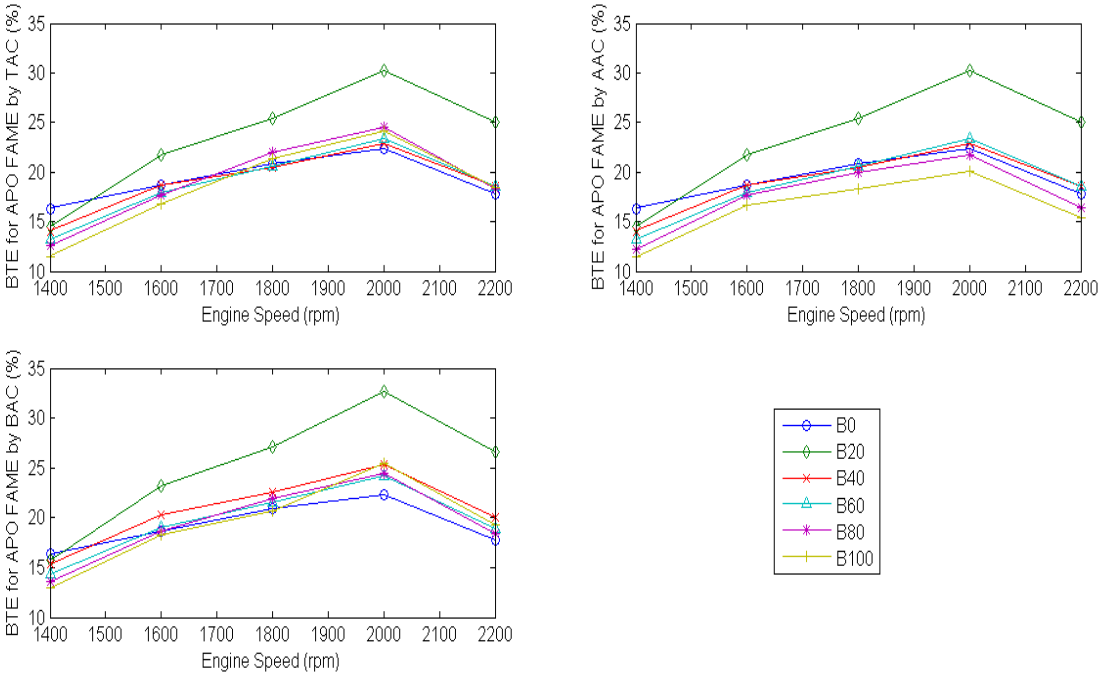

Figure 4.95a: Variation of brake thermal efficiency (BTE) with engine speed for APO FAME.

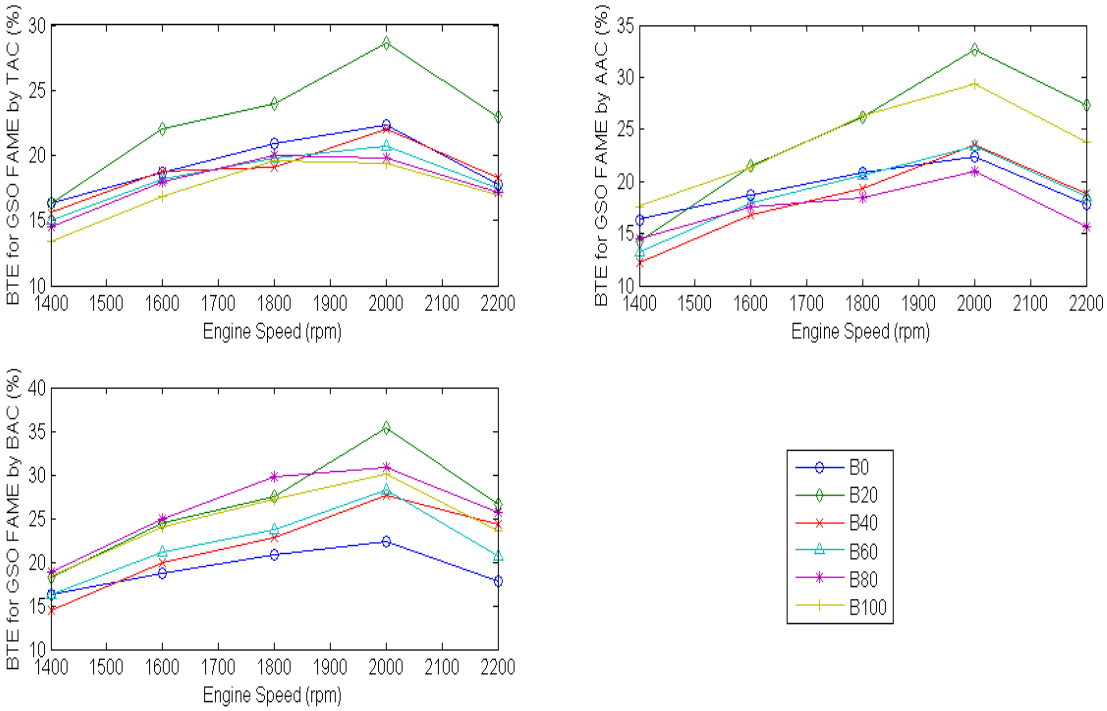

Figure 4.95b: Variation of brake thermal efficiency (BTE) with engine speed for APO FAME.

4.17.3 Variation of brake power (BP) with engine speed

Brake power is the engine net output. From Figures 4.96 (a & b), it could be observed that brake power continues to increase as the speed increases at full load. This may be attributed to reduction in lubricity at higher speed. Moreover, brake power of the engine with B20 was highest while the brake power of standard diesel was higher than for biodiesel and other blends at any speed. This is due to lower calorific value of biodiesel and its blends. This is in agreement with results obtained by Abdullah et al., (2011) and Ude et al., (2017). More so, the brake power of B20 is higher than other blends and this is due to decrease in biodiesel content.It could be observed from the figures that APO FAME and GSO FAME obtained using TAC, AAC and BAC show similar trend in the variation of brake power with engine speed.

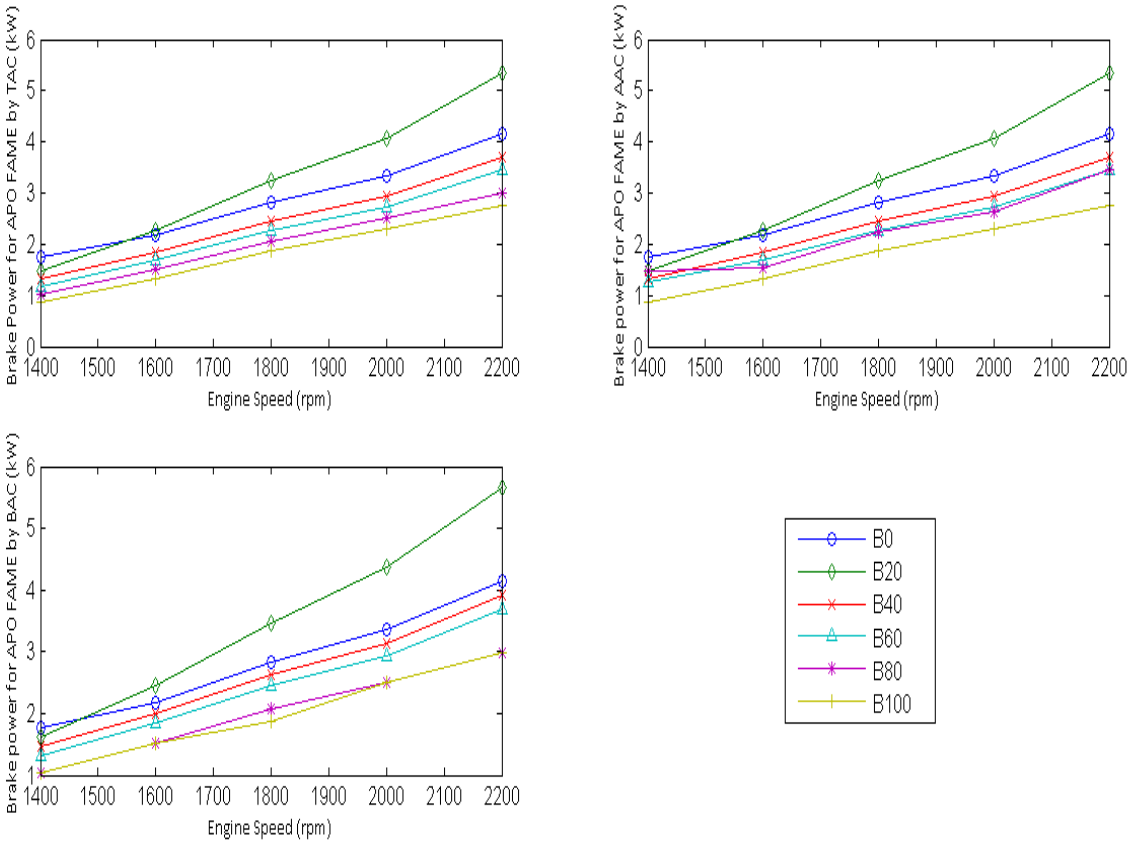

Figure 4.96a: Variation of brake power (bp) with engine speed for APO FAME.

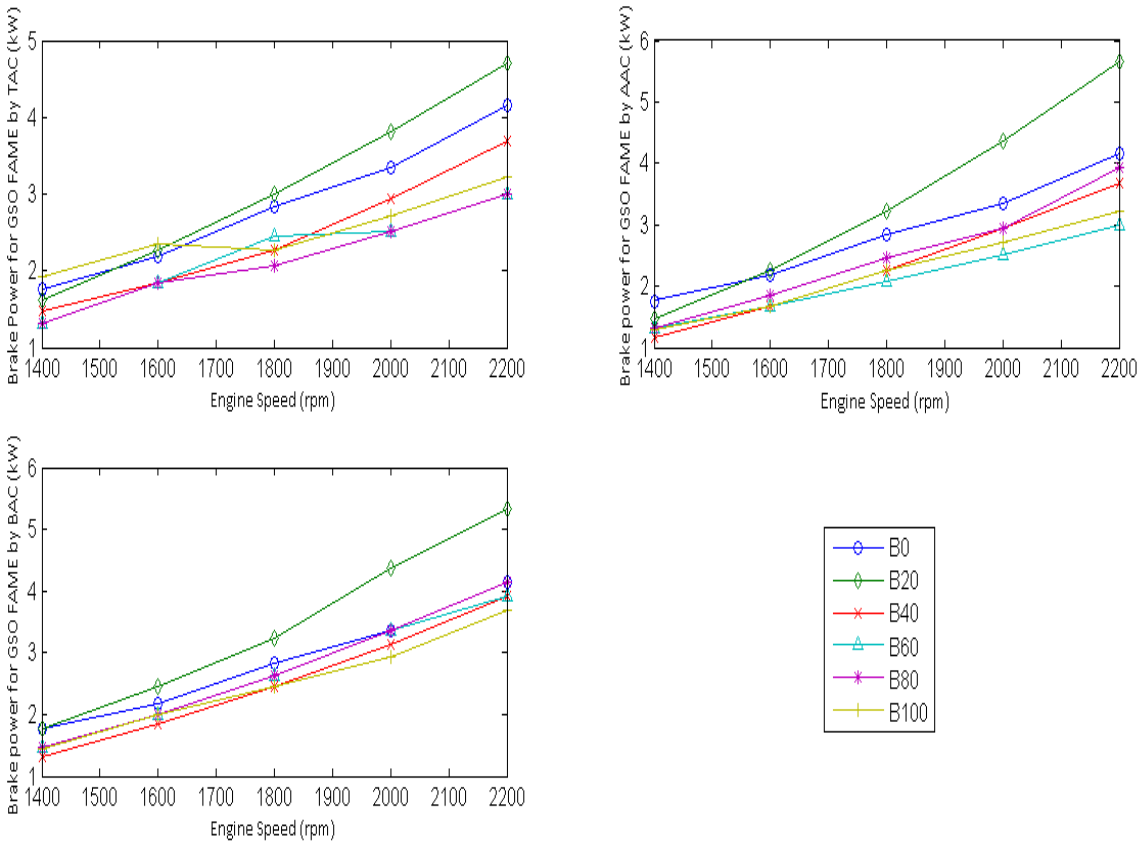

Figure 4.96b: Variation of brake power (bp) with engine speed for APO FAME.

4.17.4 Variation of brake specific fuel consumption(BSFC) with engine speed

Brake specific fuel consumption is the rate of fuel consumption per unit brake power. It is a measure of efficiency of the engine in using the fuel supplied to produce work. It is desirable to obtain a lower value of BSFC as the engine uses less fuel to produce the same amount of work. Figures 4.97 (a & b) show that fuel consumption increase when using biodiesel, but this trend will be weakened as the proportion of biodiesel reduces in the blend fuel with diesel. B100 has the highest BSFC and this may be due to its low heating value, as well as its high density and high viscosity. B20 has thelowest BSFC.The trend from the Figures 4.126 (a & b) also implies that the BSFC decreases with the increase in engine speed until minimum BSFC is found at about 2000 rpm and then increases with increase in engine speed beyond 2200. The similar trend was also reported by Azad *et al.*, (2016) with minimum BSFC found at 1600rpm and then increases until 2400rpm using FAME from Macadamia oil. Ude et al., (2017) obtained similar result using cottonseed oil FAME with minimum BSFC at 1300rpm. The difference in value may be as result of difference in feedstock used for FAME

production. BSFC of B20 from APO FAME and GSO FAME is lowest and best compared with that of standard diesel.

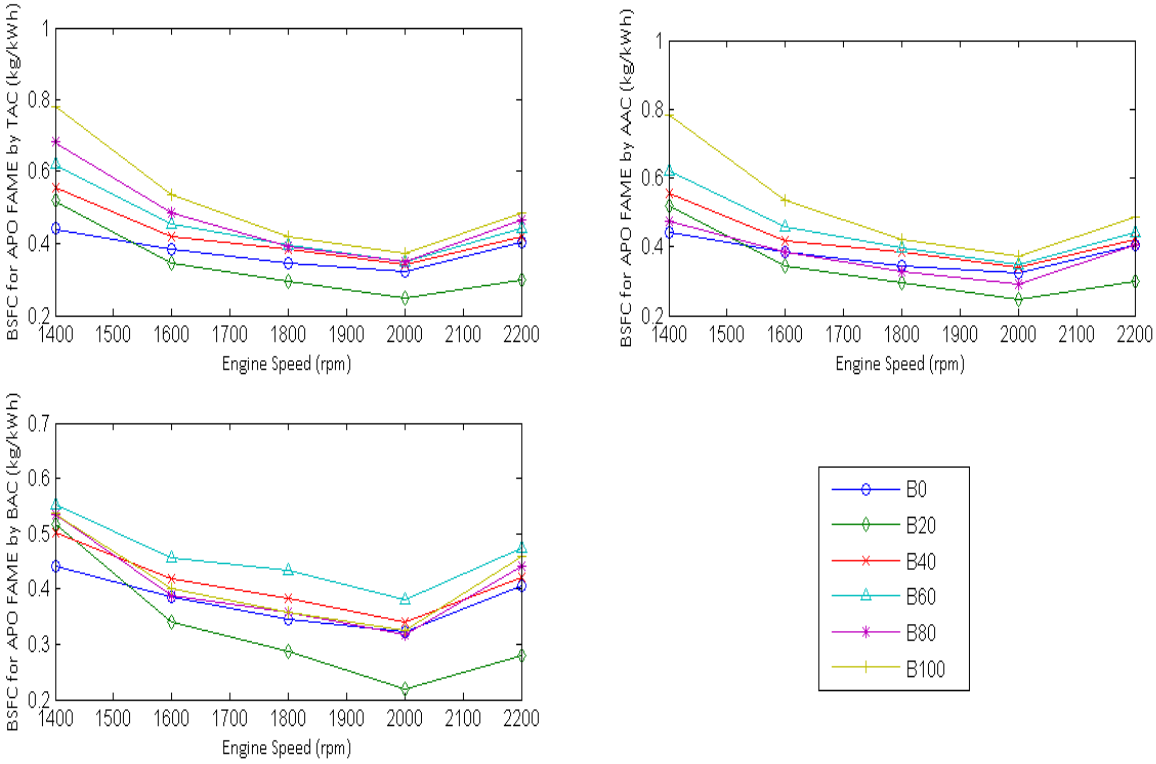

Figure 4.97a: Variation of brake specific fuel consumption (BSFC) with engine speed for APO FAME.

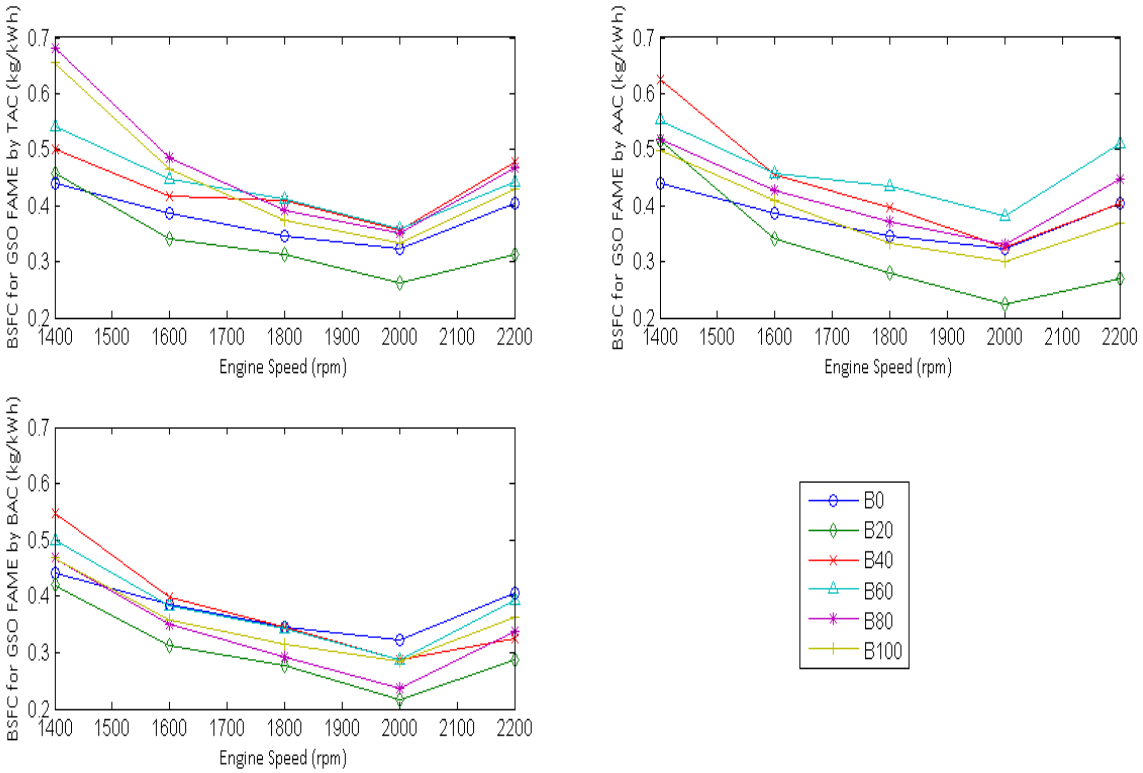

Figure 4.97b: Variation of brake specific fuel consumption (BSFC) with engine speed for GSO FAME.

4.17.5 Variation of CO emission with load

Figures 4.98 (a & b) show the variation of CO emission from APO FAME and GSO FAME produced by TAC, AAC and BAC with load in an internal combustion diesel engine. It was observed that as the engine load increases, the CO emission increases and this may be due to decrease in air-fuel ratio in the engine. Moreover, it was seen that CO emissions reduced as biodiesel content increases. This is may be attributed to high oxygen content and lower carbon to hydrogen ratio in biodiesel. The result is in consonance with that obtained by Ude et al., (2017).

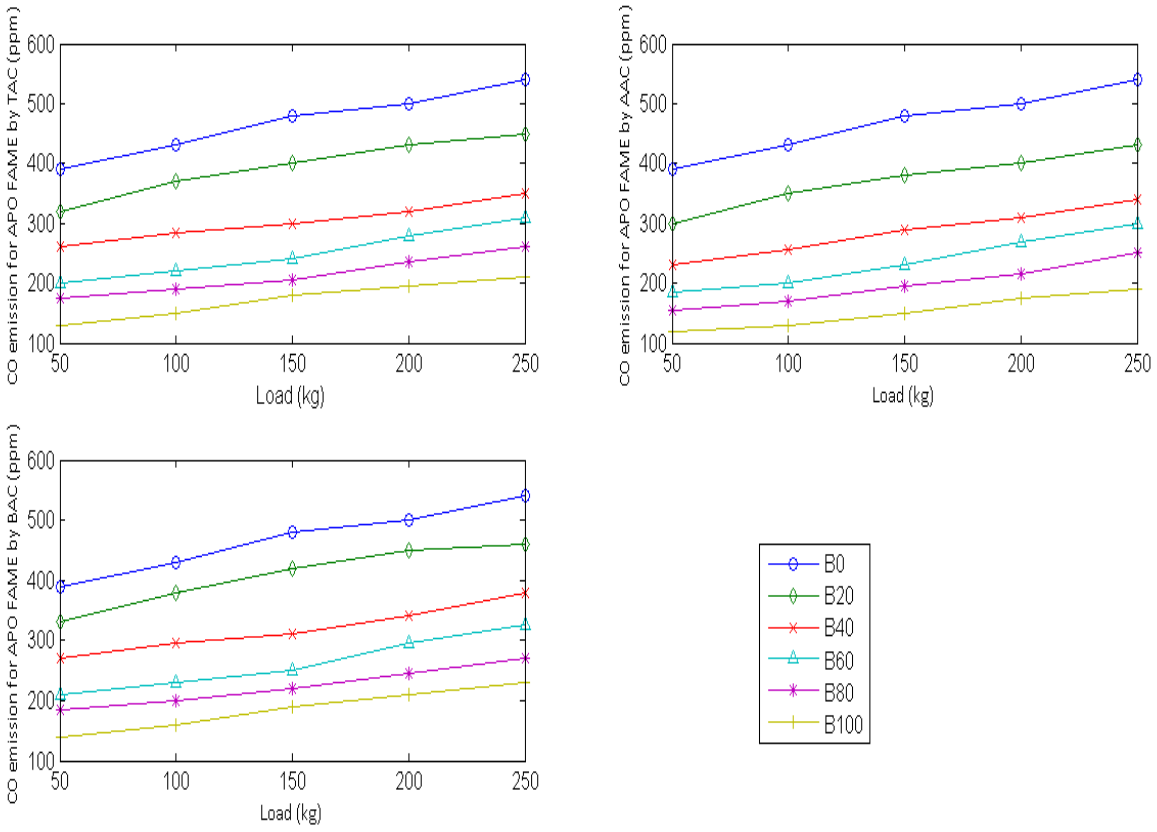

Figure 4.98a: Variation of CO emission with load for APO FAME.

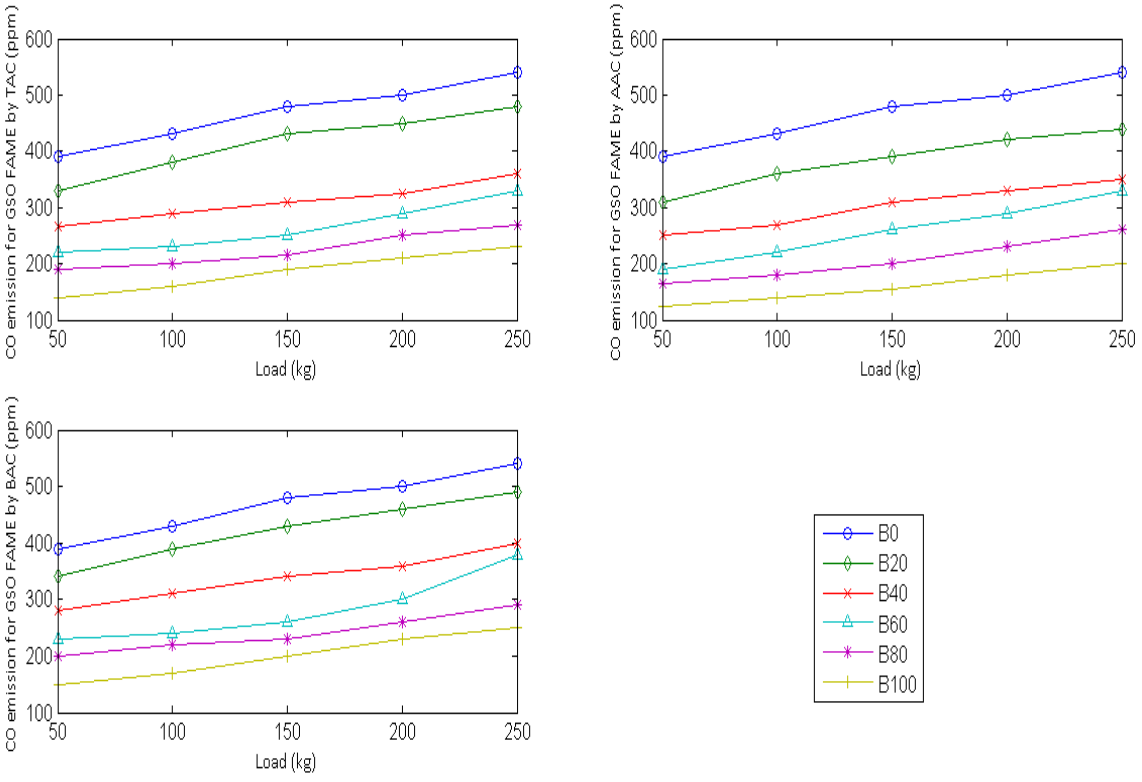

Figure 4.98b: Variation of CO emission with load for GSO FAME.

4.17.6 Variation of NO_x emission with load

Figure 4.99 (a & b) show the variation of NO_x with load from APO FAME and GSO FAME produced by TAC, AAC and BAC with load in an internal combustion diesel engine.. It was observed that NO_x emissions increases as both engine load and biodiesel content increased. This is mainly due to increase in higher combustion chambertemperature and higher fuel consumption, higher oxygencontent and cetane number in biodiesel. Similar result was obtained by Ude et al., (2017).

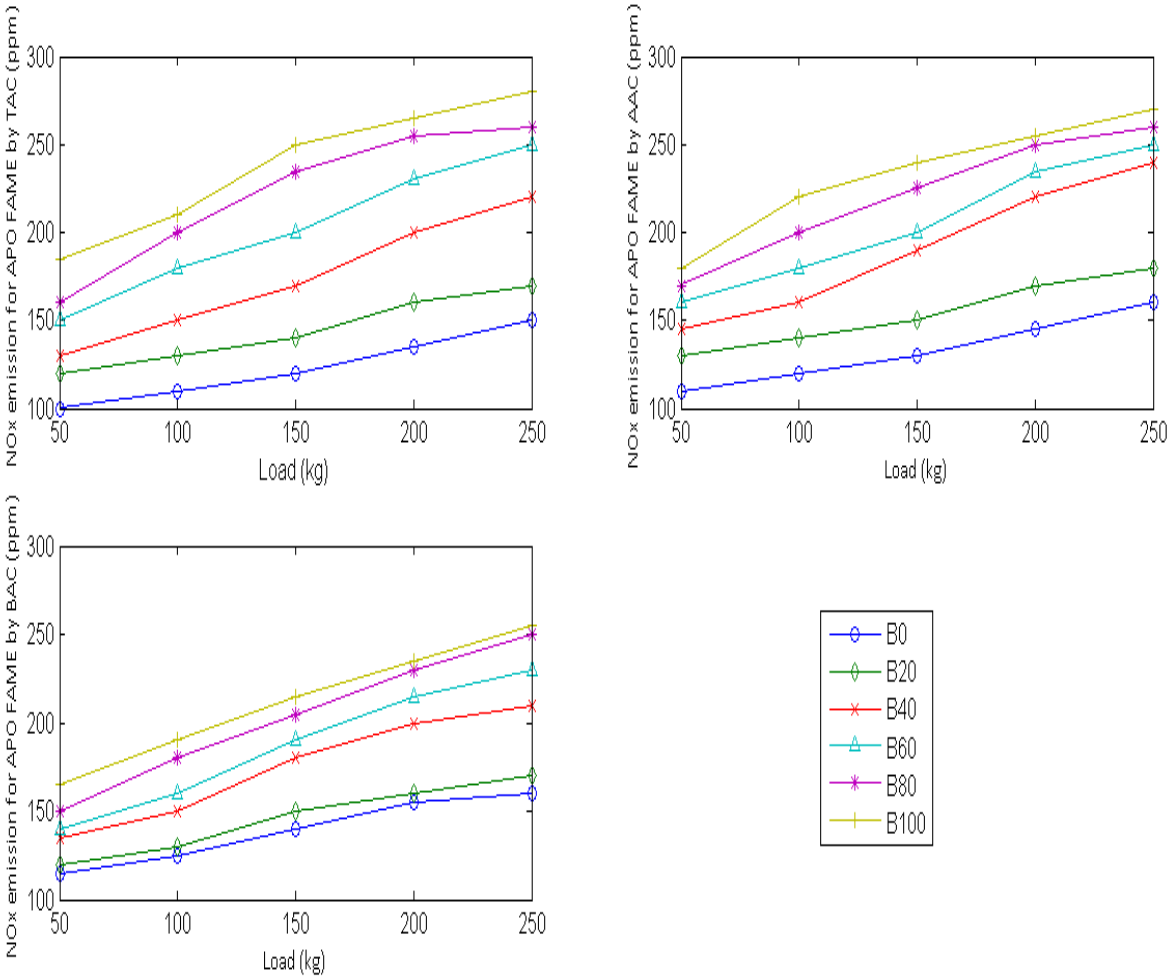

Figure 4.99a: Variation of NO_x emission with load for APO FAME.

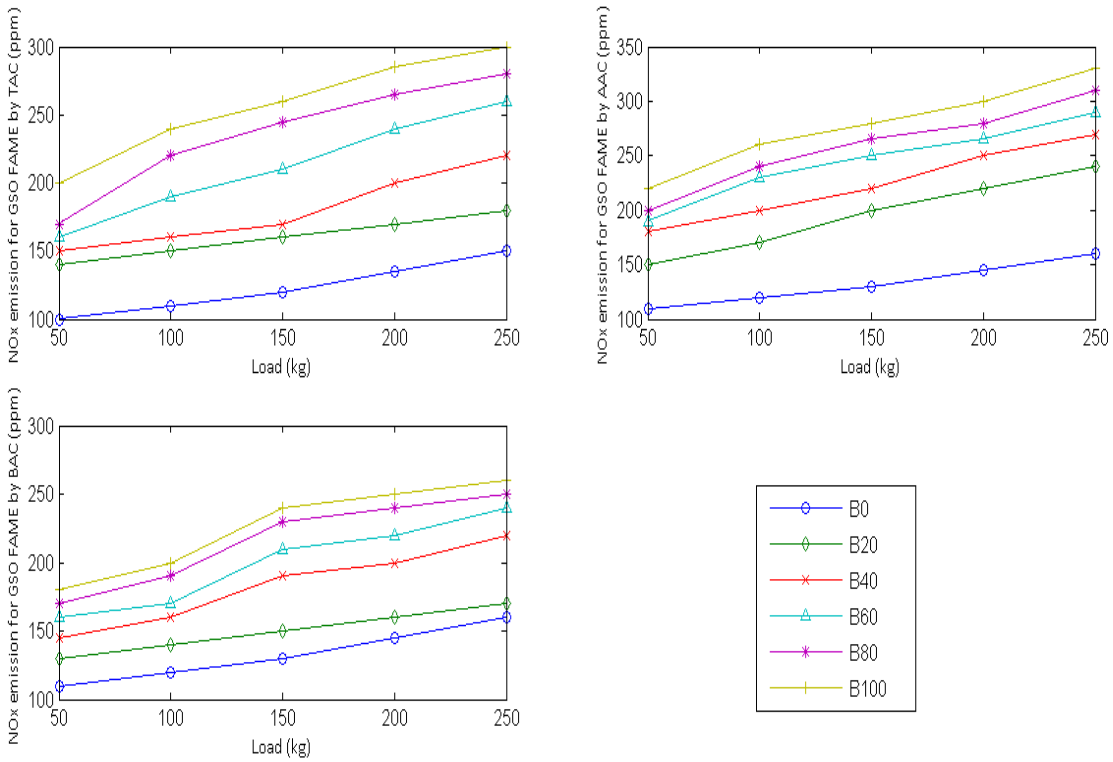

Figure 4.99b: Variation of NO_x emission with load for GSO FAME.

4.17.7 Variation of hydrocarbon (HC) emission with load

Figure 4.100 (a&b) show the variation of HC emission with loadfrom APO FAME and GSO FAME produced by TAC, AAC and BAC with load in an internal combustion diesel engine.. It shows that HC emission reduces with increase in biodiesel content. HC emission for biodiesel increases with increase in load and this may be attributed to high fuel consumption. This is in agreement with observation made by Jinlin*et al.*, (2011) and Ude et al., (2017).

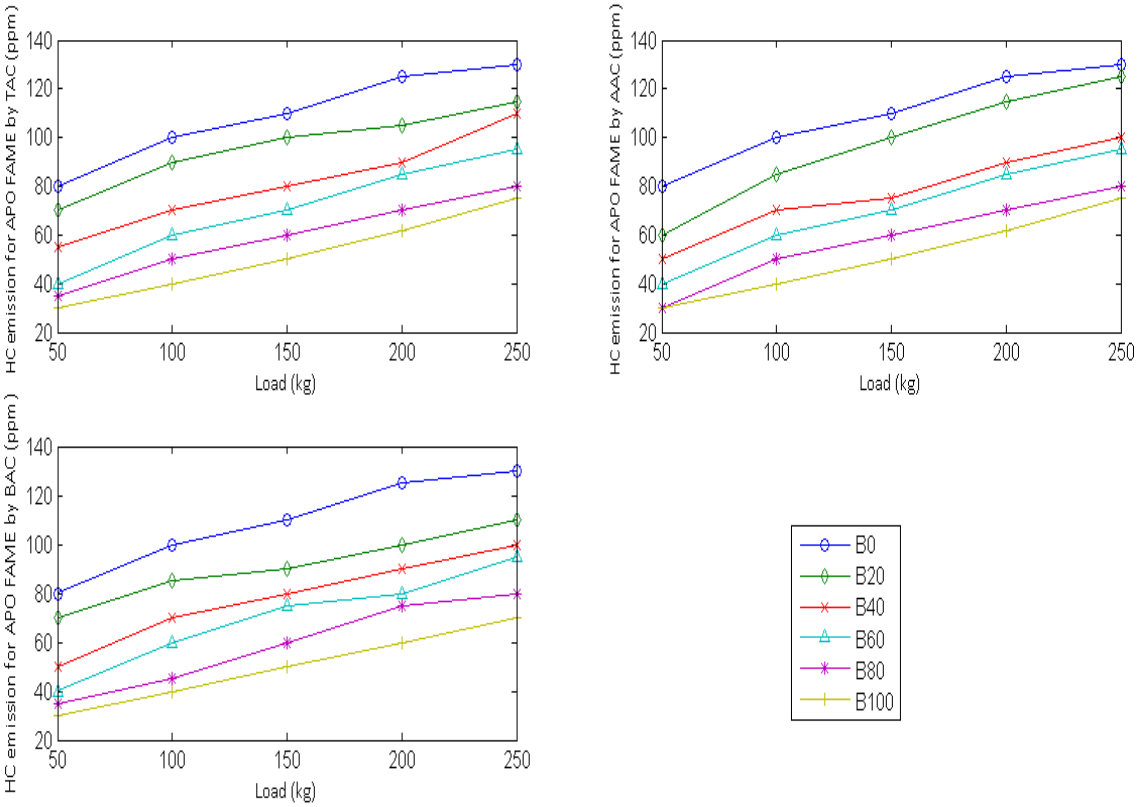

Figure 4.100a: Variation of HCemission with load for APO FAME.

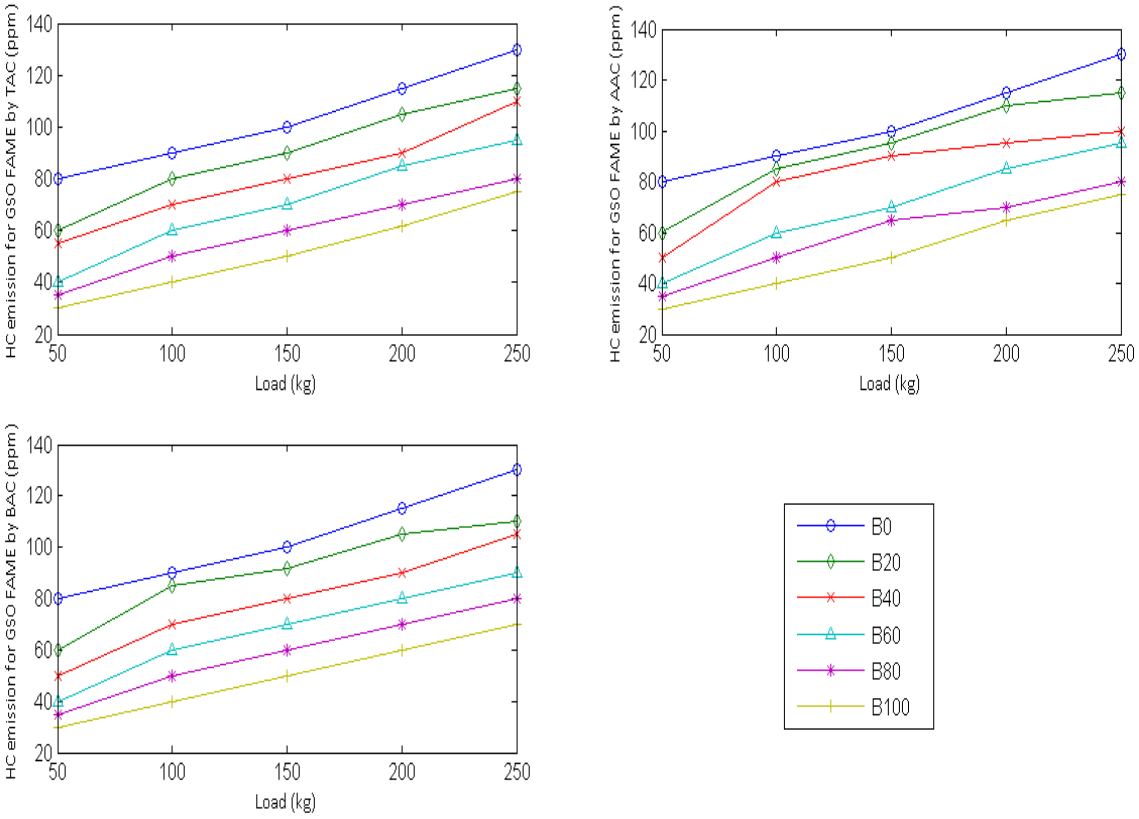

Figure 4.100b: Variation of HCemission with load for GSO FAME.

4.18 Prediction of Engine Performance of Biodiesel using ANN

ANN model was also developed to predict the performance of biodiesel from the African pear seed oil and gmelina seed oil. Necessary data used to train the network were the yields obtained from experimental responses shown in Appendices L and M. Altogether, 25 data sets of biodiesel blends and engine speed were selected to use in this study. Supervised learning was used and data sets were randomly divided by the network; 70% of the data was used for training, while 15% each was allocated for testing and validation. The maximum number of epoch was set to 1000. The epoch was set to 1000 not for any theoretical reason but to ensure that there is sufficient number of iterations during the learning process. Learning was very fast at this level and the optimum performance was obtained in all cases when the epoch was more than 20.

The network architecture consists of two input units, two hidden layers with ten hidden units (nodes) and three output unit as shown in Figure 4.101. The sigmoid transfer function was used in the processing units in the hidden layer. The input (x_1, x_2) to the neural network are the weight percentage of biodiesel blends and engine speed. The targets were the brake power, brake thermal efficiency and brake specific fuel consumption.

The performance parameters of the network in training for prediction of engine performance are shown in Figures 4.102 and 4.103 respectively. As shown in Figure 4.102, the network mean square error falls from a very high value to 0.0000014488 which is the best validation performance at epoch 21. The maximum numbers of epochs for best validation performance was 27, and also from Figure 4.103 the error histogram shows that the network errors were concentrated toward zero indicating a good performance. The network model output for the trained data sets is shown in Appendix M.

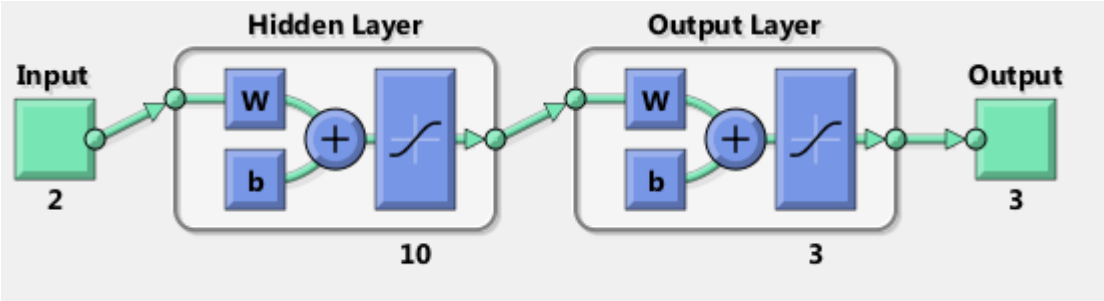

Figure 4.101: ANN architecture used in training data for engine performance prediction.

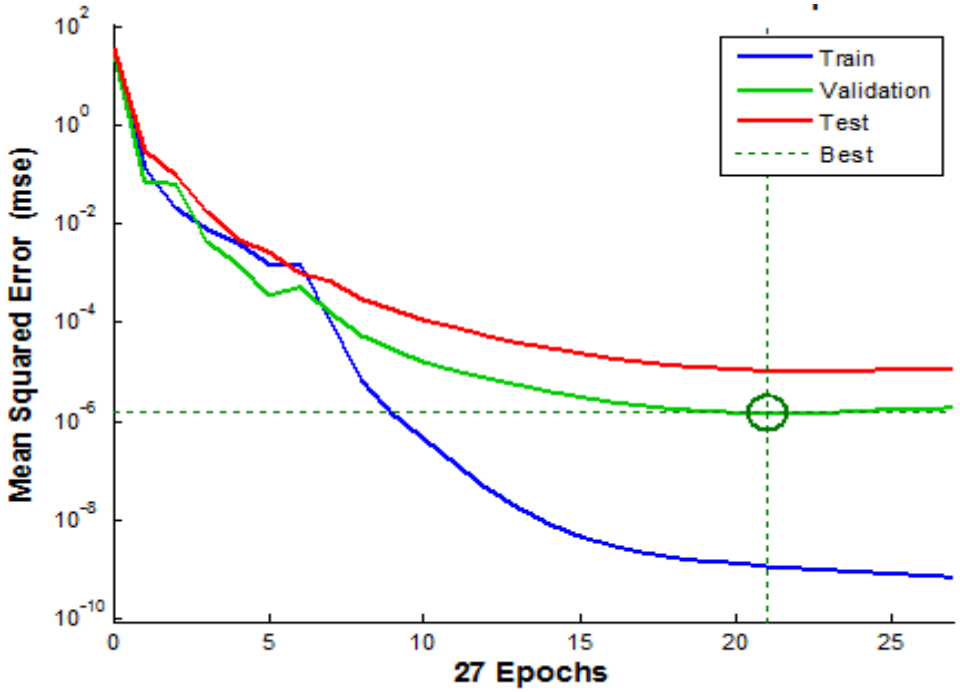

Figure 4.102: Training error (MSE) curve for engine performance prediction.

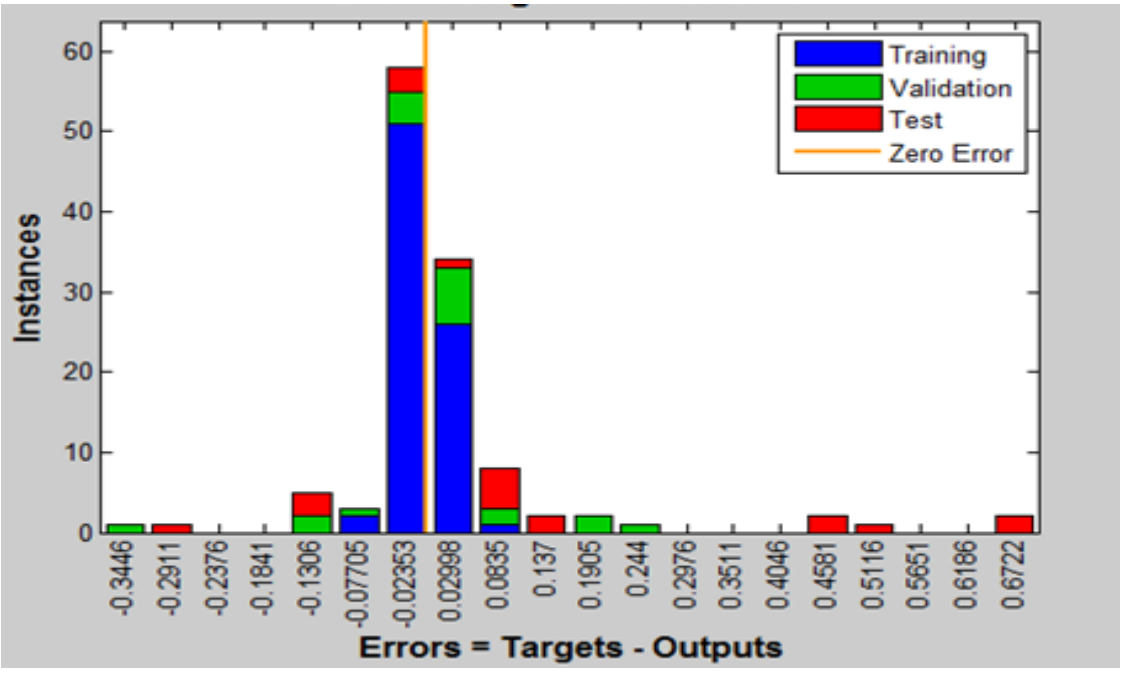

Figure 4.103: The network data sets Training Error distribution Histogram for prediction of engine performance.

A further analysis of the trained model performance was done using regression analysis as shown in Figures 4.104a, 4.104b and 4.104c. The correlation coefficient value is an indication of how far the network is able to learn the training data sets. It can be observed from the figures that there is a very high correlation between the ANN predicted values and

targeted values determined experimentally. The overall correlation coefficients for the trained model used in predicting the engine performance are 0.97369 (BP), 0.97482(BTE), 0.96892(BSFC); also the correlation coefficients for the validation and test data sets were recorded as 0.97814 and 0.9979(BP); 0.99347 and 0.99321 (BTE); 0.9501 and 0.95809 (BSFC) as shown in Figures 4.104a, 4.104b and 4.104c respectively. It could be observed that ANN was able to predict the engine performance of biodiesel produced from APO and GSO using the three heterogeneous (modified clay) catalysts and their blends.

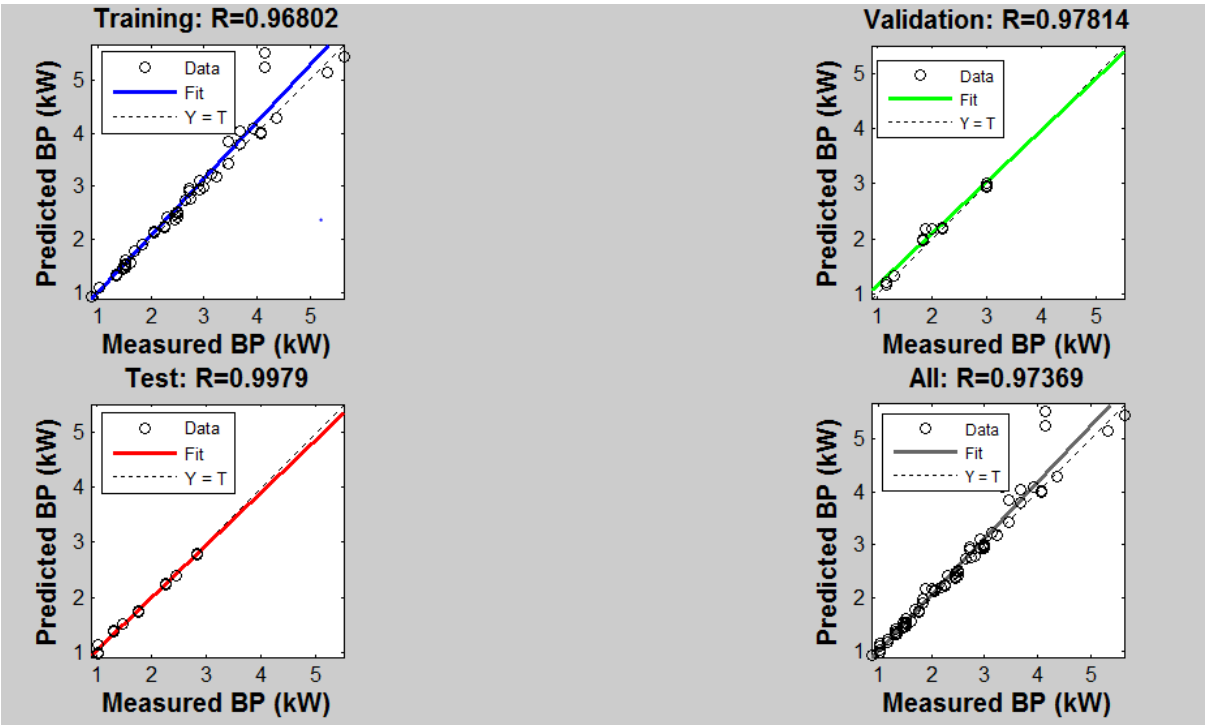

Figure 4.104a: Regression plot analysis for the trained ANN model used in prediction of brake power.

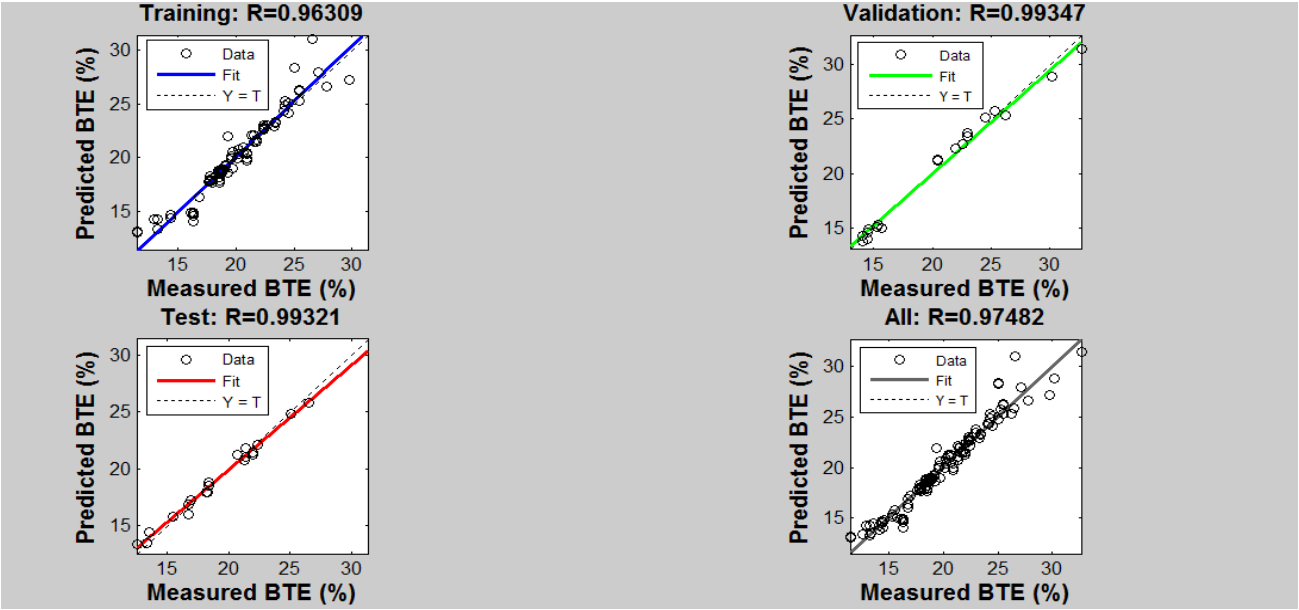

Figure 4.104b: Regression plot analysis for the trained ANN model used in prediction of brake thermal efficiency (BTE).

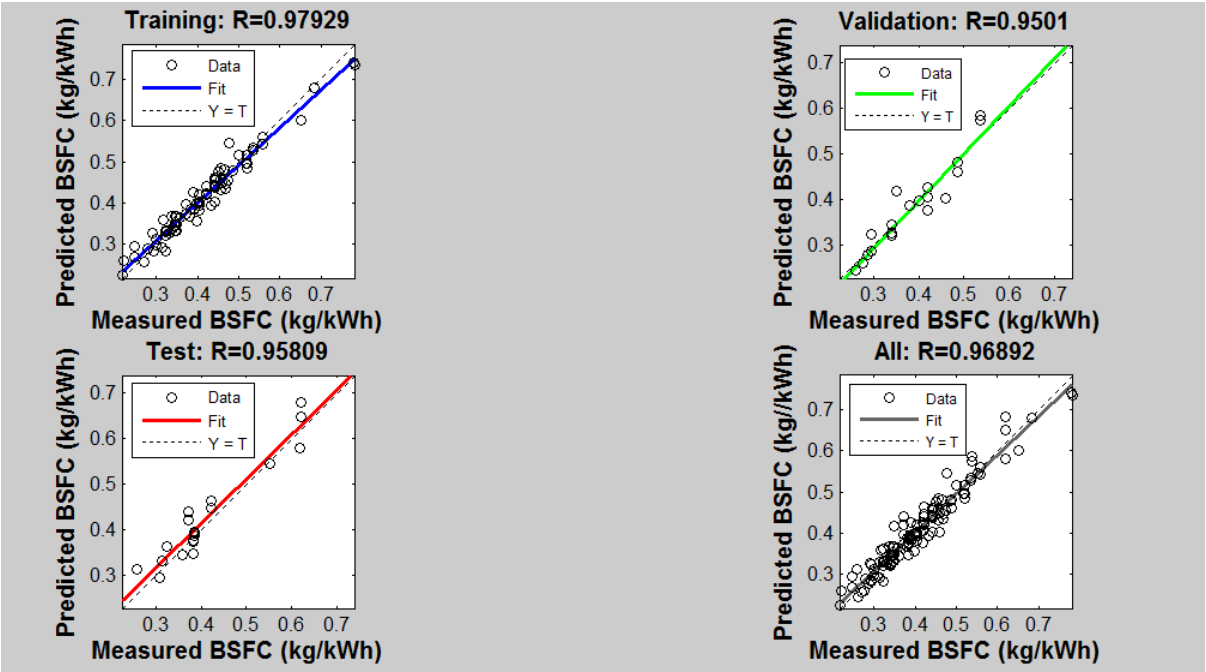

Figure 4.104c: Regression plot analysis for the trained ANN model used in prediction of brake specific fuel consumption (BSFC).

4.19 Modelling of Physical Properties of APO and GSO FAME

4.19.1 Density Model

Density of biodiesel from APO and GSO were predicted by processing the experimental data presented in Table O1 and O2 of Appendix O, using polymath statistical tools. The empirical

relationship between density and fraction of biodiesel for both APO and GSO FAMEs are shown in Eqs. (4.21 & 4.22). From the equations, it is observed that density is affected by biodiesel content as their coefficients are very large.The performance parameters results for the linear regressions model are: R^2 = 0.995, RMSE = 0.17 for APO FAME and R^2 = 0.998, RMSE = 0.107 for GSO FAMEwhich indicates good correlation between the input data, as shown in Figure 4.105. From the figure, it can be observed that density increases with increase in biodiesel content. The models are similar and this could be that biodiesel content in the blends dominated.

$$\rho_{APO\ FAME} = 839.43 + 18.14x \quad (4.21)$$

$$\rho_{GSO\ FAME} = 839.90 + 18.86x \quad (4.22)$$

Where x = biodiesel content

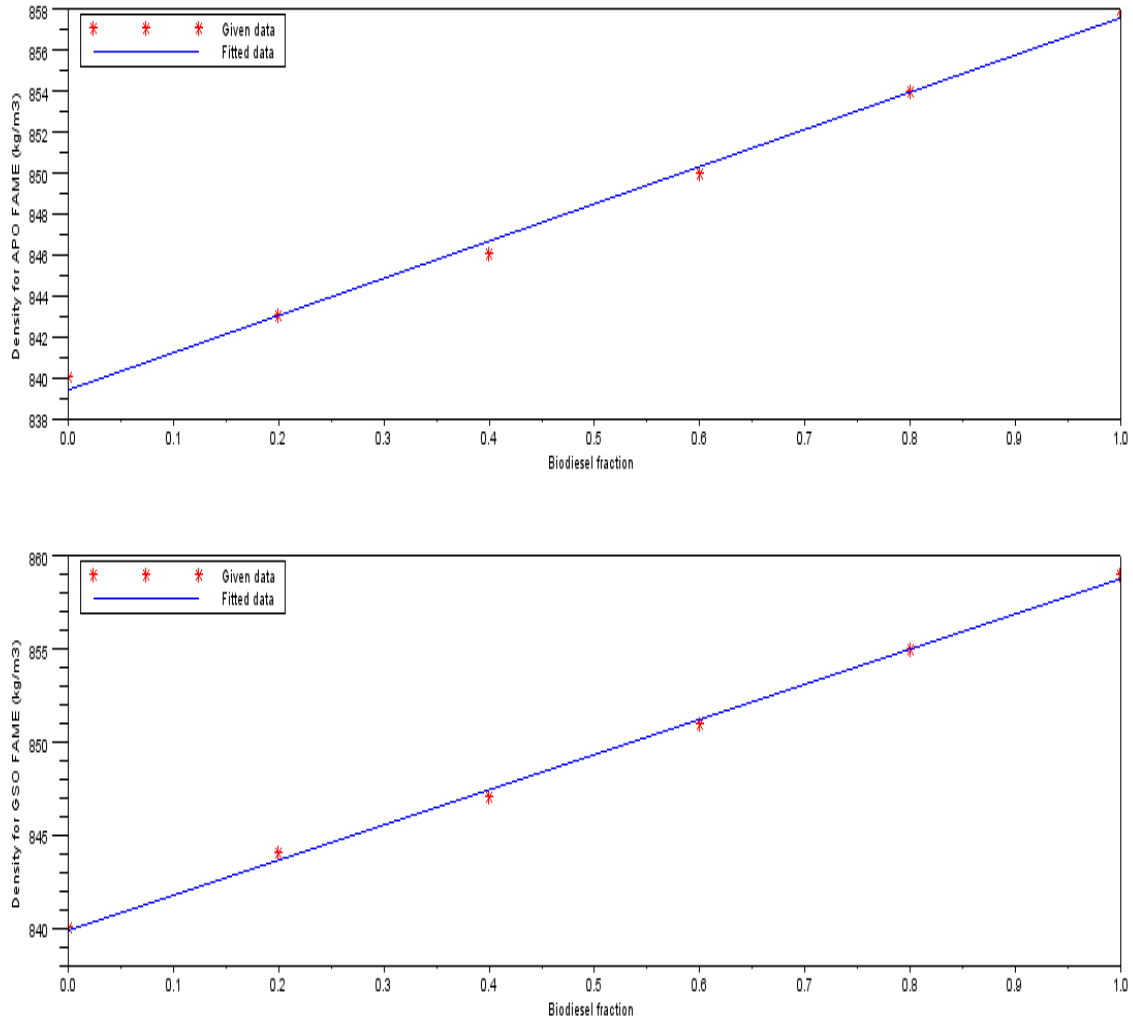

Figure 4.105: Plot of density against biodiesel fraction

4.19.2 Kinematic viscosity model

Kinematic viscosity of biodiesel from APO and GSO were predicted by processing the experimental data presented in Table O1, O2 and O3 of Appendix Ousing polymath statistical tools. The empirical relationships between kinematic viscosity and fraction of biodiesel with temperature are shown in Eqs. (4.23, 4.24, 4.25 and 4.26). From the equations, it is observed that kinematic viscosity is affected by biodiesel content and temperature as their coefficients are very large.The performance parameters results for the linear regressions model for kinematic viscosity vs biodiesel fraction are: R^2 = 0.97, RMSE = 0.04 for APO FAME and R^2 = 0.984, RMSE = 0.037 for GSO FAME whilethe performance parameters results for the linear regressions model for kinematic viscosity vs temperature are: R^2 = 0.97, RMSE = 0.04 for APO FAME and R^2 = 0.986, RMSE = 0.025 for GSO FAMEwhich indicate good correlation between the input data, as shown in Figure 4.106. It can be observed from the figure that kinematic viscosity increase as biodiesel content increases and decrease as temperature increases. The models are similar and this could be that biodiesel content in the blends did not dominate.

$$\gamma_{APO\ FAME} = 1.78 + 1.91x \quad (4.23)$$

$$\gamma_{GSO\ FAME} = 1.79 + 2.09x \quad (4.24)$$

$$\gamma_{APO\ FAME} = 25.40 - 0.072T \quad (4.25)$$

$$\gamma_{GSO\ FAME} = 24.0 - 0.068T \quad (4.26)$$

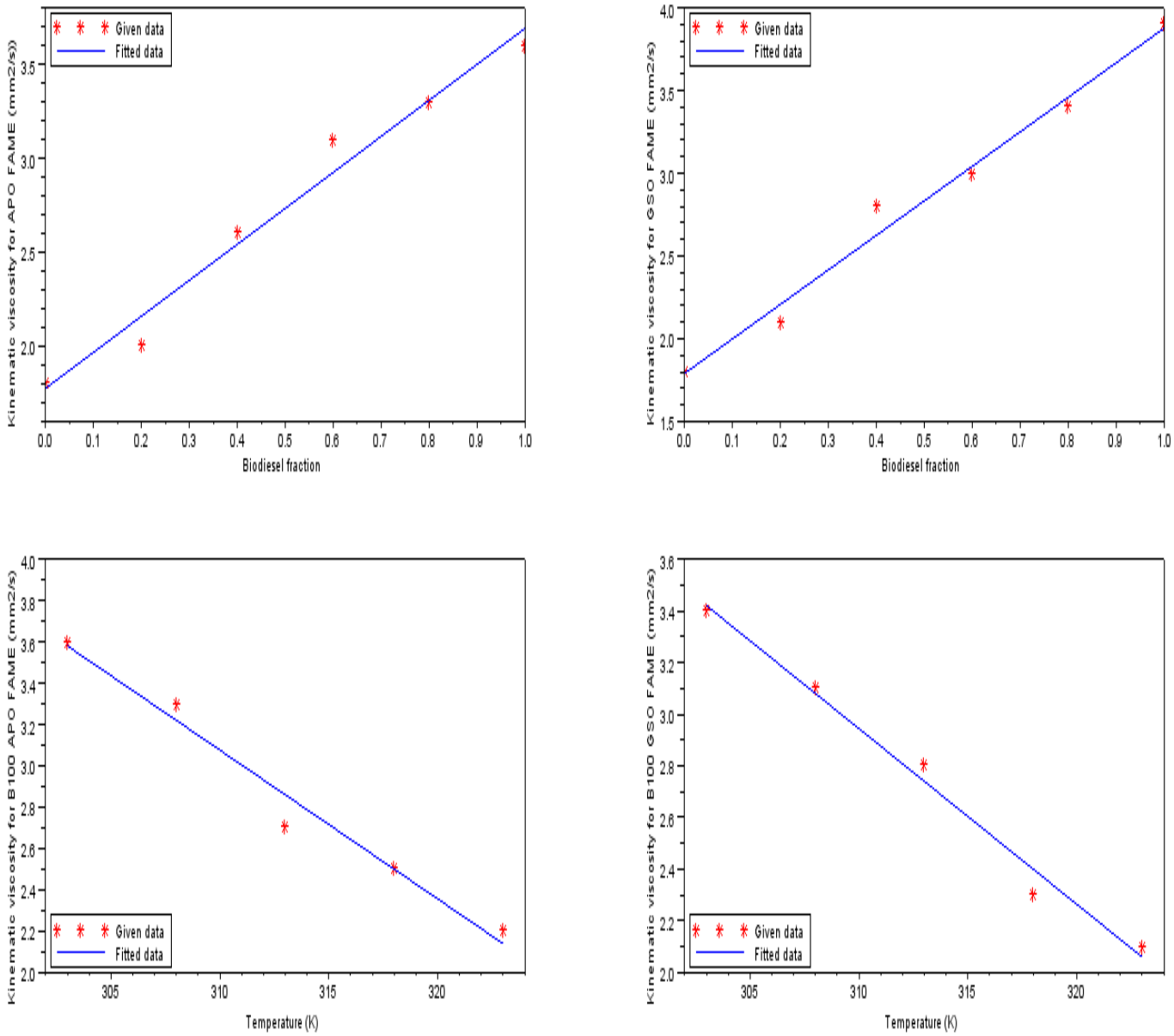

Figure 4.106: Kinematic viscosity vs biodiesel fraction and temperature:Row 1: Kinematics viscosity vs biodiesel fraction, Row 2: Kinematics viscosity vs temperature.

4.19.3 Cetane number model

The Cetane number of biodiesel was predicted from its thermal properties such as density, kinematic viscosity, flash point and lower heating value using a multiple linear regression MLR model on the experimental data shownin Tables O1 and O2 of Appendix O. Equations (4.27 & 4.28) show the empirical relationship between Cetane number and thermal properties for APO and GSO FAMEs. From the equations, it is observed that lower heating value (LHV) showed highest influence on the cetane number for APO FAME while kinematic viscosity has higher influence for GSO FAME.Figures 4.107 and 4.108 show the subplot of predicted Cetane number values against the experimental data. From the figure it can be

observed that there is a good correlation between the experimental thermal properties and predicted Cetane number. It is also observed from the figures that cetane number increases with increase in density, kinematic viscosity and flash point with decrease in lower heating value. The model performance parameters recorded are:RMSE = 0.035 and R^2 = 0.9995 (APO FAME) and RMSE = 0.19 and R^2 = 0.989 (GSO FAME),which shows that the empirical correlation proposed can be used to reproduce the Cetane number of biodiesel studied. The statistical parameters show that the model of cetane number from the thermal properties for African pear oil FAME has better fitting than gmelina seed oil FAME.

The predicted equation in terms of the coded values are:

$$CN_{APO\ FAME} = 3.73\rho + 2.49\gamma - 0.18\text{FP} + 4.30\text{LHV} - 3294.8 \quad (4.27)$$

$$CN_{GSO\ FAME} = 0.54\rho + 2.25\gamma - 0.038\text{FP} - 0.29\text{LHV} - 395.2 \quad (4.28)$$

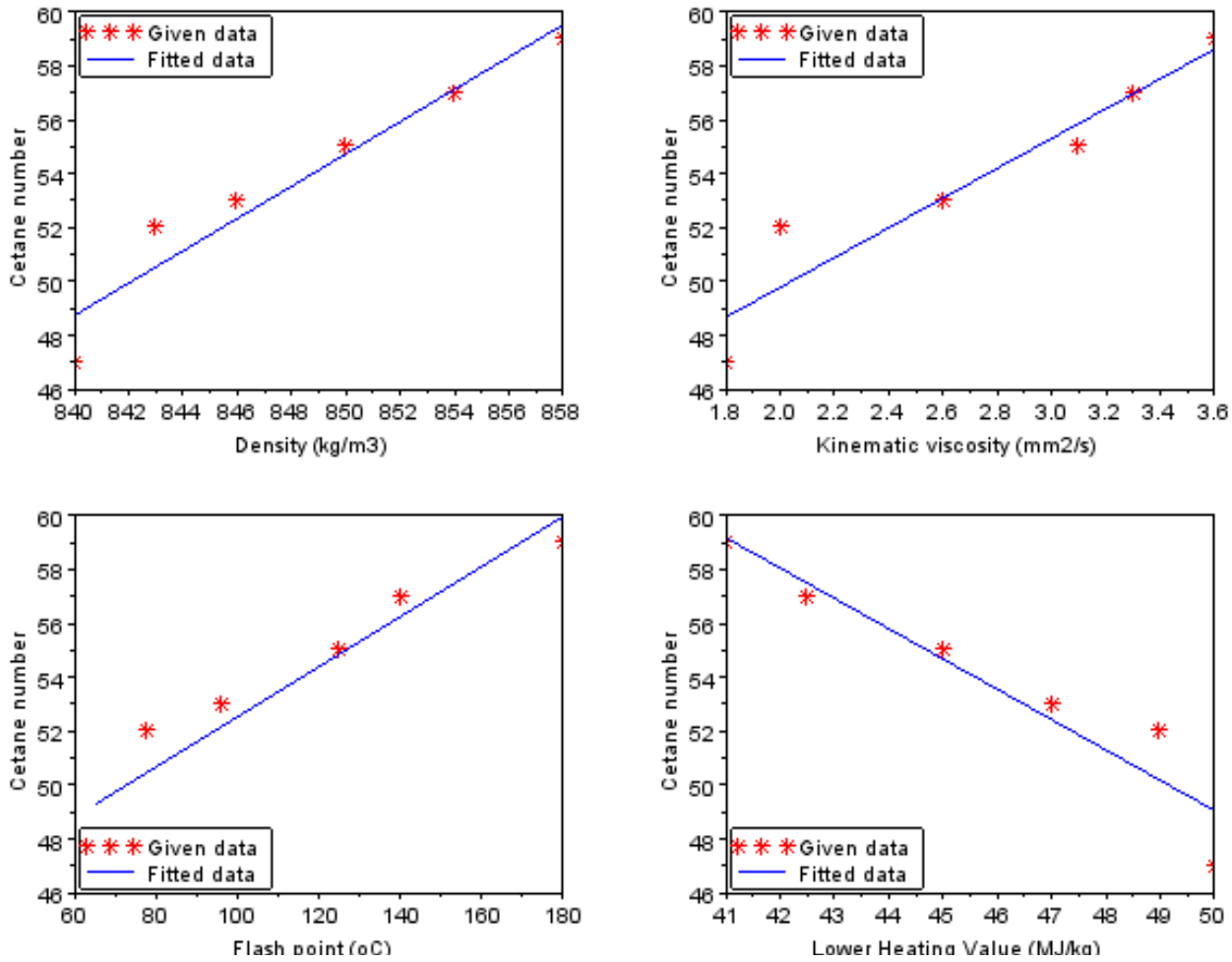

Figure 4.107: Cetane number vs thermal properties for APO FAME: (a) CN vs density (b) CN vs kinematics viscosity (c) CN vs flash point (d) CN vs lower heating value.

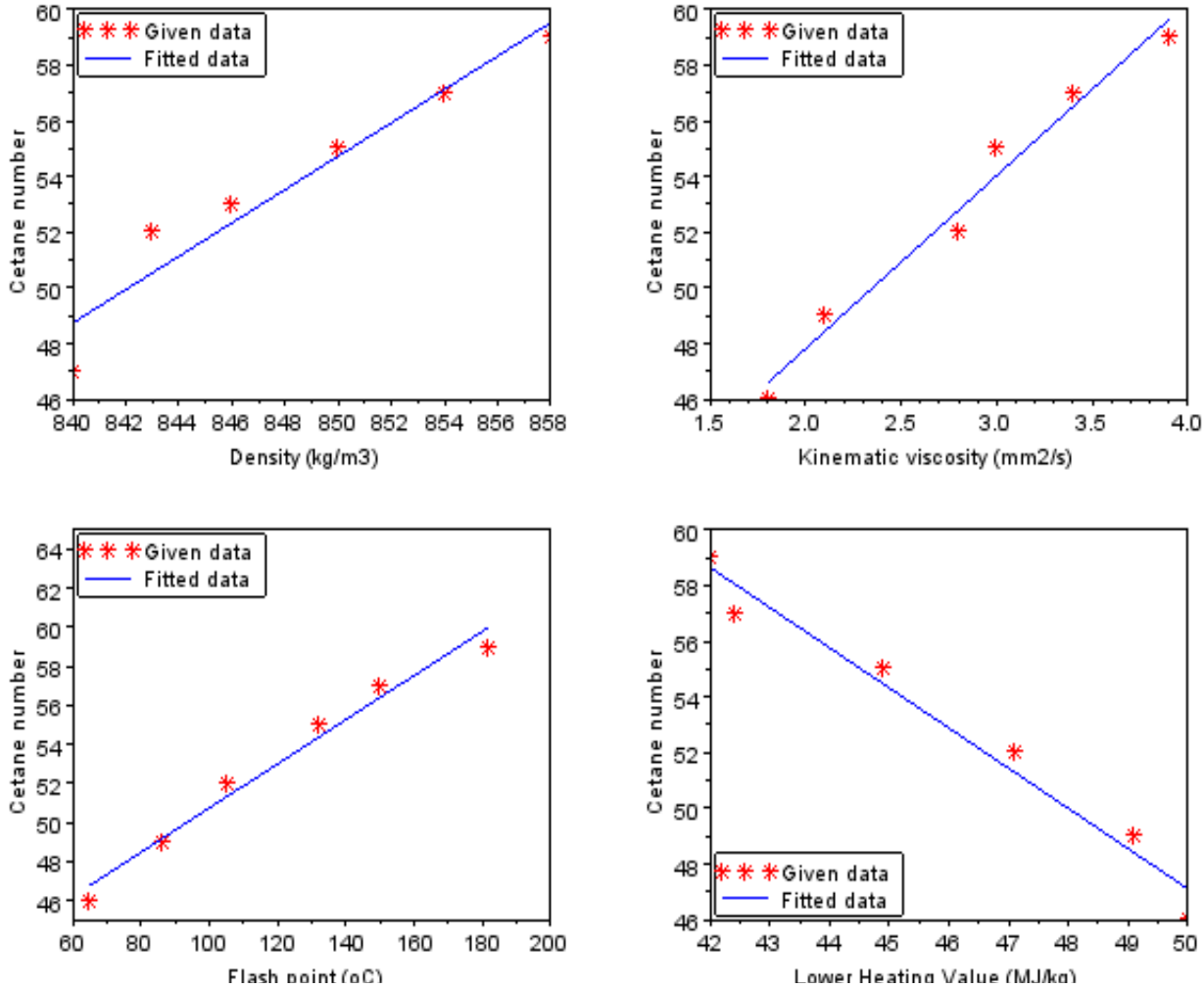

Figure 4.108: Cetane number (CN) vs thermal properties for GSO FAME: (a) CN vs density (b) CN vs kinematics viscosity (c) CN vs flash point (d) CN vs lower heating value

CHAPTER FIVE
CONCLUSION, RECOMMENDATION AND CONTRIBUTION TO KNOWLEDGE

5.1 Conclusion

The production of biodiesel from African pear seed and gmelina seed oils using heterogeneous catalysts (thermally activated clay, TAC; acid activated clay, AAC and base activated clay, BAC) and performance study of a diesel engine with biodiesel and its blends fuels were carried out. The oils from two seeds were extracted by solvent extraction methods involving two solvents (n-hexane and petroleum ether). The following conclusions were deduced from the findings of this study:

i. The yield of oil from the two seeds using the different solvents was within the quantity of oil obtained by some researchers. The low acid value, iodine value and saponification value of the oil enable it to undergo direct transesterification without treatment.

ii. The methyl ester was produced by transesterification of African pear seed and gmelina seed oils. Increase in process parameters such as reaction time, catalyst concentration, methanol/oil ratio, reaction temperature and agitation speed increase the yield of methyl ester to a reasonable point before it decreased.

iii. Optimization of the reaction parameters for biodiesel production from both oils using heterogeneous catalysts were carried out using response surface methodology and central composite design. The reaction was catalyzed with three activated clay catalysts. The effects of the reaction time, reaction temperature, catalyst concentration, methanol/oil molar ratio and agitation speed on the amount of methyl ester yields were significant parameters to predict the response values. The optimum values of the parameters for APO and GSO FAMEs using heterogeneous catalysts (TAC, BAC, AAC) were reaction time of 3hours, reaction temperature of 60^{o}C, catalyst concentration of 3%, methanol/oil molar ratio 10:1 and agitation speed of 346rpm (APO) and 326rpm (GSO) under these conditions the amount of methyl ester yields achieved were 70.5%, 69%, 77% respectively for APO and 75%, 70%, 72% respectively for GSO. The density, viscosity, cetane index, oxidative stability and higher heating values of biodiesel produced under optimized protocol in the present work meet the ASTM standard and were within the acceptable limits.

iv. The rate parameters showed that the transesterification of APO and GSO using modified clay catalysts suit LHHW reaction model with surface reaction between adsorbed of triglyceride and adsorbed methanol as RDS. It could also be observed that the rate constant for RDS increased as temperature increased from 45 to 55^{o}C. This indicates that the rate determining step of the transesterification of both APO and GSO were favoured at higher temperatures and heat is required for the reaction. The activation energies determined for APO and GSO transesterification respectively indicate that APO transesterification requires more energy than GSO transesterification and this could be because of more presence of unsaturated fatty acid in the APO.

v. The thermal efficiency and brake power of biodiesel are almost similar to conventional diesel fuel. Efficiency of B20 blends for biodiesel from African pear seed oil and gmelina seed oil with modified clay catalyst is higher than diesel fuel due to low volatility, higher viscosity and density. CO and HC emissions reduced with diesel biodiesel blended fuel, while NO_x emission increased for the diesel biodiesel blended fuel compared with the conventional diesel fuel. These suggest need for blending biodesel with petroldiesel. Models to predict both biodiesel production and the engine performance of the biodiesel using an artificial neural network (ANN) (feed forward network) were obtained. There was a very high correlation between the ANN predicted values and measured values determined experimentally with a minimum correlation coefficient above 0.95.

5.2 Recommendation

Based on the findings of this study, it is therefore recommended that:

i. Further research should be carried out to improve clay catalytic properties in order to increase the percentage yield of African pear seed oil biodiesel and gmelina seed oil biodiesel.

ii. More research should be carried out to investigate the effects of regeneration of the clay heterogeneous catalysts on the yield of biodiesel production.

iii. The environmental impact of production of biodiesel from the two seeds oil should be critically assessed.

iv. More research should be carried out to investigate use of additives to improve the oxidative stability of the biodiesel.

5.3 Contribution to Knowledge

Based on the findings in this study, the following contributions have been added to knowledge:

i. The optimal conditions for extraction of oil from both seeds using the two solvents are solvent to solid ratio 1.57ml/g, time 45 minutes, particle size 0.57mm, temperature 45^{o}C and agitation speed of 200rpm.

ii. Statistical models were developed for extraction of the oil from the seeds using both n-hexane and petroleum ether.

iii. It has been discovered that activated clay can catalyze transesterification reaction.

iv. The optimum conditions for production of biodiesel from both APO and GSO using heterogeneous clay catalysts are: reaction time of 3hours, reaction temperature of 60^{o}C, catalyst concentration of 3%, methanol/oil molar ratio 10:1 and agitation speed of 346rpm (APO) and 326rpm (GSO)

v. Statistical models were developed for transesterification of both APO and GSO using modified clay catalysts.

vi. Langmuir Hinshelwood Hougon Waston, LHHW reaction model was the best fitted kinetic model for the modified clay heterogeneous catalysis of APO and GSO with surface reaction between adsorbed of triglyceride and adsorbed methanol as RDS.

vii. The model equations for variation of physical and thermal properties of biodiesel were developed

REFERENCES

Abdullah, A., John, F. & Rob, B., (2011). The effects of using biodiesel as fuel on compression ignition (CI) engines and its production from vegetable oils. International Conference on Environmental, Biomedical and Biotechnology, IPCBEE, 16.

Adebayo G.B, Ameen O.M. &Abass L.T. (2011). Physico-chemical properties of biodiesel produced from *Jatropha Curcas* oil and fossil diesel. *Journal of Microbiology and Biotechnology Research, 1* (1), 12-16.

Adeib, I. S., Norhuda, I., Roslina, R. N. & Ruzitah, M. S. (2010). Mass transfer and solubility of *Hibiscus cannabinus* l. seed oil in supercritical carbon dioxide. *Journal of Applied Sciences, 10*(12), 1140–1145.

Aderemi, B.O.& Hameed, B. H.(2010). Production of biodiesel from palm oil. *Nigeria Society of Chemical Engineers Proceedings, 40,* 135-143.

Agarwal A. K. (2007). Biofuels (alcohols and biodiesel) applications as fuels for internal combustion engines. *Progressive Energy Combustion Science, 33*(3), 233–271.

Agarwal M.,& Garima C. (2011). Heterogeneous catalysis for Biodiesel Production: Review, International Conference on renewable energy.

Akhirevbulu, O.E. & Ogunbajo, M. I. (2011). The geotechnical properties of clay occurrences around Kutigi Central Bida Basin, Nigeria. *Ethiopian Journal of Environmental Studies and Management, 4*(1), 25-35.

Al-Widyan, M. I., Tashtoush, G. & Abu-Qudais, M. (2002). Utilization of ethyl ester of waste vegetable oils as fuel in diesel engines. *Fuel Process Technology, 76,* 91–103.

American Public Health Association (2005). Standard Methods for the Examination of Water and Wastewater, 21st ed. American Public Health Association: Washington, D.C.

Ampaitepin, S., Miyuki, K. & Tetsuo, T. (2006). Life cycle analysis of biodieselfuel production. Case study of using used cooking oil as a rawmaterial in Kyoto, Japan. *Proceeding 2nd Joint International Conference on Sustainable Energy and Environment*.

American Society for Testing and Materials. Standard test method for determination of iodine number of activated carbon. Philadelphia, PA: ASTM Committee on Standards (1986).

American Society for Testing and Materials ASTM D6751 (1973), Standard Specification for Natural (Vegetable Oil) and biodiesel, ASTM International, West Conshohocken, PA, 1973, www.astm.org.

Anthony Miraculas G, Bose N & Edwin Raj R., (2014). Optimization of process parameters for biodiesel extraction from tamanu oil using design of experiments. *Journal of Renewable and Sustainable Energy,6*(33), 1-20.

Antunes, W. M., Veloso, C. O. &Henriques, C. A. (2008). Transesterification of soybean oil with methanol catalyzed by basic solids.*Catalysis Today*, *133–135*(1-4), 548-554.

Anyanwu C.N, Mbajiorgu C.C, Ibeto C.N. & Ejikeme P.M.(2013). Effect of reaction temperature and time on neem methyl ester yield in a batch reactor. *Energy Conversion and Management, 74*, 81-87.

Attanatho, L., Magmee, S. & Jenvanitpanjakul, P., (2004). Factors affecting the synthesis of biodiesel from crude palm kernel oil. Proceedings of the Joint International Conference on Sustainable Energy and Environment (SEE), 1-3 December, 2004. Hua Hin, Thailand; 359-361.

Atadashi, I.M., Aroua, M.K. & Aziz, A.A.(2010) High quality biodiesel and its diesel engine application, a review. *Renewable and Sustainable Energy Review, 14*, 1999-2008.

Atadashi, I.M., Aroua, M. K., Abdul Aziz, R. &Sulaiman, N. M. N. (2012)The effects of catalysts in biodiesel production: A review. *Renewable and Sustainable Energy Reviews, 16*(5), 3456-3470.

Arcaklioglu, E. & Celikten, I.(2005). A diesel engine's performance and exhaust emissions. *Applied Energy*, *80*, 11-22.

Awono, A., Ndoye, O., Schreckenberg, K., Tabuna, H.& Isseri, F., (2002). Production and marketing of safou (*Dacryodes eduli*) in Cameroon and internationally: Market Development Issues. *Forest, Trees and Livelihoods, 12*, 125-147.

Aydin, H. & Bayindir, H. (2010) Performance and emission analysis of cottonseed oil methyl ester in a diesel engine. *Renewable Energy*, *35*, 588–592.

Ayhan, D., (2009). Biodiesel from waste cooking oil via base-catalytic and supercritical methanol transesterification. *Energy Conversion and Management*, 50, 923-927.

Azad, A. K., Mohammad Rasul & Masud Khan M., (2016). Production of FAME using nano alkaline catalyst and its emission effect.*Australia1st International Conference on Energy and Power*, ICEP2016, 14-16.

Azam M. M., Waris A.& Nahar N. M. (2005). Prospects and potential of fatty acid methyl esters of some non-traditional seed oils for use as biodiesel in India. *Biomass Bioenergy, 29,* 293–302.

Bai, R., Shu Wang, Fuming Mei, Tao Li & Guangxing Li.(2011). Synthesis of glycerol carbonate from glycerol and dimethyl carbonate catalyzed by KF modified hydroxyapatite.*Journal of Industrial and Engineering Chemistry*, *17,* 777-781.

Balat, M. & Balat, H. (2010). Progress in biodiesel processing. *Applied Energy*, *87*(6), 1815–1835.

Barakos, N., Pasias, S. &Papayannakos, N. (2008). Transesterification of triglycerides in high and low quality oil feeds over an HT2 hydrotalcite catalyst.*Biosource Technology, 99,* 5037-5042.

Basumatary, S., Deka, Dinesh C. & Deka, Dibakar C. (2012) Composition of biodiesel from *Gmelina arborea* seed oil. *Advanced and Applied Science Research*, *3*(5), 2745–2753.

Behzadi, S.&Farid, M. M.(2009). Production of biodiesel using a continuous gas-liquid reactor**.** *Bioresources Technology*, *100*(2), 683-689.

Biodiesel Handling and Use Guide 2009. National Reneweable Energy Laboratory, NREL/TP-540-43672.

Boehman, A. L.,(2005). Biodiesel production and processing.*Fuel Processing Technology, 86,* 1057-1058.

Bozbas, K.(2008).Biodiesel as an alternative motor fuel: Production and policies in the European Union. *Renewable and Sustainable Energy Reviews*, *12*(2), 542-552.

Brennan, L., Owende, P. (2010). Biofuels from microalgae a review of technologies for production, processing,and extractions of biofuels and co-products. *Renewable & Sustainable Energy Reviews*, *14*, 557–577.

Brigatti, M.F., Galan, E., Theng, B.K.G., 2006. *Structures and mineralogy of clay minerals*. In: Bergaya, F., Theng, B.K.G., Lagaly, G. (Eds.), *Handbook of clay science. Developments in Clay Science*, 1. Elsevier, pp. 19–86.

Bruno, W., Maicon, T., Aparecido, M. and Alexander, K. (2006). Modelling chemical kinetics of soybean oil transesterification process for biodiesel production: An analysis of molar ratio between alcohol and soybean oil temperature changes on the process conversion rate. *Journal of Bioautomation, 5*,13-22.

Bryan R. M. (2009). Biodiesel production, properties, and feedstocks. In vitro cell development biological—*Plant, 45*, 229–266.

Cardoso, A. L., Cristina, S., Neves, G., Da Silva, M. J., (2009). Esterification of oleic acid

for biodiesel production catalyzed by $SnCl_2$: A kinetic investigation.*Energies,1*, 79-92.

Calgaroto, C., Calgaroto, S., Mazutti, M., A., de Oliveira, D., Sibele Pergher, S. J., & Vladimir de Oliveira, J. V.(2013). Production of biodiesel from soybean and *Jatropha curcas* oils with ksf and amberlyst 15 catalysts in the presence of co-solvents. *Sustainable Chemical Processes*, 1, 17-22.

Canakci M. & Gerpen J. V. (1999) .The effect of yellow grease methyl ester on engine performance and emissions. Final Report: Recycling andReuse Technology Transfer Center. Publication 2000-134.

Canakc, M.I., Erdil, A. & Arcaklioglu, E., (2006). Performance and exhaust emissions of a biodiesel engine. *Applied Energy*, *83*, 594-605.

Cao, H., Zhang, Z., Wu, X. & Miao, X., (2013). Direct biodiesel production from Wet microalgae biomass of chlorella pyrenoidosa through in situ Transesterification.*Biomedical Resources International*, 1–6.

Cao, P., Dubé, M. A. &Tremblay, A. Y., (2008). High-purity fatty acid methyl ester production from canola, soybean, palm, and yellow grease lipids by means of a membrane reactor. *Biomass Bioenergy*, *32*(11), 1028–1036.

Carraretto, C., Macor, A., Mirandola, A., Stoppato, A. & Tonon, S. (2004) Biodiesel as alternative fuel: experimental analysis and energetic evaluations. *Energy*, *29*, 2195–2211.

Casas, A., Ramos, M. J. &Pe´rez, A., (2011). New trends in biodiesel production: Chemical inter-esterification of sunflower oil with methyl acetate.*Biomass and Bioenergy*, *35*(5), 1702-1709.

Casimir, C.A., Shu-wei, C., Guan-chiun, L.& Shaw, J. (2007). Enzymatic approach to biodiesel production. *Journal of Agricultural & Food Chemistry*, *55*(22), 8995-9005.

Chai, F., Cao, F. Zhai, F., Chen, Y., Wang, X. & Su, Z. (2007). Transesterification of vegetable oil to biodiesel using a heteropolyacid solid catalyst. *Advanced Synthesis and Catalysis*, *349* (7), 1057-1065.

Chementator, Biodiesel Production Using aHeterogeneous Catalyst, January 2017 bhttp://www.axens.net/upload/news/fichier/chemical_engineering.pdfN (2004).

Chhetri, A.B., Watts, K.C.& Islam, M.R. (2008).Waste cooking oil as an alternate feedstock for biodiesel production. *Energies,1*(1), 3-18.

Chongkhong, S., Tongurai, C. &Chetpattananondh, P. (2009). Continuous esterification for biodiesel production from palm fatty acid distillate using economical process. *Renewable Energy*, *34*, 1059-1063.

Choudhury, P. P. (2012). Toxicity of heart wood extract of *Gmelina arborea* against stored grain pests. *Agricultural Scienceand Resource Journal*,*2*(3), 131 – 133.

Chung, K. H., (2010). Transesterification of *Camellia japonica* and *Vernicia fordii* seed oils on alkali catalysts for biodiesel production. *Journal of Industrial and Engineering Chemistry*, *16*(4), 506-509.

Chung, K.H., Chang, D. & Park, B.(2008). Removal of free fatty acid in waste frying oil by esterification with methanol on zeolite catalysts. *Bioresouroces Technology*,*99*, 7438–7443.

Chung, K. H.& Park, B. G. (2009). Esterification of oleic acid in soybean oil on zeolite catalysts with different acidity. *Journal of Industrial and Engineering Chemistry*, *15*(3)388-392.

Darnoko D., Cheryan M. (2000). Kinetics of palm oil transesterification in a batch reactor. *Journal of American Oil Chemists Society*,*77*, 1263-1267.

Davies, W. (2005). Biodiesel Technologies and Plant Design,davies@sn2.com.au , August 2005.

Dang, T. H., Chen, B. H. & Lee, D. J. (2013). Application of kaolin-based catalysts in biodiesel production viatransesterification of vegetable oils in excess methanol. *Bioresource Technology*, *145*, 175-181.

Demirbas, A. (2006). Biodiesel production via non-catalytic SCF method and biodiesel fuel characteristics. *Energy Conversion and Management*, *47*(15-16), 2271-2282.

Demirbas, A., (2009). Progress and recent trends in biodiesel fuels. *Energy Conversion and Management*,*50*, 14-34.

Demirbas, A. (2011). Biodiesel from olgae, biofixation of carbon dioxide by microalgae: A solution to pollution problems. *Applied Energy*, *88*(10), 3541-3547.

Dey, G., Mitra, A., Banerjee, R. & Maiti, B. (2001). Enhanced production of amylase by optimization of nutritional constituents using response surface methodology. *Biochemical Engineering Journal*, *7*, 227-231.

Di Serio, M., Ledda, M. Cozzolino, M., Minutillo, G., Tesser, R. &Santacesaria, E. (2006). Transesterification of soybean oil to biodiesel by using heterogeneous basic catalysts. Journal of *Industrial and Engineering Chemistry Research*, *45*(9), 3009-3014.

Di Serio, M., Tesser, R., Pengmei, L. & Santacesaria, E.(2007). Heterogeneous catalysts for biodiesel production. *Energy and Fuels*,*22*, 207-217.

Dossin, T. F., Reyniers, M. F., Berger, R. J. &Marin, G. B. (2006). Simulation of heterogeneouslyMgO-catalyzed transesterification for fine-chemical and biodiesel industrial production. *AppliedCatalysis B-Environmental***,** *67,* (1-2), 136-148.

Dossin T. F., Reyniers, M. &Marin G. B. (2006). Kinetics of heterogeneously MgO-catalyzed transesterification. *Applied Catalysis B: Environmental*, *62*,35-45.

Dubios, P., Pollet E., Delcourt C. & Alexandre M. (2006). Transesterification catalysts to improve clay exfoliation in synthetic biodegradable polyester nanocomposites,*European Polymer Journal*,*42*, 1330-1341.

Duran, S., Laputerta, M. &Rodriguez- Fernadez, J.(2005). Neural networks estimation of diesel particulate matter composition from transesterified waste oils blends. *Journal of Fuel*, *84*(16), 2080-2085.

Dwivedi, J. S. & Sharma, M.P. (2011). Impact analysis of biodiesel on engine performance—areview. *Renewable and Sustainable Energy Reviews*, *15*, 4633–4641.

Eromosele I. C., Eromosele C. O., Akinloye A. O. & Komolafe F. O. (1994). Characterization of oils and chemical analyses of seeds of wild plants. *Plant Foods and Humanity Nutrition*, *46*, 361-365.

Fan, X., (2008). Optimization of biodiesel production from crude cottonseed oil and waste vegetable oil: Conventional and ultrasonic irradiation methods. *All dissertations*, 310. https://tigerprints.clemson.edu/all_dissertation

Fan, X., Wang, X. & Chen, F., (2011). Biodiesel production from crude cottonseed oil; An optimization process using response surface methology. *The Open Feuls and Energy Science Journal*, 4, 1-8.

Fanguli, Ma. & Milford, A.H., (1999). Biodiesel production, a review. *Bioresource Technology*, 70, 1-15.

Ferella,F., Di Celso,G.M., De Michelis, I., Stanisci, V.,&Vegliò, F. (2010) Optimization of the transesterification reaction in biodiesel. *Fuel*,*89*(1), 36-42.

Fogler, H. S. (2011)Element of chemical reaction engineering, 4thEdition, Pearson Education, Inc., Upper Saddle River, New Jersey, U.S.A., pp. 655-703.

Freedman, B., Pryde, E.N.& Mounts, T.L. (1984). Variables affecting the yield of fattesters from transesterified vegetable oils. *Journal of American Oil Chemist Society*,*61*(10), 1638-1643.

Furuta, S., Matsuhasbi, H.&Arata, K. (2004). Biodiesel fuel production with solid superacid catalysis in fixed bed reactor under atmospheric pressure. *Catalytic Communication*, *5*, 721-723.

Galan E., Aparico, P. &Mirals, A. (2005). Bioleaching of copper, cobalt and zinc from black shale by *Penicillium notatum*. *African Journal of Biotechnology, 8*(19), 5038-5045.

Georgogianni, K. G., Kontominas, M. G., Pomonis, P.J., Avlonitis, D. & Gergis, V. (2008). Alkalineconventional and in situ transesterification of cottonseed oil for the production of biodiesel. *Energy& Fuels*, *22,* 2110–2115.

Georgogianni, K. G., Katsoulidis, A. P., Pomonis,P. J.& Kontominas, M. G. (2009) Transesterification of soybean frying oil to biodiesel using heterogeneous catalysts:*Fuel Processing Technology*, *90*,671-676.

Gep, B., Hunter, W. G. & Hunter J. S. (2005). Statistics for Experimenters: An Introduction to Design, Data Analysis, and Model Building.2nd edition. John Wiley & Sons, New York.

Gerpen, J.V., (2005). Bio-diesel processing and production. *Fuel Processing Technology, 86*, 1097-1107.

Ghetsi, G. F., De macedo, J. L., Parente, V. C. I., Dias, J. A. & Dias, S. C. L.(2009). Synthesis, characterisation and reactivity of Lewis acid/surfactant cerium trisdodecylsulfate catalyst for transesterification and esterification reaction. *Applied CatalysisA; General355*, 139-147.

Ghobadian, B., Rahimi, H., Nikbakht, A. M., Najafi, G.,& Yusaf, T. F. (2009) Diesel engine performance and exhaust emission analysis using waste cooking biodiesel fuel with an artificial neural network. *Renewable Energy, 34*, 976– 982.

Gumus, M. & Kasifoglu, S. (2010) Performance and emission evaluation of a compression ignition engine using a biodiesel (apricot seed kernel oil methyl ester) and its blends with diesel fuel. *Biomass & Bioenergy*, *34*, 134– 139.

Guru, M., Koca, A., Can, O., Cınar, C. & Sahin, F. (2010) Biodiesel production from waste chicken fat based sources and evaluation with Mg based additive in a dieselengine. *Renewable Energy*, *35*, 637– 643.

Hameed, B. H., Lai, L. F. & Chin, L. H. (2009). Production of biodiesel from palm oil (*Elaeis guineensis*) using heterogeneous catalyst: An optimized process. *Fuel Processing Technology*, 90(4), 606-610.

Hansen, A. C., Gratton, M. R. & Yuan, W. (2006) Diesel engine performance and NOx emissions from oxygenated biofuels and blends with diesel fuel. *Trans ASABE, 49*, 589–595.

Haq, N. B., Hanif, M. A. &Qasim, M., Ata-ur-Rehman, (2008).Biodiesel production from waste tallow. *Fuel,87*, 2961-2966.

Hasimog˘lua, C., Ciniviz, M.,Ozsert, I˙., Icingur, Y., Parlak, A. & Salman, M. C. (2008) Performance characteristics of a low heat rejection diesel engine operating with biodiesel. *Renewable Energy, 33*, 1709– 1715.

Hattori, H., Shima, M. & Kabashima, H. (2000). Alcoholysis of ester and epoxide catalyzed by solid bases. *Studies on Surface Science and Catalysis*, *130*, 3507-3512.

Hayes, B. L. (2004). Recent advances in microwave-assisted synthesis. *Aldrichimica Actacta*., *37* (2), 66–77.

Hazar, H. (2009) Effects of biodiesel on a low heat loss diesel engine. *Renewable Energy, 34*, 1533– 1537.

Helwani, Z., Othman, M. R., Aziz, N., Fernando, W. J. N.& Kim, J. (2001).Technologies for production of biodiesel focusing on green catalytic techniques: a review. *Fuel ProcessingTechnology*, *90*, 1502–1514.

Hertz, J., Krogh, A. & Palmer, R.G.(1991). *Introduction to the theory of neural Computation*. Addison-Wesley Publishing Company, Redwood City, New Jersey.

Hideki, F., Akihiko, K. & Hideo, N. (2001). Biodiesel fuel production by transesterification of oils. *Journal of Bioscience and Bioengineering*, *92*(5), 405-416.

Hsin, S. H., Chen, W. M. & Chang, J. S. (2010).*Scenedesmus obliquus* CNW-N as a potentialcandidate for CO_2 mitigation and biodiesel production. *Bioresource Technology*, *101*(22), 8725-8730.

Huang Y.& Chang, J.I. (2010). Biodiesel production from residual oils recovered from spent bleaching earth.*Renewable Energy 35*, 269-274.

Igbokwe, P. & Ogbuagu, J. (2003). Effects of process parameters on the extraction of alumina from indigenous kaolinitic clay deposit. *Nigerian Journal of Engineering Research and Development*, *2*(2), 23-26.

Ilgen, O. &Akin, A. N. (2009).Development of alumina supported alkaline catalyst used for biodiesel production. *Turkish Journal of Chemistry*, *33*(2),281-287.

Isaac, I. O. & Ekpa, O. D. (2009). Minerals and anti-nutrients in two varieties of African pear (*Dacroyodes edulis*). *Journal of Food Technology, 7*(4), 106 – 110.

Isaac, I. O., Ekpa, O. D. &Ekpe, U.J. (2014). Extraction, characterization of African pear

(*Dacryodes edulis*) oil and its application in synthesis and evaluation of surface coating driers.*International Journal of Advanced Research in Chemical Science, 1*(4), 14-22.

Isah, Y., Yousif, A. A., Feroz, K. K., Suzana, Y., Ibraheem, A. & Soh, A. C. (2015). Comprehensive characterization of napier grass as feedstock forthermochemical conversion.*Energies Journal, 8,* 3403-3417.

Issariyakul, T. (2006). Production of biodiesel from fryer grease (Unpublished master's thesis). University ofSaskatchewan.

Janaun, J.& Ellis, N. (2010). Perspectives on biodiesel as a sustainable fuel. *Renewable & Sustainable Energy Review, 14*(4), 1312–1320.

Jimoh, A., Abdulkareem, A. S., Afolabi, J. O. & Odigure Odili, U. C. (2012). Production and characterization of biofuel from refined groundnut oil.*International Journal of Advanced Research in Chemical Science, 1*,10–12.

Jinlin Xuea, Tony E. Grift & Alan C. Hansen (2011). Effect of biodiesel on engine performances and emissions.*Renewable and Sustainable Energy Reviews,15,* 1098–1116.

Jitputti, J., Kitiyanan, B., Rangsunvigit, P., Bunyakiat, K., Attanatho, L. &Jenvanitpanjakul, P. (2006). Transesterification of crude palm kernel oil and crude coconut oil by different solid catalysts. *Chemical Engineering Journal, 116*(1), 61-66.

John, C. (2000). Interpretation of infrared spectra, a practical approach.*Encyclopedia of Analytical chemistry,* 10815–10837.

Kalam, M. A. &Masjuki, H. H. (2008) Testing palm biodiesel and NPAA additives to control NOx and CO while improving efficiency in diesel engines. *Biomass & Bioenergy, 32,* 1116– 1122.

Kalligeros, S., Zannikos, F., Stournas, S., Lois E., Anastopoulos, G., Teas, C.H. & Sakellaropoulos, C.(2003). An investigation of using biodiesel/marine diesel blends on the performance of a stationary diesel engine. *Biomass Bioenergy,24,* 141-149.

Kalogirou, S.A.(2003). Artificial intelligence for the modelling and control of combustion processes: a review. *Progressive Combustion and Energy Science,29,* 515-66.

Kalogirou, S.A. & Panteliou, S.(2000). Thermosiphon solar domestic water heating systems; long-term performance prediction using artificial neural network. *Solar Energy, 69,* 163-174.

Karmee, S.K., Chandna, D., Ravi, R. & Chadha, A. (2006). Kinetics of base catalyzed transesterification of triglycerides from pongamia oil. *Journal of American Oil Chemists Society,83*, 873-877.

Karabektas, M. (2009) The effects of turbocharger on the performance and exhaust emissions of a diesel engine fuelled with biodiesel. *Renewable Energy, 34*, 989–993.

Kathlene, J., Gopinath, R., Meher, L. C. &Kumar, A. D.(2008). Solid acid catalyzed biodieselproduction from waste cooking oil.*Applied Catalysis B: Environmental, 85,* 86–91.

Kaya, C., Hamamei, C., Baysal, A., Akba, O., Erdogan, S. & Sayduct, A.(2009). Methyl ester of peanut (*Arachis hypogeal* L.) seed oil as potential feedstock for biodiesel production. *Reneweable Energy,34*, 1257-1260.

Keskin, A., Gu¨ru¨, M.,Altiparmakc, D. &Aydin, K.(2008). Using of cotton oil soapstock biodiesel–diesel fuel blends as an alternative diesel fuel. *Renewable Energy,33*(4), 553-557.

Keskin, A., Guru, M. & Altıparmak, D. (2008) Influence of tall oil biodiesel withMgandMo based fuel additives on diesel engine performance and emission. *Bioresource Technology, 99,* 6434– 6438.

Khan, A.(2007). Evaluating biodiesel catalysts. Retrieved on May, 2017 from www.eptq.com.

Khan, N. A. & el Dessouky, H. (2009). Prospect of biodiesel in Pakistan. *Renewable & Sustainable Energy Review, 13*(6–7), 1576–1583.

Kim,S.S., Kim,K.H., Shin,S.C. & Yim, E.S.(2007). Current Status of Policy and Market forBiodiesel in Korea. *Journal of Industrial and Engineering Chemistry, 18*(5) 401-406.

Kim,S.J., Park,M.J., Jung,K.D.& Joo, O. S. (2004).Catalytic performance of metal-substituted ZSM-5 zeolites for vapor phase Beckmann rearrangement of cyclohexanone oxime. *Journal of Industrial and Engineering Chemistry*, *10*(6), 995-1002.

Kouzu, M., Kasuno, T., Tajika, M., Sugimoto, Y., Yamanaka, S. & Hidaka, J.(2008). Calcium oxide as a solid base catalyst for transesterification of soybean oil and its application to biodiesel production. *Fuel, 87,* 2798-2806.

Kumar, J. & Bansal, A.(2007). Selection of best neural network for estimating properties of diesel-biodiesel blends. In:Proceedings of the 6th WSEAS International Conference on Artificial Intelligence, Knowledge Engineering and Data Bases, Corfu, Island, Greece.

Labeckas, G. & Slavinskas, S.(2006). The effect of rapeseed oil methyl ester on direct injection diesel engine performance and exhaust emissions. *Energy Conversion and Management, 47,* 1954-1967.

Lapuerta, M., Herreros, J. M., Lyons, L. L., Garcia-Contreras, R. & Brice, Y. (2008) Effect of

the alcohol type used in the production of waste cooking oil biodiesel on diesel performance and emissions. *Fuel, 87*, 3161– 3169.

Lau, C.(1991). Neural Networks: Theoretical Foundation and Analysis. IEEE Press, Piscataway, New Jersey, USA.

Lee, S. B., Han, K.H., Lee, J.D.& Hong,I.K. (2010). Optimum process and energy density analysis of canola oil biodiesel synthesis.*Journal of Industrial and Engineering Chemistry, 16,* 1006-1010.

Lee,S.B., Lee, J.D.& Hong, I.K. (2011). Ultrasonic energy effect on vegetable oil based biodiesel synthetic process. *Journal of Industrial and Engineering Chemistry*, *17*(1), 138 – 143.

Lee, K.W., Yu, J.X., Mei,J.H., Yan, L., Kim, Y.W. &Chung,K.W. (2007).A kinetic study on the of glyceril monooleate and soybean used frying oil to biodiesel.*Journal of Industrial and Engineering Chemistry,13,* 799-807.

Lee, D., Park, Y. & Lee, K., (2009). Heterogeneous base catalysts for transesterification in Biodiesel Synthesis. *Catalysis Survey from Asia ,13*(2), 63-77.

Leng, T.Y., Mohamed, A. R. & Bhatia, S.(1999). Catalytic conversion of palm oil to fuels and chemicals. *Canadian Journal of Chemical Engineering, 77*, 156 – 161.

Leung, D. Y. C. &Guo, Y. (2006). Transesterification of neat and used frying oil: Optimization for biodiesel production. *Fuel Processing Technology, 87,* 883-890.

Leung, D. Y. C., Wu, X. & Leung, M. K. H. (2010). A review on biodiesel production using catalyzed transesterification. *Applied Energy, 87,* 1083-1095.

Levenspiel, O. (2000). *Chemical Reaction Engineering,* 4th Edition. John Wiley & Sons, New York, 178-191.

Li, H., Shen, B., Jabalu, J. C. & Nchare, M.(2009). Enhancing the production of biodiesel from cottonseed oil by fixed-fluidized bed catalytic cracking.*Renewable Energy, 34*, 1033-1039.

Liauw, M. Y., Natan, F. A., Widiyanti, P., Ikasari, D., Indraswati, N.& Soetaredjo, F. E. (2008). Extraction of neem oil (*Azadirachta indica A. Juss*) using n-hexane and ethanol: Studies of oil quality, kinetic and thermodynamic. *Journal of Engineering and Applied Sciences*, *3*(3), 49–54.

Lim, B. P., Maniam,G. P. &Hamid, S. A.(2009). Biodiesel from adsorbed waste oil on spent bleaching clay using CaO as a heterogeneous catalyst. *European Journal of Scientific Research, 33*(2), 347-357.

Lin, B. F., Huang, J. H. & Huang, D. Y. (2009) Experimental study of the effects of vegetable oil methyl ester on DI diesel engine performance characteristics and pollutantemissions. *Fuel, 88*, 1779–1785.

Liu, D. H., Wei, D., Xu, Y.Y., & Jing, Z. (2004). Novozyrn 435-catalysed transesterification of crude soy bean oils for biodiesel production in a solvent-free medium,*Biotechnology and Applied Biochemistry,40*, 187-190.

Liu, X., He H., Wang, Y., Zhu, S. & Piao, X. (2008). Transesterification of soybean oil to biodiesel using CaO as a solid base catalyst. *Fuel, 87*, 216-221.

Lo´pez, D. E., Goodwin, J. G., Jr. & Bruce, D. A. (2007). Transesterification of triacetin with methanol on nafion acid resins. *Journal of Catalysis,245*, 381-390.

Lopez, D. E., Bruce, Jr D. A. & Lotero, J. G. E. (2005). Transesterification of triacetin with methanol on solid acid and base catalysts. *Applied Catalysis A : General, 295*,97–105.

Ma, F. & Hanna, M.A.(1999). Biodiesel production: a review. *Bioresource Technology,70*, 1– 15.

MacLeod, C. S., Harvey, A. P., Lee, A. F.& Wilson, K. (2008). Evaluation of the activity and stability of alkali-doped metal oxide catalysts for application to an intensified method of biodiesel production. *Chemical Engineering Journal, 135*, (1-2), 63-70.

Madejová, J., (2003). FTIR techniques in clay mineral studies.*Vibrational Spectroscopy,31* (1), 1 – 10.

Madras, G., Kolluru, C. & Kumar, R. (2004). Synthesis of biodiesel in supercritical fluids. *Fuel, 83*(14-15), 2029-2033.

Manjunath, H., Omprakash, H.& Hemachandra, R. K.(2015). Process optimization for biodiesel production from simarouba, mahua, and waste cooking oils.*International Journal of Green Energy, 12* (4), 424-430.

Manuit, J. & Statit, P.(2007). Biodiesel synthesis from transesterification by clay-based catalyst. *Chiang Mai Journal Science*, *34*(2), 201-207.

Marchetti, J.M.& Errazu, A.F.(2008). Esterification of free fatty acid using sulphuric acid as catalyst in the presence of triglycerides. *Biomass and Bioenergy,32*(9), 892-895.

Marchetti, J.M., Miguel, V.U. & Errazu, A.F.(2007). Possible methods for biodiesel production. *Renewable Sustainable Energy Reviews, 11*,1300-1311.

Mariscal, R., Alonso, D. M., Moreno-Tost, R., Poves, M. D. Z. & Granados, M. L. (2007). Potassium leaching during triglyceride transesterification using K/γ-Al_2O_3catalysts. *Catal*ytic *Commun*ication, *8*, 2074-2080.

Martino, D., Tesser, R., Pengmei, L. &Santacesaria, E., (2008). Heterogeneous catalysts for biodiesel production. *Energy Fuels*,*22*, 207-217.

Masato, K., Takekazu, K., Masahiko, T., Yoshikazu, S., Shinya, Y. & Jusuke, H. (2008). Calcium oxide as a solid base catalyst for transesterification of soybean oil and its application to biodiesel production. *Fuel, 87*,2798–2806.

Mata,T. M., Martins, A. A.& Ceatano, N. S. (2010). Microalgae for biodiesel production and Lather applications: A review. *Renewable and Sustainable Energy Review, 14*, 217-232.

Meher, L.C., Dharmagadda, V.S.S. & Naik, S.N.(2006). Optimization of alkali-catalyzed transesterification of *Pongamia pinnata* oil for production of biodiesel. *Bioresource Technology, 97*,1392-1397.

Melvin Jose, D. F., Edwin Raj, R., Durga Prasad, D., Robert Kennedy, Z, & Mohammed Ibrahim, A. (2011). A multi-variant approach to optimize process parameters for biodiesel extraction from rubber seed oil.*Applied Energy*, *88*(6): 2056-2063.

Meyer, O., Rößner, F., Rakoczy, R. A. &Fischer, R. W. (2008). A new heterogenous process catalyst for the biodiesel production DGMK Conference September 29 –October- 1, 2008 Berlin, Germany.

Mittelbach, M., Silberholz, A. &Koncar, M. (1996). In novel aspects concerning acid-catalyzed alcoholysis of triglycerides, oils-fats-lipids. Proceedings of the 21st World Congress of the International Society for Fats Research, October 1-6, 1996, Hague, Netherlands, pp: 497-499.

Mittelbach, M. & Remschmidt, C. (2004). *Biodiesel Comprehensive Handbook*. pp 102-120.

Murillo, S., Mıguez, J. L., Porteiro, J., Granada, E., &Moran, J. C. (2007) Performance and exhaust emissions in the use of biodiesel in outboard diesel engines. *Fuel, 86*, 1765–1771.

Mythili, R., Venkatachalam, P., Subramanian, P.& Uma, D.(2014). Production characterization and efficiency of biodiesel: a review. *International Journal of Energy Research*, 38, 1233–1259.

Monyem, A., Van Gerpen, J. H. & Canakci, M. (2001) The effect of timing and oxidation on emissions from biodiesel-fueled engines. *Trans ASAE*, 44, 35–42.

Moser, B.R.(2009). Biodiesel production, properties and feedstocks. *In Vitro Cell Development Biology-Plant,45*, 229-266.

Naik, S. N., Vaibhav, V. G., Prasant, K. R.& Ajay, K. D. (2010). Production of first and second generation biofuels: a comprehensive review. *Renewable & Sustainable Energy Revision, 14*, 578–597.

Ngo, H. L., Nicholas, A. Zafiropoulos, Thomas, A., Foglia, Edward T., Samulski, W. L. (2010). Mesoporous silica-supported diarylammonium catalysts for esterification of free fatty acids in greases. *Journal of the American Oil Chemists Society, 87*, 445-452.

Nie, K., Xie, F., Wang, F. & Tan, T. (2006). Lipase catalyzed methanolysis to produce biodiesel: Optimization of the biodiesel production. *Journal Molecular Catalysis B: Enzymatic, 43*(1-2), 142-147.

Noureddini, H. & Zhu, D. (1997) Kinetics of transesterification of soybean oil. *Journal of the American Oil Chemists' Society,74*, 1457-1463.

Nwabanne, J. T. & Igbokwe, P. K. (2011). Copper (II) uptake by adsorption using palmyra palm nut. *Advances in Applied Science Research,2*(6): 166-175.

Obaje, S. O., Omada, J. I. & Dambatta, U. A. (2013). Clays and their industrial applications: Synoptic Review. *International Journal of Science and Technology, 3*(5), 264-290.

Ogunsuyi, H.O. (2012). Acid and base catalysed transesterification of mango (*Mangifera Indica*) seed oil to biodiesel. *IOSR Journal Applied Chemistry (IOSRJAC)*, 18-22.

Ogunsuyi, H.O. & Daramola, B. M. (2013). Evaluation of almond seed oil as viable feedstock for biodiesel fuel. *International Journal of Biotechnology Resources,1*(8), 120-127.

Ogunsuyi, H.O. &Oyewo, I.O.(2013). Evaluation of African pear (*Dacryodes edulis)* seeds-oil as aviable feedstock for biodiesel fuel.*Research Journal in Engineering and Applied Sciences,4*(3) 106-113.

O˘guz, H., O˘gut, H. & Eryilmaz, T. (2007) Investigation of biodiesel production, quality and performance in Turkey. *Energy Source; Part A, 29*, 1529– 1535.

Oh, K. K., Kim, Y. S., Yoon, H. H. &Tae, B. S. (2002) Pretreatment of lignocellulosic biomass using combination of ammonia recycled percolation and diluted-acid process. *Journal of Industrial and Engineering Chemistry,8* (1), 64-68.

Okolie, P.N., Ajekwene, A.E. & Uaboi, Egbeni (2012). Extraction and characterization of oil from *Jatropha curcas* seed. *World Journal of Agricultural Science, 8*(4), 359–365.

Okoroigwe, E., Li, Z., Stuecken, T., Saffron, C.M. & Onyegegbu, S. (2012)Pyrolysis of *Gmelina arborea* wood for bio-oil/biochar production: Physical and chemical characterization of the products.*Journal of Applied Sciences,12*(4), 369-374.

Olutoye, M. A., Hameed, B. H. (2016) Kinetics and deactivation of a dual-site heterogeneous oxide catalyst during the transesterification of crude jatropha oil with methanol. Journal of Taibah University for Science, 10(5), 685 – 699.

Oner, C. & Altun, S. (2009) Biodiesel production from inedible animal tallow and an experimental investigation of its use as alternative fuel in a direct injection diesel engine. *Applied Energy, 86*, 2114– 2120.

Onukwuli, O. D., Ngomo, H. M., Susu, A. A. (1999) Reforming of n-octane on a Pt/Al_2O_3 catalyst.1. product distribution and kinetics analysis. *Petroleum Science & Technology*, 17 (7-8): 711-735.

Ozsezen, A. N., Canakci, M., Turkcan, A. & Sayin, C. (2009) Performance and combustion characteristics of a DI diesel engine fueled with waste palm oil and canola oilmethyl esters. *Fuel, 88*, 629–636.

Paula, B., Shahar, N.& Zeev, W. (2011). Castor oil biodiesel and its blends as alternative fuel.*Biomass and Bioenergy, 35*, 2861-2866.

Park, H.J., Dong,J. I., Jeon, J.K., Yoo, K.S., Yim, J.H., Sohn,J.M.& Park,Y.K. (2007). Conversion of the pyrolytic vapor of radiata pine over zeolites.*Journal of Industrial and Engineering Chemistry*, *13*(2), 182-189.

Pal, A., Verma, A., Kachhwaha, S. S. & Maji, S. (2010) Biodiesel production through hydrodynamic cavitation and performance testing. *Renewable Energy, 35*, 619– 624.

Palligarnai, V. T. & Briggs M. (2008). Biodiesel production–current state of the art and challenges. *Journal of Industrial Microbiology and Biotechnology*, *35*, 421–430.

Pizarro, A.V.L. & Park, E.Y. (2003). Lipase-catalyzed production of biodiesel fuel from vegetable oils contained in waste activated bleaching earth.*Process Biochemistry*, *38*(7), 1077-1082.

Puna, J.F., Gomes, J. F., Joana, M.,Correia, N., Soares Dias, A. P. &Bordado, J. C. (2010). Advances on the development of novel heterogeneous catalysts for transesterification of triglycerides in biodiesel. *Fuel*,*89*(11), 3602-3606.

Prakash, B. S. J., Reddy, C.R., Iyengar, P.& Nagendrappa, G. (2005). Esterification of dicarboxylic acids to diesters over Mn^{+}- montmorillonite clay catalysts. *CatalysisLetter*, *101*, 87-91.

Qi, D. H., Geng, L. M., Chen, H., Bian, Y. Z. H., Liu, J. &Ren, X. C. H. (2009) Combustion and performance evaluation of a diesel engine fueled with biodiesel produced from soybean crude oil. *Renewable Energy, 34*, 2706– 2713.

Raheman, H. & Phadatare, A. G. (2004) Diesel engine emissions and performance from blends of karanja methyl ester and diesel. *Biomass & Bioenergy, 27*, 393– 397.

Ramadhas, A. S., Jayaraj, S. &Muraleedharan, C. (2004).Use of vegetable oils as I.C. engine fuels: A Review. *Renewable Energy, 29*(5), 727-742.

Ramadhas, A.S.. Jayaraj, S. &Muraleedharan,C.(2006). Biodiesel production from high FFA rubber seed oil. *Fuel, 84*(4), 335-340.

Ramadhas, A. S., Muraleedharan, C.& Jayaraj, S. (2005) Performance and emission evaluation of a diesel engine fueled with methyl esters of rubber seed oil. *Renewable Energy*,30, 1789–1800.

Ramos M. J., Casas, A., Rodrı´guez, L., Romero, R. &Pe´rez, A. (2008). Transesterification of sunflower oil over zeolites using different metal loading: A case of leaching and agglomeration studies.*Applied Catalysis A: General,346*, 79-85.

Rashid, U., Farooq, A. & Gerhard, K. (2009). Evaluation of biodiesel obtained from Cottonseed oil. *Fuel Processing Technology*,*90*(9), 1157-1163.

Refaat, A.A., El Sheltawy, S.T. & Sadek, K.U. (2008). Optimum reaction time, performance and exhaust emissions of biodiesel produced by microwave irradiation. *International Journal of Environmental Science & Techology, 5*(3), 315-322.

Rutto, H. (2013). The use of thermally modified koalin as a heterogeneous catalyst for producing biodiesel. *Materials and processes for energy: communicating current research and technological developments*: In A. Méndez-Vilas, Ed., 399-406.

Saeid, B., Aroua,M.K., Abdul Raman, A.& Sulaiman,N. M. N. (2008). Density of palm oil-based methyl ester.*Journal of Chemical and Engineering Data,53*(3), 877-880.

Sahoo, P. K., Das, L. M., Babu, M. K. G. & Naik, S.N., (2008). Biodiesel development from high acid value polanga seed oil and performance evaluation in a CI engine. *Fuel, 86,* 448–454.

Saifuddin, N. &Chua, K. H.(2004). Production of ethyl ester (biodiesel) from used frying oil: Optimization of transesterification process using microwave irradiation. *Malaysian Journal of Chemistry, 6*(1)077-082.

Saka, S. &Isayama, Y. (2009).A new process for catalyst-free production of biodiesel using supercritical methyl acetate. *Fuel,88*(7), 1307-1313.

Salahi, A., Mohsen, A. & Toraj M. (2010). Permeate flux decline during UF of oily wastewater:experimental and modeling. *Desalination,251*, 153–160.

Salis, A., Pinna, M., Monduzzi, M. & Solinas, V. (2008). Comparison among immobilised

lipases on macroporous polypropylene toward biodiesel synthesis. *Journal of Molecular Catalysis B: Enzymatic*, *54*(1-2), 19-26.

Sani, Y. M., Daud, W. M. A. W. & AbdulAziz, A. R. (2014). Activity of solid acid catalysts for biodiesel production: A critical review. *Applied Catalysis A: General*, *470*, 140 – 161.

Sanjay, B., Dinesh, C. D., Dibakar, C. D.(2012). Composition of biodiesel from *Gmelina arborea* seed oil. *Advances in Applied Science Research*, *3*(5), 2745-2753.

Schizaki dos Santos, P. R., Wypych, F., Pedersen Voll, F. A., Hamerski, F. &Corazza, M. L. (2016). Kinetics of ethylic esterification of lauric acid on acid activated montmorillonite (STx1-b) as catalyst. *Fuel*, *181*, 600-609.

Schulze, K. Makowski, W., Chyzy, R., Dziembaj, R. & Geismar, G. (2001). Nickel doped hydrotalcites as catalyst precursors for the partial oxidation of light paraffins. *Applied Clay Sciience*, *18*(1-2), 59-69.

Schwarzer, R. (2006). Esterification of acetic acid with methanol: A kinetic study on Amberlyst 15. A Masters Thesis, University of Pretoria.

Shah, S., Sharma, S. &Gupta, M. N., (2004).Biodiesel preparation by lipase-catalyzed transesterification of *Jatropha*oil.*Energy Fuels*,*18*(1), 154-159.

Sharma,Y. C.& Singh, B. (2009). Development of biodiesel: current scenario. *Renewable and Sustainable Energy Review*,*13*(6–7), 1646–1651.

Sharma,Y. C., Singh, B.& Upadhyay, S. N. (2008). Advancements in development and characterizationof biodiesel: a review. *Fuel*,*87*(12), 2355–2373.

Sharma, Y. C., Singh, B. &Korstad, J.(2011). Latest developments on application of heterogeneous basic catalysts for an efficient and eco friendly synthesis of biodiesel: a review. *Fuel*, *90*(4), 1309-1324.

Shieh, C. J., Liao, H.F. & Lee, C.C. (2003). Optimization of lipase-catalyzed biodiesel by response surface methodology. *Bioresource Technology*,*88*(2), 103-106.

Shumaker, J. L., Crofcheck, C., Tackett, S. A.,Santillan- Jimenez, E., Morgan, T., Ji, Y., Crocker, M. & Toops,T. J. (2008).Biodiesel synthesis using calcined layered double hydroxide catalysts.*Appied Catalysis B: Environmental*, *82*(1), 120-130.

Shuit, S.H., Lee, K.T., Kamaruddin, A.H. & Yusup, S. (2010). Reactive extraction of *Jatropha curcas* seed for production of biodiesel. *Process Optimization Study*, 4361–4367.

Siano, D., Nastasi, M., Santacesaria, E., Di Serio, M., Tesser, R., Minutillo, G., Ledda, M. & Tenore, T. (2006). Process for producing esters from vegetable oils and animal fats by using heterogeneous catalysts. *WO 5*(1), 09 - 25.

Silmara B. S.,Marcio A. M., Ana L. C., Paulo Rafael M. A.& Jane Sélia dos R. C. (2015). Kinetics and thermodynamics of oil extraction from Jatropha curcas using ethanol as a solvent. *International Journal of Chemical Engineering*, Article ID 871236, http://dx.doi.org/10.1155/2015/871236.

Singh, S.P. & Singh, D. (2010). Biodiesel production through the use of different sources and characterization of oils and their esters as the substitute of diesel, a review. *Renewable and Sustainable Energy Reviews, 14*(1), 200-216.

Singh, J. & Gu, S. (2010). Commercialization potential of microalgae for biofuel production. *Renewable and sustainable Energy Reviews*, *14*(9), 2596-2610.

Sivaraosa, K.R., Milkey, A.R., Samsudin, A. K., & Dubey, P. K. (2014). Comparison between Taguchi method and response surface methodology (RSM) in modelling CO_2 laser machining. *Jordan Journal of Mechanical and Industrial Engineering,8*(1), 1995 – 665.

Soetaredjo, F. E., Ayucitra, A., Ismadji, S. & Maukar, A. L. (2011). KOH/bentonite catalysts for transesterification of palm oil to biodiesel. *Applied Clay Science, 53*, 341-346.

Song, J. T. & Zhang, C. H. (2008) An experimental study on the performance and exhaust emissions of a diesel engine fuelled with soybean oil methyl ester. *P I Mech Eng D-J Aut, 222*,2487– 2496.

Sonntag, A. (2012). Reaction of fats and fatty acids In Balley's industrial oil and fat Products, New York: John Willey and Sons.

Srivastava, A.& Prasad, R. (2000). Triglycerides-based diesel fuels. *Renewable and Sustainable Energy Review*, *4*(2), 111–133.

Sulaiman, S., Abdul Aziz, A. R. & Aroua, M. K. (2013). Optimization and modeling of extraction of solid coconut waste oil. *Journal of Food Engineering, 114*(2), 228–234.

Supamathanon, N., Wittayakun, J. &Prayoonpoka, S. (2011). Properties of *jatropha* seed oil from Northeastern Thailand and its transesterification catalyzed by potassium supported on NaY zeolite. *Journal of Industrial and Engineering Chemistry,17*(2), 182-185.

Supareak, S., Wongmaneenil, P. &Jongsomjit, B.(2010). Investigation of different modifiers for nanocrystal zirconia on W/ZrO2 catalysts via esterification. *Journal of Industrial & Engineering Chemistry*, *16*, 935-940.

Suppes, G. J., Dasari, M. A., Doskocil, E. J., Mankidy, P. J. & Goff, M. J. (2004). Transesterification of soybean oil with zeolite and metal catalysts. *Applied Catalysis, A, 257*, 213 - 221.

Sunil, K., Jasvinder S., Nanoti, S. M. & Garg, M. O.(2012). A comprehensive life cycle assessment (LCA) of jatropha biodiesel production in India. *Bioresource Technology, 110,* 723-729.

Surbhi, S., Ajay, K. A., Rajendra, P. B.&Deepak, K. T. (2011). Biodiesel production using heterogeneous catalysts. *Bioresource Technology*, *102* (3), 2151-2161.

Sureshkumara, K., Velraj, R. & Ganesana, R. (2008). Performance and exhaust emission characteristics of a CI engine fuelled with *pongamia pinnata* methyl ester (PPME) and its blends with diesel. *Renewable Energy,33,* 2294-2302.

Szczesna A. M., Kubiak, A., Antcza, T. & Bieleck, S., (2009). Enzymatic biodiesel synthesis – Key factors affecting efficiency of process. *Renewable Energy, 34*, 1185-1194.

Szulczyk, K.R. &McCarl,B.A. (2010).Market penetration of biodiesel.*Renewable and Sustainable Energy Reviews,14*(8), 2426-2433.

Tan, T., Lu, J., Nie, K., Deng, L.& Wang, F. (2010). Biodiesel production with immobilized lipase: A review.*Biotechnology Advancement, 28*(5), 628-634.

Thiam, L. C. &Bhatia, S. (2008). Catalytic processes towards the production of biofuels in a palm oil and oil palm biomass-based bio-refinery. *Bioresources Technology, 99*, 7911-7922.

Tiwari, A. K., Kumar, A. &Raheman, H. (2007). Biodiesel production from jatropha oil (*Jutropha curcas*) with high free fatty acids: an optimized process. *Biomass Bioenergy, 31*(8), 569-575.

Tse-Ming, H., Senniang, C., Enruo, G., Chih- Hsiang, T., Marek, P. & Lin, V. Y. S (2010). Calcium containing silicate mixed oxide-based heterogeneous catalysts for biodiesel production. *Topics in Catalysis, 53*(11-12), 746-754.

Ude, C. N., Onukwuli, O. D., Nwobi –Okoye, C., Anisiji, O. E., Atuanya, C. U. & Menkiti, M. C. (2017). Performance evaluation of cottonseed oil methyl esters produced using CaO and prediction with an artificial neural network.*Biofuels*, DOI: 10.1080/17597269.2017.1345355.

Uma, B. H.& Kim, Y.S. (2009).A chance for Korea to advance algal-biodiesel technology Review: *Journal of Industrial and Engineering Chemistry,15*, 1-7.

Umer, R. Anwara, F., Moser, B.R.& Ashrafa, S. (2008). Production of sunflower oil methyl esters by optimized alkali-catalyzed methanolysis.*Biomass Bioenergy, 32*(12), 1202-1205.

Umoti, U. & Okyi, D. A.(1987). Characteristics and composition of oil and cake of African pear. *Journal of Science, Food and Agriculture,38,* 67 – 72.

Usta, N. (2005) Use of tobacco seed oil methyl ester in a turbocharged indirect injection diesel engine. *Biomass & Bioenergy, 28*, 77–86.

Usta, N., Ozturk, E., Can, O., Conkur, E. S., Nas, S. & Con, A. H. (2005) Combustion of biodiesel fuel produced from hazelnut soapstock/waste sunflower oil mixture in a diesel engine. *Energy Conversion & Management, 46*, 741– 755.

Utlu, Z., Kocak, M. S. (2008) The effect of biodiesel fuel obtained from waste frying oil on direct injection diesel engine performance and exhaust emissions. *Renewable Energy, 33*, 1936–1941.

Uzoh, F. C. & Onukwuli, D. O. (2014).Extraction and characterization of gmelinaseed oil; Kinetics and optimization studies. *Open Journal of Chemical Engineering and Science, 1*(2), 1-18.

Van Gerpen, J., Shanks, B., Pruszko, R., Clements, D. &Knothe, G.(2004). Biodiesel Production Technology, NREL/SR-510- 36244 August 2002–January 2004.

Veeraprasad, G.& Srinivas I.(2012). The ethanolosis of *Pongamia pinnata* oil by a Two-stage Acid-base catalyst transesterification process for production of biodiesel. *Energy Sources, Part A: Recovery, Utilization, and Environmental Effects*, *34*(16), 1550-1558.

Verma, P., Sharma, M.P., Dwivedi, G.(2016). Evaluation and enhancement of cold flow properties of palm oil and its biodiesel. *Energy Reproduction, 2*, 8–13.

Vijayakumar, B., Iyengar, P., Nagendrappa, G.,& Prakash, B. S. J. (2005). An eco-friendly method for the synthesis of aryl and alkyl esters of carboxylic acids using acid activated Indian bentonite , *Journal of Indian ChemicalSociety,82***,** 922-925.

Vicente G., Martinez M., Aracil J. & Esteban A. (2005b). Kinetics of sunflower oil methanolysis. *Industrial Engineering and Chemistry Research,44*, 5447-5454.

Vicente, G., Martinez, M. &Aracil, J. (2004).Integrated biodiesel production: A comparison of different homogeneous catalysts systems. *Bioresource Technology*, *92*(3), 297-305.

Wang, Y., Ou, S., Liu, P. &Zhang, Z.(2007). Preparation of biodiesel from waste cooking oil via two step catalyzed process. *Energy Conversion and Management, 48*, 184-188.

Wang, L. Y. &Yang, J. C.(2007). Transesterification of soybean oil with nano-MgO or not in supercritical and subcritical methanol. *Fuel*, *86*(3), 328-333.

Watanabe, Y., Shimada, Y., Sugihara, A., Noda, H., Hideki, F. & Tominaga, Y. (2000). Continuous production of biodiesel fuel from vegetable oil using immobilized *Candida antarctica* lipase. *Journal of the American Oil Chemists' Society*, *77*(4), 335-360.

Wen, Z., Yu, X., Tu, S. T., Yan, J. &Dahlquist, E. (2010). Synthesis of biodiesel from vegetable oil with methanol catalyzed by Li-doped magnesium oxide catalysts. *Applied Energy, 87*(3), 743-748.

Willis, R. D., Blanchard, F. T. & Connor, T. L. (2002). *Guidelines for the Application of SEM/EDX Analytical Techniques to Particulate Matter Samples*.U.S. Environmental Protection Agency #600/R-02/070.

Wongmaneenil, P., Bunjerd,J.& Piyasan, P, (2010). Solvent effect on synthesis of zirconia support for tungstated zirconia catalysts. *Journal of Industrial and Engineering Chemistry*, *16*(3), 327-333.

Xie, W., Peng, H. &Chen, L.(2006). Calcined Mg-Al hydrotalcites as solid base catalysts for methanolysis of soybean oil.*Journal of Molecular Catalysis A: Chemical*,*246*(1-2), 24-32.

Younis, M. N., Saeed, M. S., Khan, S., Furqan, M. U., Khan, R. U. & Saleem, M.(2009). Production and characterization of biodiesel, from waste and vegetable oils. *Journal of Quality and Technology Management, 5*(1), 111-121.

Zatta, L., Ramos, L. P. & Wypych, F. (2013). Acid-activated montmorillonites as heterogeneous catalysts for the esterification of lauric acid withmethanol. *Applied Clay Science*, *80–81*, 236–244.

Zabeti, M., Daud, W.M.A.W.& Aroua,M.K. (2009). Optimization of the activity of CaO/Al2O3 catalyst for biodiesel production using response surface methodology. *Fuel*,*366*, 154-159.

Zabeti, M., Daud, W.M.A.W.& Aroua,M.K. (2009).Activity of solid catalysts for biodiesel production: a review. *Fuel Processing Technology, 90*, 770-777.

Zabeti, M., Daud, W. M. A. W. &Aroua,M. K. (2010). Biodiesel production using alumina supported calcium oxide: an optimization study. *Fuel Processing Technology*, 91(2), 243–248.

Zeng, H. Y., Feng, Z., Deng, X.& Li, Y. Q. (2008). Activation of Mg-Al hydrotalcite catalysts for transesterification of rape oil. *Fuel*,*87*(13-14), 3071-3076.

Zhang,Y., Dube, M. A., McLean, D. D. & Kates, M.(2003). Biodiesel production from waste cooking oil: 2. Economic assessment and sensitivity analysis. *Bioresource Technology*, *90*, 229–40.

Zhang, Y., Dube, M. A., McLean, D. D. &Kates, M. (2003). Biodiesel production from waste cooking oil: 1. Process design and technological assessment.*Bioresources Technology*, *89*(1), 1-16.

Zullaikah,S., Lai, C., Vali, S.R.&Ju, Y.(2005). A two-step acid-catalyzed process for the production of biodiesel from rice bran oil. *Bioresource Technology*, *96*(17), 1889-1896.

Appendix A

Optimization of oil extraction

Table A: Design matrix result of oil extraction

A	B	C	D	E	$Y_{APO\ by\ n\text{-}hex}$	$Y_{GSO\ by\ n\text{-}hex}$	$Y_{APO\ by\ PE}$	$Y_{GSO\ by\ PE}$
1.0	30	40	0.40	250	38.0	37.0	39.0	30.0
2.0	30	40	0.40	150	40.0	32.5	42.5	32.0
1.0	60	40	0.40	150	37.0	27.8	42.4	33.0
2.0	60	40	0.40	250	38.0	28.5	35.0	31.0
1.0	30	60	0.40	150	45.0	37.0	37.0	34.0
2.0	30	60	0.40	250	47.0	30.0	37.2	34.5
1.0	60	60	0.40	250	38.0	32.0	36.5	32.0
2.0	60	60	0.40	150	40.0	33.5	39.0	36.0
1.0	30	40	0.70	150	40.3	33.0	37.0	34.0
2.0	30	40	0.70	250	40.8	35.0	41.0	38.0
1.0	60	40	0.70	250	43.5	36.0	40.0	37.0
2.0	60	40	0.70	150	42.0	31.5	41.0	39.0
1.0	30	60	0.70	250	37.0	28.0	36.3	31.0
2.0	30	60	0.70	150	40.5	33.0	38.0	32.0
1.0	60	60	0.70	150	37.0	29.0	39.5	33.0
2.0	60	60	0.70	250	39.5	33.0	45.0	39.0
0.5	45	50	0.55	200	45.0	40.0	41.5	38.0
2.5	45	50	0.55	200	48.0	39.0	44.2	43.0
1.5	15	50	0.55	200	41.0	34.5	42.0	33.0
1.5	75	50	0.55	200	38.0	31.0	45.0	37.0
1.5	45	30	0.55	200	45.0	40.0	42.5	39.0
1.5	45	70	0.55	200	46.0	38.0	40.0	38.0
1.5	45	50	0.25	200	43.0	35.5	41.0	37.0
1.5	45	50	0.85	200	43.0	35.0	44.0	42.0
1.5	45	50	0.55	100	40.0	32.0	39.0	32.0
1.5	45	50	0.55	300	39.0	32.5	37.5	32.0
1.5	45	50	0.55	200	53.0	49.0	52.0	52.0
1.5	45	50	0.55	200	53.5	49.0	51.0	50.0
1.5	45	50	0.55	200	53.0	51.0	50.0	51.0
1.5	45	50	0.55	200	54.0	52.0	51.0	50.0
1.5	45	50	0.55	200	53.0	51.0	52.0	49.0

Appendix B

Kinetics of oil Extraction

Table B1: Kinetics of oil at 30^{o}C

S/N	Time (Minutes)	$Y_{(APO)}$ n-hexane	ln $Y_{(APO)}$ n-hexane	$Y_{(GSO)}$ n-hexane	ln $Y_{(GSO)}$ n-hexane	$Y_{(APO)}$ petroleum ether	ln $Y_{(APO)}$ petroleum ether	$Y_{(GSO)}$ petroleum ether	ln $Y_{(GSO)}$ petroleum ether
1	20	35	3.56	27	3.30	33	3.50	25	3.22
2	30	40	3.67	30	3.40	38	3.64	28	3.33
3	40	42	3.74	35	3.56	40	3.69	31	3.43
4	50	44	3.78	36	3.58	42	3.74	33	3.50
5	60	45	3.81	38	3.64	43	3.76	34	3.53

Table B2: Kinetics of oil at 40^{o}C

S/N	Time (Minutes)	$Y_{(APO)}$ n-hexane	ln $Y_{(APO)}$ n-hexane	$Y_{(GSO)}$ n-hexane	ln $Y_{(GSO)}$ n-hexane	$Y_{(APO)}$ petroleum ether	ln $Y_{(APO)}$ petroleum ether	$Y_{(GSO)}$ petroleum ether	ln $Y_{(GSO)}$ petroleum ether
1	20	38	3.64	30	3.40	35	3.56	28	3.33
2	30	41	3.71	33	3.50	39	3.66	30	3.40
3	40	44	3.78	36	3.58	41	3.71	32	3.47
4	50	44	3.78	36.5	3.60	42	3.74	34	3.53
5	60	44	3.78	37	3.61	43	3.76	35	3.56

Table B3: Kinetics of oil at 50^{o}C

S/N	Time (Minutes)	$Y_{(APO)}$ n-hexane	ln $Y_{(APO)}$ n-hexane	$Y_{(GSO)}$ n-hexane	ln $Y_{(GSO)}$ n-hexane	$Y_{(APO)}$ petroleum ether	ln $Y_{(APO)}$ petroleum ether	$Y_{(GSO)}$ petroleum ether	ln $Y_{(GSO)}$ petroleum ether
1	20	40	3.69	31	3.43	36	3.58	30	3.40
2	30	42	3.74	34	3.53	40	3.69	32	3.47
3	40	45	3.81	36	3.58	43	3.76	33	3.50
4	50	46	3.83	37	3.61	44	3.78	35	3.56
5	60	46	3.83	37	3.61	45	3.81	38	3.64

Table B4: Activation energy determination

Oil/solvent	Temperature, T (K)	1/T (1/K)	k(min^{-1})	Lnk
APO n-hexane	303	0.0033	0.006	-5.12
	313	0.0032	0.003	-5.81
	323	0.0031	0.003	-5.81
GSO n-hexane	303	0.0033	0.008	-4.83
	313	0.0032	0.005	-5.30
	323	0.0031	0.004	-5.52
APO petroleum ether	303	0.0033	0.006	-5.12
	313	0.0032	0.005	-5.30
	323	0.0031	0.005	-5.30
GSO petroleum ether	303	0.0033	0.007	-4.96
	313	0.0032	0.005	-5.30
	323	0.0031	0.005	-5.30

Table B5: Activation energy value

Oil/Solvent	Ea (kJ/mol)	Arrhenius constant, A
APO n-hexane	28.68	235
GSO n-hexane	28.68	340
APO petroleum ether	7.48	0.094
GSO petroleum ether	14.13	1.29

Thermodynamics determination

$$K = \frac{Y_{Le}}{Y_{Se}} = \frac{45}{32.07} = 1.4$$

Table B6: Thermodynamics parameter determination

Oil/solvent	Temperature, T (K)	1/T (1/K)	Y_{Se}	K	lnK
APO n-hexane	303	0.0033	32.07	1.40	0.336
	313	0.0032	36.53	1.20	0.182
	323	0.0031	37.8	1.22	0.199
GSO n-hexane	303	0.0033	23.38	1.20	0.457
	313	0.0032	27.94	1.32	0.278
	323	0.0031	29.25	1.58	0.182
APO petroleum ether	303	0.0033	30.51	1.41	0.344
	313	0.0032	32.92	1.31	0.270
	323	0.0031	33.03	1.36	0.307
GSO petroleum ether	303	0.0033	21.89	1.55	0.438
	313	0.0032	25.08	1.40	0.336
	323	0.0031	26.7	1.42	0.351

Appendix C

FTIR and GCMS characterization results

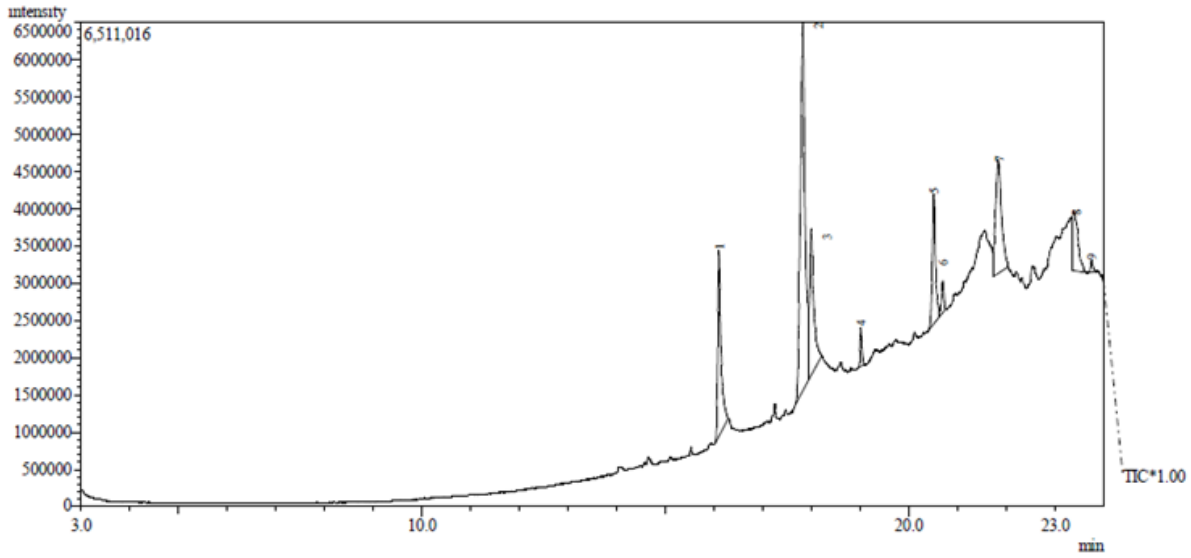

Figure C1: GC-MS of African Pear Seed Oil (*D. edulis*).

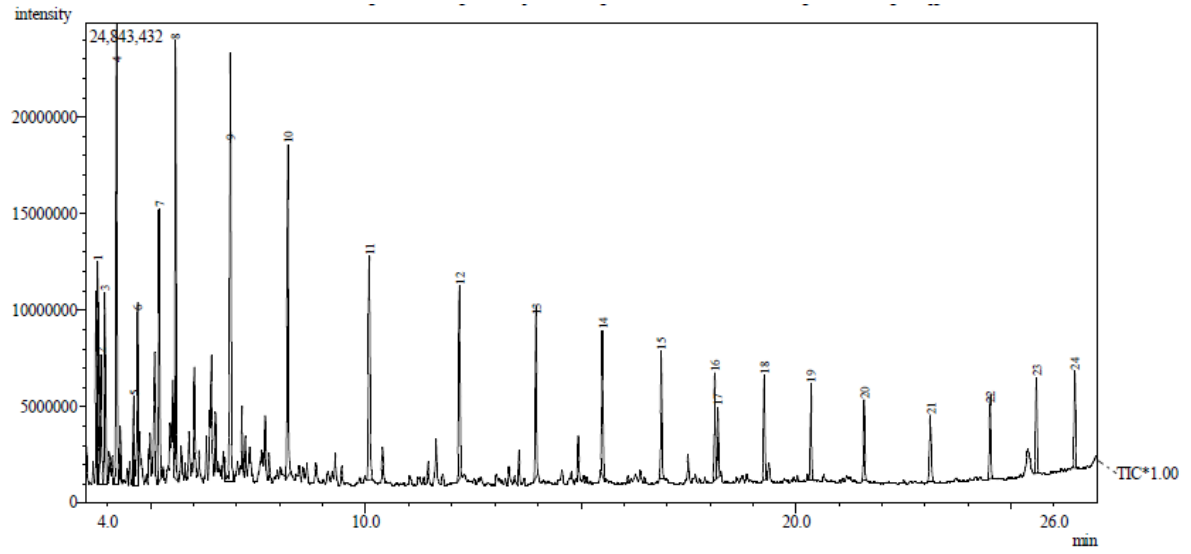

Figure C2: GC-MS of Gmelina seed oil.

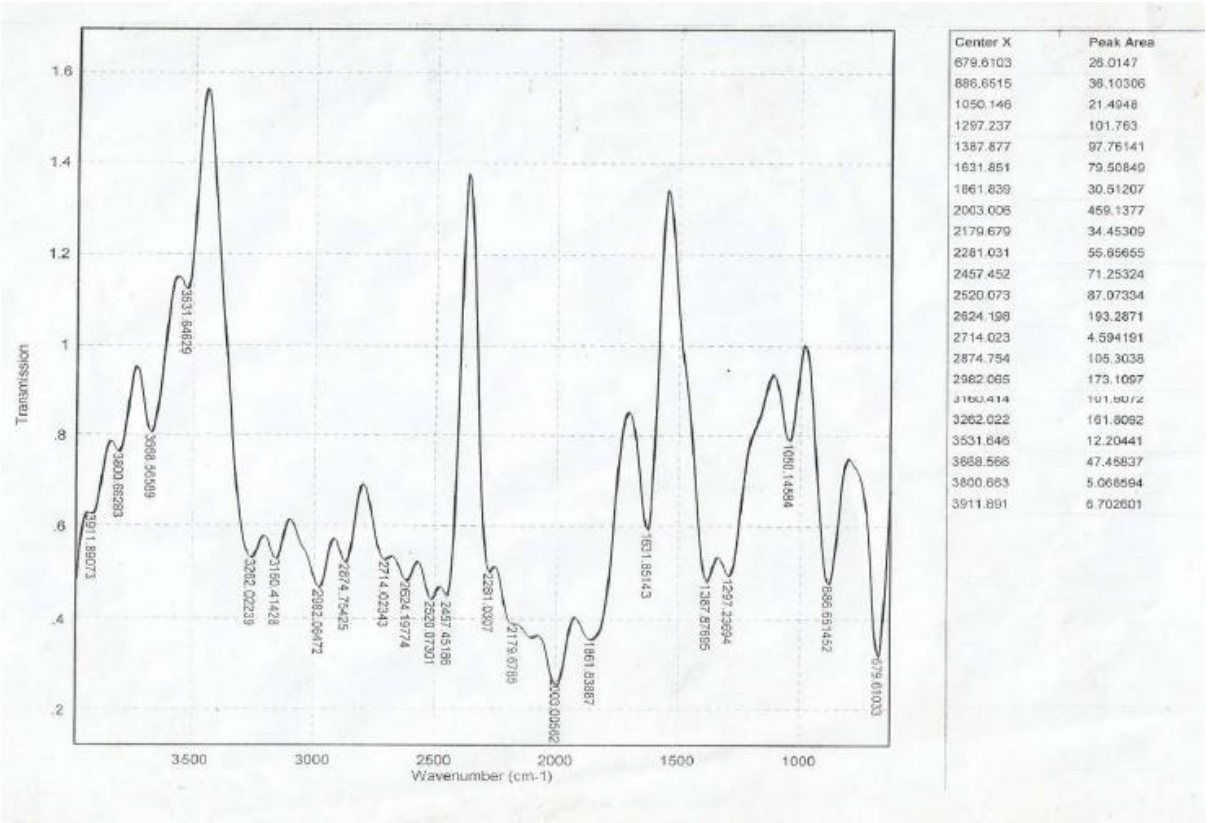

Center X	Peak Area
679.6103	26.0147
886.6515	38.10306
1050.146	21.4948
1297.237	101.763
1387.877	97.76141
1631.851	79.50849
1861.839	30.51207
2003.006	459.1377
2179.679	34.45309
2281.031	55.85655
2457.452	71.25324
2520.073	87.07334
2624.198	193.2871
2714.023	4.594191
2874.754	105.3038
2982.065	173.1097
3160.414	161.8092
3262.022	12.20441
3531.646	47.46837
3688.566	5.068594
3800.663	6.702601
3911.891	

Figure C3: FTIR spectrum of African pear seed oil (*D.edulis*).

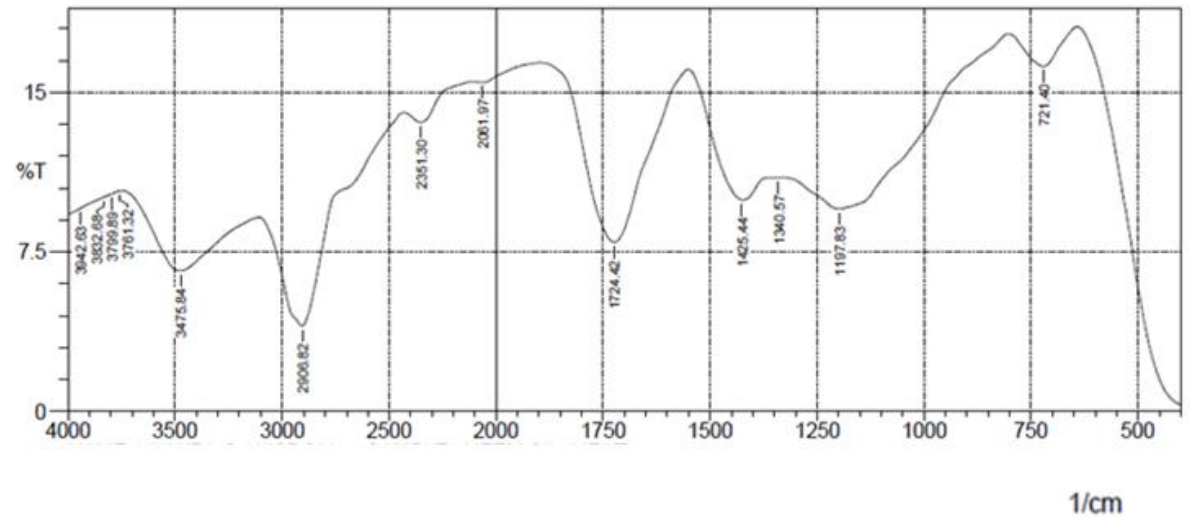

Figure C4: FTIR spectrum of Gmelina seed oil.

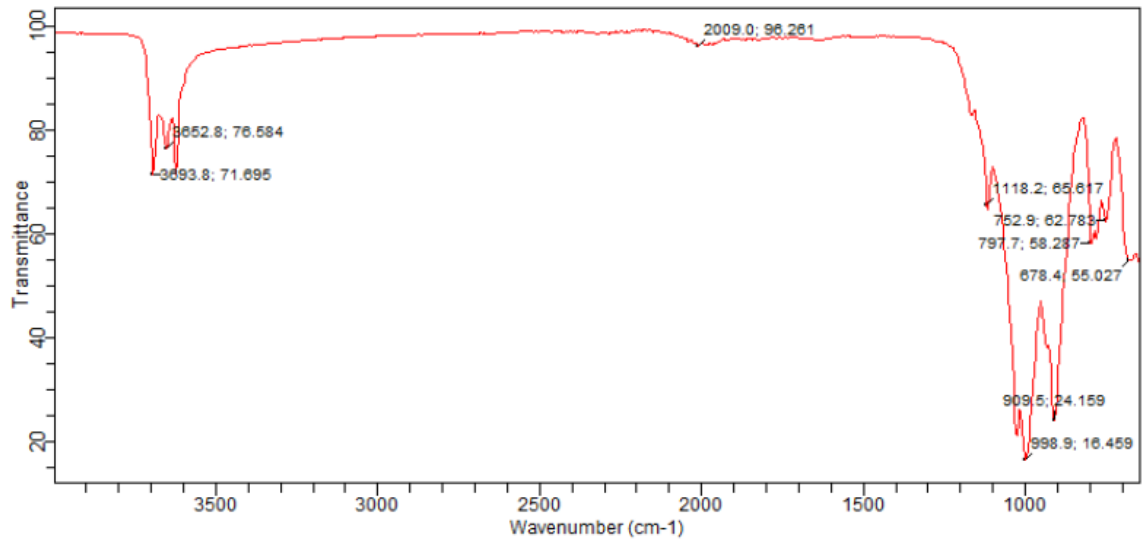

Figure C5: FTIR of raw clay

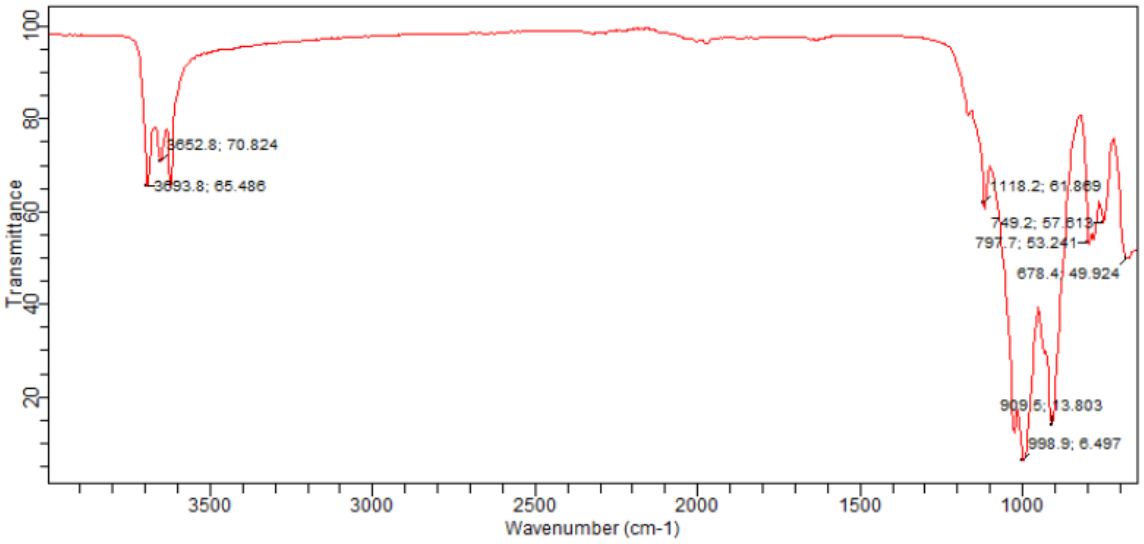

Figure C6: FTIR of thermally activated clay (TAC) catalyst.

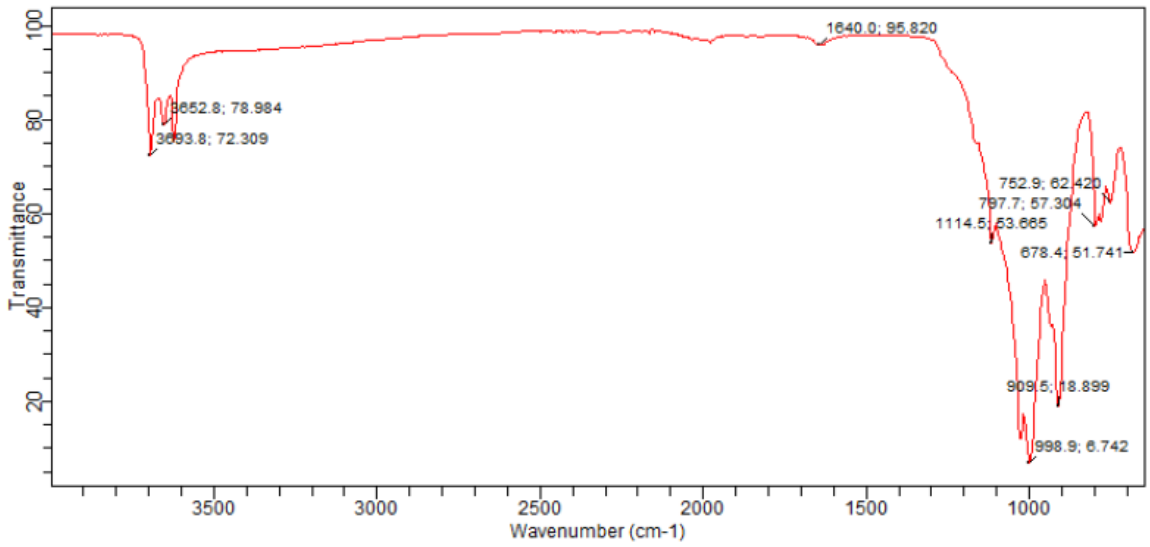

Figure C7: FTIR of acid activated clay (AAC) catalyst.

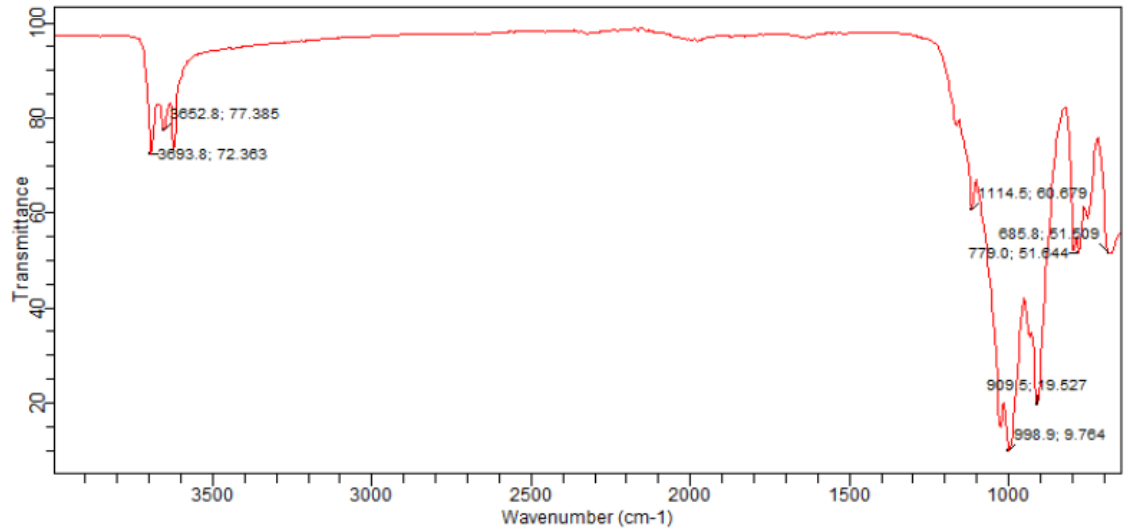

Figure C8: FTIR of base/alkaline activated clay (BAC) catalyst.

Appendix D

XRF result of clay catalyst

Table D1: XRF of raw clay

Oxford Instruments

OPERATOR: INSTRUMENT MANAGER

SAMPLE: CLAY RAW

ANALYSED: 25/09/2017 4:49:03 AM

Analysis Method: Minerals (2)

Analyte Concentration Table

Element	Concentration
Na2O	0.000 Wt %
MgO	0.321 Wt %
Al2O3	23.123 Wt %
SiO2	57.115 Wt %
P2O5	0.310 Wt %
SO3	0.246 Wt %
Cl	0.018 Wt %
K2O	0.080 Wt %
CaO	0.756 Wt %
TiO2	4.217 Wt %
Cr2O3	0.028 Wt %
Mn2O3	0.055 Wt %
Fe2O3	13.682 Wt %
ZnO	0.023 Wt %
SrO	0.025 Wt %

Table D2: XRF of thermally activated clay

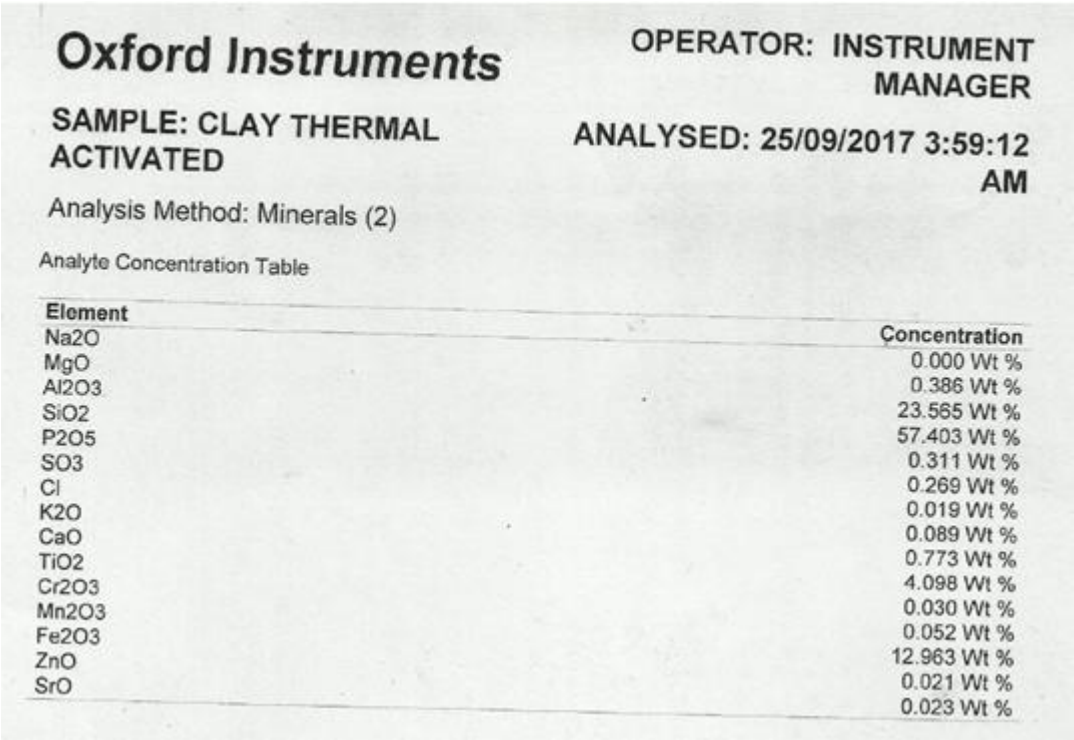

Oxford Instruments

OPERATOR: INSTRUMENT MANAGER

SAMPLE: CLAY THERMAL ACTIVATED

ANALYSED: 25/09/2017 3:59:12 AM

Analysis Method: Minerals (2)

Analyte Concentration Table

Element	Concentration
Na2O	0.000 Wt %
MgO	0.386 Wt %
Al2O3	23.565 Wt %
SiO2	57.403 Wt %
P2O5	0.311 Wt %
SO3	0.269 Wt %
Cl	0.019 Wt %
K2O	0.089 Wt %
CaO	0.773 Wt %
TiO2	4.098 Wt %
Cr2O3	0.030 Wt %
Mn2O3	0.052 Wt %
Fe2O3	12.963 Wt %
ZnO	0.021 Wt %
SrO	0.023 Wt %

Table D3: XRF of acid activated clay

Oxford Instruments

OPERATOR: INSTRUMENT MANAGER

SAMPLE: CLAY ACID ACTIVATED

ANALYSED: 25/09/2017 4:41:09 AM

Analysis Method: Minerals (2)

Analyte Concentration Table

Element	Concentration
Na2O	0.000 Wt %
MgO	0.326 Wt %
Al2O3	27.642 Wt %
SiO2	64.556 Wt %
P2O5	1.118 Wt %
SO3	0.303 Wt %
Cl	0.010 Wt %
K2O	0.122 Wt %
CaO	0.024 Wt %
TiO2	3.606 Wt %
Cr2O3	0.029 Wt %
Mn2O3	0.013 Wt %
Fe2O3	2.230 Wt %
ZnO	0.003 Wt %
SrO	0.019 Wt %

Table D4: XRF of base/alkaline activated clay

Oxford Instruments

OPERATOR: INSTRUMENT MANAGER

SAMPLE: CLAY BASE ACTIVATED

ANALYSED: 25/09/2017 4:24:29 AM

Analysis Method: Minerals (2)

Analyte Concentration Table

Element	Concentration
Na2O	0.163 Wt %
MgO	0.235 Wt %
Al2O3	25.743 Wt %
SiO2	67.197 Wt %
P2O5	0.286 Wt %
SO3	0.343 Wt %
Cl	0.017 Wt %
K2O	0.114 Wt %
CaO	0.020 Wt %
TiO2	3.644 Wt %
Cr2O3	0.028 Wt %
Mn2O3	0.014 Wt %
Fe2O3	2.178 Wt %
ZnO	0.002 Wt %
SrO	0.017 Wt %

Appendix E

Determination of best condition for synthesis of clay catalyst using biodiesel yield

Conditions: Catalyst conc. = 3wt%, time = 3 hours, temperature = 55oC, speed of agitation = 300rpm, methanol/oil molar ratio = 10:1.

Volume of oil used = 50ml

Yield of biodiesel = $\frac{Volume\ \ of\ biodiesel\ \ produced}{volume\ \ of\ oil\ used} * 100\ = \frac{32.5}{50} * 100 = 65\%$

Table E1: Thermal activation of clay

S/N	Activation Temperature (^oC)	Volume of biodiesel in African seed oil (ml)	Yield of biodiesel in African seed oil (%)	Volume of biodiesel in Gmelina seed oil (ml)	Yield of biodiesel in Gmelina seed oil (%)
1	500	32.5	65	30	60
2	600	35	70	32.5	65
3	700	41	80	38	76
4	800	37.5	75	36.5	73
5	900	36	72	33.5	67
6	1000	34	68	32	64

Table E2: Acid activation of clay

S/N	Clay to H_3PO_4 (Acid) ratio (g/ml)	Volume of biodiesel in African seed oil (ml)	Yield of biodiesel in African seed oil (%)	Volume of biodiesel in Gmelina seed oil (ml)	Yield of biodiesel in Gmelina seed oil (%)
1	1:1	35	70	34	68
2	1:2	37.5	75	36	72
3	1:3	39.5	79	38	76
4	1:4	41	82	40	80
5	1:5	38	76	37.5	75

Table E3: Base/Alkaline activation of clay

S/N	Clay to NaOH (Alkaline) ratio (g/ml)	Volume of biodiesel in African seed oil (ml)	Yield of biodiesel in African seed oil (%)	Volume of biodiesel in Gmelina seed oil (ml)	Yield of biodiesel in Gmelina seed oil (%)
1	1:1	31.5	63	29	58
2	1:2	34	68	32.5	65
3	1:3	37	74	34	70
4	1:4	35	70	35	69
5	1:5	33	66	32	64

Appendix F

Effect of process parameter on biodiesel yield by heterogeneous catalysts

Effect of time

Table F1: Effect of time on African pear seed oil FAME Yield

Conditions: Catalyst conc. = 3wt%, temperature = 55^{o}C, speed of agitation = 300rpm, methanol/oil molar ratio = 12:1.

Runs	Time (hour)	Volume of biodiesel by NAC (ml)	Volume of biodiesel by TAC (ml)	Volume of biodiesel by AAC (ml)	Volume of biodiesel by BAC (ml)	Yield of biodiesel by NAC (%)	Yield of biodiesel by TAC (%)	Yield of biodiesel by AAC (%)	Yield of biodiesel by BAC (%)
1	1	6	18	19.2	17.4	20	60	64	58
2	2	9.6	20.4	21.0	19.5	32	68	70	65
3	3	11.1	21.3	22.8	20.7	40	75	77	72
4	4	12	22.5	24.0	21.6	37	71	75	69
5	5	10.5	21	21.9	20.1	35	70	73	67

NB: NAC = non activated clay, TAC = thermally activated clay, AAC = acid activated clay, BAC = Base/alkaline activated clay.

Table F2: Effect of time on Gmelina seed oil FAME yield

Conditions: Catalyst conc. = 3wt%, temperature = 55^{o}C, speed of agitation = 300rpm, methanol/oil molar ratio = 12:1.

Runs	Time (hour)	Volume of biodiesel by NAC (ml)	Volume of biodiesel by TAC (ml)	Volume of biodiesel by AAC (ml)	Volume of biodiesel by BAC (ml)	Yield of biodiesel by NAC (%)	Yield of biodiesel by TAC (%)	Yield of biodiesel by AAC (%)	Yield of biodiesel by BAC (%)
1	1	5.7	19.2	18.0	15.9	19	64	60	53
2	2	6.6	20.7	19.2	17.4	22	69	64	58
3	3	8.4	23.1	21.0	19.2	28	77	70	64
4	4	7.5	21.6	20.1	18.0	25	72	67	60
5	5	6.3	20.4	18.6	16.5	21	68	62	55

Effect of catalyst concentration

Table F3: Effect of catalyst concentration on African pear seed oil FAME Yield

Conditions: Temperature = 55^{o}C, speed of agitation = 300rpm, methanol/oil molar ratio = 12:1, time = 3h.

Runs	Catalyst conc.(wt%) /wt (g)	Volume of biodiesel by NAC (ml)	Volume of biodiesel by TAC (ml)	Volume of biodiesel by AAC (ml)	Volume of biodiesel by BAC (ml)	Yield of biodiesel by NAC (%)	Yield of biodiesel by TAC (%)	Yield of biodiesel by AAC (%)	Yield of biodiesel by BAC (%)
1	1(0.279)	6.3	16.8	18.0	17.4	21	58	60	56
2	2(0.558)	8.4	19.2	21.9	20.4	28	68	73	64
3	3(0.837)	9.9	21.0	23.4	21.9	33	73	78	70
4	4(1.116)	9.0	20.1	21.3	21.0	30	70	71	67
5	5(1.395)	7.8	18.6	19.8	19.5	26	65	66	62

NB: NAC = non activated clay, TAC = thermally activated clay, AAC = acid activated clay, BAC = Base/alkaline activated clay.

Table F4: Effect of catalyst conc on Gmelina seed oil FAME yield

Conditions: Temperature = 55^{o}C, speed of agitation = 300rpm, methanol/oil molar ratio = 12:1, time = 3h.

Runs	Catalyst conc. (wt%)/ wt(g)	Volume of biodiesel by NAC (ml)	Volume of biodiesel by TAC (ml)	Volume of biodiesel by AAC (ml)	Volume of biodiesel by BAC (ml)	Yield of biodiesel by NAC (%)	Yield of biodiesel by TAC (%)	Yield of biodiesel by AAC (%)	Yield of biodiesel by BAC (%)
1	1(0.279)	6.0	16.8	18.6	19.5	20	56	62	56
2	2(0.558)	6.9	18.0	19.8	20.7	23	60	66	60
3	3(0.837)	8.7	18.9	21.3	22.5	29	63	71	63
4	4(1.116)	7.8	17.4	20.7	21.3	26	58	69	58
5	5(1.395)	6.3	15.9	19.5	20.1	21	57	65	57

Effect of methanol/oil molar ratio

Wt of oil used= 30 * 0.938 = 28.14g

Wt of Methanol= $\frac{6*32*28.14}{868.8}$ = 6.22g (using methanol/oil molar ratio of 6:1)

Average Molecular weight of African seed oil = [(2.52 * 214.3) + (3.148 * 228.3) + (10.88 * 294.48) + (74.78 * 296) + (8.105 * 266.43) + (0.567 * 290)] * $\frac{1}{100}$ = 289.6

Molecular weight of African seed oil = 3 * average molecular weight = 3 * 289.6 = 868.8

Volume of Methanol= $\frac{6.22}{0.7914}$ = 7.9ml

Table F5: Effect of methanol/oil molar ratio on African pear seed oil FAME Yield
Conditions: Temperature = 55^{o}C, speed of agitation = 300rpm, catalyst conc. = 3wt%, time = 3h.

Runs	Methanol/oil molar ratio (mol/mol)/ volume of methanol (ml)	Volume of biodiesel by NAC (ml)	Volume of biodiesel by TAC (ml)	Volume of biodiesel by AAC (ml)	Volume of biodiesel by BAC (ml)	Yield of biodiesel by NAC (%)	Yield of biodiesel by TAC (%)	Yield of biodiesel by AAC (%)	Yield of biodiesel by BAC (%)
1	6:1(7.9)	6.0	18.0	18.9	17.1	22	60	63	57
2	8:1(10.5)	8.4	19.5	20.4	18.9	28	65	68	63
3	10:1(13.1)	9.3	21.6	22.5	20.7	31	72	75	72
4	12:1(15.7)	7.8	20.4	21.3	19.8	26	68	71	68
5	14:1(18.3)	6.6	19.2	20.1	18.0	22	64	67	64

NB: NAC = non activated clay, TAC = thermally activated clay, AAC = acid activated clay, BAC = Base/alkaline activated clay.

Wt of oil used= 30 * 0.895 = 26.85g

Wt of Methanol= $\frac{6*32*26.85}{826.63}$ = 6.24g (using methanol/oil molar ratio of 6:1)

Average Molecular weight of Gmelina seed oil = [(1.72 * 160) + (8.62 * 228.3) + (14.84 * 240) + (38.78 * 296.51) + (14.15 * 266.43) + (12.75 * 298.51) + (6.82 * 292.51) + (0.64 * 290) + (1.67 *296)] * $\frac{1}{100}$ = 275.54

Molecular weight of Gmelina seed oil = 3 * average molecular weight = 3 * 275.54 = 826.63

Volume of Methanol= $\frac{6.24}{0.7914}$ = 7.9ml

Table F6: Effect of methanol/oil molar ratio on Gmelina seed oil FAME yield

Conditions: Temperature = 55^{o}C, speed of agitation = 300rpm, catalyst conc. = 3wt%, time = 3h.

Runs	Methanol/oil molar ratio (mol/mol)/ volume of methanol (ml)	Volume of biodiesel by NAC (ml)	Volume of biodiesel by TAC (ml)	Volume of biodiesel by AAC (ml)	Volume of biodiesel by BAC (ml)	Yield of biodiesel by NAC (%)	Yield of biodiesel by TAC (%)	Yield of biodiesel by AAC (%)	Yield of biodiesel by BAC (%)
1	6:1(7.5)	5.4	21.0	20.4	18.0	18	70	68	60
2	8:1(10.28)	7.2	22.2	21.3	18.9	24	74	71	63
3	10:1(12.85)	8.1	24.0	23.7	21.0	27	80	79	70
4	12:1(15.42)	7.5	22.8	22.2	19.8	25	76	74	66
5	14:1(17.99)	6.9	21.6	21.0	18.6	23	72	70	62

Effect of temperature

Table F7: Effect of temperature on African pear seed oil FAME Yield

Conditions: Speed of agitation = 300rpm, catalyst conc. = 3wt%, time = 3h, methanol/oil molar ratio = 10:1.

Runs	Temperature (^{o}C)	Volume of biodiesel by NAC (ml)	Volume of biodiesel by TAC (ml)	Volume of biodiesel by AAC (ml)	Volume of biodiesel by BAC (ml)	Yield of biodiesel by NAC (%)	Yield of biodiesel by TAC (%)	Yield of biodiesel by AAC (%)	Yield of biodiesel by BAC (%)
1	45	6.0	18.6	19.5	17.4	20	62	65	58
2	50	7.5	20.4	21.0	19.5	25	68	70	65
3	55	8.4	22.2	23.4	21.0	28	74	78	70
4	60	9.0	23.1	24.0	21.9	30	77	80	73
5	65	8.1	21.6	22.8	19.8	27	72	76	66
6	70	6.9	19.5	20.1	18.0	23	65	67	60

NB: NAC = non activated clay, TAC = thermally activated clay, AAC = acid activated clay, BAC = Base/alkaline activated clay.

Table F8: Effect of temperature on Gmelina seed oil FAME yield

Conditions: Speed of agitation = 300rpm, catalyst conc. = 3wt%, time = 3h, methanol/oil molar ratio = 10:1.

Runs	Temperature (^oC)	Volume of biodiesel by NAC (ml)	Volume of biodiesel by TAC (ml)	Volume of biodiesel by AAC (ml)	Volume of biodiesel by BAC (ml)	Yield of biodiesel by NAC (%)	Yield of biodiesel by TAC (%)	Yield of biodiesel by AAC (%)	Yield of biodiesel by BAC (%)
1	45	5.7	18.0	16.8	15.0	19	60	56	50
2	50	6.9	19.5	18.0	17.1	23	65	60	57
3	55	7.8	20.1	19.2	18.3	26	67	64	61
4	60	9.0	21.6	20.4	19.5	30	72	68	65
5	65	8.1	20.7	19.5	18.0	27	69	65	60
6	70	7.2	18.9	18.3	17.4	24	63	61	58

NB: NAC = non activated clay, TAC = thermally activated clay, AAC = acid activated clay, BAC = Base/alkaline activated clay.

Effect of agitation speed

Table F9: Effect of agitation speed on African pear seed oil FAME Yield

Conditions: Catalyst conc. = 3wt%, time = 3h, methanol/oil molar ratio = 10:1, temperature = 60^oC

Runs	Agitation speed (rpm)	Volume of biodiesel by NAC (ml)	Volume of biodiesel by TAC (ml)	Volume of biodiesel by AAC (ml)	Volume of biodiesel by BAC (ml)	Yield of biodiesel by NAC (%)	Yield of biodiesel by TAC (%)	Yield of biodiesel by AAC (%)	Yield of biodiesel by BAC (%)
1	100	6.9	18.3	19.8	17.1	23	61	66	57
2	200	8.7	20.4	21.0	19.5	29	68	70	65
3	300	9.9	21.6	23.1	20.4	33	72	77	68
4	400	7.8	21.0	22.2	19.8	26	70	74	66
5	500	6.3	19.2	20.4	18.0	21	64	68	60

NB: NAC = non activated clay, TAC = thermally activated clay, AAC = acid activated clay, BAC = Base/alkaline activated clay.

Table F10: Effect of speed of agitation on Gmelina seed oil FAME yield

Conditions: Catalyst conc. = 3wt%, time = 3h, methanol/oil molar ratio = 10:1, temperature = 60^{o}C.

Runs	Agitation speed (rpm)	Volume of biodiesel by NAC (ml)	Volume of biodiesel by TAC (ml)	Volume of biodiesel by AAC (ml)	Volume of biodiesel by BAC (ml)	Yield of biodiesel by NAC (%)	Yield of biodiesel by TAC (%)	Yield of biodiesel by AAC (%)	Yield of biodiesel by BAC (%)
1	100	6.3	20.1	18.9	18.0	21	67	63	60
2	200	7.5	21.3	20.7	19.2	25	71	69	64
3	300	8.4	23.4	22.8	21.0	28	78	76	70
4	400	7.8	22.5	21.6	20.4	26	75	72	68
5	500	6.9	21.6	21.0	19.5	23	72	70	65

NB: NAC = non activated clay, TAC = thermally activated clay, AAC = acid activated clay, BAC = Base/alkaline activated clay.

Appendix G

Optimization of biodiesel production using African pear oil

TAC = thermally activated clay catalyst, AAC = acid activated clay catalyst, BAC = base/alkaline activated clay catalyst,

Table G1: Design matrix result using heterogeneous catalysts

Run order	Catalyst conc. A	Methanol/ Oil molar ratio B	Temperature C	Time D	Agitation Speed E	Yield of FAME by TAC	Yield of FAME by AAC	Yield of FAME by BAC
	wt%	mol/mol	(^{o}C)	Hours	rpm	(%)	(%)	(%)
1	2	8	50	2	400	50	55	48
2	4	8	50	2	200	55	59	52
3	2	12	50	2	200	57	61	54
4	4	12	50	2	400	53	57	51
5	2	8	70	2	200	57	61	52
6	4	8	70	2	400	55	60	50
7	2	12	70	2	400	63	66	58
8	4	12	70	2	200	65	69	58
9	2	8	50	4	200	54	58	50
10	4	8	50	4	400	66	70	60
11	2	12	50	4	400	63	67	57
12	4	12	50	4	200	54	56	51
13	2	8	70	4	400	53	55	51
14	4	8	70	4	200	59	65	57
15	2	12	70	4	200	52	58	51
16	4	12	70	4	400	59	63	56
17	1	10	60	3	300	53	55	49
18	5	10	60	3	300	56	59	53
19	3	6	60	3	300	55	57	51
20	3	14	60	3	300	59	61	55
21	3	10	40	3	300	60	66	57
22	3	10	80	3	300	62	70	59
23	3	10	60	1	300	59	65	55
24	3	10	60	5	300	60	66	57
25	3	10	60	3	100	67	71	65
26	3	10	60	3	500	69	74	66
27	3	10	60	3	300	71	76	69
28	3	10	60	3	300	70	77	70
29	3	10	60	3	300	71	76	69
30	3	10	60	3	300	70	75	70
31	3	10	60	3	300	70	76	68.5
32	3	10	60	3	300	71	77	69

Table G2: Predicted and residual values for Yield of FAME by TAC

Run	FAME by TAC (%)	Predicted (%)	Resid	Std Resid
1	50.000	50.239	-0.239	-1.46
2	55.000	55.072	-0.072	-0.44
3	57.000	57.239	-0.239	-1.46
4	53.000	52.989	0.011	0.07
5	57.000	57.155	-0.155	-0.95
6	55.000	54.905	0.095	0.58
7	63.000	63.072	-0.072	-0.44
8	65.000	64.905	0.095	0.58
9	54.000	54.239	-0.239	-1.46
10	66.000	65.989	0.011	0.07
11	63.000	63.155	-0.155	-0.95
12	54.000	53.989	0.011	0.07
13	53.000	53.072	-0.072	-0.44
14	59.000	58.905	0.095	0.58
15	52.000	52.072	-0.072	-0.44
16	59.000	58.822	0.178	1.09
17	53.000	52.481	0.519	1.74
18	56.000	56.314	-0.314	-1.06
19	55.000	54.814	0.186	0.62
20	59.000	58.981	0.019	0.06
21	60.000	59.648	0.352	1.18
22	62.000	62.148	-0.148	-0.50
23	59.000	58.814	0.186	0.62
24	60.000	59.981	0.019	0.06
25	67.000	66.814	0.186	0.62
26	69.000	68.981	0.019	0.06
27	71.000	70.534	0.466	1.08
28	70.000	70.534	-0.534	-1.24
29	71.000	70.534	0.466	1.08
30	70.000	70.534	-0.534	-1.24
31	70.000	70.534	-0.534	-1.24
32	71.000	70.534	0.466	1.08

Table G3: Predicted and residual values for Yield of FAME by AAC

Run	FAME by AAC	Predicted	Resid	Std Resid
1	55.000	55.140	-0.140	-0.67
2	59.000	58.807	0.193	0.92
3	61.000	60.973	0.027	0.13
4	57.000	57.140	-0.140	-0.67
5	61.000	60.973	0.027	0.13
6	60.000	60.140	-0.140	-0.67
7	66.000	66.307	-0.307	-1.46
8	69.000	68.973	0.027	0.13
9	58.000	57.890	0.110	0.52
10	70.000	70.057	-0.057	-0.27
11	67.000	67.223	-0.223	-1.06
12	56.000	55.890	0.110	0.52
13	55.000	55.223	-0.223	-1.06
14	65.000	64.890	0.110	0.52
15	58.000	58.057	-0.057	-0.27
16	63.000	63.223	-0.223	-1.06
17	55.000	54.720	0.280	0.73
18	59.000	59.053	-0.053	-0.14
19	57.000	57.053	-0.053	-0.14
20	61.000	60.720	0.280	0.73
21	66.000	66.053	-0.053	-0.14
22	70.000	69.720	0.280	0.73
23	65.000	64.886	0.114	0.30
24	66.000	65.886	0.114	0.30
25	71.000	71.386	-0.386	-1.01
26	74.000	73.386	0.614	1.60
27	76.000	76.205	-0.205	-0.37
28	77.000	76.205	0.795	1.43
29	76.000	76.205	-0.205	-0.37
30	75.000	76.205	-1.205	-2.17
31	76.000	76.205	-0.205	-0.37
32	77.000	76.205	0.795	1.43

Table G4: Predicted and residual values for Yield of FAME by BAC

Run	Yield of FAME by BAC	Predicted	Resid	Std Resid
1	48.000	48.017	-0.017	-0.11
2	52.000	52.184	-0.184	-1.17
3	54.000	54.100	-0.100	-0.64
4	51.000	51.100	-0.100	-0.64
5	52.000	52.017	-0.017	-0.11
6	50.000	50.017	-0.017	-0.11
7	58.000	57.934	0.066	0.42
8	58.000	58.100	-0.100	-0.64
9	50.000	50.017	-0.017	-0.11
10	60.000	60.017	-0.017	-0.11
11	57.000	56.934	0.066	0.42
12	51.000	51.100	-0.100	-0.64
13	51.000	50.850	0.150	0.96
14	57.000	57.017	-0.017	-0.11
15	51.000	50.934	0.066	0.42
16	56.000	55.934	0.066	0.42
17	49.000	49.133	-0.133	-0.47
18	53.000	52.799	0.201	0.70
19	51.000	50.966	0.034	0.12
20	55.000	54.966	0.034	0.12
21	57.000	56.799	0.201	0.70
22	59.000	59.133	-0.133	-0.47
23	55.000	54.799	0.201	0.70
24	57.000	57.133	-0.133	-0.47
25	65.000	64.799	0.201	0.70
26	66.000	66.133	-0.133	-0.47
27	69.000	69.261	-0.261	-0.63
28	70.000	69.261	0.739	1.79
29	69.000	69.261	-0.261	-0.63
30	70.000	69.261	0.739	1.79
31	68.500	69.261	-0.761	-1.85
32	69.000	69.261	-0.261	-0.63

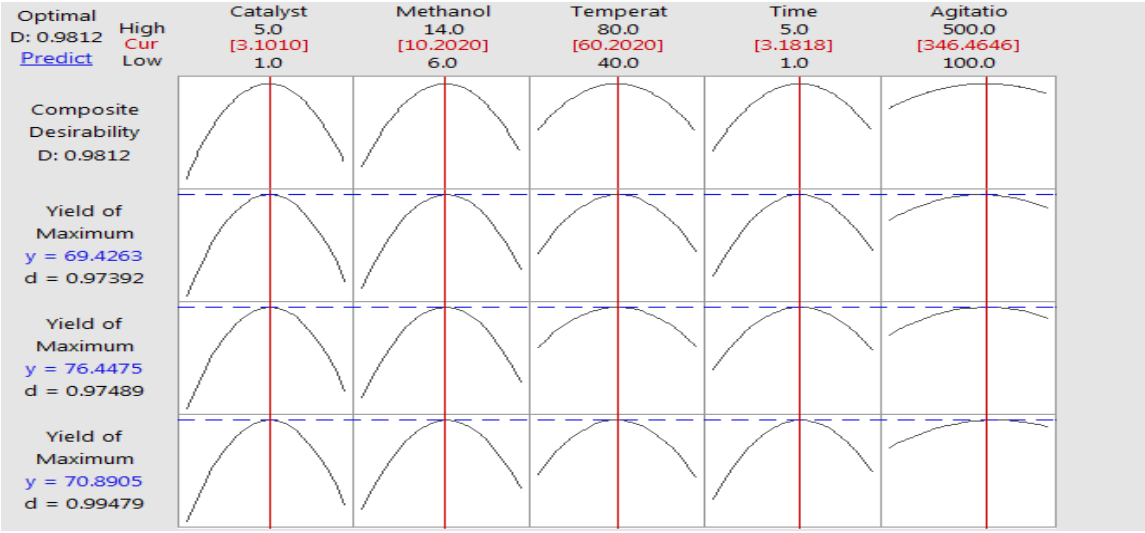

Figure G1: Optimization plot for biodiesel from African seed oil by BAC, AAC & TAC

Appendix H

Optimization of biodiesel production using Gmelina seed oil

TAC = thermally activated clay catalyst, AAC = acid activated clay catalyst, BAC = base/alkaline activated clay catalyst,

Table H1: Design matrix result using heterogeneous catalysts

Run order	Catalyst conc. A	Methanol/Oil molar ratio B	Temperature C	Time D	Agitation Speed E	Yield of FAME by TAC	Yield of FAME by AAC	Yield of FAME by BAC
	wt%	mol/mol	(^{o}C)	Hours	Rpm	(%)	(%)	(%)
1	2	8	50	2	400	54	50	47
2	4	8	50	2	200	59	54	51
3	2	12	50	2	200	60	58	54
4	4	12	50	2	400	57	53	50
5	2	8	70	2	200	62	57	51
6	4	8	70	2	400	61	56	50
7	2	12	70	2	400	66	62	56
8	4	12	70	2	200	68	64	57
9	2	8	50	4	200	59	54	50
10	4	8	50	4	400	71	65	61
11	2	12	50	4	400	67	61	56
12	4	12	50	4	200	56	52	51
13	2	8	70	4	400	55	53	51
14	4	8	70	4	200	65	60	57
15	2	12	70	4	200	59	52	50
16	4	12	70	4	400	64	58	55
17	1	10	60	3	300	54	53	49
18	5	10	60	3	300	58	55	52
19	3	6	60	3	300	57	54	51
20	3	14	60	3	300	60	58	54
21	3	10	40	3	300	65	60	57
22	3	10	80	3	300	70	62	58
23	3	10	60	1	300	66	60	55
24	3	10	60	5	300	68	61	57
25	3	10	60	3	100	70	66	64
26	3	10	60	3	500	72	68	65
27	3	10	60	3	300	74	71	70
28	3	10	60	3	300	75	72	70
29	3	10	60	3	300	75	72	69
30	3	10	60	3	300	75	73	70
31	3	10	60	3	300	75	72	70
32	3	10	60	3	300	74	72	70

Table H2: Predicted and residual values for Yield of FAME by TAC

Run	Yield of FAME by TAC	Predicted	Resid	Std Resid
1	54.000	54.110	-0.110	-0.69
2	59.000	58.777	0.223	1.41
3	60.000	59.943	0.057	0.36
4	57.000	57.027	-0.027	-0.17
5	62.000	62.027	-0.027	-0.17
6	61.000	61.110	-0.110	-0.69
7	66.000	66.277	-0.277	-1.75
8	68.000	67.943	0.057	0.36
9	59.000	58.860	0.140	0.89
10	71.000	70.943	0.057	0.36
11	67.000	67.110	-0.110	-0.69
12	56.000	55.777	0.223	1.41
13	55.000	55.193	-0.193	-1.22
14	65.000	64.860	0.140	0.89
15	59.000	59.027	-0.027	-0.17
16	64.000	64.110	-0.110	-0.69
17	54.000	53.739	0.261	0.91
18	58.000	58.239	-0.239	-0.83
19	57.000	57.072	-0.072	-0.25
20	60.000	59.905	0.095	0.33
21	65.000	65.239	-0.239	-0.83
22	70.000	69.739	0.261	0.91
23	66.000	65.905	0.095	0.33
24	68.000	68.072	-0.072	-0.25
25	70.000	70.405	-0.405	-1.41
26	73.000	72.572	0.428	1.49
27	74.000	74.670	-0.670	-1.61
28	75.000	74.670	0.330	0.79
29	75.000	74.670	0.330	0.79
30	75.000	74.670	0.330	0.79
31	75.000	74.670	0.330	0.79
32	74.000	74.670	-0.670	-1.61

Table H3: Predicted and residual values for Yield of FAME by AAC

Run	Yield of FAME by AAC	Predicted	Resid	Std Resid
1	50.000	50.095	-0.095	-0.41
2	54.000	53.761	0.239	1.02
3	58.000	58.261	-0.261	-1.12
4	53.000	53.011	-0.011	-0.05
5	57.000	56.761	0.239	1.02
6	56.000	55.511	0.489	2.10
7	62.000	62.011	-0.011	-0.05
8	64.000	63.678	0.322	1.38
9	54.000	54.178	-0.178	-0.76
10	65.000	64.928	0.072	0.31
11	61.000	61.428	-0.428	-1.84
12	52.000	52.095	-0.095	-0.41
13	53.000	52.928	0.072	0.31
14	60.000	59.595	0.405	1.74
15	52.000	52.095	-0.095	-0.41
16	58.000	57.845	0.155	0.67
17	53.000	52.519	0.481	1.13
18	55.000	55.686	-0.686	-1.62
19	54.000	54.519	-0.519	-1.22
20	58.000	57.686	0.314	0.74
21	60.000	59.519	0.481	1.13
22	62.000	62.686	-0.686	-1.62
23	60.000	60.352	-0.352	-0.83
24	61.000	60.852	0.148	0.35
25	66.000	66.186	-0.186	-0.44
26	68.000	68.019	-0.019	-0.04
27	71.000	71.966	-0.966	-1.57
28	72.000	71.966	0.034	0.06
29	72.000	71.966	0.034	0.06
30	73.000	71.966	1.034	1.69
31	72.000	71.966	0.034	0.06
32	72.000	71.966	0.034	0.06

Table H4: Predicted and residual values for Yield of FAME by BAC

Run	Yield of FAME by BAC	Predicted	Resid	Std Resid
1	47.000	47.231	-0.231	-1.34
2	51.000	51.064	-0.064	-0.37
3	54.000	54.314	-0.314	-1.82
4	50.000	50.064	-0.064	-0.37
5	51.000	51.148	-0.148	-0.86
6	50.000	49.898	0.102	0.59
7	56.000	56.148	-0.148	-0.86
8	57.000	56.981	0.019	0.11
9	50.000	49.981	0.019	0.11
10	61.000	60.731	0.269	1.56
11	56.000	55.981	0.019	0.11
12	51.000	50.814	0.186	1.08
13	51.000	50.814	0.186	1.08
14	57.000	56.648	0.352	2.04
15	50.000	49.898	0.102	0.59
16	55.000	54.648	0.352	2.04
17	49.000	48.663	0.337	1.07
18	52.000	52.496	-0.496	-1.58
19	51.000	51.163	-0.163	-0.52
20	54.000	53.996	0.004	0.01
21	57.000	56.830	0.170	0.54
22	58.000	58.330	-0.330	-1.05
23	55.000	54.496	0.504	1.61
24	57.000	57.663	-0.663	-2.11
25	64.000	63.996	0.004	0.01
26	65.000	65.163	-0.163	-0.52
27	70.000	69.807	0.193	0.43
28	70.000	69.807	0.193	0.43
29	69.000	69.807	-0.807	-1.78
30	70.000	69.807	0.193	0.43
31	70.000	69.807	0.193	0.43
32	70.000	69.807	0.193	0.43

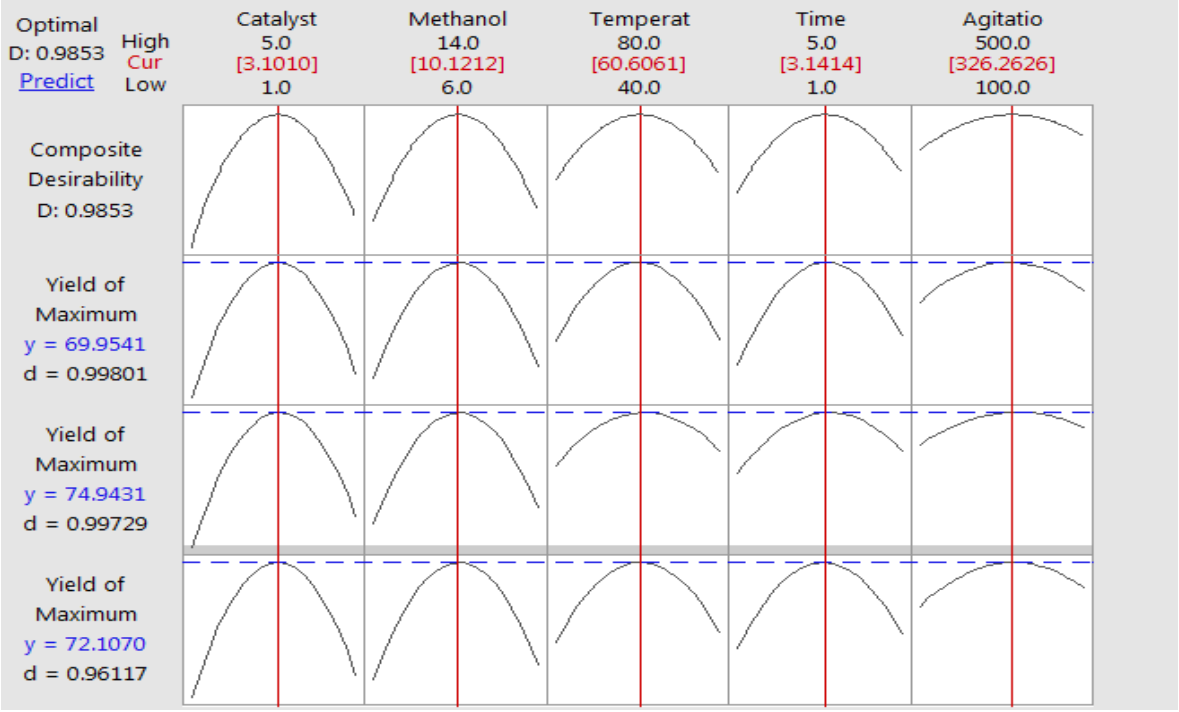

Figure H1: Optimization plot for biodiesel from Gmelina seed oil by BAC, TAC & AAC

Appendix I

Kinetics studies

APO FAME

At 45°C, [T] = 6.74 – 2.36t -0.26t^2 + 0.12t^3 ; Rate = $\frac{d[T]}{dt} = -2.36 - 0.52t - 0.36t^2$

At 50°C, [T] = 4.3 – 1.75t + 0.40t^2 - 0.031t^3 ; Rate = $\frac{d[T]}{dt} = -1.75 + 0.80t - 0.09t^2$

At 55°C, [T] = 0.505 + 5.75t – 3.58t^2+ 0.54t^3 ; Rate = $\frac{d[T]}{dt} = 5.75 - 7.16t + 1.62t^2$

At 45°C, [B] = 0.644 + 5.88t – 3.78t^2+ 0.58t^3 ; Rate = $\frac{d[B]}{dt} = 5.88 - 7.56t + 1.74t^2$

At 50°C, [B] = 1.36 + 11.38t – 3.58t^2 + 0.41t^3 ; Rate = $\frac{d[B]}{dt} = 11.38 - 7.16t + 1.23t^2$

At 55°C, [B] = 0.41 + 2.10t + 0.18t^2 + 0.074t^3 ; Rate = $\frac{d[B]}{dt} = 2.10 - 0.36t + 0.22t^2$

GSO FAME

At 45°C, [T] = 6.72 – 2.59t - 0.12t^2+ 0.095t^3 ; Rate = $\frac{d[T]}{dt} = -2.59 - 0.24t + 0.29t^2$

At 50°C, [T] = 4.10 – 0.485t - 0.212t^2 - 0.049t^3 ; Rate = $\frac{d[T]}{dt} = -0.485 - 0.424t - 0.147t^2$

At 55°C, [T] = 0.632 + 5.56t – 3.54t^2+ 0.147t^3 ; Rate = $\frac{d[T]}{dt} = 5.56 - 7.08t + 0.441t^2$

At 45°C, [B] = 0.65 + 5.95t – 3.85t^2+ 0.59t^3 ; Rate = $\frac{d[B]}{dt} = 5.95 - 7.70t + 1.77t^2$

At 50°C, [B] = 1.53 + 12.36t – 1.91t^2 + 0.093t^3 ; Rate = $\frac{d[B]}{dt} = 12.36 - 3.82t + 0.279t^2$

At 55°C, [B] = 0.18 + 6.31t – 1.92t^2 + 0.199t^3 ; Rate = $\frac{d[B]}{dt} = 6.31 - 5.76t + 0.597t^2$

Table I 1: Concentration for kinetics of APO biodiesel produced by TAC catalyzed reaction

Temp (^{o}C)	Time (Hour)	[T] (g/L)	[A] (g/L)	[D] (g/L)	[M] (g/L)	[B] (g/L)	[G] (g/L)	Rate	
45	0	6.82	4.20	0	0	0	0	2.36	
	0.5	5.28	3.80	3.56	3.97	9.06	2.35	2.71	
	1.0	4.25	2.77	3.03	3.10	9.11	2.45	3.24	
	1.5	3.50	2.30	2.81	2.89	10.73	3.45	3.95	
	2.0	1.60	2.20	1.50	1.03	12.05	4.48	4.84	
	2.5	0.90	2.10	0.80	0.70	14.06	5.50	5.91	
	3.0	0.50	1.70	0.40	0.30	15.20	6.80	7.16	
	3.5	0.50	1.70	0.40	0.30	15.20	6.80	7.17	
	4.0	0.50	1.70	0.40	0.30	15.20	6.80	7.18	
50	0	6.82	4.20	0	0	0	0	2.59	
	0.5	5.10	3.60	3.87	3.99	10.10	3.16	2.64	
	1.0	4.20	3.48	2.97	3.20	12.50	4.90	2.54	
	1.5	3.30	3.10	2.50	2.78	14.23	5.88	3.30	
	2.0	1.50	2.90	1.40	1.10	18.50	6.36	4.91	
	2.5	0.85	2.10	0.70	0.60	21.48	7.20	4.38	
	3.0	0.45	2.05	0.30	0.25	25.70	7.40	7.70	
	3.5	0.45	1.89	0.30	0.25	25.70	7.40	7.75	
	4.0	0.45	1.89	0.30	0.25	25.70	7.40	7.76	
55	0	6.82	4.20	0	0	0	0	2.63	
	0.5	4.98	3.80	4.00	3.33	10.50	2.78	2.70	
	1.0	4.10	3.60	3.80	3.10	14.60	4.20	2.61	
	1.5	3.20	3.40	2.50	2.75	16.93	4.81	3.38	
	2.0	1.40	3.20	1.30	1.40	22.98	4.90	4.99	
	2.5	0.60	3.00	0.60	0.77	31.87	5.12	5.46	
	3.0	0.20	2.80	0.25	0.15	33.24	5.14	8.77	
	3.5	0.20	2.80	0.25	0.15	33.24	5.14	8.78	
	4.0	0.20	2.80	0.25	0.15	33.24	5.14	8.79	

Table I 2: Concentration for kinetics of APO biodiesel produced by AAC catalyzed reaction

Temp (^{o}C)	Time (Hour)	[T] (g/L)	[A] (g/L)	[D] (g/L)	[M] (g/L)	[B] (g/L)	[G] (g/L)	Rate	
45	0	6.82	4.20	0	0	0	0	2.46	
	0.5	5.50	3.90	3.73	3.86	9.53	2.51	2.63	
	1.0	4.30	3.50	3.21	3.52	10.23	2.70	3.43	
	1.5	2.50	2.80	2.70	2.72	11.45	3.60	4.22	
	2.0	1.50	2.50	1.80	1.52	13.01	4.50	5.0	
	2.5	0.80	2.10	0.90	0.70	15.53	5.80	5.63	
	3.0	0.40	1.80	0.35	0.40	16.60	6.90	6.71	
	3.5	0.40	1.80	0.35	0.40	16.60	6.90	7.34	
	4.0	0.40	1.80	0.35	0.40	16.60	6.90	7.56	
50	0	6.82	4.20	0	0	0	0	2.65	
	0.5	5.81	3.80	3.90	3.88	11.20	3.40	2.89	
	1.0	4.20	3.20	3.30	3.45	13.60	3.90	3.58	
	1.5	2.40	2.60	2.80	2.63	14.90	4.80	4.41	
	2.0	1.20	2.30	1.45	1.50	19.50	5.60	5.10	
	2.5	0.70	2.00	0.60	0.50	22.50	6.50	6.82	
	3.0	0.30	1.90	0.35	0.25	26.10	6.70	7.81	
	3.5	0.30	1.90	0.35	0.25	26.10	6.70	7.53	
	4.0	0.30	1.90	0.35	0.25	26.10	6.70	8.23	
55	0	6.82	4.20	0	0	0	0	2.72	
	0.5	5.23	3.70	3.90	3.50	12.13	2.98	2.83	
	1.0	4.30	3.50	3.65	3.20	14.80	3.63	3.66	
	1.5	2.80	3.30	2.43	2.80	17.52	4.20	4.45	
	2.0	1.50	3.10	1.56	1.30	23.40	4.70	6.00	
	2.5	0.50	2.90	0.55	0.60	32.60	4.90	6.56	
	3.0	0.15	2.70	0.25	0.10	35.20	5.20	7.85	
	3.5	0.15	2.70	0.25	0.10	35.20	5.20	8.16	
	4.0	0.15	2.70	0.25	0.10	35.20	5.20	8.24	

Table I 3: Concentration for kinetics of APO biodiesel produced by BAC catalyzed reaction

Temp (^{o}C)	Time (Hour)	[T] (g/L)	[A] (g/L)	[D] (g/L)	[M] (g/L)	[B] (g/L)	[G] (g/L)	Rate	
45	0	6.82	4.20	0	0	0	0	2.26	
	0.5	5.80	3.80	3.82	3.85	9.40	2.8	2.57	
	1.0	5.10	3.60	3.40	3.50	10.21	3.10	3.56	
	1.5	3.70	2.90	2.90	2.60	12.30	3.67	4.44	
	2.0	1.80	2.60	1.70	1.80	12.80	4.80	4.98	
	2.5	1.10	2.20	1.00	0.90	15.30	5.50	5.54	
	3.0	0.60	1.70	0.55	0.50	16.40	6.10	6.69	
	3.5	0.60	1.70	0.55	0.50	16.40	6.10	7.34	
	4.0	0.60	1.70	0.55	0.50	16.40	6.10	8.51	
50	0	6.82	4.20	0	0	0	0	2.61	
	0.5	5.90	3.70	3.80	3.75	10.68	3.50	2.70	
	1.0	4.30	3.00	3.20	3.60	12.80	3.80	3.63	
	1.5	2.50	2.50	2.90	2.50	14.50	4.30	4.41	
	2.0	1.40	2.30	1.60	1.70	18.20	5.80	5.00	
	2.5	0.80	2.10	0.80	0.80	20.70	6.40	6.62	
	3.0	0.45	2.00	0.40	0.50	24.60	6.80	7.77	
	3.5	0.45	2.00	0.40	0.50	24.60	6.80	8.14	
	4.0	0.45	2.00	0.40	0.50	24.60	6.80	8.18	
55	0	6.82	4.20	0	0	0	0	2.67	
	0.5	5.70	3.60	3.80	3.40	11.50	3.00	2.77	
	1.0	4.80	3.50	3.60	2.80	13.80	3.40	3.69	
	1.5	3.10	3.20	2.50	2.50	15.70	3.80	5.41	
	2.0	1.40	3.00	1.60	1.80	18.40	4.20	6.12	
	2.5	0.70	2.90	0.80	0.90	24.80	4.60	6.63	
	3.0	0.30	2.80	0.40	0.50	28.90	5.00	7.89	
	3.5	0.30	2.80	0.40	0.50	28.90	5.00	8.17	
	4.0	0.30	2.80	0.40	0.50	28.90	5.00	8.43	

Table I 4: Concentration for kinetics of GSO biodiesel produced by TAC catalyzed reaction

Temp (^{o}C)	Time (Hour)	[T] (g/L)	[A] (g/L)	[D] (g/L)	[M] (g/L)	[B] (g/L)	[G] (g/L)	Rate	
45	0	6.50	4.20	0	0	0	0	2.46	
	0.5	5.40	4.00	3.41	3.99	9.03	2.41	3.33	
	1.0	4.50	3.72	3.20	3.20	9.00	2.60	4.22	
	1.5	3.80	2.60	2.83	2.78	10.53	3.47	5.13	
	2.0	2.10	2.30	1.70	1.05	11.85	4.50	5.76	
	2.5	1.60	2.10	1.40	0.90	13.86	5.60	6.41	
	3.0	0.50	1.80	0.60	0.45	14.89	7.00	6.56	
	3.5	0.50	1.80	0.60	0.45	14.89	7.00	7.11	
	4.0	0.50	1.80	0.60	0.45	14.89	7.00	8.01	
50	0	6.50	4.20	0	0	0	0	2.32	
	0.5	5.30	3.80	3.89	4.00	10.00	3.60	3.24	
	1.0	4.40	3.68	2.99	3.50	12.30	4.95	4.15	
	1.5	3.80	3.30	2.58	2.87	14.01	5.98	5.02	
	2.0	1.70	2.95	1.50	1.30	17.50	6.65	5.61	
	2.5	0.98	2.30	0.80	0.80	21.48	6.20	6.18	
	3.0	0.50	2.15	0.40	0.35	22.50	8.40	6.50	
	3.5	0.50	1.99	0.40	0.35	22.50	8.40	7.03	
	4.0	0.50	1.99	0.40	0.35	22.00	8.40	7.19	
55	0	6.50	4.20	0	0	0	0	2.33	
	0.5	5.50	3.90	3.90	3.35	10.10	2.85	3.30	
	1.0	4.30	3.70	3.80	3.23	11.90	4.82	4.21	
	1.5	3.60	3.50	2.70	2.90	13.30	4.81	5.11	
	2.0	1.80	3.50	1.80	1.60	18.98	4.90	5.78	
	2.5	0.70	3.00	0.80	0.79	23.87	6.02	6.25	
	3.0	0.60	2.80	0.30	0.25	28.24	6.02	6.64	
	3.5	0.60	2.80	0.30	0.25	28.24	6.02	7.19	
	4.0	0.60	2.80	0.30	0.25	33.24	6.02	8.01	

Table I 5: Concentration for kinetics of GSO biodiesel produced by AAC catalyzed reaction

Temp (^{o}C)	Time (Hour)	[T] (g/L)	[A] (g/L)	[D] (g/L)	[M] (g/L)	[B] (g/L)	[G] (g/L)	Rate	
45	0	6.50	4.20	0	0	0	0	2.39	
	0.5	5.70	4.00	3.90	3.98	9.80	2.80	3.34	
	1.0	4.60	3.80	3.32	3.60	10.84	2.90	4.26	
	1.5	2.80	2.90	2.80	2.83	12.10	3.80	5.14	
	2.0	1.90	2.60	1.90	1.64	13.84	4.90	5.68	
	2.5	0.85	2.20	1.00	0.80	16.10	6.00	6.36	
	3.0	0.50	1.90	0.45	0.50	17.50	7.10	6.60	
	3.5	0.50	1.90	0.45	0.50	17.50	7.10	7.24	
	4.0	0.50	1.90	0.45	0.50	17.50	7.10	7.64	
50	0	6.50	4.20	0	0	0	0	2.61	
	0.5	5.95	3.90	4.00	3.94	11.60	3.30	3.52	
	1.0	4.50	3.50	3.80	3.65	13.80	3.80	4.47	
	1.5	2.80	2.80	2.95	2.83	15.10	4.50	5.31	
	2.0	1.70	2.60	1.65	1.90	18.50	5.30	5.86	
	2.5	0.80	2.30	0.70	0.80	21.80	6.30	6.43	
	3.0	0.40	1.95	0.45	0.35	25.50	6.50	6.81	
	3.5	0.40	1.95	0.45	0.35	25.50	6.50	7.12	
	4.0	0.40	1.95	0.45	0.35	25.50	6.50	7.29	
55	0	6.50	4.20	0	0	0	0	2.70	
	0.5	5.45	3.80	3.93	3.60	12.00	3.00	3.65	
	1.0	4.70	3.60	3.75	3.30	14.50	3.75	4.53	
	1.5	2.92	3.40	2.56	2.90	18.12	4.30	5.43	
	2.0	1.65	3.20	1.78	1.50	24.40	4.80	6.21	
	2.5	0.60	2.95	0.85	0.80	30.50	4.90	6.57	
	3.0	0.25	2.80	0.35	0.20	33.10	5.50	6.78	
	3.5	0.25	2.80	0.35	0.20	33.10	5.50	7.38	
	4.0	0.25	2.80	0.35	0.20	33.10	5.50	8.15	

Table I 6: Concentration for kinetics of GSO biodiesel produced by BAC catalyzed reaction

Temp (^{o}C)	Time (Hour)	[T] (g/L)	[A] (g/L)	[D] (g/L)	[M] (g/L)	[B] (g/L)	[G] (g/L)	Rate	
45	0	6.50	4.20	0	0	0	0	2.57	
	0.5	5.60	3.85	3.91	3.95	9.20	2.85	3.48	
	1.0	5.00	3.70	3.50	3.70	10.01	3.15	4.36	
	1.5	3.60	2.95	3.00	2.80	12.00	3.72	4.43	
	2.0	1.50	2.70	2.40	1.90	12.50	4.85	5.82	
	2.5	1.20	2.30	1.50	0.95	15.10	5.70	6.30	
	3.0	0.70	1.80	0.65	0.55	16.00	6.00	6.63	
	3.5	0.70	1.80	0.65	0.55	16.00	6.00	7.23	
	4.0	0.70	1.80	0.65	0.55	16.00	6.00	7.31	
50	0	6.50	4.20	0	0	0	0	2.72	
	0.5	5.80	3.80	3.90	3.85	10.51	3.40	3.64	
	1.0	4.40	3.30	3.50	3.70	12.30	3.80	4.52	
	1.5	2.90	2.60	2.95	2.80	13.80	4.20	5.21	
	2.0	1.60	2.40	1.80	1.95	17.40	5.60	6.13	
	2.5	0.90	2.30	0.95	0.85	19.50	6.40	6.24	
	3.0	0.40	2.10	0.50	0.45	23.40	6.50	6.63	
	3.5	0.40	2.10	0.50	0.45	23.40	6.50	7.13	
	4.0	0.40	2.10	0.50	0.45	23.40	6.50	7.14	
55	0	6.50	4.20	0	0	0	0	2.68	
	0.5	5.90	3.65	3.75	3.60	11.20	3.10	3.54	
	1.0	5.20	3.50	3.63	2.90	13.40	3.50	4.31	
	1.5	3.40	3.30	2.52	2.60	15.60	3.70	5.26	
	2.0	1.80	3.10	1.90	1.90	18.20	4.30	6.13	
	2.5	0.90	3.00	0.85	0.79	23.50	4.70	7.04	
	3.0	0.32	2.90	0.45	0.51	27.80	5.40	7.16	
	3.5	0.32	2.90	0.45	0.51	27.80	5.40	8.13	
	4.0	0.32	2.90	0.45	0.51	27.80	5.40	8.23	

APPENDIX J

Rate constants and equilibrium constants determination for LHHW kinetic mechanism

Table J 1: Equilibrium and rate constants values for heterogeneous catalysis (TAC) of African pear seed oil at 45^{o}C

	Methaol adsorption	TG adsorption	Surface rxn b/w TG and methanol	Surface rxn b/w DG and methanol	Surface rxn b/w MG and methanol	Desorption of Biodiesel	Desorption of DG	Desorption of MG	Desorption of GL
K1		10.11	11.61	7.11	9.35	10	10	8.67	46.54
K2	9.99		10.54	9.83	9.48	10	10	9.46	41.24
K3	9.84	9.64				10	10		
K4				6.05				9.48	
K5									22.92
K6	9.87	9.67	8.79	13.53	10.78		10	10.55	22.21
K7	9.84	9.64	8.85	13.97	10.83	10			10.28
K8	18.55	14.12	15.6	3.40	7.84	10	10		9.73
K9	8.87	6.37	12.33	24.90	275.61	10	10	12.68	
k_f	0.00999	0.0113	0.008887	0.0141	0.0109	0.01	0.01	0.01	0.0103
k_b	0.000983	0.00113	0.000796	0.00233	0.0119	0.001	0.001	0.000862	0.0000222
σ^2	0.793	0.338	0.3178	0.6076	0.735	0.984	0.680	0.735	0.666
R^2	0.651	0.556	0.901	0.887	0.831	0.721	0.598	0.698	0.715

Table J2: equilibrium and rate constants values for heterogeneous catalysis (TAC) of African pear seed oil at 50^{o}C

	Methaol adsorption	TG adsorption	Surface rxn b/w TG and methanol	Surface rxn b/w DG and methanol	Surface rxn b/w MG and methanol	Desorption of Biodiesel	Desorption of DG	Desorption of MG	Desorption of GL
K1		11.32	10.5	10	10	10	10	14.95	2.72
K2	8.34		11.3	10	10	10	10	6.11	19.50
K3	11.50	9.94				10	10		
K4								14.95	
K5									7.21
K6	9.91	10.30	10.23	10	10		10	11.73	7.41
K7	12.8	14.6	8.97	10	10	10		8.23	9.97
K8	10.30	8.60	9.89	10	10	10	10		10.03
K9	9.87	9.45	10.3	10	10	10	10	393.54	
k_f	0.0101	0.010	0.00937	0.01	0.01	0.01	0.01	0.00999	0.009968
k_b	0.000989	0.00131	0.000938	0.001	0.001	0.001	0.001	0.0000127	0.0000322
R^2	0.561	0.655	0.922	0.857	0.730	0.623	0.512	0.614	0.742
σ^2	0.428	0.691	0.348	0.7664	0.691	0.654	0.766	0.692	0.546

Table J3: Equilibrium and rate constants values for heterogeneous catalysis (TAC) of African pear seed oil at 55^{o}C

K	Methaol adsorption	TG adsorption	Surface rxn b/w TG and methanol	Surface rxn b/w DG and methanol	Surface rxn b/w MG and methanol	Desorption of Biodiesel	Desorption of DG	Desorption of MG	Desorption of GL
1		7.36	10.18	10	10	10	10	12	9.95
2	9.46		16.60	10	10	10	10	11.20	9.74
3	6.89	8.65				10	10		
4								10.12	
5									10.43
6	8.56	9.87	6.9	10	10			9.45	21.56
7	9.91	14.51	11.75	10	10	10		8.78	7.94
8	11.30	7.89	10.94	10	10	10			10.36
9	15.36	6.20	8.91	10	10	10	10	9.15	
k_f	0.012	0.011	0.009990	0.01	0.01	0.01	0.01	0.013	0.0123
k_b	0.00118	0.00105	0.000708	0.001	0.001	0.001	0.001	0.00163	0.00105
R^2	0.615	0.555	0.956	0.759	0.731	0.764	0.514	0.597	0.689
σ^2	0.581	0.425	0.345	0.684	0.785	0.891	0.965	0.756	0.856

Table J4: Equilibrium and rate constants values for heterogeneous catalysis (AAC) of African pear seed oil at 45^{o}C

	Methaol adsorption	TG adsorption	Surface rxn b/w TG and methanol	Surface rxn b/w DG and methanol	Surface rxn b/w MG and methanol	Desorption of Biodiesel	Desorption of DG	Desorption of MG	Desorption of GL
K1		9.10	10	8.56	15.12	10	10	10	8.50
K2	9.89		9.86	9.23	8.76	10	10	10	13.4
K3	11.23	10.68				10	10		
K4								10	
K5									10.1
K6	10.63	12.60	8.25	10.2	12.4		10	10	8.85
K7	9.65	8.56	9.42	14.3	10.5	10		10	8.7
K8	13.04	9.97	21.2	6.1	8.20	10	10		9.63
K9	15.20	10.50	12.41	10.2	12.3	10	10	10	
k_f	0.0098	0.012	0.0089	0.0106	0.0112	0.01	0.01	0.01	0.018
k_b	0.000983	0.00152	0.00103	0.0013	0.00165	0.001	0.001	0.000862	0.0018
R^2	0.598	0.596	0.930	0.877	0.834	0.743	0.538	0.682	0.757
σ^2	0.423	0.645	0.256	0.789	0.864	0.946	0.971	0.746	0.694

Table J5: K values for heterogeneous catalysis (AAC) of African pear seed oil at 50^{o}C

	Methaol adsorption	TG adsorption	Surface rxn b/w TG and methanol	Surface rxn b/w DG and methanol	Surface rxn b/w MG and methanol	Desorption of Biodiesel	Desorption of DG	Desorption of MG	Desorption of GL
K1		7.51	9.99	10.14	10	10	10	9.4	9.6
K2	8.10		9.75	9.86	10	10	10	14.5	7.8
K3	6.7	9.15				10	10		
K4								9.10	
K5									15.8
K6	13.4	20.46	13.4	10.5	10		10	15.15	10.8
K7	8.60	12.4	18.3	6.7	10	10		10.8	12.50
K8	25.3	11.5	31.4	8.9	10	10	10		10.30
K9	45.87	18.40	12.4	5.6	10	10	10	13.4	9.86
k_f	0.0099	0.013	0.0095	0.014	0.01	0.01	0.01	0.011	0.015
k_b	0.000884	0.00103	0.00117	0.00188	0.001	0.001	0.001	0.00126	0.00152
R^2	0.611	0.663	0.902	0.897	0.856	0.698	0.579	0.619	0.699
σ^2	0.754	0.546	0.223	0.681	0.945	0.861	0.764	0.678	0.876

Table J6: Equilibrium and rate constant values for heterogeneous catalysis (AAC) of African pear seed oil at 55^{o}C

	Methaol adsorption	TG adsorption	Surface rxn b/w TG and methanol	Surface rxn b/w DG and methanol	Surface rxn b/w MG and methanol	Desorption of Biodiesel	Desorption of DG	Desorption of MG	Desorption of GL
K1		10.10	9.15	10.60	8.51	10	10	9.45	8.50
K2	11.30		8.19	8.70	9.15	10	10	10.32	14.03
K3	9.06	13.5				10	10		
K4								8.90	
K5									10.65
K6	9.45	10.68	7.20	11.4	8.65		10	11.37	9.82
K7	8.12	11.54	10.4	15.05	14.72	10		6.8	8.20
K8	6.5	9.71	15.9	5.25	12.30	10	10		11.23
K9	7.8	5.80	16.6	10.34	9.86	10	10	17.4	
k_f	0.0103	0.011	0.00998	0.0106	0.0132	0.01	0.01	0.0161	0.0145
k_b	0.000844	0.00115	0.00105	0.00079	0.00126	0.001	0.001	0.00189	0.00171
R^2	0.652	0.557	0.919	0.889	0.868	0.768	0.599	0.698	0.724
σ^2	0.560	0.786	0.312	0.861	0.778	0.984	0.872	0.861	0.561

Table J7: Equilibrium and rate constants values for heterogeneous catalysis (BAC) of African pear seed oil at 45^{o}C

	Methaol adsorption	TG adsorption	Surface rxn b/w TG and methanol	Surface rxn b/w DG and methanol	Surface rxn b/w MG and methanol	Desorption of Biodiesel	Desorption of DG	Desorption of MG	Desorption of GL
K1		9.51	10.53	9.86	8.15	10	10	9.67	8.5
K2	7.86		7.70	8.34	12.3	10	10	13.23	14.4
K3	9.15	8.07				10	10		
K4								6.10	
K5									12.1
K6	10.31	10.50	7.25	30.2	11.14		10	21.6	8.50
K7	12.5	5.6	8.42	13.3	12.5	10		15.40	14.8
K8	13.04	9.5	15.2	7.1	11.20	10	10		15.2
K9	12.20	11.40	12.41	10.2	12.3	10	10	9.5	
k_f	0.0098	0.0099	0.0088	0.0103	0.011	0.01	0.01	0.0106	0.0103
k_b	0.000981	0.00124	0.000917	0.00113	0.000815	0.001	0.001	0.000846	0.001195
R^2	0.646	0.592	0.920	0.875	0.840	0.657	0.600	0.629	0.778
σ^2	0.456	0.498	0.234	0.572	0.678	0.523	0.861	0.786	0.869

Table J8: Equilibrium and rate constants values for heterogeneous catalysis (BAC) of African pear seed oil at 50^{o}C

	Methaol adsorption	TG adsorption	Surface rxn b/w TG and methanol	Surface rxn b/w DG and methanol	Surface rxn b/w MG and methanol	Desorption of Biodiesel	Desorption of DG	Desorption of MG	Desorption of GL
K1		8.05	11.10	8.95	8.21	10	10	9.99	10
K2	8.11		9.45	9.35	10.10	10	10.2	10	8.99
K3	6.70	8.9				10	10		
K4								10	
K5									9.98
K6	12.5	18.50	13.40	10.5	15.3		10	10.3	10.1
K7	7.60	11.56	28.3	6.7	8.21	10		9.98	10.20
K8	10.3	10.5	11.4	9.5	8.56	10	10		6.01
K9	12.87	15.23	12.3	15.6	20.4	10	10.1	10.4	
k_f	0.00991	0.00999	0.0095	0.0123	0.0131	0.01	0.01	0.011	0.013
k_b	0.000806	0.00097	0.00147	0.00166	0.000977	0.001	0.001	0.0011	0.00126
R^2	0.766	0.656	0.932	0.788	0.823	0.732	0.698	0.634	0.599
σ^2	0.356	0.468	0.301	0.584	0.595	0.612	0.579	0.654	0.786

Table J9: Equilibrium and rate constants values for heterogeneous catalysis (BAC) of African pear seed oil at 55^{o}C

	Methaol adsorption	TG adsorption	Surface rxn b/w TG and methanol	Surface rxn b/w DG and methanol	Surface rxn b/w MG and methanol	Desorption of Biodiesel	Desorption of DG	Desorption of MG	Desorption of GL
K1		8.99	9.20	16.7	9.65	10.10	10.0	11.3	9.85
K2	9.98		12.89	9.27	10.45	10.0	9.89	10.0	15.3
K3	11.4	9.56				9.99	10.2		
K4								9.1	
K5					11.21				10.5
K6	10.1	8.59	6.20	17.6		10	10	12.5	11.4
K7	5.12	9.54	11.4	10.05	14.72		9.99	8.6	7.20
K8	7.5	8.61	14.9	8.25	15.30	10.7		10.23	9.45
K9	9.1	8.10	15.6	12.34	25.15	10.0	10.10	17.6	9.86
k_f	0.010	0.00999	0.00992	0.012	0.015	0.01	0.011	0.109	0.135
k_b	0.000952	0.000942	0.000973	0.00127	0.00149	0.001	0.001	0.00619	0.0000222
R^2	0.686	0.762	0.909	0.802	0.701	0.715	0.601	0.611	0.623
σ^2	0.465	0.341	0.245	0.521	0.589	0.671	0.712	0.814	0.799

Table J10: Determination of activation energy for APO FAME

S/N	Temperature (K)	Rate constant k_f (1/s)			1/T (1/K)	lnln k_f		
		TAC	AAC	BAC		TAC	AAC	BAC
1	318	0.008887	0.008910	0.008800	0.00314	-4.72	-4.72	-4.73
2	323	0.009370	0.009500	0.009500	0.00310	-4.67	-4.66	-4.66
3	328	0.009990	0.009980	0.009920	0.00305	-4.61	-4.61	-4.61

Table J11: Equilibrium and rate constants values for heterogeneous catalysis (TAC) of Gmelina seed oil at 45^{o}C

	Methaol adsorption	TG adsorption	Surface rxn b/w TG and methanol	Surface rxn b/w DG and methanol	Surface rxn b/w MG and methanol	Desorption of Biodiesel	Desorption of DG	Desorption of MG	Desorption of GL
K1		9.61	11.11	6.61	8.85	10	10	8.17	16.04
K2	9.49		10.04	9.33	8.98	10	10	8.96	10.74
K3	9.34	9.14				10	10		
K4								8.98	
K5									12.42
K6	9.37	9.17	8.29	13.03	10.28		10	10.05	11.71
K7	9.34	9.14	8.35	13.47	10.33	10		-0.5	9.78
K8	18.05	13.62	15.1	2.9	7.34	10	10		9.23
K9	8.37	5.87	11.83	24.4	275.11	10	10	12.18	
k_f	0.00891	0.0123	0.00879	0.0121	0.0119	0.01	0.01	0.013	0.0105
k_b	0.000922	0.0013	0.000825	0.00218	0.00138	0.001	0.001	0.00117	0.000164
R^2	0.665	0.6576	0.915	0.859	0.831	0.689	0.691	0.608	0.707
σ^2	0.693	0.328	0.308	0.612	0.725	0.974	0.670	0.715	0.646

Table J12: Equilibrium and rate constant values for heterogeneous catalysis (TAC) of Gmelina seed oil at 50^{o}C

K	Methaol adsorption	TG adsorption	Surface rxn b/w TG and methanol	Surface rxn b/w DG and methanol	Surface rxn b/w MG and methanol	Desorption of Biodiesel	Desorption of DG	Desorption of MG	Desorption of GL
K1		10.82	10	10	10	10	10	14.45	12.22
K2	7.84		10.8	10	10	10	10	5.61	19
K3	11	9.44				10	10		
K4								14.45	
K5								-0.5	6.71
K6	9.41	9.8	9.73	10	10		10	11.23	6.91
K7	12.3	14.1	8.47	10	10	10		7.73	9.47
K8	9.8	8.1	9.39	10	10	10	10		9.53
K9	9.37	8.95	9.8	10	10	10	10	10.5	39.02
k_f	0.011	0.0131	0.00921	0.01	0.01	0.01	0.01	0.00988	0.00978
k_b	0.00113	0.00183	0.00097	0.001	0.001	0.001	0.001	0.000126	0.000251
R^2	0.501	0.543	0.945	0.879	0.813	0.688	0.568	0.608	0.730
σ^2	0.418	0.591	0.328	0.756	0.682	0.666	0.867	0.703	0.645

Table J13: Equilibrium and rate constants values for heterogeneous catalysis (TAC) of Gmelina seed oil at 55^{o}C

	Methaol adsorption	TG adsorption	Surface rxn b/w TG and methanol	Surface rxn b/w DG and methanol	Surface rxn b/w MG and methanol	Desorption of Biodiesel	Desorption of DG	Desorption of MG	Desorption of GL
K1		6.86	9.68	10	10	10	10	11.5	9.45
K2	8.96		16.1	10	10	10	10	10.7	9.24
K3	6.39	8.15				10	10		
K4								9.62	
K5									9.93
K6	8.06	9.37	6.4	10	10		10	8.95	21.06
K7	9.41	14.01	11.25	10	10	10		8.27	7.44
K8	10.8	7.39	10.44	10	10	10	10		9.86
K9	14.86	5.7	8.41	10	10	10	10	8.65	
k_f	0.013	0.0112	0.00978	0.01	0.01	0.01	0.01	0.0121	0.0125
k_b	0.00134	0.00112	0.000718	0.001	0.001	0.001	0.001	0.00162	0.00112
R^2	0.598	0.665	0.939	0.807	0.864	0.732	0.567	0.697	0.743
σ^2	0.571	0.433	0.356	0.686	0.795	0.819	0.956	0.764	0.866

Table J14: Equilibrium and rate constants values for heterogeneous catalysis (AAC) of Gmelina seed oil at 45^{o}C

	Methaol adsorption	TG adsorption	Surface rxn b/w TG and methanol	Surface rxn b/w DG and methanol	Surface rxn b/w MG and methanol	Desorption of Biodiesel	Desorption of DG	Desorption of MG	Desorption of GL
K1		8.6	9.5	8.06	14.62	10	10	10	8
K2	9.39		9.36	8.73	8.26	10	10	10	12.9
K3	10.73	10.18			-0.5	10	10		
K4					-0.5			10	
K5									9.6
K6	10.13	12.1	7.75	9.7	11.9		10	10	8.35
K7	9.15	8.06	8.92	13.8	10	10		10	8.2
K8	12.54	9.47	20.7	5.6	7.7	10	10		9.13
K9	14.7	10	11.91	9.7	11.8	10	10	10	9.5
k_f	0.0099	0.011	0.00888	0.012	0.0111	0.01	0.01	0.01	0.013
k_b	0.00105	0.00149	0.00109	0.00157	0.00177	0.001	0.001	0.001	0.00137
R^2	0.651	0.664	0.911	0.813	0.845	0.671	0.567	0.619	0.726
σ^2	0.433	0.654	0.266	0.797	0.856	0.967	0.918	0.765	0.649

Table J15: Equilibrium and rate constants values for heterogeneous catalysis (AAC) of Gmelina seed oil at 50^{o}C

	Methaol adsorption	TG adsorption	Surface rxn b/w TG and methanol	Surface rxn b/w DG and methanol	Surface rxn b/w MG and methanol	Desorption of Biodiesel	Desorption of DG	Desorption of MG	Desorption of GL
K1		7.01	9.49	9.64	10	10	10	8.9	9.1
K2	7.6		9.25	9.36	10	10	10	14	7.3
K3	6.2	8.65				10	10		
K4								8.6	
K5									15.3
K6	12.9	19.96	12.9	10	10		10	14.65	10.3
K7	8.1	11.9	17.8	6.2	10	10		10.3	12
K8	24.8	11	30.9	8.4	10	10	10		9.8
K9	45.37	17.9	11.9	5.1	10	10	10	12.9	9.36
k_f	0.0093	0.012	0.00960	0.013	0.01	0.01	0.01	0.013	0.0112
k_b	0.000869	0.000992	0.00126	0.00187	0.001	0.001	0.001	0.00158	0.0012
R^2	0.612	0.662	0.914	0.823	0.841	0.649	0.579	0.718	0.633
σ^2	0.745	0.565	0.234	0.627	0.964	0.818	0.748	0.687	0.868

Table J16: Equilibrium and rate constants values for heterogeneous catalysis (AAC) of Gmelina seed oil at 55^{o}C

	Methaol adsorption	TG adsorption	Surface rxn b/w TG and methanol	Surface rxn b/w DG and methanol	Surface rxn b/w MG and methanol	Desorption of Biodiesel	Desorption of DG	Desorption of MG	Desorption of GL
K1		9.6	8.65	10.1	8.01	10	10	8.95	8
K2	10.8		7.69	8.2	8.65	10	10	9.82	13.53
K3	8.56	13				10	10		
K4								8.4	
K5									10.15
K6	8.95	10.18	6.7	10.9	8.15		10	10.87	9.32
K7	7.62	11.04	9.9	14.55	14.22	10		6.3	7.7
K8	6	9.21	15.4	4.75	11.8	10	10		10.73
K9	7.3	5.3	16.1	9.84	9.36	10	10	16.9	7.96
k_f	0.013	0.012	0.00999	0.0113	0.0123	0.01	0.01	0.0111	0.0123
k_b	0.00111	0.00132	0.00111	0.000876	0.00124	0.001	0.001	0.00139	0.00155
R^2	0.721	0.645	0.935	0.856	0.823	0.754	0.688	0.675	0.700
σ^2	0.650	0.876	0.213	0.681	0.877	0.894	0.782	0.867	0.643

Table J17: Equilibrium and rate constants values for heterogeneous catalysis (BAC) of Gmelina seed oil at 45^{o}C

	Methaol adsorption	TG adsorption	Surface rxn b/w TG and methanol	Surface rxn b/w DG and methanol	Surface rxn b/w MG and methanol	Desorption of Biodiesel	Desorption of DG	Desorption of MG	Desorption of GL
K1		9.01	10.03	9.36	7.65	10	10	9.17	8
K2	7.36		7.2	7.84	11.8	10	10	12.73	13.9
K3	8.65	7.57				10	10		
K4								5.6	
K5									11.6
K6	9.81	10	6.75	29.7	10.64		10	21.1	8
K7	12	5.1	7.92	12.8	12	10		14.9	14.3
K8	12.54	9	14.7	6.6	10.7	10	10		14.7
K9	11.7	10.9	11.91	9.7	11.8	10	10	9	
k_f	0.0099	0.00999	0.00899	0.0121	0.0131	0.01	0.01	0.0112	0.0131
k_b	0.00104	0.00134	0.000988	0.00140	0.00101	0.001	0.001	0.000931	0.00161
R^2	0.641	0.546	0.932	0.884	0.873	0.699	0.600	0.701	0.687
σ^2	0.531	0.553	0.213	0.576	0.699	0.578	0.889	0.768	0.896

Table J18: Equilibrium and rate constants values for heterogeneous catalysis (BAC) of Gmelina seed oil at 50^{o}C

	Methaol adsorption	TG adsorption	Surface rxn b/w TG and methanol	Surface rxn b/w DG and methanol	Surface rxn b/w MG and methanol	Desorption of Biodiesel	Desorption of DG	Desorption of MG	Desorption of GL
K1		7.55	10.6	8.45	7.71	10	10	9.49	9.5
K2	7.61		8.95	8.85	9.6	10	10.2	9.5	8.49
K3	6.2	8.4				10	10		
K4								9.5	
K5									9.48
K6	12	18	12.9	10	14.8		10	9.8	9.6
K7	7.1	11.06	27.8	6.2	7.71	10		9.48	9.7
K8	9.8	10	10.9	9	8.06	10	10		5.51
K9	12.37	14.73	11.8	15.1	19.9	10	10.1	9.9	9.85
k_f	0.01	0.011	0.00923	0.0112	0.0122	0.01	0.01	0.0103	0.0102
k_b	0.000847	0.00112	0.00155	0.00162	0.000945	0.001	0.001	0.00108	0.00104
R^2	0.589	0.514	0.954	0.818	0.832	0.713	0.598	0.631	0.734
σ^2	0.556	0.668	0.312	0.684	0.695	0.662	0.795	0.861	0.867

Table J19: Equilibrium and rate constants values for heterogeneous catalysis (BAC) of Gmelina seed oil at 55^{o}C

	Methaol adsorption	TG adsorption	Surface rxn b/w TG and methanol	Surface rxn b/w DG and methanol	Surface rxn b/w MG and methanol	Desorption of Biodiesel	Desorption of DG	Desorption of MG	Desorption of GL
K1		8.49	8.7	16.2	9.15	10.10	10.0	10.8	9.35
K2	9.48		12.39	8.77	9.95	10.0	9.89	9.5	14.8
K3	10.9	9.06				9.99	10.2		
K4								8.6	
K5									10
K6	9.6	8.09	5.7	17.1	9.6		10	12	10.9
K7	4.62	9.04	10.9	9.55	14.22	10		8.1	6.7
K8	7	8.11	14.4	7.75	14.8	10.7	10.0		8.95
K9	8.6	7.6	15.1	11.84	24.65	10.0	10.10	17.1	
k_f	0.0101	0.012	0.00999	0.0121	0.0113	0.01	0.011	0.0113	0.0122
k_b	0.00101	0.00119	0.00103	0.00135	0.00106	0.001	0.0011	0.00116	0.0013
R^2	0.633	0.555	0.940	0.800	0.799	0.621	0.528	0.618	0.715
σ^2	0.565	0.441	0.321	0.653	0.987	0.871	0.762	0.884	0.899

Table J20: Determination of activation energy for GSO FAME

S/N	Temperature (K)	Rate constant k_f (1/s)			1/T (1/K)	lnln k_f		
		TAC	AAC	BAC		TAC	AAC	BAC
1	318	0.00879	0.00888	0.00899	0.00314	-4.73	-4.72	-4.71
2	323	0.00921	0.00960	0.00923	0.00310	-4.69	-4.65	-4.69
3	328	0.00978	0.00999	0.00999	0.00305	-4.63	-4.61	-4.61

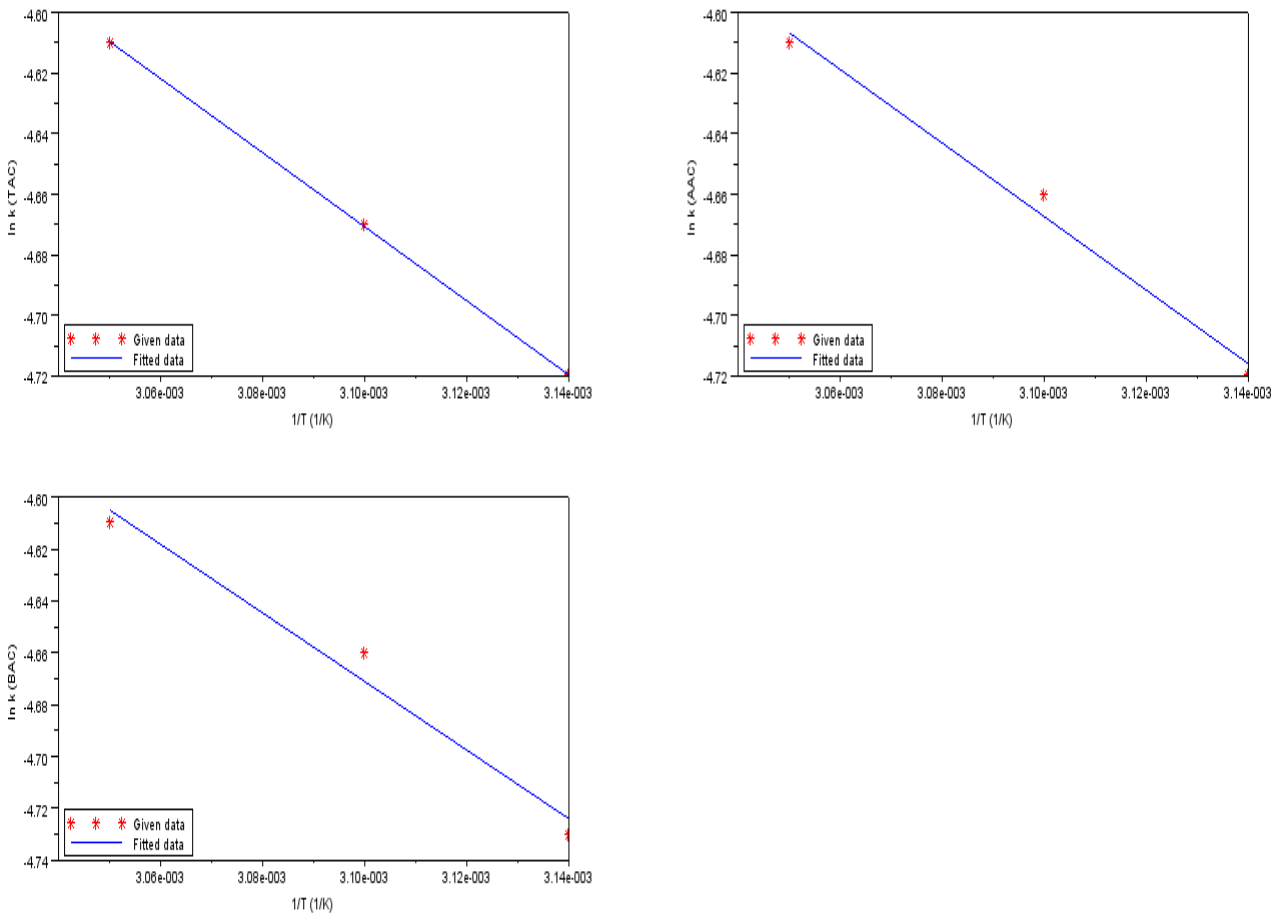

Figure J1: Activation energy determination for APO FAME.

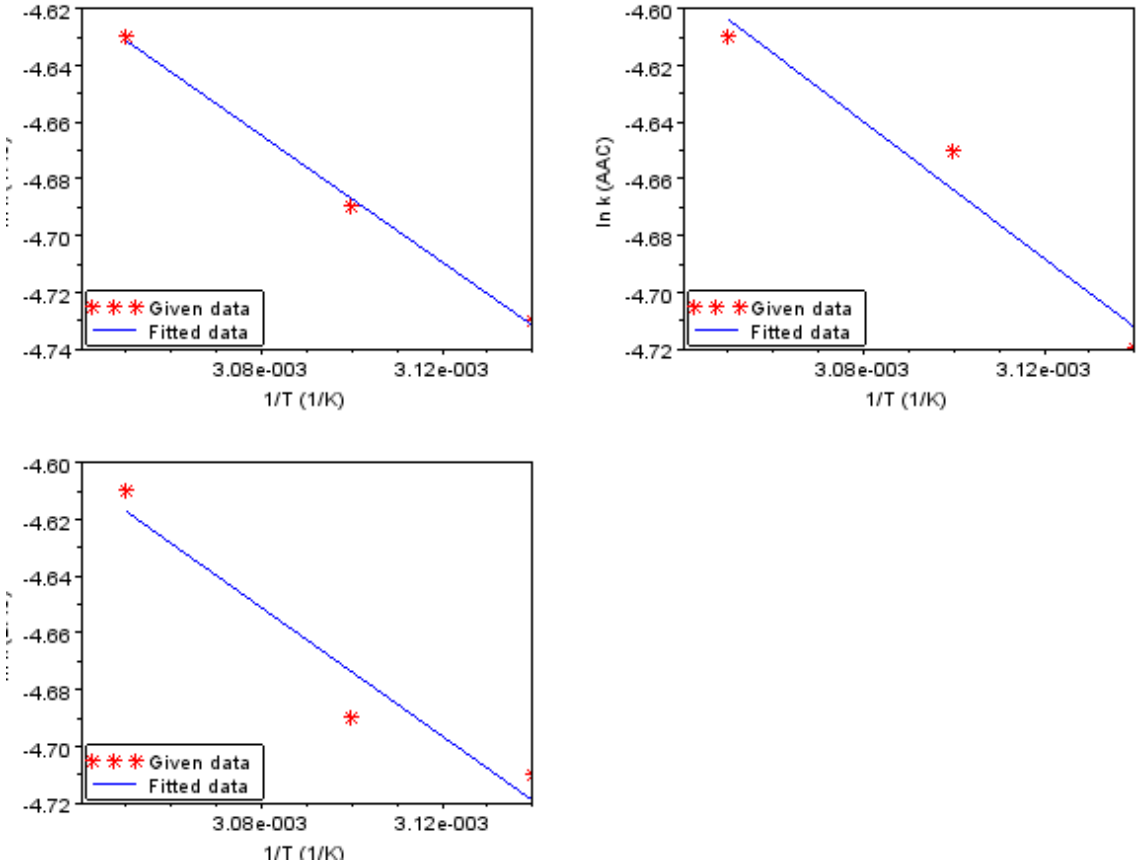

Figure J2: Activation energy determination for GSO FAME.

Table J21: Conversion from experimental and predicted rate using rate eqation 3 (APO) for LHHW model

TAC				AAC				BAC			
45^{o}C											
r_e	r_p	X_e	X_p	r_e	r_p	X_e	X_p	r_e	r_p	X_e	X_p
2.36	2.2	0	0	2.46	2.38	0	0	2.26	2.00	0	0
3.43	3.0	0.23	0.21	3.43	3.31	0.198	0.19	3.56	3.10	0.17	0.18
4.84	4.0	0.32	0.31	5.0	4.87	0.553	0.51	4.98	4.51	0.29	0.27
7.16	6.1	0.47	0.44	6.71	6.45	0.731	0.68	6.69	5.99	0.40	0.32
7.71	6.8	0.56	0.50	7.56	7.11	0.751	0.71	8.51	7.2	0.49	0.46
7.50	6.9	0.57	0.51	7.60	7.23	0.751	0.70	8.49	7.24	0.56	0.50
50^{o}C											
2.59	2.40	0	0	2.65	2.59	0	0	2.61	2.51	0	0
3.54	2.80	0.24	0.22	3.58	3.42	0.21	0.20	3.63	3.41	0.21	0.19
4.91	3.99	0.33	0.31	5.10	4.92	0.57	0.55	5.00	4.89	0.35	0.31
7.70	7.30	0.49	0.46	7.81	7.35	0.75	0.71	7.77	6.89	0.49	0.45
7.76	7.40	0.60	0.56	8.23	7.89	0.77	0.72	8.18	7.99	0.59	0.58
7.78	7.40	0.60	0.56	8.23	7.88	0.77	0.70	8.19	7.98	0.68	0.62
55^{o}C											
2.63	2.10	0	0	2.72	2.61	0	0	2.67	2.62	0	0
3.61	3.51	0.24	0.22	3.66	3.41	0.24	0.22	3.69	3.58	0.29	0.28
4.99	4.70	0.33	0.30	6.00	5.88	0.63	0.59	6.12	5.98	0.39	0.38
8.77	8.20	0.53	0.48	7.85	7.12	0.79	0.76	7.89	7.75	0.49	0.44
8.79	8.40	0.68	0.52	8.24	7.98	0.80	0.78	8.43	8.20	0.59	0.54
8.80	8.41	0.69	0.53	8.24	7.98	0.80	0.77	8.43	8.20	0.69	0.55

Table J22: Conversion from experimental and predicted rate using rate eqation 3 (GSO) for LHHW model

TAC				AAC				BAC			
45^{o}C											
r_e	r_p	X_e	X_p	r_e	r_p	X_e	X_p	r_e	r_p	X_e	X_p
2.46	1.56	0	0	2.39	2.17	0	0	2.57	2.31	0	0
4.22	3.12	0.21	0.20	4.26	3.45	0.24	0.21	4.36	3.87	0.22	0.19
5.76	5.41	0.45	0.42	5.68	4.67	0.42	0.39	5.82	4.45	0.39	0.31
6.56	6.41	0.52	0.51	6.60	5.89	0.57	0.54	6.63	5.84	0.53	0.49
8.01	7.89	0.63	0.62	7.24	6.98	0.67	0.66	7.31	6.25	0.65	0.61
8.01	7.89	0.63	0.62	7.25	6.99	0.68	0.67	7.32	6.26	0.65	0.62
50^{o}C											
2.32	2.10	0	0	2.61	2.21	0	0	2.72	2.12	0	0
4.15	3.40	0.19	0.18	4.47	3.81	0.26	0.22	4.52	3.87	0.22	0.20
5.61	4.80	0.29	0.27	5.86	4.50	0.48	0.45	6.13	5.45	0.43	0.38
6.50	5.65	0.39	0.34	6.81	5.98	0.60	0.59	6.61	5.86	0.56	0.48
7.19	6.93	0.55	0.51	7.29	6.88	0.68	0.62	7.14	6.73	0.67	0.59
7.20	6.94	0.66	0.64	7.30	6.90	0.69	0.61	7.15	6.73	0.68	0.59
55^{o}C											
2.33	2.14	0	0	2.70	2.40	0	0	2.68	2.22	0	0
4.21	3.98	0.25	0.23	4.53	4.10	0.28	0.23	4.31	3.79	0.28	0.24
5.78	5.65	0.45	0.41	6.21	5.99	0.49	0.40	6.13	5.61	0.45	0.39
6.64	6.23	0.57	0.55	6.78	6.32	0.65	0.61	7.16	6.23	0.57	0.53
8.01	7.65	0.67	0.63	8.15	7.88	0.70	0.67	8.23	7.14	0.71	0.68
8.02	7.65	0.69	0.64	8.17	7.88	0.71	0.67	8.23	7.15	0.71	0.69

Table J23: Conversion from experimental and predicted rate using rate eqation 2 (APO) for ER model

TAC				AAC				BAC			
45°C											
r_e	r_p	X_e	X_p	r_e	r_p	X_e	X_p	r_e	r_p	X_e	X_p
2.36	1.99	0	0	2.46	2.12	0	0	2.26	1.89	0	0
3.43	2.81	0.23	0.17	3.43	3.00	0.198	0.16	3.56	2.88	0.17	0.15
4.84	3.40	0.32	0.28	5.0	4.61	0.553	0.48	4.98	4.00	0.29	0.21
7.16	5.88	0.47	0.35	6.71	5.87	0.731	0.60	6.69	6.00	0.40	0.30
7.71	6.00	0.56	0.48	7.56	6.13	0.751	0.61	8.51	7.30	0.49	0.38
7.50	6.10	0.57	0.48	7.60	6.81	0.751	0.61	8.49	7.31	0.56	0.51
50°C											
2.59	2.30	0	0	2.65	2.42	0	0	2.61	2.40	0	0
3.54	2.60	0.24	0.19	3.58	3.31	0.21	0.18	3.63	3.13	0.21	0.19
4.91	3.71	0.33	0.31	5.10	4.78	0.57	0.49	5.00	4.41	0.35	0.29
7.70	7.00	0.49	0.41	7.81	6.89	0.75	0.69	7.77	6.51	0.49	0.40
7.76	7.10	0.60	0.57	8.23	7.10	0.77	0.71	8.18	6.89	0.59	0.51
7.78	7.12	0.60	0.58	8.23	7.10	0.77	0.71	8.19	7.00	0.68	0.60
55°C											
2.63	1.97	0	0	2.72	2.43	0	0	2.67	2.56	0	0
3.61	3.12	0.24	0.17	3.66	3.21	0.24	0.18	3.69	3.24	0.29	0.20
4.99	3.89	0.33	0.28	6.00	5.54	0.63	0.48	6.12	5.26	0.39	0.28
8.77	6.45	0.53	0.41	7.85	6.89	0.79	0.59	7.89	6.53	0.49	0.37
8.79	6.88	0.68	0.52	8.24	7.34	0.80	0.68	8.43	7.13	0.59	0.48
8.80	7.00	0.69	0.52	8.24	7.35	0.80	0.70	8.43	7.14	0.69	0.57

Table J24: Conversion from experimental and predicted rate using rate eqation 2 (GSO) for ER model

TAC				AAC				BAC			
45^{o}C											
r_e	r_p	X_e	X_p	r_e	r_p	X_e	X_p	r_e	r_p	X_e	X_p
2.46	1.66	0	0	2.39	2.01	0	0	2.57	2.25	0	0
4.22	3.24	0.21	0.19	4.26	3.25	0.24	0.20	4.36	3.36	0.22	0.18
5.76	5.14	0.45	0.35	5.68	4.46	0.42	0.37	5.82	4.29	0.39	0.28
6.56	5.89	0.52	0.48	6.60	5.74	0.57	0.51	6.63	5.31	0.53	0.47
8.01	6.97	0.63	0.59	7.24	6.67	0.67	0.60	7.31	6.16	0.65	0.57
8.01	7.02	0.63	0.59	7.25	6.68	0.68	0.60	7.32	6.17	0.65	0.58
50^{o}C											
2.32	2.00	0	0	2.61	2.18	0	0	2.72	2.10	0	0
4.15	3.10	0.19	0.16	4.47	3.56	0.26	0.19	4.52	3.76	0.22	0.19
5.61	4.00	0.29	0.22	5.86	4.43	0.48	0.38	6.13	5.34	0.43	0.35
6.50	5.54	0.39	0.30	6.81	5.61	0.60	0.47	6.61	5.45	0.56	0.47
7.19	6.12	0.55	0.48	7.29	6.23	0.68	0.59	7.14	6.17	0.67	0.56
7.20	6.14	0.66	0.59	7.30	6.24	0.69	0.59	7.15	6.17	0.68	0.57
55^{o}C											
2.33	2.20	0	0	2.70	2.34	0	0	2.68	2.13	0	0
4.21	3.59	0.25	0.19	4.53	3.88	0.28	0.20	4.31	3.56	0.28	0.21
5.78	5.46	0.45	0.38	6.21	5.78	0.49	0.36	6.13	5.43	0.45	0.36
6.64	6.10	0.57	0.46	6.78	6.12	0.65	0.49	7.16	6.37	0.57	0.49
8.01	7.23	0.67	0.58	8.15	7.24	0.70	0.58	8.23	6.98	0.71	0.57
8.02	7.34	0.69	0.60	8.17	7.23	0.71	0.59	8.23	7.11	0.71	0.60

Appendix K

Rate and equilibrium constants for heterogeneous reaction using Eley-Rideal (ER) model

Table K 1:Rate and equilibrium constants for TAC heterogeneous catalyzed reaction of APO using Eley-Rideal (ER) model at 45^{o}C

	Methaol adsorption	Surface rxn b/w TG and adsorbed methanol	Surface rxn b/w DG and adsorbed methanol	Surface rxn b/w MG and adsorbed methanol	Desorption of DG	Desorption of MG	Desorption of GL
K1		11.59	12.29	12.95	10	10	10
K2	33.10				10	10	10
K3							
K4	6.94					10	10
K5	96.8	7.97	88.65	7.54		10	10
K6	13.59	72.40	82.93	75.31	10		10
K7	70.85	16.27	7.45	97.94	10	10	
k_f	0.015	0.0086	0.0113	0.0098	0.01	0.01	0.01
k_b	0.000487	0.001	0.000904	0.00078	0.001	0.001	0.001
R^2	0.565	0.912	0.661	0.672	0.508	0.651	0.621
σ^2	0.658	0.512	0.6076	0.657	0.680	0.735	0.654

Table K 2:Rate and equilibrium constants for TAC heterogeneous catalyzed reaction of APO using Eley-Rideal (ER) model at 50^{o}C

	Methaol adsorption	Surface rxn b/w TG and adsorbed methanol	Surface rxn b/w DG and adsorbed methanol	Surface rxn b/w MG and adsorbed methanol	Desorption of DG	Desorption of MG	Desorption of GL
K1		11.02	13.20	12.36	10	10	10
K2	31.30				10	10	10
K3							
K4	8.40					10	10
K5	88.6	8.79	79.65	9.45		10	10
K6	14.32	93.37	80.78	85.13	10		10
K7	71.32	15.4	8.95	87.49	10	10	
k_f	0.012	0.00917	0.0134	0.0123	0.01	0.01	0.01
k_b	0.000427	0.001	0.00115	0.000906	0.001	0.001	0.001
R^2	0.651	0.932	0.615	0.602	0.611	0.598	0.600
σ^2	0.585	0.512	0.667	0.688	0.608	0.715	0.624

Table K 3:Rate and equilibrium constants for TAC heterogeneous catalyzed reaction of APO using Eley-Rideal (ER) model at 55^{o}C

	Methanol adsorption	Surface rxn b/w TG and adsorbed methanol	Surface rxn b/w DG and adsorbed methanol	Surface rxn b/w MG and adsorbed methanol	Desorption of DG	Desorption of MG	Desorption of GL
K1		10.87	12.50	13.61	10	10	10
K2	30.30				10	10	10
K3							
K4	8.85					10	10
K5	83.6	9.06	81.71	10.42		10	10
K6	13.20	79.47	83.65	87.88	10		10
K7	69.86	14.38	9.41	90.21	10	10	
k_f	0.0109	0.00933	0.015	0.0119	0.01	0.01	0.01
k_b	0.000376	0.001	0.00142	0.000831	0.001	0.001	0.001
R^2	0.515	0.921	0.712	0.671	0.538	0.647	0.698
σ^2	0.599	0.543	0.669	0.699	0.618	0.764	0.687

Table K 4:Rate and equilibrium constants for AAC heterogeneous catalyzed reaction of APO using Eley-Rideal (ER) model at 45^{o}C

	Methanol adsorption	Surface rxn b/w TG and adsorbed methanol	Surface rxn b/w DG and adsorbed methanol	Surface rxn b/w MG and adsorbed methanol	Desorption of DG	Desorption of MG	Desorption of GL
K1		11.75	14.30	10.31	10	10	10
K2	27.56				10	10	10
K3							
K4	6.96					10	10
K5	84.21	7.51	80.51	11.32		10	10
K6	14.30	57.03	78.25	89.74	10		10
K7	73.40	15.82	8.14	89.24	10	10	
k_f	0.0099	0.00845	0.0116	0.0141	0.01	0.01	0.01
k_b	0.000299	0.001	0.00104	0.000926	0.001	0.001	0.001
R^2	0.555	0.932	0.623	0.665	0.518	0.621	0.645
σ^2	0.503	0.465	0.669	0.701	0.523	0.577	0.601

Table K 5:Rate and equilibrium constants for AAC heterogeneous catalyzed reaction of APO using Eley-Rideal (ER) model at 50^{o}C

	Methanol adsorption	Surface rxn b/w TG and adsorbed methanol	Surface rxn b/w DG and adsorbed methanol	Surface rxn b/w MG and adsorbed methanol	Desorption of DG	Desorption of MG	Desorption of GL
K 1		11.22	12.40	10.58	10	10	10
K 2	26.45				10	10	10
K 3							
K 4	8.13					10	10
K 5	81.21	8.46	85.10	12.21		10	10
K 6	13.60	71.83	76.51	90.21	10		10
K 7	75.40	15.48	8.36	86.45	10	10	
k_f	0.0142	0.00899	0.0112	0.0111	0.01	0.01	0.01
k_b	0.00045	0.001	0.00109	0.000707	0.001	0.001	0.001
R^2	0.513	0.923	0.689	0.772	0.588	0.698	0.556
σ^2	0.569	0.531	0.686	0.722	0.713	0.777	0.689

Table K 6:Rate and equilibrium constants for AAC heterogeneous catalyzed reaction of APO using Eley-Rideal (ER) model at 55^{o}C

	Methanol adsorption	Surface rxn b/w TG and adsorbed methanol	Surface rxn b/w DG and adsorbed methanol	Surface rxn b/w MG and adsorbed methanol	Desorption of DG	Desorption of MG	Desorption of GL
K1		10.87	12.40	10.24	10	10	10
K2	24.51				10	10	10
K3							
K4	8.86					10	10
K5	81.98	9.04	90.10	13.40		10	10
K6	12.99	77.78	77.30	88.87	10		10
K7	76.10	15.17	9.6	85.29	10	10	
k_f	0.0123	0.00934	0.0122	0.0136	0.01	0.01	0.01
k_b	0.00038	0.001	0.0011	0.00058	0.001	0.001	0.001
R^2	0.654	0.941	0.620	0.615	0.524	0.599	0.600
σ^2	0.589	0.449	0.691	0.740	0.685	0.679	0.789

Table K 7:Rate and equilibrium constants for BAC heterogeneous catalyzed reaction of APO using Eley-Rideal (ER) model at 45^{o}C

	Methanol adsorption	Surface rxn b/w TG and adsorbed methanol	Surface rxn b/w DG and adsorbed methanol	Surface rxn b/w MG and adsorbed methanol	Desorption of DG	Desorption of MG	Desorption of GL
K1		11.82	14.87	11.32	10	10	10
K2	24.61				10	10	10
K3							
K4	7.07					10	10
K5	84.97	7.19	82.30	11.65		10	10
K6	13.62	91.96	78.64	87.45	10		10
K7	73.76	15.02	7.88	90.23	10	10	
k_f	0.0098	0.00839	0.0145	0.0132	0.01	0.01	0.01
k_b	0.000305	0.00101	0.00136	0.00084	0.001	0.001	0.001
R^2	0.544	0.918	0.666	0.772	0.608	0.701	0.645
σ^2	0.565	0.502	0.676	0.713	0.623	0.677	0.619

Table K 8:Rate and equilibrium constants for BAC heterogeneous catalyzed reaction of APO using Eley-Rideal (ER) model at 50^{o}C

	Methanol adsorption	Surface rxn b/w TG and adsorbed methanol	Surface rxn b/w DG and adsorbed methanol	Surface rxn b/w MG and adsorbed methanol	Desorption of DG	Desorption of MG	Desorption of GL
K 1		11.42	13.60	11.85	10	10	10
K 2	23.51				10	10	10
K 3							
K 4	7.98					10	10
K 5	75.10	7.81	81.10	12.56		10	10
K 6	12.30	94.30	74.15	86.41	10		10
K 7	70.14	14.05	9.32	77.65	10	10	
k_f	0.0123	0.00879	0.0133	0.0101	0.01	0.01	0.01
k_b	0.000407	0.001	0.00117	0.000615	0.001	0.001	0.001
R^2	0.665	0.911	0.681	0.672	0.578	0.657	0.626
σ^2	0.612	0.523	0.674	0.714	0.697	0.667	0.699

Table K 9:Rate and equilibrium constants for BAC heterogeneous catalyzed reaction of APO using Eley-Rideal (ER) model at 55^{o}C

	Methanol adsorption	Surface rxn b/w TG and adsorbed methanol	Surface rxn b/w DG and adsorbed methanol	Surface rxn b/w MG and adsorbed methanol	Desorption of DG	Desorption of MG	Desorption of GL
K 1		11.49	10.40	10.87	10	10	10
K 2	20.51				10	10	10
K 3							
K 4	8.12					10	10
K 5	78.75	7.34	89.12	12.14		10	10
K 6	11.34	88.26	78.56	80.54	10		10
K 7	72.15	13.63	8.67	77.56	10	10	
k_f	0.0106	0.00884	0.0120	0.0117	0.01	0.01	0.01
k_b	0.00039	0.00101	0.000976	0.000822	0.001	0.001	0.001
R^2	0.665	0.952	0.689	0.711	0.558	0.621	0.599
σ^2	0.678	0.534	0.617	0.717	0.650	0.669	0.702

Table K 10:Rate and equilibrium constants for TAC heterogeneous catalyzed reaction of GSO using Eley-Rideal (ER) model at 45^{o}C

	Methaol adsorption	Surface rxn b/w TG and adsorbed methanol	Surface rxn b/w DG and adsorbed methanol	Surface rxn b/w MG and adsorbed methanol	Desorption of DG	Desorption of MG	Desorption of GL
K1		12.12	11.29	12.15	10	10	10
K2	23.12				10	10	10
K3							
K4	7.35					10	10
K5	86.8	8.23	87.51	7.89		10	10
K6	12.91	75.60	80.32	65.32	10		10
K7	60.52	15.12	8.54	75.32	10	10	
k_f	0.013	0.00878	0.0103	0.0118	0.01	0.01	0.01
k_b	0.00063	0.000979	0.000896	0.000861	0.001	0.001	0.001
R^2	0.665	0.922	0.611	0.612	0.687	0.710	0.578
σ^2	0.648	0.498	0.605	0.655	0.670	0.725	0.644

Table K 11:Rate and equilibrium constants for TAC heterogeneous catalyzed reaction of GSO using Eley-Rideal (ER) model at 50^{o}C

	Methaol adsorption	Surface rxn b/w TG and adsorbed methanol	Surface rxn b/w DG and adsorbed methanol	Surface rxn b/w MG and adsorbed methanol	Desorption of DG	Desorption of MG	Desorption of GL
K1		12.56	12.20	13.34	10	10	10
K2	21.30				10	10	10
K3							
K4	8.74	8.74				10	10
K5	78.6	8.88	71.15	8.64		10	10
K6	13.20	83.37	70.10	81.40	10		10
K7	62.41	16.10	8.56	71.35	10	10	
k_f	0.0110	0.00901	0.0123	0.0113	0.01	0.01	0.01
k_b	0.000607	0.00097	0.00115	0.00092	0.001	0.001	0.001
R^2	0.561	0.942	0.652	0.663	0.529	0.643	0.627
σ^2	0.576	0.531	0.657	0.669	0.613	0.615	0.643

Table K 12:Rate and equilibrium constants for TAC heterogeneous catalyzed reaction of GSO using Eley-Rideal (ER) model at 55^{o}C

	Methanol adsorption	Surface rxn b/w TG and adsorbed methanol	Surface rxn b/w DG and adsorbed methanol	Surface rxn b/w MG and adsorbed methanol	Desorption of DG	Desorption of MG	Desorption of GL
K1		11.76	13.10	12.51	10	10	10
K2	20.40				10	10	10
K3							
K4	8.68					10	10
K5	71.56	8.99	78.31	11.52		10	10
K6	12.34	80.71	75.5	68.24	10		10
K7	67.41	16.38	8.41	70.51	10	10	
k_f	0.0119	0.0092	0.0122	0.0108	0.01	0.01	0.01
k_b	0.00062	0.00096	0.00109	0.00082	0.001	0.001	0.001
R^2	0.569	0.930	0.691	0.678	0.598	0.687	0.589
σ^2	0.621	0.514	0.658	0.678	0.620	0.715	0.631

Table K 13:Rate and equilibrium constants for AAC heterogeneous catalyzed reaction of GSO using Eley-Rideal (ER) model at 45^{o}C

	Methanol adsorption	Surface rxn b/w TG and adsorbed methanol	Surface rxn b/w DG and adsorbed methanol	Surface rxn b/w MG and adsorbed methanol	Desorption of DG	Desorption of MG	Desorption of GL
K1		12.45	12.30	11.14	10	10	10
K2	18.35				10	10	10
K3							
K4	7.01					10	10
K5	70.31	9.10	75.14	10.21		10	10
K6	13.45	60.32	56.32	78.01	10		10
K7	61.56	14.39	9.42	68.24	10	10	
k_f	0.0110	0.00839	0.0105	0.0131	0.01	0.01	0.01
k_b	0.000375	0.00095	0.000997	0.00115	0.001	0.001	0.001
R^2	0.625	0.922	0.681	0.676	0.698	0.756	0.6310
σ^2	0.503	0.498	0.657	0.701	0.612	0.667	0.681

Table K 14:Rate and equilibrium constants for AAC heterogeneous catalyzed reaction of GSO using Eley-Rideal (ER) model at 50^{o}C

	Methanol adsorption	Surface rxn b/w TG and adsorbed methanol	Surface rxn b/w DG and adsorbed methanol	Surface rxn b/w MG and adsorbed methanol	Desorption of DG	Desorption of MG	Desorption of GL
K 1		11.99	11.60	12.21	10	10	10
K 2	16.51				10	10	10
K 3							
K 4	7.98					10	10
K 5	76.11	9.45	75.10	13.42		10	10
K 6	12.10	73.31	65.23	56.42	10		10
K 7	67.10	15.45	9.12	75.32	10	10	
k_f	0.0131	0.00868	0.0102	0.0131	0.01	0.01	0.01
k_b	0.00062	0.001	0.000829	0.00093	0.001	0.001	0.001
R^2	0.634	0.9120	0.672	0.632	0.631	0.681	0.563
σ^2	0.687	0.511	0.698	0.734	0.723	0.754	0.678

Table K 15:Rate and equilibrium constants for AAC heterogeneous catalyzed reaction of GSO using Eley-Rideal (ER) model at 55^{o}C

	Methanol adsorption	Surface rxn b/w TG and adsorbed methanol	Surface rxn b/w DG and adsorbed methanol	Surface rxn b/w MG and adsorbed methanol	Desorption of DG	Desorption of MG	Desorption of GL
K 1		11.23	11.50	11.35	10	10	10
K 2	23.25				10	10	10
K 3							
K 4	9.10					10	10
K 5	71.96	9.70	81.40	12.54		10	10
K 6	11.64	70.84	75.10	13.67	10		10
K 7	64.53	15.10	8.97	71.42	10	10	
k_f	0.0134	0.00899	0.0111	0.0125	0.01	0.01	0.01
k_b	0.00063	0.001	0.000895	0.000885	0.001	0.001	0.001
R^2	0.565	0.912	0.661	0.672	0.508	0.651	0.621
σ^2	0.597	0.419	0.615	0.690	0.612	0.655	0.789

Table K 16:Rate and equilibrium constants for BAC heterogeneous catalyzed reaction of GSO using Eley-Rideal (ER) model at 45^{o}C

	Methanol adsorption	Surface rxn b/w TG and adsorbed methanol	Surface rxn b/w DG and adsorbed methanol	Surface rxn b/w MG and adsorbed methanol	Desorption of DG	Desorption of MG	Desorption of GL
K1		12.32	13.46	12.54	10	10	10
K2	26.25				10	10	10
K3							
K4	7.78					10	10
K5	75.26	8.21	72.50	12.36		10	10
K6	12.46	88.60	68.41	67.45	10		10
K7	64.57	15.62	8.86	71.31	10	10	
k_f	0.0099	0.00859	0.0125	0.0122	0.01	0.01	0.01
k_b	0.000444	0.001	0.000904	0.00078	0.001	0.001	0.001
R^2	0.565	0.912	0.661	0.672	0.508	0.651	0.621
σ^2	0.516	0.512	0.668	0.689	0.697	0.678	0.664

Table K 17:Rate and equilibrium constants for BAC heterogeneous catalyzed reaction of GSO using Eley-Rideal (ER) model at 50^{o}C

	Methanol adsorption	Surface rxn b/w TG and adsorbed methanol	Surface rxn b/w DG and adsorbed methanol	Surface rxn b/w MG and adsorbed methanol	Desorption of DG	Desorption of MG	Desorption of GL
K1		12.04	12.30	13.14	10	10	10
K2	21.31				10	10	10
K3							
K4	8.02					10	10
K5	65.10	8.67	71.10	10.24		10	10
K6	11.30	78.9	64.15	70.63	10		10
K7	60.14	15.4	8.98	65.21	10	10	
k_f	0.0103	0.00871	0.0113	0.0132	0.01	0.01	0.01
k_b	0.000534	0.00102	0.000645	0.0000512	0.001	0.001	0.001
R^2	0.558	0.912	0.661	0.665	0.517	0.620	0.601
σ^2	0.697	0.502	0.665	0.741	0.672	0.656	0.617

Table K 18:Rate and equilibrium constants for BAC heterogeneous catalyzed reaction of GSO using Eley-Rideal (ER) model at 55^{o}C

	Methanol adsorption	Surface rxn b/w TG and adsorbed methanol	Surface rxn b/w DG and adsorbed methanol	Surface rxn b/w MG and adsorbed methanol	Desorption of DG	Desorption of MG	Desorption of GL
K1		12.01	12.65	11.54	10	10	10
K2	21.32				10	10	10
K3							
K4	8.55					10	10
K5	71.53	7.98	76.31	11.54		10	10
K6	12.45	82.60	65.42	70.25	10		10
K7	70.12	14.30	9.12	67.84	10	10	
k_f	0.0116	0.00886	0.0132	0.0129	0.01	0.01	0.01
k_b	0.00052	0.000996	0.00111	0.00096	0.001	0.001	0.001
R^2	0.655	0.939	0.619	0.687	0.598	0.689	0.699
σ^2	0.698	0.513	0.678	0.721	0.638	0.697	0.778

Appendix L

Engine Performance for APO biodiesel/blends

i. Brake Power

bp = $\frac{TxN}{9549.3}$, N= speed, T= torque

bp= $\frac{1400x12}{9549.3}$ =1.76kW

ii. Brake Thermal Efficiency

n_{bt} = $\frac{bp}{m_f\ x\ LHV}$ x 100

n_{bt} = $\frac{1.76}{0.215x10^{-3}\ x\ 50000}$ x 100 = 16.37%

iii. Brake Specific Fuel Consumption, BSFC

BSFC = $\frac{feul\ used\ (\frac{kg}{h})}{brake\ \ power\ \ (kw)}$ = $\frac{3600xm_f}{bp}$ = $\frac{3600x\ 0.215x10^{-3}}{1.76}$ = 0.44kg/kwh

Table L1: Test Rig Result for B0

Volume of fuel = 50cm^3, ρ = 840kg/m^3, LHV = 50000J/kg

S/N	Time (s)	Q x 10^{-7} m^3/s	Speed (rpm)	Torque (Nm)	Exhaust Temp. ^{o}C	Air-fuel ratio	mf (kg/s) x10^{-3}
1	195	2.56	1400	12	255	77.67	0.215
2	180	2.77	1600	13	298	92.56	0.233
3	155	3.23	1800	15	350	92.61	0.271
4	140	3.57	2000	16	399	91.07	0.300
5	90	5.56	2200	18	450	65.45	0.467

Table L2a: Test Rig Result for APO B20 by TAC

Volume of fuel = 50cm^3, ρ = 845kg/m^3, LHV = 4800kJ/kg

S/N	Time (s)	Q x 10^{-6} m^3/s	Speed (rpm)	Torque (Nm)	Exhaust Temp. ^{o}C	Air-fuel ratio	mf (kg/s) x10^{-3}
1	200	0.250	1400	10	253	79.20	0.211
2	195	0.256	1600	12	300	99.68	0.217
3	160	0.313	1800	14	351	95.03	0.264
4	150	0.333	2000	15	399	96.99	0.282
5	95	0.526	2200	17	458	68.68	0.445

Table L2b: Test Rig Result for APO B20 by AAC

Volume of fuel = 50cm^3, ρ = 843kg/m^3, LHV = 4900kJ/kg

S/N	Time (s)	Q x 10^{-6} m^3/s	Speed (rpm)	Torque (Nm)	Exhaust Temp. ^{o}C	Air-fuel ratio	mf (kg/s) x10^{-3}
1	201	0.249	1400	11	254	79.78	0.210
2	196	0.255	1600	13	301	100.43	0.215
3	162	0.309	1800	15	352	96.45	0.260
4	155	0.323	2000	16	398	100.47	0.272
5	97	0.515	2200	18	457	70.29	0.435

Table L2c: Test Rig Result for APO B20 by BAC

Volume of fuel = 50cm^3, ρ = 845kg/m^3, LHV = 4700kJ/kg

S/N	Time (s)	Q x 10^{-6} m^3/s	Speed (rpm)	Torque (Nm)	Exhaust Temp. ^{o}C	Air-fuel ratio	mf (kg/s) x10^{-3}
1	205	0.244	1400	12	254	81.18	0.206
2	198	0.253	1600	14	301	101.22	0.213
3	168	0.298	1800	16	352	99.79	0.251
4	160	0.313	2000	17	398	103.46	0.264
5	100	0.500	2200	19	457	72.30	0.423

Table L3a Test Rig Result for APO B40 by TAC

Volume of fuel = 50cm^3, ρ = 848kg/m^3, LHV = 46000kJ/kg

S/N	Time (s)	Q x 10^{-6} m^3/s	Speed (rpm)	Torque (Nm)	Exhaust Temp. ^{o}C	Air-fuel ratio	mf (kg/s) x10^{-3}
1	207	0.212	1400	9	258	81.97	0.204
2	197	0.254	1600	11	300	100.71	0.214
3	162	0.309	1800	13	351	96.22	0.261
4	152	0.329	2000	14	400	98.29	0.278
5	98	0.510	2200	16	450	70.85	0.431

Table L3b Test Rig Result for APO B40 by AAC

Volume of fuel = 50cm^3, ρ = 846kg/m^3, LHV = 47000kJ/kg

S/N	Time (s)	Q x 10^{-6} m^3/s	Speed (rpm)	Torque (Nm)	Exhaust Temp. ^{o}C	Air-fuel ratio	mf (kg/s) x10^{-3}
1	208	0.240	1400	10	258	82.27	0.203
2	200	0.250	1600	12	300	102.12	0.212
3	170	0.294	1800	14	351	100.85	0.249
4	160	0.313	2000	15	400	103.34	0.264
5	102	0.490	2200	17	450	73.65	0.415

Table L3c: Test Rig Result for APO B40 by BAC

Volume of fuel = 50cm^3, ρ = 847kg/m^3, LHV = 46000kJ/kg

S/N	Time (s)	Q x 10^{-6} m^3/s	Speed (rpm)	Torque (Nm)	Exhaust Temp. ^{o}C	Air-fuel ratio	mf (kg/s) x10^{-3}
1	210	0.238	1400	11	258	82.96	0.202
2	205	0.244	1600	13	300	104.55	0.207
3	175	0.286	1800	15	351	103.70	0.242
4	165	0.303	2000	16	400	106.44	0.257
5	105	0.476	2200	18	450	75.73	0.403

Table L4a: Test Rig Result for APO B60 by TAC

Volume of fuel = 50cm^3, ρ = 852kg/m^3, LHV = 44000kJ/kg

S/N	Time (s)	Q x 10^{-6} m^3/s	Speed (rpm)	Torque (Nm)	Exhaust Temp. ^{o}C	Air-fuel ratio	mf (kg/s) x10^{-3}
1	210	0.238	1400	8	255	95.68	0.202
2	200	0.250	1600	10	301	111.60	0.212
3	170	0.294	1800	12	347	106.06	0.249
4	160	0.313	2000	13	397	109.35	0.265
5	100	0.500	2200	15	448	75.56	0.424

Table L4b: Test Rig Result for APO B60 by AAC

Volume of fuel = 50cm^3, ρ = 850kg/m^3, LHV = 45000kJ/kg

S/N	Time (s)	Q x 10^{-6} m^3/s	Speed (rpm)	Torque (Nm)	Exhaust Temp. ^{o}C	Air-fuel ratio	mf (kg/s) x10^{-3}
1	208	0.240	1400	9	255	94.55	0.204
2	198	0.253	1600	11	301	110.23	0.215
3	168	0.298	1800	13	347	104.57	0.253
4	158	0.316	2000	14	397	107.73	0.269
5	98	0.510	2200	16	448	73.87	0.434

Table L4c: Test Rig Result for APO B60 by BAC

Volume of fuel = 50cm^3, ρ = 853kg/m^3, LHV = 44500kJ/kg

S/N	Time (s)	Q x 10^{-6} m^3/s	Speed (rpm)	Torque (Nm)	Exhaust Temp. ^{o}C	Air-fuel ratio	mf (kg/s) x10^{-3}
1	211	0.237	1400	10	255	95.57	0.202
2	202	0.248	1600	11	301	112.06	0.211
3	174	0.287	1800	12	347	107.92	0.245
4	163	0.306	2000	13	397	110.75	0.262
5	104	0.481	2200	15	448	78.12	0.410

Table L 5a Test Rig Result for APO B80 by TAC

Volume of fuel = 50cm^3, ρ = 855kg/m^3, LHV = 42000kJ/kg

S/N	Time (s)	Q x 10^{-6} m^3/s	Speed (rpm)	Torque (Nm)	Exhaust Temp. ^{o}C	Air-fuel ratio	mf (kg/s) x10^{-3}
1	220	0.227	1400	7	260	99.42	0.194
2	210	0.238	1600	9	300.5	116.22	0.204
3	190	0.263	1800	11	347.8	117.57	0.225
4	175	0.286	2000	12	395	118.62	0.244
5	110	0.455	2200	13	448	82.43	0.389

Table L 5b: Test Rig Result for APO B80 by AAC

Volume of fuel = 50cm^3, ρ = 854kg/m^3, LHV = 42500kJ/kg

S/N	Time (s)	Q x 10^{-6} m^3/s	Speed (rpm)	Torque (Nm)	Exhaust Temp. ^{o}C	Air-fuel ratio	mf (kg/s) x10^{-3}
1	215	0.227	1400	8	260	99.42	0.194
2	205	0.238	1600	10	300.5	116.22	0.204
3	185	0.263	1800	12	347.8	117.57	0.225
4	170	0.286	2000	13	395	118.62	0.244
5	105	0.455	2200	14	448	82.43	0.389

Table L 5c: Test Rig Result for APO B80 by BAC

Volume of fuel = 50cm^3, ρ = 856kg/m^3, LHV = 41500kJ/kg

S/N	Time (s)	Q x 10^{-6} m^3/s	Speed (rpm)	Torque (Nm)	Exhaust Temp. ^{o}C	Air-fuel ratio	mf (kg/s) x10^{-3}
1	221	0.226	1400	10	260	99.75	0.194
2	218	0.229	1600	11	300.5	120.51	0.196
3	192	0.260	1800	13	347.8	118.67	0.223
4	180	0.278	2000	14	395	121.87	0.238
5	110	0.455	2200	15	448	82.33	0.389

Table L 6a: Test Rig Result for APO B100 by TAC

Volume of fuel = 50cm^3, ρ = 860kg/m^3, LHV = 40100kJ/kg

S/N	Time (s)	Q x 10^{-6} m^3/s	Speed (rpm)	Torque (Nm)	Exhaust Temp. ^{o}C	Air-fuel ratio	mf (kg/s) x10^{-3}
1	225	0.222	1400	6	260	101.32	0.191
2	215	0.233	1600	8	303	118.57	0.200
3	195	0.256	1800	10	345	120.24	0.221
4	180	0.278	2000	11	419	121.58	0.239
5	115	0.435	2200	12	445	85.88	0.374

Table L 6b: Test Rig Result for APO B100 by AAC

Volume of fuel = 50cm^3, ρ = 858kg/m^3, LHV = 41000kJ/kg

S/N	Time (s)	Q x 10^{-6} m^3/s	Speed (rpm)	Torque (Nm)	Exhaust Temp. ^{o}C	Air-fuel ratio	mf (kg/s) x10^{-3}
1	222	0.252	1400	7	260	99.97	0.193
2	213	0.235	1600	9	303	117.47	0.201
3	193	0.259	1800	10	345	119.01	0.222
4	178	0.281	2000	12	419	120.23	0.241
5	113	0.442	2200	13	445	84.38	0.380

Table L 6c: Test Rig Result for APO B100 by BAC

Volume of fuel = 50cm^3, ρ = 859kg/m^3, LHV = 41000kJ/kg

S/N	Time (s)	Q x 10^{-6} m^3/s	Speed (rpm)	Torque (Nm)	Exhaust Temp. ^{o}C	Air-fuel ratio	mf (kg/s) x10^{-3}
1	224	0.223	1400	8	262	100.87	0.192
2	215	0.233	1600	9	303	118.57	0.200
3	194	0.258	1800	11	345	119.62	0.221
4	180	0.278	2000	12	420	121.58	0.238
5	115	0.435	2200	14	446	85.88	0.373

Table L 7a: Variation of Engine Speed with Brake Power for APO biodiesel/blends by TAC

S/N	Speed (rpm)	Brake Power (KW)					
		B0	B20	B40	B60	B80	B100
1	1400	1.76	1.47	1.32	1.17	1.03	0.880
2	1600	2.18	2.26	1.84	1.68	1.51	1.34
3	1800	2.83	3.23	2.45	2.26	2.07	1.88
4	2000	3.35	4.08	2.93	2.72	2.51	2.30
5	2200	4.15	5.34	3.69	3.46	2.99	2.76

Table L 7b: Variation of Engine Speed with Brake Power for APO biodiesel/blends by AAC

S/N	Speed (rpm)	Brake Power (KW)					
		B0	B20	B40	B60	B80	B100
1	1400	1.76	1.47	1.32	1.27	1.47	0.880
2	1600	2.18	2.26	1.84	1.68	1.54	1.34
3	1800	2.83	3.23	2.45	2.26	2.25	1.88
4	2000	3.35	4.08	2.93	2.72	2.63	2.30
5	2200	4.15	5.34	3.69	3.46	3.46	2.76

Table L 7c: Variation of Engine Speed with Brake Power for APO biodiesel/blends by BAC

S/N	Speed (rpm)	Brake Power (KW)					
		B0	B20	B40	B60	B80	B100
1	1400	1.76	1.61	1.47	1.32	1.03	1.03
2	1600	2.18	2.45	2.01	1.84	1.51	1.51
3	1800	2.83	3.46	2.64	2.45	2.07	1.88
4	2000	3.35	4.36	3.14	2.93	2.51	2.51
5	2200	4.15	5.65	3.92	3.69	2.99	2.99

Table L 8a: Variation of Engine Speed with Brake Thermal Efficiency for APO biodiesel/blends by TAC

S/N	Speed (rpm)	Brake Thermal Efficiency (%)					
		B0	B20	B40	B60	B80	B100
1	1400	16.34	14.46	14.05	13.20	12.57	11.51
2	1600	18.67	21.75	18.68	17.96	17.64	16.75
3	1800	20.87	25.45	20.42	20.61	21.94	21.37
4	2000	22.34	30.20	22.93	23.35	24.50	24.11
5	2200	17.78	25.01	18.59	18.52	18.35	18.48

Table L 8b: Variation of Engine Speed with Brake Thermal Efficiency for APO biodiesel/blends by AAC

S/N	Speed (rpm)	Brake Thermal Efficiency (%)					
		B0	B20	B40	B60	B80	B100
1	1400	16.34	14.46	14.05	13.20	18.24	11.48
2	1600	18.67	21.75	18.68	17.96	22.62	16.71
3	1800	20.87	25.45	20.42	20.61	26.49	21.32
4	2000	22.34	30.20	22.93	23.35	29.71	24.05
5	2200	17.78	25.01	18.59	18.52	21.40	18.44

Table L 8c: Variation of Engine Speed with Brake Thermal Efficiencyfor APO biodiesel/blends by BAC

S/N	Speed (rpm)	Brake Thermal Efficiency (%)					
		B0	B20	B40	B60	B80	B100
1	1400	16.34	15.69	15.34	14.35	13.57	12.95
2	1600	18.67	23.25	20.23	19.08	18.64	18.26
3	1800	20.87	27.11	22.57	21.53	21.94	20.68
4	2000	22.34	32.69	25.28	24.22	24.50	25.43
5	2200	17.78	26.56	20.09	18.89	18.35	19.24

Table L 9a: Variation of Engine Speed with Brake Specific Fuel Consumption for APO biodiesel/blends by TAC

S/N	Speed (rpm)	Brake Specific Fuel Consumption (kg/kWh)					
		B0	B20	B40	B60	B80	B100
1	1400	0.441	0.519	0.557	0.620	0.682	0.780
2	1600	0.386	0.345	0.419	0.456	0.486	0.537
3	1800	0.345	0.295	0.383	0.397	0.391	0.421
4	2000	0.322	0.248	0.341	0.350	0.350	0.373
5	2200	0.405	0.300	0.421	0.442	0.467	0.487

Table L 9b: Variation of Engine Speed with Brake Specific Fuel Consumption for APO biodiesel/blends by AAC

S/N	Speed (rpm)	Brake Specific Fuel Consumption (kg/kWh)					
		B0	B20	B40	B60	B80	B100
1	1400	0.441	0.519	0.557	0.620	0.476	0.782
2	1600	0.386	0.345	0.419	0.456	0.383	0.537
3	1800	0.345	0.295	0.383	0.397	0.327	0.421
4	2000	0.322	0.248	0.341	0.350	0.292	0.373
5	2200	0.405	0.300	0.421	0.442	0.405	0.487

Table L 9c: Variation of Engine Speed with Brake Specific Fuel Consumption for APO biodiesel/blends by BAC

S/N	Speed (rpm)	Brake Specific Fuel Consumption (kg/kWh)					
		B0	B20	B40	B60	B80	B100
1	1400	0.441	0.517	0.501	0.552	0.534	0.536
2	1600	0.386	0.340	0.419	0.456	0.389	0.402
3	1800	0.345	0.288	0.383	0.434	0.357	0.359
4	2000	0.322	0.220	0.341	0.380	0.317	0.324
5	2200	0.405	0.279	0.421	0.474	0.441	0.460

Table L 10a: Variation of CO with load for APO biodiesel/blends by TAC

S/N	Load (kg)	CO (ppm)					
		B0	B20	B40	B60	B80	B100
1	50	400	320	260	200	175	130
2	100	480	370	285	220	190	150
3	150	510	400	300	240	205	180
4	200	560	430	320	280	235	195
5	250	600	450	350	310	260	210

Table L 10b: Variation of CO with load for APO biodiesel/blends by AAC

S/N	Load (kg)	CO (ppm)					
		B0	B20	B40	B60	B80	B100
1	50	380	300	230	185	155	120
2	100	410	350	255	200	170	130
3	150	470	380	290	230	195	150
4	200	520	400	310	270	215	175
5	250	550	430	340	300	250	190

Table L 10c: Variation of CO with load for APO biodiesel/blends by BAC

S/N	Load (kg)	CO (ppm)					
		B0	B20	B40	B60	B80	B100
1	50	410	330	270	210	185	140
2	100	490	380	295	230	200	160
3	150	520	420	310	250	220	190
4	200	570	450	340	295	245	210
5	250	610	460	380	325	270	230

Table L 11a: Variation of NO_x with load for APO biodiesel/blends by TAC

S/N	Load (kg)	NO_x (ppm)					
		B0	B20	B40	B60	B80	B100
1	50	100	120	130	150	160	185
2	100	110	130	150	180	200	210
3	150	120	140	170	200	235	250
4	200	135	160	200	230	255	265
5	250	150	170	220	250	260	280

Table L 11b: Variation of NO_x with load for APO biodiesel/blends by AAC

S/N	Load (kg)	NO_x (ppm)					
		B0	B20	B40	B60	B80	B100
1	50	110	130	145	160	170	180
2	100	120	140	160	180	200	220
3	150	130	150	190	200	225	240
4	200	145	170	220	235	250	255
5	250	160	180	240	250	260	270

Table L 11c: Variation of NO_x with load for APO biodiesel/blends by BAC

S/N	Load (kg)	NO_x (ppm)					
		B0	B20	B40	B60	B80	B100
1	50	115	120	135	140	150	165
2	100	125	130	150	160	180	190
3	150	140	150	180	190	205	215
4	200	155	160	200	215	230	235
5	250	160	170	210	230	250	255

Table L 12a: Variation of HC with load for APO biodiesel/blends by TAC

S/N	Load (kg)	HC (ppm)					
		B0	B20	B40	B60	B80	B100
1	50	80	70	55	40	35	30
2	100	100	90	70	60	50	40
3	150	110	100	80	70	60	50
4	200	125	105	90	85	70	62
5	250	130	115	110	95	80	75

Table L 12b: Variation of HC with load for APO biodiesel/blends by AAC

S/N	Load (kg)	HC (ppm)					
		B0	B20	B40	B60	B80	B100
1	50	70	60	50	40	30	30
2	100	95	85	70	60	50	40
3	150	110	100	75	70	60	50
4	200	125	115	90	85	70	62
5	250	130	125	100	95	80	75

Table L 12c: Variation of HC with load for APO biodiesel/blends by BAC

S/N	Load (kg)	HC (ppm)					
		B0	B20	B40	B60	B80	B100
1	50	70	60	50	40	30	25
2	100	90	85	70	60	50	40
3	150	100	90	75	70	60	50
4	200	115	100	90	80	70	60
5	250	130	110	100	90	80	70

Appendix M

Engine Performance for GSO biodiesel/blends

Table M 1a: Test Rig Result for GSO B20 by TAC

Volume of fuel = 50cm^3, ρ = 846kg/m^3, LHV = 48100kJ/kg

S/N	Time (s)	Q x 10^{-6} m^3/s	Speed (rpm)	Torque (Nm)	Exhaust Temp. ^{o}C	Air-fuel ratio	mf (kg/s) x10^{-3}
1	206	0.243	1400	11	253	81.47	0.205
2	198	0.253	1600	12	300	101.10	0.214
3	163	0.307	1800	13	351	96.70	0.260
4	153	0.327	2000	14	399	98.82	0.276
5	99	0.505	2200	15	458	71.49	0.427

Table M 1b: Test Rig Result for GSO B20 by AAC

Volume of fuel = 50cm^3, ρ = 844kg/m^3, LHV = 49100kJ/kg

S/N	Time (s)	Q x 10^{-6} m^3/s	Speed (rpm)	Torque (Nm)	Exhaust Temp. ^{o}C	Air-fuel ratio	mf (kg/s) x10^{-3}
1	201	0.249	1400	10	254	79.68	0.210
2	197	0.254	1600	12	301	100.83	0.214
3	168	0.298	1800	14	352	99.90	0.251
4	155	0.323	2000	16	398	100.35	0.272
5	100	0.500	2200	18	457	72.38	0.422

Table M 1c: Test Rig Result for GSO B20 by BAC

Volume of fuel = 50cm^3, ρ = 846kg/m^3, LHV = 47100kJ/kg

S/N	Time (s)	Q x 10^{-6} m^3/s	Speed (rpm)	Torque (Nm)	Exhaust Temp. ^{o}C	Air-fuel ratio	mf (kg/s) x10^{-3}
1	206	0.243	1400	11	254	81.47	0.205
2	199	0.251	1600	13	301	101.61	0.213
3	170	0.294	1800	14	352	100.85	0.249
4	162	0.309	2000	16	398	104.63	0.261
5	99	0.505	2200	17	457	71.49	0.427

Table M 2a Test Rig Result for GSO B40 by TAC

Volume of fuel = 50cm^3, ρ = 849kg/m^3, LHV = 46100kJ/kg

S/N	Time (s)	Q x 10^{-6} m^3/s	Speed (rpm)	Torque (Nm)	Exhaust Temp. ^{o}C	Air-fuel ratio	mf (kg/s) x10^{-3}
1	208	0.240	1400	10	258	81.98	0.204
2	199	0.251	1600	11	300	101.25	0.213
3	165	0.303	1800	12	351	97.54	0.257
4	158	0.316	2000	13	400	101.69	0.269
5	99	0.505	2200	14	450	71.23	0.429

Table M 3b: Test Rig Result for GSO B40 by AAC

Volume of fuel = 50cm^3, ρ = 847kg/m^3, LHV = 47100kJ/kg

S/N	Time (s)	Q x 10^{-6} m^3/s	Speed (rpm)	Torque (Nm)	Exhaust Temp. ^{o}C	Air-fuel ratio	mf (kg/s) x10^{-3}
1	208	0.240	1400	8	258	82.17	0.204
2	200	0.250	1600	10	300	102.00	0.212
3	170	0.294	1800	12	351	100.74	0.249
4	160	0.313	2000	14	400	103.21	0.265
5	102	0.490	2200	16	450	73.57	0.415

Table M 2c: Test Rig Result for GSO B40 by BAC

Volume of fuel = 50cm^3, ρ = 848kg/m^3, LHV = 45500kJ/kg

S/N	Time (s)	Q x 10^{-6} m^3/s	Speed (rpm)	Torque (Nm)	Exhaust Temp. ^{o}C	Air-fuel ratio	mf (kg/s) x10^{-3}
1	211	0.237	1400	10	258	83.26	0.201
2	208	0.240	1600	11	300	105.95	0.204
3	180	0.278	1800	13	351	106.54	0.236
4	170	0.294	2000	15	400	109.54	0.249
5	120	0.417	2200	16	450	86.45	0.353

Table M 3a: Test Rig Result for GSO B60 by TAC

Volume of fuel = 50cm^3, ρ = 853kg/m^3, LHV = 44200kJ/kg

S/N	Time (s)	Q x 10^{-6} m^3/s	Speed (rpm)	Torque (Nm)	Exhaust Temp. ^{o}C	Air-fuel ratio	mf (kg/s) x10^{-3}
1	215	0.233	1400	9	255	97.38	0.198
2	205	0.244	1600	10	301	113.72	0.208
3	180	0.278	1800	11	347	111.64	0.237
4	170	0.294	2000	12	397	115.50	0.251
5	110	0.455	2200	13	448	82.62	0.388

Table M 3b: Test Rig Result for GSO B60 by AAC

Volume of fuel = 50cm^3, ρ = 851kg/m^3, LHV = 44900kJ/kg

S/N	Time (s)	Q x 10^{-6} m^3/s	Speed (rpm)	Torque (Nm)	Exhaust Temp. ^{o}C	Air-fuel ratio	mf (kg/s) x10^{-3}
1	209	0.238	1400	8	255	95.34	0.203
2	205	0.250	1600	10	301	111.21	0.213
3	185	0.294	1800	11	347	105.69	0.250
4	178	0.313	2000	12	397	108.96	0.266
5	110	0.500	2200	13	448	75.29	0.426

Table M 3c: Test Rig Result for GSO B60 by BAC

Volume of fuel = 50cm^3, ρ = 854kg/m^3, LHV = 44400kJ/kg

S/N	Time (s)	Q x 10^{-6} m^3/s	Speed (rpm)	Torque (Nm)	Exhaust Temp. ^{o}C	Air-fuel ratio	mf (kg/s) x10^{-3}
1	210	0.238	1400	10	255	95.01	0.203
2	200	0.250	1600	12	301	110.82	0.214
3	170	0.294	1800	14	347	105.31	0.251
4	160	0.313	2000	15	397	108.58	0.267
5	100	0.500	2200	16	448	75.02	0.427

Table M 5 a Test Rig Result for GSO B80 by TAC

Volume of fuel = 50cm^3, ρ = 856kg/m^3, LHV = 42100kJ/kg

S/N	Time (s)	Q x 10^{-6} m^3/s	Speed (rpm)	Torque (Nm)	Exhaust Temp. ^{o}C	Air-fuel ratio	mf (kg/s) x10^{-3}
1	225	0.222	1400	9	260	101.56	0.190
2	215	0.233	1600	10	300.5	118.85	0.199
3	200	0.250	1800	11	347.8	123.61	0.214
4	185	0.270	2000	12	395	125.25	0.231
5	115	0.435	2200	13	448	86.08	0.372

Table M 3b: Test Rig Result for GSO B80 by AAC

Volume of fuel = 50cm^3, ρ = 855kg/m^3, LHV = 42400kJ/kg

S/N	Time (s)	Q x 10^{-6} m^3/s	Speed (rpm)	Torque (Nm)	Exhaust Temp. ^{o}C	Air-fuel ratio	mf (kg/s) x10^{-3}
1	220	0.227	1400	7	260	99.42	0.194
2	215	0.233	1600	9	300.5	118.99	0.199
3	195	0.256	1800	11	347.8	120.66	0.219
4	182	0.275	2000	12	395	123.37	0.235
5	105	0.476	2200	13	448	78.68	0.407

Table M 3c: Test Rig Result for GSO B80 by BAC

Volume of fuel = 50cm^3, ρ = 857kg/m^3, LHV = 41400kJ/kg

S/N	Time (s)	Q x 10^{-6} m^3/s	Speed (rpm)	Torque (Nm)	Exhaust Temp. ^{o}C	Air-fuel ratio	mf (kg/s) x10^{-3}
1	225	0.222	1400	8	260	101.44	0.190
2	220	0.227	1600	10	300.5	121.47	0.195
3	200	0.250	1800	11	347.8	123.47	0.214
4	195	0.256	2000	13	395	131.87	0.220
5	110	0.455	2200	15	448	82.23	0.390

Table M 4a: Test Rig Result for GSO B100 by TAC

Volume of fuel = 50cm^3, ρ = 859kg/m^3, LHV = 41000kJ/kg

S/N	Time (s)	Q x 10^{-6} m^3/s	Speed (rpm)	Torque (Nm)	Exhaust Temp. ^{o}C	Air-fuel ratio	mf (kg/s) x10^{-3}
1	230	0.217	1400	8	260	103.45	0.187
2	220	0.227	1600	9	303	121.19	0.195
3	200	0.250	1800	10	345	123.18	0.215
4	185	0.270	2000	11	419	124.81	0.232
5	120	0.417	2200	12	445	89.51	0.358

Table M 4b: Test Rig Result for GSO B100 by AAC

Volume of fuel = 50cm^3, ρ = 859kg/m^3, LHV = 41000kJ/kg

S/N	Time (s)	Q x 10^{-6} m^3/s	Speed (rpm)	Torque (Nm)	Exhaust Temp. ^{o}C	Air-fuel ratio	mf (kg/s) x10^{-3}
1	235	0.252	1400	7	260	105.70	0.183
2	225	0.235	1600	9	303	123.95	0.191
3	205	0.259	1800	10	345	126.26	0.210
4	190	0.281	2000	12	419	128.19	0.226
5	130	0.442	2200	13	445	96.96	0.330

Table M 4c: Test Rig Result for GSO B100 by BAC

Volume of fuel = 50cm^3, ρ = 860kg/m^3, LHV = 41000kJ/kg

S/N	Time (s)	Q x 10^{-6} m^3/s	Speed (rpm)	Torque (Nm)	Exhaust Temp. ^{o}C	Air-fuel ratio	mf (kg/s) x10^{-3}
1	226	0.221	1400	8	262	101.65	0.190
2	220	0.227	1600	9	303	121.19	0.195
3	200	0.250	1800	10	345	123.18	0.215
4	190	0.263	2000	11	420	128.19	0.226
5	120	0.417	2200	14	446	89.51	0.358

Table M 5a: Variation of Engine Speed with Brake Power for GSO biodiesel/blends by TAC

S/N	Speed (rpm)	Brake Power (KW)					
		B0	B20	B40	B60	B80	B100
1	1400	1.76	1.61	1.47	1.32	1.32	1.93
2	1600	2.18	2.26	1.84	1.84	1.84	2.36
3	1800	2.83	2.99	2.26	2.45	2.07	2.26
4	2000	3.35	3.81	2.93	2.51	2.51	2.72
5	2200	4.15	4.71	3.69	2.99	2.99	3.23

Table M 5b: Variation of Engine Speed with Brake Power for GSO biodiesel/blends by AAC

S/N	Speed (rpm)	Brake Power (KW)					
		B0	B20	B40	B60	B80	B100
1	1400	1.76	1.47	1.17	1.32	1.31	1.30
2	1600	2.18	2.26	1.67	1.68	1.84	1.68
3	1800	2.83	3.23	2.26	2.07	2.45	2.26
4	2000	3.35	4.36	2.93	2.51	2.93	2.72
5	2200	4.15	5.65	3.69	2.99	3.92	3.23

Table M 7c: Variation of Engine Speed with Brake Power for GSO biodiesel/blends by BAC

S/N	Speed (rpm)	Brake Power (KW)					
		B0	B20	B40	B60	B80	B100
1	1400	1.76	1.76	1.32	1.47	1.46	1.45
2	1600	2.18	2.45	1.84	2.01	2.01	2.00
3	1800	2.83	3.23	2.45	2.63	2.64	2.45
4	2000	3.35	4.36	3.14	3.35	3.35	2.93
5	2200	4.15	5.34	3.92	3.92	4.15	3.69

Table M 6a: Variation of Engine Speed with Brake Thermal Efficiency for APO biodiesel/blends by TAC

S/N	Speed (rpm)	Brake Thermal Efficiency (%)					
		B0	B20	B40	B60	B80	B100
1	1400	16.34	16.33	15.58	15.05	14.48	13.40
2	1600	18.67	22.01	18.74	18.22	17.99	16.83
3	1800	20.87	23.99	19.07	19.78	20.01	19.55
4	2000	22.34	28.66	21.98	20.66	19.80	19.40
5	2200	17.78	22.92	18.32	17.48	17.12	16.91

Table M 6b: Variation of Engine Speed with Brake Thermal Efficiency for APO biodiesel/blends by AAC

S/N	Speed (rpm)	Brake Thermal Efficiency (%)					
		B0	B20	B40	B60	B80	B100
1	1400	16.34	14.22	12.23	13.20	14.50	17.61
2	1600	18.67	21.51	16.80	17.96	17.54	21.41
3	1800	20.87	26.15	19.28	20.61	18.50	26.33
4	2000	22.34	32.59	23.52	23.35	21.04	29.38
5	2200	17.78	27.29	18.85	18.52	15.67	23.81

Table M 6c: Variation of Engine Speed with Brake Thermal Efficiencyfor APO biodiesel/blends by BAC

S/N	Speed (rpm)	Brake Thermal Efficiency (%)					
		B0	B20	B40	B60	B80	B100
1	1400	16.34	18.19	14.43	16.24	18.89	18.31
2	1600	18.67	24.48	19.87	21.21	24.93	23.99
3	1800	20.87	27.52	22.86	23.66	29.75	27.20
4	2000	22.34	35.42	27.68	28.28	30.84	30.11
5	2200	17.78	26.54	24.36	20.65	25.71	23.53

Table M 7a: Variation of Engine Speed with Brake Specific Fuel Consumption for APO biodiesel/blends by TAC

S/N	Speed (rpm)	Brake Specific Fuel Consumption (kg/kWh)					
		B0	B20	B40	B60	B80	B100
1	1400	0.441	0.458	0.501	0.541	0.682	0.655
2	1600	0.386	0.340	0.417	0.447	0.486	0.466
3	1800	0.345	0.312	0.409	0.411	0.391	0.373
4	2000	0.322	0.262	0.355	0.359	0.350	0.333
5	2200	0.405	0.312	0.479	0.442	0.467	0.430

Table M 7b: Variation of Engine Speed with Brake Specific Fuel Consumption for APO biodiesel/blends by AAC

S/N	Speed (rpm)	Brake Specific Fuel Consumption (kg/kWh)					
		B0	B20	B40	B60	B80	B100
1	1400	0.441	0.516	0.625	0.553	0.519	0.499
2	1600	0.386	0.341	0.455	0.457	0.428	0.410
3	1800	0.345	0.280	0.396	0.435	0.372	0.333
4	2000	0.322	0.225	0.325	0.381	0.331	0.299
5	2200	0.405	0.269	0.405	0.511	0.447	0.369

Table M 7c: Variation of Engine Speed with Brake Specific Fuel Consumption for APO biodiesel/blends by BAC

S/N	Speed (rpm)	Brake Specific Fuel Consumption (kg/kWh)					
		B0	B20	B40	B60	B80	B100
1	1400	0.441	0.420	0.548	0.499	0.468	0.468
2	1600	0.386	0.312	0.398	0.382	0.349	0.357
3	1800	0.345	0.278	0.346	0.343	0.292	0.315
4	2000	0.322	0.216	0.286	0.287	0.236	0.285
5	2200	0.405	0.288	0.325	0.392	0.338	0.364

Table M 8a: Variation of CO with load for GSO biodiesel/blends by TAC

S/N	Load (kg)	CO (ppm)					
		B0	B20	B40	B60	B80	B100
1	50	390	330	265	220	190	140
2	100	430	380	290	230	200	160
3	150	480	430	310	250	215	190
4	200	500	450	325	290	250	210
5	250	540	480	360	330	270	230

Table M 8b: Variation of CO with load for GSO biodiesel/blends by AAC

S/N	Load (kg)	CO (ppm)					
		B0	B20	B40	B60	B80	B100
1	50	390	310	250	190	165	125
2	100	430	360	270	220	180	140
3	150	480	390	310	260	200	155
4	200	500	420	330	290	230	180
5	250	540	440	350	330	260	200

Table M 8c: Variation of CO with load for GSO biodiesel/blends by BAC

S/N	Load (kg)	CO (ppm)					
		B0	B20	B40	B60	B80	B100
1	50	390	340	280	230	200	150
2	100	430	390	310	240	220	170
3	150	480	430	340	260	230	200
4	200	500	460	360	300	260	230
5	250	540	490	400	380	290	250

Table M 9a: Variation of NO_x with load for GSO biodiesel/blends by TAC

S/N	Load (kg)	NO_x (ppm)					
		B0	B20	B40	B60	B80	B100
1	50	110	140	150	160	170	200
2	100	120	150	160	190	220	240
3	150	130	160	170	210	245	260
4	200	145	170	200	240	265	285
5	250	160	180	220	260	280	300

Table M 9b: Variation of NO_x with load for GSO biodiesel/blends by AAC

S/N	Load (kg)	NO_x (ppm)					
		B0	B20	B40	B60	B80	B100
1	50	110	150	180	190	200	220
2	100	120	170	200	230	240	260
3	150	130	200	220	250	265	280
4	200	145	220	250	265	280	300
5	250	160	240	270	290	310	330

Table M 9c: Variation of NO_x with load for GSO biodiesel/blends by BAC

S/N	Load (kg)	NO_x (ppm)					
		B0	B20	B40	B60	B80	B100
1	50	110	130	145	160	170	180
2	100	120	140	160	170	190	200
3	150	130	150	190	210	230	240
4	200	145	160	200	220	240	250
5	250	160	170	220	240	250	260

Table M 10a: Variation of HC with load for APO biodiesel/blends by TAC

S/N	Load (kg)	HC (ppm)					
		B0	B20	B40	B60	B80	B100
1	50	80	60	55	40	35	30
2	100	90	80	70	60	50	40
3	150	100	90	80	70	60	50
4	200	115	105	90	85	70	62
5	250	130	115	110	95	80	75

Table M 10b: Variation of HC with load for APO biodiesel/blends by AAC

S/N	Load (kg)	HC (ppm)					
		B0	B20	B40	B60	B80	B100
1	50	80	60	50	40	35	30
2	100	90	85	80	60	50	40
3	150	100	95	90	70	65	50
4	200	115	110	95	85	70	65
5	250	130	115	100	95	80	75

Table M 10c: Variation of HC with load for APO biodiesel/blends by BAC

S/N	Load (kg)	HC (ppm)					
		B0	B20	B40	B60	B80	B100
1	50	80	60	50	40	35	30
2	100	90	85	70	60	50	40
3	150	100	92	80	70	60	50
4	200	115	105	90	80	70	60
5	250	130	110	105	90	80	70

Appendix N

Artificial Neural Network Model for prediction of Biodiesel Production and Engine Performance

Artificial Neural Network Model for prediction of Biodiesel Production

```
% Solve an Input-Output Fitting problem with a Neural Network
% Script generated by Neural Fitting app
% Created Thu Feb 01 16:16:16 WAT 2018
%
% This script assumes these variables are defined:
%
%   Input1 - input data.
%   Output1 - target data.

x = Input1;
t = Output1;

% Choose a Training Function
% For a list of all training functions type: help nntrain
% 'trainlm' is usually fastest.
% 'trainbr' takes longer but may be better for challenging problems.
% 'trainscg' uses less memory. NFTOOL falls back to this in low memory
situations.
trainFcn = 'trainlm';  % Levenberg-Marquardt

% Create a Fitting Network
hiddenLayerSize = 25;
net = fitnet(hiddenLayerSize,trainFcn);

% Setup Division of Data for Training, Validation, Testing
net.divideParam.trainRatio = 70/100;
net.divideParam.valRatio = 15/100;
net.divideParam.testRatio = 15/100;

% Train the Network
[net,tr] = train(net,x,t);

% Test the Network
y = net(x);
e = gsubtract(t,y);
performance = perform(net,t,y)

% View the Network
view(net)

% Plots
% Uncomment these lines to enable various plots.
%figure, plotperform(tr)
%figure, plottrainstate(tr)
%figure, plotfit(net,x,t)
%figure, plotregression(t,y)
%figure, ploterrhist(e)
```

```
% Solve an Input-Output Fitting problem with a Neural Network
% Script generated by Neural Fitting app
% Created Sun Apr 15 16:20:47 WAT 2018
%
% This script assumes these variables are defined:
%
%   Input - input data.
%   Output1 - target data.

x = Input;
t = Output1;

% Choose a Training Function
% For a list of all training functions type: help nntrain
% 'trainlm' is usually fastest.
% 'trainbr' takes longer but may be better for challenging problems.
% 'trainscg' uses less memory. NFTOOL falls back to this in low memory
situations.
trainFcn = 'trainlm';  % Levenberg-Marquardt

% Create a Fitting Network
hiddenLayerSize = 10;
net = fitnet(hiddenLayerSize,trainFcn);

% Setup Division of Data for Training, Validation, Testing
net.divideParam.trainRatio = 70/100;
net.divideParam.valRatio = 15/100;
net.divideParam.testRatio = 15/100;

% Train the Network
[net,tr] = train(net,x,t);

% Test the Network
y = net(x);
e = gsubtract(t,y);
performance = perform(net,t,y)

% View the Network
view(net)

% Plots
% Uncomment these lines to enable various plots.
%figure, plotperform(tr)
%figure, plottrainstate(tr)
%figure, plotfit(net,x,t)
%figure, plotregression(t,y)
%figure, ploterrhist(e)
```

Appendix O

Variation of biodiesel physical properties with fraction of biodiesel

Table O 1: Physical properties with blends for APO FAME

Blends	Density (kg/m^3)	Kinematics viscosity (mm^2/s)	Flash point (^oC)	Lower heating value (MJ/kg)	Cetane Number
B0	840	1.8	65	50	47
B20	843	2.0	78	49	52
B40	846	2.6	96	47	53
B60	850	3.1	125	45	55
B80	854	3.3	140	42.5	57
B100	858	3.6	180	41	59

Table O 2: Physical properties with blends for GSO FAME

Blends	Density (kg/m^3)	Kinematics viscosity (mm^2/s)	Flash point (^oC)	Lower heating value (MJ/kg)	Cetane Number
B0	840	1.8	65	50	46
B20	844	2.1	86	49.1	49
B40	847	2.8	105	47.1	52
B60	851	3.0	132	44.9	55
B80	855	3.4	150	42.4	57
B100	859	3.9	182	42	59

Table O 3: FAME (B100) Kinematic viscosity with temperature

Temperature (K)	APO FAME Kinematics viscosity (mm^2/s)	GSO FAME Kinematics viscosity (mm^2/s)
303	3.6	3.4
308	3.3	3.1
313	2.7	2.8
318	2.5	2.3
323	2.2	2.1

Appendix P
Development of models for physical properties of FAME

POLYMATH Results
03-29-2018

Linear Regression Report

Model: Density APO FAME = a0 + a1*x

Variable	Value	95% confidence
a0	839.42857	1.0467282
a1	18.142857	1.7286148

General
Regression including free parameter
Number of observations = 6

Statistics

R^2 =	0.9953101
R^2adj =	0.9941376
Rmsd =	0.1736627
Variance =	0.2714286

POLYMATH Results
03-30-2018

Linear Regression Report

Model: Density GSO FAME = a0 + a1*x

Variable	Value	95% confidence
a0	839.90476	0.6502912
a1	18.857143	1.0739205

General
Regression including free parameter
Number of observations = 6

Statistics

R^2 =	0.9983193
R^2adj =	0.9978992
Rmsd =	0.1078898
Variance =	0.1047619

POLYMATH Results
03-30-2018

Linear Regression Report

Model: Kinematic viscosity for APO FAME = a0 + a1*x

Variable	Value	95% confidence
a0	1.7761905	0.262324
a1	1.9142857	0.4332138

General
Regression including free parameter
Number of observations = 6

Statistics

R^2 =	0.9741049
R^2adj =	0.9676311
Rmsd =	0.0435222
Variance =	0.0170476

POLYMATH Results
03-30-2018

Linear Regression Report

Model: Kinematic viscosity for GSO FAME= a0 + a1*x

Variable	Value	95% confidence
a0	1.7904762	0.2205245
a1	2.0857143	0.3641842

General
Regression including free parameter
Number of observations = 6

Statistics

R^2 =	0.9844212
R^2adj =	0.9805265
Rmsd =	0.0365872
Variance =	0.0120476

POLYMATH Results
03-30-2018

Linear Regression Report

Model: Kinematic viscosity for APO FAME = a0 + a1*x

Variable	Value	95% confidence
a0	1.7761905	0.262324
a1	1.9142857	0.4332138

General
Regression including free parameter
Number of observations = 6

Statistics

R^2 =	0.9741049
R^2adj =	0.9676311
Rmsd =	0.0435222
Variance =	0.0170476

POLYMATH Results
03-30-2018

Linear Regression Report

Model: Kinematic viscosity for APO FAME = a0 + a1*T

Variable	Value	95% confidence
a0	25.396	6.9020155
a1	-0.072	0.0220455

General
Regression including free parameter
Number of observations = 5

Statistics

R^2 =	0.972973
R^2adj =	0.963964
Rmsd =	0.0379473
Variance =	0.012

POLYMATH Results
03-30-2018

Linear Regression Report

Model: Kinematic viscosity for GSO FAME = a0 + a1*T

Variable	Value	95% confidence
a0	24.024	4.6013436
a1	-0.068	0.014697

General
Regression including free parameter
Number of observations = 5

Statistics

R^2 =	0.9863481
R^2adj =	0.9817975
Rmsd =	0.0252982
Variance =	0.0053333

POLYMATH Results
03-30-2018

Multiple linear regression

Model: CN for APO FAME = a0 + a1*Density + a2*Kinematic_viscosity + a3*FP + a4*LHV

Variable	Value	95% confidence
a0	-3294.7826	3250.9984
a1	3.7309767	3.6065918
a2	2.4910104	8.9639265
a3	-0.182401	0.2522792
a4	4.3031072	5.2766338

Number of independent variables = 4
Regression including free parameter
Number of observations = 6

R^2 =	0.9995053
R^2adj =	0.9975264
Rmsd =	0.0349397
Variance =	0.0439481

POLYMATH Results
03-31-2018

Multiple linear regression

Model: CN = a0 + a1*Density + a2*Kinematic_viscosity + a3*FP + a4*LHV

Variable	Value	95% confidence
a0	-395.18589	1.639E+04
a1	0.5409426	19.206667
a2	2.2526062	54.656119
a3	-0.0376528	2.6443183
a4	-0.2857082	12.557891

Number of independent variables = 4
Regression including free parameter
Number of observations = 6

R^2 =	0.9891721
R^2adj =	0.9458606
Rmsd =	0.191558
Variance =	1.3210009

Appendix Q

Pictures of experimental set up

Figure Q1: Set-up for synthesis of catalyst.

Figure Q2: Set-up for engine performance.